SENSITIVITY AND CLAY MINERALOGY OF WEATHERED TEPHRA-DERIVED SOIL MATERIALS IN THE TAURANGA REGION

A thesis

submitted in partial fulfilment

of the requirements for the degree

of

Master of Science in Earth Sciences

at

The University of Waikato

by

JUSTIN WYATT

THE UNIVERSITY OF
WAIKATO
Te Whare Wānanga o Waikato

The University of Waikato

2009

Abstract

Soil sensitivity is defined as the ratio of peak to remoulded shear strength. Problem soil materials are those that show large strength losses on disruption, resulting in catastrophic failure, liquefaction and long run-out distances. This study focussed on sensitive, weathered, mainly tephra-fall derived soils of mid-Pleistocene age in the Tauranga region. The liquefiable character of these soils is well known, but little detailed study has been directed towards the reasons for sensitivity. The objective of this work was to examine soil sensitivity by investigating geomechanical properties, clay mineralogy, and microfabric, and to determine how these factors combine to develop sensitivity. To achieve these objectives a combination of both field and laboratory investigations was undertaken.

Field investigations indicated that sensitive soils are common in the Tauranga region. Sampling was undertaken at sites in Tauriko and Otumoetai. Selected samples ranged across high (76) and low (≈ 8) field sensitivity. Stratigraphically, samples from Otumoetai lie below the Rangitawa Tephra (ca. 0.34 Ma), and those from Tauriko underlie the Te Ranga Ignimbrite (ca. 0.27 Ma).

Geomechanical investigation revealed that the sensitive soils had high moisture contents (> 60 %), low dry bulk density (< 966 kg m^{-3}), and high porosity (> 60 %). Liquidity index values ranged between 0.27 and 2.41. Plasticity index values ranged from 13.2 % to 42.7 %, with all samples plotting below the A line. Strength tests indicated effective friction angles from 25.7 ° to 38.5 °, effective cohesion from 4.7 kPa to 34.5 kPa, residual friction angles of 19.34 ° to 33.18 °, and cohesions of 0 kPa to 4.87 kPa. Remoulded vane shear strengths ranged between 1 kPa and 36 kPa.

Clay minerals were dominantly hydrated halloysite. Scanning electron microscopy indicated that clay morphology was in the form of hollow tubes, spheres, plates, and platy vermiforms ('books'). Tubes and spheres represent characteristic forms of halloysite in soils, plates are less common, and books have never previously been observed. Hence, these books represent a new morphology for halloysite. Individual plates in each of the books appear to show structural Fe enrichment (~ 5 . 2 %). This enrichment indicates that Fe had replaced Al in octahedral positions reducing the mismatch with the tetrahedral sheet, lessening layer curvature and thus generating flat plates.

All microfabrics were continuous with larger sand and silt grains supported in a background of clay minerals. Microfabrics ranged from extremely open with components being loosely packed to those which were dense and tightly packed. A feature common to all structural types was an abundance of extremely small pores (< 20 μm) which are capable of tightly retaining water. The loosely packed microfabrics had void ratios that allowed moisture content to exceed liquid limits, producing a liquidity index > 1. These open microfabrics are probably a result of quick burial by subsequent pyroclastic beds; hence weathering to clays occurred as a process of subsurface diagenesis. Dense microfabrics with low void ratios and high liquid limits did not have liquidity indexes > 1. These dense microfabrics arose as a result of the deposits being at, or near, the land surface for a considerable time, thus allowing strong pedogenic processes to occur, which promoted clay formation and clay migration (illuviation) and reduced void ratios.

Liquidity index was a major control on remoulded strength and sensitivity. Liquidity index is controlled by clay type and content, void ratio, and natural moisture content. When remoulded, structures with natural moisture contents exceeding the liquid limit release a large amount of water, which both dilutes the plasticity of binding clays and supports grains and broken aggregates of clay, allowing the material to flow. The development of sensitivity with low remoulded strength requires a number of factors. These include: a void ratio that is sufficiently high to allow natural moisture content to exceed the liquid limit; the presence of halloysite, which encourages samples to retain a coherent structure when saturated and to ensure the liquid limit remains sufficiently low so that it can be exceeded by natural moisture content; and a saturated environment, which ensures the liquid limit is exceeded.

Acknowledgements

Firstly, thanks are due to the Broad Memorial Trust and those who administer the University of Waikato Masters' Research Scholarships. Your financial support was much appreciated and enabled me to undertake my field work in Tauranga.

A special mention must go to my supervisors, Dr. Vicki Moon and Prof. David Lowe. Vicki, thank you for suggesting a topic that has proved both enjoyable and challenging. Although, I am sure you will agree, I did always seem to attract the challenging bits most often. Also your encouragement, expertise, open door and superb editing skills were much appreciated. David, I am in awe of your vast knowledge on all things tephra related, and I have appreciated your support, encouragement and am thankful for your time spent reading and editing. A big thank you must go to Dr Jock Churchman for the advice on halloysite; your input has been invaluable. Assoc. Prof. Roger Briggs, thank you for introducing me to the interesting and informative world that is volcanic petrology.

Thank you to Mr and Mrs French of Otumoetai for allowing me to undertake minor earthworks on your property. Also, thank you to Simon Maxwell, James Bilkie, Dave Morton, Brett Harlem and Diggs for letting me "*fill my boots"* with more than enough material from Tauriko. Mr and Mrs Montgomery of Ngapeke and Mr and Mrs Waugh from Oropi – thank you for letting me explore your properties. Ross Pedon, I appreciated your support in providing access to geotechnical reports held on Tauranga City Council files. At Opus International Consultants, Stan Lim is thanked for discussions on all things triaxial, and Jonathon Cahm and the guys at the Tauranga laboratory are thanked for letting me have a brief look around the slip at Tauriko. I must thank Marion O'Halleron from Ice Consultants for an early thesis-project tour and the benefit of a geotechnical engineer's perspective.

Dr. Dave Campbell is thanked for agreeing to let "someone else" take care of my allophane determinations. Thank you to Tom Dutton from Landcare Research for being that other person. Carolyn Hedley, also from Landcare Research, is thanked for sending ceramic tiles when it seemed no one in the Waikato area had any. Thank you to all the technical and support staff at the University of Waikato. Jacinta Parenzee, I would have been lost without your help. Renat Radosinsky, thank you for buying new things to replace those which I broke. However, the triaxial is now all yours. Helen Turner, many thanks for assistance with the SEM. Dr Ganqing Xu, thank you for help with the XRD and in preparing grain mounts. I also thank Peter Jarman, Annette Rodgers, Chris McKinnon, Craig Hosking, and Sydney Wright for all the other odds and ends.

Steve, Ange and Ryan – thank you for giving this travelling Earth scientist a place to rest. Glen, thanks for the couple of days in the field and the odd dinner or two. To all the other budding Earth scientists – you know who you are – cheers for the good times and banter. I am sure all of you are at the start of what will be illustrious careers. To all my family thanks for keeping it real and reminding me, when all seems pear shaped, what life is really about. Hopefully, I can make up for the missed events… Heartfelt thanks must go to Leah, for your kind words, encouragement and amazing support at the end, it has meant so much. Finally, we're free! Mum, thanks for giving me the determination to make it to the end – I'm sure you'd be proud.

Table of contents

Chapter Three

Chapter Four

Chapter Five

Chapter Six

Chapter Seven

Chapter Eight

List of figures

Chapter One

Chapter Two

Chapter Three

Chapter Four

Chapter Five

Chapter Six

Chapter Seven

Chapter Eight

List of Tables

Chapter Two

Chapter Three

Chapter Four

Chapter Five

Chapter Six

Chapter Seven

Chapter Eight

Chapter 1
Introduction

1.1 Introduction

Sensitivity is defined as the ratio of peak to remoulded shear strength, and many naturally coherent soils show sensitivity on disturbance (Mitchell & Soga 2005). Particularly Problematic and hazardous soils are those which show large strength losses on disruption, through low remoulded strength, allowing soil liquefaction, long run out distances, and retrogressive failures (Lefebvre 1996). However, soils with high shear strength will allow steep slopes to form, which may show a dramatic strength decrease on disruption, failing catastrophically (Torrance 1996). Whilst the soil may not liquefy, high sensitivities will be recorded.

Most research focusing on sensitive soils has been directed towards the glaciomarine clays of Scandanavia and Canada (Selby 1993; Lefebvre 1996; Rannka *et al.* 2004). These soils typically have extremely low remoulded strength and are often called “quick clays” (Lefebvre 1996). “Quick clays” typically have retrogressive failures with long run out distances (Gregersen 1981; Geertsema & Torrance 2005; Geertsema *et al.* 2006b). The works of numerous authors have been summarised into both pre- and post-depositional requirements for the development of sensitivity (Torrance 1983; 1995; 1996), and also basic factors which contribute to sensitivity (Mitchell & Soga 2005), in glaciomarine clays.

Receiving less international interest are sensitive soils observed in weathered, clayey pyroclastic material from New Zealand (Smalley *et al.* 1980; Jacquet 1987; 1990; Cong 1992; Keam 2008). Work which has specifically investigated the sensitive volcanic/pyroclastic deposits of the Taranaki and Waikato regions suggested that sensitivity manifests as high undisturbed rather than low remoulded strength (Jacquet 1987; Torrance 1992; 1995; 1996), with soils having a non-liquid-like character once remoulded. However, in the clayey pyroclastic deposits of the Bay of Plenty, the long run out distances and liquefiable character of mass wasting events suggest that sensitivity manifests as low remoulded strength. Many authors have made mention of the sensitivity of

pyroclastic deposits and associated volcaniclastic sediments of the Tauranga region (Prebble 1983; 1986; 2001), typically during the course of investigation into mass wasting events (Gibb 1979; Tonkin & Taylor 1980; Bird 1981; Hatrick 1982; Oborn *et al.* 1982; Oborn 1988; Burns & Cowburne 2003; Hegan & Wesley 2005; Wesley 2007). Locations of studies which have identified sensitive soils in volcanic ash material are presented in Figure 1.1.

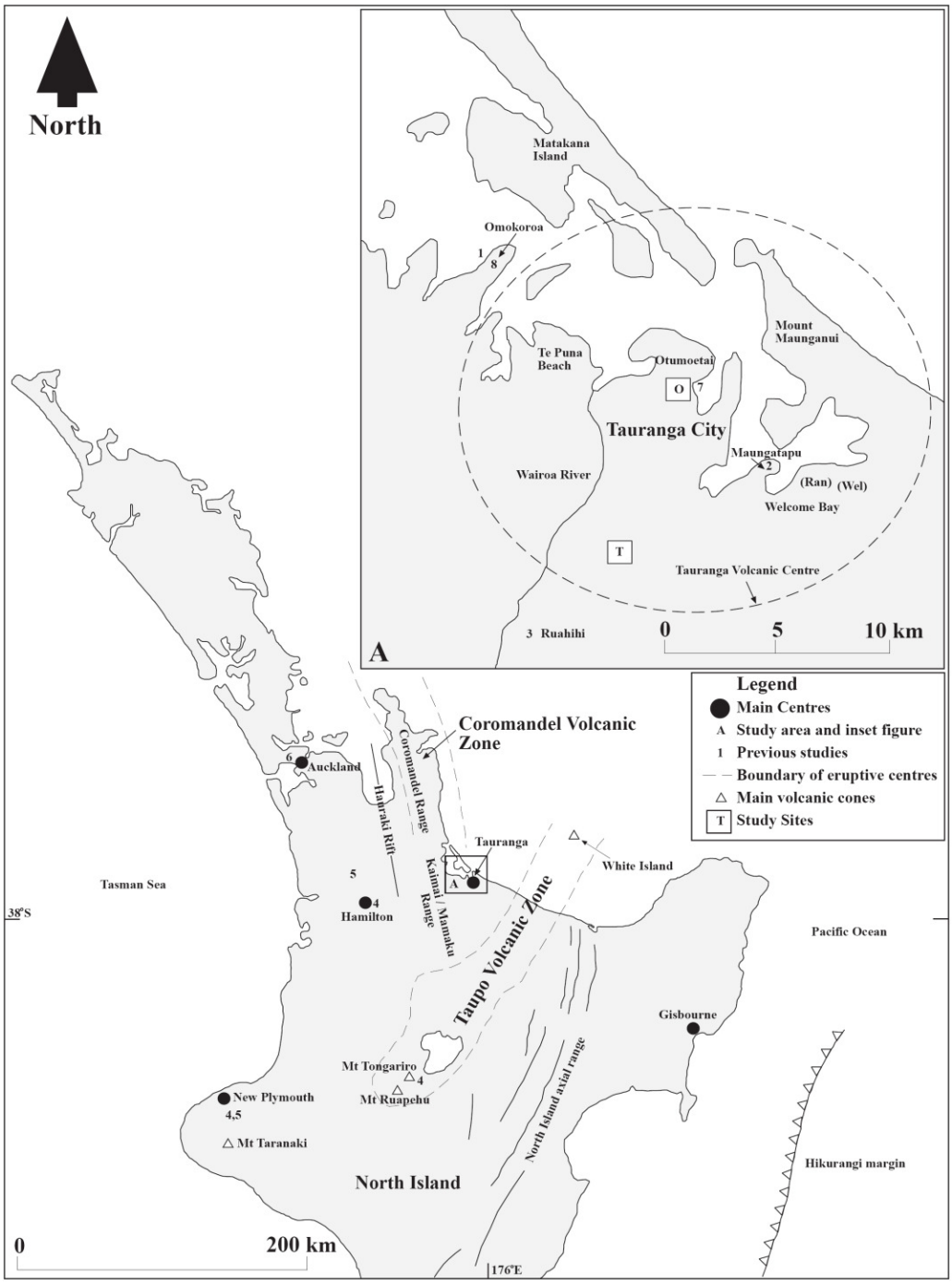

Figure 1.1: Map of the upper North Island, New Zealand, showing the proximity of the study area (Inset A) to the Coromandel and Taupo volcanic zones. In both the main figure and inset, the numbered locations indicate previous studies which mention sensitive volcanic deposits. These are (1) Gibb (1979), Tonkin & Taylor (1980), Smalley *et al.* (1980); (2) Bird (1981); (3) Hatrick (1982), Oborn *et al.* (1982); (4) Jacquet (1987); (5) Jacquet (1990); (6) Cong (1992); (7) Wesley (2007); (8) Keam (2008). These studies are discussed in Chapter 2. The principal study sites are located at Tauriko [T] and Otumoetai [O]. Geomorphic mapping and slip descriptions were undertaken at Ranginui Road (Ran) and Welcome Bay (Wel) (Chapter 4).

1.2 Thesis aims

The aim of this thesis is to develop an understanding of the causes of sensitivity in volcanic/pyroclastic deposits from the Tauranga region. Furthermore, an underlying aim is to provide a geotechnical characterisation of these soils.

Objectives to achieve this aim are to:

1) identify a number of highly sensitive soils in the field;

2) determine a range of geomechanical properties of selected sensitive soils using a combination of standard field and laboratory analyses;

3) qualitatively assess the mineralogy of selected sensitive soils, in both the clay-size (< 2 μm) fraction and bulk sample (includes clay, silt and sand);

4) describe the microstructure of selected sensitive soils using scanning electron microscopy; and

5) indentify the key aspects of geomechanics, mineralogy and microstructure which control sensitivity, especially that which manifests in low remoulded strength.

1.3 Study setting

The study area is in the Tauranga region (Figure 1.1). It comprises a portion of the Tauranga Basin and is at an approximate mid-point between the Late Miocene to Pliocene Coromandel Volcanic Zone (CVZ) to the north and the currently active Taupo Volcanic Zone (TVZ) to the south (Briggs *et al.* 2005) (Figure 1.1). Transition between these two volcanic zones occurred between 1.90 and 1.55 Ma (Briggs *et al*. 2005). The study area lies within the Tauranga Volcanic Centre, which was active between 2.69–1.90 Ma (Briggs *et al.* 2005) (Figure 1.1 (Inset A)). To the west of the study area is the Kaimai Range which represents and upfaulted block of Miocene–Pliocene basaltic to rhyolitic rocks (Briggs *et al.* 1996). The small Kaimai Volcanic Centre (2.87 – 2.09 Ma; Briggs *et al.* 2005) is also located within these ranges. To the east of the study area is the

barrier island, Matakana Island, which confines the shallow estuary of Tauranga Harbour (Figure 1.1, Inset A).

The close proximity to several volcanic centres has resulted in the study area being dominated by volcanic and pyroclastic materials. These include older andesitic lavas and breccias, Pliocene–Quaternary ignimbrites, which are intercalated with Quaternary volcaniclastic sediments, and a thick cover of younger Pleistocene–Holocene silicic tephras (Briggs *et al.* 2005). Of most interest in this study are mid to late Pleistocene pyroclastic deposits (including ash fall or pyroclastic flow deposits), either primary or reworked, which have become weathered.

Within the study area a number of NE and NNE trending terraces exist which typically extend as peninsulas into the Tauranga Harbour (e.g. Omokoroa, and Otumoetai) (Figure 1.1, Inset A). These terraces are typically between 20–40 m high, are intersected by broad valleys and terminate seawards in the form of shallow cliffs and steep slopes (Briggs *et al.* 1996).

1.4 Thesis outline

In Chapter 2 a literature review discusses sensitivity in overseas glaciomarine sediments, describes clay mineralogy and sensitivity in volcanic ash soils, and provides details of the stratigraphy of the study area and notable mass wasting events within the region. Both field and laboratory methods are described in Chapter 3. A summary of field investigations, including justification for site selection, site stratigraphy and field strength and sensitivity results, is presented in Chapter 4.

The main results are given in chapters 5, 6 and 7. In Chapter 5, results from geotechnical characterisation of samples, including effective strength testing, are outlined. Qualitative mineralogical analyses of both bulk material (clay, silt and sand) and clay-size fractions (< 2 μm) for each sample are presented in Chapter 6. The results of microfabric investigations undertaken using scanning electron microscopy are described in Chapter 7.

Chapter 8 is a discussion drawing together all the main findings of this study. The discussion describes the nature and geological development of each unit sampled, relationships between measured and observed properties, and concludes with a possible explanation for the development of sensitivity. Chapter 9 concludes the study and presents a summary of findings in regards to the main aims and objectives, followed by recommendations for further research

Chapter 2
Literature review

2.1 Introduction

Sensitive soils have unique properties which are a result of their mode of origin and subsequent geological history. The aim of this chapter is to introduce the idea of sensitivity both internationally and on a local scale. The chapter is divided into six sections: (1) defining sensitivity; (2) classical glaciomarine quick clays; (3) the volcanic stratigraphy of the study area; (4) the structure of typical clay minerals (allophane and halloysite) derived from volcanic parent materials. Sections 3 and 4 will clearly differentiate the soils of this study from classical quick clays; (5) sensitivity in volcanic soils both internationally and locally; (6) sensitive soils already observed within the study area and their relationship with notable mass wasting events.

2.2 Soil sensitivity

2.2.1 General Definition

Sensitive soils remain stable for thousands of years, and then suddenly lose strength, often with catastrophic consequences. Disturbance can occur with little increase in moisture content (Selby 1993). When remoulded strength is very low, disturbed material behaves as a fluid, moving away from the failure scarp leaving the new slope unsupported. Subsequent failures may then occur (Lefebvre 1996). However, high undisturbed strengths allow steep slopes to form and to be stable. These soils may not liquefy on failure but the subsequent loss in strength can be catastrophic (Torrance 1995). Therefore, two types of sensitive soils exist:

1) those which show a large loss of strength on remoulding, but may not necessarily liquefy; and

2) those which display very low, liquid-like remoulded strength.

2.2.2 Numerical definition of sensitivity

Sensitivity can be defined as the ratio of undisturbed strength over remoulded strength (Selby 1993) and is presented by the equation:

$$Sensitivity\ (S_t) = \frac{Undisturbed\ ,\ undrained\ \ strengt\ h\ (\tau_u)}{\underset{(at\ the\ same\ \ moisture\ \ content\ )}{Remoulded\ ,\ undrained\ \ strengt\ h\ (\tau_r)}} \qquad (2.1)$$

Because equation 2.1 is simply a ratio, soil materials with identical sensitivities may exhibit different undisturbed and remoulded strengths (Torrance 1987). Within the literature a wide range of terminologies and divisions between different levels of sensitivity exists (i.e. non-sensitive, medium and quick) (Skempton & Northey 1952; Rosenqvist 1953; Norsk Geoteknisk Forening 1974; Rankka *et al.* 2004; New Zealand Geotechnical Society 2005). In all studies samples which display values of unity (1) are termed insensitive. Because this study is being undertaken in New Zealand the classification system set out by the New Zealand Geotechnical Society (2005) will be used (Table 2.1).

Table 2.1: Soil sensitivity categories as determined by the New Zealand Geotechnical society (2005).

Descriptive term	**Shear strength ratio** (Undisturbed strength / Remoulded strength)
Insensitive, normal	<2
Moderately sensitive	2-4
Sensitive	4-8
Extra sensitive	8-16
Quick	>16

One problem with the New Zealand classification is that it does not have an upper limit for remoulded strength. This is important when deciding whether the clay being examined is actually "quick" and hence flows on disturbance (Torrance 1983), because in a classical sense, clay becomes "quick" not because undisturbed strength is very high but because remoulded strength is extremely low (Mitchell & Soga 2005). Swedish and Canadian authors use an upper value for remoulded strength of 0.4 kPa (Karlsson & Hansbo 1989; Rannka *et al.* 2004) or 0.5 kPa (Torrance 1996), typically combined with a sensitivity value of between 30 and 50, when defining a soil as quick. A Swedish drop or sensitive laboratory vane are typically used to derive such low values (Rannka *et al.* 2004; Geertsema & Torrance 2005). Whilst it is recognised that low remoulded strength values are important, the field vane used in this study to directly measure remoulded strength (Chapter 3) was unable to measure such low values (Chapter 4). Therefore, a

classification which uses the upper limits of remoulded strength suggested by previous authors could not be employed.

2.3 International sensitive soils

Internationally, highly sensitive sediments have been observed in fine grained, post-glacial marine and brackish water sediments of eastern Canada, Scandinavia and Alaska (Torrance 1996; Mitchell & Soga 2005). Sensitive glacial clays of freshwater origin have also been reported (Soderblom 1966). Sensitive Holocene age volcanic materials deposited in a marine environment have been observed in Ariake Bay, Japan (Torrance & Ohtsubo 1995). Sensitivities up to 1500 and 895, often quick in nature, have been reported in Canadian glacial marine Leda clay (Smalley 1971) and Ariake Bay sediments (Torrance & Ohtsubo 1995), respectively. The following will describe the causes and origins of sensitivity in these soils.

Glacial marine clays are geologically young, typically deposited in pre-glacial and post-glacial bodies of water during the retreat of the Wisconsin ice sheet some 18 000 to 6 000 ^{14}C years before present (Lefebvre 1996). Unloading and subsequent isostatic rebound has meant these soils are above present-day sea-level (Lefebvre 1996). The erosive activity of rivers has cut into these uplifted sediments, exposing sensitive material and allowing retrogressive slope failure to occur (Torrance 1996).

Slow sedimentation in a marine or brackish environment has promoted an open, flocculated structure (Smalley *et al.* 1984), with initially high salt concentrations in soil pore water (Torrance 1987; 1992). Mitchell & Soga (2005) described the fabric of sensitive clays as having a "metastable" structure. This description implies clay particles are in edge-to-edge and edge-to-face contacts, forming an open cardhouse arrangement. This structure can carry effective stresses at a void ratio higher than if particles were in a parallel array (Mitchell & Soga 2005). Sensitivity is also enhanced by the linking of large particles (i.e. sand, silt and clay aggregates) with unstable connectors (Mitchell & Soga 2005).

Sensitive marine clays are dominated by low activity (< 0.5) minerals. These include the clay minerals illite, chlorite and sometimes kaolinite. Non-clay

minerals, typically representing glacial flour, are quartz, feldspar, amphiboles and carbonates (Torrance 1992; Mitchell & Soga 2005). Often primary minerals are in greater abundance in the clay-size fraction than phyllosilicates (Torrance 1996). In contrast, sediments at Araike Bay, Japan, are dominated by low swelling and low-activity smectite with lesser amounts of kaolinite, illite and vermiculite (Egashira & Ohtsubo 1982; Torrance 1996). An abundance of low activity material will result in a system dominated by short-range bonds, as opposed to long-range bonding typical of high activity clays. Short range bonds are weak and are lost when particles lose contact (Smalley 1971). This bond loss promotes dramatic strength decrease on disturbance. Furthermore, leaching (discussed below) may decrease long-range bonding encouraging short-range bonds to dominate and sensitivity to occur (Smalley 1971). The concept of short-range bonding contributing to sensitivity has been termed the "inactive particle theory" (Smalley *et al.* 1980).

A post-depositional reduction in remoulded strength leading to high sensitivity is often attributed to salt leaching from pore water (Torrance 1992). Three leaching processes exist, including water from rain and snow percolating through a deposit, water seeping upwards as a result of artesian pressure, and diffusion of salt along a concentration gradient (Rankka *et al.* 2004). A reduction in salinity affects both individual particles and the forces between them; however, the flocculated structure is largely preserved (Brand & Brenner 1981). Leaching can reduce the liquid limit of the soil but water content and void ratio will remain constant (Torrance 1983; 1987; Mitchell & Soga 2005). Leaching affects the ability of particles to re-flocculate into large aggregates following remoulding (Rannka *et al.* 2004), thus causing a large loss in strength (Torrance 1987; 1992).

Other lesser factors also contribute to sensitivity. A high proportion of the ions Na^+ and K^+, in comparison with Ca^{2+} and Mg^{2+}, in pore water solutions will promote high sensitivity. The abundance of these monovalent ions will lead to a large double diffuse layer around clay particles which will result in larger repulsive forces between particles, hence preventing re-flocculation following remoulding (Rannka *et al.* 2004).

Cementation increases undisturbed strength but by itself is not enough to produce highly sensitive clays because it does not affect remoulded strength (Torrance 1983; 1987). Cementing agents may include carbonates, iron oxides, alumina and organic matter, and these bind soil material together at inter-particle contacts (Mitchell & Soga 2005). Addition of organic or inorganic dispersants to a low activity soil can lower the liquid limit, decreasing remoulded strength (Torrance 1983; 1987). Organic dispersants were believed to have decreased the liquid limit of a freshwater glacial deposit, enhancing its sensitivity (Soderblom 1966).

The shape of clay particles may also be important for the development of quick clay. Pusch (1962), as cited in Rannka *et al.* (2004), stated that large, thin plates will become more dispersed on remoulding than particles with more uniform dimensions.

In glacial marine clays, the following factors inhibit the development of quick clay; presence of swelling minerals, high degree of weathering, presence of high valence cations, deep burial and consolidation (Torrance 1987). In glacial marine clays, weathering to produce a soil alters mineralogy, structure, sensitivity and strength. Typically both undisturbed and remoulded strength increase with progressed weathering.

2.4 Stratigraphy of the Tauranga region

The classic quick clays frequently described in international literature have a different geological history and mineralogy than soils observed in the study area. Thus, the following section will introduce the volcanic stratigraphy of the study area. Furthermore, this stratigraphy is important in later sections where mass wasting events and sensitivity in the Tauranga region are discussed.

Strata observed in the Tauranga Basin include deposits of both primary volcanic origin (including pyroclastic) and reworked volcanic materials. All the primary deposits were derived from eruptive events occurring in the southern Coromandel Volcanic Zone (CVZ), the Tauranga Volcanic Centre, the Kaimai Volcanic Centre and the Taupo Volcanic Zone (TVZ), and appear to be dominantly rhyolitic in composition. The eruptive events, especially pyroclastic

flows (density currents) that produced ignimbrites, were often voluminous, providing material to be reworked by fluvial, lacustrine and estuarine processes, which were then redeposited in sequences intercalated with primary volcanic deposits (Briggs *et al.* 1996). Figure 2.1 presents a graphical summary of the stratigraphic sequence which occurs in the Tauranga region. This sequence is then discussed in the following section with the most emphasis placed on the tephra-fall deposits and Matua Subgroup material.

2.4.1 Volcanics

The underlying volcanics range from early andesitic lavas (Otawa Volcanics, 2.95 to 2.54 Ma) and volcanic breccias through to materials of dacitic to rhyolitic composition (Figure 2.1). These are, however, of little significance to this study.

2.4.2 Ignimbrites

Ignimbrite sheets are prominent features in the Tauranga region forming a series of extensive plateaux (Briggs *et al.* 2005). The Waitekauri Ignimbrite is the oldest (2.18 to 2.13 Ma) and underlies the Tauranga Basin to depths of 50 – 150 m. It is encountered in drill holes throughout the Tauranga Harbour and urban area (Briggs *et al.* 2005). The Papamoa Ignimbrite consists of multiple flow and interbedded tephra-fall deposits (Briggs *et al.* 2005).

The Ongatiti Ignimbrite (1.34 Ma) was erupted from the Mangakino Volcanic Centre and in the Tauranga region it is typically partially to densely welded (Briggs *et al.* 1996). The Te Puna Ignimbrite (0.93 Ma) is non to partially welded and is derived either locally (Briggs *et al.* 1996; 2005) or is a correlative with Kidnappers Ignimbrite (Keam 2008).

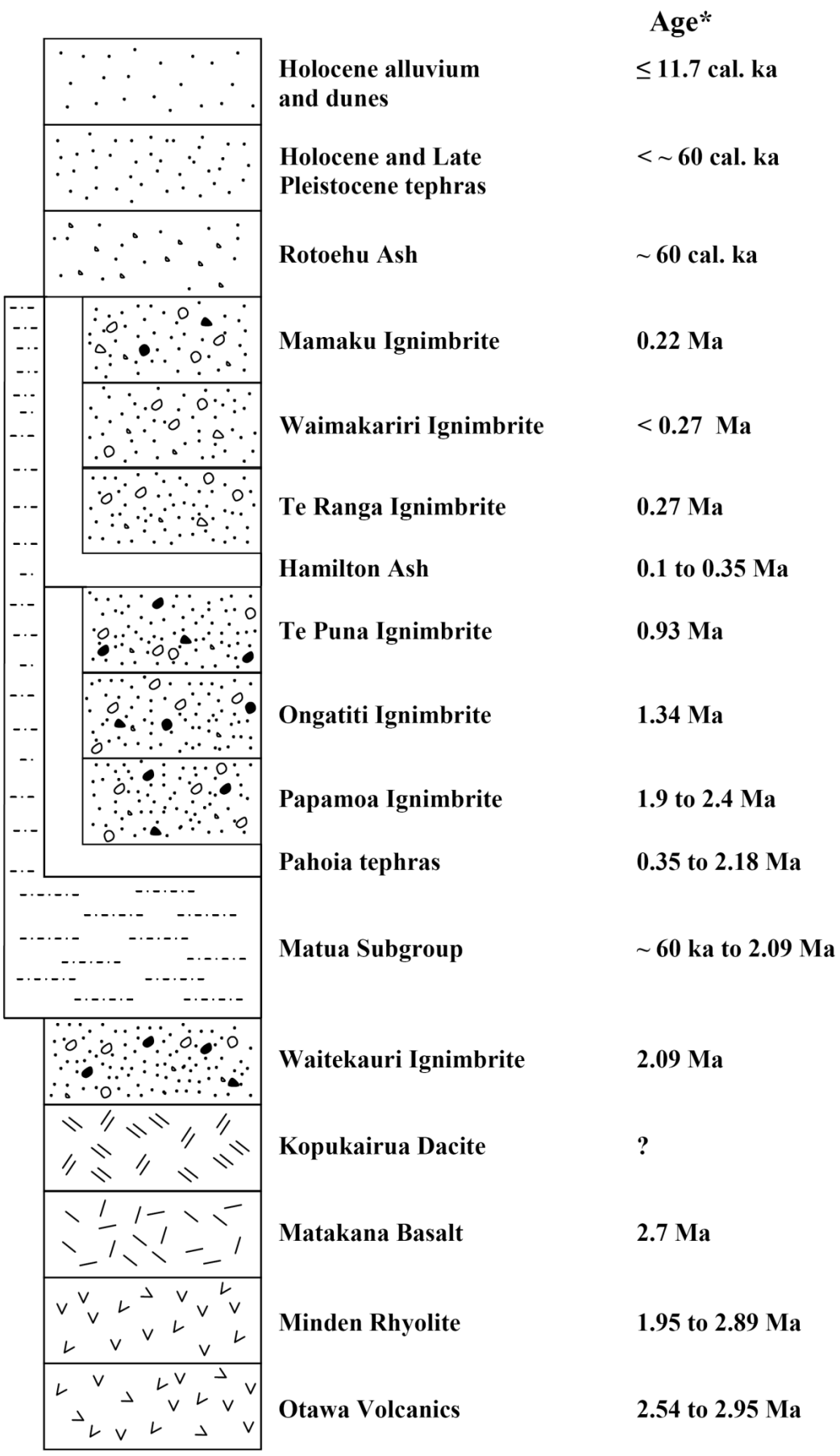

Figure 2.1: Stratigraphy of the Tauranga Region after Briggs *et al.* (1996), Briggs *et al.* (2005), and Briggs *et al.* (2006). *Ma = millions of years ago, ka = thousands of years ago.

The Te Puna ignimbrite is eroded and overlain by cross bedded fluvial pumiceous sands, lacustrine diatomaceous silts and sand, lignites and tephra fall beds (Pahoia tephras, Hamilton Ash) (Briggs *et al.* 1996). The Te Ranga (0.27 Ma) ignimbrite is a light grey, non welded, crystal-poor, sandy textured ignimbrite. This ignimbrite is not known outside the central Tauranga Basin and is therefore suggested to be locally derived (Briggs *et al.* 1996). The Te Ranga Ignimbrite has been observed intercalated with lacustrine silts, overlying Matua Subgroup (~ 60 ka to 2.09 Ma) materials and also overlain by the Hamilton Ash Formation (0.1 to 0.35 Ma) and Rotoehu Ash (~ 60 ka) (Briggs *et al.* 1996; 2005). The Waimakariri Ignimbrite (0.22 to 0.32 Ma) is a large volume, welded ignimbrite (Briggs et al. 1996). The Mamuku Ignimbrite (0.22 Ma) is a partially to weakly welded unit and, with the Waimakariri Ignimbrite, forms the upper surface of the Mamaku Plateau which dips 1 – 2 º northwards towards the Tauranga Basin (Briggs *et al.* 2005).

2.4.3 Matua Subgroup

The Matua Subgroup (~ 60 ka to 2.09 Ma) is a member of the Tauranga Subgroup (as defined by Kear & Schofield 1978) and includes all terrestrial and estuarine sedimentary materials deposited after the emplacement of the Waitekauri Ignimbrite (2.09 ± 0.03 Ma) and before Rotoehu Ash deposition (~ 60 ka). This excludes those fluvial and other sediments of the late Pleistocene and Holocene age (Brigg *et al.* 1996). Briggs *et al.* (1996) defined the upper limit of the Matua Subgroup as the Mamaku Ignimbrite. However, at Maketu, Briggs *et al.* (2006) extended it to the base of the Rotoiti Tephra, of which Rotoehu Ash is a member. The Matua Subgroup was deposited during a period of intense and voluminous activity in both the CVZ and TVZ (Briggs *et al.* 2006).

A range of lithologies occurs within the Matua subgroup including fluvial pumiceous and rhyolitic silts, sands and gravels, lacustrine and estuarine muds, lignites and peats intercalated with tephra fall units and thin distal ignimbrites (Briggs *et al.* 1996). Sedimentary structures include cross-bedding, planar stratified and massive units, and massive slump and water escape structures mostly derived from reworked volcaniclastic material (Briggs *et al.* 1996). Matua Subgroup materials infill the Tauranga Basin to a depth of ~ 150 m (Harmsworth 1983) and form terraces up to 80 m high (Briggs *et al* 1996). Matua Subgroup

sediments are exposed in sections at Maungatapu, Matapihi, Omokoroa and at the the base of Mt Maunganui (Briggs *et al.* 1996).

2.4.4 Pahoia tephras

Pahoia tephras (0.35 to 2.18 Ma), originally named tuffs by Pullar & Birrell (1973), is a portmanteau term for highly weathered ashes older than the Hamilton Ash. Pahoia tephras are believed to be rhyolitic (Harmsworth 1983). Kirkman & Pullar (1978) observed 13 beds with associated paleosols near Opotiki. These were light coloured (pink, white and pale yellow) and comprised almost entirely of halloysite. Harmsworth (1983) observed 14 light coloured clayey to sandy tephra beds at Omokoroa Peninsula which formed a sequence ~ 5 metres thick. Paleosols were observed in four units. Across the Tauranga Basin the sequence has been recorded between 1 and 15 metres thick, and included both tephra fall but also pyroclastic flow deposits (ignimbrites) (Harmsworth 1983). The Pahoia tephras are often intercalated with the Matua Subgroup materials and distal ignimbrites (Briggs *et al.* 1996).

The Pahoia tephras may in part, represent correlatives of the Kauroa Ash Formation (≥ 0.78 to 2.24 Ma; Lowe *et al.* 2001) (Briggs *et al.* 1996). The Kauroa Ash sequence is well known in the Waikato region (Ward 1967; Salter 1979; Briggs *et al.* 1994) and is up to 12 m thick and includes multiple tephra deposits and associated paleosols sometimes interbedded with loess material (Briggs *et al.* 1994; Lowe *et al.* 2001). The beds are assumed to be predominantly rhyolitic and possibly relate to either late CVZ or early TVZ eruptions, or both (Lowe *et al.* 2001).

The Pahoia tephras have been observed at Greerton, Maungatapu, Matapihi, the base of Mount Maunganui, along the Waikareao expressway, Matua and Omokoroa (Brigg *et al.*1996).

2.4.5 Hamilton Ash

The Hamilton Ash Formation (~ 0.1 to 0.35 Ma) is a sequence of highly weathered clayey ash beds, with associated paleosols, which were originally identified in the Waikato region (Ward 1967) and which are also recognised in the South Auckland and Coromandel regions (Bakker *et al.* 1996; Lowe *et al* 2001).

In the Waikato region this sequence is up to 6 m thick and comprises up to 7 members (H1 – H7). At some sites, fall deposits may be intercalated with loess beds (Lowe *et al.* 2001; 2008c). Only the origin of member H1 is known with any certainty, and it is a correlative of the Rangitawa Tephra. The Rangitawa Tephra is a correlative of the Whakamaru-group ignimbrites derived from the Whakamaru caldera volcano (0.35 – 0.32 Ma; Lowe *et al.* 2001). Whilst the source of the remaining members is unknown (H2 – H7), they are thought to be of rhyolitic origin (Lowe & Percival 1993; Briggs *et al.* 1994; Lowe *et al.* 2001). In the Waikato region, Shepherd & Gibbs (1984) suggested an origin in the rhyolitic Taupo – Maroa volcanic centres. Lowe *et al.* (2001) stated that a number of rhyolitic centres in the TVZ were active during the emplacement of the Hamilton Ash sequence and hence the beds may have multiple origins.

In the Tauranga region a similar composite sequence, up to 2.5 m thick, has been observed so the term Hamilton Ash has also been employed (Briggs *et al.* 1996; 2005). These beds often appear yellowish to dark brown in which paleosols are developed with a polyhedral to blocky structure (Harmsworth 1983).

2.4.6 Rotoehu Ash

The Rotoehu Ash is a shower bedded tephra-fall unit overlying the Hamilton Ash beds and typically found at depths of between ~ 1.2 and ~ 2.2 m in the Tauranga region. Multiple white to greyish beds 0.02 to 0.2 m thick are observed which have a sandy texture (Harmsworth 1983). The Rotoehu Ash has an age of ~ 60 ka (c. calendar [cal] ka) and is derived from the Okataina Volcanic Centre (Froggatt & Lowe 1990; Lowe & Hogg 1995; Wilson *et al.* 2007). Part of the unit may have been deposited from phreatic eruptions when the co-eval Rotoiti Ignimbrite entered the sea (Walker 1979 as cited in Briggs *et al.* 1996).

2.4.7 Post-Rotoehu Ash tephras

Overlying the Rotoehu Ash sequence is a cover of tephra deposits which represent the dominant pedological soil forming parent materials in the Tauranga region. These tephras have been summarised in Briggs *et al.* (1996) (see also Briggs *et al.* 2006) and include: Mangaone (0.6 to 3 m), Kawakawa (0.3 to 0.6 m), Te Rere (0.15 to 0.3 m), Okareka (0.15 to 0.5 m), Rotorua (0.15 to 0.45 m), Mamaku (0.1 m), Tuhua (0.1 m), Taupo (0.1 m) and Kaharoa (0.1 m) tephras. The

tephras, with the exception of the Tuhua, are from the Okataina and Taupo volcanic centres. The Tuhua is from Mayor Island (Briggs *et al.* 1996). All ages are summarised in Froggat & Lowe (1990) and Lowe *et al.* (2008c).

2.4.8 Holocene sediments

Holocene sediments comprise a number of deposits, including sediments deposited in the large barrier-enclosed estuary of Tauranga Harbour, progradational dune ridges which tie the tombolos of Mt Maunganui and Bowentown to the mainland, and alluvial deposits which have formed low terraces of Holocene and late-Pleistocene age. These sediments are composed of silts, sands, clays, gravels and carbonaceous material (Briggs *et al.* 1996).

2.5 Clay minerals, structures and formation

Pyroclastic materials comprise a variety of materials, including non-crystalline volcanic glass, feldspars, quartz and heavy minerals including Fe-Ti oxides and ferromagnesian minerals (Churchman 2000). Following dissolution, neogenesis and then crystallisation a variety of clay minerals is formed from dissolution products of these materials. Clay minerals typically associated with central and upper North Island volcanic deposits include both halloysite and allophane (Salter 1979; Shepherd 1984; Lowe & Nelson 1983; Lowe & Percival 1993; Lowe 1995). The following section will discuss the structure of kaolinite, because of its importance to this study, and then halloysite and allophane. The subsequent section will then explain the formation of both allophane and halloysite.

2.5.1 Clay mineral structures

2.5.1.1 Kaolinite

The structure of kaolinite comprises a single 1:1 layer consisting of a Si^{4+} tetrahedral sheet and Al^{3+} octahedral sheet (Figure 2.2). However, the ideal lateral dimension of Si tetrahedral sheet is larger than the Al octahedral sheet, causing a size misfit in the *b* dimension (Bates *et al.* 1950; White & Dixon 2002). The misfit in size is overcome by either alternate tetrahedra rotating in opposite directions, tilting or changes in their ideal shape (White & Dixon 2002). This 'misfit response' results in 1:1 layers which are flat.

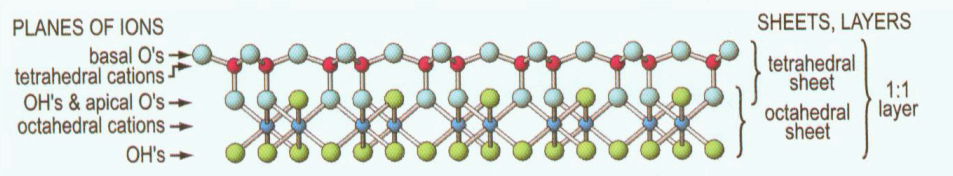

Figure 2.2: The typical structure of a 1:1 layer, in this instance the octahedral cation is Al^{3+} (blue sphere) and the tetrahedral cation is Si^{4+} (red sphere). This layer structure represents that typically observed in kaolinite and dehydrated halloysite and has a thickness of 7 Å (0.7 nm) (image adapted from Schultz 2002). Note that the apex of the individual tetrahedra point inwards towards the octahedral sheet.

In a kaolinite crystal the flat 1:1 layers stack above each other (Olson *et al.* 2000; Schultze 2002). The stacks of layers are held together by hydrogen bonding between basal oxygens of the tetrahedral sheet (shown as light blue spheres in Figure 2.2) and the hydroxyls of the adjacent plane of the octahedral sheet (shown as light green spheres in Figure 2.2) (Schultze 2002; White & Dixon 2002). Because the misfit in size of sheets is corrected, stacks of 1:1 kaolinite are commonly observed as pseudo hexagonal plates or in some cases vermiforms (books) (White & Dixon 2002).

2.5.1.2 Halloysite

Halloysite has the same structure as kaolinite (Figure 2.2). However, in hydrated halloysite a water molecule is intercalated between adjacent 1:1 layers (Olson *et al.* 2000; Schultze 2002). Thus, a single water molecule and a 1:1 layer give hydrated halloysite, a thickness of 10 Å (1 nm). However, this water molecule is easily lost, causing halloysite cell layer thickness to reduce to 7 Å, forming dehydrated halloysite (Olson *et al.* 2000). Dehydrated halloysite has the same unit thickness as kaolinite (7 Å).

Unlike kaolinite, hydrated halloysite is typically observed as spheres and tubes (Schultze 2002). This curvature and hence layer rolling is believed to originate from the misfit in size between the octahedral and tetrahedral sheets, which, unlike kaolinite, is not corrected (Churchman 2000). A mechanism which facilitates layer rolling is the water between the adjacent 1:1 layers. This water relaxes the hydrogen bonding between adjacent 1:1 layers and acts as a lubricant, allowing the halloysite crystal to curl (Costanzo & Giese 1985; Singh 1996). Rolling is also assisted by interlayer water blocking tetrahedral rotation (Bailey 1990). Blocking tetrahedral rotation means the structural changes which prevent

layer rolling in kaolinite cannot occur. This disruption results in the larger tetrahedral sheet curling around the outside of the octahedral sheet (Bates *et al.* 1950; Singh 1996; Churchman 2000), forming the common tube-like morphology.

2.5.1.3 Allophane

The structure of allophane differs from that of kaolinite and halloysite because it has a short-range order. In New Zealand three types of allophane exist (Parfitt 1990; Lowe 1995):

1) **Al-rich allophane** with an *Al:Si* molar ratio of ≥ 2 and sometimes referred to as imogolite-like allophane.

2) **Si-rich allophane** with an *Al:Si* ratio ≈ 1, often referred to as halloysite-like allophane.

3) **Stream-deposit allophane** with an *Al:Si* ratio ≈ 0.9 to 1.8, often called hydrous feldspathoid allophane.

Both the Al- and Si-rich variety are found in soils, but the Al-rich allophane is predominant in New Zealand soils (Parfitt 1990). The structure of both Al- and Si-rich allophane consist of small imogolite-like fragments. These fragments combine to form a hollow porous spherule which is 4 – 5 nm (40 – 50 Å) in diameter and has water molecules in the centre of the spherules and also adsorbed onto their surface (Lowe 1995). Rao (1995) stated that the water within the spheres is inactive during soil deformation and has no influence on the mechanical behaviour of allophane. The structure of Al-rich allophane is shown schematically in Figure 2.3.

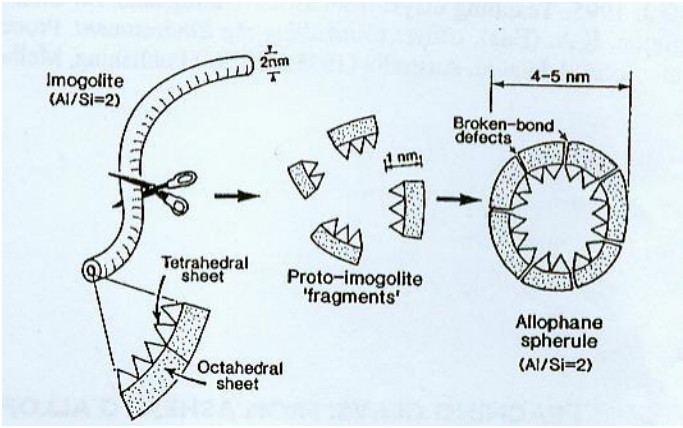

Figure 2.3: Schematic diagram indicating how imogolite fragments make up Al-rich allophane. The triangles represent Si^{4+} tetrahedra and the shaded rectangles represent Al^{3+} octahedra. The schematic diagram is from Lowe (1995).

2.5.2 Allophane and halloysite formation

In volcanic deposits the most important factors involved in the process of clay formation are environmental conditions coupled with the composition of parent material (Lowe 1986). Environmental conditions are exceptionally important for allophane and halloysite considering it is possible for them to weather directly from the same primary mineral (Churchman 2000; Joussien *et al.* 2005).

2.5.2.1 Allophane

Concentrations of silicon in soil are a significant factor in determining whether, and which type of allophane, will form (Lowe 1995);

1) Where Si in soil solution is low (< 10 g m^{-3}), Al-rich allophane may be formed;

2) Where Si in soil solution is high (> 10 g m^{-3}), halloysite or Si-rich allophane may form.

Silica in soil solution is controlled mainly by drainage and leaching, the latter governed mainly by rainfall. For example, Parfitt *et al.* (1984) considered at least ~ 250 mm yr^{-1} of through drainage is important for the formation of Al-rich allophane because this will leach sufficient Si to favour Al-rich allophane forms. Parent material is also important because rhyolitic tephras are more siliceous (and less Al-rich) than andesitic tephras (Lowe 1986), creating an environment of potentially high Si content. Under the same rainfall conditions and drainage, soils of andesitic origin will typically yield Al-rich allophane whereas those of rhyolitic origin may yield halloysite (Harsh *et al.* 2002). The rate of weathering (dissolution) in andesitic glass is faster than that of rhyolitic glass under similar conditions (Lowe 1995). Therefore more Si will be released into soil solution quicker by weathering of andesite glass compared to rhyolitic glass (and hence liable to loss in drainage waters) which will affect the rate of allophane formation (Churchman 2000). The amount of Al available to precipitate can affect allophane formation. For example, Dahlgren *et al.* (1993) (as cited in Lowe 1995) indicated that metal-humus complexes (found in soils rich in organic matter especially in Japan, for example) effectively compete for Al (the so called anti-allophane affect). This competition can leave very little Al in the soil available for

inorganic allophane formation, mostly being bound on Al-humus complexes. Allophane forms at pH > 4.8 (Lowe 1995).

2.5.2.2 Halloysite

The weathering sequence volcanic ash → allophane → hydrated (10 Å) halloysite → dehydrated (7 Å) halloysite → kaolinite, has been reported on many occasions (Joussien *et al.* 2005). Prior to 1980, the transformation of allophane to halloysite was largely accepted, however more recently this transformation has been overturned (Parfitt *et al.* 1980; Lowe *et al.* 1986; Churchman 2000; Joussien *et al.* 2005). Allophane and halloysite have been shown to form directly from similar volcanic parent material (Joussien *et al.* 2005) and transformation would require the reorganization of atomic structures involving the re-precipitation and dissolution of both Al and Si (Parfitt 1990; Lowe & Percival 1993; Joussien *et al.* 2005). Reorganisation of structure to form halloysite from allophane is required because in allophone, the tetrahedra occur on the inner surface of hollow spheres and their apices point away from the octahedral sheet (Figure 2.3). This is reverse to their situation in kandic clays (Figure 2.2) (Lowe 1986; Churchman 2000). Thus it is more likely that halloysite will form directly from dissolution of primary minerals rather than via an allophane transitional step.

The formation of halloysite directly from volcanic materials is related to a Si-rich environment (Harsh *et al.* 2002; Joussien *et al.* 2005). McIntosh (1979) showed halloysite could form in very young (~1800 year old) tephra material under certain conditions in New Zealand. Environmental conditions which favour the formation of halloysite include a humid tropical climate, a short dry season (1 to 3 months) and moderate rainfall regimes. Moderate rainfall regimes will lead to less desilication when compared with high rainfall conditions which promote strong leaching (Joussien *et al.* 2005). An essential requirement for the formation of hydrated halloysite is the abundance of water (Churchman 2000; Joussien *et al.* 2005) and hence halloysite is more common in the lower wetter parts of soil profiles (Churchman 1990). Halloysite formation is also believed to be favoured by a 'stagnant' moisture regime and a thick depositional over-burden (Wada 1989). The stagnant moisture regime ensures that Si in soil solution will not be leached thus remaining high. Wada (1989) suggested the thick overburden acts as a silica source for the resilication of allophane, which may then form halloysite.

However, considering the comments regarding the transformation of allophane to halloysite, this overburden may act as a rich source of silica for the direct formation of halloysite (Lowe 1986).

2.6 Sensitivity in volcanic ash materials

The following will describe sensitivity in volcanic ash material both internationally and in New Zealand.

2.6.1 Internationally sensitive volcanic ash

Sensitivity in volcanic ash soils is not widely reported in the engineering geology literature. Furthermore, it seems that volcanic soils typically have very good engineering properties. For example, slopes in volcanic ash soils tend to be steeper than deposits with similar clay contents in sedimentary soils (Wesley 1973). Furthermore, Wesley & Matuschka (1988) stated that, typically, volcanic ash soils are of high strength and low compressibility, with properties which are not greatly influenced by natural water content or Atterberg limits.

Volcanic ash materials which have subsequently weathered to soils dominated by either allophane or halloysite have been recorded with sensitivities of ~ 1 and ~ 2, respectively, in the soils of Indonesia (Wesley 1973). These soils have high clay contents, 70 – 90 %, and can maintain the same amount of water year round regardless of environmental conditions. However, Wesley (1973) indicated that volcanic ash soils with sensitivities up to 20 occur in Indonesia.

Investigating the tropical volcanic soils of Teneriefe, Gonzalez *et al.* (1981), without recording sensitivity values, suggested large strength decreases following remoulding occurred in soils containing halloysite but not in those dominated by montmorillonite. The authors suggested that the strength decrease in halloysite was a result of the disruption of a highly organised interwoven fabric. It was believed that disturbance caused little alteration to the already random fabric observed in montmorillonite-containing soils.

Volcanic ashes from Papua New Guinea, containing allophane, have been reported with sensitivities between reported between 2 and 6. This sensitivity

manifested in high undisturbed strength, as soils were observed supporting cuttings up to 10 m high (Moore & Styles 1988).

2.6.2 New Zealand

Jacquet (1987) summarised a comprehensive bibliography by stating that volcanic ash soils in New Zealand have unique properties. These include sensitivity, physical changes on drying (aggregation and loss of plasticity), high liquidity indexes, high preconsolidation pressures and elevated moisture contents. These properties were a consequence of either structure or mineralogy, or both. Allophane, and to a lesser extent, halloysite were considered to contribute to the unusual properties observed, with imogolite and ferrihydrite playing a role in some cases.

In Jacquet's (1987) bibliography, sensitivities in material of mostly andesitic origin ranged between 4 and 21. However, extreme values of 60 and 140 at Ruahihi and Omokoroa, respectively in the Tauranga area were reported (more detail on these soils is presented in section 2.7). It was concluded that in their undisturbed state, volcanic ash soils behave very well as engineering soils, but that structural collapse and water release on remoulding resulted in large strength losses (Jacquet 1987).

Following the bibliography of Jacquet (1987) the only study which has exclusively investigated sensitivity in New Zealand volcanic ash soils is that by Jacquet (1990). However, his ideas have been developed and discussed by Torrance (1992, 1995, 1996). The study of Jacquet (1990) focused on the allophane- and halloysite-dominated soils from the Taranaki and Waikato regions. Jacquet (1990) reported sensitivities between 5 and 55. The presence or abundance of either clay mineral did not explain the sensitivity encountered (Jacquet 1990).

The peak shear strengths recorded (28 to 190 kPa) in Jacquet's (1990) study occurred for a number of reasons, including aggregation of allophane particles (Torrance 1992), the fibre reinforcing effect of imogolite (Jacquet 1990), and the tubular shape of halloysite particles promoting physical interaction of aggregates (Torrance 1992; 1996). Furthermore, Jacquet (1990) found a positive

relationship between ferrihydrite and apparent over-consolidation ratio indicating a cementing action.

Void ratios in Jacquet`s (1990) samples were high, between 2.11 and 3.59. The high void ratio was a consequence of tephra fall origin, loss of soluble material during diagenesis and weathering, and high strength created by clay bonding (Jacquet 1990; Torrance 1992; 1996). The maintenance of high void ratio potentially predisposed soil to low remoulded strength upon disturbance (Torrance 1992).

Remoulded shear strengths between 1.5 and 8.5 kPa were reported by Jacquet (1990) with the lowest value being from a halloysite-bearing sample. A decrease in strength resulted from the rupture of electrostatic bonds in halloysite and allophane. This rupture resulted in the structure being completely destroyed. Destruction of the imogolite network, observed during scanning electron microscopy (SEM), in allophane rich samples also assisted in strength reduction (Jacquet 1990). Whilst natural moisture contents in his samples were high (55 to 108 %), these values did not exceed liquid limits (63 – 127 %), and therefore remoulded material did not flow (Jacquet 1990). Furthermore, strength was analysed using a uniaxial compression apparatus (shear strength = uniaxial compressive strength / 2; see Chapter 3), indicating remoulded samples were at least plastic and able to form coherent specimens. Considering the upper limit for remoulded strength suggested in section 2.2.2, Jacquet's (1990) soils were not "quick" clays in an international sense. Therefore, it has been concluded that volcanic ash soils manifest sensitivity in high remoulded strength (Torrance 1996).

In summarising the work of Jacquet (1990), Torrance (1992) presented a basic model for the development of sensitivity in volcanic ash soil (Table 2.2), giving both depositional and post-depositional factors. One error in this model is that it indicates that allophane is present on deposition and then transforms to halloysite. This can not be the case, because normally one would expect primary material to be present initially (i.e. glass, pumice, feldspar, rock fragments and heavy minerals) and then weather to form either allophane or halloysite or both depending on conditions.

Table 2.2: Depositional and post depositional factors causing the manifestation of sensitivity in volcanic ash soils, after Torrance (1992).

Depositional	Post depositional
Factors producing a high undisturbed strength	
Mineralogy: • Allophanic*	Diagenesis and weathering to produce: • Halloysite • Imogolite • Ferrihydrite
Factors producing a low remoulded strength	
Fall out origin: • To produce a high void ratio	Void ratio increase: • Dissolution of soluble material during weathering and diagenisis
Mineralogy: • Allophanic	Dispersing agents

*see text.

2.7 Landslides and sensitivity in the Tauranga region

Most of the studies involving sensitive soils in the Tauranga region were undertaken during the investigation of landslides, so are not to the same detail as the studies by Jacquet (1990). Furthermore, remoulded strengths in Tauranga soils are typically more liquid-like than those presented by Jacquet (1990). The liquid-like remoulded strength typically results in mass wasting events which flow. Therefore the following section will discuss the more notable mass wasting events in the Tauranga region, making comment on the contribution of sensitivity and unique soil properties where appropriate.

2.7.1 General observations

Undertaking a relict slip investigation, Houghton & Hegan (1980) divided mass wasting events of the Tauranga region into two categories: deep seated and superficial failures. Both failure types were associated with intense periods of precipitation. Superficial failures were more widespread and occurred in regolith material < 2 m deep. Deep-seated failures were confined to high sea cliffs occurring within "older volcanic ashes", where failed material flowed out like a flat tongue. The term "older volcanic ashes" referred to deposits older than the Rotoehu Ash, i.e. the tephra beds and associated buried soils of the Hamilton Ash and Pahoia tephras. One example of a deep-seated failure was the large August 1979 failure at Bramley Drive, Omokoroa. Deep-seated failures resulted from the liquefaction of deep sensitive soil layers, due to pore water pressure (PWP)

increase, in the "older volcanic ashes". Because these sensitive layers were below the water table, Houghton & Hegan (1980) concluded that a small change in ground water conditions initiated failure condition. In conclusion, Houghton & Hegan (1980) defined a cliff top regression hazard zone with a ratio of 1V:2H, measured from the base of the slope. Adding to this hazard zone, Bell *et al*. (2003) suggested a runout angle ratio of 1V:4H, measured from the scarp crest to failure toe, to account for landslide mobility.

2.7.2 Omokoroa

Reports indicated that Omokoroa Peninsula has a history of mass wasting events following intense rainfall (Tonkin & Taylor 1980; Shrimpton & Lipinski 1998; Keam 2008). The event at Bramley Drive during August 1979 was the largest in recent history. The landslide occurred in a 40 m high cliff section which comprised ~ 25 m of volcanic ash materials overlying ~ 15 m of volcanic breccias and weathered ignimbrite. The slip was retrogressive and deep-seated, being ~ 50 m wide, ~ 30 m deep with a run out lobe of ~ 150 m. Keam (2008), using the classification of Cruden & Varnes (1996), termed the failure as complex with a transition from compound earth slide to flow. Coastal erosion was ruled out as a causal factor because it was too slow (0.15 m yr^{-1}) (Gibbs 1979). During investigation, the impermeable basal ash bed within the Pahoia tephras was observed dipping 15° towards the centre of the scarp, indicating an ancient stream gully, and a paleo-topographical control of ground water (Gibbs 1979).

Investigation undertaken during landslide investigations (Tonkin & Taylor 1980; Smalley *et al.* 1980) and an MSc thesis project (Keam 2008) recorded some interesting soil properties at Omokoroa Peninsula. Sensitive soils had high natural moisture contents (60 to > 100 %) which were typically above their respective liquid limits (Tonkin & Taylor 1980; Smalley *et al.* 1980; Keam 2008). Sensitivity was typically > 16 but values up to 140 were reported (Tonkin & Taylor 1980). Keam (2008) reported remoulded strength as low as 2 kPa. A highly sensitive unit investigated by Tonkin & Taylor (1980) was composed of 85 % hydrated halloysite. The halloysite plotted below the A line, therefore having properties of silt. Halloysite crystals were small (~0.2 μm), spherical, and had an *Al:Si* ratio of 1 (Smalley *et al.* 1980; Tonkin & Taylor 1980). Cementation was absent and the halloysite occurred as single crystals rather than aggregates.

Fabric was termed metastable (see section 2.3) with water loosely held in voids (Tonkin & Taylor 1980). Smalley *et al*. (1980) attributed the high sensitivity and low activity of the halloysite to slight inter-particle interactions between halloysite crystals (see inactive particle theory section 2.3). This weak bonding allowed brittle failure and structural collapse. Furthermore, an abundance of water supported material once failure had occurred. Tonkin & Taylor (1980) stated that PWP pressure increase facilitated the Bramley Drive event, as a result of the delicate sensitive material becoming overstressed and creating a basal slip plane.

Keam (2008) suggested that irregularly shaped spherical material similar to that described by Tonkin & Taylor (1980) represented small, crystalline quartz grains. This material had an open porous nature, delicate structure, low plasticity and cohesion. Therefore, Keam (2008) suggested that in an undisturbed state, negative pore pressures or electrostatic forces, or both, provide temporary strength for sensitive material. On saturation and disturbance negative pore water pressures are lost within sensitive material and basal slip planes are formed. Keam (2008) also stated that on failure the porous nature of pumice adds moisture to the debris, enhancing its runout distance.

2.7.3 Maungatapu

Two authors have investigated mass wasting at Maungatapu Peninsula. Bird (1981) indicated that coastal cliff mass wasting events were facilitated by tide- and wave-driven basal erosion which caused cliff retreat and steepening. Subsequent failure occurred during long wet periods, as pore water pressure built up in lensoidal silty sands overlying an impermeable clay bed, and this process culminated in failure following intense rainfall events. Oliver (1997) identified four types of failure across the peninsula, including; 1) large scale block failures, 2) piping-triggered block failures, 3) wave-erosion triggered block failure, and 4) shallow regolith failures. The piping-triggered block failures resulted from aquifer recharge, increasing PWP, and discharge at the cliff face. The pressure from discharge caused piping up to 5 metres deep, which reduced support for the overlying block. These failures typically do not involve the full height of the slope (Oliver 1997).

Hydrated halloysite has been identified as the dominant clay mineral at Maungatapu Peninsula (Bird 1981; Oliver 1997). Oliver (1997) recorded allophane using NaF testing in Hamilton Ash and Matua Subgroup material. Only Bird (1981) discussed sensitivity. Sensitive materials were identified in clayey marker beds, possibly the Pahoia tephras, with values up to 200 and remoulded strengths down to ~ 0.5 kPa. However, the remoulded strength may have been much lower because of laboratory equipment limitations. Rapidity number values suggested a large amount of energy was required to liquefy samples, indicating that the sensitivity of the clays played little part in the instigation of mass movement (Bird 1981). Oliver (1997) stated that the flow-like nature of failures was a result of soils moisture content and tide height.

2.7.4 Ruahihi

A less natural mass wasting event, but heavily influenced by an abundance of water, was the canal collapse at Ruahihi during September 1981 (Oborn 1988). This event destroyed 600 m of the canal and caused more than one million cubic metres of liquid mud and rubble to flow over adjacent farmland into the Wairoa River (Hatrick 1982). The physical properties of volcanic soils (including the clay lining and underlying material) and paleotopographic controls influenced canal failure (Oborn 1988; Burns & Cowburne 2003).

Materials within the failure chasm were identified as tephra (Hamilton Ash material and younger) which overlayed non-welded ignimbrite (Oborn *et al.* 1982; Oborn 1988; Burns & Cowburne 2003). Allophane occurred in material younger than the Hamilton Ash. The Hamilton Ash was considered the most stable material and had the highest clay content. The non-welded ignimbrite had low clay content and consisted of spherical hydrated halloysite, arranged with a large amount of porosity both between individual grains and aggregates (Oborn *et al.* 1982). Soils had high natural water contents, porosities, sensitivity and low bulk density. Moisture values often exceeded liquid limits allowing soils to liquefy and flow on disturbance (Parton & Olsen 1980). Subaerial deposition and low particle density produced materials with low dry bulk density (Oborn 1988). Prebble (1983) reported high sensitivities in stiff to brittle clay seams within the ignimbrite, but, Oborn *et al.* (1982) indicated that many of the units at Ruahihi are sensitive. Sensitivities reached values up to 60, but had remoulded strength of 1 to

2 kPa (Oborn *et al.* 1982; Prebble 1983). Sensitivity was attributed to the metastable fabric and poor cementation (as described in section 2.3) (Oborn *et al.* 1982). Prebble (1986) suggested that the open, porous, honeycomb like structure of halloysite and allophane at Ruahihi may collapse when disturbed. Furthermore, high sensitivity may have been produced as a result of intervening cycles of weathering (Prebble 1986).

2.7.5 Otumoetai

Following a large storm during May 2005, a number of landslides occurred across the Tauranga region, most notably in the suburb of Otumoetai. Typically slips had the attributes of shallow arc features, which did not occur across the full height of the slope (Wesley 2007). An exception was one large slip which occurred behind a property on Vale Road, Otumoetai. It had a more bowl shape or deep-seated character (Figure 2.4). Failures occurred in relict coastal cliffs and valley heads, typically where overland flow was concentrated. Debris disintegrated as they moved, became intermixed with water, and thus flowed. Run out distances fell within the 1V:4H line projected by Bell *et al*. (2003).

Wesley (2007) examined a slip at 198 Grange Road in some detail. He observed sensitivities between 3.5 and 97, with remoulded strengths between 1 and 60 kPa. The highest sensitivities occurred in light coloured material between dark brown buried soil horizons, below the Rangitawa Tephra (H1). The darker buried soil units were considered to have good engineering properties much like typical brown ashes (see Wesley 1973; 1977) and the Hamilton Ash Formation. It was believed that the dominant clay mineral was predominantly either halloysite or kaolinite, with very little allophanic material (Hegan & Wesley 2005). Highly sensitive material had natural moisture contents which were close to or exceeded liquid limits (60 – 96 %). The ease of sample disturbance ranged between a lot of applied pressure and very little (Wesley 2007).

Figure 2.4: Slip at Vale Road, Otumoetai. Note little debris remains in the scarp and the house with the red roof has been pushed off its foundations (Photo courtesy of Tauranga City Council).

Wesley (2007) stated that the role of sensitive soils in slope instability is not very well understood. It is clear that sensitivity influences post-failure behaviour, through liquefaction and flow. However, sensitive soils do not lose strength when they become wet nor do they liquefy. Failure was believed to occur as a result of increasing PWP, which is consistent with other observations. Wesley (2007) added that sensitivity is an interesting property of Tauranga soils and promotes the flow-like nature of slides. He suggested much work could be undertaken investigating their geomechanical properties and weathering histories.

2.8 Summary

Sensitivity is defined as the decrease in strength on remoulding. Remoulded strength has an effect on the characteristics of post-failure behaviour, i.e. soils with extremely low strength will flow. Sensitivity is reasonably well understood in the chlorite- and illite-dominated glacial marine clays of the Northern Hemisphere. Less is known about the sensitive volcanic soils of New Zealand. Glacial marine clays are young and have been deposited in a saline environment, then isostatically uplifted. Sensitive volcanic clays are derived by weathering of pyroclastic fall materials experiencing minimal consolidation.

Therefore, each has different properties. Clay fractions of volcanic soils are typically comprised of allophane and halloysite. It is unknown whether allophane or halloysite offers a greater contribution to sensitivity. However, in the Tauranga region halloysite is associated with those mass wasting events which flow on failure. The remoulded strength of volcanic ash soils has yet to be recorded with sufficiently low strength to be considered "quick clay" in an international sense. Therefore, past authors considered that the sensitivity in volcanic ash soils manifests as high undisturbed strength. To date little work has provided reliable and specific laboratory data on sensitive volcanic soils in the Tauranga region. Furthermore, little is known about the weathering pathways which lead to sensitivity and the liquid-like nature of these soils.

Chapter 3
Methods

3.1 Introduction

This chapter will give a description of the methods used in the field and laboratory. Emphasis will be placed on testing which has followed non-standard practice, or is derived from in-house methods.

3.2 Field methods

This section describes methods used in the field during the initial stages of this study. These methods, especially sensitivity testing, played an essential role in the selection of samples for later analysis. Methods involved field logging, shear vane testing and geomorphic mapping.

3.2.1 Soil description

Engineering geological soil descriptions were undertaken at all potential sites and followed the guidelines set out in "Field Description of Soils and Rocks" published by the New Zealand Geotechnical Society (2005). Descriptions of soils included the logging of soil colour, grain size, moisture content, strength and plasticity. Weathering terms were derived from the guidelines set out in Bell & Pettinga (1984). For ease in the field, basic terms and requirements for description were summarised in a flow chart (Appendix 3.1).

3.2.2 Penetration resistance

A pocket penetrometer (Figure 3.1 (A)) was used to measure the penetration resistance of selected units during soil profile description. Readings were taken every 30 cm down a profile, or at smaller intervals when units became noticeably thinner. Results are reported in kilograms on a scale of 1 to 10 but these values should be considered approximates because the penetrometer was not recently calibrated. Data were internally consistent and thus gave relative penetration values.

3.2.3 Vane shear strength

A direct field measurement of undrained shear strength was obtained using a calibrated Geotechnics shear vane (Figure 3.1 (B)), following the methods presented by the New Zealand Geotechnical Society (2001). As with penetration resistance, shear strength was recorded every 30 cm down the profile or at smaller intervals when units were noticeably thinner or different. The vane was pushed into the soil approximately 70 – 80 mm and rotated at the rate of one revolution per minute. On most occasions the 19 mm vane (Figure 3.1 (C)) was used. However, in particularly weak soils the 33 mm vane was used (Figure 3.1 (D)). As the vane was turned, a spring inside became tighter providing greater force for shear. The soil then failed once its yield strength was reached. The strength value recorded from the face of the vane at failure was converted to kPa by multiplication with the shear strength constant determined during calibration. Shear strength constants were 1.562 and 0.289 for the 19 and 33 mm vanes respectively.

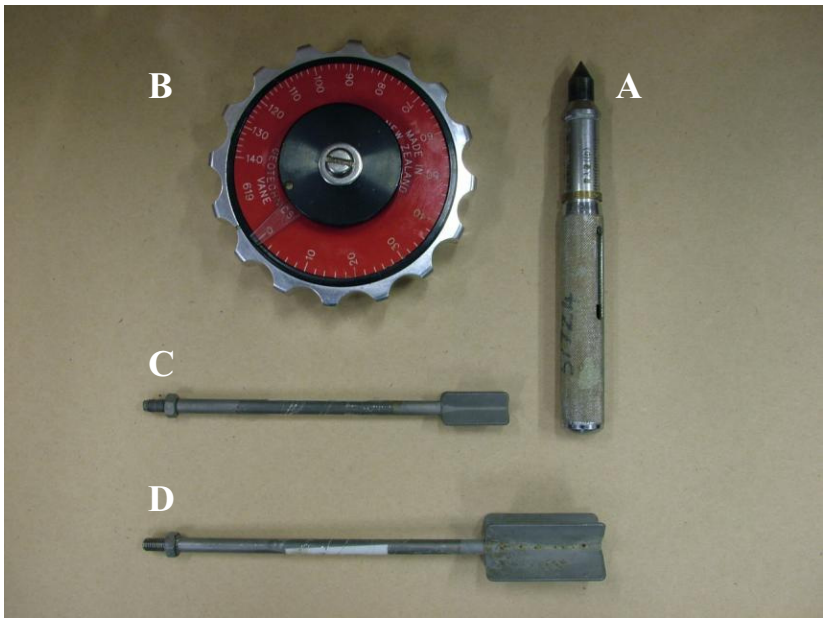

Figure 3.1: Image displaying a pocket penetrometer (A) and a Geotechnics shear vane (B) with 19 (C) and 33 mm (D) vanes.

3.2.4 Field sensitivity testing

Sensitivity represents the ratio of undisturbed to remoulded strength. In this study two methods were employed for field sensitivity testing. The first followed the methods set out by the New Zealand Geotechnical Society (2001), and hereafter will be called the **standard** method. The second was developed after discussion with a colleague at Auckland University (L. Wesley *pers. comm.* 2008)

and will be called the **adapted** method. Once sensitivity was measured it was correlated with standards from the New Zealand Geotechnical Society (2005), as presented in the Table 2.1 in Chapter 2.

Both sensitivity methods used the shear vane, and undisturbed strength was determined by the same means as the vane shear strength method outlined in section 3.2.3. However, the difference between methods occurs at the remoulding stage of the test. The following will outline the techniques used for each type of test:

Standard method

1. The soil was sheared as per section 3.2.3;
2. Once the soil had sheared the vane was turned five complete rotations at a speed of approximately one rotation every 10 seconds, in the same direction that shearing occurred;
3. Rotation was ceased for ~ 30 seconds to allow pore water pressures to dissipate;
4. The sample was re-sheared as per the method in section 3.2.3.

Adapted method

1. The soil was sheared as per section 3.2.3;
2. The vane was removed and a rubber mallet and block of wood were used to gently insert a 10cm long steel ring;
3. The ring and intact core were extracted and the sample was then pushed into a plastic sample bag;
4. The sample was remoulded in the bag for approximately 1 minute, or until it was clear that the structure had been completely disturbed;
5. If after remoulding the sample was a soft paste or almost liquid it was placed into the steel ring. However if it was of thicker consistency it was placed back into the hole from which it was extracted;
6. The soil was then sheared as per section 3.2.3, either inside the ring or hole.

Because two methods were used to measure sensitivity some basic testing was undertaken to determine the comparability of the results. A silty CLAY unit which appeared homogenous and did not display extreme sensitivities was divided

into a grid of 12 blocks (4 x 3). Within each block either a standard or adapted sensitivity test was undertaken, with a total of 6 tests being completed for each method. Raw results are presented in Appendix 3.2. A summary of the results from comparison testing is presented in Figures 3.2, 3.3 and 3.4.

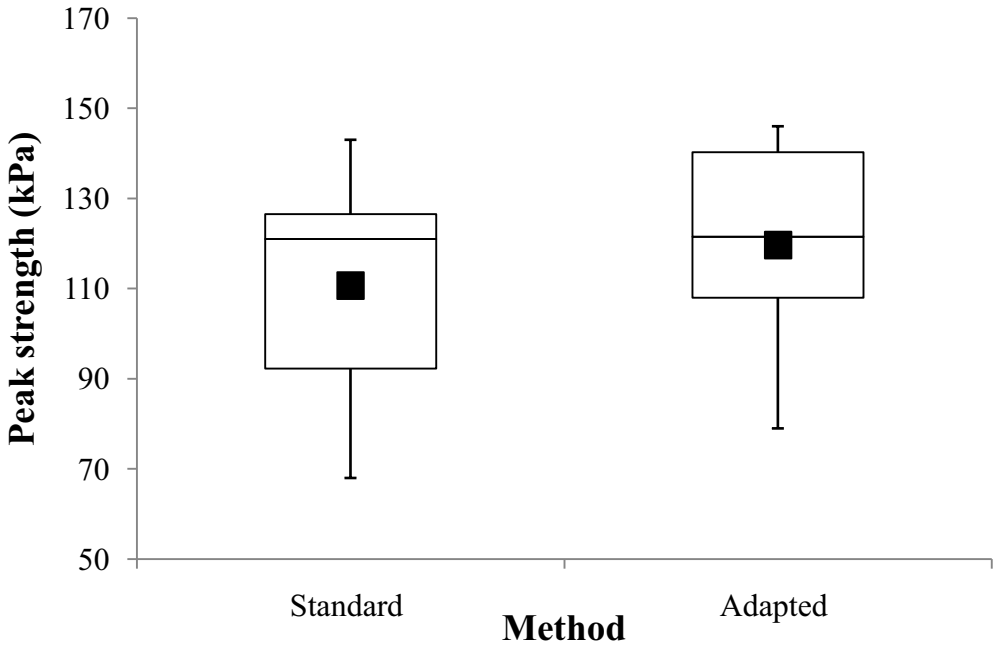

Figure 3.2: Peak vane strength results from comparison testing in a homogenous silty CLAY unit from Tauriko, Tauranga. The black square indicates the mean value.

The range of peak strength values recorded for both the standard and adapted method of testing was similar (Figure 3.2). However, the mean, and data which occurred between the first and third quartile were slightly higher for the adapted method than the standard method. Because the methods to measure peak strength were identical, the variation could only arise from either variation in the unit examined or the small sample size. However, a t-test indicated that the two sets of data were not significantly different ($p = 0.58$).

When the same material was remoulded (Figure 3.3) the standard method recorded a lower mean, first and third quartile, and minimum value than the adapted method. The standard method also displayed a greater range of values than the adapted method. The narrow range of values recorded for adapted remoulded strength compared to the standard method may indicate that the adapted method provided a more consistent measure of remoulded strength (Figure 3.3). A t-test indicates that the data for remoulded strength were not significantly different ($p = 0.29$).

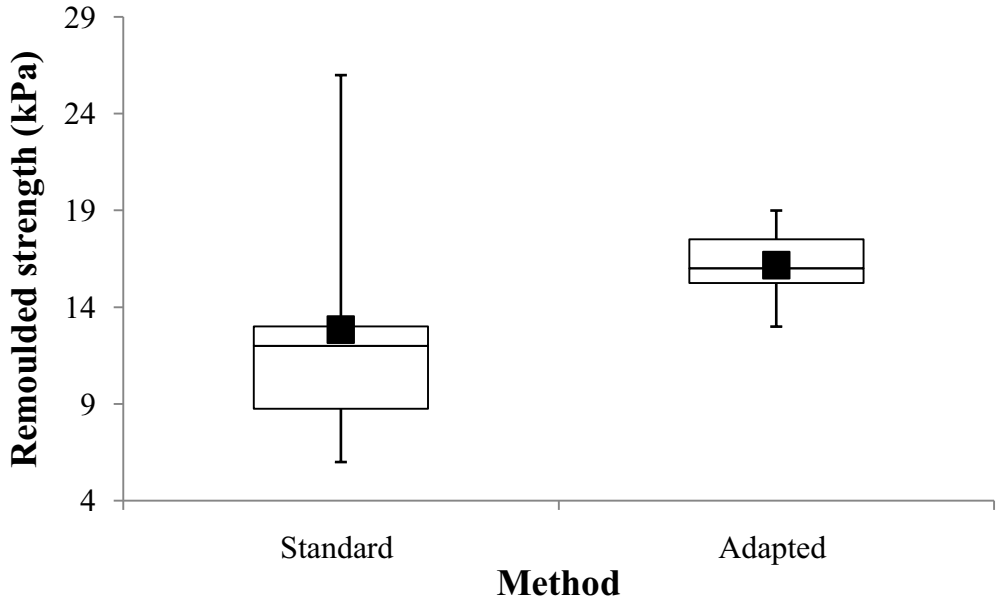

Figure 3.3: Remoulded strength results from comparison testing in a homogenous silty CLAY unit from Tauriko, Tauranga. The black square indicates the mean value.

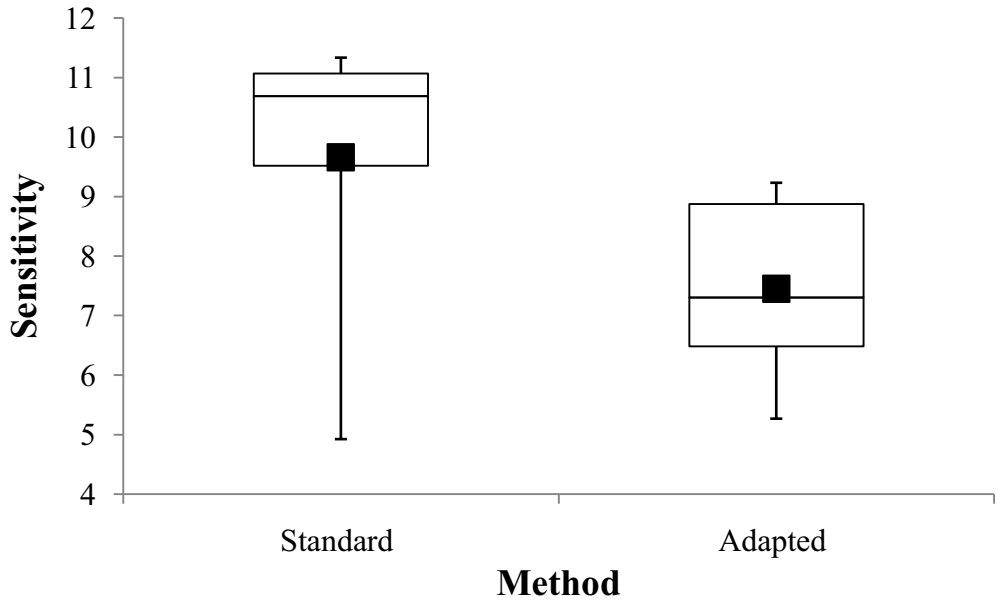

Figure 3.4: Sensitivity results from comparison testing in a homogenous silty CLAY unit from Tauriko, Tauranga. The black square indicates the mean value.

When sensitivity was calculated for the material in Figures 3.2 and 3.3 the mean and data between the first and third quartile were higher in the standard than the adapted method (Figure 3.4). The Range of values was also greater for the standard method. The large relative distance which occurred between the first quartile and minimum value for the standard method indicated a possible outlier which had pulled the mean value towards a lower sensitivity than if the outlier was not present (Figure 3.4). Examination of the raw data indicated that most

manual sensitivity values lay between 10 and 11 however, one value of was 5 reported. The influence of a single low value is a consequence of small sample size. Considering all values measured a t-test indicated that the data were not significantly different at the 95% confidence interval ($p = 0.09$), indicating that, based on the data collected, the adapted method was comparable with the standard method and was an acceptable way of measuring sensitivity.

Whilst undertaking field work it was noted that the adapted method often appeared more sensitive, recording more extreme values than the standard method. For example, in a profile at Grange Road Otumoetai (Figure 3.5), three instances of extremely high sensitivity were identified by the adapted but not the standard method. In each of these cases, material was highly dilatant when extracted and remoulded giving a much lower remoulded strength by the adapted method. It is possible that the standard method does not remould the soil enough to cause the required amount of disturbance. For example, Lancelotta (1995) recommended the shear vane be turned 25 times before remoulded strength is recorded, whilst Keam (2008) rotated the vane 30 times before taking a remoulded measurement (compared with the 5 revolutions used here as per the standard method).

The adapted method ensures that soil structure is completely destroyed, which is analogous to a highly disruptive failure event. Furthermore, sensitivity was determined after physical remoulding of samples in unconfined compression (Head 1994), triaxial compression Fredericksen (1988), cone penetration (Kezdi 1980; Bird 1981) and shear box tests (Chandler & Rogers 1980). Craig (1997) states that remoulding for test purposes is normally brought about by the process of kneading. Therefore it is logical that sensitivity using a field shear vane should, where possible, be determined by physically remoulding the sample. In this study, both methods were used in the field but because the adapted method clearly destroyed the structure of the soil, it was heavily consulted for the selection of samples for further laboratory work.

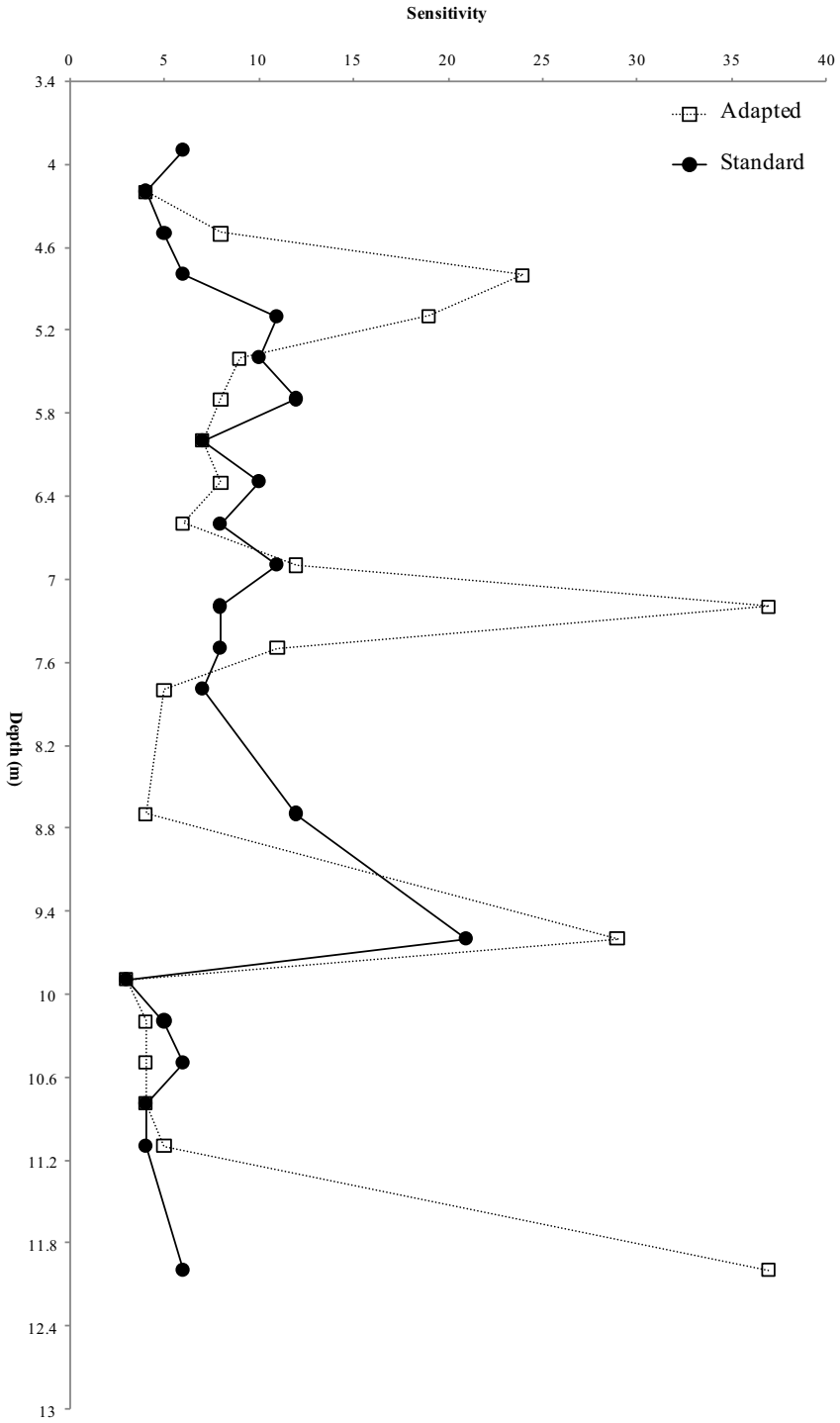

Figure 3.5: Comparison of sensitivity values for the standard and adapted method down a soil profile at Grange Road, Otumoetai. The graph indicates that on 9 occasions the adapted method recorded higher sensitivities than the standard and on 8 occasions the standard method was higher than the adapted. Note the peak strength values were identical because the remoulded material for the adapted method was removed from the same location as the standard method. This means that any variation in sensitivity will manifest in remoulded strength.

3.2.5 Geomorphic mapping

At sites of interest, geomorphic mapping was undertaken. This was done to give the area investigated a landscape perspective. The symbols used in the production of a geomorphic map were taken from Gardiner & Dackombe (1983)

and are summarised in Appendix 3.3. Slope profiling for geomorphic mapping was undertaken using a Suunto optical reading clinometer. Because field investigation was undertaken independently a rigid steel pole was used for sighting which had specific eye level markings.

3.2.6 Field sampling

Samples taken in the field for laboratory analysis included bulk samples for moisture content, Atterberg limits, and mineralogy, and core samples for strength testing. Description of the protocol followed during sample collection can be found in Appendix 3.4.

3.3 Laboratory methods

The following section presents laboratory methods used to characterise samples that were selected as a result of field testing.

3.3.1 Moisture content

Field moisture content was determined using the method set out in New Zealand Standard (NZS) 4402 (2.1) (1986). The procedure followed was for fine soils, because greater than 90% of the sample would have passed through a 2mm sieve. Moisture content was calculated by:

$$Moisture\ content = \frac{loss\ in\ weight\ of\ soil}{oven\ dry\ weight\ of\ soil} \times 100\ (\%) \qquad (3.1)$$

Moisture factor was calculated for converting wet to dry bulk density. Moisture factor was calculated by:

$$Moisture\ factor = \frac{moist\ weight\ of\ soil}{oven\ dry\ weight\ of\ soil} \qquad (3.2)$$

3.3.2 Bulk density

New Zealand Standard 4402 (5.1.3) (1986) was followed as closely possible for the determination of bulk density. In the laboratory fine sand was used to correct for the absence of any missing soil; this is not a requirement of NZS 4402. Bulk density was calculated from:

$$\rho = \frac{mass\ of\ soil}{volume\ of\ soil}\ (kg\ m^{-3}) \tag{3.3}$$

3.3.3 Particle density

The method used for soil particle density was outlined by both Head (1992) and Vickers (1978). The density bottle method was used as it is suited to soils with particles of less than 2 mm in diameter (Head 1992). Particle density was found by the equation:

$$Particle\ density\ (\rho_s) = \frac{mass\ of\ dry\ soil}{volume\ of\ particles}\ (kg\ m^{-3}) \tag{3.4}$$

3.3.4 Porosity

Porosity was calculated using dry bulk density and average particle density for each sample (McLaren & Cameron 1996). Porosity was calculated by:

$$Soil\ porosity = 1 - \left(\frac{bulk\ density\ (kg\ m^{-3})}{particle density\ (kg\ m^{-3})} \right) (\%) \tag{3.5}$$

Note that void ratio is inversely related to porosity through the equation:

$$e = \frac{\varepsilon}{1-\varepsilon} \quad \text{and} \quad \varepsilon = \frac{e}{1+\varepsilon} \tag{3.6}$$

where;

e = void ratio;

ε = porosity.

3.3.5 Degree of saturation

The degree of saturation represents the volume of water contained in void spaces between soil particles and is expressed as a percentage of total voids (Head 1994):

$$S_r = \frac{w\rho_s}{e}\ (\%) \tag{3.7}$$

where;

S_r = the saturation ratio (typically expressed as a %);

ρ_s = particle density (kg m^{-3});

w = moisture content (%).

3.3.6 Particle size

A Malvern Mastersizer laser particle sizer was used to measure particle sizes. An in-house method was used for sample preparation, which involved the removal of organic matter using H_2O_2 and dispersion of clay particles with calgon (Appendix 3.5). Following analysis, particle sizes were categorized using size classes from NZS 4402 (1986) (Table 3.1).

Table 3.1: Particle size divisions which are in accordance with NZS 4402 (1986).

Description	Particle Size (mm)	Particle Size (µm)
Clay	0.000060 - 0.002	0.060 – 2
Silt	0.002 – 0.06	2 – 60
Sand	0.06 - 2	60 - 2000

Because the Malvern Mastersizer measures particles as equivalent spheres results are volume based. This is important because one would need one thousand 1 µm particles to have the same volume as a single 10 µm particle. Furthermore results from sieving and sedimentation are based on the narrowest dimension and total surface area respectively.

When using the Mastersizer it is important to optimise the experimental method and calculation constants for the material being examined. In particular, optical parameters and sample size (obscuration) must be considered, as changes in these can have a large impact on apparent size distributions. These parameters will be discussed in turn.

The Malvern Mastersizer uses the Mie theory to predict the light scattering behaviour of particles (Malvern 1999). A requirement of this theory is that the material properties of refractive indices (RI) and adsorption (A) must be entered into the Mastersizer. The Mastersizer then creates an optical model using the RI

and A parameters. The selection of appropriate RI and A values is important because variations in optical properties can significantly alter estimated grain size distributions (Sperazza *et al.* 2004). RI values for single materials can be found in the manual provided with the instrument (Malvern 1997). Because the soils in this study were comprised of a variety of minerals, with different optical properties, no single value was appropriate. The Mastersizer has default optical parameters for soil with an RI of 1.56 and an A of 0. Unfortunately the A value of 0 implies that all particles in the samples are semi transparent and perfectly spherical, which is typically not the case for soil samples (Bryn McDonagh *pers. comm.* 2008). Therefore the default soil settings in the Mastersizer were initially employed and then improved using the data fit package supplied with the machine.

The data fit program calculates the residuals between fitted (from the optical model) and measured data. The fit package also compares residuals from weighted and unweighted data, where weighting takes into account the fact that smaller particles scatter less light than larger ones. Values are presented numerically as weighted and un-weighted residuals and also graphically. The graphical plot displays light energy recorded by each detector in the Mastersizer and presents lines of measured and fitted data. These can be used to decide which parameters (i.e. RI or A) need altering; typically the closer the lines are to each other the better the fit. The general rule is that a bad fit in low detector channels indicates a poor choice of RI, and a bad fit in high detector channels represents a poor choice of A. An example showing a good fit with low residuals (~ 0.5) is presented in Figure 3.6.

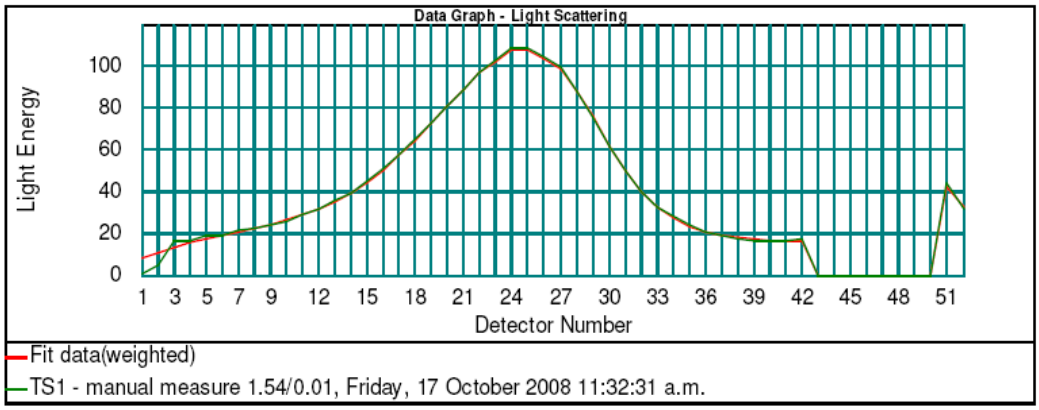

Figure 3.6: Graph of detector number versus light energy showing plots of measured (green line) and fit data (red line) for a soil sample from Tauriko Tauranga.

Numerically a good fit occurs when the weighted and unweighted residuals are of similar magnitude and both are low, e.g. a value of < 1 is adequate (Malvern 1999). However the results derived must be believable, in terms of what is being examined. For example, a sample which is visibly sandy (quartz grains etc) should not display a distribution of entirely clay.

Table 3.2 indicates the impact of changing optical parameters on estimated clay fraction material (<2 μm), for soils of this study. Table 3.2 indicates that the residual values provided by the default model (RI = 1.56) are good but can be improved by adjusting RI to 1.57 and A to 0.01. This adjustment increased the clay fraction by ~ 3 % (Table 3.2). Interestingly if RI was changed to 1.38 and the clay fraction increased by ~ 76%, the residuals recorded were very bad. This exceptionally high value indicates the importance of selecting appropriate optical properties. Therefore, for the sample in Table 3.2 an RI of 1.57 and an A of 0.01 was employed.

Table 3.2: Effect of changing the optical parameters RI and A for a sample of material from Tauriko examined in this study.

Refractive Index	Absorption	Residual	Weighted Residual	< 2 μm material recorded (%)
1.56	0	0.405	0.461	4.81
1.57	0.01	0.180	0.178	7.21
1.44	0.01	0.255	0.916	26.87
1.38	0.01	2.705	7.083	80.75

All samples in this study were tested at RI values between 1.52 and 1.57, with an A of 0.01. The RI values chosen gave very good unweighted and weighted residual fits, with maximum values of 0.757 and 0.966 respectively. The RI values used are sensible considering that volcanic glass, feldspar and quartz have RI values of 1.50, 1.52 – 1.59, 1.54 – 1.56 respectively (Malvern 1997). These materials were recorded by XRD in samples of this study (see Chapter 6). No RI value for halloysite, also observed in this study, could be found but an associated kaolin group mineral, kaolinite, has an RI between 1.53 and 1.57 (Malvern 1997).

Obscuration represents the amount of sample added to the Mastersizer chamber. The manual recommends that for samples with a diverse size range,

such as soil, obscuration should be ~ 25% (Malvern 1999). The general guideline at Waikato University is to never test samples at an obscuration above 20%, due to the risk of re-scattering light. However, re scattering of light does not typically occur until obscuration is > 30 % (Bryn McDonagh *pers. comm.* 2008). Investigating fine grained sediments, Sperazza *et al.* (2004) found that results were most repeatable at an obscuration of ~ 20%.

Because of this contradiction all samples were examined across a range of obscuration values, typically 0 – 35 %, to see if this had an impact on the mass median diameter (d = 0.5). Using a manual analysis material was added to the mastersizer chamber at obscuration increments of 2 %. After each increment of material was added to the sample chamber a reading was taken. The sample chamber was not flushed out between subsequent 2 % increments of material. Not flushing the sample chamber meant material which was measured at 2 % obscuration was still present for a measurement at 32 %. The results from this examination were then plotted as obscuration versus median diameter. An example is presented in Figure 3.7 and results for each sample are presented in Appendix 3.6.

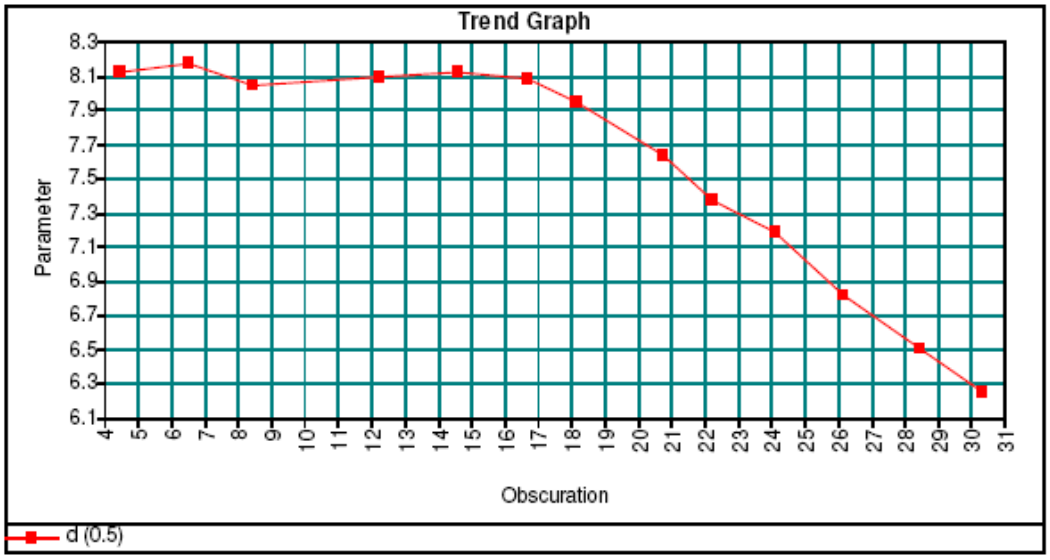

Figure 3.7: Graph of obscuration versus median particle size (d = 0.5) for a soil sample taken from Tauriko.

With the exception of one sample, it was found that at low obscuration median particle size was greater than that observed at higher obscurations. Often, as shown in Figure 3.7, median particle size would remain stable until a certain

obscuration (17 % in Figure 3.7) and then suddenly decrease. However, one sample from Tauriko displayed a steady decrease in median particle size from low to high obscuration (Figure 3.8). A sample from Otumoetai displayed a sudden decrease in median particle size at and obscuration of ~ 16 % (Figure 3.9), yet the overall trend displayed a decrease.

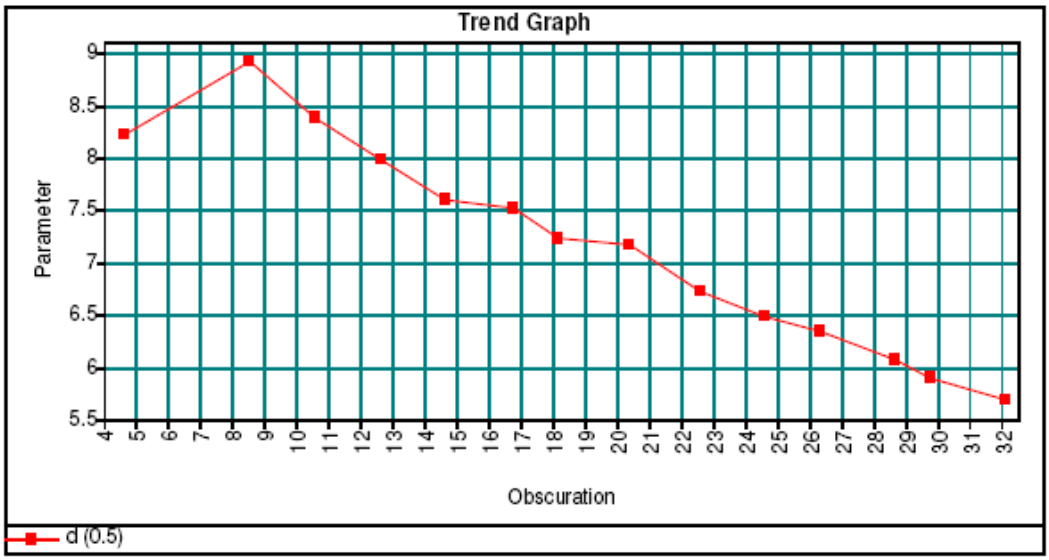

Figure 3.8: Graph of obscuration versus median particle size (d = 0.5) for a soil sample taken from Tauriko.

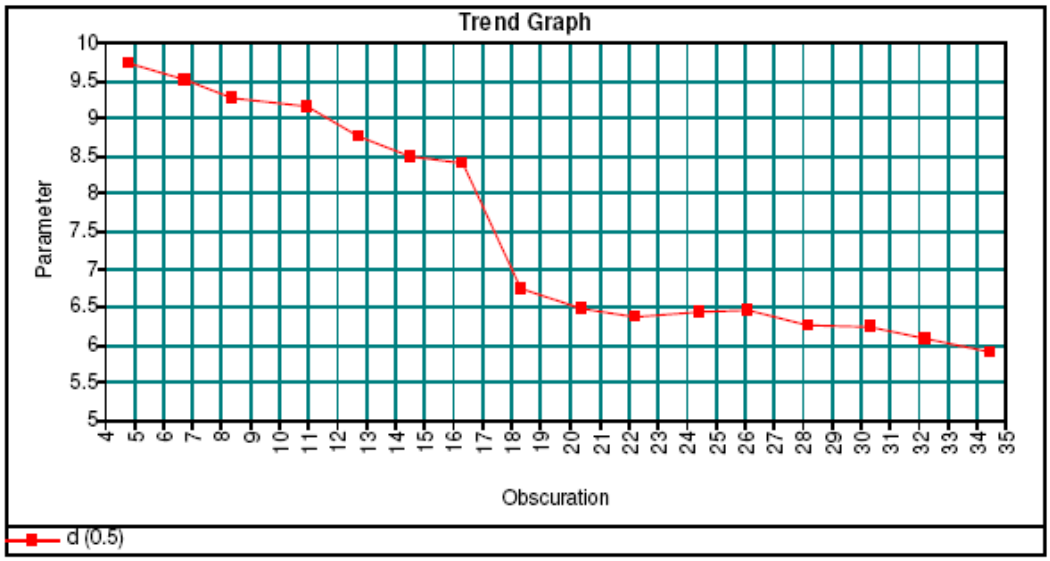

Figure 3.9: Graph of obscuration versus median particle size (d = 0.5) for a soil sample taken from Otumoetai.

This phenomenon is potentially the result of smaller particles being more significant, on a volumetric basis, at higher levels of obscuration. This is a problem when samples with a range of size classes are being investigated (Bryn

McDonagh *pers. com.* 2008). To determine the obscuration value to test samples at, a number of methods were employed depending on the shape of the obscuration versus median particle size graph. The following method was used to determine the obscuration to analyse samples which displayed the phenomenon observed in Figure 3.7, and an example is given in Figure 3.10. Two lines were drawn, one along the flat section of the graph and then another along the sloped section. The point where these two lines intersected represented the inflection of the curve. This point was used to determine the obscuration to test samples at (Figure 3.10). This method ensured that the samples were tested at the highest possible obscuration to ensure a fair representation of grain sizes, but not to represent a point where estimated mean diameter was unstable.

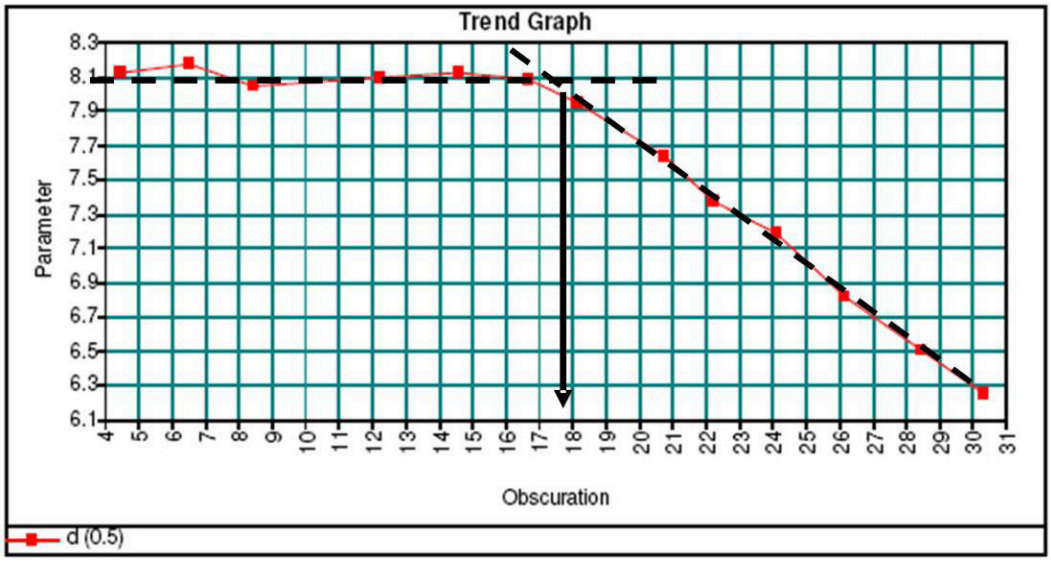

Figure 3.10: Graph of obscuration versus median particle size (d = 0.5) for a soil sample taken from Tauriko showing the method used to determine the obscuration to be used for particle size analysis.

Where the median size steadily decreased or remained the same across a range of obscuration, samples were analysed at obscuration values between 22 and ~ 24 %. These obscuration levels took into consideration the values recommended by Malvern (1999) (25 %) and the findings of Sperazza *et al.* (2004) (20 %).

Following the determination of optical parameters and obscuration levels new samples were prepared and tested at the values calculated. Each test was repeated 3 to 5 times, depending on sample availability, and results were averaged to account for the variability within samples.

3.3.7 Atterberg limits

Atterberg limits were determined following methods outlined by both Head (1992) and NZS 4402 (1986). Soils were not sieved because particle size analysis indicated that, with the exception of one sample, ~ 95% of material would pass through a 425 μm test sieve. In the one exception 90 % of material would have passed through a 425 μm test sieve. This soil was tested unaltered because the value was not exceptionally low and it was more representative to analyse the material as a whole soil. Furthermore, soils were not dried because the content of allophane was not known with any certainty and it was thought that air drying may have an irreversible effect on Atterberg limits (Allbrook 1983).

3.3.7.1 Plastic limit

NZS 4402 (2.3) (1986) was used to determine the plastic limit, which is the moisture content were the soil passes from a plastic to solid state (Head 1992). In this method the temperature of the hands was used to decrease the moisture content of the sample so it sheared longitudinally and laterally when rolled into a 3mm thread.

3.3.7.2 Liquid limit

The liquid limit was determined using the cone penetration limit as set out in NZS 4402 (2.5), which was also found in Head (1992) specifically as a liquid limit test. Liquid limit is the theoretical water content when a soil passes from a plastic to a liquid state (Selby 1993), and is found at moisture content when the cone penetrates 20 mm into the sample. Cone penetration measurements at different moisture contents above and below the liquid limit (20 mm) were taken. The values were plotted on a graph of moisture content versus cone penetration and a line of best fit was plotted. The moisture content at 20 mm penetration representing the liquid limit was then read off the graph.

3.3.7.3 Plasticity Index

Plasticity index was calculated following the guideline in NZS 4402 (2.4) and is the numerical difference between the liquid and plastic limit (sections 3.3.7.1 and 3.3.7.2). This is presented in the equation below:

Plasticity index (PI) = liquid limit (LL) – plastic limit (PL) (3.8)

3.3.7.4 Liquidity index

Liquidity index compares the soil's field moisture content with its plasticity index (Selby, 1993). If the liquidity index is 0 then the soil is at its plastic limit, at 1 the soil is at its liquid limit, and above 1 means the natural moisture content of the soil is greater than its liquid limit. Liquidity index is calculated from:

$$Liquidity\ Index = \frac{natural\ moisture\ content\ (NMC) - PL}{PI} \tag{3.9}$$

3.3.8 Activity

Activity measures the plasticity of clay-size particles in a sample, and is calculated from the following equation:

$$Activity = \frac{PI}{\%\ clay\ content} \tag{3.10}$$

3.3.9 Rapidity number

Whilst the basic classification of sensitivity has been set out in Chapter 2, it does not take into account the energy required to mobilise soil material. Soderblom (1975) developed the rapidity number which gives an estimate of the amount of energy required to produce the drop in strength, from peak to remoulded, indicated by a classification number (Table 3.3). A low value indicates a large amount of energy would be required to cause sample disturbance, whereas a high number indicates only a small amount of energy is required. The importance of this is that an exposed, highly rapid layer would be more likely to transport material than a layer of equal sensitivity, but lower rapidity (Geertsema *et al.* 2006b).

In this study the determination of rapidity number was undertaken using the method outlined by Soderblom (1975). An undisturbed core sample (40mm in height and 60mm in diameter) was dropped from a height of 10 mm 250 times, using Casagrande's liquid limit device. The degree of disturbance was then classified on a scale of 1- 10 (Table 3.3).

Table 3.3: Rapidity number classification scale, where 1 represents a sample which is hardly affected after 250 blows in the Casagrande device and 10 indicates the sample has completely liquefied. Table is taken from Soderblom (1975).

Rapidity number R_n	Degree of Disturbance
1	Samples not visually affected.
2	Hardly visually affected.
3	About 1 mm of the bottom part deformed to a gelatinous mass.
4	About 5 mm of bottom part deformed, gelatinous mass formed. Upper part usually visually unchanged.
5	About 5mm of the bottom part deformed, gelatinous mass and liquid mass formed. Upper part visually unchanged.
6	About 10mm of bottom part deformed, gelatinous mass of liquid formed. Upper part visually unchanged.
7	Bottom part highly deformed, liquid mass formed. Upper part visually unchanged.
8	Whole sample begins to deform, liquid mass formed. Sharp edges and irregularities disappear.
9	Whole sample highly deformed, liquid mass forms and begins to flow out of the vessel.
10	Whole sample transformed into a liquid mass.

3.3.10 X-ray diffraction

X-ray diffraction (XRD) was used to identify crystalline species present in the clay and bulk fraction of each sample. The method relies on the principle that each crystalline substance has a characteristic arrangement of atoms which diffracts x-rays in a unique pattern (Whitton & Churchman, 1987). Observed patterns are then correlated with known patterns to determine the mineral species present. The machine used was a Philips PW analytical defractometer. The scanning range in the study was from 2° to 40° 2θ. Each bulk sample was analysed including all sand, silt and clay size classes. The clay fraction of each sample was also investigated separately.

No pre-treatment was undertaken on bulk samples as they were dried and crushed before testing in aluminium holders. In preparing the clay fraction Whitton & Churchman (1987) recommend perioxidation using H_2O_2 and deferration by dithionite (CBD) extraction to remove organic matter and Fe oxides respectively. Because of the volcanic origin of the soil in this study, these treatments were not used as it was thought that the chemicals may cause degradation and dissolution of constituent clay minerals (Lowe 1981; Lowe &

Nelson, 1983). Samples intended for XRD analysis of the clay fraction were separated using settling towers and Stokes law. In order to disperse samples, prior to placing in the settling tower, samples were soaked in calgon and mixed in an end-over-end shaker overnight and then treated with ultra-sonication for 5 minutes. Once samples were placed in the settling tower Stokes law was used to determined the time it would take for only clay sized material (< 2 μm) to remain in the top 12 cm of the tube. Stokes law is represented by the following equation:

$$V = \frac{2}{9}\frac{(\gamma_s - \gamma_L)g.r^2}{\eta} \tag{3.11}$$

where;

V = velocity of the falling particle (cm/s);

γ_s = mass density of particles (g/cm^3);

γ_L = mass density of the water (g/cm^3);

g = acceleration due to gravity (cm/s^2);

r = radius of the particle (cm);

η = viscosity of the liquid (poise or g/cm/s).

Once the calculated time had elapsed the top 12 cm was decanted off the settling tower into a separate beaker. The solution in the beaker was saturated with MgCl to encourage flocculation as per the method of Whitton and Churchman (1987).

Once the clay fraction was separated and flocculated, an eye dropper was used to place samples on glass slides and porous ceramic tiles. The glass plates were dried over distilled water for ~ 24 hours to ~ 48 hours in an attempt to stop low temperature dehydration of 10 Å to 7 Å halloysite (Kirkman & Pullar 1978; Lowe 1981). Ceramic tiles were used because their high porosity meant that any free water was drawn away from the surface of the clay and thus samples could be scanned in a field-moist condition. Samples prepared on ceramic tiles also appeared in better condition than those on glass. For example samples on glass slides tended to crack, which is a consequence of the dropper on glass slide method (Lowe & Nelson 1983) while those on ceramic tiles remained whole.

The benefit of preventing sample dehydration allows differentiation between species of halloysite and kaolinite. Samples can also be assessed in their actual field hydration state (Lowe 1981). Once halloysite inter-layer water is lost the mineral cannot be rehydrated with the application of water (Joussein *et al.* 2006).

Following sample preparation of the clay fraction and bulk sample a number of treatments were undertaken to help with identification of different minerals, these are presented in table 3.4. Treatment 1 (Table 3.4) was a scan of the dried bulk fraction in an aluminium holder. Treatment 2 in Table 3.4 involved sample heating; this helped to determine the types of kaolin species present and excluded the presence of mica, chlorites, smectites and vermiculite (Brindley & Brown, 1980; Lowe and Neslon, 1983; Mitchell & Soga 2005). The application of formamide following the methods of Churchman *et al.* (1984), as in treatment 3, enabled the distinction between kaolinite and dehydrated halloysite.

Table 3.4: Three different treatment types which each sample was subject to. Each sample began analyses at step 1 and then proceeded through to steps 2, 3, 4 etc. until analysis was complete.

Treatment	Step 1	Step 2	Step 3	Step 4	Step 5	Step 6
1	Dried Bulk Sample untreated	Scan Sample				
2	MgCl saturated clay + air	Scan Sample	Heated to 110°C for 1 hr	Scan Sample	Heated to 550°C for 1 hr	Scan Sample
3	MgCl saturated clay + air	Scan Sample	1 drop of formamide added	Scan Sample		

Classification of peaks, and hence mineralogy, was interpreted using tables and text presented in Brindley & Brown (1980), Lowe & Nelson (1983) and Moore & Reynolds (1997).

3.3.11 Allophane and Ferrihydrite identification

The testing of soil samples for the determination of allophane and ferrihydrite was undertaken by Landcare Research in Palmerston North. The basic laboratory methods used by Landcare and the calculations used to determine allophane and ferrihydrite will be described in the following section.

3.3.11.1 Allophane

In the laboratory a quantitative estimation of allophane was obtained using acid oxalate Al and Si extraction (Parfitt 1990). XRD analysis indicates that acid oxalate is an effective reagent for dissolving allophane (Campbell & Schwertmann 1985). Imogolite also dissolves in acid oxalate but the amount in New Zealand soils is usually very small (Parfitt 1990; Lowe & Percival 1993). To account for organically bound Al, pyrophosphate extractable Al was measured (Parfitt 1990). All measured values were used in the following equation to calculate the *Al:Si* ratio of each sample:

$$Al{:}Si = \frac{(Al_o - Al_p)}{Si_o} \qquad (3.12)$$

where:

Al:Si = Al to Si ratio;

Al_o = Acid oxalate extractable Al;

Al_p = Pyrophosphate extractable Al;

Si_o = Acid oxalate extractable Si.

The *Al:Si* ratio was used to find the factor in Table 3.5 which was multiplied by acid oxalate extractable Si to determine allophane content (%) in each sample.

Table 3.5: *Al:Si* atomic ratios of allophane and the factor (A) to be used in estimating allophane table taken from Parfitt (1990).

Al:Si	Factor[A]	Al:Si	Factor[A]
1.0	5	2.5	10
1.5	6	3.0	12
2.0	7	3.5	16

3.3.11.2 Ferrihydrite

Ferrihydrite was estimated by multiplying acid oxalate extractable Fe by 1.7 as described by Parfitt & Childs (1988).

3.3.12 Grain mounts

Grain mounts were used to analyse mineralogy, especially non-clay minerals. Grain mounts were made from the fine sand fraction of each sample. To separate out the fine sand fraction (60 – 200 μm) samples were dispersed using similar preparation techniques as particle size (see Appendix 3.5) and then wet sieved. Samples were mounted in resin on a glass slide and then viewed using a petrographic microscope.

3.3.13 Scanning electron microscopy

The Scanning Electron Microscope (SEM) has the ability to allow description of clay, sand and silt particles and their interactions directly. Therefore the SEM was used in this study to help determine both mineralogy and microstructure of the samples under investigation.

Because the SEM requires an evacuated sample chamber, specimens were observed in a dry state. Specimens were mounted on carbon tape as either crushed powder, for mineralogy, or as intact blocks, for microstructure and mineralogy. Following mounting, carbon paint was applied to the edges of the intact block and all samples were coated with platinum. The use of platinum coating, carbon paint and carbon tape prevents charging and loss of resolution by providing a conduction pathway for electrons. Initially samples were tested at an acceleration rate of 20 kV, however the high porosities meant charging was a problem so the acceleration rate was decreased to 5 kV.

A number of samples, especially clay minerals, were investigated using energy dispersive x-ray analysis. This technique allowed the determination of elemental compositions of material under investigation. However, for this to be undertaken the sample had to be scanned at an accelerating voltage of 20 kV, which had a detrimental impact on image quality.

3.3.14 Unconfined compressive strength

Unconfined compressive strength of a sample was measured using a drained triaxial cell following the method of Head (1994) and NZS 4402 (1986). Samples tested were 100 mm tall with a diameter of 50 mm and tested at a compression rate of 2 mm min^{-1}, which is the appropriate speed for a sample of the stated diameter (Head 1994). Because the number of specimens was limited each sample was tested only once.

Load was recorded using an electronic cell and failure was considered to occur at peak stress. All calculations were completed by the WINCLISP program. The WINCLISP programme converted unconfined compressive strength to shear strength using the equation from Head (1994):

$$C_u = \frac{1}{2} q_u \tag{3.13}$$

where:

C_u = unconfined compressive shear strength (kPa);

q_u = unconfined compressive strength (kPa).

3.3.15 Calculated determination of remoulded shear strength

During field testing the remoulded strength was often very low (< 1 kPa), making accurate measurement difficult. The method of Sharma & Bora (2003; 2005) was employed to estimate undrained shear strength of a remoulded soil based on moisture content, liquid and plastic limit (Sharma & Bora 2003). The method assumes that the undrained shear strength for any soil at its liquid limit is 1.7 kNm^2 (Sharma & Bora 2003; 2005). The equation is presented below:

$$Log\,\tau = Log\,\tau_{LL} + \frac{2}{Log(w_L / w_P)} \times Log(w_L / w) \tag{3.14}$$

where:

τ = Undrained shear strength (kPa);

τ_{LL} = Undrained shear strength at the liquid limit (kPa);

w = Water content (%);

w_L = Liquid limit (%);

w_P = Plastic limit (%).

Sharma and Bora (2003) recommend that a 3.92 N, 30 degree cone is used for plastic limit and a 0.59 N, 60 degree cone is used to determine liquid limit. However these were not available at the University of Waikato, so the values entered into the equation are based on liquid limits derived from a 0.78 N, 30 degree cone. Plastic limits have been derived from the "worm" method as described in section 3.3.7.1. Therefore results should be considered estimates.

3.3.16 Direct shear test

An important property of soil is its strength. One simple measure of this is the determination of the Mohr-Coulomb parameters cohesion (c) and friction angle (ϕ) using a laboratory shear box. Cohesion is dependent on inter particle forces and friction angle is dictated by structural roughness within a specimen. Whilst effective stresses can be measured with the shear box only total stresses were required for this study, thus undrained unconsolidated tests were undertaken.

A Wykeham Farrence shear box was used (model number 25000), which sheared 60 mm circular samples along a predetermined horizontal plane. Sample slippage was prevented by placing two grooved plates perpendicular to the direction of shear. Shear strength was measured using a calibrated proving ring and vertical deformation was measured with a dial gauge. Specimen analysis was undertaken at a strain rate of 0.3 mm min^{-1}. Detailed shear box methods can be found in Chandler & Rodgers (1980), however the following will outline the determination of normal load and area correction applied.

Normal load was applied through a dead weight system directly above the specimen. Selection of the normal load was based on what would best bracket *in situ* overburden pressure. For example sample OS4 is 8 m deep; considering approximate wet bulk density above the sample (~ 1400 kg m^3) the *in situ* over burden pressure was calculated as ~109 kN m^{-2}. Therefore specimens were tested at approximately 7, 20, 50, 100 and 180 kN m^{-2}. The lower normal loads (~ 7 and ~ 20 kN m^{-2}) were used in an attempt to accurately estimate cohesion (c), the value at 100 kN m^{-2} was close to the estimated overburden value. The upper load (~ 180 kN m^{-2}) was ~ 50% larger than the estimated *in situ* value. However, consideration was given to the fact that the material under investigation may be at

a different depth at other locations. Other shallower units were tested at similar values. Full equations are given in Appendix 3.7.

Because the area of soil to soil contact decreases during shear, an area correction was applied to allow for the displacement of material at either end of the specimen. Area corrections were only applied to the shear stress readings; the calculation used is presented below and can be found in Bareither *et al.* (2008):

$$A_{CS} = A_I \left[\frac{1}{90} \times \cos^{-1}\left(\frac{\delta_h}{D}\right) - \frac{2}{\pi} \times \frac{\delta_h}{D} \times \sqrt{1 - \left(\frac{\delta_h}{D}\right)^2} \right] \tag{3.15}$$

where:

A_{CS} = Corrected area (mm^2);

A_I = Initial area (mm^2);

δ_h = horizontal displacement (mm);

D = diameter of the shear box (mm).

3.3.17 Triaxial

A triaxial apparatus was used to obtain both effective and total strength parameters for selected samples. The triaxial allows control of stresses along three principal axes and stress application under conditions of axial symmetry (Craig, 1997). Unlike the shear box, the triaxial does not impose a plane of failure on a sample and allows the characteristics of natural failure to be closely observed (Bird 1981). The general principles and methods followed for triaxial testing in this study are comprehensively discussed in British Standard (BS) 1377 (1990) and Head (1994; 1998). It should be noted that all samples tested had a height of ~ 100 mm and a diameter of ~ 50 mm giving a height to diameter ratio of 2. The following section will briefly outline the system used, give justification to the type of test undertaken, and describe the production of Mohr-Coulomb parameters.

3.3.17.1 Apparatus description

Testing was conducted using a VJ tech strain controlled triaxial. The test is strain controlled because the base platen is driven up at a predetermined rate of displacement, so that the sample is deformed at a constant rate of strain (Head

1998). The system was fully electronic with load, strain, volume change and pore water pressure readings all being recorded on a 16 Channel VJ Tech MPX3000 data logger. De-aired water was supplied from a DeNold Deaerator, water was considered completely de-aired when bubbles had ceased to appear in the closed vacuum cell. Using a Mettler Toledo oxygen meter dissolved oxygen was measured at 1.38 ± 0.15 mg/L (or ppm), which is below the 2 ppm maximum recommended for de-aired water (Head 1998).

Cell and back pressure were provided by two air-water cells with butyl rubber bladders. A regulated level of compressed air was passed into the butyl rubber bladders which inflated to increase either cell or back pressure. Compressed air was provided via a piped line from a main supply. However, this supply did not provide enough pressure (750 kPa) to undertake certain pre-test checks required in BS 1377 (1990), nor did it allow enough cell pressure to be applied following saturation and consolidation. This was overcome by installing a 2:1 in-line air pressure amplifier.

The pore water pressure (PWP) transducer was calibrated using a DHT 920 portable calibrator. Both zero (0 bar and 0 mV) and maximum output (10 bar and 100 mV) were applied using the calibrator to determine the span of the PWP transducer. The recorded values were entered into the data logger which divided the span value by 1000 kPa (10 bar). Originally both cell and back pressure were read off a dial gauge on the wall; this could not be calibrated either individually or with the PWP transducer. This proved problematic because during the saturation stage both readings from the dial gauge and PWP transducer were entered into an equation to calculate the pore pressure coefficient B. To have confidence in this calculation all pressure measurement devices should be calibrated. To overcome this problem, it was decided to connect the cell and back pressure lines into the calibrated PWP transducer as shown in Figure 3.11. During operation, taps could be closed to isolate either the pore water, back or cell pressure systems. This represents a modification of the original VJ Tech apparatus

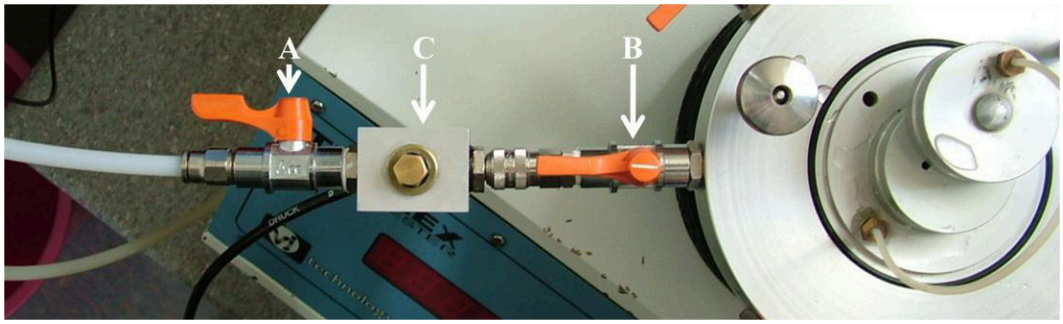

Figure 3.11: Image of Pore Water Pressure transducer with inlet taps A and B. Tap A is closed and B is left open to make a PWP pressure measurement. However to make a cell or back pressure measurement tap A is closed and B is opened. C represents the block which the PWP transducer is attached to.

3.3.17.2 Triaxial test type

Three standard triaxial tests were attempted during this study; unconsolidated undrained (UU), consolidated undrained (CU) and consolidated drained (CD). The main differences between each test type are outlined in Table 3.6.

Table 3.6: The main differences between unconsolidated undrained, consolidated undrained and consolidated drained for triaxial testing. Parameters entered under each category are compiled from Craig (1997) and Head (1994; 1998).

	Unconsolidated Undrained	**Consolidated Undrained**	**Consolidated Drained**
Pore water pressure measurement, during testing	No	Yes	Yes
Saturate Sample until B = 95%	No	Yes	Yes
Consolidate until 95% PWP dissipation	No	Yes	Yes
Drainage	No	Only during consolidation	During consolidation and shear.
Normal stresses	Cell Pressure	Cell Pressure – Back Pressure	Cell Pressure – Back Pressure
Strain rate	Failure within minutes	Slow enough to allow pore water pressure equalisation and measurement	Slow enough to prevent pore water pressure build up.
Duration test time per sample	Minutes to Hours	Day to days	Days to a week
Cohesion	Total	Total and Effective	Total and Effective
Friction Angle	Total	Total and Effective	Total and Effective

The UU method, whilst quick, only allows the measurement of total stress parameters c and ϕ. Because soils under investigation were almost fully saturated (see Chapter 5) ϕ was very low. An example of this is presented in Figure 3.12 where the sample has a friction angle of 4.5° and cohesion of 10 kPa.

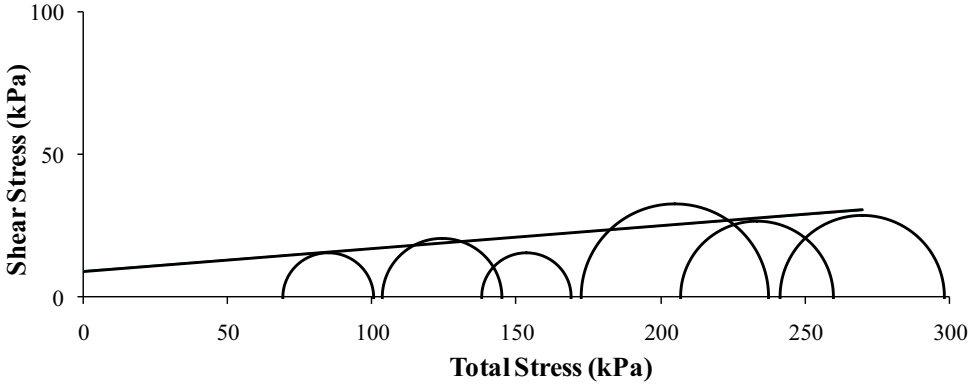

Figure 3.12: Mohr circle plot from an unconsolidated undrained triaxial test of a saturated sample examined during the course of this study.

The phenomenon presented in Figure 3.12 is not uncommon in saturated samples tested under UU conditions, because in a saturated undrained test deviator stress ($\sigma_1 - \sigma_3$) at failure is independent of cell pressure (Bishop & Henkel 1962). When cell pressure is increased the response from PWP within the saturated specimen is almost identical. Therefore, no matter the amount of increase in cell pressure the effective stresses in the specimen will remain unchanged. Because the effective stresses are the same deviator stress will remain the same, or similar, across a range of confining pressures (σ_3). This results in Mohr circles of similar sizes at different positions along the total stress axis (Craig 1997). Therefore UU tests were not undertaken on samples in this study. Furthermore, total stress values can be obtained from both consolidated undrained and drained tests.

The consolidated drained (CD) test provides long term values of shear strength (Selby 1993), however it was not used to test more than one sample. The results of this test were not analysed. Because the test times were long (one specimen took a week) in all three specimens examined, peak deviator stress was not reached before 20 % strain. Considering that up to 7 samples were intended to be tested, the operator was relatively inexperienced, and the time frame for this study, it was decided that this type of test was inappropriate.

Consolidated undrained (CU) tests were relatively quick (1 – 2 days per specimen) and a peak in deviator stress was observed in most samples. Therefore, consolidated undrained tests were undertaken on all samples and provide both effective and total strength parameters examined in this study. Whilst drained tests are relevant for slope failures which are slow and progressive, consolidated undrained tests are more appropriate for rapid failures (Selby 1993). This is applicable to the Tauranga region as failures are typically rapid (Tonkin & Taylor 1980; Hatrick 1982; Wesley 2007). Furthermore, results from consolidated undrained tests are typically similar to those of a drained test (Selby 1993); differences become most apparent in heavily consolidated clays (Head 1998).

3.3.17.3 General test protocol

The type of CU test employed was a single stage multiple specimen test as opposed to a multiple stage single specimen test. CU triaxial testing has three main steps, including saturation, consolidation and compression. A brief outline of the processes followed is presented here, but more detail and equations are available in both BS 1377 (1990) and Head (1998).

During testing, specimens were typically saturated using increments of cell and back pressure. The aim of this process was to dissolve any air remaining in the pore system of the sample (Craig 1997) and also eliminate any air bubbles in the drainage line and pore pressure connections (Head 1998). Cell and back pressure increases were stopped when the pore water pressure coefficient (B) was > 95%, as required by BS 1377 (1990). BS 1377 (1990) recommends the use of side drains to speed up the saturation process, but these were not required for our samples due to the high porosity (see Chapter 5). Once saturation was complete, effective stress was applied. Effective stress is the difference between the back pressure and the cell pressure. Typically back pressure was always at 300 kPa or greater during consolidation and testing as required by BS 1377 (1990). Effective confining pressures were based on *in situ* conditions, and the same principles were followed as for the shear box. However, for some specimens, higher confining pressures (> 300 kPa) were limited by the ability of the system to supply adequate pressure.

Specimens were consolidated under isotropic conditions until 95% PWP dissipation had been achieved. Time to failure was estimated from the consolidation curve. Test run times were calculated from both time to failure and an estimated value of strain at failure, which was typically less than 5 %. Specimens in this study consolidated rapidly often having time to failure values of < 10 minutes, and hence very quick test times. Because BS 1377 (1990) recommends that specimens are not be allowed to fail until compression has proceeded for ~ 2 hours, the test times were dramatically increased from those calculated. This gave test speeds between ~ 0.015 and 0.030 mm min^{-1}. The slow compression speeds ensured PWP equalisation through the specimen, so effective stresses could be calculated with accuracy (Head 1998). During compression testing information was logged about every 3 minutes. This logging time meant that up 350 individual measurements of strain, PWP and deviator stress were taken during each test.

Compression of each specimen was run until 20% axial strain was achieved (BS 1377 1990; Head 1998). Above 20% strain the specimen may become severely distorted and can result in dubious values of calculated axial stress (Head 1998). Typically, during the first ~ 0.5 % of axial strain no deviator stress recording occurred. Deviator stress remained at 0 because a small gap existed between the load cell and triaxial frame at test start up. Therefore it took a small amount of compression travel before any increase in deviator stress was recorded. The effect of this gap is shown as a flat section on the stress strain curve in Figure 3.13. Because a number of equations, corrections and interpretations require accurate values of axial strain during certain times of the test this flat section was always subtracted from the total axial strain recorded.

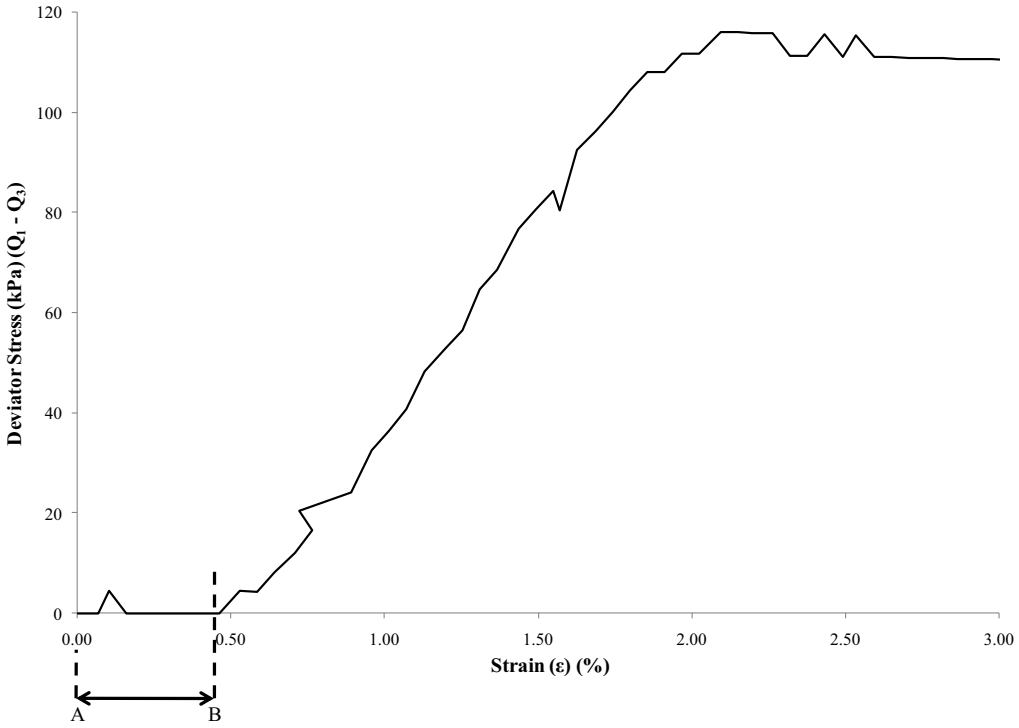

Figure 3.13: Axial strain which needs to be subtracted for stress strain curves. Example is from a sample from Otumoetai tested at a confining stress of 25 kPa. A and B represent the excess strain which was deleted during triaxial calculations.

Upon test completion a correction had to be applied to the calculated deviator stress value which accounted for the restraining effect of the membrane used. BS 1377 (1990) presented a chart of correction values versus axial strain. However the chart presented was difficult to read with accuracy and was not suitable when corrections for large data sets were required. Therefore, a third order polynomial equation was developed which replicates this graph, and is presented below:

$$Mc = 4 \times 10^{-5}\left(\varepsilon^3\right) - 4.7 \times 10^{-3}\left(\varepsilon^2\right) + 0.1596 \times \varepsilon \qquad (3.16)$$

where:

Mc = membrane correction;

ε = strain (%).

The value derived from equation 3.16 was then subtracted from the raw deviator stress values.

3.3.17.4 Mohr-Coulomb plots

Ultimately the most important parameters derived from a triaxial test are the effective and total cohesion (c', c) and friction angle (ϕ', ϕ) values. The typical way to derive these parameters is by drawing stress circles for each specimen analysed, at least 3, and then plotting a line tangential to the circles (e.g. Figure 3.12). Plotting tangents is subjective, causing questionable accuracy especially when stress circles do not form an idealised failure envelope. In this study total stress parameters at failure were plotted using $s = [{}^1/_2(\sigma_1 + \sigma_3)]$ and $t = [{}^1/_2 (\sigma_1 - \sigma_3)]$. Effective stress parameters are plotted as $s' = [{}^1/_2(\sigma_1' + \sigma_3')]$ and $t' = [{}^1/_2 (\sigma_1 - \sigma_3)]$. Deviator stress $(\sigma_1 - \sigma_3)$ is the same for both total and effective stresses because PWP cancels out, therefore the same calculation is used for t and t' in both plots (Head 1998).

The "s and t" method presented a single point for each sample analysed rather than a stress circle. Once a series of analyses were completed a line of best fit, which treats all samples equally, was plotted (Frederickson 1988). This line is termed the K_f line having a slope of θ and an intercept of t_o (Head 1998). An example for a single stress circle (specimen) is given in Figure 3.14.

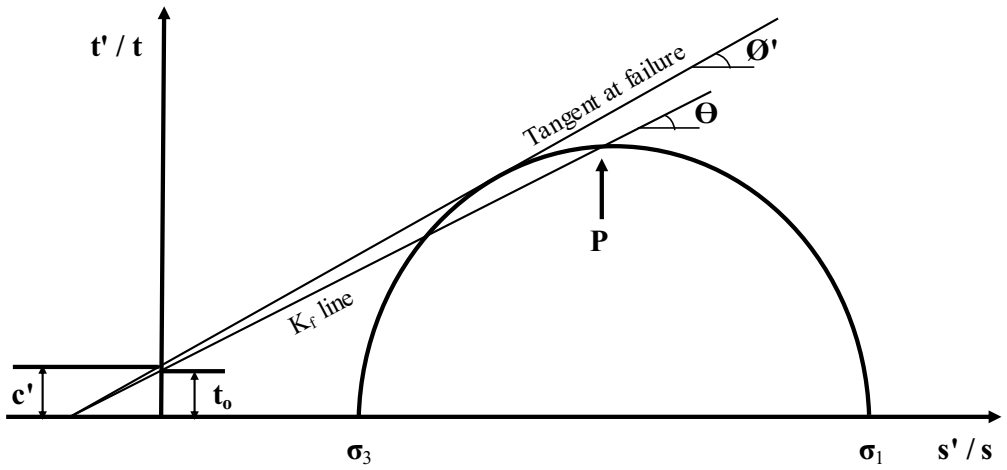

Figure 3.14: "S and t" plot showing a K_f line which plots through the top most point of the circle at point P denoted by $s` = {}^1/_2(Q_1' + Q_3')$ and $t = {}^1/_2 (Q_1 - Q_3)$. For total stress, s becomes $s = {}^1/_2(Q_1 + Q_3)$ and t does not change (refer to text). Also presented is the Mohr-coulomb line plotted as a tangent to the stress circle.

Figure 3.14 indicates that the K_f line passes through the apex of the circle whereas the stress circle line passes at a tangent. Therefore, the slope and intercept values

of the K_f and tangental line are different. The slope and intercept calculated from the K_f line has a mathematical relationship with both total and effective c and ϕ (see Head 1998). Therefore the Mohr parameters can be derived from the K_f line using the following equations (BS 1377 1990):

$$\phi' = \sin^{-1}(\tan\theta) \tag{3.17}$$

$$c' = \frac{t_o}{\cos \emptyset'} \tag{3.18}$$

where:

t_o = y axis intercept of the K_f line;

θ = slope of the K_f line.

The total stress parameters c and ϕ can be derived from similar equations using a plot of s and t.

3.3.18 Ring shear test

Ring shear testing enables the measurement of residual shear strength parameters on remoulded soil specimens for the determination of effective residual cohesion (c_r) and friction angle (ϕ_r) (Law 1980). Unlike the shear box, the ring shear allows unlimited deformation to be applied. Furthermore the rate of displacement applied is not critical because the fully drained condition will be reached eventually (Head 1994).

A Wykeham Farrence, model number 25850, ring shear apparatus was used, which confines a 5mm thick specimen vertically between two bronze platens and radially between two concentric rings (Head 1994). Shearing occurs close to the upper platen in an annulus (circular) mould with an internal diameter of 70 mm and an outer diameter of 100 mm. The thin specimen size allows perfect and rapid pore pressure dissipation (Law 1980).

Specimens were set up following methods laid out by Law (1980) and Head (1994). Before testing, the specimens were dried to just above the plastic limit. Head (1994) recommended that specimens should be tested at moisture contents wetter than the plastic limit. On testing volcanic ash soils Wesley (1992)

adjusted the moisture content to just above the plastic limit. It seems the main reason for doing this is that excessively wet specimens will extrude from the annular cavity when consolidated and sheared, therefore this method was adopted in this study.

The following two sections will set out methods for specimen consolidation and strain rate selection, because a brief survey of laboratory manuals (Law 1980; Bromhead 1986; Head 1994) indicated that there was no clear method which should be followed.

3.3.18.1 Sample Consolidation

Specimen consolidation immediately followed test preparation and required the application of normal loads to be used during testing. Normal loads used were those which best bracket *in situ* conditions. The method of load selection was the same as for the shear box and the equation used to derive the appropriate normal load weights can be found in Appendix 3.7.

Under conditions of consolidation the specimen was compressed vertically between platens by means of a 10:1 lever loading system loaded with dead weights (Law 1980). Specimen compression readings were taken using a vertical dial. Readings were frequent at first (e.g. 2, 6, 15 seconds), to accurately capture the start of the consolidation curve, and then became more spaced as consolidation progressed (e.g. 45, 60, 90 minutes). Recordings were then plotted as settlement versus square root time. The equation used to convert time recorded during consolidation to root time is presented below:

$$\sqrt{t} = \sqrt{\left(\frac{x}{60}\right)} \qquad (3.19)$$

where:

$\sqrt{t}$ = root time;

x = recorded time (seconds).

A specimen was considered to be fully consolidated when the vertical dial reading remained constant over a period of at least one hour.

3.3.18.2 Strain rate selection

Specimens in the ring shear were tested under drained conditions; therefore the rate of shearing was slow enough to allow any pore water pressure generated to escape from the specimen (Bromhead 1986). To determine the rate of shear, a time to failure was calculated. Bromhead (1986) recommended the equation given in Bishop & Henkel (1962) which is typically used for calculating the time to failure for a triaxial specimen with drainage from both ends. The equation is:

$$T_f = \frac{H^2}{3Cv(1-\overline{U}_f)} \tag{3.20}$$

where:

T_f = time to failure;

H = half the sample height;

Cv = coefficient of consolidation;

U_f = pore pressure conditions allowed at failure.

Allowing 5% pore water to remain (U_f= 0.95), as recommended by Bromhead (1986), the equation becomes more simply:

$$T_f = \frac{20H^2}{3Cv} \tag{3.21}$$

The consolidation coefficient (Cv) was calculated using the t_{90} root time method presented in Craig (1997). The equation used for C_v is:

$$Cv = \frac{0.848H^2}{t_{90}} \tag{3.22}$$

Where:

t_{90} = time for 90% consolidation;

H = half sample height;

0.848 = time factor.

The t_{90} component was found using the following method, which is shown graphically in Figure 3.15. A line was drawn down the linear portion of the

consolidation graph, representing the line AB. Starting at point A another line was drawn with an abscissa 1.15 times that of line AB, which is line AC. The time on the x axis where line AC intersects the settlement curve represents $\sqrt{t_{90}}$. Because the actual time measurement for $\sqrt{t_{90}}$ is required in equation 3.22 it must be squared before use.

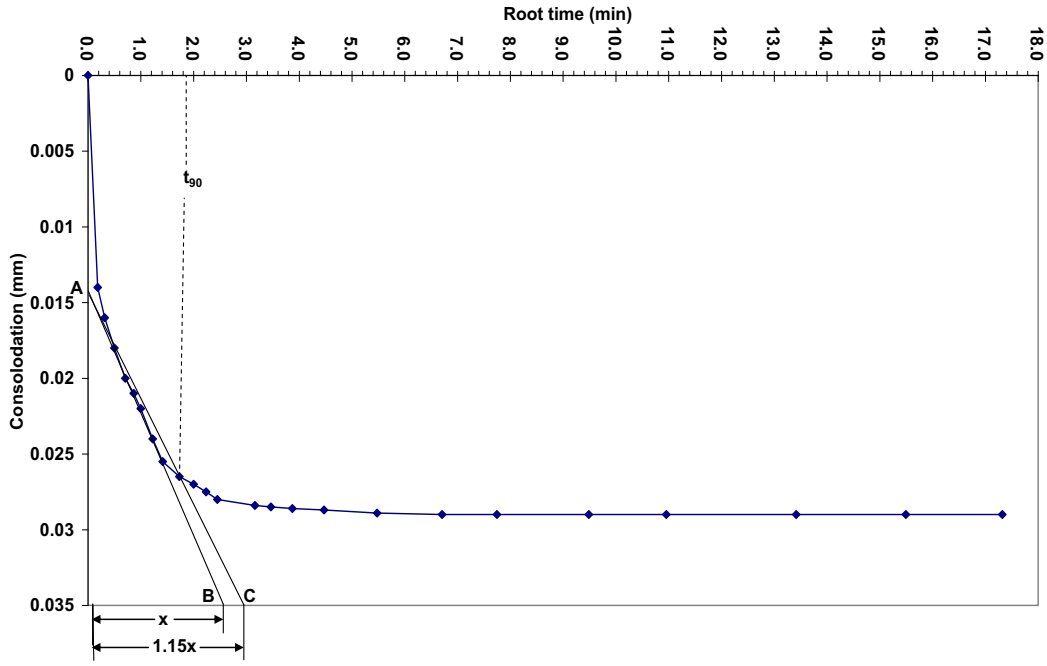

Figure 3.15: Example of consolidation versus root time graph showing how to determine t_{90}.

Most specimens fail at a displacement of 2 mm or less, which represents a rotation of 2.7° in the ring shear apparatus (Law 1980). This was used in combination with the estimated time to failure to derive a speed at which to run the ring shear.

Because a large number of the specimens being tested were highly compressible, it was often difficult to differentiate between initial compression and the linear section of primary consolidation, making determining t_{90} difficult. When this occurred, a strain rate of 0.048 deg min^{-1} was used. A strain of 0.048 deg min^{-1} has been indicated by both Bromhead (1986) and Head (1994) as a safe speed which provides a safety factor against strain sensitivity. Once the testing programme was complete it was found that other workers used strain rates as high as 0.12 deg min^{-1} with no regard to consolidation rates, stating that the influence on measured strengths is negligible (Skempton 1985; Wesley 1992).

A check on strain rate sensitivity during testing was made by stopping the drive motor for one hour after testing had commenced, if the reading did not drop significantly over this period the strain rate was deemed acceptable (Head 1994). Unfortunately the value which corresponds to significant change is not defined by Head (1994). For this study, a > 2 % decrease in the proving ring reading was considered to be significant. This never occurred during the course of this study.

3.3.18.3 Sample Shearing

Before the shear stage was run, a shear plane was formed. Normally the sample would be set up in the evening with a rate of strain set at 0.048 deg. min^{-1}. and let run overnight unrecorded (Bromhead 1986). This method was followed because it was found that a fast manual shear as recommended by Law (1980) caused a large amount of sample extrusion.

Once a shear plane was formed the torque was released from the proving rings and the sample was let sit for at least the period taken to achieve t_{90}. This let any excess pore water pressure generated during the shear stage dissipate. Following this the proving ring and vertical dials were set to zero and the test was begun proper. The proving ring and vertical dials were read at regular intervals (between 30 seconds and 5 minutes), however the frequency of readings decreased once failure had occurred (the proving ring readings were no longer increasing). As the test proceeded results were plotted on a stress strain graph. Residual strength was determined at the point where the value recorded by the individual proving rings remained relatively stable.

3.3.18.4 Further application of normal load

The specimens were run as multistage tests where the same sample was tested under increasing normal loads. Detail of this process can be found in Law (1980) and Head (1994). At least three readings were taken to derive a Mohr-Coulomb plot. These were then used to calculate residual friction angle and cohesion.

3.3.19 Error treatment

Errors are presented as:

$$x \pm \Delta x \tag{3.23}$$

where:

x = is the best estimate of the true value;
Δx = is the precision of this value.

Chapter 4
Stratigraphy and field properties

4.1 Introduction

This chapter presents information collected during field investigations. This information includes the purpose of field investigations, justification for site selection, and the stratigraphy and geomechanical properties of selected sites. The aim of this chapter is to provide detailed field information regarding the samples collected for laboratory investigation.

4.2 Initial field investigations

The main purpose of field investigations was to locate sites with soils of high sensitivity, especially those which are categorised as "quick" (sensitivity > 16) and have low, dilatant, remoulded strength. The identification of highly sensitive soils then provided the basis for site selection. Through the course of field investigation, the geomorphology of three slips which displayed soils of elevated sensitivity were investigated in detail in an attempt to add information regarding the role of sensitive soils in mass wasting events in the Tauranga area. These results are also presented in this section. Methods employed during field investigation can be found in Chapter 3. Field logs and geomorphic maps are presented in Appendix 4.1.

4.2.1 Sensitivity observations

Highly sensitive soils were observed in weathered pyroclastic and associated deposits in cuttings at McLarens Falls, Tauriko and Pyes Pa; in slips at Oropi, Welcome Bay, and Otumoetai; and at a coastal cliff section at Omokoroa (Appendix 4.1).

Sensitivity values ranged from 2 to 29 using the standard method and 2 to 160 using the adapted method. However, sensitivities between 5 and 10 were typical at most sites, with values up to 15 not uncommon. Both the maximum standard (29) and adapted (160) sensitivity values occurred at Tauriko, but were

not recorded in the same unit. Extremely high sensitivities (> 30) measured using the adapted method were typically the result of low remoulded strength (< 3 kPa). Unfortunately, low remoulded strength (< 3 kPa) values were close to the limit of precision for the shear vane and could only be considered estimates. However, it was obvious from visual investigation that remoulded material in these samples was extremely soft and liquid-like (Figure 4.1). During adapted sensitivity method remoulding samples took varying degrees of effort to liquefy, with some requiring a full minute of kneading before they were fully softened. Samples which became liquid-like on remoulding were typically pale coloured (pale orange, greys, browns and pinks) and very wet. These soils ranged across both SILT and CLAY textures.

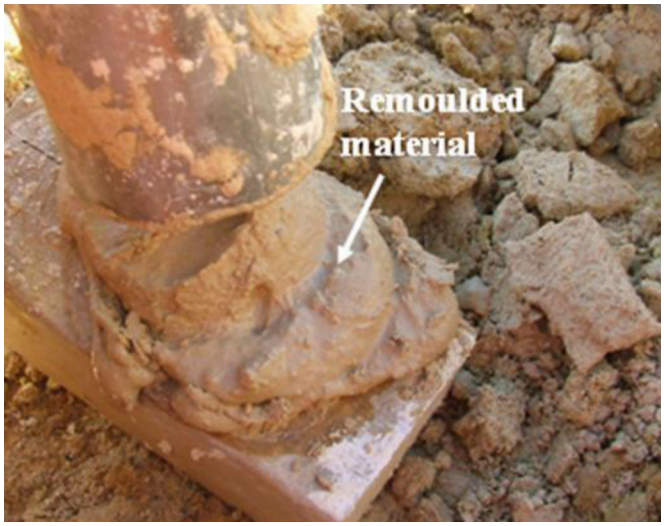

Figure 4.1: Remoulded clayey SILT (labelled) from Tauriko showing a dilatant character.

Redoximorphic features, including manganese (pyrolusite) concretions (Vepraskas 1994) (also known as redox segregations: Hewitt 1998) were observed in soils of both high and low sensitivity. Manganese dioxides (presumably mainly pyrolusite, MnO_2) were expected because many soils in the Tauranga region, with the exception of material near the surface, are close to saturation for a large part of the year (Wesley 2007) but dry sufficiently for oxidation to occur and hence concretionary material to form.

4.2.2 Geomorphic observations

The following presents the geomorphic information of three slips at Welcome Bay, which occurred during a storm event in May 2005. Field logs and geomorphic maps for each are presented in Appendices 4.1 and 4.2, respectively.

The first slip at Ranginui Road (**U14 927 817**; Appendix 4.2a) (grid references of the 1: 50,000 New Zealand topographical map series NZMS 260) was a deep bowl shape (Figure 4.2). During failure, material slumped, disintegrated and flowed. Run out distance was ~ 20 m, with material lapping against an adjacent slope. However, material also flowed ~ 55 m down slope (< 10 º) to the west of the scarp. The slip had a width of ~ 20 m and a length of ~ 22 m, with a near vertical head scarp of ~ 5 m. The failure occurred with a slope of ~ 27 º. Within the scarp, both the Rotoehu Ash and Hamilton Ash beds were identified (Figure 4.2). The basal slip plane was ~ 3.5 m below the contact between the Hamilton and Rotoehu Ash beds. Sensitivity increased towards the base of the slip. At the base, a light yellowish brown clay with a peak vane strength of 42 kPa and an adapted sensitivity of 42 was encountered (remoulded strength = 1 kPa). The centre of the slip scarp was water logged and muddy.

Figure 4.2: Slip at Ranginui Road. The dashed line represents the contact between the Rotoehu Ash and Hamilton Ash Formation.

The other slips occurred on a property adjacent to Welcome Bay Road (**U14 937 818**; Appendix 4.2b) and are referred to as slip 1 and slip 2 (Figure 4.3).

Both slips occurred as single events and had steep translational appearances (Figure 4.3). Figure 4.3 indicates that both slips liquefied following failure, with run out lobes of up to 90 m. The inclination of the failed surface in slip 1 was ~ 30 º. Slip 1 had a width of ~ 12 m, a length of 24 m and a back scarp of ~ 2 m. However, the slip walls were up to 3.5 m high. Slip 2 was wider at ~ 19

m, with a length of ~ 14 m, and was up to 2 m high. Both slips occurred from unfailed surfaces of ~ 30 º. Sensitivities at Welcome Bay Road were lower than those at Ranginui Road. Sensitivities up to 10 were recorded in slip 1 and values up to 28 were recorded near the base of slip 2. The lowest remoulded strength recorded was 3 kPa.

Figure 4.3: Slips on Welcome Bay Road at Welcome Bay. Note the distinction between slip 1 and slip 2 and the run out distances of each slip (Photo courtesy of Tauranga City Council).

The general features of the slip at Otumoetai are not further discussed here because information has already been presented by Wesley (2007) and comments are made in section 4.4.2. Limited detailed information was collected on the slips at Oropi or Omanawa.

As noted in Chapter 2, the slips observed in this study occurred as a single event associated with intense rainfall (and thus pore water pressure increase), typically flowed on failure leaving little debris in the scarp, had units of elevated sensitivity, occurred from steep slopes and were small with either a bowl shape or shallow translational appearance.

4.3 Site selection

Two sites were selected for further analysis; a cutting at an earthworks site in Tauriko (**U14 832 789**), and a slip at Grange Road, Otumoetai (**U14 875 863**). The slip at Otumoetai is a remnant of the May 2005 storm event. The location of these two sites relative to the rest of the study area is presented in Figure 1.1. For the remainder of this thesis, the sampling sites will be referred to as **Tauriko** and **Otumoetai**.

Tauriko was selected because it had units of high sensitivity which manifested in low remoulded strength (based on the adapted method). The site was easily accessible and, being an earthworks site, an unlimited amount of freshly exposed material could be sampled. The abundant amount of material provided the basis for establishing a laboratory programme, especially triaxial testing.

Otumoetai had units of high and low sensitivity in close vertical proximity (within ~ 1 metre) and represented a site of previous investigations (see Wesley 2007). The fluid nature of slip material meant that little debris remained in the scarp zone, ensuring that undisturbed samples could be collected with minor excavation. Finally, Otumoetai and Tauriko represented sites in different geographic locations and age.

4.4 Site geomorphology

4.4.1 Tauriko

The site at Tauriko was formerly agricultural land, which was being excavated and developed at the time of sampling. The general area is dominated by a number of plateaux which fall away, often steeply, to broad shallow valleys. These raised areas represent pyroclastic constructional surfaces which have been modified by erosion (Briggs *et al*. 1996). At the base of the broad valleys a number of small natural watercourses were observed, including the Kopurererua Stream near the Tauriko site. The cutting investigated at Tauriko was on an elevated plateau surface, was approximately 30 m high and had a north-easterly aspect.

4.4.2 Otumoetai

The site at Otumoetai is on a NE-trending peninsula which extends into the Tauranga Harbour. The surface of the peninsula is an elevated plateau largely covered by residential development. The site under investigation was the scarp of a slip generated during the May 2005 storm event, which occurred in a remnant sea cliff bounding the peninsula. The remnant sea cliff was about 20 m high and the base was separated from the harbour by approximately 600 m of terrestrial and aquatic vegetation. The slip under investigation occurred on the lower half of the coastal cliff and had a shallow circular appearance. A small slip also occurred on the upper half of the cliff however, this had been covered by a retaining structure and vegetation. The lower slip was relatively free of debris because much of the material disintegrated and flowed into the marshy area below, having a run out distance of approximately 100 m. Slips are not uncommon in this location, with three others recorded within 500 m of the sampling site following the May 2005 storm event.

4.5 Site stratigrahpy

The stratigraphy of the sampling sites at Tauriko and Otumoetai are presented in Figures 4.4 and 4.5, respectively, and described in the following section. It should be noted that the depths recorded are based on actual measured distances and have not been corrected for slope inclination. Furthermore, manganese dioxides were observed in most units at both Tauriko and Otumoetai, the exceptions typically being units dominated by sand.

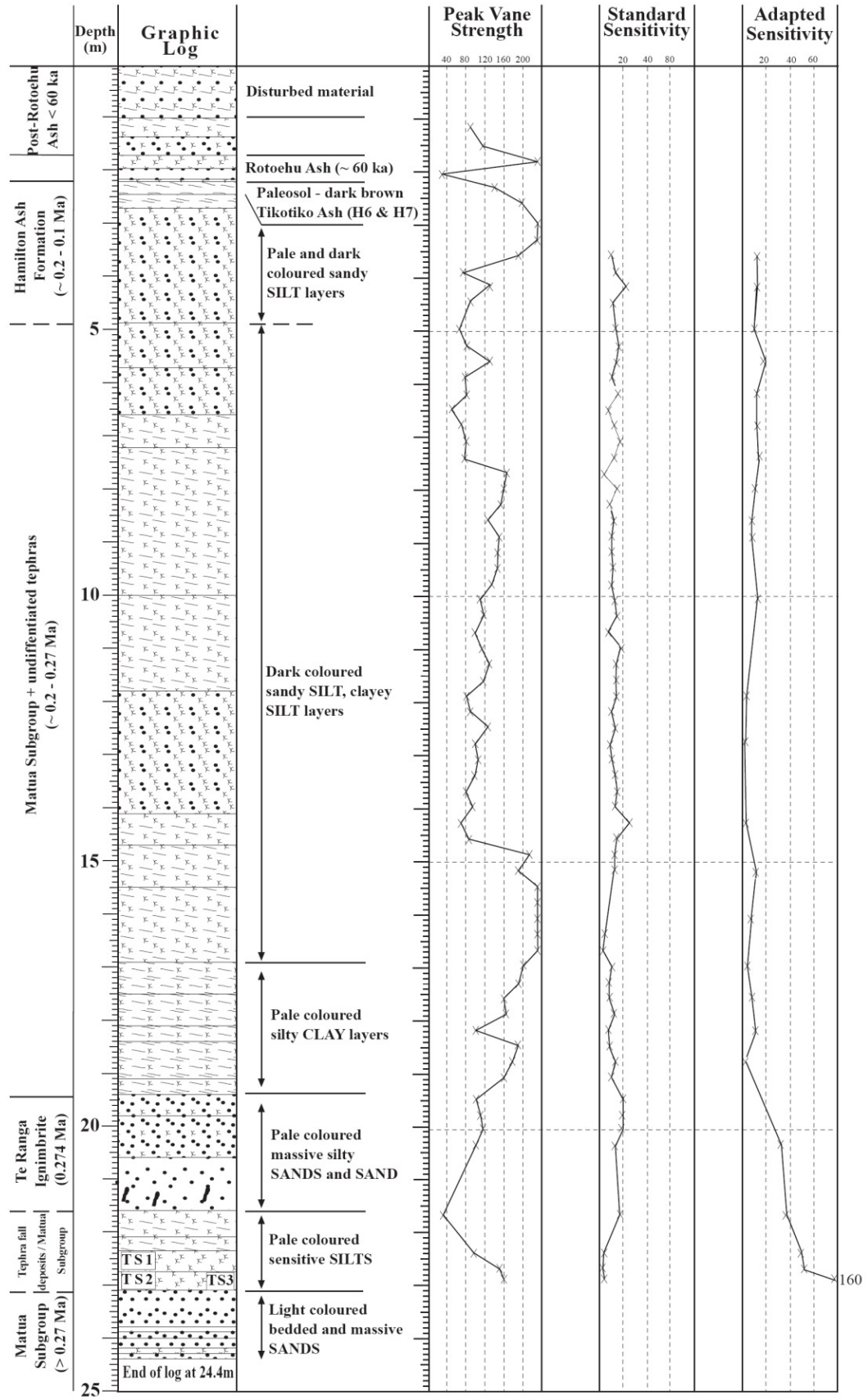

Figure 4.4: Stratigraphic column from Tauriko. Also included are peak vane strength and adapted and remoulded sensitivity values for each unit. TS represents the approximate Tauriko sample position

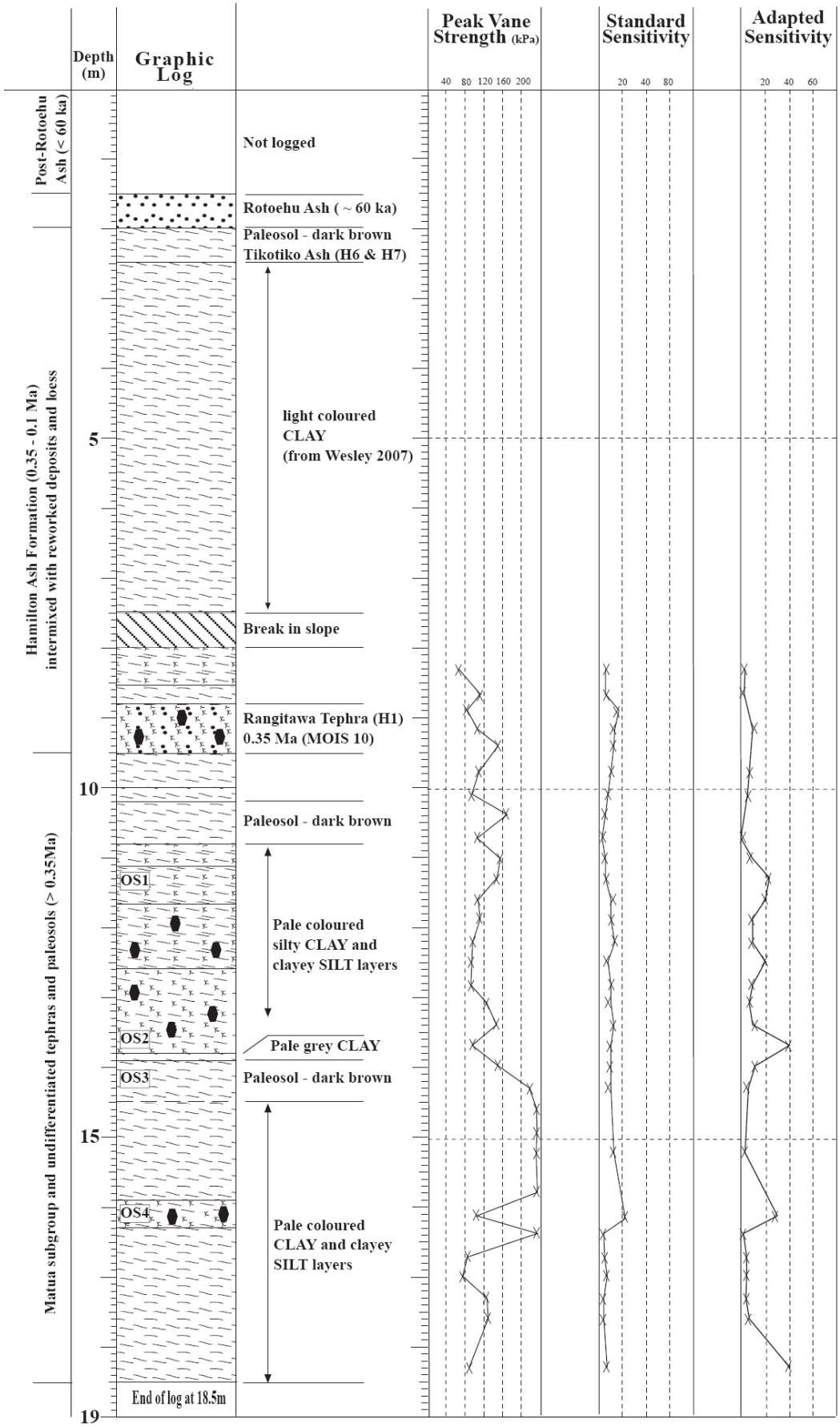

Figure 4.5: Stratigraphic column from Otumoetai. Also included are peak vane strength and adapted and remoulded sensitivity values for each unit. MOIS = marine oxygen isotope stage (see text), OS = Otumoetai sample positions, the black hexagons represent flakes of micaceous material.

4.5.1 Tauriko

At Tauriko, the Rotoehu Ash (c. 60 calendar [cal] ka) was represented by a thin (0.2 m) well-sorted, fine to coarse SAND which lay between two thin (0.25 m and 0.05 m) SILT units. Underlying the Rotoehu Ash was a dark brown clayey paleosol (Figures 4.4 and 4.6) representing a strongly-developed buried soil on the uppermost member of the Hamilton Ash sequence, possibly the Tikotiko Ash Member (H6 and H7) (Lowe *et al.* 2001). The dark paleosol represents development probably during the Last Interglacial (Briggs *et al*. 2006; Lowe 2008a). The base of the Hamilton Ash Formation could not be defined, and the entire unit was expected to be no thicker than about 2.5 m (Briggs *et al.* 1996). Figure 4.6 displays light and dark coloured beds making up part of the Hamilton Ash Formation. The Hamilton Ash sequence, which may include loess beds at some locations, has an age range estimated between ~350 ka at the base (H1 or Rangitawa Tephra, not observed at Tauriko) and ~100 ka at the top (Lowe *et al.* 2001; Lowe 2008a).

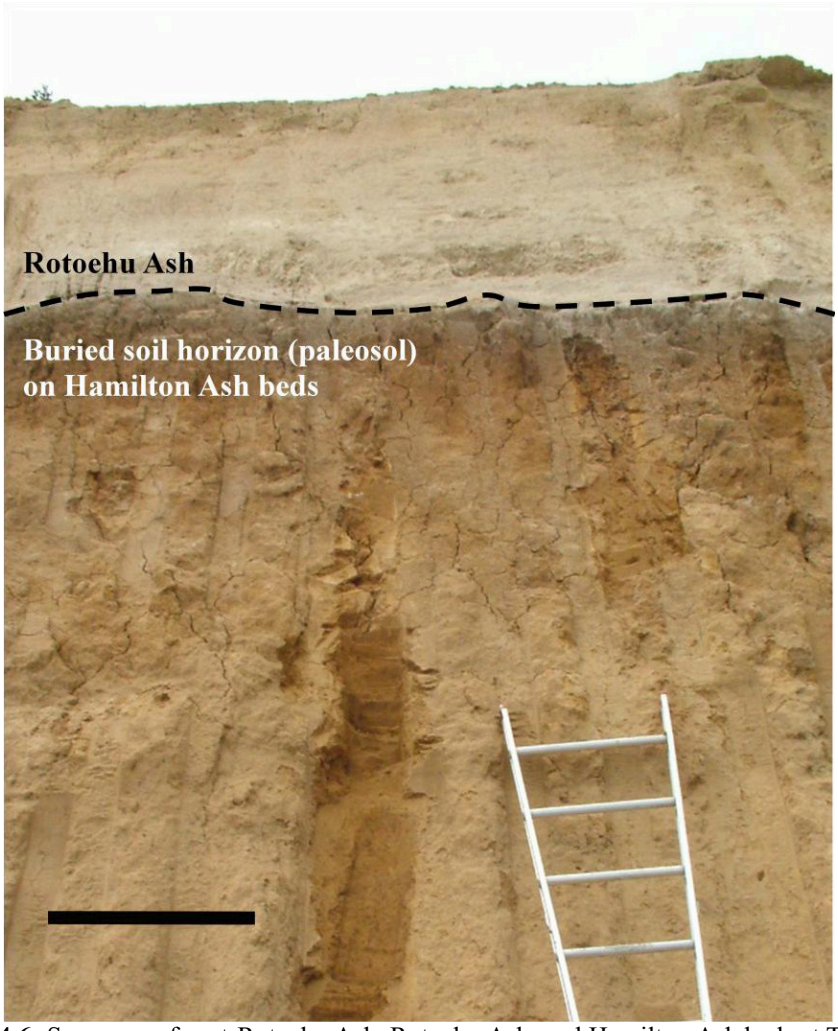

Figure 4.6: Sequence of post-Rotoehu Ash, Rotoehu Ash amd Hamilton Ash beds at Tauriko.

Below the Hamilton Ash beds was a ~16 m thick unit comprising alternating sandy SILTS, clayey SILTS, and silty CLAYS (Figure 4.4). These layers were not correlated and were reported as undifferentiated weathered tephric (pyroclastic) material derived from tephra fall deposits, pyroclastic flow deposits, reworked material, or combinations of these. This sequence could, in effect, represent part of the Matua Subgoup (60 cal. ka to 2.1 Ma; Briggs *et al.* 1996; 2006). Within the undifferentiated material changes in peak strengths did not always correlate with different layers based on colour and texture (Figure 4.4). The maximum sensitivity value in the undifferentiated material was 29 (Figure 4.4) (derived from the standard method) and it had a remoulded strength of 3 kPa. This same sample, on extraction and remoulding following the adapted method, did not have a liquid-like consistency, and returned a remoulded strength of 15 kPa.

Underlying the undifferentiated material was a sequence of light grey, massive, silty SAND and SAND units (Figure 4.4). These sands totalled ~ 2 m in thickness, and charcoaled logs, up to 0.3 metres long, were identified at the base (Figure 4.7). The presence of charcoal represents hot emplacement and a pyroclastic flow origin (Briggs *et al.* 1996). Charcoal is typical of the Te Ranga Ignimbrite (0.274 Ma) which is found in the Tauriko region (Briggs *et al.* 1996).

Further investigation of this unit using thin sections identified coarse glass shards with lunate, cuspate and platy textures, showing little deformation (Figure 4.8). These glass shard textures are characteristic of the Te Ranga Ignimbrite (Briggs *et al.* 1996) and so this identification was ascribed to the unit at Tauriko. The Te Ranga Ignimbrite overlay a sequence of light coloured sensitive SILT units (Figure 4.4) up to 0.5m thick (Figure 4.9).

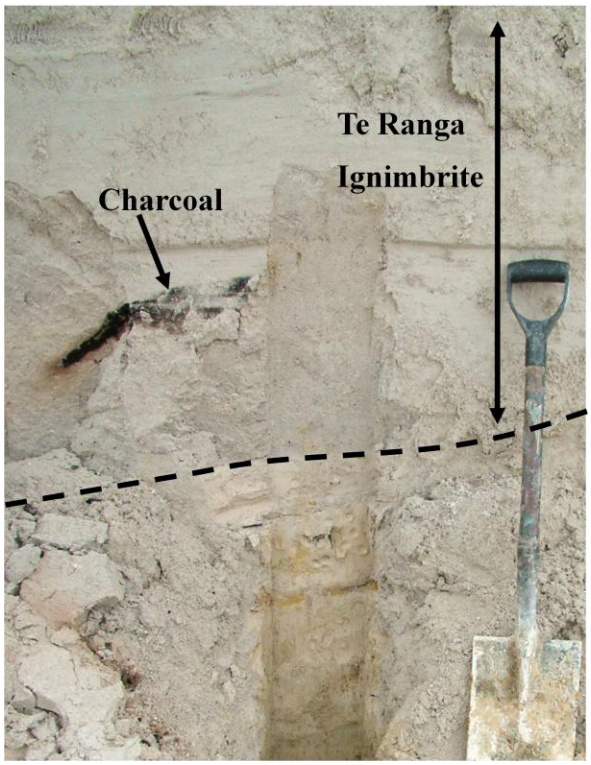

Figure 4.7: Base of Te Ranga Ignimbrite (0.274 Ma) at Tauriko overlying sensitive silt deposits. Note the piece of charcoal to the left of the image. The spade is approximately 1.2 m long.

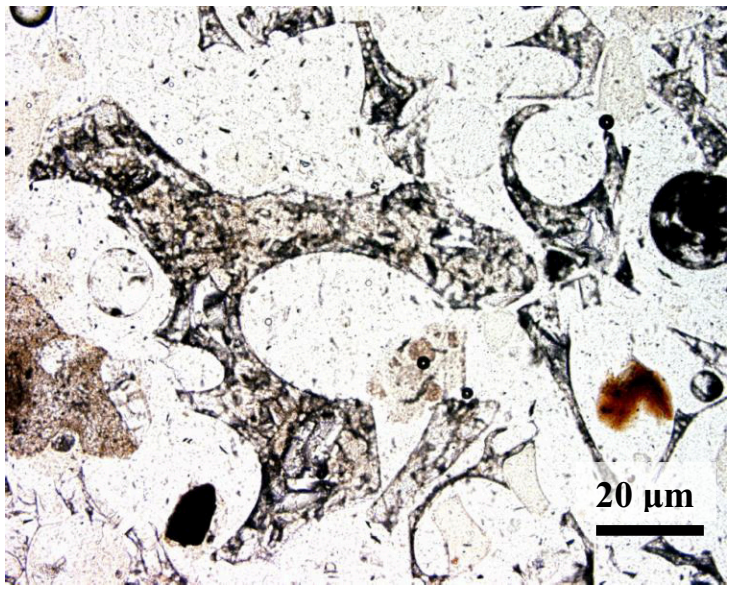

Figure 4.8: Glass shard textures from the Te Ranga Ignimbrite at Tauriko. Note the coarse y-shaped shard in the centre of the image.

Assuming the charcoal layers represent the base of the Te Ranga Ignimbrite, the underlying sensitive silt layers may represent either fallout tephras associated with the Te Ranga eruptive sequence which deposited the ignimbrite, or fall deposits, from an earlier unrelated eruption. If the sensitive material is not associated with the Te Ranga Ignimbrite then it represents a unit of the Matua Subgroup (60 cal. ka to 2.1 Ma; Briggs *et al.* 1996; 2006). This material was soft

to firm, became extremely dilatant on remoulding, and had adapted sensitivities up to 160 (Figure 4.1); samples were collected from this unit.

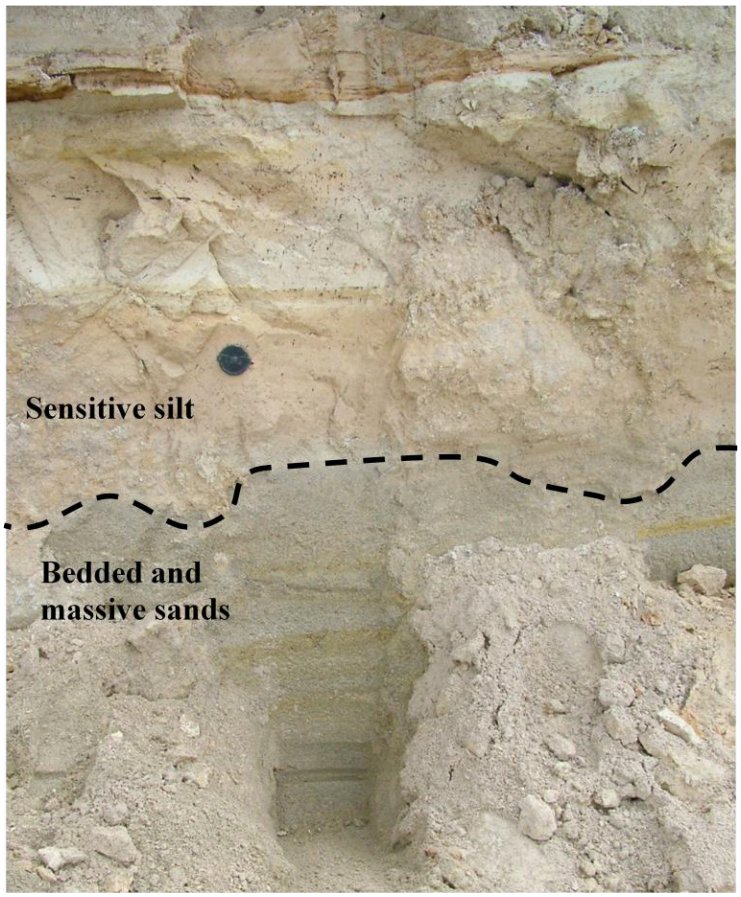

Figure 4.9: Sensitive silt from Tauriko overlying bedded and massive sands. Note the camera lens cap (~ 5 cm) for scale.

The silt units unconformably overlay a sequence of dense pumiceous SANDS (Figures 4.4 and 4.9), each less than 0.2 m thick. Sedimentary structures observed within these sands included both massive units and laminar planar bedded layers. These sand units represent fluvially derived members of the Matua Subgroup, and are most likely derived from reworked rhyolitic ignimbrites and tephra fall units (Briggs *et al.* 1996; 2006).

4.5.2 Otumoetai

The full stratigraphic sequence of the relict coastal cliff could not be obtained in this study because vegetation and a retaining structure obscured the upper section (section 4.4.2). Fortunately, before the retaining structure was built, Wesley (2007) investigated the site and described the sequence. He identified the top of the Hamilton Ash Formation and stated that it was mostly likely overlain by

the Rotoehu Ash (a widespread and distinctive unit in the area). These units have been included in Figure 4.5.

The following description comes from investigations made during this study (see also Wesley 2007) and focuses only on the lower slip (see section 4.4.2). The description presented herein will proceed from the break in slope, which represents the top of the lower slip; both are identified in Figure 4.5.

At the top of the lower slip (8 m depth in Figure 4.5) two thin, silty CLAY and CLAY units were observed and classified as moderately sensitive. Neither unit displayed dilatancy following remoulding. Below these units was a pale yellow, non-plastic sandy SILT unit, with distinctive golden sand-sized flakes. These features are indicative of the Rangitawa Tephra (~350 ka) and the golden flakes are likely to be 2:1:1 partially random interstratified micaceous-kaolinite intergrades (T.G Shepherd in Lowe and Percival 1993). Furthermore, Wesley (2007) identified this unit as the Rangitawa Tephra. The Rangitawa tephra represents the earliest member (H1) of the Hamilton Ash Formation (Lowe *et al.* 2001). Based on Wesley's (2007) identification of the topmost unit of Hamilton Ash Formation at ~ 2 m, it appeared that the sequence of beds was ~ 7 m thick. This is thicker than the typical maximum of 2.5 m (Briggs *et al.* 1996) in the area and therefore reworked tephra material and possibly weathered loess (e.g. as described by Briggs *et al.*, 2006, at Maketu) are likely to be included within the unit described as Hamilton Ash. It is also possible that the thickness of Hamilton Ash beds have been exaggerated because the individual beds are inclined rather than flat.

Below the Rangitawa Tephra, alternating layers of two dark brown CLAY paleosols and paler CLAYS, silty CLAYS and clayey SILTS were observed (Figures 4.5 and 4.10). Paleosols may indicate periods of either warm interglacial climates (when topdown soil formation is likely to result in strongly developed pedogenic features) or soil formation that has occurred during upbuilding pedogenesis on accumulating loess and/or thin ash beds during glacial climates (Manning 1996; Lowe *et al.* 2008c). Paleosols also represent periods of hiatus in volcanic activity (or when any deposits are sufficiently thin to be subsumed into the surface soil horizon). Because the Rangitawa Tephra has been correlated with

the end of Marine Oxygen Isotope Stage (MOIS) 10 (Kohn *et al.* 1992; Lowe *et al.* 2001), the upper and lower paleosols can be tentatively associated with MOIS 11 and 12, respectively (ca. 360–470 ka). These paleosols and associated sediments are best referred to as components of the Matua Subgroup, which includes in effect the Pahoia tephras or tuffs (Briggs *et al.* 1996).

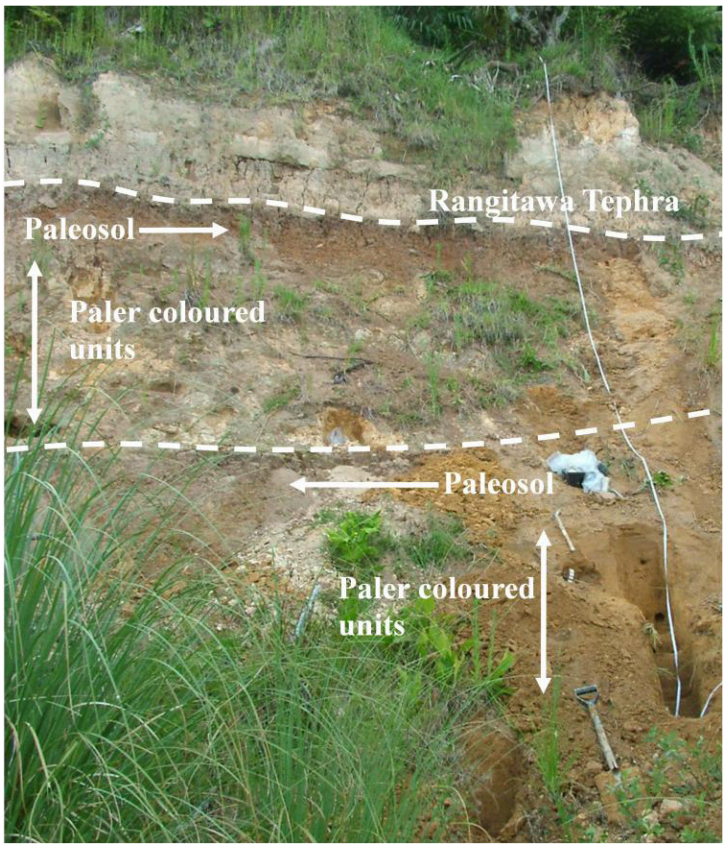

Figure 4.10: Site at Otumoetai, displaying location of the Rangitawa Tephra (~ 0.35 Ma), underlying two paleosols and paler coloured units. The spade at the base of the image is ~ 1.2 m in length.

Typically the paleosols were very stiff and had sensitivities between 4 and 11, using both adapted and standard methods (Figure 4.5). However, sensitivity manifested in high undisturbed strength (107 to 214 kPa) rather than low remoulded strength (13 to 32 kPa). The paler units ranged between firm and very stiff, displayed a range of sensitivities and some contained micaceous flakes (Figure 4.5). Using the standard and adapted method, sensitivity ranged between 3 to 21 and 3 to 37, respectively. A number of the high (29 to 37) adapted sensitivity measurements were a result of low remoulded strength (≤ 3 kPa).

Between the paleosol at 13.9 m depth and the overlying pale unit, a thin (~ 0.1 m) pale grey clay layer was observed (Figures 4.5 and 4.11). This pale layer contained extensive coatings of manganese dioxide (pyrolusite), indicating that

redox conditions have originated partly because of the lower permeability of the underlying paleosol. High sensitivity (37) (Figure 4.5) with low remoulded strength (2 kPa) was recorded directly above this unit.

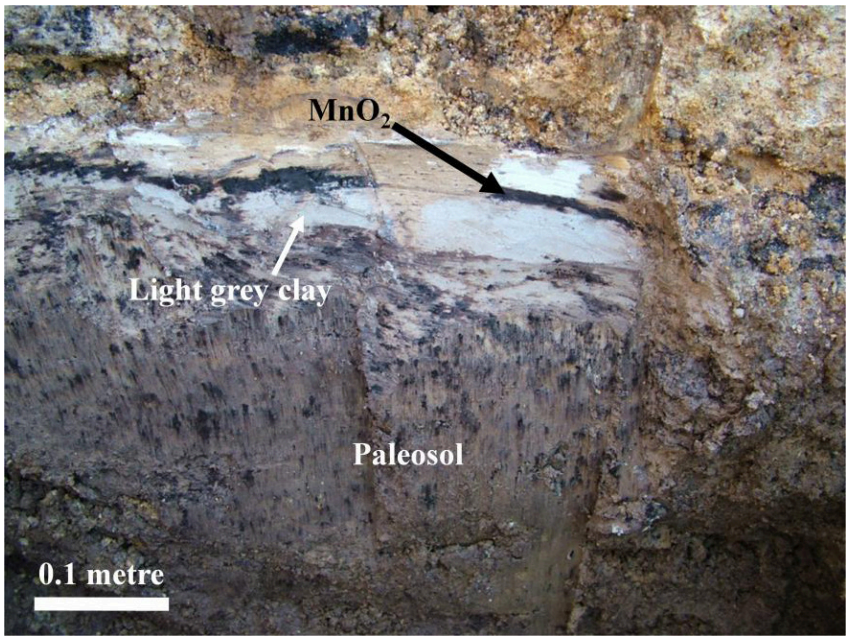

Figure 4.11: Light grey clay and manganese dioxide (pyrolusite) layer above the paleosol unit at 13.9 metres depth at Otumoetai.

4.6 Field geomechanical properties

Soil logging, strength and sensitivity testing were undertaken for each sample during collection. This investigation occurred sometime after initial logging which was used to compile Figures 4.4 and 4.5, and hence results may be slightly different. The results from this investigation are presented in the following section, and raw values can be found in Appendix 4.3.

4.6.1 Tauriko

Three samples were collected from Tauriko and these were labelled as TS1, TS2 and TS3. TS3 was from below the Te Ranga Ignimbrite (Figure 4.4). TS1 and TS2 were from a location ~ 150 m north of TS3 and were vertically only ~ 300 mm apart in a unit which was wetter than TS3. Like TS3, TS1 and TS2 were from a SILT unit below the Te Ranga Ignimbrite. At the time of sampling, both TS1 and TS2 were considered to be extremely wet lateral correlatives of TS3.

Samples from Tauriko were selected because of their depth below the ground surface (Table 4.1), silt texture, firm undisturbed strength, high sensitivity, and dilatancy following remoulding.

All samples collected from Tauriko had similar field characteristics, being pale grey, slightly plastic, clayey SILTS (Table 4.1). TS1 and TS2 were very wet and firm but became dilatant after remoulding. The dilatancy of TS1 and TS2 was typical of silt. However, both samples were very sticky, indicating high layer-silicate clay content. TS3 had the highest plasticity, peak vane strength (151 kPa) and cone penetration (9.5 kg) of all three samples (Table 4.1). Like the other samples, TS3 became dilatant after remoulding.

Table 4.1: Depth, mean vane shear strength (kPa), cone penetrometer (Pen.) readings and field soil descriptions for samples collected from Tauriko. Vane shear strength values presented in parentheses represent the range of values recorded. Sensitivities described in text are from the standard method in keeping with NZGS (2005). For peak vane strength the minimum error accepted was 3 kPa which represents 2 divisions on the vane.

Label	Depth (m)	Vane shear strength (kPa)	Pen. (kg)	Description
TS1	~ 22.6	58 ± 3 (49 – 62)	4	Clayey SILT, trace fine sand, light pink with black flecks (MnO_2), firm but soft on remoulding, very wet, non-plastic, extra sensitive, dilatant without the addition of water, very weakly allophanic, moderately weathered, coarse pebbles which represent pumiceous flecks are present but these disintegrate on contact
TS2	~ 22.9	45 ± 3 (39 – 50)	4	Clayey SILT, light pink with black flecks (MnO_2), firm but soft on remoulding, very wet, non-plastic, quick, dilatant without the addition of water, very weakly allophanic, moderately weathered, coarse pebbles which represent pumiceous flecks are present but these disintegrate on contact
TS3	~ 22.9	151 ± 3 (149 – 152)	9.5	Clayey SILT, trace fine sand, light grey becoming light yellow with depth, firm but soft on remoulding, moist to wet, very slightly plastic, sensitive, dilatant without the addition of water, very weakly allophanic, moderately weathered, coarse pebbles which represent pumiceous flecks are present but these disintegrate on contact

Remoulding and sensitivity testing indicated that all samples from Tauriko had extremely low strength (1 – 2 kPa) after extraction and remoulding (Table 4.2). This low strength resulted in extremely high adapted sensitivities (50 – 76) (Table 4.2). Using the standard method, TS2 recorded low remoulded strength (2 kPa), thus resulting in high sensitivity (20). TS3 had the highest remoulded values yet it recorded the highest adapted sensitivity (Table 4.2), a result of high peak strength (Table 4.1).

Table 4.2: Remoulded vane strength and sensitivity values and ranges derived from the standard and adapted method for samples from Tauriko. For remoulded vane strength, the minimum error accepted was 3 kPa which represents 2 divisions on the vane. The errors for sensitivity are calculated as a combination of peak and remoulded vane strength values. For TS2 and TS3 the ranges for each category are the same as the mean because one test was undertaken.

Sample	Adapted remoulded vane strength	Standard sensitivity	Adapted remoulded vane strength	Adapted sensitivity
TS1				
• ***Range***	5 – 8	8 – 10	1	58 – 60
• ***Mean***	6 ± 3	9 ± 0.5	1 ± 3	59 ± 3
TS2				
• ***Range***	2	20	1	50
• ***Mean***	2 ± 3	20 ± 1.5	1 ± 3	50 ± 3
TS3				
• ***Range***	34	5	2	76
• ***Mean***	34 ± 3	5 ± 0.5	2 ± 3	76 ± 1.5

4.6.2 Otumoetai

Four samples were collected from Otumoetai, OS1, OS2, OS3 and OS4. Sampling locations are presented in Figure 4.5. Using Figure 4.5 as the basis of sample collection, OS1, OS2 and OS4 were selected because they were "quick" (> 16) using adapted sensitivity. Furthermore, these samples typically had low remoulded strength and were dilatant when disturbed. Contrastingly, OS3 represented a paleosol unit which was sensitive (8 – 11), but which had high undisturbed strength (> 227 kPa). Whilst OS3 had different strength and sensitivity properties, it may also be from the same depostional event as OS4. Therefore, OS3 was selected to provide comparison between samples of both low and high remoulded strength.

OS3 had the greatest strength of all samples from Otumoetai (>227 kPa) and was the most plastic, representing a clayey paleosol unit. Comparatively OS1, OS2 and OS4 were siltier, had lower plasticity, peak vane strength and showed greater strength variability (Table 4.3). For example, OS2 had maximum and minimum vane shear strength values ~ 38 % either side of the mean (Table 4.3). This wide range reflects the variable geomechanical nature of deposits under investigation.

Table 4.3: Depth, mean vane shear strength, cone penetrometer (Pen.) readings and field soil descriptions for samples collected from Otumoetai. Vane shear strength values presented in parentheses represent the range of values recorded. Depths are recorded from below the top of the bench rather than the top of the slope (as in Figure 4.5). Sensitivities described in text are from the standard method in keeping with NZGS (2005). For peak vane strength the minimum error accepted was 3 kPa which represents 2 divisions on the vane.

Label	Depth (m)	Vane shear strength (kPa)	Pen. (kg)	Description
OS1	4	101 ± 6 (73 – 123)	7.5	Silty CLAY, trace coarse sand, light orange-ish brown with black flecks (MnO_2), firm, wet, slightly plastic, sensitive – extra sensitive, dilatant without the addition of water, highly weathered, sticky, flakes of micaceous material ('mica flakes').
OS2	6.3	125 ± 7 (78 – 172)	NR	Clayey SILT, trace fine sand, light yellowish brown with black flecks (MnO_2), grades to whitish grey immediately above next unit (OS3), firm, wet, non-plastic, extra sensitive, slightly dilatant without the addition of water, highly weathered, flakes of micaceous material present, roots present which may affect the strength of the sample
OS3	6.9	>227	>10	CLAY, dark greyish brown with black flecks (MnO_2), very stiff, wet, homogenous, highly plastic, sensitive, highly weathered, paleosol
OS4	8	72 ± 8 (58 – 84)	9.5	Silty CLAY, trace fine sand, light yellowish brown with black flecks (MnO_2), stiff, very wet, very slightly plastic, extra sensitive, dilatant without the addition of water, highly weathered, flakes of micaceous material present

OS3 had the highest remoulded vane shear strength values using both the adapted and standard method (Table 4.4). Much like peak shear strength, variability in remoulded strength was high, resulting in sensitivities with a large range of values (Table 4.4). For example, OS1, using the adapted method, displayed remoulded strengths between 2 kPa and 11 kPa. Thus it appeared that sensitivity was not only variable between units but also within them.

Table 4.4: Remoulded vane strength and sensitivity values and ranges derived from the standard and adapted method for samples from Otumoetai. For remoulded vane strength, the minimum error accepted was 3 kPa which represents 2 divisions on the vane. The errors for sensitivity are calculated as a combination of peak and remoulded vane strength values.

Sample	Standard remoulded vane strength	Standard sensitivity	Adapted remoulded vane strength	Adapted sensitivity
OS1				
• ***Range***	10 – 23	5 – 11	2 – 11	10 – 51
• ***Mean***	13 ± 4	8 ± 0.5	7 ± 3	23 ± 0.5
OS2				
• ***Range***	6 – 21	6 – 15	3 – 8	13 – 33
• ***Mean***	15 ± 3	10 ± 0.5	7 ± 3	19 ± 0.5
OS3				
• ***Range***	34 – 37	> 6 – > 7	23 – 49	> 5 – > 10
• ***Mean***	36 ± 3	> 6	36 ± 18	> 8
OS4				
• **Range**	5	12 – 17	1 – 2	42 – 62
• **Mean**	5 ± 3	14 ± 0.5	2 ± 3	52 ± 1.5

4.7 Normal load above samples

The following will present a brief description of *in situ* consolidation pressures experienced by each sample. These values are then employed during direct shear, triaxial and ring shear testing.

4.7.1 Tauriko

Because the cutting at Tauriko was broken into sloped batters the actual depth to each sample was less than that measured and presented in Table 4.1. Instead of ~ 22 m, it was estimated that the depth to Tauriko samples was between 16 and 18 m. Considering a wet bulk density of ~ 1400 kg m^{-3}, the *in situ* overburden was between 220 and 250 kPa.

4.7.2 Otumoetai

The break in slope at Otumoetai represented a flat benched section of ~ 8 m width, thus depths to each sample were measured from the top of this flat section and are presented in Table 4.3. Considering a wet bulk density of ~ 1400 kg m^{-3}, the *in situ* overburdens for OS1, OS2, OS3 and OS4 were 55, 86, 94 and 109 kPa, respectively. These overburdens may even be less as the slip scarp had a slight inclination (thus depth to the samples was less), especially below OS1.

4.8 Summary

Field investigations indicated that sensitive soils were common in the Tauranga region and those which had high adapted sensitivity values (> 30) typically had low remoulded strength (< 3 kPa). The landslides observed and mapped occurred as a single event and were associated with heavy rainfall and flowed on failure. Sites at Tauriko and Otumoetai were selected for further laboratory analysis, and seven samples in total were collected. Tauriko represented a large cutting and Otumoetai was a slip site. Samples from Tauriko underlay the Te Ranga Ignimbrite (0.274 Ma) and those from Otumoetai were below the Rangitawa Tephra (0.35 Ma). A large amount of variability in both peak vane strength and sensitivity was observed between and within single samples. At both Otumoetai and Tauriko peak strengths ranged from 45 kPa to > 227 kPa and sensitivities were between > 6 to 76. Considering the adapted method, samples TS1, TS2, TS3 and OS4 had low remoulded strengths (< 2 kPa), OS1 and OS2 moderate remoulded strength (7 kPa), and OS3 high remoulded strength (36 kPa). Those samples with low and moderate remoulded strength were dilatant on disturbance.

Chapter 5
Geotechnical Properties

5.1 Introduction

This chapter presents geotechnical data for sampled units from Tauriko (TS1, TS2, TS3) and Otumoetai (OS1, OS2, OS3, OS4). The aim of this chapter is to geotechnically characterise these sensitive soils. Values for particle size, moisture content, bulk density, particle density and Atterberg limits are reported, as are strength data from unconfined compression, direct shear, ring shear and triaxial testing.

5.2 Particle size

Samples from Tauriko and Otumoetai have been divided into clay (< 2 μm), silt (2-60 μm) and sand (60-2000 μm) size fractions; these values are presented in Table 5.1. Silt is divided into fine (2 – 6 μm), medium (6 – 20 μm) and coarse (20 – 60 μm) fractions. Sand has also been divided into fine (60 – 200 μm), medium (200 – 600 μm) and coarse (600 – 2000 μm) size distributions. Raw particle size distributions can be found in Appendix 5.1.

Table 5.1: Clay, silt and sand particle fractions, as a volume percentage, from Tauriko and Otumoetai, including division into fine, medium and coarse size classes for sand and silt (size classes are presented in the text).

	Clay (>2μm)	**Silt (2 - 60μm)**				**Sand (60 – 2000μm)**			
Sample	**Total (%)**	***Fine* (%)**	***Medium* (%)**	***Coarse* (%)**	**Total (%)**	***Fine* (%)**	***Medium* (%)**	***Coarse* (%)**	**Total (%)**
TS1	**5.70**	*24.37*	*38.48*	*18.36*	**81.22**	*7.20*	*4.78*	*1.10*	**13.08**
TS2	**7.21**	*25.56*	*40.10*	*17.20*	**82.86**	*6.85*	*3.01*	*0.07*	**9.93**
TS3	**8.30**	*30.78*	*34.10*	*15.47*	**80.35**	*9.98*	*1.32*	*0.05*	**11.34**
OS1	**9.98**	*14.64*	*23.11*	*27.64*	**65.39**	*15.08*	*6.86*	*2.58*	**24.52**
OS2	**6.39**	*7.40*	*14.22*	*18.98*	**40.59**	*25.84*	*22.21*	*4.87*	**52.91**
OS3	**33.54**	*18.58*	*21.40*	*14.95*	**54.93**	*6.64*	*3.04*	*1.25*	**10.93**
OS4	**1.98**	*8.81*	*17.19*	*25.15*	**51.15**	*30.53*	*14.17*	*2.17*	**46.87**

All samples have high silt contents (> 40 %) (Table 5.1). OS3 had the highest clay content with ~ 34 %, whilst all other samples have < 10 % (Table 5.1). Silt content is higher in Tauriko samples (~ 81 %) than Otumoetai samples (~53 %). OS2 had the highest sand content (~ 53 %) and samples from Otumoetai typically have higher sand content than those from Tauriko (Table 5.1). Typically, the coarse sand fraction comprised only a low proportion of all samples (< 5%). In all Tauriko samples, ~ 70 % of the particle size distribution was less than 20 μm (Table 5.1). Approximately 50 % of the particle size distribution for the paleosol in OS3 was less than 6 μm and ~ 70 % was less than 20 μm (Table 5.1). Field texture for OS1 and OS4 have been recorded as dominantly clay, however particle size results contradict this (see Chapter 4).

5.3 Moisture, bulk density and porosity

The following section will describe moisture content (*w)*, wet bulk density (ρ), dry bulk density (ρ_D), particle density (ρ_s), porosity (*n*), void ratio (*e*) and saturation state (*Sr*) of each sample. Measured values are presented in Table 5.2, described and then compared with published values which have been summarised in Table 5.3. All raw data can be found in Appendix 5.2.

Table 5.2: Bulk soil properties for samples collected from Tauriko and Otumoetai.

Sample	*w* (%)	ρ (kg m^{-3})	ρ_D (kg m^{-3})	ρ_s (kg m^{-3})	*n* (%)	*e*	*Sr (%)*
TS1	115 ± 0.5	1280 ± 24	656 ± 41	2532 ± 9	74.1	2.86	102.2
TS2	109 ± 0.7	1273 ± 18	589 ± 13	2591 ± 5	77.3	3.40	83.5
TS3	64 ± 0.9	1581 ± 15	966 ± 10	2542 ± 5	62.0	1.63	99.3
OS1	104 ± 3	1358 ± 8	656 ± 8	2636 ± 8	75.1	3.02	91.1
OS2	69 ± 4	1497 ± 30	893 ± 51	2664 ± 8	66.5	1.98	93.0
OS3	66 ± 3	1515 ± 19	920 ± 15	2667 ± 2	65.5	1.90	92.4
OS4	86 ± 0.3	1407 ± 9	743 ± 9	2686 ± 3	72.3	2.62	87.8

Moisture contents between ~ 64 % to > 100 % have been measured across both sites (Table 5.2). The lowest value occurred in sample TS3 and the highest in TS1. Table 5.3 indicated that it was not unusual for volcanic silts and clay to have moisture contents close to and exceeding 100 %.

Wet bulk density values ranged from ~ 1273 kg m^{-3} to ~ 1581 kg m^{-3}. Dry bulk densities were between ~ 45 % and ~ 60 % of wet values. TS1 and TS2 results were lower than the wet and dry bulk density values presented for volcanic

silts in Table 5.3. All samples had wet bulk densities within the range of those presented for volcanic soils overall (Table 5.3). Dry bulk densities for all samples except TS2 fell within the range of values previously reported for volcanic soils (Table 5.3). The clayey OS3 had wet and dry density properties which fell in the range for those presented in Table 5.3 for the Hamilton Ash.

Table 5.3: Published index values for volcanic silts, allophane (Al) and halloysite (Ha) clays and Hamilton Ash. NR indicates that no results could be found.

Material	Dominant mineral	Location	*w* (%)	ρ (kg m^{-3})	ρ_D (kg m^{-3})	ρ_s (kg m^{-3})	*n (%)*
Volcanic silt[1]	Ha	Auckland, Tauranga	32–106	1348-1820	759–972	2275–2365	43 –70
Volcanic clay[2]	Ha	Indonesia, Waikato	31–89	NR	1084–1313	2720–2890	53 –61
Volcanic clay[3]	Al	Indonesia, Taranaki	55–180	NR	610–965	2580-2880	66 - 80
Hamilton Ash[4]	Ha, Al	Waikato, Waihi	29-109	1250-1680	790-1210	2200–2700	36 - 69

Notes:
1) Values from Keam (2008) and Cong (1992)
2) Values from Wesley (1973) and Jacquet (1990)
3) Values from Wesley (1973) and Jacquet (1990)
4) Values from Nicholson (1986)

Particle density values presented in Table 5.2 from Tauriko were lower than those for Otumoetai, with mean values of 2555 kg m^{-3} and 2662 kg m^{-3} respectively. All samples had higher particle densities than volcanic silts and values lower than volcanic halloysite clays presented in Table 5.3. All values except TS3 fell within the range of particle density values presented for allophanic clays. Particle densities for all samples fit into the wide range of values listed for the Hamilton Ash (Table 5.3).

Porosity values from both sites were high, ranging from ~62 % to ~77 %. Porosities were at the upper limit or greater than those presented for volcanic silts and volcanic halloysite clays in Table 5.3, and were more analogous to allophanic clays. OS3 fell into the wide range of values presented for the Hamilton Ash.

Void ratios presented in Table 5.2 were within the range of values (0.5 to 4.0) considered by Mitchell & Soga (2005) to be the normal range for typical mineral soils. However, Hillel (2004) stated that void ratios typically range

between 0.3 and 2.0 and Azizi (2000) indicated that sands typically have void ratios between 0.5 and 0.8, with clays ranging between 0.7 and 1.3. Considering these values it would seem that all samples in this study had high void ratios, yet TS1, TS2, OS1 and OS4 had extremely high values. Jacquet (1990) reported void ratios between ~ 2.1 and ~ 3.6 for allophane and halloysite dominated volcanic soils; only samples TS3, OS2 and OS3 did not fall within this range.

Saturation states for samples were high with all values between ~ 84 % and > 100 %. Considering that 100 % represents a fully saturated soil then all samples were either completely or almost saturated and had either a small amount or no air filled porosity. Saturated soils in the Tauranga region are not uncommon, with Meyer *et al.* 2005 reporting ~ 100 % saturation at depths between 2.5 and 5.8 metres. These high results are interesting considering samples were collected at the end of summer. However samples from Tauriko were collected from depths of ~ 16 to 18 m so it possible these samples were below the water table before the cutting was exposed; this was not case for Otumoetai samples.

Compared with similar published values, these samples from Tauriko and Otumoetai were characterised by low bulk density, yet relatively high particle density and thus very high porosity and void ratio. *In situ* materials were at or near full saturation.

5.4 Atterberg limits

The following section will present Atterberg limits and associated indices for samples from Tauriko and Otumoetai. Values are presented in Table 5.4 and raw data can be found in Appendix 5.3.

Table 5.4: Atterberg limit values for samples collected from Tauriko and Otumoetai.

Sample	Liquid Limit (%)	Plastic Limit (%)	Plasticity Index (%)	Liquidity Index (%)	Activity
TS1	81.25	56.89	24.36	2.39	4.27
TS2	72.67	46.66	26.01	2.41	3.61
TS3	51.97	38.74	13.23	1.88	1.59
OS1	90.02	47.32	42.70	1.33	4.28
OS2	57.40	32.44	24.96	1.46	3.91
OS3	96.40	54.41	41.99	0.27	1.25
OS4	72.96	36.80	36.18	1.35	18.27

Liquid and plastic limits ranged from ~ 52 % to ~ 97 % and ~ 32 % to ~ 57 % respectively. Liquid limit had a much greater range of values than plastic limit (Table 5.4). Plasticity index values ranged from ~ 13 % to ~ 42 %. The high clay (~ 34 %) paleosol sample (OS3) represented the upper bound for liquid and plastic limits. OS1 also had a comparable liquid and plastic limits yet it had low clay content (~ 10 %). TS3 had lower liquid limit and plasticity index values than all other samples. OS2, with a clay content of ~ 6 %, also had low liquid and plastic limits; interestingly it had the highest sand content. Most soils, except OS3, had liquidity indexes greater than 1 indicating that natural moisture content was higher than the liquid limit at both Tauriko and Otumoetai. Typically all low clay (< 10 %) samples are highly active with values greater than 2 (Head 1992). OS4 had an exceptionally high value of 18. Selby (1993) stated that soils with an activity >1.25 are dominated by either allophane or smectite. OS3 is the only sample which had activity in the range of normal clays (0.75 – 1.25) (Head, 1992).

When the values from Table 5.4 were plotted on a plasticity chart (Figure 5.1) values ranged from high to extremely high plasticity and fell below the A line, in the silt category, regardless of clay content.

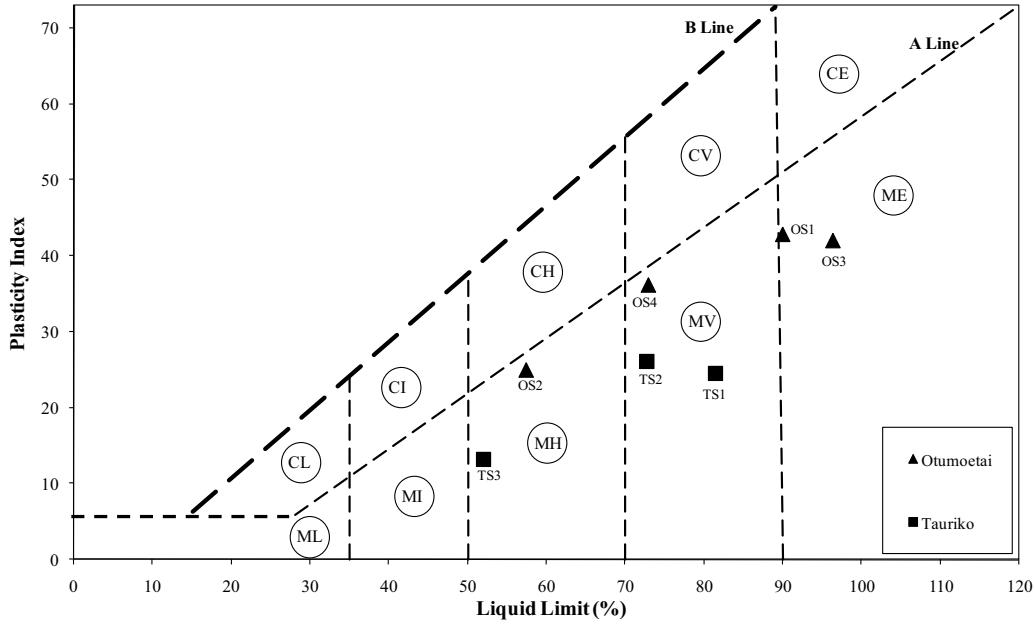

Figure 5.1: Samples from Tauriko and Otumoetai Atterberg values, (Table 5.4), plotted on a plasticity chart. The A line represents a differentiation between silt (M) and clay (C) and the B line represents an upper limit for all soils. The graph is divided into plasticity based on liquid limit with extremely high (E), very high (V), high (H), intermediate (I) and low (L). The basis of the plasticity division is that liquid limit is based on the total surface area of clay particles, which links to clay content. Thus a higher liquid limit indicates greater clay content and hence higher plasticity.

It is not uncommon for volcanic ash soils to plot below the A line, as Figure 5.2 shows.

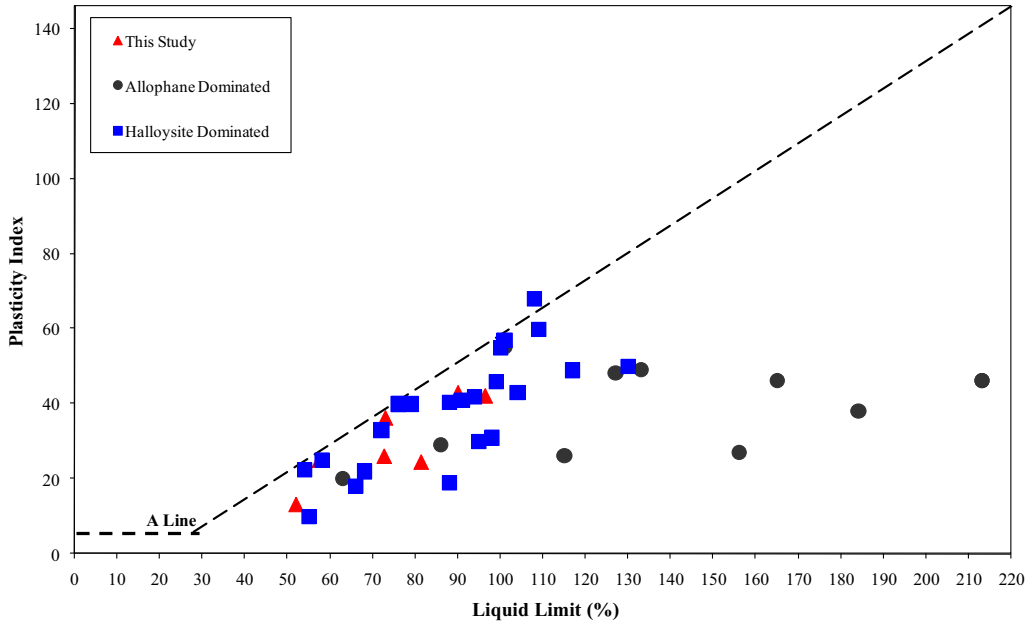

Figure 5.2: Liquid limit and plasticity index values obtained for volcanic ash soils, from local and international sources. These materials have been divided into those dominated by either allophane or halloysite. Data were obtained from this study, Wesley (1973, 1977), Jacquet (1990), Nicholson (1986) and Keam (2008).

When plotted against published Atterberg limit data for both allophane and halloysite dominated materials, samples from this study occupied a similar position to soils dominated by halloysite (Figure 5.2), though a distinction between allophane and halloysite dominated soils was not definite.

5.5 Rapidity number

Table 5.5 presents rapidity number values for all samples from Tauriko and Otumoetai.

Table 5.5: Rapidity numbers for samples collected from Tauriko and Otumoetai. 1 represents minimal disturbance and 10 indicates complete liquefaction after 250 blows of the Casagrande apparatus. Also included are moisture contents taken from samples immediately after testing.

Sample	Rapidity number	Moisture (%)
TS1	3	110.6
TS2	4	96.96
TS3	2	61.32
OS1	3	101.16
OS2	2	61.84
OS3	2	52.28
OS4	3	67.34

Rapidity numbers were low ranging from 2 (hardly visually affected) to 4 (about 5 mm of bottom part deformed to a gelatinous mass, upper part visually unchanged). However, all of the moisture contents presented in table 5.5 are lower than those presented in table 5.2 (between 2 and 13 % difference), this lower moisture content may make the samples less rapid than they actually are. In keeping with this study, Bird (1981) also reported rapidity numbers between 3 and 5 for volcaniclastic materials from the Tauranga region. Bird (1981) suggested a large amount of energy would be required for mobilisation when low rapidity values are reported.

5.6 Unconfined compressive strength

Unconfined compressive strength (UCS) was used to compare the strength of individual samples. Failed specimens were remoulded and retested in an attempt to derive sensitivity values. Values obtained from UCS testing of undisturbed and remoulded specimens are presented in Table 5.6, raw results can be found in Appendix 5.4. Too few samples were available for repeat measurements, so values are presented with unknown error values.

Table 5.6: Peak unconfined compressive strength (UCS) values for undisturbed and remoulded values for samples from Tauriko (TS1 and TS3) and Otumoetai (OS1, OS2, OS3 and OS4) *.

Sample	Peak UCS (C_u) (kPa)	Remoulded UCS (C_u) (kPa)	UCS Sensitivity	Undisturbed failure type
TS1	27.93	NR	NR	Shear
TS3	81.04	NR	NR	Shear
OS1	56.74	NR	NR	Shear
OS2	50.54	0.87	58	Shear
OS3	42.35	40.55	1	Shear
OS4	40.46	NR	NR	Shear

*Remoulded UCS shear strength values have been obtained in an attempt to derive sensitivity. Failure type is also presented and uses the descriptions provided by Head (1994). It should be noted that shear strength (C_u) is used rather than compressive strength (q_u) for data derived from UCS testing (see Chapter 3 section 3.3.14 for calculation). NR represents no recording, because samples were too soft to form a remoulded specimen.

Peak UCS ranged from ~ 27 kPa to ~ 81 kPa. The highest measured value was recorded for TS3 (~ 81 kPa). In this study, failure type was divided into three groups; barrel, intermediate and shear failures (schematic examples are presented in Figure 5.3). All samples showed shear or brittle type failure. Figure 5.4 presents TS1 (Tauriko) and OS4 (Otumoetai) as examples of shear failure.

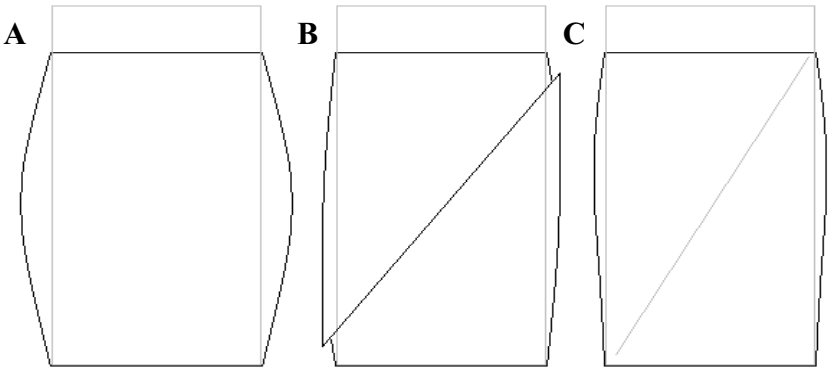

Figure 5.3: Schematic diagram depicting modes of failure resulting from compression testing. These are (A) barrel failure where the sample bulges into a barrel shape, (B) shear failure where the specimen shear along one or more clearly defined surfaces, and (C) intermediate failure which is a combination of both barrel and shear failures. Adapted from Head (1994).

Figure 5.4: UCS samples from TS1 (Tauriko) and OS4 (Otumoetai) showing brittle type failure patterns. OS4 displays some vertical cracking to the right of the sample.

Only OS2 and OS3 were measured in their remoulded state, as all other samples were extremely dilatant (liquid-like) and could not form self supporting cores (Figure 5.5). The sensitivities of OS2 (58) and OS3 (1), from Table 5.6, would be categorised as quick (> 16) and insensitive (< 2) respectively under the guideline presented by the New Zealand Geotechnical Society (2005). Figure 5.5 shows samples from TS1 and OS4 after remoulding, highlighting their inability to form cores for testing and giving an indication of extremely low remoulded strength.

Figure 5.5: Remoulded UCS samples from TS1 (Tauriko) and OS4 (Otumoetai) displaying an inability to support cores because of extremely low remoulded strength. When tested with the shear vane both these samples had remoulded strength of < 2 kPa.

Previous workers have reported a range of compressive strength values for volcanic soils (Table 5.7). Results from this study (Table 5.6) were similar to UCS peak shear strength data for allophanic soils, yet at the lower end of halloysite soils (Table 5.7). Remoulded strength for OS3 (~ 41 kPa) was much higher than remoulded strength values for both allophanic and halloysite dominated volcanic materials. Interestingly, the highest sensitivity recorded by Jacquet (1990) for halloysite soils was similar to the sensitivity recorded for OS2; however OS2 had lower remoulded strength than any of the reported halloysite soils (Table 5.7).

Table 5.7: Uniaxial compressive strength and sensitivity values for allophanic and halloysite soils from the Taranaki (Jacquet 1990), Waikato (Jaquet 1990), Bay of Plenty (Keam 2008) and Auckland (Cong 1992) regions.*

Dominant Mineral	Peak UCS (Cu) (kPa)	Remoulded UCS (Cu) (kPa)	UCS Sensitivity	Reference
Allophane	28 - 58	1.5 – 8.5	5 - 39	Jacquet (1990)
Halloysite	75 - 190	4 – 9.5	8 - 55	Jacquet (1990)
Halloysite	16 - 363	-	-	Cong (1992)
Halloysite	141 - 310	-	-	Keam (2008)

*Note that shear strength (C_u) is used rather than compressive strength (q_u) for data derived from UCS testing (see chapter 3 for calculation).

5.7 Remoulded strength calculation

The following presents remoulded strength using the calculations from Sharma and Bora (2003; 2005), which are based on moisture content, liquid limit and plastic limit.

Table 5.8 indicates that most samples, with the exception of OS3, have very low remoulded strengths (< 1 kPa). The high value for OS3 is consistent with field testing and remoulded UCS values. Tauriko samples have lower remoulded strengths that those from Otumoetai this is consistent with field testing. Low remoulded strengths are not uncommon in Tauranga soils as reported in chapter 2.

Table 5.8: Remoulded strength calculations using the equation of Sharma and Bora (2003; 2005).

Sample	Remoulded Strength (kPa)
TS1	< 0.3
TS2	< 0.3
TS3	< 0.3
OS1	0.6
OS2	0.4
OS3	35.9
OS4	0.6

5.8 Shear box

Unconsolidated undrained shear box data was obtained for samples TS1 and TS3 from Tauriko and all samples from Otumoetai (OS1, OS2, OS3 and OS4). Basic data from testing is presented in Table 5.9 and raw results are presented in Appendix 5.5. It should be noted that for shear box, triaxial and ring shear TS2 has been omitted due to time constraints. TS2 was omitted because field logging, early laboratory results, and scanning electron microscopy indicated that it was similar to TS1.

Table 5.9: Unconsolidated undrained shear box values including the number of samples tested, normal loads applied, shear displacement at failure and the range of peak shear stress with the area correction applied (see Chapter 3, section 3.3.16).

Site	Number of Samples tested	Range of σ_n (kPa)	Range of peak τ_f (kPa) with area correction
TS1	7	15.2 – 188.7	26.59 – 142.38
TS3	5	15.2 – 216.4	25.75 – 167.4
OS1	5	20.1 – 150.5	41.72 – 113.44
OS2	5	20.3 – 154.0	38.76 – 124.79
OS3	5	35 – 150.5	36.71 – 144.8
OS4	6	7.5 – 181.7	29.2 – 146.5

The number of specimens tested in the shear box ranged between 5 and 7 (Table 5.9). This was primarily dictated by sample availability and the requirement to obtain at least three peak strength values at different normal loads to define the Mohr-Coulomb failure envelope. Normal load selection for Otumoetai samples was based on an attempt to represent *in situ* confining pressures (Chapter 3, section 3.3.16). Estimated *in situ* normal loads for Tauriko samples (TS1 and TS3) were extremely high (220 kPa); the upper limits of the load required during testing could not be replicated on the device used.

Strain at failure was typically higher at larger normal loads (Table 5.10). All samples had tests which failed at strains of less than ~ 3 mm, which typically occurred at normal loads of < 50 kPa (Table 5.10). Shear displacement at failure for OS1 and OS3 remained low even at high confining pressures (Table 5.10). In TS1, TS3 and OS4 a number of specimens typically tested at confining pressures above 50 kPa failed at strain rates > 8 mm (Table 5.10). These specimens displayed continued strain hardening and did not show a peak in shear stress, thus failure was taken when the shear box reached the end of its travel (Head 1994). Figure 5.6 is presented as an example.

Table 5.10: Values of shear displacement (mm) at failure across different normal loads for specimens from Tauriko and Otumoetai. All stress versus strain plots can be found in Appendix 5.5.

Approximate normal loads (σ_n) (kPa)	**TS1**	**TS3**	**OS1**	**OS2**	**OS3**	**OS4**
10						3.28
15	1.49	2.85				
20	2.18		2.58	5.62	2.47	2.92
30	7.6			2.98		
40	5.79				2.28	
50		2.87	4.34	3.34	2.31	6.23
70	8.05		4.09			
100		3.51		6.72	2.56	8.49
120			3.01			
135	9.72					
150		8.23	2.98	6.09	3.04	8.86
180	9.66					9.63
190						
215		8.27				

Specimens from all samples tested at different normal loads typically displayed compaction before failure. All samples had at least one specimen which

displayed at least minor dilation before peak shear stress. Figure 5.7 from Otumoetai is presented as an example of dilation and compaction. Specimens which displayed dilation prior to peak shear stress only occurred at confining pressures < 50 kPa.

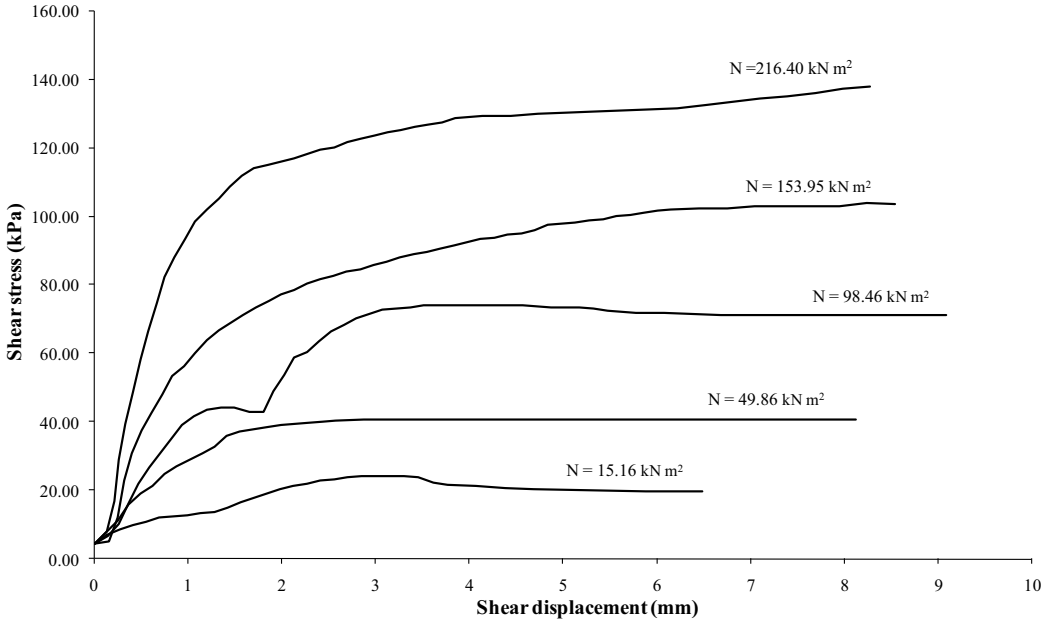

Figure 5.6: Shear displacement versus (mm) versus shear stress (kPa) for shear box tests from sample TS3 Tauriko. The specimens tested at confining pressures of 153.95 and 216.4 kPa do not display a peak in shear strength.

Following failure, compacted specimens typically continued to decrease in volume. All specimens analysed at or above confining pressures of 150 kPa always continued to compact sharply (Figures 5.7 and 5.8). Typically all specimens analysed below 150 kPa either compacted sharply or flattened. Figure 5.7 from OS1 is presented as an example of post failure volume change. Only samples TS3, OS2 and OS4 had specimens which dilated following failure, this occurred at normal loads below (50 kPa) (Figure 5.8) and only in 5 out of 34 specimens.

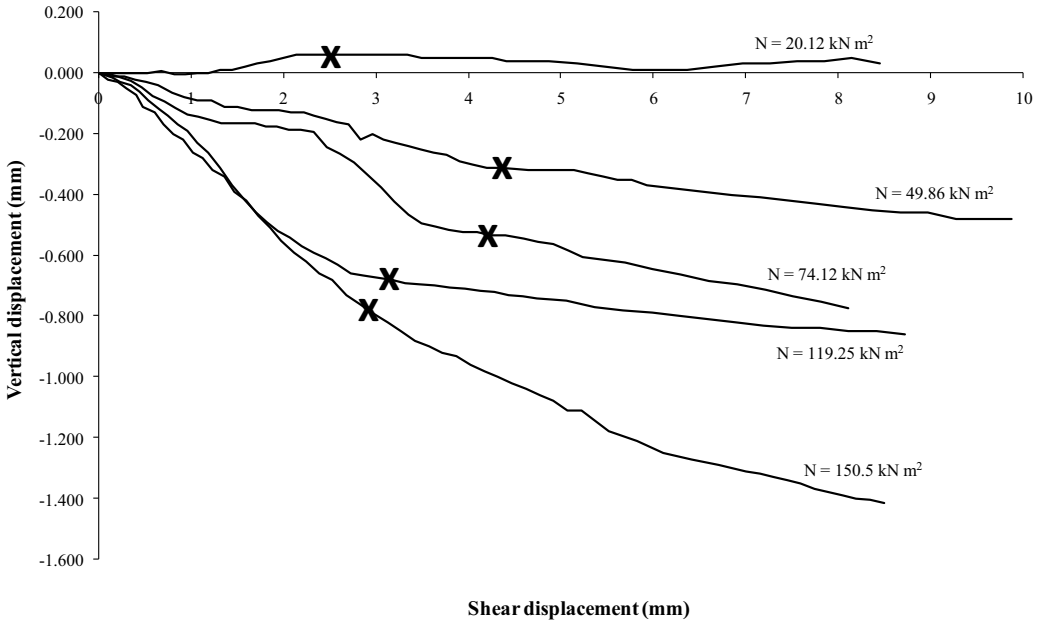

Figure 5.7: Shear displacement (mm) versus vertical displacement (mm) for shear box tests from sample OS1. The crosses (**x**) indicate failure. Specimens tested at normal loads of 49.86, 74.12, 119.25 and 150.5 kPa represent compaction prior to failure. The specimen tested at a normal load of 20.12 kPa displays dilation prior to failure. Following failure (x), all specimens compact on further shearing. Following failure sample 150.5 kPa displays the strongest compaction.

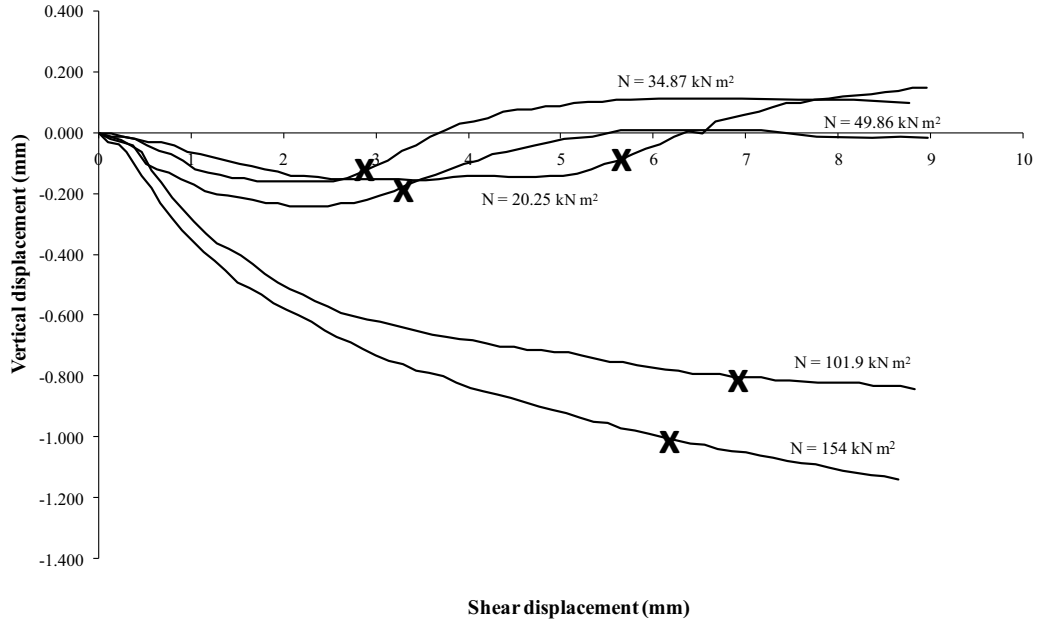

Figure 5.8: Shear displacement versus (mm) versus vertical displacement (mm) for shear box tests from sample OS2. Specimens observed dilating following failure are those with confining pressures of 20.25, 34.87, and 49.86 kPa.

Mohr – Coulomb parameters for the unconsolidated undrained shear box tests were based on the area corrected data and presented in Table 5.11. Samples from Tauriko (TS1 and TS3) had lower cohesion (mean of 13 kPa) than those from Otumoetai (mean 26 kPa). While OS3 had the largest clay content of all samples (34%), it had the highest friction angle (~ 42º) of all samples, and was at

the lower end of cohesion. Friction angles for most samples were similar to each other (32 – 36º) with the exception of OS3 (Table 5.11).

Table 5.11: Mohr-Coulomb strength parameters for shear box data for samples from Tauriko and Otumoetai. All Mohr – Coulomb plots are presented in Appendix 5.5.

Sample	c (kPa)	ϕ (º)	r^2
TS1	15.34	33.93	0.99
TS3	11.27	35.90	1.00
OS1	33.71	32.62	0.95
OS2	27.99	33.16	0.99
OS3	16.64	42.49	0.95
OS4	24.73	33.38	0.99

Most investigations employing the shear box have measured effective cohesion and friction angle (for example Bird 1981; Nicholson 1986; Oliver 1996) rather than total values as measured here. However, in the Waikato region Frederickson (1988) measured total cohesion and friction angle values from allophanic material above the Rotoehu Ash (c. 60 calender (cal) ka). Results for field moist samples had a friction angle of 36° and cohesion of 16 kPa. The friction angle presented by Frederickson (1988) was similar to most samples except OS3, and cohesion was similar to TS1 and OS3 (Table 5.11).

5.9 Triaxial

The following section presents total and effective strength parameters measured using a triaxial device for samples TS1 and TS3 and all samples from Otumoetai. Triaxial results are divided into separate sections: initial sample properties and testing conditions, consolidation characteristics, compression testing results and Mohr-Coulomb strength parameters. Triaxial samples were tested under consolidated undrained (CU) conditions using a strain controlled triaxial apparatus. All raw data for triaxial testing can be found in Appendix 5.6

5.9.1 Triaxial sample properties and testing conditions

Initial testing conditions and the properties of samples obtained for triaxial testing are presented in Table 5.12. The following will compare triaxial sample values in Table 5.12 with original field samples in Table 5.2. This will add to the data presented in Table 5.2 and confirm that material collected for triaxial testing is similar, with some natural variation, to original samples. This is important

because samples were collected from what appeared to be the same units but at different time periods.

Table 5.12: Bulk soil properties for samples from Tauriko (TS1 and TS3) and Otumoetai (OS1, OS2, OS3 and OS4) measured as a result of triaxial testing.*

Sample	Samples tested	Range of σ_3' (kPa)	*w* (%)	ρ (kg m^3)	ρ_D (kg m^3)	*e*	*Sr (%)*
TS1	3	50 - 300	98 ± 3	1409 ± 10	711 ± 12	2.56 ± 0.06	97 ± 2
TS3	3	100 – 300	58 ± 7	1530 ± 47	971 ± 74	1.6 ± 0.2	90 ± 1
OS1	5	25 - 150	102 ± 9	1368 ± 19	679 ± 39	2.9 ± .2	93 ± 2
OS2	4	25 – 150	79 ± 10	1475 ± 18	831 ±59	2.2 ± 0.2	92 ± 4
OS3	3	25 - 160	62 ± 0.4	1541 ± 8	952 ± 4	1.78 ± 0.01	91.9 ± 0.9
OS4	4	20 – 150	77 ± 3	1432 ± 18	808 ± 22	2.34 ± 0.09	89.3± 0.6

* This table includes the number of samples tested and the range of confining pressures (σ_3) used during testing. The values presented are directly comparable to those in Table 5.2.

The number of triaxial test results obtained for each sample ranged between 3 and 5 (Table 5.12). The effective confining pressures used (σ_3') were based on the same justification as normal loads selected for the shear box.

Moisture contents for triaxial samples presented in Table 5.12 were similar to those in Table 5.2. TS1 had the largest moisture difference when compared with Table 5.2, showing a decrease of ~ 17 % in the triaxial specimen. Samples were collected at different times so the variations may be the result of antecedent moisture regimes. However, samples were saturated during testing so this difference was negated.

Wet density values, with the exception of TS1, displayed < 4% difference between results presented in Table 5. 2 and those in Table 5.12. The wet bulk density for the TS1 triaxial sample was ~ 10 % higher than the original value. Samples TS1, OS2 and OS4 recorded > 5% variation in mean dry bulk densities between original and triaxial samples. These differences were + 8, - 7 and + 9 % respectively. Frederickson (1988), citing sample disturbance as a reason, stated that triaxial samples with dry bulk density values showing > 5% variation from the original sample should be discarded. Using a t-test to investigate the difference between original and triaxial dry bulk densities for TS1, OS2 and OS4 p values of 0.21, 0.40 and 0.03 were calculated respectively. The p values indicated that the original and triaxial values from TS1 and OS2 were from the

same population but those from OS4 were not. However, because of the variability observed within individual samples in the field (see Chapter 4) it was possible that the difference observed in OS4 represented natural variation rather than sampling error.

Typically, triaxial samples were greater than or close to the required saturation state of 95% (Table 5.12), which was consistent with Table 5.2. Even though saturation values were naturally high, samples were still saturated by way of back pressure. Saturation times were rapid and samples often reached a B value of 0.95 within a matter of hours.

5.9.2 Consolidation conditions

As a requirement of the CU test, specimens were consolidated under isotropic stress conditions after saturation. A range of values were measured. Highly sensitive material (TS1, TS3, OS1, OS2 and OS4) had coefficient of consolidation (C*v*) values between 45 and 6944 m^2 yr and coefficient of compressibility (M*v*) results were between 0.01 and 0.64 m^2 MN. Ranges of C*v* and M*v* values for the paleosol sample (OS3) were 3.93 to 1346.7 m^2 yr and 0.03 to 0.1 m^2 MN respectively.

Compared to other sensitive material from the Tauranga region (TCC 2005; OPUS 2006), also tested with a triaxial apparatus, the upper limit of values in this study were very high. Previous C*v* and M*v* results range from 3.2 to 590 m^2 yr and 0.12 to 0.22 m^2 MN respectively (TCC 2005; OPUS 2006). The high values in this study may be expected considering porosity and void ratio results. However, the upper limit of C*v* (6944 m^2 yr) for this study is an order of magnitude greater than those previously reported.

5.9.3 Undrained compression results

The following will describe results and trends from the compression stage of triaxial testing. The parameters examined in this section will include deviator stress (σ_1- σ_3), pore water pressure (PWP), axial strain, stress paths, PWP coefficient at failure (A_f) and maximum effective principle stress ratio (σ_1'/ σ_3').

5.9.3.1 Stress strain characteristics

The following presents stress versus axial strain characteristics from triaxial compression.

5.9.3.1.1 Peak characteristics

Two distinctively different forms of stress stain curves can be recognised from triaxial specimens. When peak deviator stress occurred at strains of approximately < 3%, the stress strain curve increased steadily, reached a peak and then the curve abruptly flattened, resulting in an angular appearance suggesting brittle type failure. When axial strain at peak deviator stress increased, the curvature of the stress strain relationship increased. Slight curvature occurred for axial strains at peak deviator stresses of between ~3 and ~7 %, and strong curvature was observed beyond this. Increasing axial strain and curvature at peak deviator stress suggested a greater amount of strain hardening during compression and plastic type failures. Figure 5.9 presents examples of angular and curved stress strain relationships from sample OS2 tested at confining pressures of 150 and 25 kPa respectively.

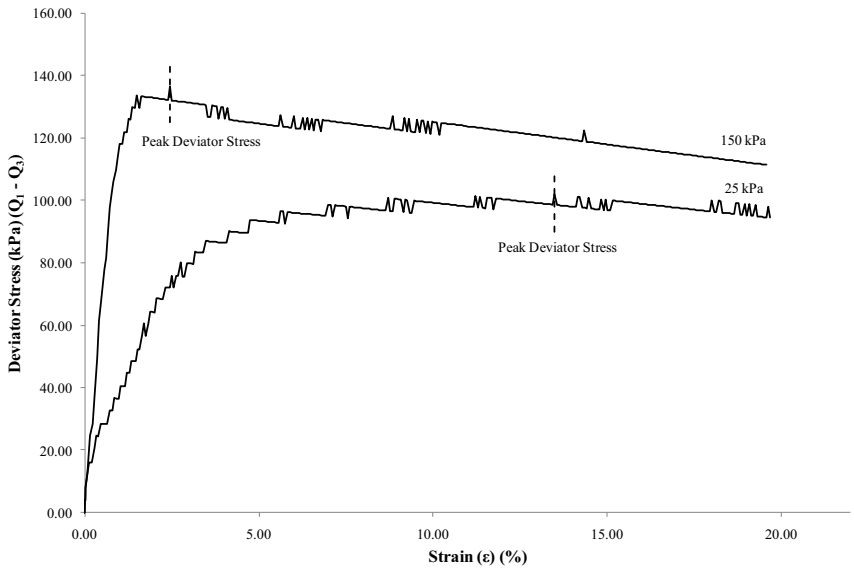

Figure 5.9: Deviator stress ($\sigma_1 - \sigma_3$) (kPa) versus strain (ε) (%) for consolidated undrained triaxial tests at confining pressures of 150 kPa and 25 kPa for sample OS2. The sample tested at 25 kPa displays a highly curved stress strain curve, failing at an axial strain of 13.65 %. The sample tested at a confining pressure of 150 kPa displays a sharp transition from increasing deviator stress to a post failure flattening; failure has occurred at an axial strain of 2.47 %.

Curve shape and strain at failure for all specimens is summarised in Table 5.13. In samples TS1, OS2 and OS4 sharp stress strain curves were typically observed in tests with confining pressures (σ_3') greater than 50 kPa. Curved or

highly curved shapes are exhibited at confining pressures below 50 kPa. OS1 displayed sharp stress strain curves for all specimens. The stress strain curves for OS3 all exhibited strong curvature.

Table 5.13: Description of stress strain curve shape, axial strain at peak deviator stress and the value for peak deviator stress at each confining pressure for samples from Tauriko (TS1 and TS3) and Otumoetai (OS1, OS2, OS3, OS4).The letters indicate the shape of the stress strain curve; S indicates the transition from a linear increase in deviator stress to post failure is sharp, C indicates there is some curvature in the stress strain curve, and HC indicates that the stress strain curve is highly curved. Axial strain (%) at peak deviator stress is shown in parentheses. Peak deviator stress (kPa) is presented below both curve shape and axial strain at failure..*

Approximate confining pressure (kPa)	TS1	TS3	OS1	OS2	OS3	OS4
20	-	-	S (1.8) 116.4	HC (13.7) 102.4	HC (20.1) 144.3	C (3.0) 64.2
50	C (4.9) 73.4	-	-	HC (11.7) 116.6	HC (13.2) 285.4	C (4.5) 81.4
80	-	-	S (2.3) 136	-	HC (20.2) 234	-
100	-	C (6.4) 196.5	S (2) 169.6	S (2.8) 129.6	-	S (1.8) 114.10
150	-	-	C (3.4) 157.2	S (2.5) 137.3	HC (17.6 & 15.7) 249.4 & 368.4	S (1.7) 144.33
200	S (2.4) 141.2	C (7.2) 250.6	-	-	-	-
300	S (2.1) 191.6	C (5.1) 294.5	-	-	-	-

* Note confining pressure is only approximate and actual values may deviate up to 5 kPa. Sample OS3 at a confining pressure of ~150 kPa includes two specimens the first test at 150 kPa and the second at 160 kPa. All stress strain curves are presented in Appendix 5.6. The line represents a division between specimens which were tested above and below estimated *in situ* confining pressures.

Sample TS1, OS1, OS4, and OS2 tested at high confining pressures displayed peak deviator stress prior to 5% axial strain which is synonymous with brittle soils (Head, 1998). Furthermore, axial strain at peak deviator stress for TS3 was only just above 5 %, with values of 5.1, 7.2 and 6.4 %, suggesting that failure at peak deviator stress was more brittle than plastic. Considering strains at peak deviator stress, TS3 displayed a more plastic manner than TS1 (Table 5.13). OS2 and OS3, tested low confining pressures, reached peak deviator stress at strains between ~ 12 and 20 % (Table 5.13). According to Head (1998) failure strains of 8 to 15 % are associated with compacted sandy silts and those between 15 and 20% have properties of normally consolidated clays. Sample OS3 tested at $\sigma_3' =$

20 and 50 kPa did not reach peak deviator stress before 20 % axial strain, which is the test termination point recommended by BS1377 (1990) and Head (1998). Failure strains > 20 % are associated with over-consolidated clays (Head 1998).

Table 5.13 clearly shows that, within each sample, different confining pressure (σ_3) influences axial strain at failure and as a corollary the shape of each stress strain curve. Although the relationship was not particularly clear, Table 5.13 indicated that peak deviator stress was likely to occur at lower axial strains when a higher confining pressure was applied. The obvious exception to this was sample OS1 which showed a higher axial strain at larger confining pressures (Table 5.13).

Peak deviator stress ($\sigma_1 - \sigma_3$) values recorded in each test are presented in Table 5.13. As expected, deviator stress typically increased positively with increases in confining pressure. Interestingly, the largest σ_1 - σ_3 was for sample OS3, even though the maximum confining pressures were less than those for Tauriko (Table 5.13). This suggested that OS3 had the greatest undisturbed strength, which was consistent with field vane shear testing but not unconfined compressive strength results.

5.9.3.1.2 Post failure curves

Stress versus strain curves for specimens from Otumoetai and Tauriko typically displayed little reduction in strength following peak deviator stress. The curves would characteristically flatten and then decrease slowly. The rate or amount of strain softening following peak deviator stress did not appear to be affected by effective confining pressure. Post failure flattening is typical in consolidated undrained triaxial tests (Bishop & Henkel 1962; Craig 1997). An example from TS3 is presented in Figure 5.10.

OS1 tested at a confining pressure (σ_3') of 100 kPa was the only sample which displayed a pronounced deviator stress peak at failure followed by a sudden reduction (Figure 5.11). The large amount of strain softening following peak deviator stress implies either dense sands or over-consolidated clay (Craig 1997; Head 1998; Azizi 2000). However Table 5.12 indicated that OS1 had the lowest dry density (~ 679 kg m^{-3}) and was predominantly silt. Furthermore, axial strain at failure was less than what is normally considered applicable to over-consolidated clays (Head 1998).

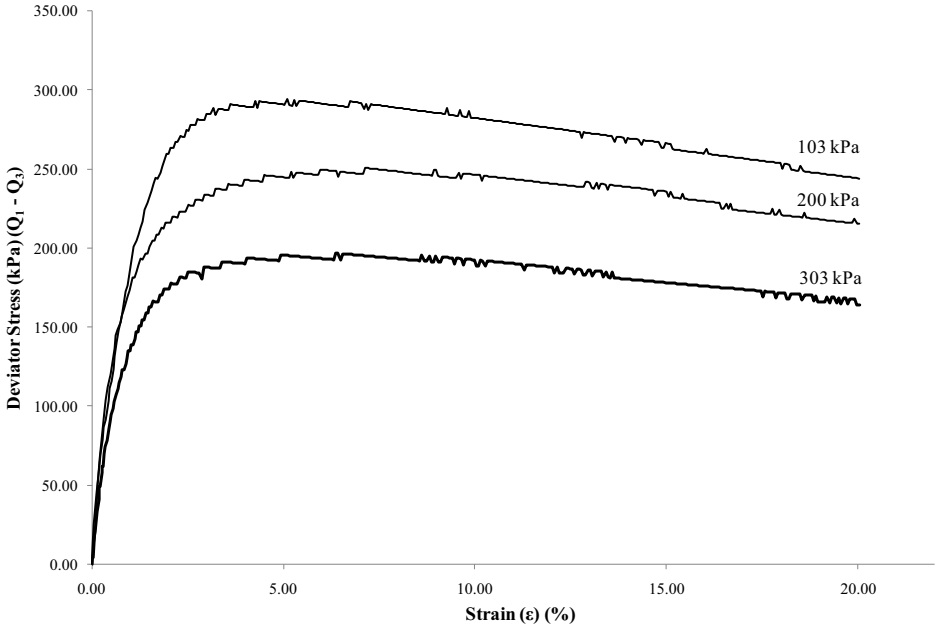

Figure 5.10 Deviator stress ($\sigma_1 - \sigma_3$) (kPa) versus strain (ε) (%) for TS3 from Tauriko. Values of σ_3' include 103, 200 and 303 kPa.

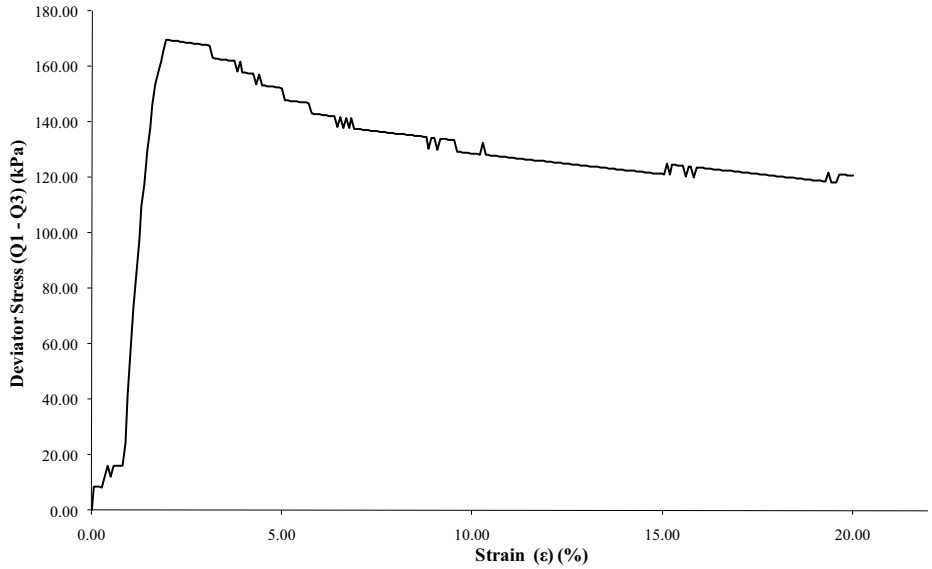

Figure 5.11: Deviator stress ($\sigma_1 - \sigma_3$) (kPa) versus strain (ε) (%) for samples OS1 from Otumoetai tested at an effective confining pressure (σ_3') of 100 kPa displaying a pronounced peak in deviator stress followed by sudden strain softening.

5.9.3.2 Pore water pressure characteristics

Pore water pressure (PWP) characteristically increased steadily during compression testing and then flattened. An example from TS3 is presented in Figure 5.12. The PWP characteristics indicate sample compaction and are similar to those observed for normally consolidated clays (Craig 1997).

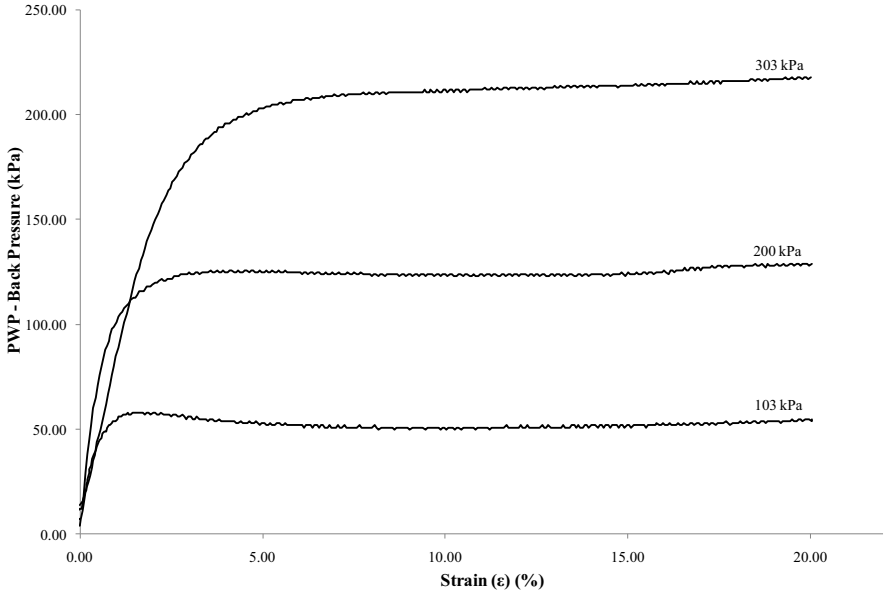

Figure 5.12: PWP (kPa) less back pressure (kPa) as a datum versus strain (ε) (%) for TS3 from Tauriko. Values of σ_3' include 103, 200 and 303 kPa.

Some specimens diverged from the typical PWP characteristics observed in Figure 5.12. Otumoetai samples OS1, OS2 and OS4 tested at low confining pressures (σ_3'), between 20 and 25 kPa, displayed a definite peak in pore water pressure followed by a steady decrease. This phenomenon was also observed in all triaxial tests for OS3. In sample OS2 tested at σ_3' = 25 kPa and two tests for OS3 (σ_3' = 25 and 55 kPa) PWP decreased below the initial back pressure value, becoming negative. The test from OS2 (σ_3' = 25 kPa) is given as an example in Figure 5.13.

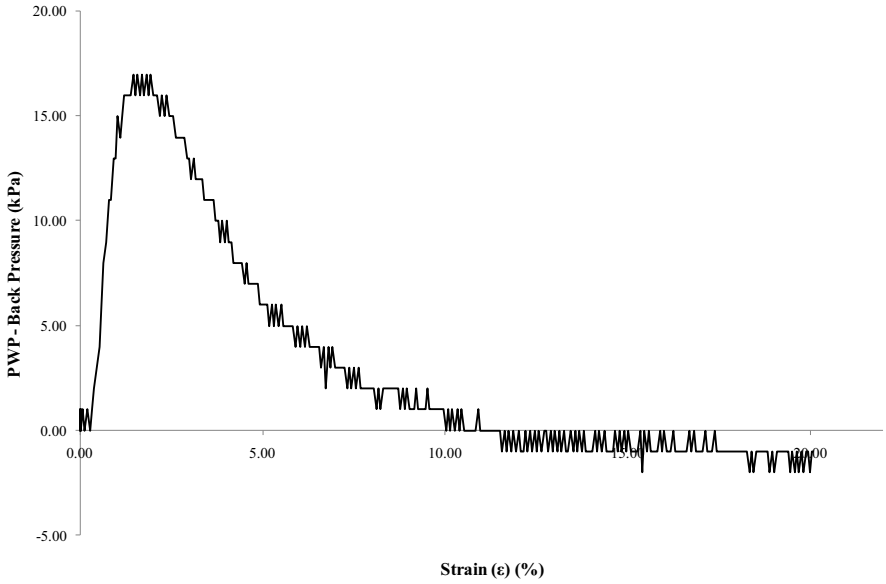

Figure 5.13: PWP (kPa) less back pressure (kPa) as a datum versus strain (ε) (%) for OS2 from Otumoetai tested at a σ_3' of 25 kPa.

A decrease in PWP following a clear peak indicates compaction followed by dilation. This phenomenon is not unique to this study, as Fredrickson (1988) observed similar PWP patterns in allophanic soils from the Waikato, where during tests at low confining pressures (σ_3' = 6 kPa) PWP became negative following an obvious peak (Fredrickson 1988). This behaviour is often interpreted as a characteristic of over-consolidated clays. Larger decreases in pore water pressure represent higher over-consolidation ratios (Craig 1997). However in the case of Frederickson (1988) this was attributed to desiccation rather than geological history.

5.9.3.3 Stress path characteristics

A stress path can be represented by a series of Mohr circles, in a plot of s' versus t', or in a less confusing way as a series of points which form a line. This line presents a clear representation of successive states of stress during testing (Craig 1997). Stress path plots are generally indicative of the stress history of the soil being tested (Frederickson 1988). Thus the shape of the stress path plot is typically used to describe consolidation, or compaction and dilation characteristics during analysis.

A total stress path always plots as a 45° line and the horizontal difference between the total and effective stress path represents the value of PWP at the stresses in question (Head 1998). If the effective stress path deviates to the left this indicates an increase in PWP as a result of compaction which is associated with normal consolidation. Alternatively, if the effective stress path deviates to the right this indicates a decrease in PWP due to dilatancy and over-consolidation(Head 1998). Examples of typical stress path plots are given in Figure 5.14.

Stress paths from Tauriko and Otumoetai, displayed a number of characteristics. Figure 5.15 indicated that when TS1 was tested at high confining pressures (σ_3' = 207 and 297 kPa) stress paths curved heavily to the left, more than all other samples. A left trending curvature indicates properties of normally consolidated clays and possibly sensitive soils. In sensitive soils the heavy left trending curve occurs because as the soil shears its structure is destroyed and collapses causing excessive pore pressures to develop (Frederickson 1988).

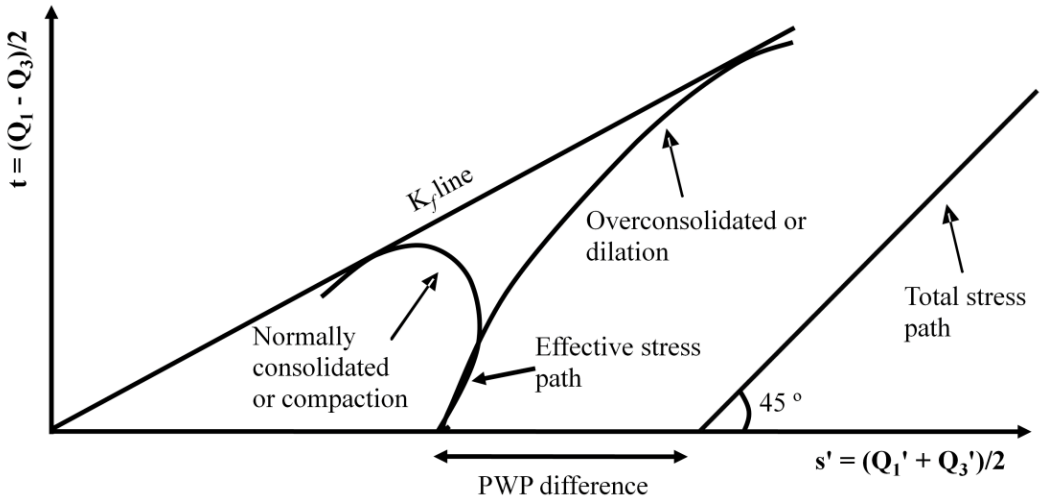

Figure 5.14: Example of a total and effective stress path plots (s' versus t). The space between the two represents the difference in PWP. The effective stress path plot can deviate in two directions from the total stress path. Deviation to the left indicates compaction and normal consolidation and to the right indicates dilation and over-consolidation.

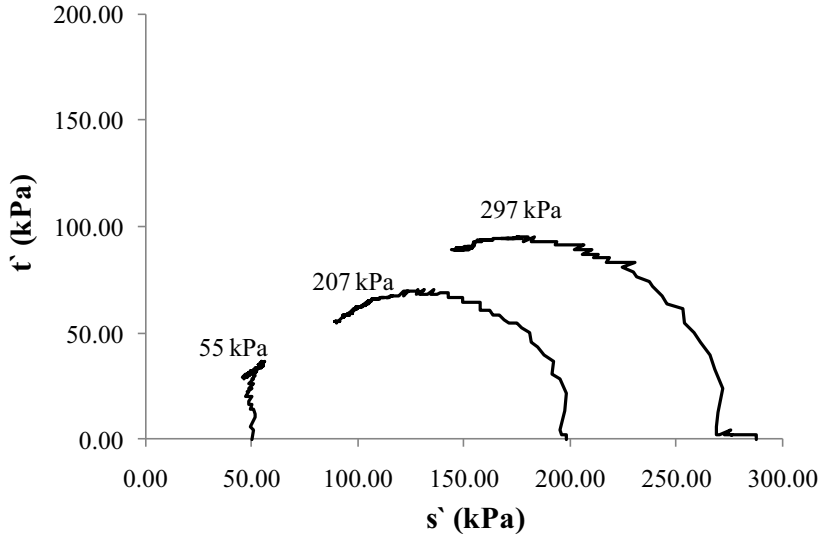

Figure 5.15: Stress path plot from TS1 (Tauriko) for triaxial specimens analysed at confining pressures (σ_3') of 55, 207 and 297 kPa.

OS3 from Otumoetai displayed stress paths which all trended to the right which typically suggests over-consolidation and dilation (Figure 5.16). This indicated that prior to and after failure pore water pressure decreased as a result of sample dilation. Figure 5.16 indicated that the magnitude of curvature was similar for all specimens.

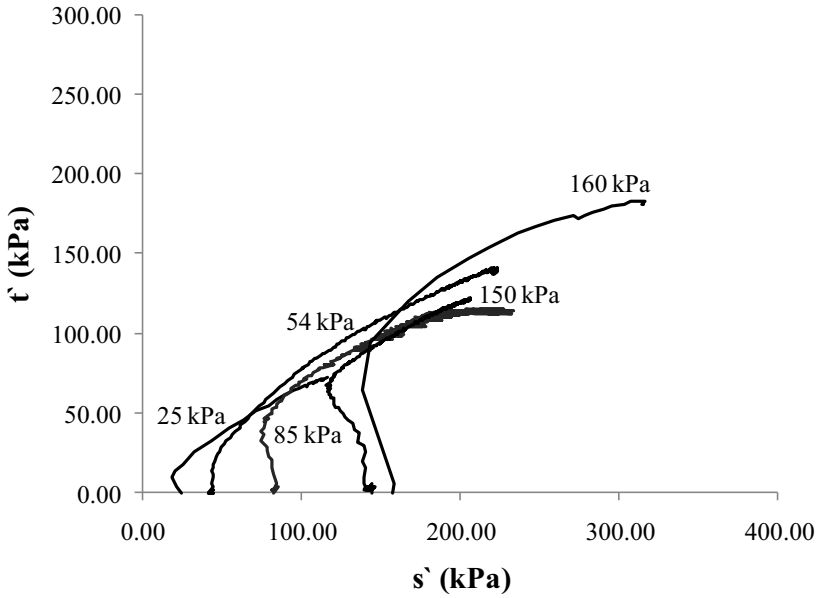

Figure 5.16: Stress path plot from OS3 (Otumoetai) for specimens analysed at confining pressures (σ_3') of 25, 54, 85, 150 and 160 kPa.

Aside from the two extremes presented in Figures 5.15 and 5.16 all other samples followed a typical pattern. Figure 5.17 presents OS2 as an example. It appeared that specimens analysed at low confining pressures (σ_3'), typically < 50 kPa, displayed properties of over-consolidated clays and hence dilation, whereas those tested at higher confining pressures displayed properties of normally consolidated clays and hence compaction. Interestingly, curvature was less pronounced in specimens analysed at intermediate confining pressures, possibly representing a transition between normal (compaction) and over-consolidated (dilation) stress path states.

Table 5.14 is presented to summarise all stress path plots from each specimen. Aside from what has been previously described it appeared that, with the exception of OS3, all specimens tested at high confining pressures tended to compact having properties of normally consolidated clays. As confining pressures decrease stress paths are more likely to represent dilation.

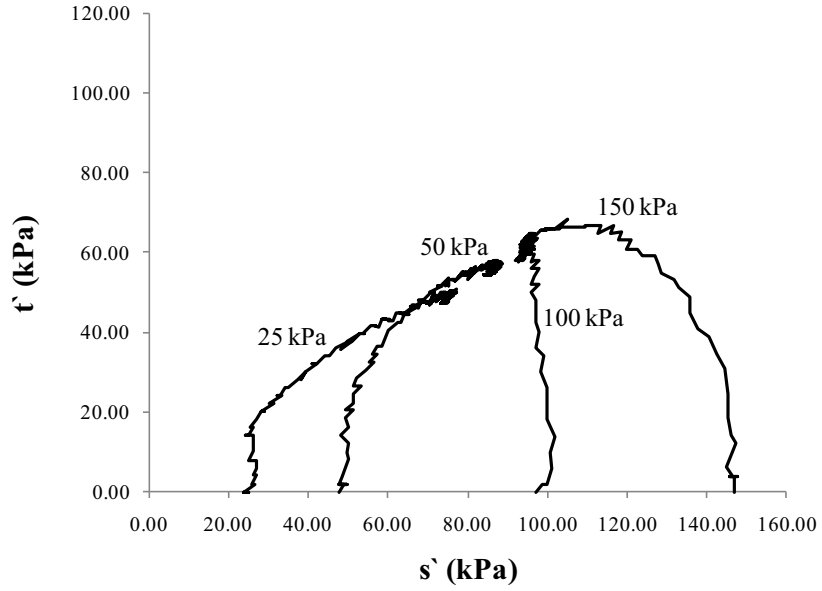

Figure 5.17: Stress path plot from OS2 (Otumoetai) for triaxial tests run at confining pressures (σ_3') of 25, 50, 100 and 150 kPa.

Table 5.14: Description of stress path (s` and t`) plots, indicating samples which dilated (dilat.) during analysis appearing to have properties of over-consolidated (OC) specimens and those which compacted (comp.) appearing to have properties of normally consolidated (NC) clays. Specimens with an M in parentheses had a less pronounced curve, as shown for σ_3' = 100 kPa in Figure 5.17.*

Approximate confining pressure (kPa)	TS1	TS3	OS1	OS2	OS3	OS4
20	-	-	OC dilat.	OC dilat.	OC dilat.	OC dilat.
50	OC dilat.	-	-	OC dilat.	OC dilat.	(M) OC dilat.
80	-	-	(M) OC dilat.	-	OC dilat.	-
100	-	OC dilat.	(M) OC dilat.	(M) NC comp.	-	NC comp.
150	-	-	NC comp.	NC comp.	OC dilat.	NC comp.
200	NC comp.	(M) OC dilat.	-	-	-	-
300	NC comp.	NC comp.	-	-	-	-

* All effective stress path plots are presented in Appendix 5.6. The line represents a division between specimens which were tested above and below estimated *in situ* confining pressures.

Table 5.14 indicated that compaction was more likely to occur in samples tested above their estimated *in situ* confining pressure and dilation was more likely to occur below.

5.9.3.4 Pore water pressure coefficient at failure (Af)

The pore water pressure coefficient at failure (A_f) adds to the data obtained from stress path testing, because it numerically describes the condition of PWP at the time of failure. Therefore A_f is often used to define stress history and hence apparent consolidation states (Head 1998). The pore water pressure coefficient at failure is calculated as:

$$A_f = \frac{\Delta u_f}{(\Delta\sigma_1 - \Delta\sigma_3)_f} \quad (5.1)$$

where:

A_f = pore water pressure coefficient (A) at failure;

Δu_f = change in PWP;

$(\Delta\sigma_1\text{-}\Delta\sigma_3)_f$ = change in deviator stress at failure.

Typical values, from Head (1998), are presented in Table 5.15 and will be compared with values from this study presented in Table 5.16

Table 5.15: Typical values of pore pressure coefficient A_f for a range of saturated soils (taken from Head (1998) after Skempton (1954)).

Type of Soil	Volume Change due shear	A_f
Highly sensitive clay	Large contraction	+ 0.75 to + 1.5
Normally consolidated clay	Contraction	+ 0.5 to + 1
Compacted Sandy Clay	Slight contraction	+ 0.25 to + 0.75
Lightly over-consolidated clay	None	0 to + 0.5
Compacted clay gravel	Expansion	- 0.25 to + 0.25
Heavily over-consolidated clay	Expansion	-0.5 to 0

Interpreting Table 5.15 further, negative values indicate that at peak deviator stress pore water pressure is less than the applied back pressure, while large positive values indicate that PWP pressure has increased to a level well above back pressure. Table 5.15 also presents descriptions of volume change due to shear which relate to the pore water pressure coefficient at failure (A_f). The association relies on the assumption that a sample will change in volume on the application of deviator stress. In a saturated soil tested under drained conditions, volume change will result in either water being expelled or sucked into the sample. In an undrained test volume change is prohibited because drainage is blocked. Therefore any volume change which would have occurred is represented

by a change in PWP. Typically, loose sands and soft clays collapse (compact) causing a positive change in PWP and dense sands and stiff clays expand (dilate) resulting in a decrease in PWP (Head 1998).

Table 5.16: Values of pore pressure coefficient (A_f) for a range of saturated samples examined during triaxial testing at a range of confining pressures (σ_3'). HSC = highly sensitive clay, NC = normally consolidated clay, LOC = lightly over-consolidated clay, HOC = highly over-consolidated clay, as per table 5.15.*

Approximate confining pressure (kPa)	TS1	TS3	OS1	OS2	OS3	OS4
20	-	-	LOC 0.18	HOC - 0.01	HOC - 0.13	LOC 0.12
50	LOC 0.49	-	-	LOC 0.18	LOC 0.03	LOC 0.44
80	-	-	LOC 0.41	-	LOC 0.26	-
100	-	LOC 0.25	LOC 0.45	NC 0.52	-	NCC 0.62
150	-	-	NC 0.69	HSC 0.82	LOC 0.089	HSC 0.80
200	HSC 1.01	LOC 0.49	-	-	-	-
300	HSC 1.09	NC 0.69	-	-	-	-

*The line represents a division between specimens which were tested above and below estimated *in situ* confining pressures.

All samples had at least one triaxial specimen which displayed some degree of apparent over-consolidation (Table 5.16), which was most evident in samples from Otumoetai. Typically, as confining pressure (σ_3') increased so did the pore water pressure coefficient A_f, with the exception of OS3. The observed positive relationship may indicate that under low confining pressure (σ_3') it was easier for the soil to dilate, because less energy is required for expansion against low pressures than high (Mitchell & Soga 2005).

Specimens TS1 (σ_3 = 200 and 300 kPa), OS2 and OS4 (σ_3 = 150 kPa) had very high PWP coefficient ratios which fell into the category of sensitive clays (A_f > 0.75) (Table 5.16). This indicates that during shear there is a large increase in pore water pressure resulting from a large amount of compaction.

Samples OS2 and OS3 at low confining pressures (σ_3' = 20 kPa) displayed negative pore water pressure coefficient values (Table 5.16). Negative values indicate that the tendency to dilate is so strong pore water pressure at failure has fallen below the initial value of back pressure (Head 1998). This is not desirable because air which was originally dissolved in pore water may start coming back out of solution.

Plots of PWP versus axial strain, stress paths, and the pore water pressure coefficient A_f at failure value all indicated that Otumoetai samples tested at low σ_3' and all of OS3 behaved like over-consolidated clays and dilate during shear. Firstly, all samples, with the exception of OS3, had high silt contents, so the classification of clay may be slightly misleading. Secondly, an over-consolidated state in these samples is unusual, because the material being investigated has not been subjected to a large overburden pressure which has been subsequently eroded. Jacquet (1990) reported volcanic soils comprised of either allophane or halloysite with over-consolidation ratios between 2.5 and 17. It was suggested that the apparent over-consolidation was caused by a positive relationship with ferrihydrite content rather than geological history. Furthermore the over-consolidation reported may simply represent dilation during testing and not the consolidation state. Thus the over-consolidation reported here should be termed apparent over-consolidation.

5.9.3.5 Principal effective stress ratio (σ_1'/σ_3')

The principal effective stress ratio (σ_1'/σ_3') represents the ratio of the major (σ_1') to minor (σ_3') effective principal stresses at any point during compression testing. In some instances the principal effective stress ratio is used instead of peak deviator stress to define failure (Head 1998). In this study (σ_1'/σ_3') was plotted against axial strain during testing. A summary of peak principal stress ratios for all samples from Tauriko and Otumoetai is presented in Table 5.17. Typically the peak principal effective stress ratio is between 4 and 5 for Tauriko samples and 4 and 9 for Otumoetai samples. However, sample OS1 tested at a confining pressure of ~ 20 kPa recorded a principal effective stress ratio of 38.3.

Table 5.17: Values of peak effective stress ratio (σ_1'/σ_3') for samples from Tauriko and Otumoetai. OS3 analysed at a confining pressure of ~150 kPa includes two samples: the first tested at 150 kPa, and the second at 160 kPa.*

Approximate confining pressure (kPa)	TS1	TS3	OS1	OS2	OS3	OS4
20	-	-	38.3	8.1	8.23	6.9
50	4.9	-	-	5.9	8.01	6.0
80	-	-	6.6	-	4.48	-
100	-	5	8.7	5.1	-	6.21
150	-	-	5.17	5.3	4.5 & 6.41	4.53
200	4.3	4.3	-	-	-	-
300	4.39	4.1	-	-	-	-

*All effective stress ratio versus axial strain plots presented in Appendix 5.6. The line represents a division between specimens which were tested above and below estimated *in situ* confining pressures.

Figure 5.18 presents an example of an effective stress ratio versus axial strain plot. Two tests from different confining pressures are displayed. The first at a σ_3' of 82 kPa represents a typical effective stress ratio plot with a peak value of 6.6. The second represents the plot which produced the extremely high value of 38.3 which was tested at a σ_3' of 25 kPa.

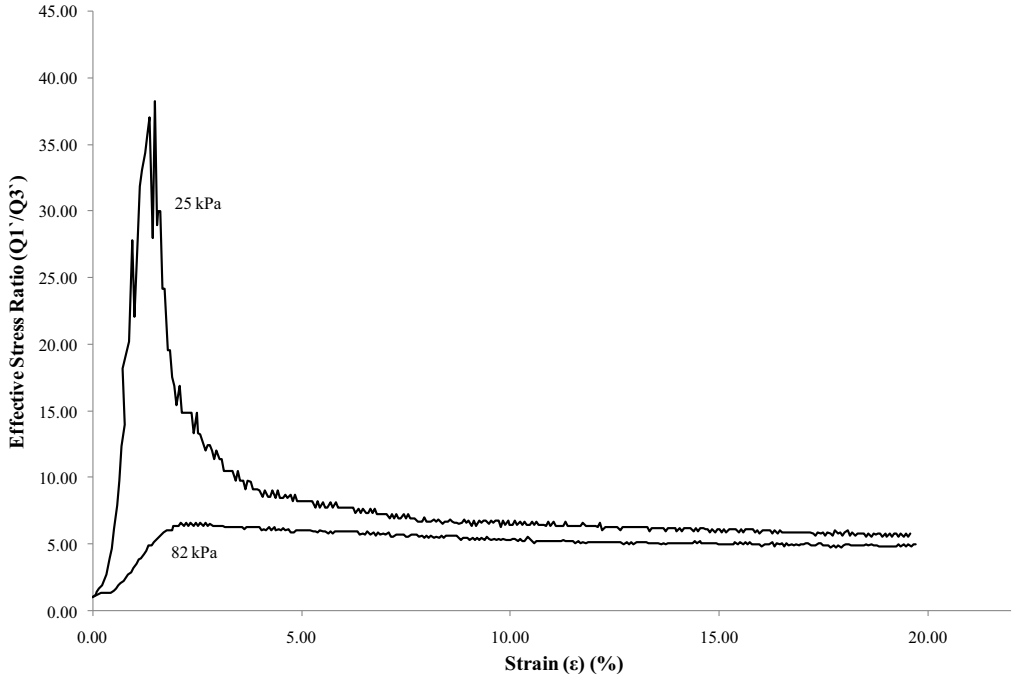

Figure 5.18: Effective stress ratio (σ_1'/σ_3') versus strain for sample OS1 tested at an effective confining pressure of σ_3` = 25 kPa and 82 kPa.

The exaggerated peak in Figure 5.18 was a result of the low effective confining pressure, deviator stress (σ_1- σ_3), and PWP. In this situation effective confining pressure was ~ 25 kPa; as compression proceeded, both PWP and σ_1- σ_3 increased. When PWP increased σ_3' decreased; in this example the σ_3' for the 25 kPa test presented in Figure 5.18 was reduced to 4 kPa. When σ_3' decreased, σ_1- σ_3 and hence σ_1 increased at a rate similar to specimens tested at higher effective confining pressures. The very high σ_3' combined with an increasing σ_1- σ_3 caused the effective stress ratio to increase to an exceptional value (~38). This value then decreased as σ_1- σ_3 settled and PWP decreased. This phenomenon occurred, to a lesser extent, in samples OS2, OS3 and OS4 tested at low confining pressures. This suggested that a high effective stress ratio was the result of increasing deviator stress and PWP combined with low confining pressure during the initial stages of the test, therefore, making it a property of test conditions rather than the specimen.

5.9.4 Specimen failure condition

Failure type is considered to be a significant feature of soil properties (Head 1994) but there seems to be little published material which outlines what this significance is. In this study failure type was divided into three groups: barrel, intermediate and shear failures, which are the same as those used for unconfined compression testing. Schematic examples are presented in Figure 5.3. Table 5.18 described each of the failure types (Figure 5.3) for each of the specimens from Tauriko and Otumoetai.

Table 5.18 indicated the most common failure type was by barrelling, with the least common being shear failure. Specimens from Tauriko typically failed by barrelling, however one specimen from TS3 analysed at a σ_3 of 200 kPa displayed intermediate failure with both barrelling and the formation of a brittle shear plane. The angle of this shear plane was ~ 30°. Both a general plastic failure and the single intermediate failure are presented in Figure 5.19.

Table 5.18: Typical failure shapes for each sample from Otumoetai and Tauriko at different confining pressures (σ_3'). B = Barrel failure, I = intermediate failure and S = shear failure, examples of which are given in Figure 5.3. Also included in this table is axial strain at failure for each sample in parentheses.*

Approximate Confining pressure (kPa)	TS1	TS3	OS1	OS2	OS3	OS4
20	-	-	I (1.76)	I (13.65)	I (20.07)	I (3.02)
50	B (4.9)	-	-	B (11.7)	B (13.2)	B (4.5)
80	-	-	B (2.26)	-	B (20.2)	-
100	-	B (6.37)	S (1.97)	I (2.82)	-	I (1.81)
150	-	-	I (3.4)	S (2.47)	B/S (14.45)	I (1.66)
200	B (2.36)	I (7.15)	-	-	-	-
300	B (2.12)	B (5.1)	-	-	-	-

*. All failure images are included in Appendix 5.6. The line represents a division between specimens which were tested above and below estimated *in situ* confining pressures.

Figure 5.19: (A) Example of a barrel failure from TS1, σ_3 = 300 kPa, and (B) intermediate failure from TS3, σ_3 = 200 kPa.

Specimens from Otumoetai did not display any clear single failure type nor were any apparent trends observed in Table 5.18. However intermediate failures were the most common and shear failures the least. Figure 5.20 displays the three different failure types which were observed at Otumoetai. Shear planes for Otumoetai samples, when they occurred, ranged from 45 – 65°.

Figure 5.20: Examples of failure from Otumoetai including: (A) barrel failure from sample OS4 σ_3' = 55kPa: (B) intermediate failure from OS2 σ_3' = 25kPa; and (C) shear failure from OS3 σ_3' = 160.

Also presented in Table 5.18 are axial strains at peak deviator stress. One would expect shear type failures to occur when axial strain at failure is low, and barrel type failures to occur when axial strain is high, but this was not the case for the Tauriko or Otumoetai samples. Furthermore, Fredrickson (1988) observed shear type failure at low confining pressures, between 6 and 26 kPa and barrel failures between 48 and 96 kPa. Similar trends were not observed in the samples from this study. This may result from the fact that most specimens were compressed well past their axial strain at failure values of < 5% because most tests were typically terminated at 20%.

5.9.5 Mohr - Coulomb failure envelopes

5.9.5.1 Effective Mohr - Coulomb parameters

To plot Mohr-Coulomb failure envelopes for each sample, at different effective confining pressures (σ_3'), the parameter used to determine failure must be chosen. For effective stress tests BS 1377 (1990) recommended that failure can be determined under three separate stress conditions, which are: peak deviator stress ($\sigma_1 - \sigma_3$), maximum effective principal stress ratio (σ_1'/σ_3'), or when shearing continues at constant pore water pressure and shear stress. It is thought that the third option would only be used if peak deviator stress ($\sigma_1 - \sigma_3$) or maximum principal stress ratio (σ_1'/σ_3') could not be easily defined.

Unfortunately little guidance was given in the literature as to which parameter should be used and when. However, it is well known that peak deviator stress and maximum principal stress ratio seldom occur at the same axial strain

(Head 1998). Bishop & Henkel (1962) recommended the use of peak deviator stress as a failure criteria. Head (1998) presented peak deviator stress as a failure option, but Head (1998) also stated that maximum effective principal stress ratio may provide better correlation with other parameters and be suitable for tests where peak deviator stress occurs at large strains. Lambe & Whitman (1979) and Lee *et al.* (1983) recommended using peak effective stress ratio in the case of consolidated undrained tests, especially when pore water pressure decreases after peak stress ratio has been measured. This is because further increases in shear strength may be a result of the decrease in PWP (Fredrickson 1988), which in turn increases σ'_3. In some situations, previous workers have found little difference between failure envelopes created using either peak deviator stress or effective stress ratio (Lo 1962; Fredrickson 1988). In this study effective cohesion and friction angle values derived using the two methods were not comparable, thus Table 5.19 presents those derived from both peak deviator stress and maximum effective stress ratio.

Table 5.19: Mohr-Coulomb parameters of effective cohesion (c') (kPa) and friction angle (ϕ') (º) derived from peak deviator stress and maximum principal stress ratio. The table also includes r^2 values derived from s' and t' plots. All source data and raw calculations are presented in Appendix 5.6.

	Deviator Stress			**Effective Stress Ratio**		
Sample	**c' (kPa)**	**ϕ' (º)**	**r^2**	**c' (kPa)**	**ϕ' (º)**	**r^2**
TS1	11.8	27.3	0.99	4.7	36.6	0.99
TS3	24.0	31.1	0.99	20.3	32.7	1.00
OS1	34.5	25.7	0.81	31.9	27.6	0.82
OS2	4.7	38.5	0.99	9.6	36.9	0.99
OS3	8.3	35.4	0.99	4.3	43.8	0.97
OS4	13.7	28.5	0.99	9.2	34.3	0.97

Correlation coefficient (r^2) values in Table 5.19 were derived from s` and t` plots. Because c' and ϕ' were calculated from the s` and t` plots, the r^2 values were applicable and indicated that all data fit their respective trend lines well. With the exception of OS2, effective cohesion was greater for failure envelopes derived from peak deviator stress than maximum effective principle stress ratio. However, the opposite was true for effective friction angle, also with the exception of OS2 (Table 5.19). When comparing methods the difference between effective cohesion values ranged from 2.6 to 7.1 kPa and the range in friction

angle was between 1.6 and 9.3°. The greatest difference between methods for both effective friction angle and cohesion was observed in TS1 (Table 5.19).

Considering all values presented in Table 5.19, effective cohesion was incredibly variable and ranged from very low to high ~ 4 to ~ 35 kPa. All friction angles were high (> 25°); these values fell into the range of effective friction angles presented for halloysites (25 – 35°), allophanes (30 – 40°) and sands (28 – 46°) by Wesley (1973) and Selby (1993).

Tables 5.20 and 5.21 present triaxial data obtained from previous studies in the Tauranga region and will be used to make comparison with data obtained in this study. Values presented in Table 5.20 are results for specific geological units and materials, while those in Table 5.21 are for materials only. Effective strength values presented in Table 5.20 indicated that both friction angle and cohesion were spread across a range of values between and within geological units, especially the Pahoia Tephras. Friction angles in Tauranga material appeared typically high (> 21°) and material tested was dominantly silty (Tables 5.20 and 5.21). Both Tables 5.20 and 5.21 indicated that samples can have both high cohesion and friction angle.

When peak deviator stress was used as a failure criterion, Tauriko samples had effective cohesion values which were higher and friction angles which were lower than the Te Ranga ignimbrite (Table 5.20). The Pahoia tephras displayed a range of effective strength parameters, c' = 4 – 45 kPa and ϕ' = 22 to 38° (Table 5.20). Mohr-Coulomb values from Otumoetai and Tauriko (Table 5.19), with the exception of TS3, were similar to those presented for Pahoia tephras (Table 5.20). This was not surprising considering that both the Pahoia tephras and the majority of samples in this study are dominated by silt. Interestingly, OS3 had similar effective strength parameters as the Hamilton Ash and its associated paleosol, although friction angle was slightly higher for OS3. This was not unexpected as both the Hamilton Ash and OS3 have high clay contents.

Table 5.20: Peak effective cohesion and friction angle values for known geological units derived from previous studies in the Tauranga region.

Unit[1]	c' (kPa)	ϕ ' (º)	Material	Reference
Post Rotoehu Ash	0	42	Sandy SILT	Oliver (1997)[2]
	1	40	Sandy SILT	
Rotoehu Ash	0	37 – 42	SAND	Oliver (1997)[2]
Hamilton Ash Paleosol	6	31	SILT[3]	Oliver (1997)[2]
Hamilton Ash	6	33	Silty CLAY	Oliver (1997)[2]
	9	32	Silty CLAY	
Pahoia Tephra	6	37	SILT	TCC (2005)
	36	22	SILT	
	32	23	SILT	
	4	38	Silty SAND	OPUS (1998)
	12 – 45	26	SILT	OPUS (2006)
Matua Subgroup	17.5	30	Silty SAND	Oliver (1997)[2]
	3	37	Silty SAND	
	0	36 - 43	Silty SAND	
	0	34	SILT	Connell Wagner (2007)
Ignimbrite (Te Ranga)	0	38	Sandy SILT/SANDS	Connell Wagner (2000)[4]
	3	45	Sandy SILT/SANDS	

Notes:

1) Units were either directly described with test data or correlated with borehole logs.
2) Effective cohesion and friction angle values from Oliver (1997) were obtained with a shear box not a triaxial
3) In Oliver (1997) particle size indicated a high amount of sand (58%) due to aggregation of material. His field logs indicated SILT. However in this study the Hamilton ash paleosol was typically logged as CLAY or silty CLAY
4) Results presented for the Te Ranga Ignimbrite by Connell Wagner (2000) were collected from other sources but represent accepted values.

Table 5.21: Effective cohesion and friction angle values for silty CLAY material from Waikite Road (Welcome Bay) and Omokoroa, which are both in the Tauranga region.

Material	Depth (m)	c' (kPa)	ϕ ' (º)	Reference
Silty CLAY	2.5	23.5	23.8	Meyer *et al.* (2005)
	4.5	6.8	26.5	
	5.8	15.5	20.8	
Clayey SILT	22.2	0	29.5	Tonkin & Taylor (1980)

Using maximum principal effective stress ratio as the failure criteria TS1 had a c' value (~ 5 kPa) similar to the Te Ranga ignimbrite (~ 3 kPa) (Tables 5.19 and 5.20). However, ϕ' was much lower, at ~ 37° and ~ 45° for TS1 and Te Ranga ignimbrite respectively. Typically, effective Mohr – Coulomb parameters for samples in this study, with the exception of TS3, were broadly similar to values presented for the Pahoia tephras (Table 5.20). TS3, with c' ≈ 20 kPa and ϕ' ≈ 33°, had effective strength properties similar to a silty SAND from the Matua subgroup, with c' ≈ 18 kPa and ϕ' ≈ 30°. However, TS3 was predominantly silt. OS3 had lower cohesion and a much higher friction angle than those presented for the Hamilton Ash (Tables 5.19 and 5.20).

For the remainder of this study c' and ϕ' derived from deviator stress at failure will be used. This is because OS3 was the only sample which displayed a decrease in PWP, possibly increasing ($\sigma_1 - \sigma_3$), at all confining pressures. However peak deviator stress will be used for OS3 because it fits the values presented in Table 5.20 for the high clay Hamilton Ash, which appears to be a similar material.

5.9.5.2 Total Mohr - Coulomb parameters

Peak deviator stress was used as the failure criterion for total stress parameters derived from CU testing. Because PWP was not measured the difficulties encountered for effective stress failure parameter selection no longer exist. Total cohesion (c) and friction angle (ϕ) for samples from Tauriko and Otumoetai are presented in Table 5.22.

Table 5.22: Mohr-Coulomb parameters of total cohesion c (kPa) and friction angle ϕ (º) derived from peak deviator stress for samples from Tauriko and Otumoetai. The table also includes r^2 values derived from s and t plots. All source data and raw calculations are presented in Appendix 5.6.

	Peak Deviator Stress		
Sample	**c (kPa)**	**ϕ (º)**	**R^2**
TS1	18.5	11.3	0.99
TS3	60.4	11.4	0.99
OS1	46.4	9.5	0.75
OS2	44.2	6.8	0.95
OS3	44.9	23.1	0.80
OS4	19.5	13.8	0.99

Correlation coefficients (r^2) indicate an excellent fit of data for all samples except OS1 and OS3, however the lower r^2 values are still acceptable. Apparent cohesion was highest in sample TS3 (~ 60 kPa) and lowest in TS1 (~ 19 kPa). Friction angle was greatest for OS3 (~ 23 °) and lowest in OS2 (~ 7 °). TS1 and OS4 displayed similar results.

Pahoia tephra was the only material for which total strength parameters could be found for material from the Tauranga region; these values are presented in Table 5.23. OS1, with c ≈ 46 kPa and ϕ ≈ 10°, had the closest comparable values to those presented in Table 5.23.

Table 5.23: Total cohesion and friction angle values for the Pahoia tephras derived from previous studies in the Tauranga region.

Unit	**c (kPa)**	**ϕ (°)**	**Material**	**Reference**
Pahoia Tephra	2	19	SILT	TCC (2005)
	51	10	SILT	
	48	10	SILT	
	5	22	Silty SAND	OPUS (1998)
	15	15	SILT	OPUS (2006)
	56	15	SILT	

Because limited data were available to compare results from this study with those of the Tauranga region, Table 5.24 presents total stress parameters from other studies examining tephra derived soils. The friction angles from this study presented in Table 5.22, ~ 7 to ~ 23°, were typically higher than those presented for halloysite soils (Table 5.24). Cohesion values for halloysite clays were similar to samples TS3, OS1, OS2 and OS3. Allophanic soils in Table 5.24 covered a wide range of c and ϕ with values between 10 to 150 kPa and 5 to 48° for cohesion and friction angle respectively. Because of this wide range, all values in Table 5.22 are represented.

Table 5.24: Total cohesion and friction angle values derived from previous studies on volcaniclastic materials in the Waikato and Taranaki regions.

Dominant clay mineral	c (kPa)	ϕ (°)	Material	Reference
Halloysite	55	2.6	Silty CLAY	Jacquet (1990)
	50	2	Clayey SILT	
	60	9	Clayey SILT	
Allophane	150	11	Clayey/sandy SILT[1]	
	150	5	Silty/clayey SAND[2]	
	65	15	Clayey/sandy SILT[1]	
	90	10	Clayey/sandy SILT[1]	
	33 – 35	29 – 32	Clayey/sandy SILT[1]	Frederickson (1988)
	10 – 21[3]	35 – 48[3]	Clayey/sandy SILT[1]	

Notes:

1) Presented in source reference as a silt loam
2) Presented in source reference as a sandy loam
3) Results were from tests on samples of 100mm diameter.

5.9.6 Triaxial summary

Summarising triaxial results, OS3 was clearly different from all other samples. OS3 displayed peak deviator stress at higher strains (13.2 – 20.1 %) than other samples, indicating more plastic type failures (based on strain at failure). Values of peak deviator stress demonstrated that OS3 had the greatest strength. PWP activity during compression indicated that OS3 dilated at all confining pressures having the apparent property of over-consolidated clay. This tendency to dilate was so strong that PWP may have become negative.

All other samples, which had extremely high adapted sensitivities (19 to 76), typically displayed brittle failure (based on strain at failure) especially as confining pressure increased. These samples displayed sharp stress strain relationships and displayed peak deviator stress at < 5 % strain. However, OS2 at confining pressures of less than 50 kPa displayed peak deviator stress at high strains (11.7 – 13.7 %). Strain at failure for TS3 (5.1 – 7.2 %) across all confining pressures was slightly more plastic than TS1, OS1, and OS4 (1.7 – 4.9 %). Strain softening following failure was typically minimal. Examining PWP characteristics, all highly sensitive samples dilate during compression at low confining pressure, having the characteristics of over-consolidated clay. As confining pressure increased, the tendency to dilate decreased, and specimens displayed characteristics of compaction during compression. The degree of compaction at failure for TS1, OS2 and OS4, at confining pressures of 150 kPa

and above, was so great their A_f value indicated properties of highly sensitive clays. Of the highly sensitive clays, TS3 stood out failing at higher strains across all confining pressures. TS3 showed the lowest A_f and highest deviator stress values compared to all other highly sensitive samples. These characteristics indicated TS3 was structurally different to TS1, OS1, OS2 and OS4.

Using deviator stress as a failure criterion, effective cohesion and friction angles for OS3 were similar to the clayey Hamilton Ash. The remainder of samples, with the exception of TS3, were similar to the Pahoia tephras.

5.10 Ring shear

This section presents ring shear results for samples collected from Tauriko and Otumoetai, a summary of values is presented in Table 5.25. Raw results, including Mohr-Coloumb plots, are presented in **Appendix 5.7**.

Table 5.25: Ring shear ranges of normal load used (σ_n), range of peak strength (kPa), residual cohesion (c_r) and residual friction (ϕ_r) angle for samples collected from Otumoetai and Tauriko. All shear stress versus linear displacement graphs, and Mohr – Coulomb plots are presented in Appendix 5.7.

Sample	Range of σ_n (kPa)	Range of peak τ_f (kPa)	c_r (kPa)	ϕ_r	r^2
TS1	14 – 149	10 – 90	3.06	30.40	0.99
TS3	52 – 296	31 – 194	0.0[1]	33.18[1]	0.99
OS1	19 – 150	13 – 90	0.75	30.99	0.99
OS2	19 – 149	11 – 87	0.39	30.05	0.99
OS3	19 – 149	11 – 57	4.87	19.34	0.99
OS4	8 - 174	6 – 89	2.87	26.56	0.99

Notes:

1) Cohesion forced through 0 actual measured result was c_r = -3.41 (kPa) and ϕ_r = 33.82º.

Residual cohesion (c_r) values range from 0 to 4.87 (kPa). Low cohesion was expected as Craig (1997) stated that c_r is very low and can often be taken as 0. The highest C_r value was 4.87 (kPa) for sample OS3; considering this sample had the highest clay content this was not unexpected. TS3 originally had a negative c_r value, which was not realistic, but a negative cohesion had been previously reported by Keam (2008) for volcanic silts in Omokoroa, Tauranga (Table 5.26). Residual friction angles (ϕ_r) range from 19.34º to 33.18º; Craig (1997) stated that ϕ_r decreased with increasing clay content. OS3 had the highest clay content and friction angle was lowest for this soil. However, when examining volcanic ash

soils across a range of size class (Table 5.26), increasing clay content seemed to have little effect on ϕ_r angle. High silt samples (TS1, TS3, OS1, OS2 and OS4) all fell within the range of ϕ_r presented in Table 5.26. OS3, which is predominantly clay, was much lower than those values recorded for volcanic clays.

Effective friction angle results for triaxial samples TS1, TS3, OS1 were all less than residual friction angles. Furthermore, total peak friction angles for the shear box were greater than all residual friction angles.

Table 5.26: Previous ring shear values presented by other workers for volcanic ash material. NR indicates that no value was recorded.

Source	Volcanic Ash Silt		Volcanic Ash Clayey Silt		Volanic Ash Silty Clays		Volcanic ash clays	
	c_r	ϕ_r	c_r	ϕ_r	c_r	ϕ_r	c_r	ϕ_r
Ranges	0 – 15.9	16.6 - 32	NR	18 - 35	NR	31 – 37	NR	24.5 - 39
Single values	0.0	29[1]	NR	24.5[2]	NR	35[2]	0	39[3,4]
	15.9	28[1]	NR	31[2]	NR	37[2]	4	35[3,4]
	6.8	32[1]	NR	18.1[2]	NR	35[2]	0	39[3,4]
	-4.4	30.9[5]	NR	28[2]	NR	31[2]	5	24.5[3,6]
	4.3	16.6[5]	NR	34[2]	NR	37[2]		
			NR	35[2]	NR	36[2]		

Notes:
1) Values from Cong (1992)
2) Values from Wesley (1992)
3) Values from Wesley (1977)
4) Dominant clay mineral was halloysite
5) Values from Keam (2008)
6) Dominant clay mineral was allophane

5.11 Summary of geotechnical properties

Tables 5.27 and 5.28 summarise all the geotechnical properties measured for samples from Tauriko and Otumoetai. All samples with the exception of OS3 had only a small percentage of clay (< 10 %). Most samples were predominantly silt (> 50%), though this was not the case for OS2, which was dominated by sand (> 50 %). High moisture contents were typical (> 60 %); TS1, TS2 and OS1 had values over 100 %. Porosities for all samples were at the upper limit of what had been previously measured, and void ratios were also high. Dry bulk density values were within the ranges previously measured; however volcanic soils typically have low bulk density (Molloy 1998). TS3 and OS3 had the highest dry densities and lowest porosities.

Atterberg limits indicated that all samples had similar properties to halloysite and to a lesser extent allophane. High adapted sensitivity samples (TS1, TS2, TS3, OS1, OS2 and OS4) had moisture contents above their respective liquid limits as indicated by the high liquidity index values (> 1). This resulted in low remoulded strength, which was confirmed by the results from the calculation of Sharma & Bora (2003; 2005) and the inability to form cores for unconfined compressive strength testing. Even though samples had low remoulded strength the rapidity number indicated that a lot of energy was required to cause complete structural disturbance.

During shear box testing samples typically decreased in volume, which often resulted in strain hardening at high normal loads. Shear box and effective triaxial testing indicated that all samples had high friction angles. However, effective residual friction angles for samples TS1, TS3 and OS1 from ring shear testing were higher than peak values obtained from triaxial testing. Triaxial results indicated OS3 was clearly different than all other samples. OS3 displayed plastic type failure whilst all other samples were typically brittle. Furthermore OS3 dilated during compression having the properties of an over-consolidated clay at all confining pressures. In all other samples as confining pressure increased they tended toward compaction rather than dilation. At their maximum confining pressures TS1, OS2 and OS4 had the properties of highly sensitive clays. During triaxial testing TS3 appeared different to all other highly sensitive samples (TS1, OS1, OS2 and OS4) displaying elevated peak deviator stress, strains at failure and lower A_f values.

Table 5.27: Summary of Particle size results, bulk soil properties and Atterberg limit values for samples from Tauriko and Otumoetai. Bulk soil properties include; moisture content (*w)*, wet bulk density (ρ), dry bulk density (ρ_D), particle density (ρ_s), porosity (*n*), void ratio (*e*) and saturation state (*Sr*).

Sample	Particle size			Bulk Soil Properties							Atterberg limits				
	Clay (%)	Silt (%)	Sand (%)	*w* (%)	ρ (kg m^{-3})	ρ_D (kg m^{-3})	ρ_s (kg m^{-3})	*n* (%)	*e*	*Sr (%)*	Liquid limit (%)	Plastic limit (%)	Plasticity index (%)	Liquidity index (%)	Activity
TS1	5.70	81.22	13.08	115 ± 0.5	1280 ± 24	656 ± 41	2532 ± 9	74.1	2.86	102.2	81.25	56.89	24.36	2.39	4.27
TS2	7.21	82.86	9.93	109 ± 0.7	1273 ± 18	589 ± 13	2591 ± 5	77.3	3.40	83.5	72.67	46.66	26.01	2.41	3.61
TS3	8.30	80.35	11.34	64 ± 0.9	1581 ± 15	966 ± 10	2542 ± 5	62.0	1.63	99.3	51.97	38.74	13.23	1.88	1.59
OS1	9.98	65.39	24.52	104 ± 3	1358 ± 8	656 ± 8	2636 ± 8	75.1	3.02	91.1	90.02	47.32	42.70	1.33	4.28
OS2	6.39	40.59	52.91	69 ± 4	1497 ± 30	893 ± 51	2664 ± 8	66.5	1.98	93.0	57.40	32.44	24.96	1.46	3.91
OS3	33.54	54.93	10.93	66 ± 3	1515 ± 19	920 ± 15	2667 ± 2	65.5	1.90	92.4	96.40	54.41	41.99	0.27	1.25
OS4	1.98	51.15	46.87	86 ± 0.3	1407 ± 9	743 ± 9	2686 ± 3	72.3	2.62	87.8	72.96	36.80	36.18	1.35	18.27

Table 5.28: Summary of strength results for samples from Tauriko and Otumoetai which includes; rapidity numbers, peak uniaxial compression (UCS) results, values from Sharma & Bora's (2003; 2005) remoulded strength calculation, and also Mohr-Coulomb parameters from shear box, triaxial and ring shear testing. See text for discussion on omission of TS2. Triaxial effective stress parameters effective cohesion (c') and friction angle (ϕ ') are derived from peak deviator stress.

Sample	Rapidity number	Peak UCS (C_u) (kPa)	Remoulded Strength[1] (kPa)	Shear box		Triaxial				Ring shear	
				c (kPa)	ϕ (°)	c' (kPa)	ϕ ' (°)	c (kPa)	ϕ (°)	c_r (kPa)	ϕ_r
TS1	3	27.93	< 0.3	15.34	33.93	11.8	27.3	18.5	11.3	3.06	30.40
TS2	4	-	< 0.3	-	-	-	-	-	-	-	-
TS3	2	81.04	< 0.3	11.27	35.90	24.0	31.1	60.4	11.4	0.0	33.18
OS1	3	56.74	0.6	33.71	32.62	34.5	25.7	46.4	9.5	0.75	30.99
OS2	2	50.54	0.4	27.99	33.16	4.7	38.5	44.2	6.8	0.39	30.05
OS3	2	42.35	35.9	16.64	42.49	8.3	35.4	44.9	23.1	4.87	19.34
OS4	3	40.46	0.6	24.73	33.38	13.7	28.5	19.5	13.8	2.87	26.56

Notes: 1) The remoulded strength values are derived from the equation found in Sharma & Bora (2003; 2005) therefore the values only estimates based on the water content of the sample relative to liquid limit

Chapter 6
Mineralogy

6.1 Introduction

Mineral assemblages are a primary control on the physical and chemical properties of a soil. Therefore *a priori* knowledge of what minerals are in a soil provides an insight into its behaviour (Mitchell & Soga 2005). Because volcanic deposits often contain both crystalline and short-range order minerals (Lowe & Nelson 1983), and both clay and non-clay minerals were investigated in this study, a number of analytical techniques have been adopted to provide a qualitative analysis of the minerals present in each sample. Methods used to detect short-range order minerals were sodium fluoride and oxalate extractable Fe, Al and Si. X-ray diffraction (XRD) and scanning electron microscopy (SEM) were employed for the identification of both clay and non-clay minerals. All samples from Tauriko (TS1, TS2, and TS3) and Otumoetai (OS1, OS2, OS3, and OS4) were analysed for mineral assemblages.

It should be noted that **bulk soil** refers to samples which include all sand, silt, and clay. The **clay-size fraction** refers to all material < 2 μm. Material with a crystalline clay mineral structure is normally < 2 μm; however, clay minerals can also occupy larger size ranges. Material which appears characteristically clay-like under SEM investigation, but not necessarily < 2 μm, will be termed a clay mineral.

6.2 Sodium fluoride (NaF)

The use of sodium fluoride (NaF) determines the presence of reactive hydroxyl-aluminium in short-range order minerals such as allophane and ferrihydrite (Fields & Perrot 1966). However, in the field this analysis is classically used only to determine the presence of allophane. The results for bulk soil samples from Tauriko and Otumoetai are presented in Table 6.1. For each sample, Table 6.1 is divided into three categories. The first is the colour change observed as a result of the NaF reaction, the second is the pedological

classification from Milne *et al.* (1995), and the third is an estimate of allophane content based on NZS 4402 (1986).

Table 6.1 Allophane identification in samples from Tauriko (TS1, TS2 and TS3) and Otumoetai (OS1, OS2, OS3 and OS4), as indicated by application of sodium fluoride. Visual classification indicates the observed colour changes, the pedological and NZS 4402 classifications follow those of Milne *et al. (*1995) and NZS 4402 (1986).

Sample	Visual	Pedological allophane reaction	NZS 4402 allophane content (%)
TS1	Moderately pink	Very weak	5 to 7
TS2	Moderately pink	Very weak	5 to 7
TS3	Moderately pink	Weak	5 to 7
OS1	Moderately pink	Weak	5 to 7
OS2	Moderately – dark pink	Moderate	> 7
OS3A	Very light pink	Very weak	< 5
OS4B	Very light pink	Very weak	< 5

The NaF field test indicated that all samples had at least a minor amount of free aluminium (hydroxyl – aluminium in short-range order), indicating the possible presence of some allophane. OS2 from Otumoetai had the strongest reaction and hence the highest estimated allophane content (Table 6.1). Table 6.1 indicates that TS3 has the same visual characteristics as TS1 and TS2, but its final pedological result is higher. The higher result occurred because TS3 reached its final colour of 'moderately pink' quicker than TS1 and TS2.

6.3 Extractible Fe, Al and Si

Allophane and ferrihydrite contents have been quantitatively estimated from acid-oxalate extractable Fe, Al and Si combined with pyrophosphate extractable Fe and Al. It should be noted that imogolite also dissolves in acid-oxalate, but this is only a very minor constituent in New Zealand soils (Lowe & Percival 1993), so will not be discussed here. All samples from Tauriko (TS1, TS2 and TS3) and Otumoetai (OS1, OS2, OS3 and OS4) have been analysed and the results are presented in Table 6.2. Raw test values can be found in Appendix 6.1. Included in Table 6.2 is the Al:Si ratio measured from extractable Si and Al results. The Al:Si ratio determines the multiplier, found in Parfitt (1990), used to quantify allophane content. This value is then multiplied by acid-oxalate extractable Si to obtain a quantitative determination of allophane (Parfitt 1990;

Lowe & Percival 1993) (see Chapter 3). Ferrihydrite is determined by multiplying acid-oxalate extractable Fe by 1.7 (Parfitt & Childs 1988).

Table 6.2: Oxalate-extractable ferrihydrite (%) and allophane (%) contents for samples collected from Tauriko and Otumoetai. Results presented include the *Al:Si* ratio, the multiplier and the acid-oxalate extractible Si (Si_o).* Also included is acid-oxalate extractible Fe (Fe_o).

Sample	*Al:Si* ratio	Multiplier	Si_o (%)	Allophane %	Fe_o (%)	Ferrihydrite %
TS1	7.7	-	0.03	-	0.01	0.01
TS2	5.6	-	0.04	-	< 0.01	< 0.01
TS3	5.7	-	0.04	-	< 0.01	< 0.01
OS1	2.1	7	0.19	1.3	0.29	0.5
OS2	2.3	10	0.16	1.6	0.25	0.4
OS3	2.3	10	0.08	0.8	0.28	0.5
OS4	3.8	-	0.04	-	0.16	0.3

* TS1, TS2, TS3 and OS4 allophane results cannot be determined because the *Al:Si* ratio was higher than that published for any other allophane.

All *Al:Si* ratios were greater than 2:1 indicating that allophane present in samples of this study were Al-rich or imogolite-like allophane (Parfitt 1990; Lowe & Percival 1993). Al-rich allophane is the dominant form in New Zealand soils (Lowe & Percival 1993) and is likely to be present when the Si in soil solution is low (Parfitt & Kimble 1989). Interestingly, the *Al:Si* ratios of Tauriko samples were unusually high, between 5.6 and 7.7, and may be aberrant because they were much higher than the range of 0.4 to 4.0 recorded by Parfitt & Kimble (1989) for 512 allophanic samples from New Zealand.

Allophane as determined by acid-oxalate analysis was only a minor component in samples from OS1, OS2 and OS3 from Otumoetai with values ranging between 0.8 and 1.6 % (Table 6.2). These low allophane results can be accepted as reasonably accurate because Parfitt (1990) stated that the extractable Al and Si method can detect as little as 0.5 % during routine analysis. Furthermore, the *Al:Si* ratios (3.8 – 7.7) presented for samples from Tauriko and OS4 (Table 6.2) were higher than the maximum of 3.5 presented by Parfitt (1990), and therefore no multiplier is available. The Si_o values (0.03 – 0.04) were so low that allophane content was insignificant (Table 6.2).

Ferrihydrite contents were relatively low, at ≤ 0.5 % (Table 6.2). This value is at the lower end and less than the measured range of 0.5 to 8.0 % for

ferrihydrite content of New Zealand tephras (Lowe & Percival 1993). Otumoetai samples had higher ferrihydrite contents than those from Tauriko, with mean values of ~ 0.4 % and < 0.01 % respectively. Ferrihydrite is a common component of tephra-derived soils (Lowe & Percival 1993).

Allophane values derived from extractible Al and Si give a quantitative and much more reliable estimate than the field-based NaF analyses. The NaF field test does not reflect the results all that well, but do give relative amounts. Therefore, extractible Al and Si allophane results will be used in the remainder of this study.

6.4 X-ray diffraction (XRD)

XRD was used to examine both the clay-size fraction (< 2 μm) and bulk soil for all samples from Tauriko and Otumoetai. The clay-size fraction was analysed as orientated pastes, with the hope of enhancing 00*l* reflections, and the bulk sample was scanned as a randomly orientated powder.

6.4.1 Tauriko

XRD results from Tauriko are summarised in Table 6.3. All diffractograms can be found in Appendix 6.2.

Table 6.3: Minerals observed in both the clay-size fraction (< 2 μm) and bulk soil material for samples from Tauriko, as determined by XRD.

Sample	Bulk sample (sand, silt, clay) minerals	Clay-size fraction minerals (< 2 μm)
TS1	Dehydrated halloysite, low temperature tridymite, Na-Ca feldspar (plagioclase), low temperature quartz	Hydrated halloysite
TS2	Dehydrated halloysite, low temperature tridymite, Na-Ca feldspar (plagioclase), low temperature quartz	Hydrated halloysite
TS3	Dehydrated halloysite, Na-Ca feldspar (plagioclase), low temperature tridymite, low temperature quartz	Hydrated halloysite

6.4.1.1 Bulk sample

The bulk sample traces for TS1, TS2 and TS3 are shown in Figures 6.1 to 6.3. These all show strong broad 001 peaks between 7.34 Å and 7.48 Å which

indicate the presence of dehydrated halloysite. In all samples the shoulder of the dehydrated halloysite peak extends over the kaolinite position of 7.15 Å, but no peaks are observed. If halloysite is completely dehydrated one would expect a peak at ~7.2 Å which is similar to that of kaolinite. The larger spacing suggests some retained interlayer water. The retention of interlayer water further confirms the presence of dehydrated halloysite rather than kaolinite. If kaolinite is present, but only in very small amounts, it is possible that the 7.15 Å peak may be masked by the dehydrated halloysite peak.

In each sample an asymmetrical peak at ~4.48 Å extends down towards ~3.3 Å (Figures 6.1, 6.2 and 6.3). While Brindley & Brown (1980) stated that the 4.48 Å position represents disordered kaolinite, the shape of the peak is characteristic of the ~ 4.4 Å 02, 11 band of halloysite (Jock Churchman, *pers. com*. 2008). However, it should also be noted that all layer silicates typically show a peak at ~ 4.4 Å. In each sample the intensity of the 4.4 Å 02,11 band is stronger than the 001 dehydrated halloysite peak. The stronger 02,11 band suggests the presence of halloysite rather than kaolinite (Brindley & Brown 1980). In all samples the 001 and 02, 11 halloysite peaks dominate the XRD trace, indicating its abundance.

Peaks near 3.6 Å were observed in TS1 and TS2. These represent the 002 position for halloysite (Figures 6.1 and 6.2). The 003 halloysite position of 2.4 Å is closely approximated by peaks at 2.37 Å and 2.4 Å in TS1 and TS2, respectively (Figures 6.1 and 6.2). All samples have indistinct low broad peaks around 2.34 Å which represent kaolinite (Figures 6.1, 6.2 and 6.3). These peaks may indicate the presence of a small amount of kaolinite in these samples. However, these peaks are difficult to define and the absence of a 001 (7.15 Å) reflection does not clearly support the presence of kaolinite.

Plagioclase feldspar and low temperature quartz are present in all samples. Both TS2 and TS3 have strong peaks for plagioclase between 3.19 Å and 3.22 Å (Figures 6.2 and 6.3). A similarly positioned, but less intense, plagioclase peak was observed for TS1 (Figure 6.1). Alternatively, TS1 displays the strongest low temperature quartz peak at ~ 3.34 Å (Figure 6.1).

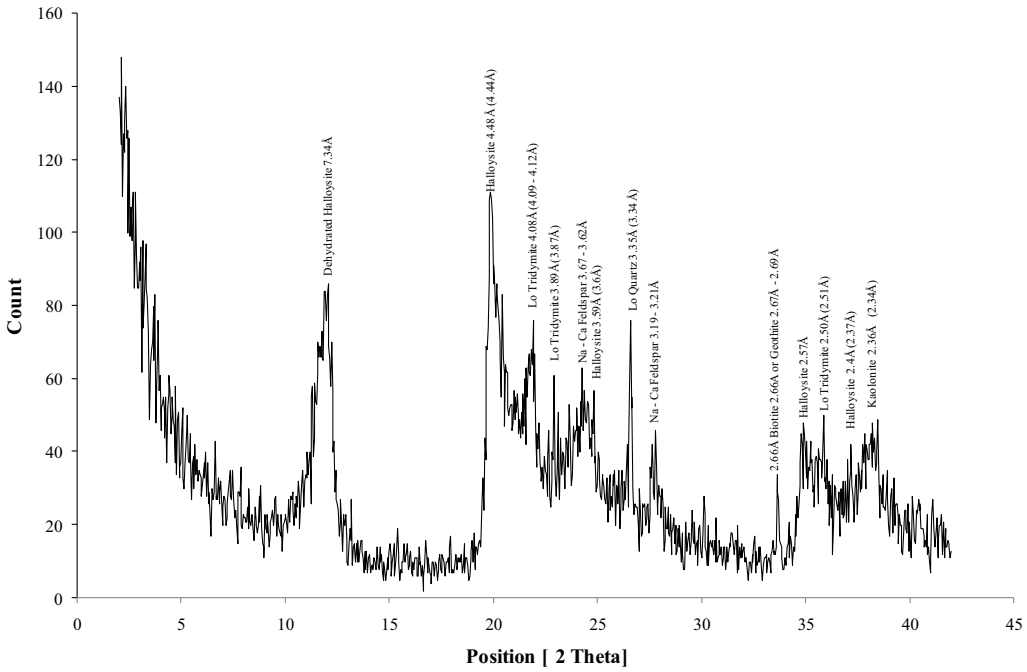

Figure 6.1: XRD diffractograms for the bulk samples from TS1 (Tauriko). All peaks are labelled with the associated mineral. Å values presented first represent those measured by the trace and Å values in parentheses represent the ideal value for the selected mineral.

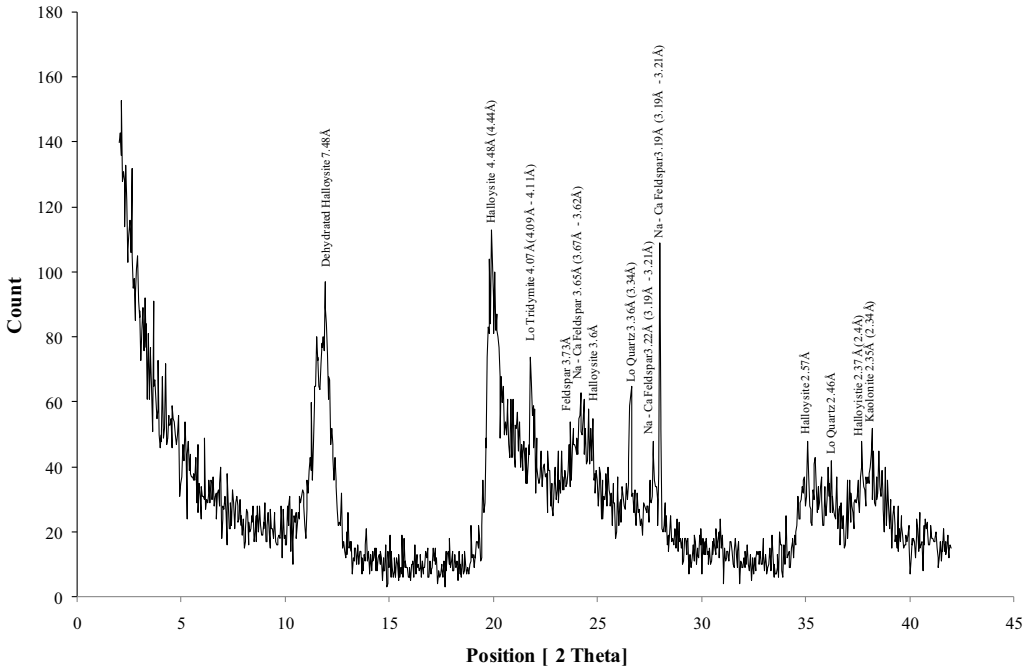

Figure 6.2: XRD diffractograms for the bulk samples from TS2 (Tauriko). All peaks are labelled with the associated mineral. Å values presented first represent those measured by the trace and Å values in parentheses represent the ideal value for the selected mineral.

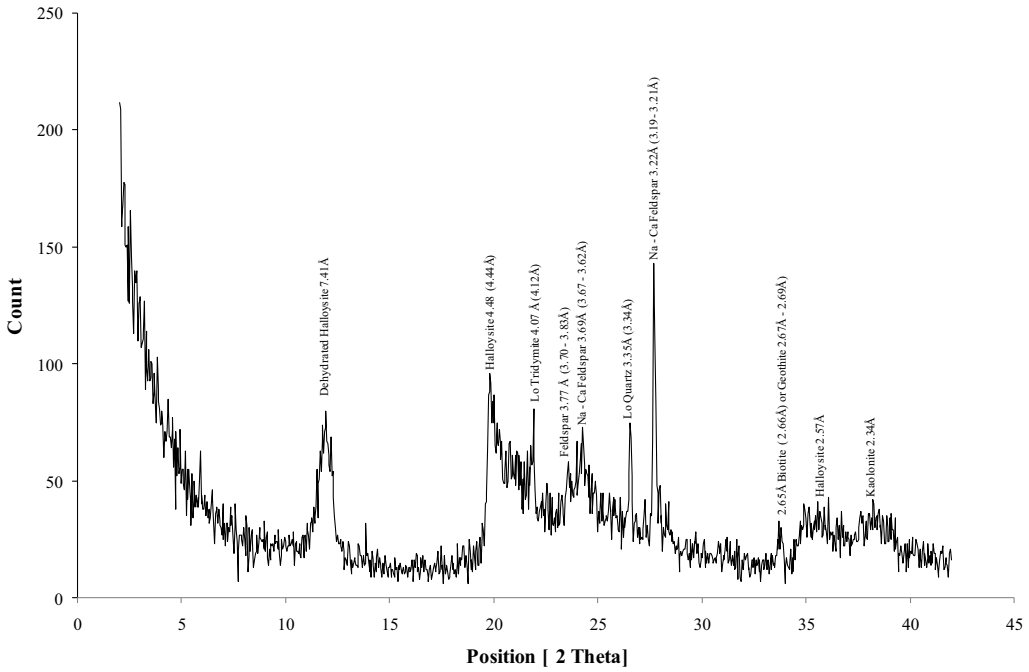

Figure 6.3: XRD diffractograms for the bulk samples from TS3 (Tauriko). All peaks are labelled with the associated mineral. Å values presented first represent those measured by the trace and Å values in parentheses represent the ideal value for the selected mineral.

In all Tauriko samples, peaks occurred between 4.07 Å and 4.08 Å (Figures 6.1, 6.2, and 6.3). These fall between values for low temperature tridymite (4.09 – 4.11 Å), opal (4.09 – 4.11 Å), plagioclase (4.02 – 4.04 Å), and low temperature cristobolite (4.04/4.05 Å). Work by Salter (1979), Lowe & Nelson (1983), Cong (1992), Lowe & Percival (1993), and Keam (2008) indicate that it is possible to find all in upper North Island weathered pyroclastics. Lowe & Nelson (1983) stated that cristobalite can not be positively identified when primary feldspar peaks are high, which is the case for TS1 and TS2. In TS1, a peak occurs at 2.51 Å which characterises low temperature tridymite. This provides confidence that the peak at 4.08 Å represents this mineral. Low temperature tridymite can also be assumed for both TS2 and TS3 because the peaks at 4.08 Å and 4.07 Å are closest to the reference values given, and because of the peak at 2.51 Å in TS1.

A peak occurred in TS1 and TS3 at ~ 2.66 Å, which may represent biotite (Brindley & Brown 1980) a micaceous mineral (Figure 6.1 and 6.3). Biotite also has a peak at ~3.3 Å (Fanning*, et al.* 1989) which is present in both samples. If biotite minerals were present then a peak at ~ 10 Å would be expected, but this was not observed. However, Fanning *et al.* (1989) indicated that if the mica

mineral comprises very thin sheets then the peak at ~ 10 Å may be absent. Micas characteristically sparkle in hand specimens as light reflects from the flakes (Fanning *et al.* 1989), but this feature was not observed in any of the Tauriko samples, so it seems unlikely that biotite is present. The peak at 2.66 Å may represent goethite as it is close to the position of 2.67 – 2.69 Å identified by Brindley & Brown (1980). Associated goethite peaks at 2.43 to 2.45 Å and 2.23 to 2.25 Å (Brindley & Brown 1980) are difficult to identify because of the high background surrounding this section of the XRD diffractograms (Figures 6.1 and 6.3). It is possible that goethite is present because it has been recorded by Shepherd (1994) in beds of the Hamilton Ash Formation (1 – 8 %) (0.08 – 0.34 Ma; Lowe *et al.* 2001) and the Kauroa Ash Formation (2 – 15 %) (0.78 – 2.24 Ma; Lowe *et al.* 2001).

6.4.1.2 Clay-size fraction (< 2 μm)

Figure 6.4 presents a clay fraction XRD trace of TS1 from Tauriko. The sample has been scanned fully hydrated on a porous ceramic tile and then scanned again after heating at 110 °C for 1 hour. Only TS1 is presented from Tauriko because all samples displayed almost identical diffraction tracings (Appendix 6.2). When scanned fully hydrated, all samples are dominated by sharp 001 hydrated halloysite peaks between ~9.82 Å and ~9.92 Å. This d spacing is close to the classical ~10.1 Å peak of hydrated halloysite. The slight difference may be the result of interlayer water loss during testing. Peak positions slightly increase to between 9.94 Å and 10.06 Å after the application of formamide (Appendix 6.2). Furthermore, the sharpness of the peaks indicates the high degree of crystallinity of the halloysite minerals (Lowe & Nelson 1983).

Figure 6.4 further confirms halloysite because the 001 peak collapsed to between ~7.3 Å and ~7.2 Å heating to 110 ºC. This collapse is characteristic of halloysite and represents a loss of interlayer water as the clay mineral transforms from its hydrated to dehydrated state (Brindley & Brown 1980). This collapse occurred in all Tauriko clay fraction samples (Appendix 6.2).

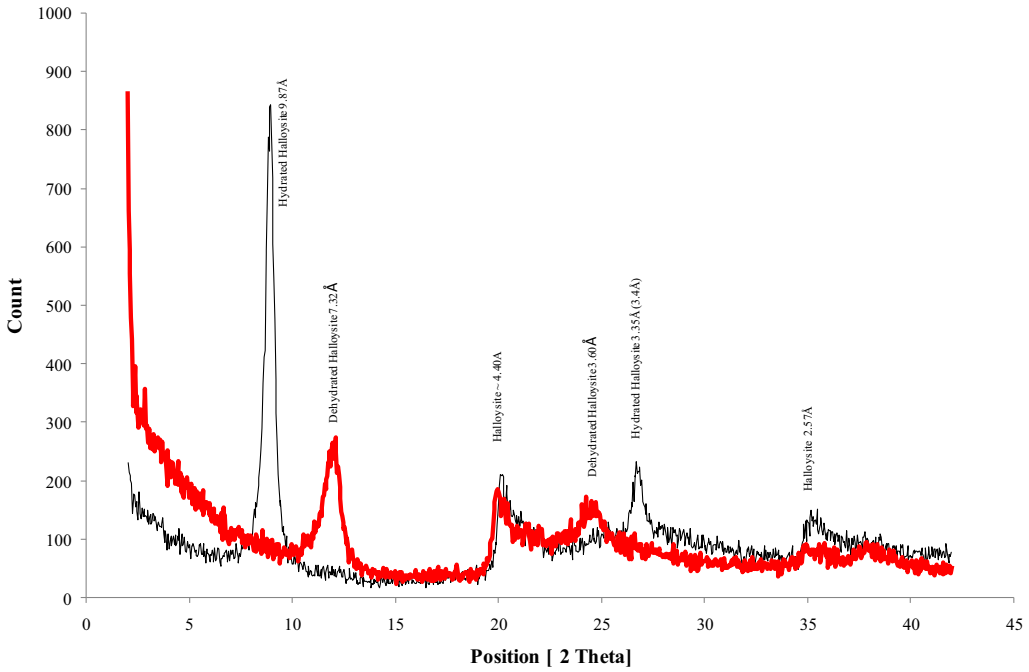

Figure 6.4: XRD diffractograms for the clay-size fraction from TS1 (Tauriko). The black line represents the trace when the sample is fully hydrated and the red line is after heating for 1 hour at 110 °C.

Further confirmation of halloysite is provided by the asymmetrical peak at ~ 4.4 Å which represents the 02, 11 band (Figure 6.4). Interestingly, in the fully hydrated state, 003 peaks for hydrated halloysite were observed between 3.32 and 3.35 Å. When air dried or after being heated to 110 ºC this peak shifted to ~ 3.6 Å indicating this peak represents halloysite rather than quartz (3.34 Å).

Figure 6.5 from TS1 is presented as an example of high temperature (~ 550 °C) peak collapse. When heated to 550 ºC, all peaks collapsed indicating that mica, smectites and chlorites were not present. Typically peaks will persist at 10 Å or 14 Å after heating if these minerals are present (Brindley & Brown 1980). Serpentines can also be excluded because they will display a low broad reflection in the 10 to 14 Å region after high temperature heating (Brindley & Brown 1980).

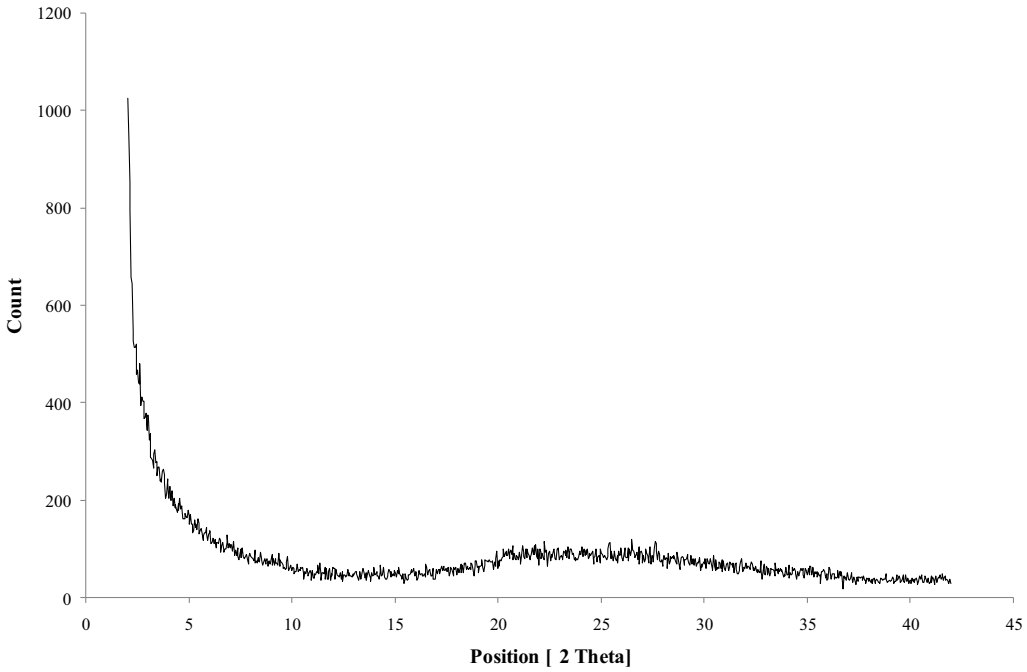

Figure 6.5: XRD diffractograms for the clay size fraction from TS1 (Tauriko) after heating for 1 hour at 550 °C.

The determination of 10.1 Å halloysite by scanning samples fully hydrated on ceramic tiles is likely to represent the natural field state of the mineral. Thus halloysite observed in the air-dried bulk sample is likely to be hydrated *in situ*, rather than dehydrated, halloysite in its natural field condition. The dehydrated state is simply a product of interlayer water loss during sample preparation (Lowe & Nelson 1983).

Peaks in the position of low temperature cristobalite (~ 4.05 Å) and tridymite (~ 4.09 Å) were present in TS1 and TS2 clay fractions, respectively. However, these peaks were only observed in samples scanned on ceramic tiles. Ceramic tile blank sample traces indicated these peaks may represent the tile rather than the sample; the blank tile trace is presented in Appendix 6.2.

6.4.2 Otumoetai

Samples OS1, OS2, OS3 and OS4 were analysed from Otumoetai and the results are summarised in Table 6.4. All XRD traces can be found in Appendix 6.2.

Table 6.4: Minerals observed in both the clay-size fraction (< 2 μm) and bulk soil material for samples from Otumoetai, as determined by XRD.

Sample	Bulk sample (sand, silt, clay) minerals	Clay-size fraction minerals (< 2 μm)
OS1	Dehydrated halloysite, low temperature quartz, low temperature cristobalite	Hydrated halloysite, low temperature tridymite, low temperature quartz
OS2	Dehydrate halloysite, low temperature quartz, Pyroxene	Hydrated halloysite
OS3	Dehydrated halloysite, low temperature quartz, low temperature cristobalite	Hydrated halloysite, kaolinite, low temperature cristobalite, low temperature quartz
OS4	Dehydrated halloysite, low temperature quartz, low temperature tridymite	Hydrated halloysite, kaolinite

6.4.2.1 Bulk sample

The bulk sample traces for OS1, OS2, OS3 and OS4 are presented in Figures 6.6, 6.7, 6.8 and 6.9. All Otumoetai bulk samples displayed broad dehydrated halloysite peaks between 7.33 Å and 7.45 Å and had a shoulder which fell over the kaolinite position of 7.15 Å. The dehydrated halloysite peak intensity is lowest in OS3. As at Tauriko, all samples displayed a number of secondary peaks for halloysite. The 02, 11 band at ~ 4.4 Å was present in all samples. Its intensity was greater than that of the 001 halloysite peak in all samples except OS4. A peak at ~ 3.6 Å was present in all samples which indicated halloysite. Following the same rationale as Tauriko, it can be concluded that the dominant clay material in the bulk sample from Otumoetai was halloysite, which was most likely to be in the hydrated (10 Ǻ) state *in situ*.

Of the non-clay minerals low temperature quartz dominated OS3, OS1 and OS4, which are listed in order of peak intensity and hence quartz abundance. OS2 was dominated by pyroxene with very sharp and intense peaks at 2.94 Å and 2.54 Å. Quartz was also present in OS2, with a peak intensity greater than that observed in OS4 but less than that observed in OS1. Low temperature cristobolite was observed in OS1 and OS3 with peaks at ~ 4.06 Å. Low temperature tridymite was observed in OS4 with a peak at 4.11 Å (Figures 6.6, 6.7, 6.8 and 6.9).

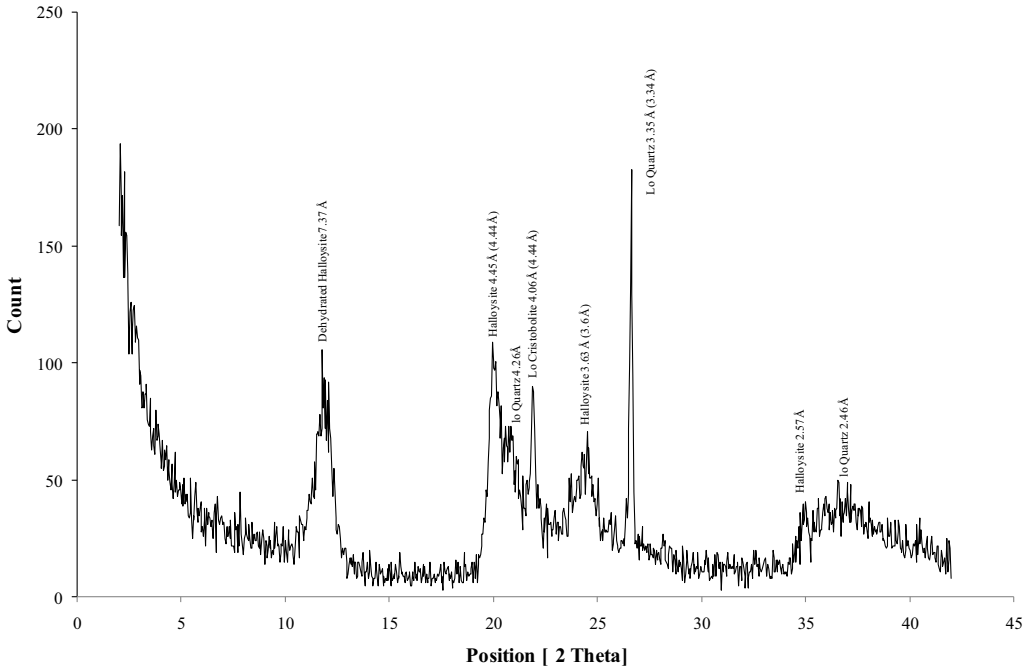

Figure 6.6: XRD diffractogram for the bulk samples from OS1 (Otumoetai). All peaks are labelled with the associated mineral. Å values presented first represent those measured by the trace and Å values in parentheses represent the ideal value for the selected mineral.

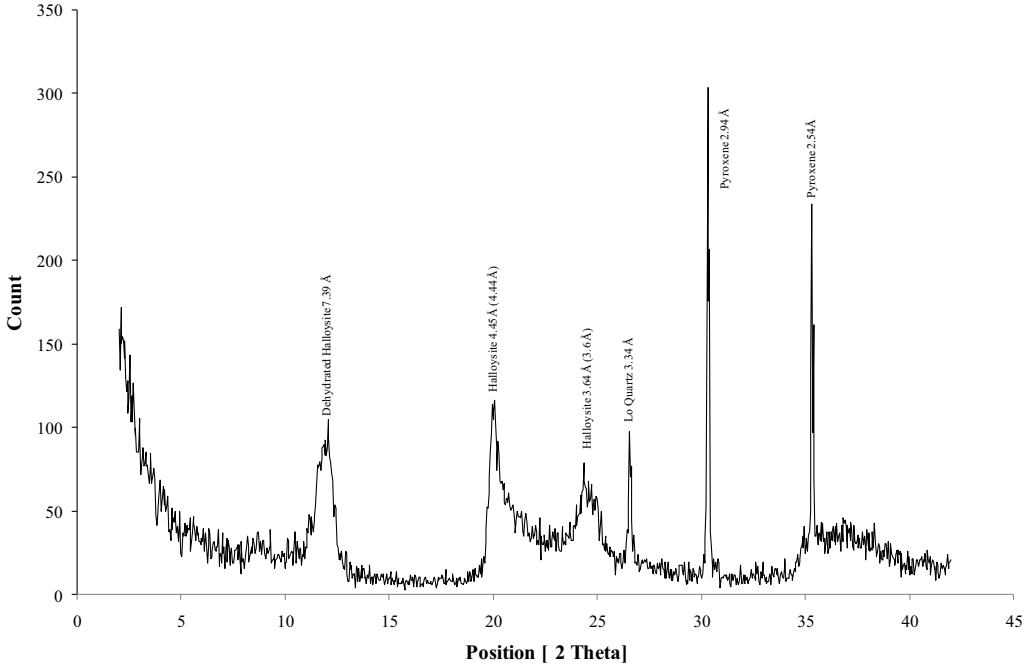

Figure 6.7: XRD diffractogram for the bulk samples from OS2 (Otumoetai). All peaks are labelled with the associated mineral. Å values presented first represent those measured by the trace and Å values in parentheses represent the ideal value for the selected mineral.

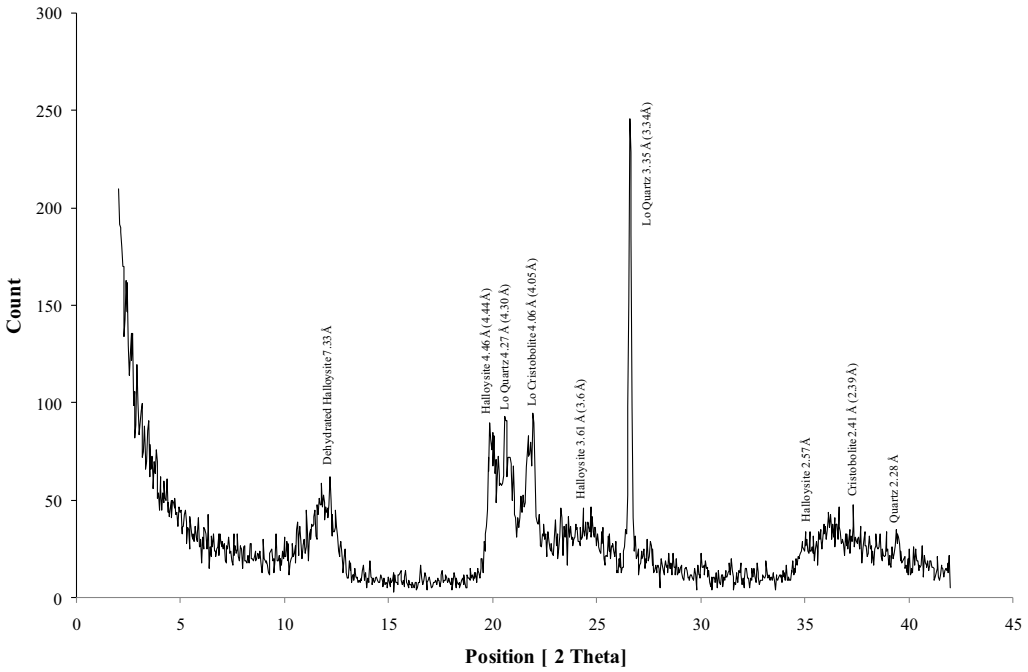

Figure 6.8: XRD diffractogram for the bulk samples from OS3 (Otumoetai). All peaks are labelled with the associated mineral. Å values presented first represent those measured by the trace and Å values in parentheses represent the ideal value for the selected mineral.

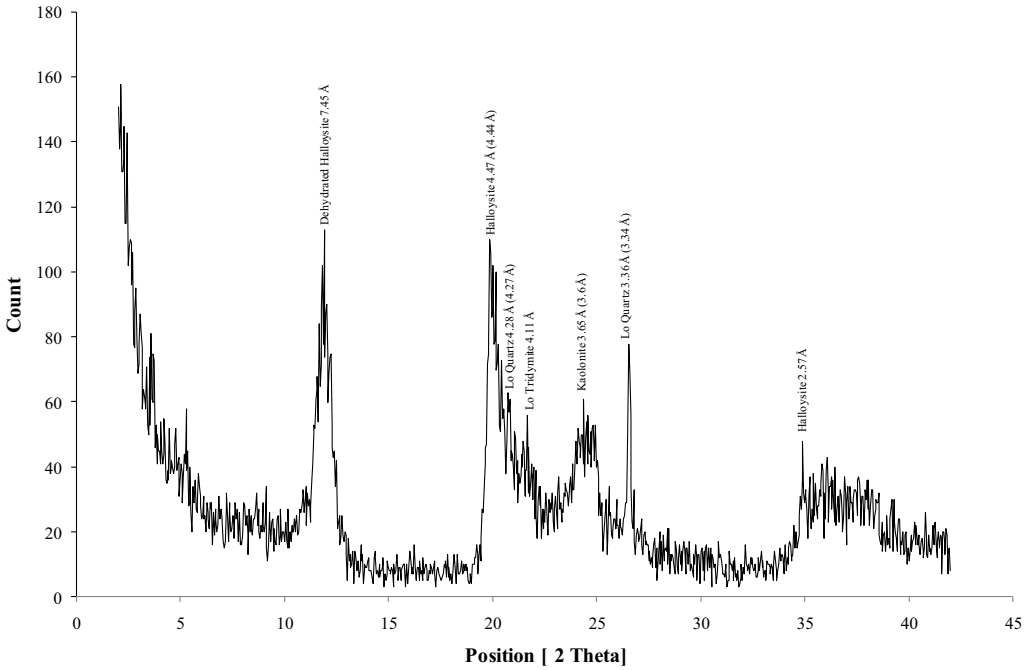

Figure 6.9: XRD diffractogram for the bulk samples from OS4 (Otumoetai). All peaks are labelled with the associated mineral. Å values presented first represent those measured by the trace and Å values in parentheses represent the ideal value for the selected mineral.

6.4.2.2 Clay fraction

The clay fraction results for samples from Otumoetai were similar to those presented for Tauriko, with all samples being dominated by hydrated halloysite. When scanned fully hydrated on ceramic tiles, sharp 001 hydrated halloysite peaks occurred between 9.85 Å and 10.02 Å. These peaks were complemented by the 02, 11 band at ~ 4.4 Å. The 001 peaks expanded to between 10.02 Å to 10.14 Å with the application of formamide (Appendix 6.2). Halloysite was further confirmed by the collapse of the ~10 Å to ~ 7.2 Å on heating at 110 ºC for 1 hour. In all samples, clay peaks disappear after heating for 1 hour at 550 ºC (Appendix 6.2), ruling out any possible micas, chlorites or smectites.

When scanned fully hydrated, OS3 displayed small peaks at ~7.15 Å indicating the presence of kaolinite. After the application of formamide, this peak decreased in size but could still be identified (Figure 6.10).

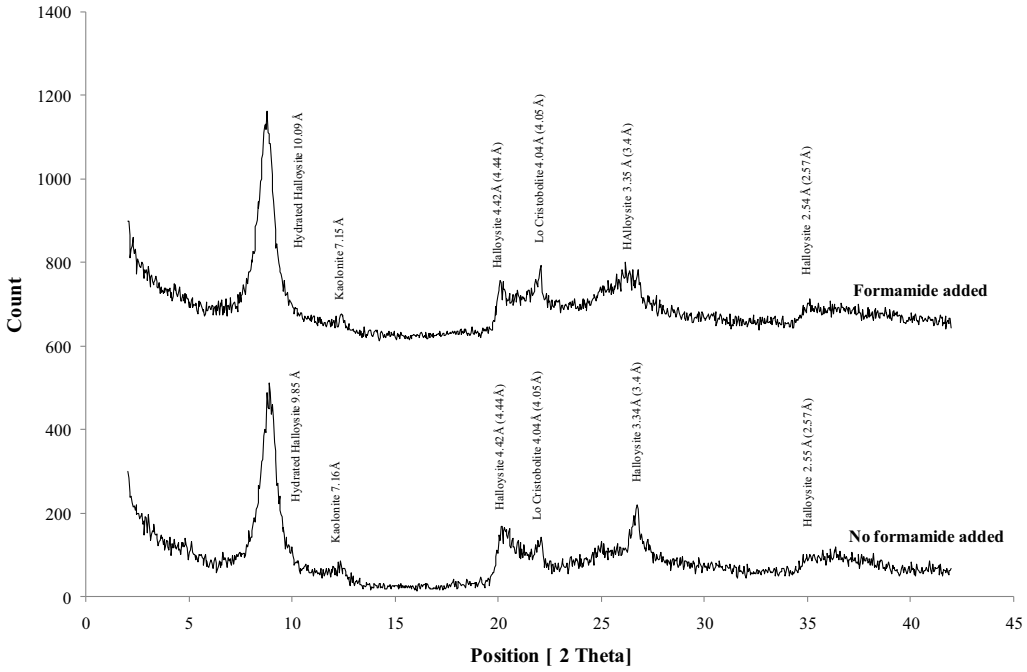

Figure 6.10: XRD diffractogram for clay size fraction for untreated and formamide treated samples from OS3 (Otumoetai). All peaks are labelled with the associated mineral. Å values presented first represent those measured by the trace and Å values in parentheses represent the ideal value for the selected mineral.

Low temperature tridymite and cristobalite peaks occurred in OS1 and OS3, respectively. The peaks observed were still present after the sample was heated to 550 ºC. A small amount of quartz is identified in OS1 and OS3, because

a small quartz peak was observed at ~ 3.34 Å even after the 003 hydrated halloysite peak had shifted to 3.6 Å following heating at 110 ºC for 1 hour (Appendix 6.2).

6.5 Scanning electron microscope

Methods such as XRD provide basic identification of any crystalline mineral. The scanning electron microscope (SEM) can add to XRD findings by providing a morphological image of minerals observed. This ability is especially important for clay when a single mineral can occur as a number of morphologies, a prime example of this polymorphism being halloysite (Joussein *et al.* 2005).

The SEM was employed to investigate both clay and non-clay minerals in samples from Tauriko (TS1, TS2 and TS3) and Otumoetai (OS1, OS2, OS3 and OS4). The SEM coupled with energy dispersive X-ray (EDX) was also used to obtain elemental compositions of certain clay morphologies.

6.5.1 Clay minerals

Because the dominant clay mineralogy was halloysite (section 6.4), SEM was employed to determine its morphology.

6.5.1.1 Tubes

Hollow tubes (Figure 6.11) were found in all samples from both sites but their abundance was greatest in samples from Otumoetai. Tube lengths in Otumoetai samples range from approximately 0.05 μm up to 2 μm (Figures 6.11 and 6.12). In a number of samples the longer tubes appeared to taper at one end (Figure 6.13). Short tubes, between 0.05 μm and 0.4 μm in length, were the dominant morphology in OS3 (Figure 6.12). Longer tubes, up to 2 μm, were the principle tube morphology in OS4 (Figure 6.11). In both OS1 and OS2 observed tubes were normally less than 1 μm in length, but some up to 2 μm long were evident.

When examined under high magnification tubes from OS1, OS3 and OS4 displayed varying degrees of fracturing. Such fracturing was most evident in OS3 (Figure 6.13). Fracturing in Figure 6.13 appeared hexagonal in nature, covered the entire tube and showed no orientation. Ece & Schroder (2007) attributed

hexagonal cracking in clay tubes to volume expansion as a result of cryogenic SEM. The tubes observed in Figure 6.13 have not been subject to cryogenic freezing. However, cracking could also occur as a result of heating under high vacuum (Jock Churchman *pers. com.* 2008).

Hollow tubes were observed in all Tauriko samples, although most abundantly in TS1. Tube sizes ranged between 0.3 µm (Figure 6.14) and 1 µm (Figure 6.15). Unfortunately it was often difficult to distinguish tubes from other matrix material, which may be attributed to their scarcity or small size, or both.

The tubes observed represent the classical morphology of halloysite (White & Dixon 2002; Joussein *et al.* 2005). Generally, tubes are derived from synthesis following the weathering of volcanic glass, pumice, feldspar and mica (Joussein *et al.* 2005). Tube lengths can range from 0.2 µm to >30 µm (Joussein *et al.* 2005). The presence of halloysite tubes in local volcanic material has been confirmed by Salter (1979) who recorded halloysite tubes as a dominant morphology in multiple units in the Kauroa Ash bed sequence. Kirkman (1981) observed tubes in both the Hamilton Ash and Kauroa Ash beds. Tubes in rhyolitic tephra from a number of locations in New Zealand including Te Puke were recorded by Churchman & Theng (1984), whereas Keam (2008) observed tubes in reworked rhyolitic material from Omokoroa, Tauranga.

Other clay minerals have tube-like morphologies. One example is serpentine. However, serpentine tubes are much smaller and have a greater aspect ratio than halloysite (White & Dixon 2002). Imogolite is also observed as packed bunches of hollow fibres. However, these fibres are normally several micrometres in length (White & Dixon 2002), and imogolite is rare in New Zealand soils (Lowe & Percival 1993) but, imogolite has been reported in sensitive soils of the Taranaki region (Jacquet 1990).

In some instances halloysite tubes, up to 0.3 µm, from Tauriko are growing from the edges of plates in books (books are described below in section 6.5.1.4) and stacked much like individual plates (Figure 6.16). These growths may represent a secondary phase of clay formation. Robertson & Eggleton (1991) reported halloysite tubes forming from kaolinite plates resulting from a loss of

structural rigidity along points of the kaolinite crystal. However, Robertson & Eggleton (1991) indicated that the original kaolinite needed freedom of movement and this may not be the case here because of the tightly packed layers in the books. Salter (1979) described clay books from Kauroa Ash beds which had halloysite tubes between and attached to the edges of individual plates. However, the books presented by Salter (1979) displayed clear delimitation, were much larger (> 200 µm long), and the tubes appeared to be more abundant than in Figure 6.16 of this study. Authigenic tube formation was observed in OS3 (Figure 6.17); interestingly the tubes have maintained the crystalline pattern of the primary mineral. Dominant tube formation is occurring parallel to the crystal face of the primary mineral.

Some tubes were observed splitting and unrolling (Figure 6.18). These features are likely to be the result of desiccation (Mitchell & Soga 2005).

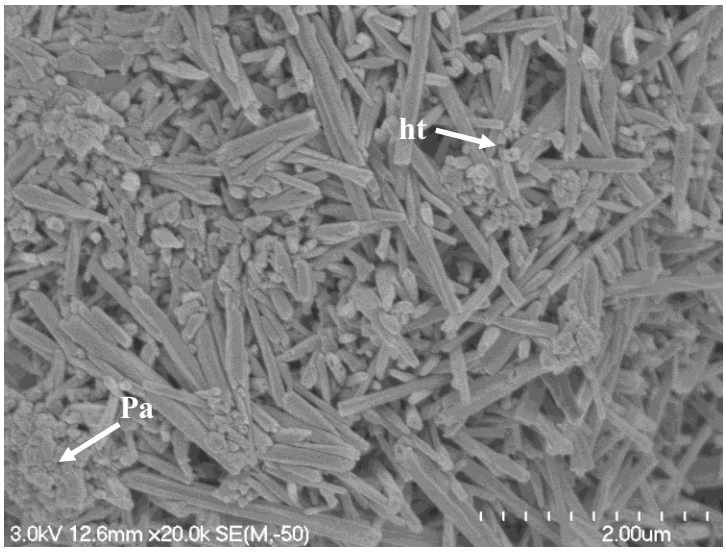

Figure 6.11: SEM image from OS4 (Otumoetai) showing loosely packed hollow tubes. The hollow nature of tubes is identified by the open end of tubes as shown at **ht**. The lengths of individual tubes range between 0.2 µm and 2 µm, longer tubes are clearly dominant. Diameters of tubes are up to 0.2 µm. Intermixed with tubular material are irregularly shaped plates or blocky 'spheres'. The irregular material is < 0.2 µm, and appears to have formed a micro aggregate in the bottom left corner of the image (**pa**). Unfortunately the small size of the non-tubular material makes it difficult to accurately define a shape.

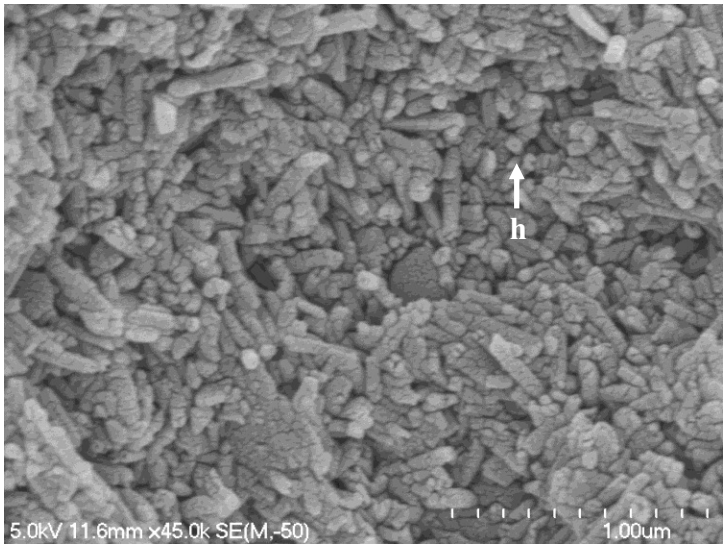

Figure 6.12: Tightly packed tubes and plates observed with scanning electron microscopy for OS3. Tubes are hollow as denoted by **h.** The lengths of individual tubes range between 0.05 µm and ~0.4 µm and have diameters up to 0.1 µm. The surface of all material in the image displays a large amount of un-orientated hexagonal fracturing.

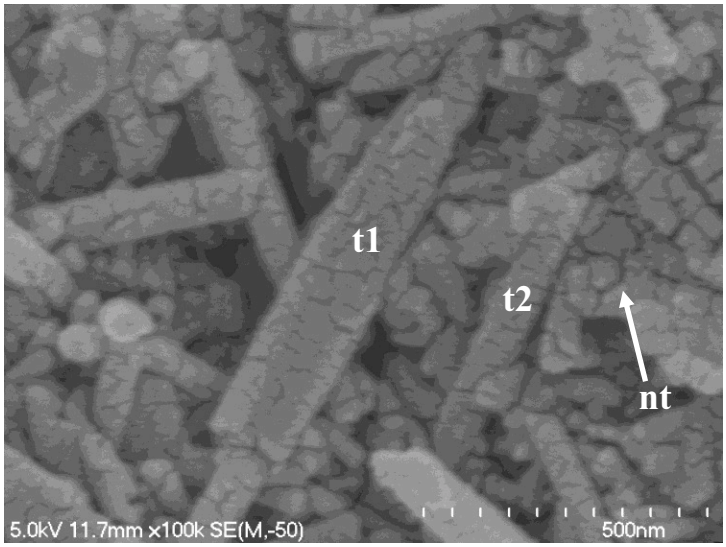

Figure 6.13: Hollow tubes from OS3 (Otumoetai) up to 1.0 µm long displaying un-orientated hexagonal fracturing which extends the entire length of each tube. Non-tubular material also displays fracturing, as indicated by **nt**. The tube located at **t1** appears to taper towards the top of the image, as does the tube at **t2**.

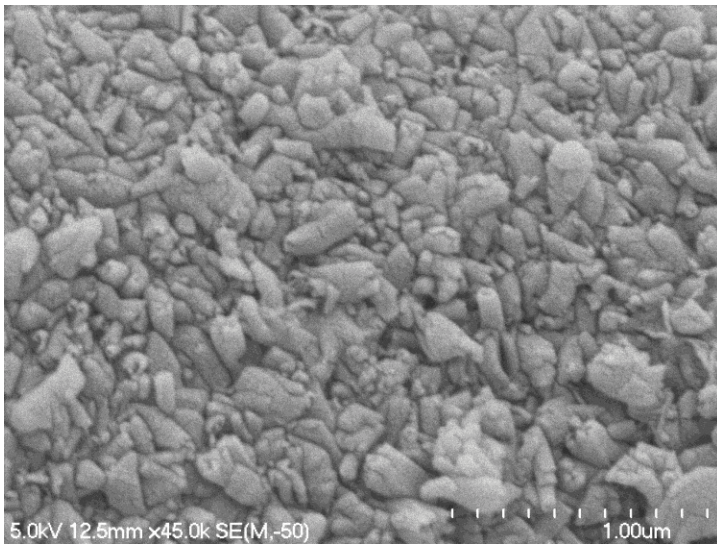

Figure 6.14: SEM image from TS1 (Tauriko) showing tubes up to 0.3 µm long. Also evident are blocky and plate-like materials having a similar range of sizes as the tubes.

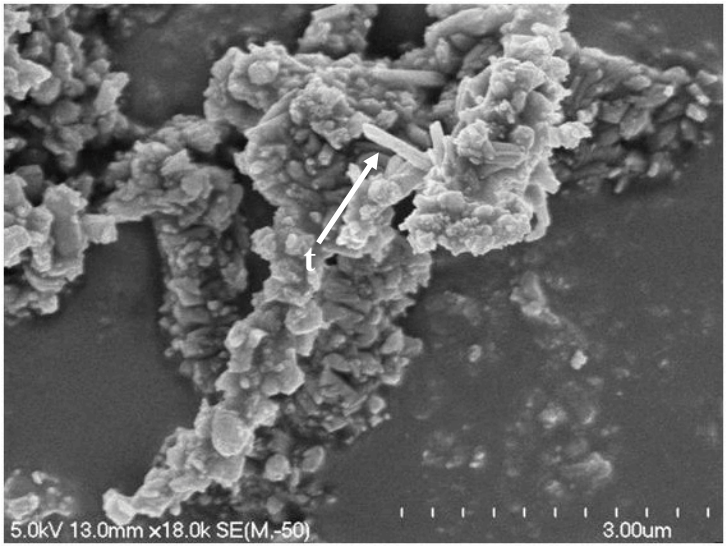

Figure 6.15: Thin hollow tubes, indicated by **t**, from TS1 (Tauriko) up to 1 µm in length and approximately 0.15 µm in diameter radiating from an aggregate of platy material.

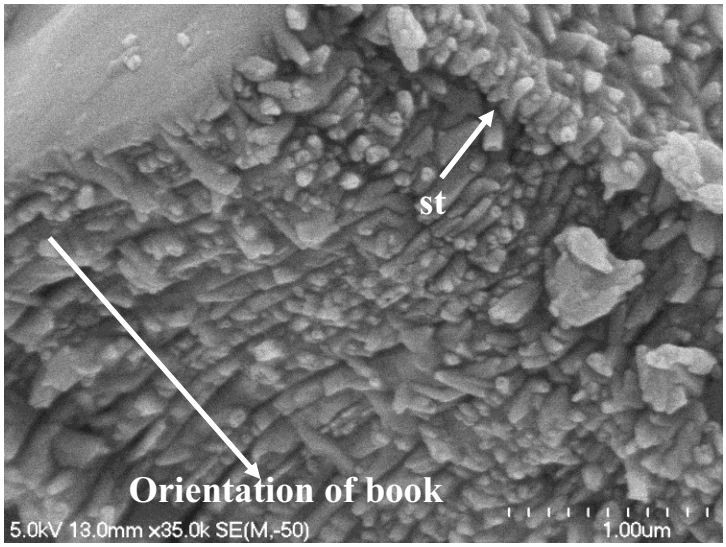

Figure 6.16: A clay book from TS2 (Tauriko) with at least 24 individual plates. The book is orientated diagonally across the image, as indicated by arrow. Interestingly, individual tubes up to 0.3 µm are growing from the edge of individual plates. In the top right hand corner, indicated by **st,** tubes are stacked much like individual plates would be.

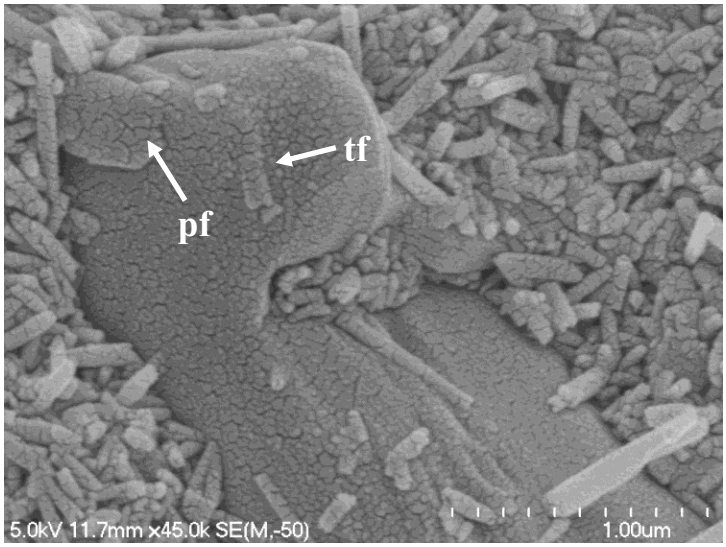

Figure 6.17: Authigenic tube formation in OS3 (Otumoetai), as shown by **tf**, occurring on an unidentified primary mineral. Evidence of plate formation may also be seen in the top left corner of the SEM image **(pf)**. Clay formation appears to be occurring parallel to the surface of the primary mineral. Authigenically formed tubes and plates appear to maintain the crystalline pattern of the parent material.

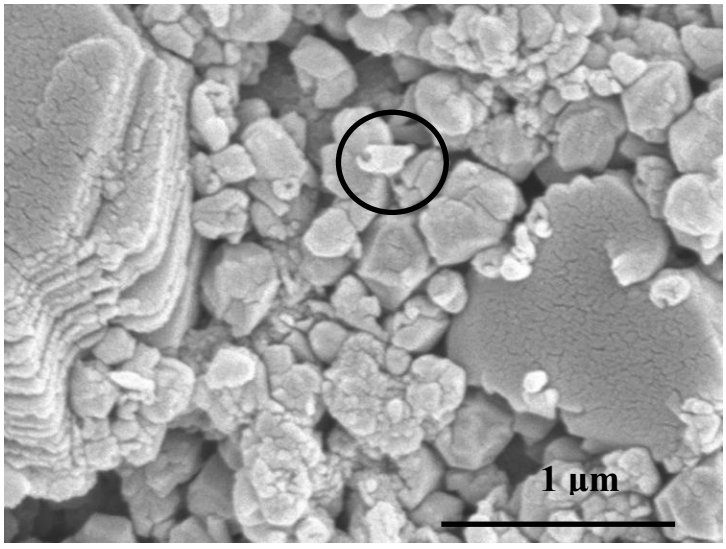

Figure 6.18: SEM images displaying a tube from TS3 splitting and unrolling (in circle).

6.5.1.2 Spheres

Small (less than ~ 0.7 μm) irregularly shaped almost blocky polygonal type spheres (Figure 6.19) were present in the clay fraction at both Tauriko and Otumoetai. In most samples it was difficult to determine whether the material was spherical rather than platy. OS2 from Otumoetai was the only sample where morphologies were clearly spherical (Figure 6.20).

Polygonal type spheres from Tauriko have diameters ranging from 0.1 μm up to ~ 0.7 μm (Figures 6.19 and 6.21). Shapes are typically blocky and never appeared perfectly round. For example, Figure 6.19 shows the flattened polygonal surfaces typically observed. Some larger spheres had surface ridges which appear much like the tubes described earlier (Figure 6.19).

Spheres in samples from Otumoetai appeared to have slightly different morphologies than those in Tauriko samples. For example, polygonal spheres in OS4 were small (0.1 μm across) and irregular with some appearing ovoid (Figure 6.22). Spheres in OS1 had a globular (cauliflower) type morphology with the appearance of a number of small (~ 0.05 μm) spheres combining to become one (Figure 6.23). The spheres in OS2 had a smooth, regular surface and the overall shape was easy to define (Figure 6.20). OS2 had the highest number of easily defined spheres.

These spherical type shapes represent another common morphology of halloysite. Joussein *et al.* (2005) stated that halloysite spheres are commonly formed in weathered volcanic ashes and pumice. It is accepted that morphology may not be perfect and some particles are more pseudo spherical (Joussein *et al.* 2005). For example, Kirkman (1977) observed multifaceted squat cylinders rather than perfect spheres in the weathered Pahoia tuffs (0.35 – 2.18 Ma: Briggs *et al.* 1996) near Opotiki. Bailey (1990) suggested that flattened morphologies may be the result of drying during sample preparation. However, OS2, which was dried during sample preparation, contained regularly shaped spheres (Figure 6.20). Interestingly, the shapes observed in the samples of this study may be linked to weathering, as Ogura *et al.* (2008) found that where weathering was more advanced the spherical shape of halloysite was more easily defined.

Small sphere sizes, as observed in the samples of this study, are not unusual. For example, spheres with diameters of < 0.1 μm have been reported in altered volcanic tuffs (Ece & Schroder 2007) and Holocene-aged volcanic ash (Ogura *et al.* 2008). More specifically, Salter (1979) identified spherical halloysite, with a mean diameter of 0.2 μm, as the dominant clay mineral in three beds from the Kauroa Ash formation. Smalley *et al.* (1980) described spheres with a mean diameter of 0.2 μm from highly sensitive volcaniclastic soils, similar to those under study in this project, at Omokoroa, Tauranga. Comparatively, the squat halloysite cylinders observed in the Pahoia tuffs by Kirkman (1977) were up to 1 μm in diameter.

Al-rich allophane also has a spherical morphology comprised of an imogolite-like structure. The fragments of this structure link to create discrete hollow porous spheres approximately 4 nm (40 Å / 0.004 μm) in diameter. Individual allophane spheres are often found clumped together in aggregates (Parfitt 1990; Lowe & Percival 1993). Because the allophane content measured by extractible Al and Si was very low and because allophane spheres are very small, it is unlikely that any of the spheres observed are allophane.

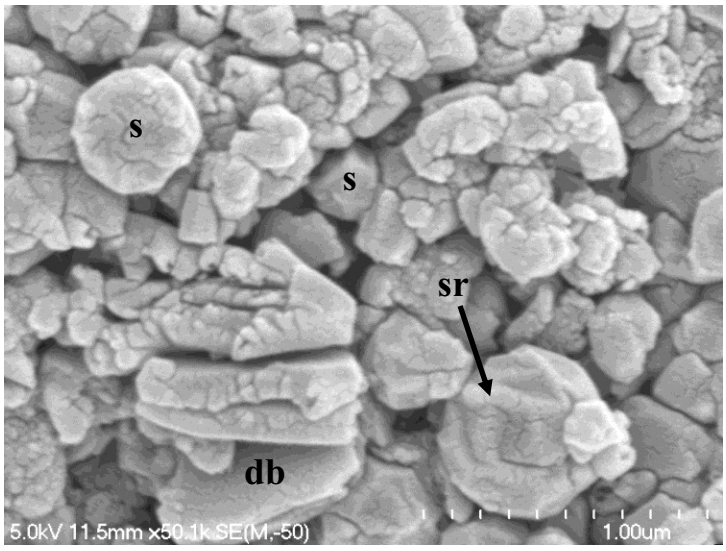

Figure 6.19: SEM image displaying polygonal spheres **(s)** from Tauriko ranging in size from 0.3 to 0.65 in diameter. The sphere at **sr** has surface ridges which appear like tubes. Surrounding the spheres is a slightly delaminated book **(db)** and a number of irregularly shaped and aggregated plates. Some plates may also represent blocky spheres.

Figure 6.20: Easily defined spheres **(s)** up to 0.5 µm in diameter from OS2 (Otumoetai). The image appears to be dominated by spheres of varying size yet some tubes **(t)** < 1.0 µm in length are also present.

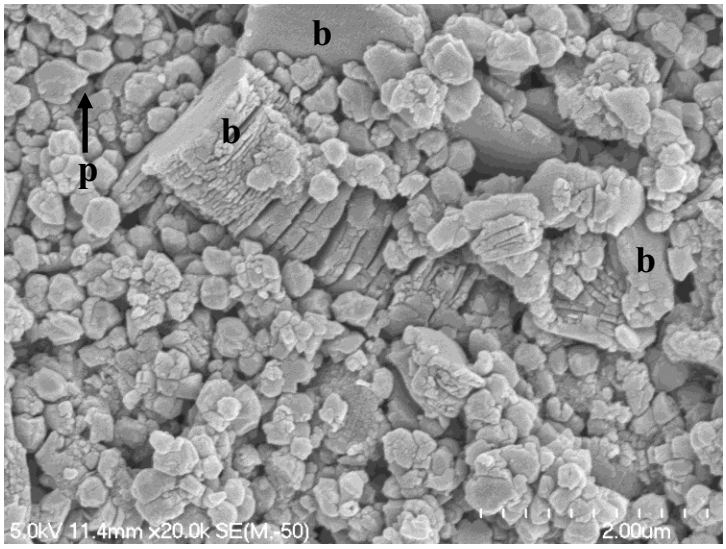

Figure 6.21: SEM image of material from TS3 (Tauriko) displaying at least 3 books **(b)** with the longest being ~ 3 µm in length. Plate thickness differs between the books and also within them. Material surrounding the books includes blocky spheres and plates **(p)**. Because the SEM images lack depth and the image is cluttered with material, it is often difficult to specifically define shapes. Blocky spheres range in size from 0.1 to 0.4 µm. In most instances spheres appear very irregular, almost blocky and have polyhedral flattened faces. Individual plates, not those included in books, are normally irregularly shaped and have diameters up to ~0.5 µm.

Figure 6.22: SEM image of material from OS4 (Otumoetai) showing very small ~0.1µm irregularly shaped spheres. Many spheres appear to be either blocky or show an ovoid shape. Intermixed with the spheres is platy material of similar size. Tubes are present in the centre of the image and appear at least 0.8 µm long.

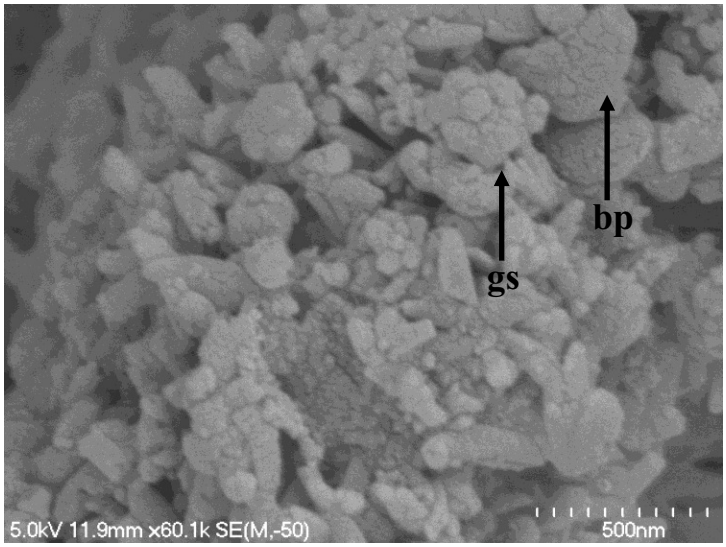

Figure 6.23: SEM image from OS1 (Otumoetai) showing a number of small spheres less than 0.1 μm in diameter forming clusters to form larger spheres (**gs**) up to 0.3 μm in diameter with a globular type appearance. Also observed in this image are narrow < 0.2 μm flat broken plates (**bp**).

6.5.1.3 Plates

Plate morphologies were present in all samples from Tauriko and in OS1, OS3 and OS4 from Otumoetai. Plates in samples from Tauriko were small (less than 0.5 μm in diameter) ranging from irregularly shaped to hexagonal and often display fracturing (Figure 6.24). Because of the lack of depth in SEM images it was difficult to distinguish between flat plates and potentially blocky spheres.

Samples OS3 and OS4 had small, 0.2 to 0.5 μm, highly-fractured irregularly shaped plates (Figure 6.25). All plates in OS3 had rounded edges, but the overall geometry was varied, with plates appearing either hexagonal, irregular, or half oval (Figures 6.25 and 6.26). Plates in OS1 were less frequent but larger than those which occurred in OS3 and OS4 with diameters up to 2 μm (Figure 6.27).

Plates, especially those which are hexagonal, are normally associated with kaolinite (Dixon 1989). However, halloysite plates have been previously associated with volcanic ash soils, tuff beds, weathered pyroclastics and lateric profiles, but are less common than spheres and tubes (Joussien *et al.* 2005). Small size is not uncommon as Noro (1986) reported flat plates of halloysite, from an altered tuff bed, having diameters of ~ 0.3 μm. In New Zealand, blocky halloysite has been reported in hydrothermally altered dacite derived soils at Kauri and rhyolitic/andesitic soils from Te Puke (Churchman & Theng 1984).

The plates from OS3 cannot be confidently identified as halloysite because of the small kaolinite peak which remained after addition of formamide during

XRD analysis (Figure 6.10). Thus it could be suggested that these plates are kaolinite. This would be logical as the plates are only a very minor fraction in both samples and the kaolinite observed in the clay size fraction XRD trace was only very small, thus indicating that kaolinite will not be very abundant if present. This is not the case for plates observed in the clay fraction of Tauriko samples because kaolinite is not identified in any of the XRD traces.

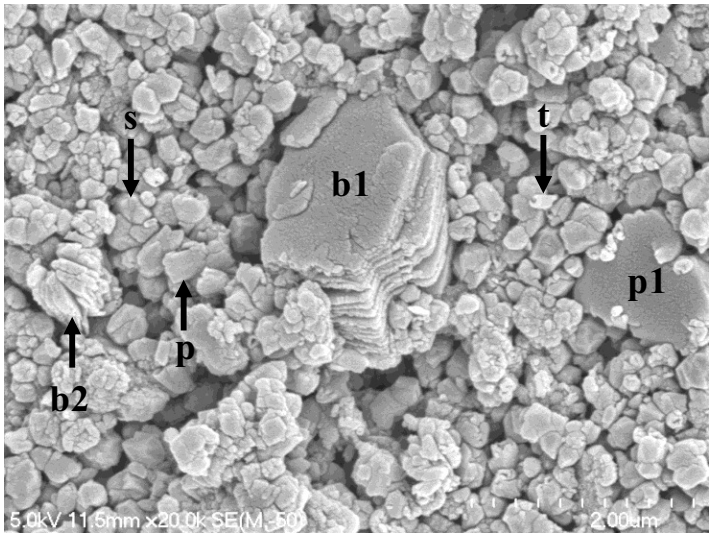

Figure 6.24: SEM image from TS3 (Tauriko) showing highly irregular spheres **(s)** and plates **(p)**. Spheres appear almost blocky with flattened polyhedral faces and diameters up to 0.3 µm. The plates intermixed with the irregular spheres have diameters up to 0.6 µm and shapes are either elongated, irregular or disk like. Tubes **(t)** are only sparsely present. Within the background of spheres, plates and tubes are books **(b1)**. Plates which make up the books are ~1 µm in diameter and appear to be pseudo hexagonal. Another smaller book is located at **(b2)** the plates in which appear slightly delaminated. The large irregular plate at **(p1)** is possibly the top of another book.

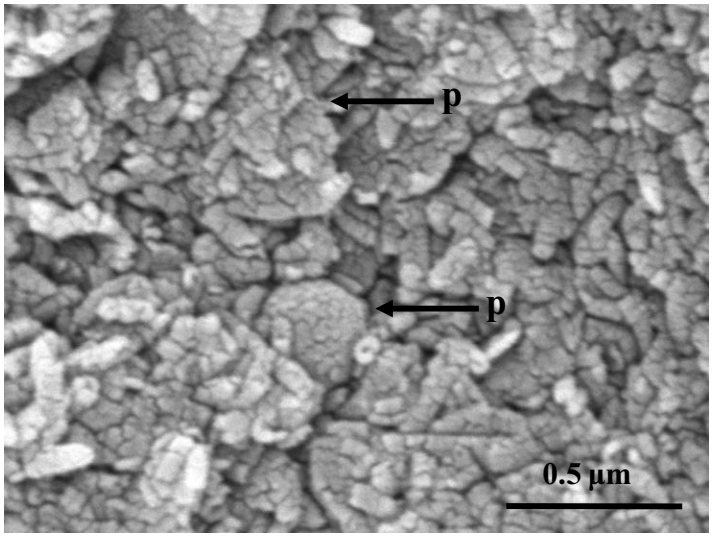

Figure 6.25: Flat plates (**p**) up to 0.5 µm in width from OS3 (Otumoetai) surrounded by short tubes up to 0.3 µm in length.

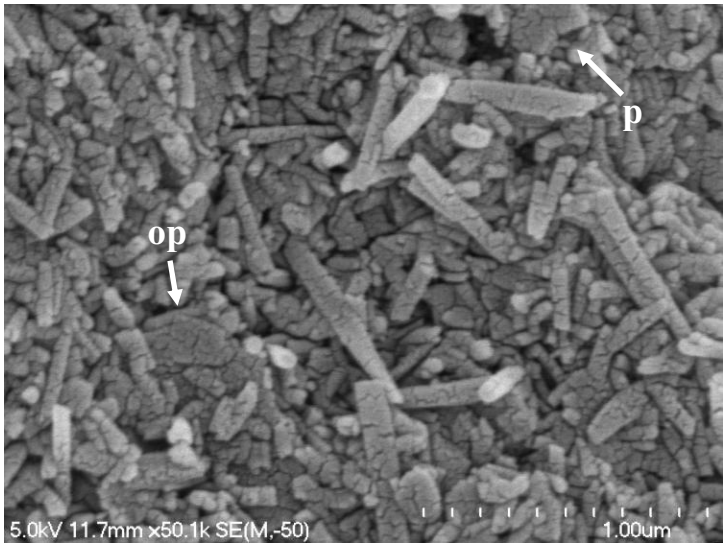

Figure 6.26: Fractured tubes and plates in OS3 (Otumoetai). Tubes are up to 0.7 μm in length. Whilst the edges of individual plates (**p**) are difficult to define they appear to be irregularly shaped and up to 0.5 μm in diameter. One plate appears to be showing an oval type shape (**op**).

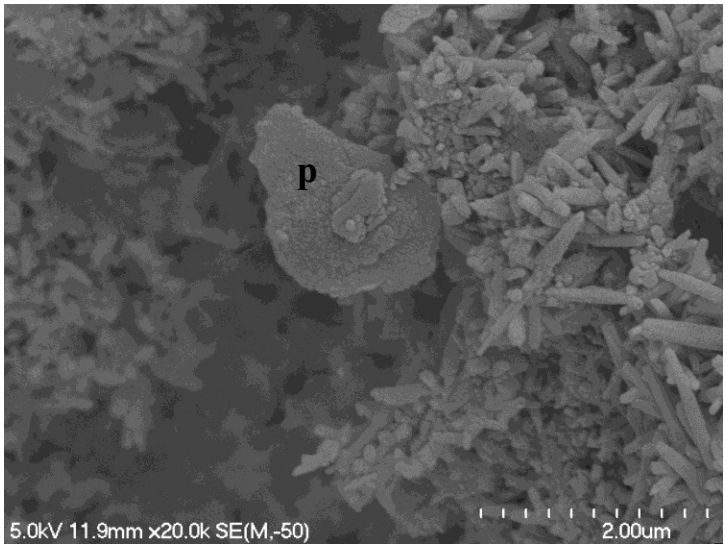

Figure 6.27: SEM image displaying a plate (**p**) from OS1 (Otumoetai) approximately 2 μm in diameter.

6.5.1.4 Books

Whilst individual plates were characteristically small (< 0.5 μm), other larger plates were present but they appeared to be stacked in vermiforms (books) (Figure 6.28). Books are only present in Tauriko samples and abundance was greatest in TS3 and least in TS2.

A variety of plate shapes occurred for each individual book. Shapes were irregular (Figure 6.28), pseudo-hexagonal (Figure 6.24) and elongated (Figure 6.29). Individual plate widths in each of the books ranged from ~ 1 μm (Figure 6.28) to ~ 20 μm (Figure 6.29). The contact between each plate was normally tight, but some books displayed minor delamination at either the edges or centre of individual plates (Figure 6.30). Some books were completely delaminated, with

infilling material (Figure 6.31). Poor clarity during SEM imaging means the material between delaminating plates was difficult to define, but this material would logically be best described as the other smaller morphologies of halloysite, i.e. tubes, spheres or small plates.

Book lengths ranged from ~ 1.5 μm long (Figure 6.32) to ~ 50 μm long. Books were generally curved, with bends and undulations of the parallel sides (Figure 6.30). Some appeared nearly U shaped (Figure 6.33) whilst others were worm shaped or weakly helical (Figure 6.34).

Clay books are a common kaolinite morphology (Dixon 1989; White & Dixon 2002), yet Bailey (1990) stated that kaolinite and halloysite cannot be distinguished by morphology alone. XRD traces of the clay-size fractions and bulk samples from Tauriko indicated strongly that the books were halloysite. Whilst halloysite can occur in a range of morphologies it has never previously been observed as books (see detailed review by Joussien *et al.* 2005). Furthermore, the infrequent yet positive identification of halloysite as plates in other soils (Churchman & Theng 1984; Noro 1986; Joussien *et al.* 2005) lends some confidence to the identification here of halloysite, uniquely, with a book morphology.

XRD traces present indisputable evidence that the book material observed in the clay-size fraction of all Tauriko samples can only be halloysite and not kaolinite. This was because peaks only occurred at ~ 10 Å, representing hydrated halloysite and not at 7.15 Å which would indicate kaolinite. To further confirm identification as halloysite alone, clay-sized fraction specimens analysed by XRD from TS3 were examined with the SEM. From this, books were observed comprising at least 10% of the sample. This was less frequent than that observed in the bulk sample (up to 30%), but if the books were kaolinite one would expect at least a minor peak at 7.15 Å. This conclusion is based on the reasoning that kaolinite gives a stronger reflection than halloysite for the same amount of material (Jock Churchman, *pers. com*. 2008). For example, Churchman *et al.* (1984) showed XRD patterns for a mixture of 60% halloysite and 40% kaolinite. After treatment with formamide the ~ 10 Å halloysite peak was lower in height than the ~ 7 Å peak for kaolinite.

Discussion in section 6.4.1.1 indicates that the 7.33 Å and 7.41 Å peaks in the bulk fraction were more likely to be dehydrated halloysite rather than kaolinite (Figures 6.1, 6.2 and 6.3). In conclusion, the books that were observed in the clay fraction were certainly halloysite and it was almost certain that those observed in the bulk sample were also halloysite.

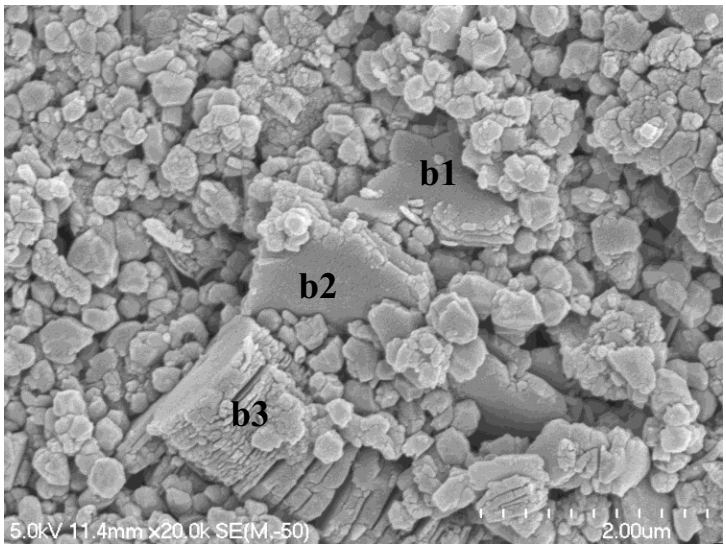

Figure 6.28: SEM image from OS3 displaying at least 3 books **(b1 – b3)**. The plates in books **b1** and **b2** appear to be irregularly shaped. The material surrounding the plates is dominated by small flat plates up to 0.5 µm in diameter. Some of this material also appears blocky, and less plate-like.

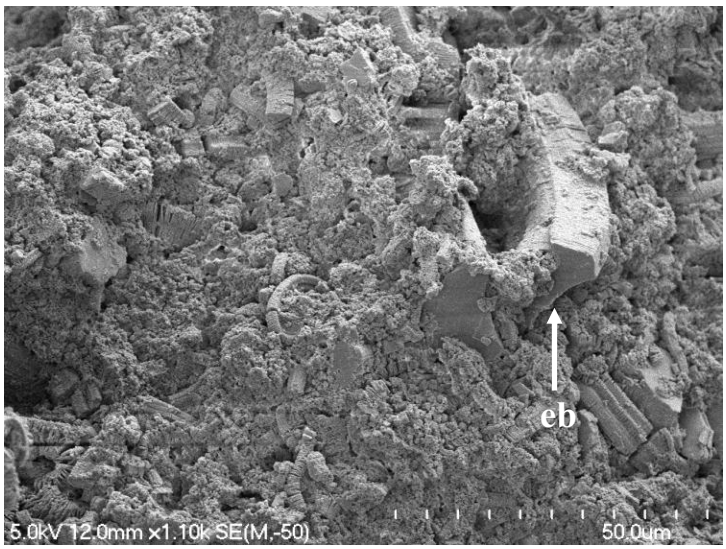

Figure 6.29: Large number of clay books from TS3 (Tauriko) supported by smaller non-book-like material. Of most interest are the books at **eb**. These books appear to be made up of highly elongated plates ~ 20 µm across.

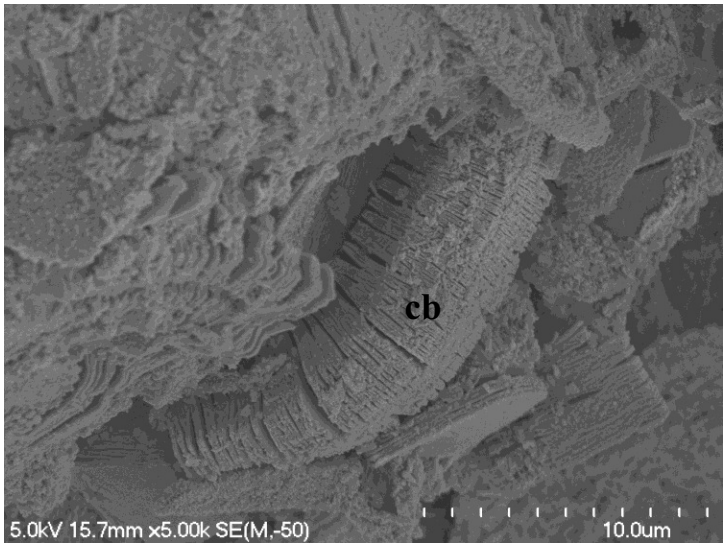

Figure 6.30: Curved book from TS1 (Tauriko) **(cb)**. The book is ~ 18 µm long and ~ 6 µm wide; plates which make up the book appear hexagonal. The book at **cb** displays minor delamination of plates both in the centre of the book and along the edges.

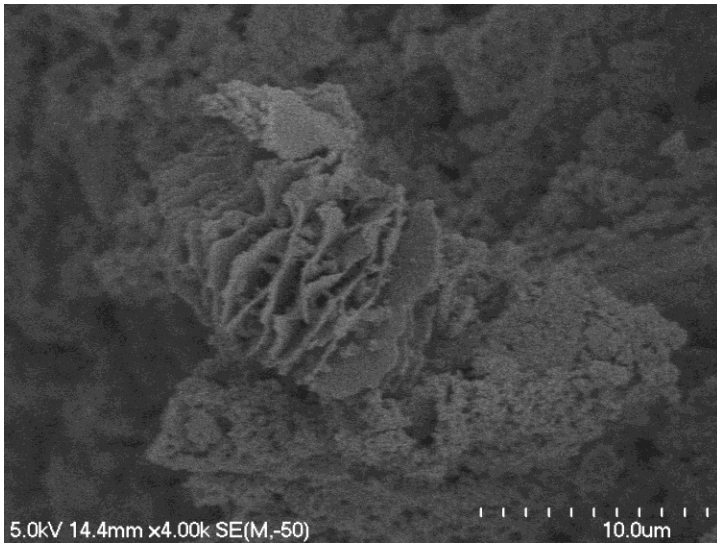

Figure 6.31: Book from TS1 (Tauriko) with plates ~ 10 µm across showing complete delamination. Materials infilling between the plates are possibly tubes, spheres and smaller plates. Unfortunately poor image clarity makes infill material hard to define.

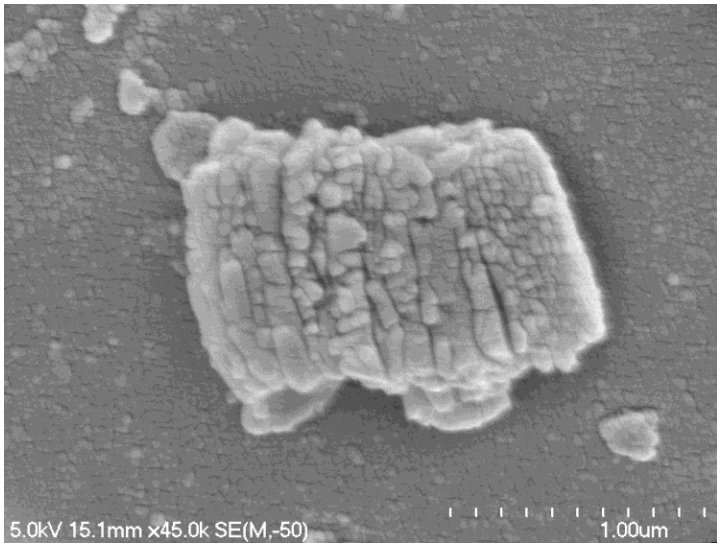

Figure 6.32: Small book ~ 1.5 µm in length. Plates are different widths and each appears highly fractured.

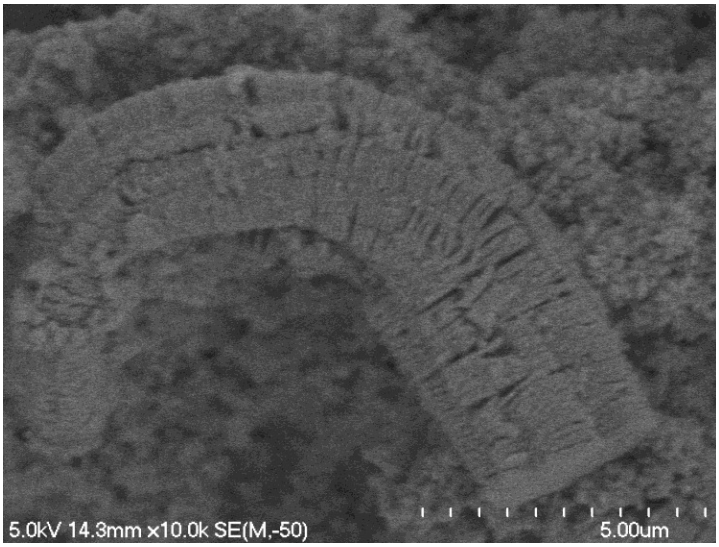

Figure 6.33: SEM image of a curved book from TS1 (Tauriko). The book is ~ 15 µm long with plates ~ 3 µm in diameter.

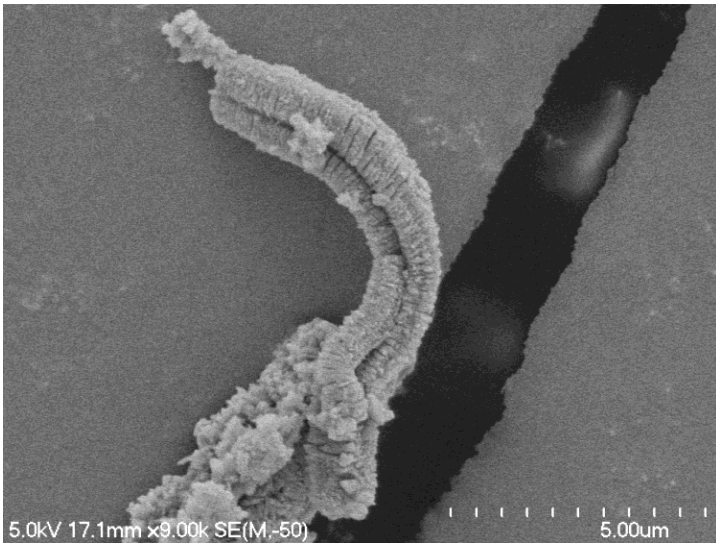

Figure 6.34: SEM image of a worm-shaped (helical) book from TS1 (Tauriko) ~ 10 µm long. Each plate appears to be ~ 1.5 µm in diameter.

6.5.1.5 Elemental analysis of clay minerals

EDX analysis was undertaken on books from Tauriko and tubes from Otumoetai in order to determine their elemental compositions. All raw EDX analysis values are presented in Appendix 6.3. Previous workers have established that structural Fe content is an important determinant of halloysite morphology especially in the case of plates and tubes (Joussien *et al.* 2005). Plates are considered to have high iron contents whilst tubes have less (Bailey 1990). By analogy one would expect books to have high structural Fe contents because they comprise many plates. Spheroidal halloysite is not included because Fe content is thought to have little influence on spheroidal morphology: Fe content can range from zero to values which are comparable with those of plates (Churchman & Theng 1984; Noro 1986; Johnson *et al.* 1990).

Seven books in total were investigated. Analysis focused on the top plate, or 'leaf', of the books. All books analysed came from the TS3 clay fraction XRD sample to ensure that the books examined were halloysite. An example of a book which was analysed is presented in Figure 6.35. A direct comparison between books and tubes in Tauriko material was not possible because tubes were too narrow for individual analysis. Furthermore, tubes were typically observed intermixed with spheriodal and platy material so could not be analysed as clusters.

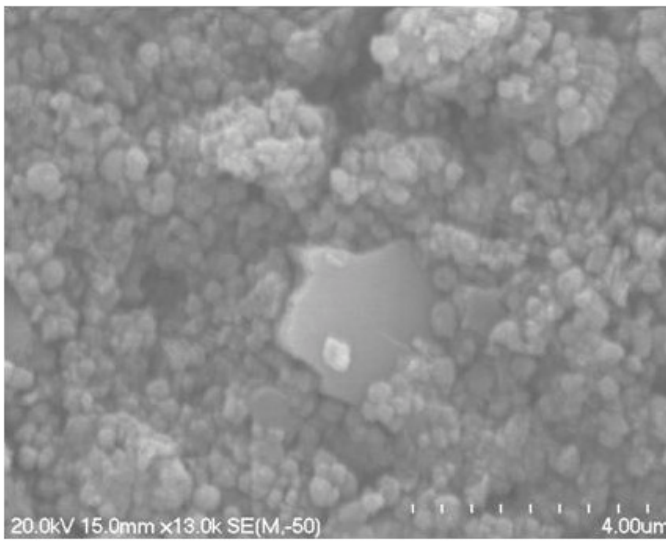

Figure 6.35: SEM image from TS3 displaying the top plate of a book which was analysed for elemental properties using EDX. Note that the area analysed included only the surface of the book. The image quality is reduced because of the high accelerating voltage (20 kV).

Because samples from Otumoetai contained a large amount of halloysite tubes it was possible to analyse these in clusters. Twelve clusters of tubes were investigated from OS4 Otumoetai and an example is presented in Figure 6.36. It is important to point out that this method does incorporate the risk of scanning some non-tubular material. Also, the accuracy of results is somewhat diminished because a flat surface was not examined. A cluster of tubes recorded an Fe content of 2.6 ± 0.32% and on replication the result was 3.8 ± 0.71%. Nevertheless a Student t-test of these two results showed the assays to be insignificantly different (95% probability). Nevertheless, the following results should be examined with some caution. It should be noted that samples have not been deferrated so are not free of possible Fe impurities. However, the method used here does focus on individual particles rather than a bulk analysis, probably eliminating this potential problem.

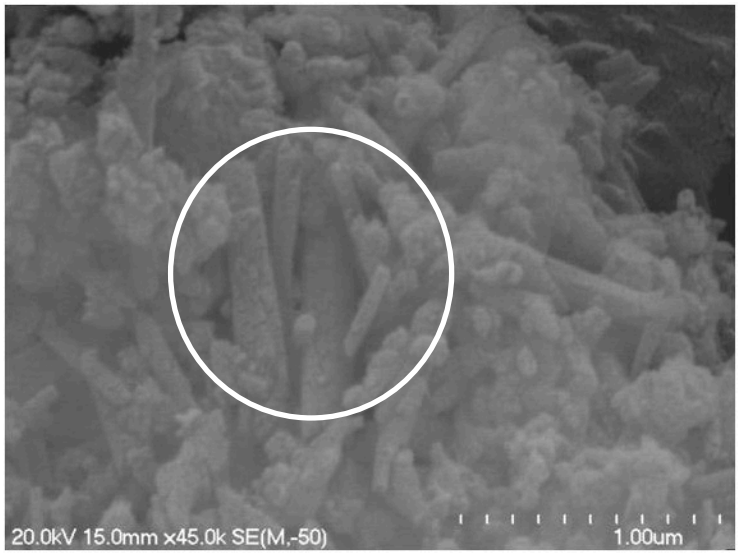

Figure 6.36: SEM image of a cluster of tubes which were investigated with EDX analysis. The analysis focused on a much closer section in the centre of the image, as indicated by the circle. Note the image quality is reduced because of the high accelerating voltage (20 kV).

Table 6.5 presents Al_2O_3, SiO_2, and Fe_2O_3 values for books from Tauriko and tubes from Otumoetai. The values presented in Table 6.5 have been stoichiometrically converted to oxides from Al, Si and Fe using multipliers of 1.889, 2.139 and 1.430, respectively, which are found in Berkman (2004). EDX analysis also recorded C and Pt. These elements were excluded from calculation because they are from sample mounting and coating material, respectively (see blank analysis in Appendix 6.3). Some samples recorded elements such as Mg, Ge and Cl, with the highest value being 1.15%. These elements may represent contaminants or material on exchange sites.

Table 6.5: Percentages of Al_2O_3, SiO_2 and Fe_2O_3 for books from Tauriko and tubes from Otumoetai.

Compound	Books	Tubes
Al_2O_3	34.1 ± 0.5	34.2 ± 1.3
SiO_2	47.7 ± 1.1	50.7 ± 2.1
Fe_2O_3*	5.2 ± 0.2	3.17 ± 0.3

*All Fe expressed as Fe_2O_3

Results presented in Table 6.5 indicate that when errors are included the mean Al_2O_3 and SiO_2 values are the same. Student t-tests indicated that there was no significant difference between the Al_2O_3 and SiO_2 values presented for tubes and books, with p values of 0.94 and 0.20, respectively. The SiO_2 values in Table 6.5 were higher than those of the Hamilton Ash (40.7 and 45.6%) (Shepherd 1984, as cited in Lowe & Percival 1993). The Al_2O_3 values (Table 6.5) were within the range of those for the Hamilton Ash (32.4 to 42.4 %). The Fe value for

books was higher (~ 5.2 %) than that presented for tubes (~ 3.2 %) (Table 6.5). A students t-test indicated that the difference in Fe_2O_3 between the books and tubes was significant ($p = 4.1 \times 10^{-5}$). Consequently it is likely that the Fe content (as Fe_2O_3) is higher in books than in tubes.

When the Fe_2O_3 data for books and tubes (Table 6.5) were presented as box and whisker plots (Figure 6.37), the upper range for tubes extended into the book values, and the total range of values was greater. This indicated the variability in tube results. However the majority of the Fe_2O_3 data, which occurred between the first and third quartile, were higher for books than tubes.

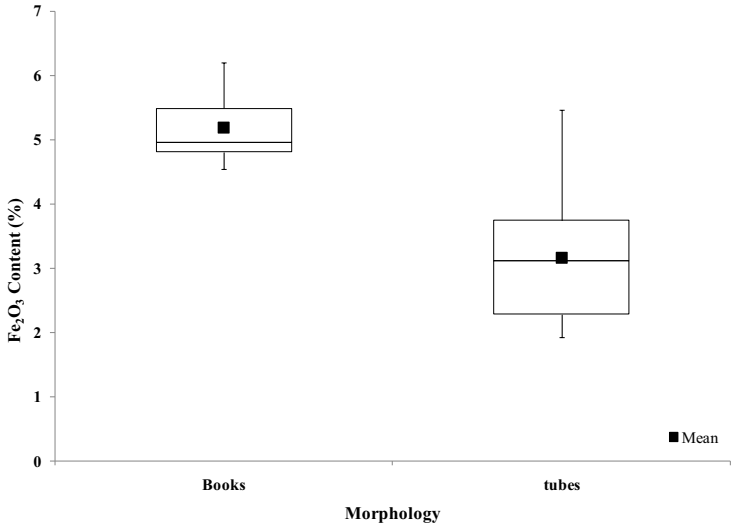

Figure 6.37: Box and whisker plot of Fe_2O_3 for two morphologies: books from Tauriko and tubes from Otumoetai. The black square represents the mean value.

The mean Fe_2O_3 content of books (~ 5.2 %) was higher than values of 3.33 % and 3.07 % (as Fe_2O_3) for untreated and deferrated halloysite plates examined by Soma *et al.* (1992), for samples from Te Puke. Tube Fe_2O_3 values (~ 3.2 %) in this study were within the values presented for untreated (0.24 % – 8.14 %) and deferrated (0.26 – 3.55 %) tubes by Soma *et al.* (1992), when his Fe values were converted to Fe_2O_3. However, their analysis examined the bulk soil fraction with XRF and the platy samples included a minor amount of tubes and spheres. Tube Fe_2O_3 content (~ 3.2 %) was higher than that presented for 'short' tubes (2.4 % to 2.6 %) and 'long' tubes (0.2 to 0.8%) by Noro (1986). However, no size range was presented for his/her tube samples.

Books are within the typical range of Fe_2O_3 (~ 2 to ~ 6%) found in plates. Tubes in this study were at the upper limit of typical values for long tubes (0 to ~

3.5 %) and were greater than the typical values for short tubes (~ 0.2 to ~ 2.8) (Figure 6.38)

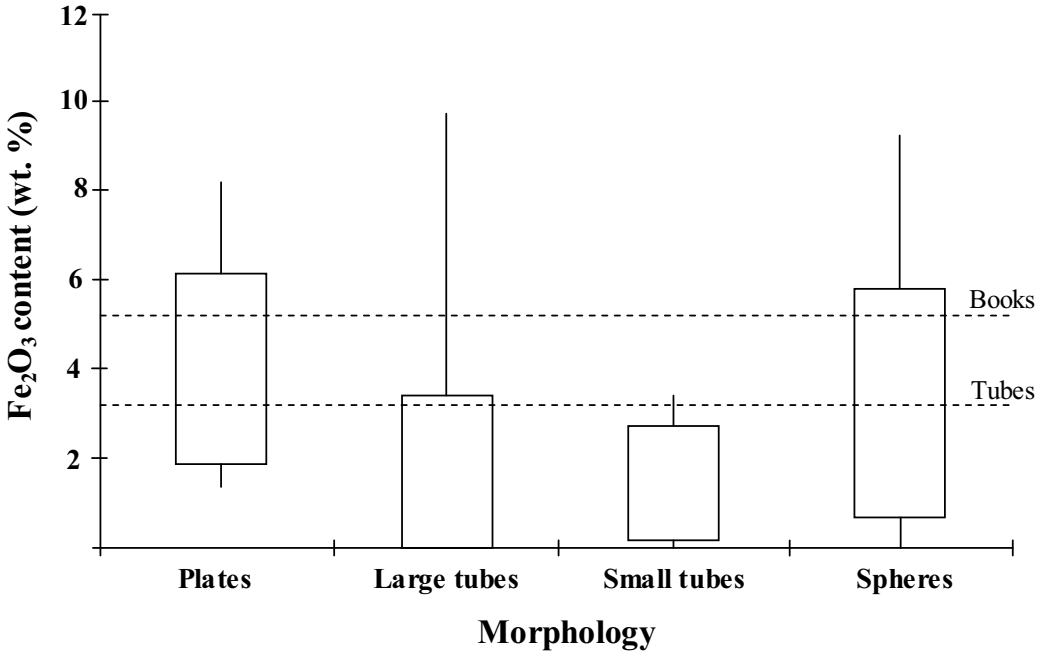

Figure 6.38: Main halloysite morphologies versus Fe content (as Fe_2O_3) from data in the literature compiled by Joussein *et al.* (2005). Included in this graph are dashed lines which represent the Fe contents measured in this study for books and tubes.

6.5.2 Non-clay material

6.5.2.1 Tauriko

Non-clay mineral grains ranged in size from 18 μm (Figure 6.39) to 420 μm (Figure 6.40) and the distribution of sizes was similar for all samples. Volcanic glass (Figure 6.41) was the most abundant non-clay mineral observed in all samples from Tauriko, using SEM analysis. Glass fragments ranged in size from 30 μm (Figure 6.41) to 330 μm (Figure 6.42), although most material was < 120 μm with the median size being ~ 75 μm. Shapes were typically angular (Figure 6.41), but flat triangular plates, long thin shards and irregular shapes were also observed (Figures 6.43, 6.44 and 6.45). Most glass fragments were dominated by conchoidal shaped depressions. These depressions represented either fracturing or the edges of vesicle walls (Figure 6.46). Internal vesicles were only observed in three glass minerals, ranging in size from 2 μm (Figure 6.41) to 180 μm (Figure 6.42). EDX analysis on three of the glass textures showed high levels of SiO2 and also the presence of Al2O3, K2O, FeO, Na2O and CaO, which are typical of

rhyolitic glass (e.g. Lowe *et al.* 2008b) (see Appendix 6.3 for EDX values of glass from this study).

Feldspar, probably plagioclase, was present in TS1 and TS3 and crystals ranged in size from 70 µm (Figure 6.47) to 420 µm (Figure 6.40). The identification of plagioclase is based on cleavage, which was observed along two axes at ~ 90º. Typically the feldspar was blocky with sub-angular edges (Figures 6.40 and 6.47).

Other mineral shapes in each sample were both angular and blocky (Figure 6.48), which may represent quartz.

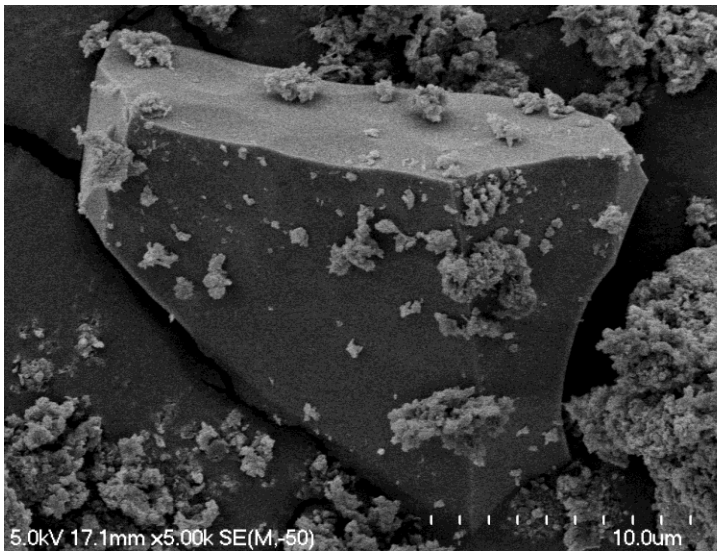

Figure 6.39: Small angular grain (possibly quartz) observed at TS1 which is ~18 µm along its longest dimension.

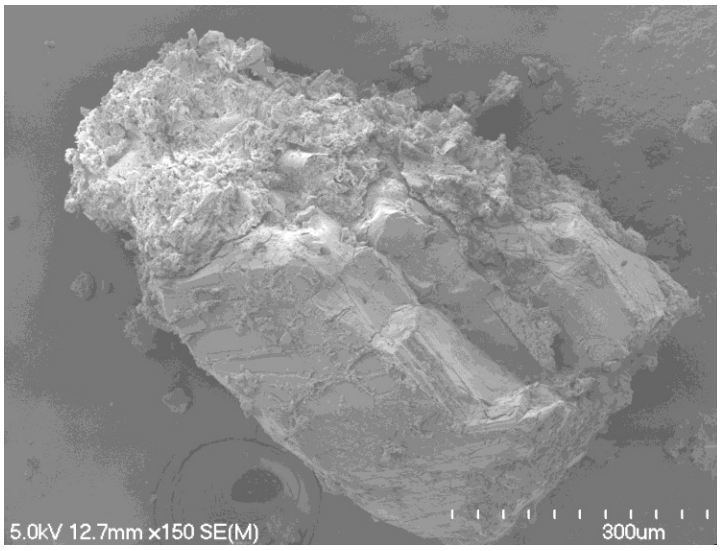

Figure 6.40: Large blocky feldspar mineral from TS3 ~ 420 µm long.

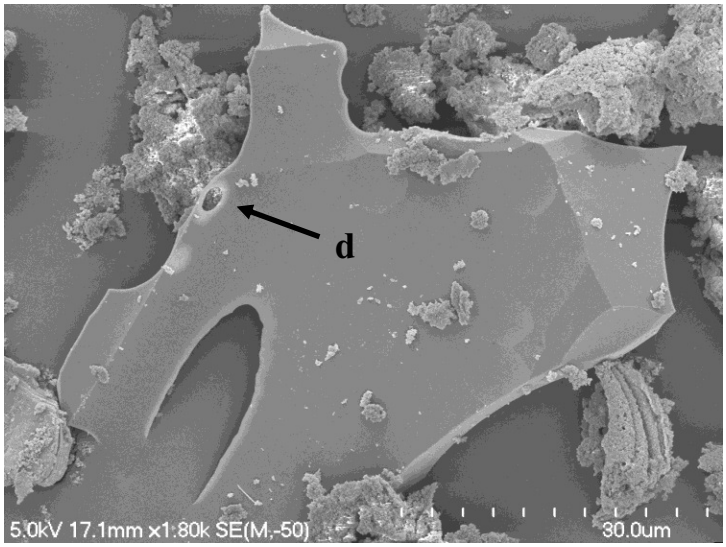

Figure 6.41: Angular glass fragment ~ 30 µm in length. Small hole (~ 2 µm) marked by **d** indicates either dissolution as a result of weathering or a small vesicle.

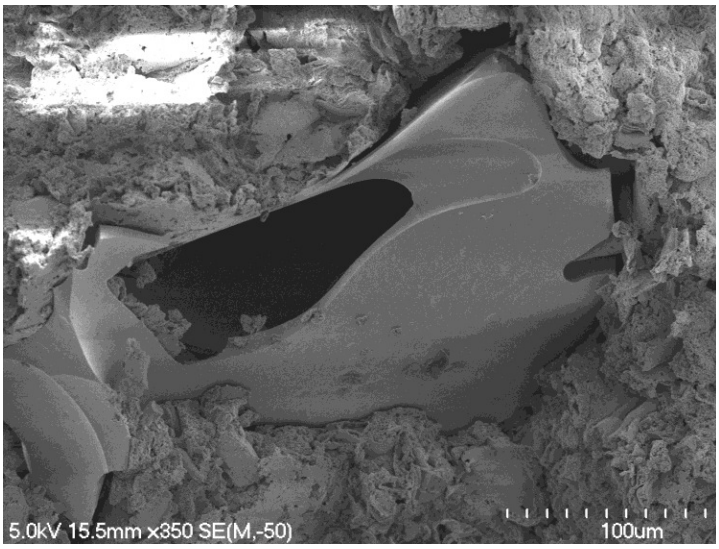

Figure 6.42: Glass fragment 330 µm in length, with a large 180 µm long elongated central vesicle displaying minor infilling.

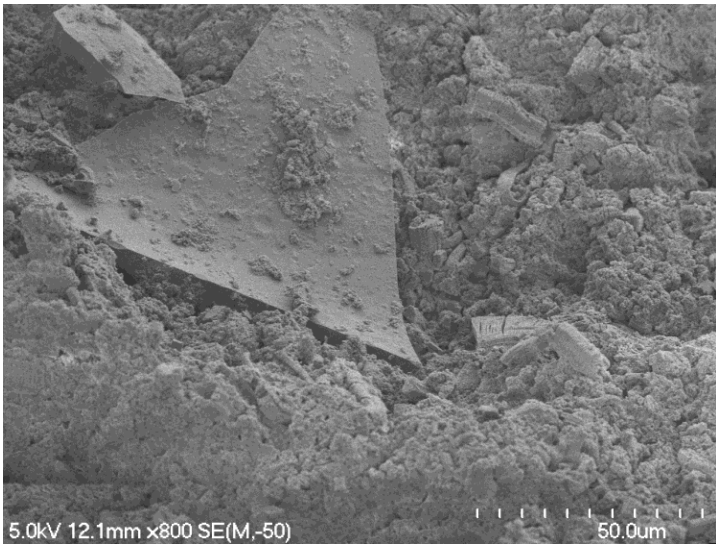

Figure 6.43: Flat triangular plate, probably volcanic glass ~ 60 µm in length.

Figure 6.44: Long slender glass shard (**gs**) ~ 80 μm long.

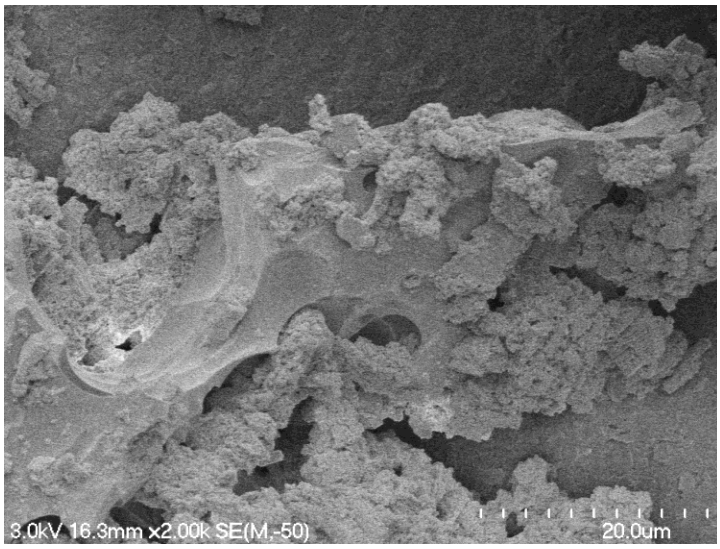

Figure 6.45: Irregularly shaped glass shard ~ 70 μm long showing conchoidal fracturing and cuspate depressions and abundant adhering surface material.

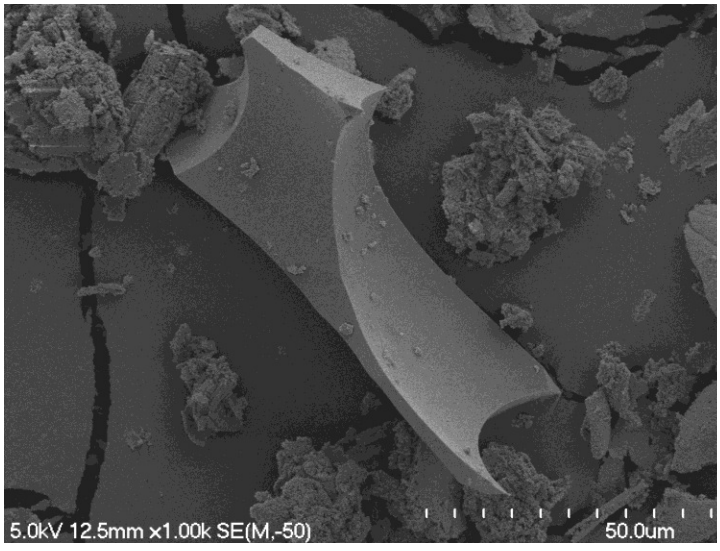

Figure 6.46: Volcanic glass fragment from Tauriko, the conchoidal fracturing represents bubble walls.

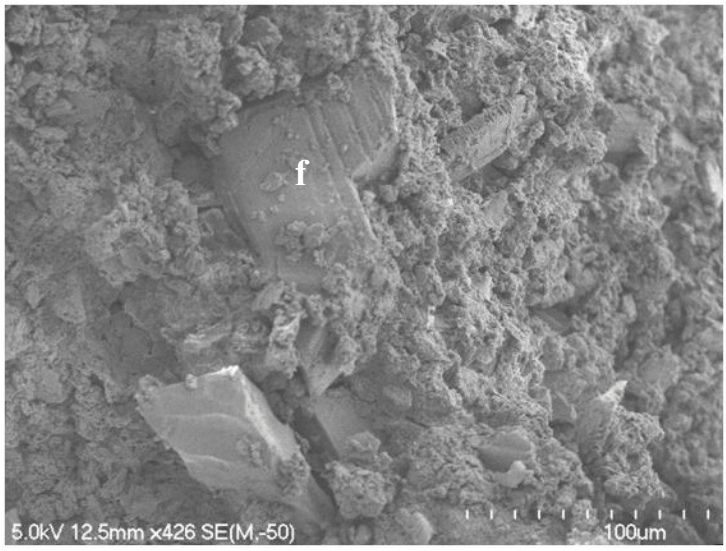

Figure 6.47: Blocky feldspar **(f)** crystal from TS3 up to 70 µm long displaying cleavage in two directions at 90º.

Figure 6.48: SEM image from TS1 Tauriko showing a blocky quartz (**q**) grain with sub angular edges which is ~ 190 µm across. Surrounding the quartz mineral are irregularly shaped materials which are likely volcanic glass fragments. Note the conchoidal depression at **con**.

6.5.2.2 Otumoetai

Across all samples, mineral sizes ranged from 3 µm to 750 µm (0.750 mm). Grains were typically smaller in OS3 when compared to other samples, with a maximum size of 60 µm (Figure 6.49). Infrequent large grains up to 750 µm and 850 µm (Figures 6.50 and 6.51) in length were observed in OS4 and OS2, respectively. The largest grain observed in OS1 was 160 µm. Shapes from all Otumoetai samples were blocky (Figure 6.52), platy (Figure 6.53) and angular (Figure 6.54). In OS1, OS2 and OS4, the edges of grains ranged between angular and sub-rounded. Alteration was not observed in OS1 and OS4, but was evident in OS2 (Figure 6.55). Grains in OS3 appeared more rounded than those in other samples and some alteration was present (Figure 6.17).

Biotite, with its distinctive hexagonal shape (Figure 6.49) and basal cleavage (Figure 6.50), was present in OS1, OS3 and OS4. Sizes observed ranged between 4 μm (Figure 6.56) and 750 μm (Figure 6.50). In OS1, OS2 and OS4 quartz was present and displayed conchiodal fracturing and had anhedral crystal faces (Figure 6.57). Volcanic glass was not positively identified using SEM in any of the samples from Otumoetai.

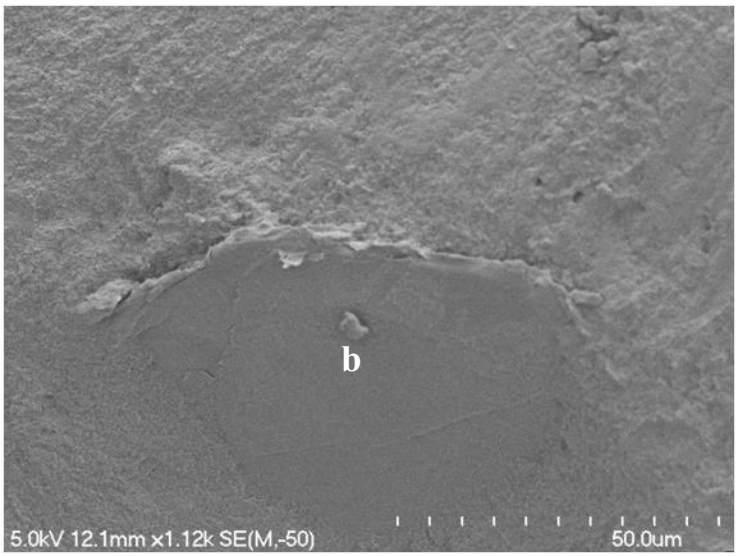

Figure 6.49: Biotite **(b)** mineral from OS3 which is at least 60 μm in diameter. A section of the typical hexagonal shape can be observed.

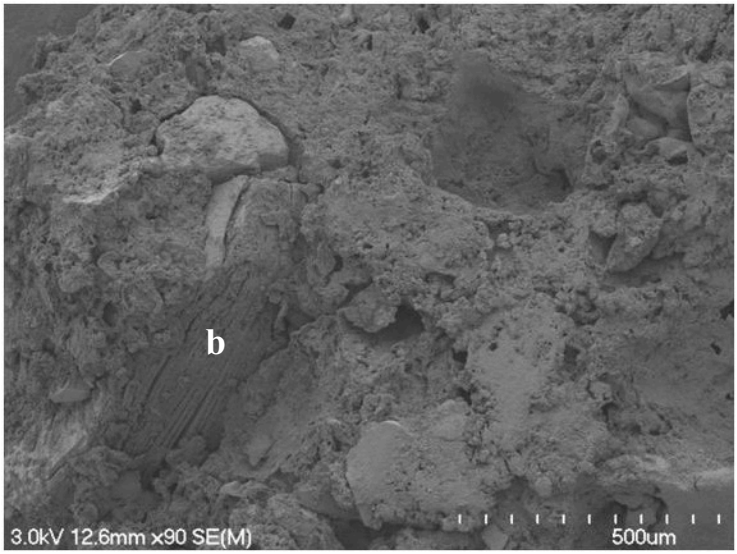

Figure 6.50: Exfoliating biotite **(b)** grain from OS4 750 micron in length.

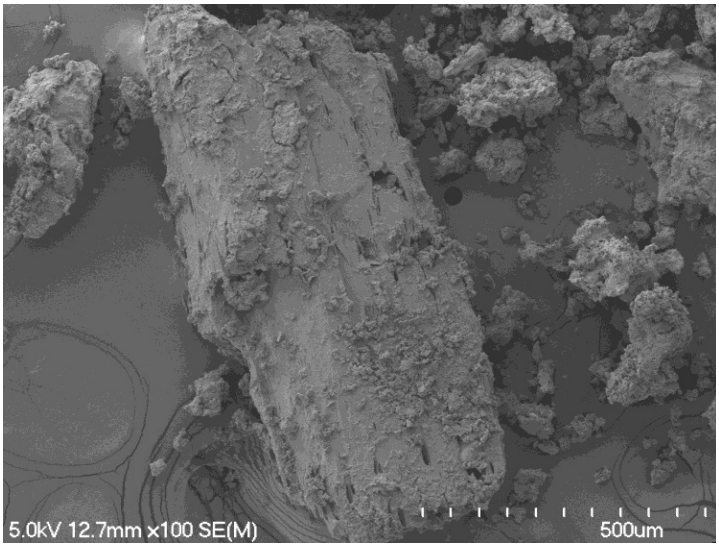

Figure 6.51: Large partly weathered crystal (850 µm in length) from OS2.

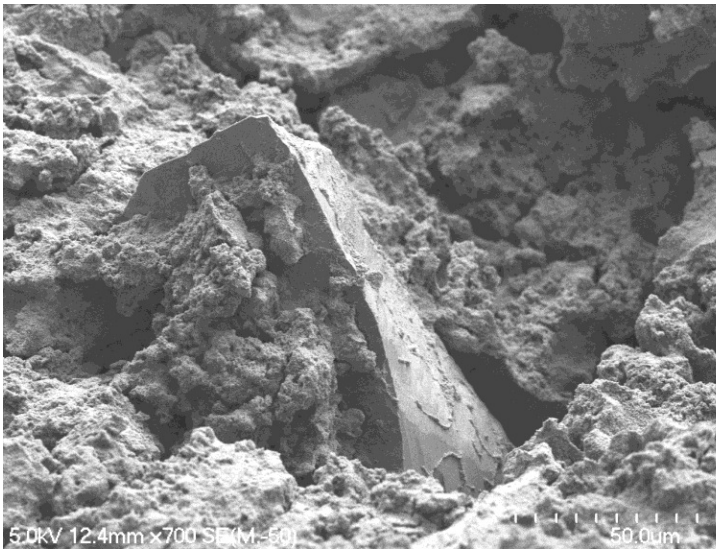

Figure 6.52: Blocky mineral from OS2. Possibly pyroxene with its columnar shape and obvious cleavage.

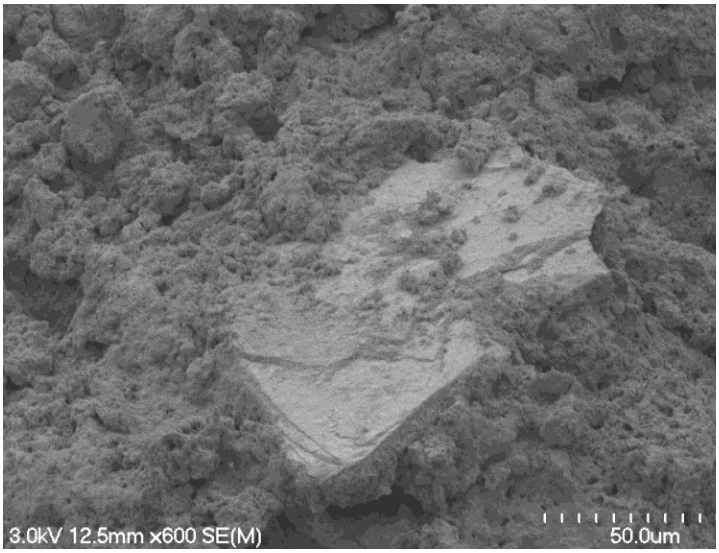

Figure 6.53: Trapezoidal platy grain from OS4. The grain appears to have a micaceous or layer-like structure.

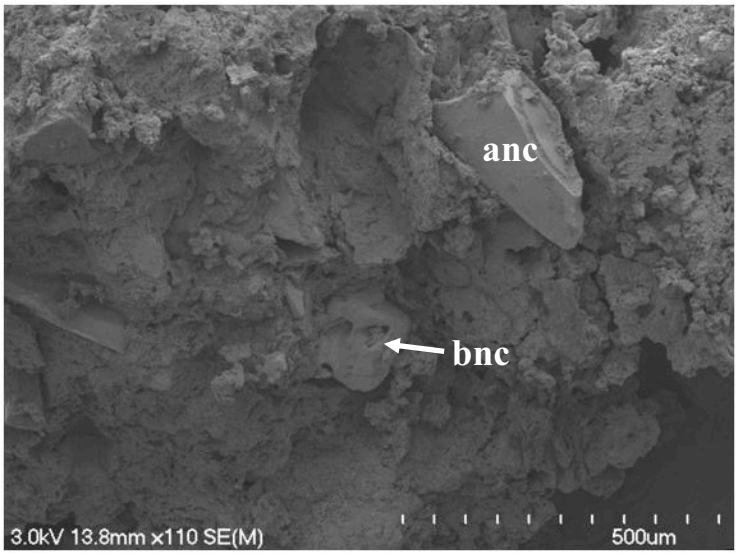

Figure 6.54: SEM image from OS4 displaying an angular non-clay (**anc**) grain and a blocky non-clay grain (**bnc**) with rounded edges.

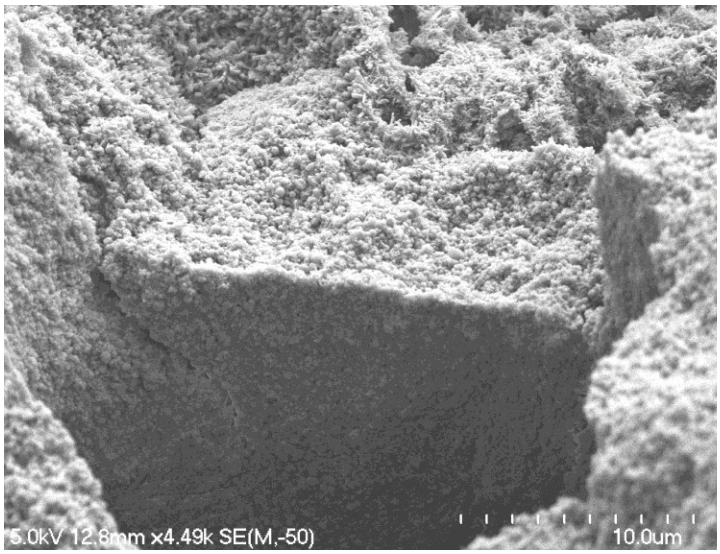

Figure 6.55: SEM image from OS2 displaying what appears to be the alteration of a blocky primary mineral to halloysite spheres. The mineral is possibly feldspar, as perpendicular sides may represent cleavage at 90º.

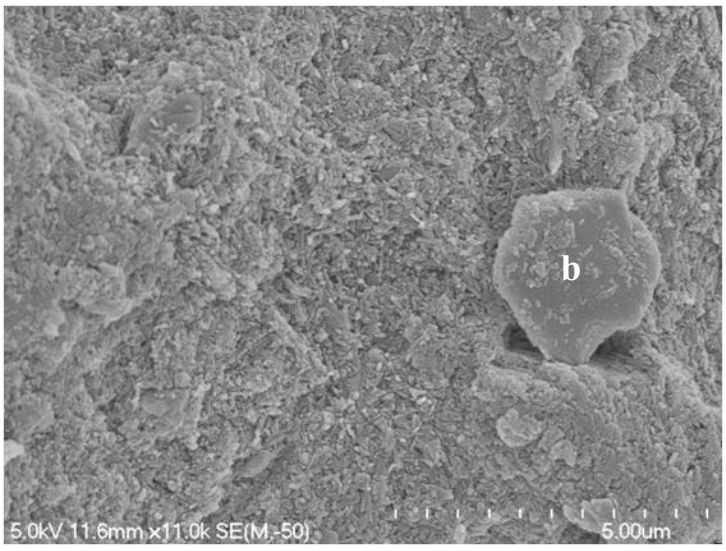

Figure 6.56: Highly weathered biotite from 0S3, ~ 4 μm in diameter (**b**). Note the hexagonal shape.

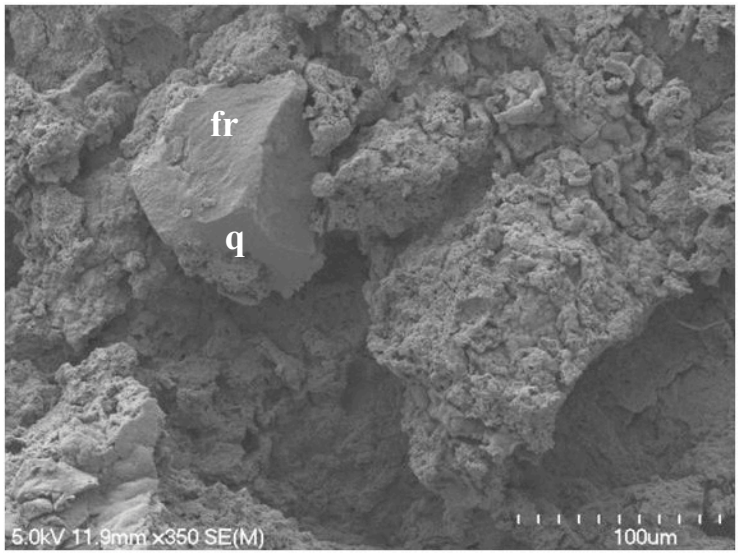

Figure 6.57: SEM image from OS1 displaying quartz **(q)** with conchoidal fracturing **(fr)** and an anhedral crystal habit.

6.6 Grain mounts

The following section presents results from grain-mount analysis, using the fine sand fraction of samples from Tauriko and Otumoetai. An estimate of mineral type and abundance in each sample is presented in Table 6. 6.

Table 6.6: Estimates of relative abundance from grain mount analysis of the fine sand fraction of samples from Tauriko (TS1, TS2, TS3) and Otumoetai (OS1, OS2, OS3 and OS4)*.

	TS1	TS2	TS3	OS1	OS2	OS3	OS4
Clay aggregates	P	A	P	A	A	P	A
Volcanic glass	A	A	A	T	T	T	T
Quartz	A	A	A	A	P	A	A
Plagioclase	A	A	A	P	P	P	P
Hornblende	P	P	P	P	C	T	P
Hypersthenes	P	P	P	P	-	T	P
Biotite	-	-	-	P	P	P	P
Titanomagnetite	P	P	P	-	C	A	T
"Limonite"	-	T	T	P	P	-	P
Zircon	-	-	-	-	-	T	-
Rock fragment	P	P	-	-	-	P	P

* Categories are divided into trace (T) < 1%, present (P) 1 – 10%, abundant (A) 10 – 25% and concentrated (C) > 25%. Note these quantities are estimates and based on visual analysis only. "Limonite" represents Fe oxides of varying compositions.

6.6.1 Tauriko

All samples from Tauriko had very similar mineralogical characteristics and were dominated by volcanic glass, quartz and plagioclase (Table 6.6). The volcanic glass was often angular, displaying curved and cuspate shapes. Some glasses show signs of devitrification, which is indicated by a brown colouration.

Quartz has the typical characteristics of low relief and an absence of cleavage. Plagioclase displays distinctive twinning characteristics optically and is identified as the only feldspar mineral. The presence of volcanic glass, quartz and plagioclase show the volcanic origin of the deposits (Assoc. Prof. Roger Briggs *pers. com.* 2008). The identification of volcanic glass, feldspar and quartz is consistent with XRD and SEM observations.

Hornblende, hypersthenes and titanomagnetite were present in moderate quantities in all of the Tauriko samples. Because titanomagentite is opaque and grain mounts were not ground or polished it was identified by its distinctive square or hexagonal shape. Weathered Fe oxides occurred only sparsely in TS2 and TS3. No biotite was observed in the Tauriko samples (c.f. Otumoetai).

Clay aggregates were present in all samples but was most abundant in TS1 and TS3. Clay aggregates display high interference colours under polarising light, and appear as husky brown fragments or elongated worm-like features. Because material was sieved to include only the fine sand fraction (60 – 200 μm), any clay observed must be present as aggregates.

6.6.2 Otumoetai

The materials observed in grain mounts of Otumoetai samples were similar to those in Tauriko samples. However, the difference lies in the proportions of material present. Most Otumoetai samples were dominated by quartz, with the exception of OS2 which had a high concentration of the heavy minerals hornblende and titanomagnetite. The concentration of heavy minerals in OS2 may be a result of reworking and sediment transport, indicating that it is a secondary deposit.

In keeping with SEM, glass was only sparsely observed in Otumoetai samples, in stark contrast to its abundance in Tauriko samples. However, combined with the presence of quartz and pyroxene, it still can be concluded that samples from Otumoetai are of volcanic origin. “Limonite” was more abundant in Otumoetai than Tauriko samples which may indicate a greater degree of weathering. Zircons were present in OS3 but only as a very minor component.

The ability to identify zircons in OS3 provides testimony to its highly weathered state, because zircons are very resilient.

The micaceous mineral biotite was present in all of the samples from Otumoetai (but not Tauriko) and was identified by its unique pseudo hexagonal shape and brown colour and perfect basal cleavage. This was consistent with field findings as a micaceous mineral was thought to be present because all samples displayed individual minerals which sparkled as light reflected from its surface. The mineral is likely to be an intergrade between biotite and kandic alteration products (as reported by T.G Shepherd in Lowe & Percival 1993, in Hamilton Ash beds).

The minerals identified in both Tauriko and Otumoetai are not uncommon in volcanic and pyroclastic materials. Salter (1979) identified hornblende and titanomagnetite in beds of the Kauroa Ash Formation. Bird (1981) observed quartz and feldspar in pre-Hamilton Ash material from Maungatapu Peninsula. The identification of volcanic glass, plagioclase, hornblende and quartz in Tauriko samples are consistent with the minerals found in the Te Ranga Ignimbrite (Briggs *et al.* 1996).

6.7 Summary

Table 6.7 summarises the components of each sample in both the clay fractions (< 2 μm) and the bulk soil samples. The most abundant clay mineral was hydrated (10 Å) halloysite. This mineral dominated the clay fraction and typically formed a strong well defined peak in the bulk sample XRD diffractograms. Halloysite was observed as tubes, irregular spheres and plates in all samples. In Tauriko, samples of halloysite occurred as books, which have never been previously observed. The halloysite books had high Fe content (~ 5.2 % as Fe_2O_3), in the typical range of halloysite plates. Allophane and ferrihydrite were insignificant in Tauriko samples but were present in very small quantities at Otumoetai. Kaolinite was present in very small quantities only in OS3.

In the bulk soil fraction, highly angular volcanic glass and plagioclase were abundant in samples from Tauriko yet make up only a minor component in bulk samples from Otumoetai. In contrast, biotite was observed in all samples

from Otumoetai, yet not in those from Tauriko. Weathered Fe oxides were more abundant in samples from Otumoetai. All samples from Tauriko appeared to have very similar compositions, yet those from Otumoetai displayed some variation. OS2 had an abundance of pyroxene in the bulk soil sample and a concentration of the heavy minerals titanomagentite and hornblende. Interestingly, OS3 appeared to have the least amount of large sand- and silt-sized grains and those which were observed appeared highly rounded and weathered. OS3 was the only sample in which zircons were observed. The Otumoetai samples are thus more weathered than those from Tauriko. Finally, the appearance of volcanic glass, quartz and plagioclase in all samples confirms that all materials are of volcanic origin.

Table 6.7 Summary of components found in each sample from both Tauriko and Otumoetai. The table presents materials found in the clay fraction and bulk sample (includes clay, silt and sand). Symbols indicate what method the component was detected with and these include: X-ray diffraction (XRD), acid-oxalate extraction (AO), grain mount analysis (GM) and scanning electron microscopy (SEM). Estimated abundances from grain-mount analyses are trace (T), present (P), abundant (A), and concentrated (C). The clay fraction XRD has either a D or S to indicate whether the mineral in question was a dominant (D) peak or only a small peak (S). The acid-oxalate extractable (AO) results have also have their measured quantities presented in parentheses. The numbers presented in parentheses beside the bulk sample XRD identifier represent the height value above background.

Mineral	TS1	TS2	TS3	OS1	OS2	OS3	OS4
Clay fraction (< 2 µm)							
Hydrated halloysite	XRD (D)	XRD (D)	XRD (D)	XRD (D)	XRD (D)	XRD (D)	XRD (D)
Kaolinite						XRD (S)	
Allophane				AO (1.3 %)	AO (1.6 %)	AO (0.8 %)	
Ferrihydrite	AO (0.01 %)	AO (< 0.01 %)	AO (< 0.01 %)	AO (0.5 %)	AO (0.4 %)	AO (0.5 %)	AO (0.3 %)
Quartz				XRD (S)		XRD (S)	
Low temperature tridymite				XRD (S)			
Low temperature cristobalite						XRD (S)	
Bulk Sample							
Halloysite	XRD (60)	XRD (71)	XRD (53)	XRD (81)	XRD (68)	XRD (38)	XRD (88)
Plagioclase	XRD (20) GM (A) SEM	XRD (84) GM (A)	XRD (120) GM (A) SEM	GM (P)	GM (P)	GM (P)	GM (P)
Low temperature quartz	XRD (50) GM (A)	XRD (40) GM (A)	XRD (50) GM (A)	XRD (156) GM (A) SEM	XRD (81) GM (P) SEM	XRD (230) GM (A) SEM	XRD (58) GM (A)
Low temperature tridymite	XRD (40)	XRD (40)	XRD (43)				XRD (53)
Low temperature cristobalite				XRD (56)		XRD (65)	
Pyroxene					XRD (295)		
Volcanic glass	GM (A) SEM	GM (A) SEM	GM (A) SEM	GM (T)	GM (T)	GM (T)	GM (T)
Hornblende	GM (P)	GM (P)	GM (P)	GM (P)	GM (C)	GM (T)	GM (P)
Hypersthene	GM (P)	GM (P)	GM (P)	GM (P)		GM (T)	GM (P)
Biotite				GM (P) SEM	GM (P)	GM (P) SEM	GM (P) SEM
Titanomagnetite	GM (P)	GM (P)	GM (P)		GM (C)	GM (A)	GM (T)
Zircon						GM (T)	
“Limonite”		GM (T)	GM (T)	GM (P)	GM (P)		GM (P)
Rock fragments	GM (P)	GM (P)				GM (P)	GM (P)

Chapter 7
Microfabric and structure

7.1 Introduction

Fabric, the arrangement of grains in sediment or soil, is influenced by grain distribution, openness of fissures, and orientation and packing of individual grains (Selby 1993). Microfabric has long been recognised as an important factor in the strength characteristics of clay-rich sedimentary soils and soft rocks (Huppert 1986, 1988; Beattie 1990; Selby 1993). More specifically, microfabric has been related to geomechanical properties of undisturbed and reworked pyroclastic material (Moon 1989, 1993; Cong 1992; Keam 2008). As a corollary to this, it is expected that microfabric will be an important factor in determining the geomechanical properties and hence sensitivity of weathered pyroclastic material from the Tauranga region.

This chapter qualitatively describes the dominant microfabric characteristics of each sample. Samples examined in the geomechanical chapter have been viewed in both undisturbed and remoulded states using a scanning electron microscope (SEM). This chapter gives a background to the terminology employed by previous studies and then describes what will be used in this study. The microfabric characteristics of the samples from Tauriko and Otumoetai are then individually described.

7.2 Terminology

7.2.1 Previously used terminology systems

Microfabric description has a long history which predates SEM use; this has been extensively reviewed by a number of workers (for example, Collins & McGown 1974; Grabowska-Olszewska *et al.* 1984; Huppert 1986; Selby 1993). Combined with their own investigations these workers outline a chronological sequence of development. Initially microstructure terminology focused on

individual particle interaction. However as time and technology progressed, other factors became important, such as electrochemical environments at time of deposition, mineralogy, and depth of burial. Later, investigations which examined different microfabric types described individual particle arrangements and realised the importance of hierarchical descriptions (Collins & McGown 1974). Whole soil microfabric arrangements were then placed into geometric classifications (Sergeyev *et al.* 1980; Grabowska-Olszewska *et al.* 1984; Huppert 1986).

These previous classification systems were largely based on sedimentary soils. Previous investigations examining pyroclastic material found it difficult, if not impossible, to describe microfabric using this terminology. For example, Moon (1989, 1993) investigated the microfabric of ignimbrites and ignored sedimentary terminology, building instead on terminology used by Carr (1981). Moon's (1989) descriptions were based on the structure of groundmass, the nature of crystals and pumice clasts, and evidence for post depositional alteration processes. The lack of clay material in Moon's (1989) investigation meant that her terminology was not completely compatible with observations in this study. Both Heiken (1972) and Heiken & Wohletz (1985) described volcanic ash material in the interpretation of eruption conditions using SEM observations. The terms may be relevant for individual clasts but they do not provide description for contacts or clay material.

Other workers have applied the terminology of sedimentary soils to volcanic material. These workers include Cong (1992) examining rhyolitic silts from Waitemata, and Keam (2008) who investigated reworked pyroclastics from the Omokoroa region. Keam (2008) stated that neither previous volcanic or sedimentary classifications were ideal for his investigation and employed a multi-faceted approach.

In this study, terms derived from both previous volcanic and sedimentary microfabric investigations have been employed. However, where necessary, these systems and terms have been modified to accommodate the unique material considered in this study.

7.2.2 Terminology employed in this study

The terminology employed in this study is based on a hierarchical system which is outlined below.

7.2.2.1 Primary Structural Elements

Primary structural elements are those particles which form the basic building blocks of the soil being examined (Beattie 1990). Previously, other workers divided this section into clay platelets and microaggregates, silt and sand grains, and authigenic phases (Huppert 1986; Beattie 1990). However, the approach in this study was much simpler and primary structural elements were classified as either clay minerals or grains.

Clay minerals represent individual units of crystalline clay, which are often observed as irregular polygonal spheres, tubes and plates and are seldom larger than 2 μm. Grains are simply all other materials which can be identified as single units, examples being volcanic glass, plagioclase and quartz. The term grain is used rather than rather than sand or silt, as in Huppert (1986) & Beattie (1990), to remove the distinction of size. It should be noted that the bulk of primary structural element description has been presented in Chapter 6 and this chapter only serves to refresh and add to this information.

7.2.2.2 Elementary Particle Arrangements

Elementary particle arrangements describe the interaction of primary structural elements discussed in section 7.2.2.1. This section is loosely based on the framework outlined by Collins & McGown (1974) and Collins (1985). The major difference is that Collins & McGown (1974) and Collins (1985) only consider the interaction of single clay morphologies, which is not the case in this study (see Chapter 6). Figure 7.1 identifies the face and edge for each clay morphology observed in this study, and presents the different types of contact between these minerals.

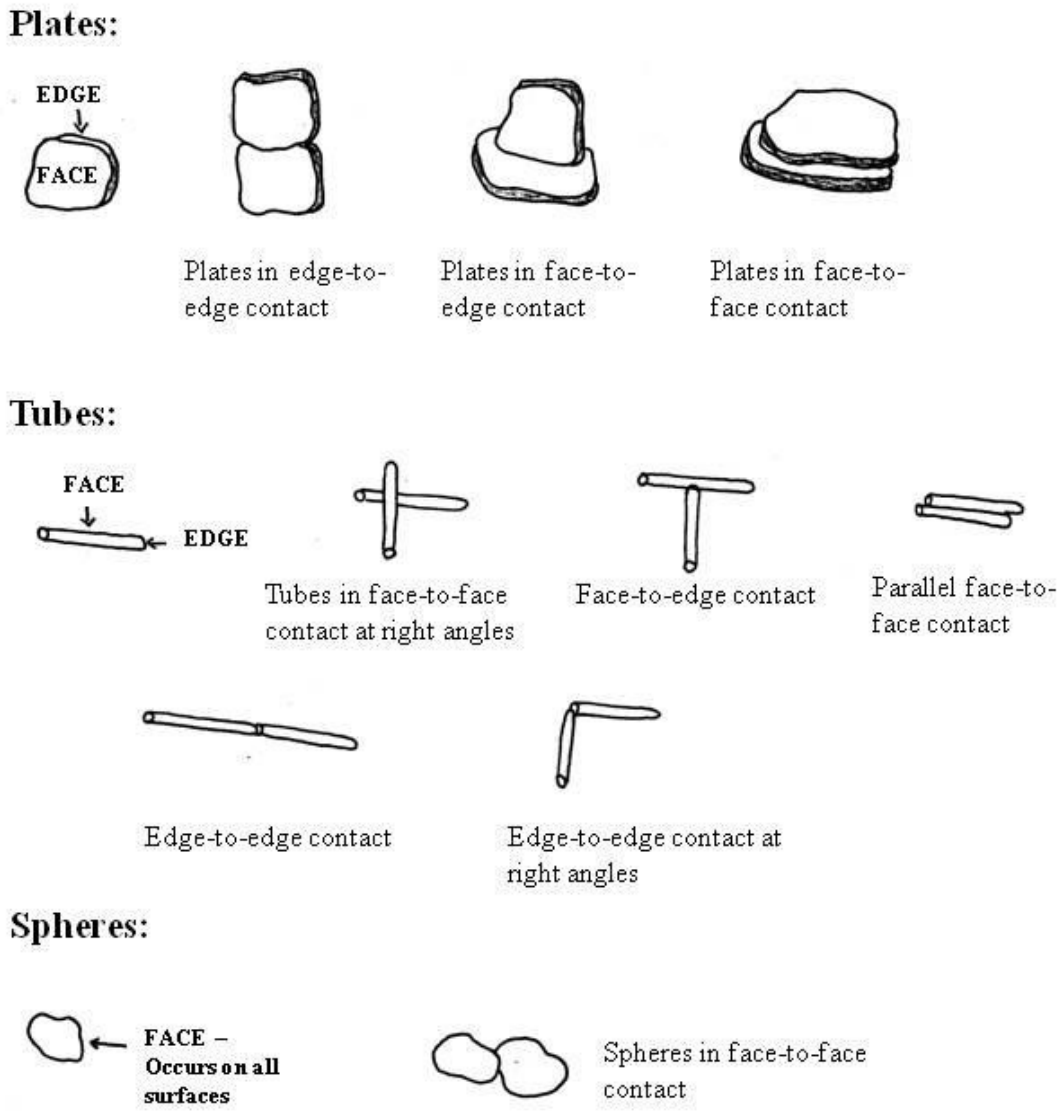

Figure 7.1: Schematic diagram (not to scale) of the three different clay morphologies observed during scanning electron microscopy. Each morphology is displayed with identification of their respective face and edges and the arrangement of contacts each is observed in.

Building on Figure 7.1, Figure 7.2 displays the typical interactions between different clay morphologies observed this study. When tubes occur in predominantly face-to-face or face-to-edge contacts at right angles, they form an open network arrangement (Figure 7.2 (A)). This arrangement appears much like the flocculated structure of Lambe (1958). When the framework of tubes in Figure 7.2 (A) is intermixed with polygonal spheres it become less open as the spheres coat and fill in the gaps between tubes (Figure 7.2 (B)). Tubes are also observed in a more subdued or regular structure which is dominated by parallel face-to-face contacts (Figure 7.2 (C)). The arrangement in Figure 7.2 (C) is much like the dispersed structure of Lambe (1958). Plates may also be intermixed with tubes

(Figure 7.2 (D)). The tight packing of tubes and tubes and plates (Figures 7.2 (C) and (D)) are very similar to the "matrix" structure of Sergeyev *et al.* 1980.

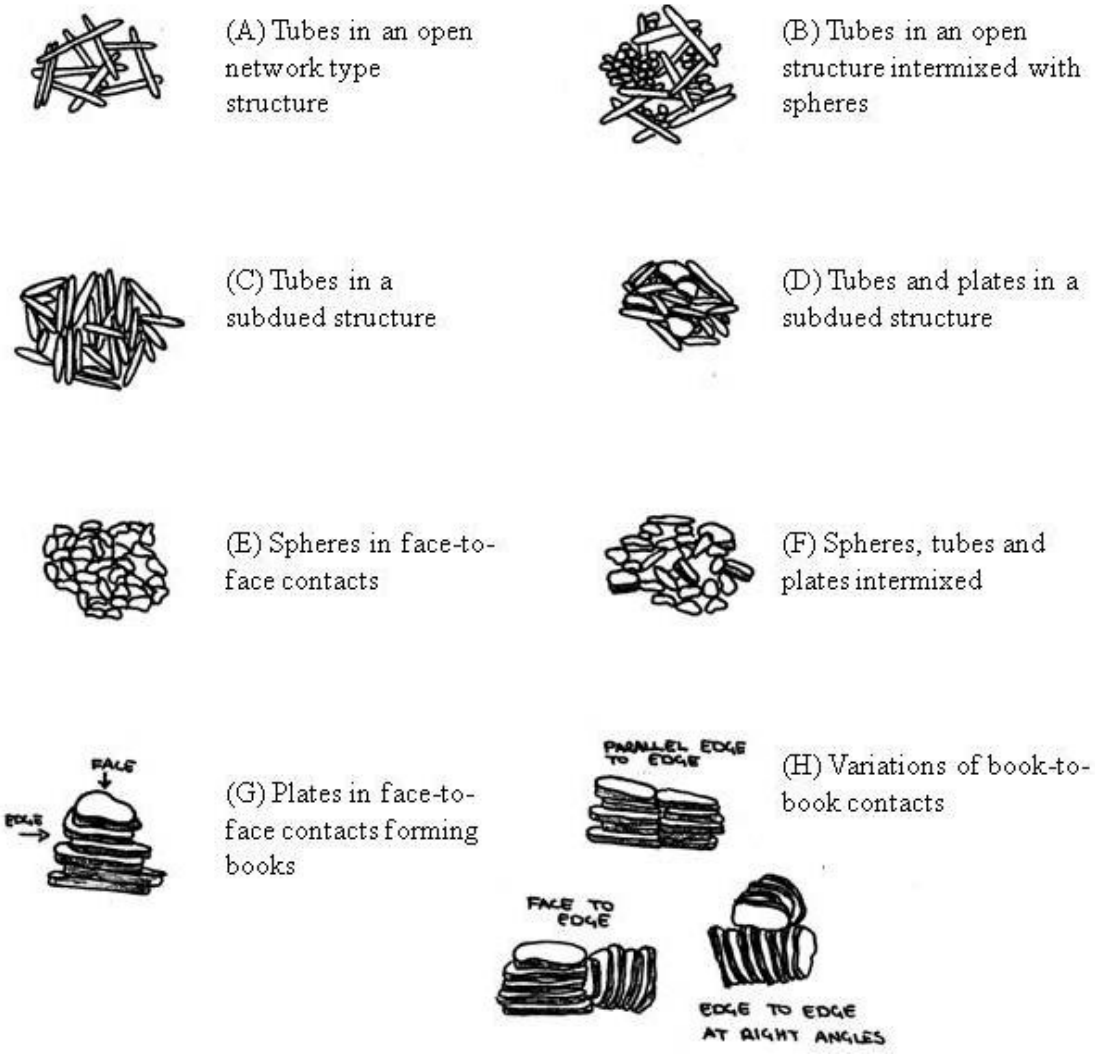

Figure 7.2: Schematic diagram (not to scale) of the contacts between individual clay minerals, which are described in the text.

When polygonal spheres interact individually (Figure 7.2 (E)) or with plates and tubes (Figure 7.2 (F)) they form a structure similar to but slightly less open than the 'honeycomb' arrangement of Terzaghi (1925). Geometrically, the structures in Figure 7.2 (E) and (F) are very similar to the 'skeletal' structure of Sergeyev *et al.* 1980. As previously described in Chapter 6, plates stack to form books (Figure 7.2 (G)) and these books interact through a range of contacts (Figure 7.2 (H)).

The arrangements displayed in Figure 7.2 form both microaggregates and groundmass material. The volcanic term "groundmass" is used in this study rather

than the sedimentary term 'matrix'. With the exception of books, the boundaries of microaggregates are difficult to define. In this study micro aggregates represent the association of clay minerals, of any morphology, in a physiochemical arrangement forming small structures (Huppert 1986) and range in size between 1.5 μm and 50 μm. The classification of microaggregates includes individual halloysite books. Groundmass refers to combinations of clay minerals which cannot be defined as microaggregates.

7.2.2.3 Overall particle associations

Particle associations represent the interaction between the grains described in section 7.2.2.1 and the particle arrangements in section 7.2.2.2. This section is loosely based on particle assemblages used by Colins & McGown (1974) and also draws terms from Moon (1989) and Beattie (1990). Terms used are presented and described in Table 7.1.

Table 7.1: Descriptions of the interaction between grains and the surrounding background material of clay minerals.

Connectors	Clusters of clay size material which forms bridges between clay microaggregates and non clay material (Collins & McGown 1974)
Embedded	Grains are completely surrounded by groundmass material
Grain Coatings	Material coats the surface of a grain along the fracture surface
Pluck mark	Grains are removed by specimen preparation techniques, leaving a distinctive hollow depression (Moon 1989)
Loose Material	Grains are observed in the groundmass but are loose with a physical separation between the two (Moon 1989)
Lapping	Groundmass material laps against the surface of the grain to form a direct contact (Moon 1989)

This section also differentiates between continuous and discontinuous microfabrics, which are terms used by Beattie (1990) in his study of Waikato coal measures. A **continuous groundmass** does not have clearly definable boundaries between structural units and individual grains are immersed within the groundmass. In contrast a **discontinuous groundmass** is one which the particle associations have definable boundaries or occur within discrete domains (Beattie 1990).

7.2.2.4 Porosity

In this study pores are classified by size, with their boundary elements and shape being considered of less importance. Pore size classification, presented in Table 7.2, is based on that of Huppert (1986). Pore sizes affect the retention of water, for example smaller pores will hold water more tightly than larger ones. Huppert (1986) stated that in sedimentary rocks, ultra-pores were filled with adsorbed and firmly bonded water, and micro- and meso-pores were associated with capillary rise. Beattie (1990) stated that macro pores were directly related to the degree of saturation.

Table 7.2: Pore size classes adapted from Huppert (1986).

Class	Size range (μm)
Ultra-pore	< 0.1
Micro-pore	0.1 to 5
Meso-pore	5 to 30
Macro-pore	> 30

In terms of boundary elements a number of studies use complex systems (e.g. Collins & McGown 1974; Grabowska-Olszewska 1984 and Huppert 1986). However in this study pores will be described as either between individual clay minerals or grains, between microaggregates or simply within the groundmass.

7.3 Tauriko Summary

The following describes primary structural elements, elementary particle arrangements, overall particle associations, and pore characterises for material from Tauriko (TS1, TS2, and TS3).

7.3.1 Primary Structural Elements

7.3.1.1 Clay Minerals

All clay minerals were positively identified as halloysite and their morphologies were comprehensively described in Chapter 6. Individual clay minerals from Tauriko were dominated by small (< 1 μm), irregular, polygonal spheres, tubes and plates which had no structural orientation (Figures 6.19, 6.21 and 6.24). The remainder of this section will refer to this material as **clay minerals**.

Large plates were typically stacked in tight face-to-face contacts forming microaggregates of books (Chapter 6, section 6.5.1.4), which are further described in section 7.3.2. Tubes were more abundant than polygonal spheres and small plates in TS1 and TS2 (Figure 7.3). In TS3, polygonal spheres and small plates were in greater abundance than tubes (Figure 7.4). Books were most abundant in TS3. In all Tauriko samples, SEM imaging indicated that small clay minerals dominated the microstructure.

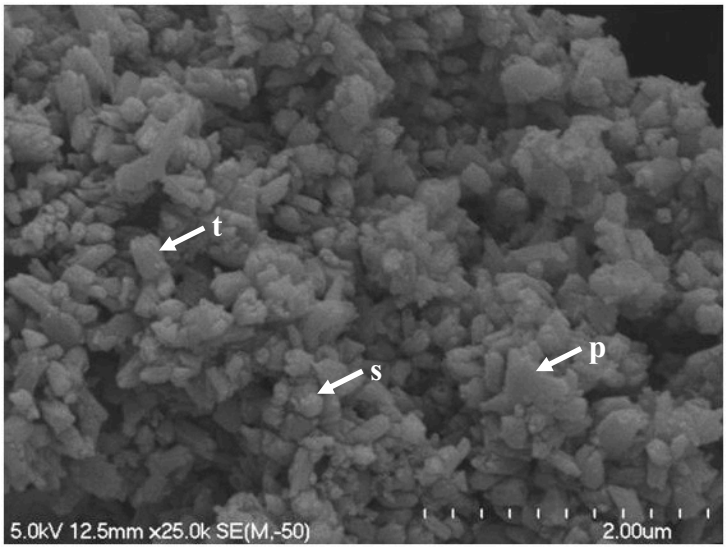

Figure 7.3: SEM image from TS1 showing a high proportion of tubes **(t)** which are intermixed with plates **(p)** and irregular spheres **(s)** to form a microaggregate. Few pores are larger than 0.4 µm, and typically result from the interaction of irregularly shaped clay minerals.

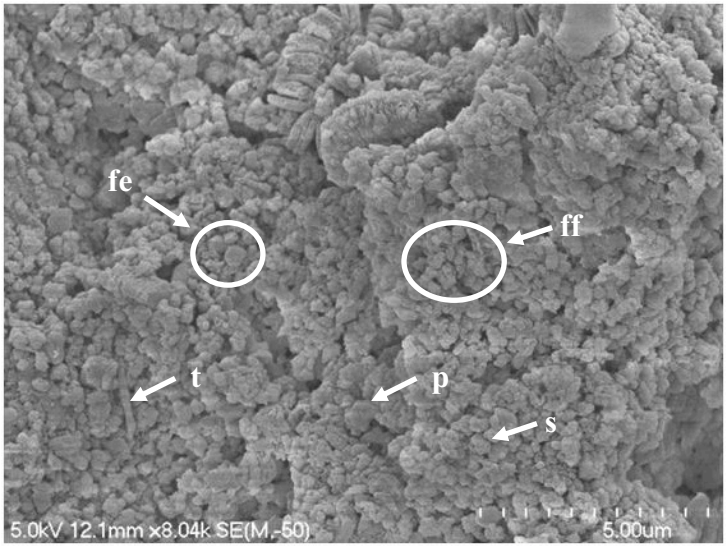

Figure 7.4: Groundmass material from TS3 showing that polygonal spheres **(s)** and irregular plates **(p)** are more abundant than tubes **(t)**. Contacts between clay minerals are typically spheres in face-to-face **(ff)** contacts. However face-to-edge contacts between spheres and plates **(fe)** are also present. Porosity is typically dictated by the interaction between irregularly shaped clay minerals. Few pores are larger than ~ 0.7 µm and many are much smaller at ~ 0.2 µm.

7.3.1.2 Grains

Grains were observed in all Tauriko samples. Both sand and silt size classes were represented and composition was predominantly quartz, feldspar and volcanic glass. Feldspar was typically blocky and glass appeared angular. Chapter

6 described in detail the abundance, size and shape of all non-clay material. The remainder of this section will refer to this material as **grains**

Grains did not display any dominant orientation (Figure 7.5) and typically did not come in contact with each other (Figure 7.6). When grains were close, small clay minerals filled the area between them (Figure 7.7). Because particle size analysis suggested there was a large amount of silt in Tauriko samples, it was possible that the small, clay sized material was clothing larger grains. Consequently, these unseen grains may be playing a more important role in the microstructure than presently observed.

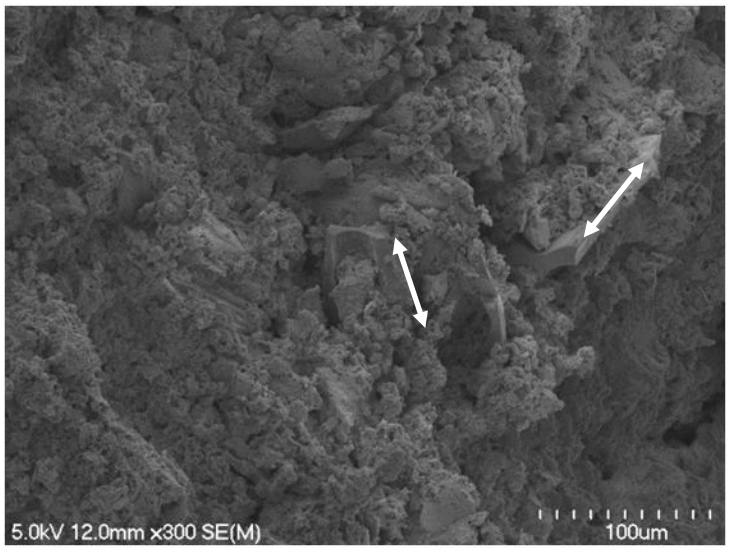

Figure 7.5: Volcanic glass from TS3 orientated in a number of different directions (as indicated by arrows) and supported in a groundmass of smaller clay sized material

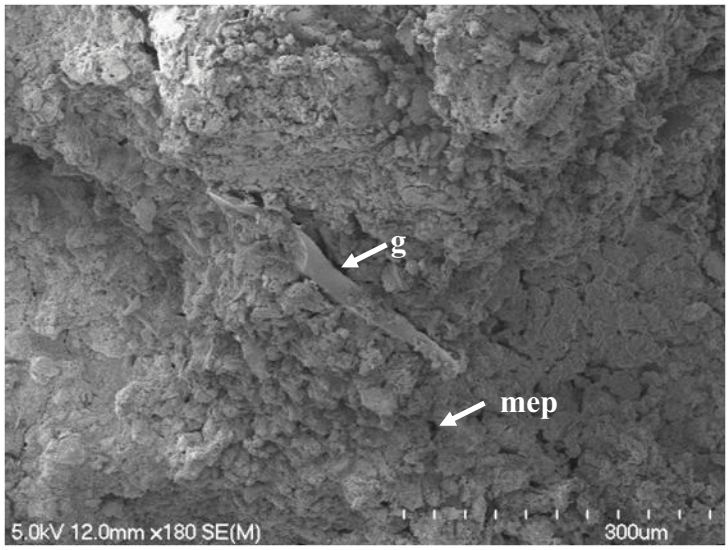

Figure 7.6: Elongated fragment of volcanic glass **(g)** ~ 200 µm long, from TS3, occurring individually and in direct contact with surrounding microfabric of clay minerals. Also present are meso-pores **(mep)** which are ~ 15 µm in diameter.

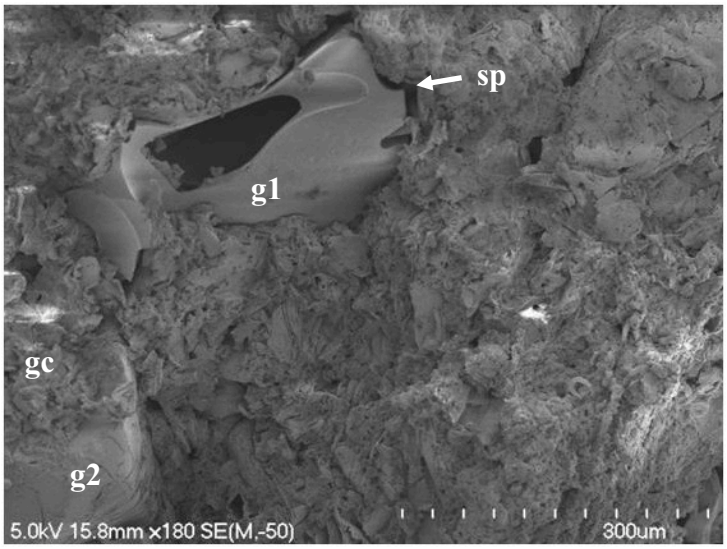

Figure 7.7: SEM image from TS1 displaying two large grains **(g1 and g2)** supported in a highly disorganised groundmass of clay minerals. Small clay sized material separates the two grains. The material surrounding the piece of volcanic glass (**g1**) is pulling away (**sp**) from the surface of the grain. Along the fracture surface the face of the volcanic glass **(g1)** is clean, however, the sand grain (**g2**) appears to have a heavy layer of grain coatings (**gc**) along one face. In the top right hand and bottom left hand corner pores of ~ 30 μm diameter are observed.

7.3.2 Elementary particle arrangements

7.3.2.1 Groundmass

In all Tauriko samples material which formed the groundmass appeared loosely packed, forming an open structure (Figure 7.8). In TS1 and TS2 the arrangement of groundmass material involved the interaction of irregular polygonal spheres, tubes and plates (Figure 7.8). Because of the diverse range of morphologies present, and their irregular shape, it was difficult to define clear particle contacts. However, tubes occurred in parallel face-to-face (FF) and face-to-edge (FE) contacts, and spheres formed FF contacts with each other (Figure 7.8). It was likely that other contacts were present but were not easily discernable.

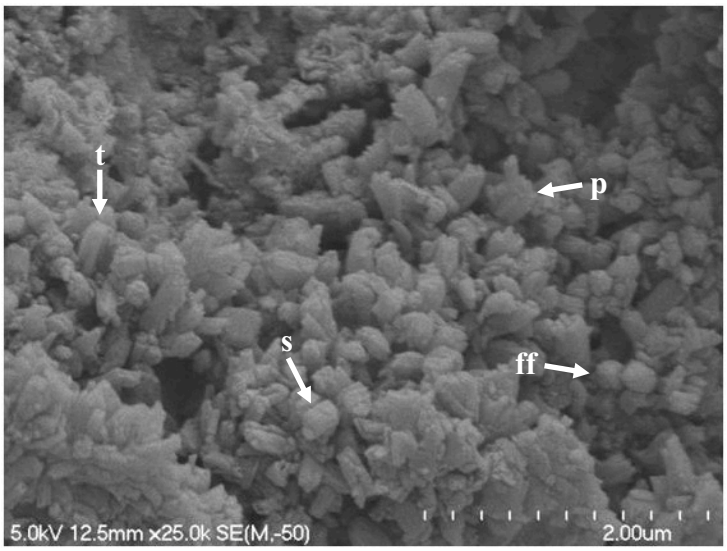

Figure 7.8: SEM image of ground mass material from TS1 which is loosely packed and includes tubes **(t)** spheres **(s)** and plates **(p).** Spheres are observed forming face-to-face contacts **(ff)** other contacts are difficult to define. Pores are abundant and up to 0.4 μm in diameter.

In TS3 irregular polygonal spheres dominated the groundmass material, plates were present and tubes were seldom observed (Figure 7.4). Spheres in FF contacts formed the dominant particle arrangement (Figure 7.4). Plates and spheres were also observed forming edge (plate) to face (sphere) contacts (Figure 7.4).

7.3.2.2 Microaggregates

Within Tauriko samples microaggregates comprised three different structures, including clusters of clay minerals with poorly defined boundaries (Figure 7.9), a streaky and wavy arrangement of clay minerals (Figure 7.10), and halloysite books (Figure 7.9).

Clusters of clay minerals, which represent individual microaggregates, were difficult to indentify because they had irregular boundaries and were comprised of the same material as the groundmass. However, when defined, the irregularly shaped microaggregates were typically less than ~ 10 μm in diameter, and were observed in all Tauriko samples (Figures 7.9, 7.11 and 7.12). Microaggregates in TS1 and TS2 were mostly comprised of un-orientated tubes, with spheres and plates being of lesser abundance (Figure 7.3). Microaggregates observed in TS3 appeared to have a lesser amount of tubes and a greater abundance of polygonal spheres and irregular plates (Figure 7.12). Microaggregates were most abundant in TS1.

Streaky and wavy material (Figure 7.10) which appeared thin walled and hollow (Figure 7.13) was abundant in TS1 (Figures 7.10 and 7.13) and TS2 (Figure 7.14), but less so in TS3. This material was up to 70 μm long and often contained a number of curved layers, either overlaying (Figure 7.10) or alongside each other (Figure 7.13). The shape of individual layers ranged from broad rolls (Figures 7.13 and 7.14) to tight curves (Figure 7.14). Layers in close proximity were orientated in the same direction (Figures 7.10 and 7.13), however in some instances adjacent material was orientated at almost right angles (Figure 7.14). The delicacy and hollow nature of this streaky and wavy material was emphasised by the wall collapse observed in Figure 7.13. Under high magnification (25 000 x) this material was dominated by tubes with a lesser amount of small plates and polygonal spheres (Figures 7.15 and 7.16). Contacts between individual

tubes occurred as parallel FF, face-to-edge (FE) and edge-to-edge (EE) (Figure 7.16). Plates formed FF contacts with the other clay minerals (Figure 7.15). All structural components formed a flat surface and each component was un-orientated across this surface (Figure 7.16).

The elongated hollow streaks and waves (Figure 7.10) may represent pipe vesicles, a feature of pumice (Heiken 1985). It was hypothesised that the original pumice texture has authigenically weathered to tubes, small plates and polygonal spheres. The pumice may have acted as a template for the structural configuration of the clay minerals which are currently present. The presence of relict pumice would suggest that the parent material is most likely rhyolitic. On examination of Kauroa Ash beds, Salter (1979) identified relict pumice textures in the fine to coarse sand fraction. These appeared partially limonitised, indicating weathering, but the textures had not completely altered to clay. The pumice like material observed in this study will herein be referred to as relict textures.

The ends of hollow tubes were observed in a number of SEM images (Figures 7.17, 7.18 and 7.19). The tubes were comprised of the same material that was found in the relict textures (Figure 7.18). Diameters of the tubes were up to ~ 8 μm and the walls were less than 1 μm (Figure 7.19). It is possible that the tubes were a cross section of a relict texture and represent pipe vesicles. However, the tubes may also represent the effects of biological activity (worms or roots) or an interesting electrostatic arrangement of clay particles.

Plates with diameters between 1 to 20 μm were observed in tight FF contacts and appeared as books (Figure 6.21). These books ranged in length from ~ 1.5 to ~ 50 μm long (Figure 6.32), were identified as halloysite and their morphology was comprehensively described in Chapter 6. The tight EE contacts of individual plates mean the books would typically behave as a large single grained clay mineral. However, as described in Chapter 6 the books displayed differing degrees of delamination (Figures 6.30 and 6.31) so were weaker than an individual grain.

Typically books in TS1 and TS2 were un-orientated, observed individually and supported in a groundmass of tubes, spheres and smaller plates (Figure 7.20).

Books in TS3 were supported in similar material but were frequently observed forming contacts with each other (Figure 7.12). In all samples, contacts between books included EE contacts, with the books orientated either parallel (Figures 7.12 and 7.21) or at right angles (Figure 7.22) to each other. In TS3, parallel EE contacts were observed most often. Figure 7.21 presents an example of at least 4 books in parallel FF contacts forming a larger microaggregate. Because of the irregular shape of the plates in each book the EE contacts at right angles form at a point with very little surface interaction (Figure 7.22), making them weaker than parallel contacts. Contacts were also observed as FE interactions (Figure 7.23) but these occurred less often than EE contacts.

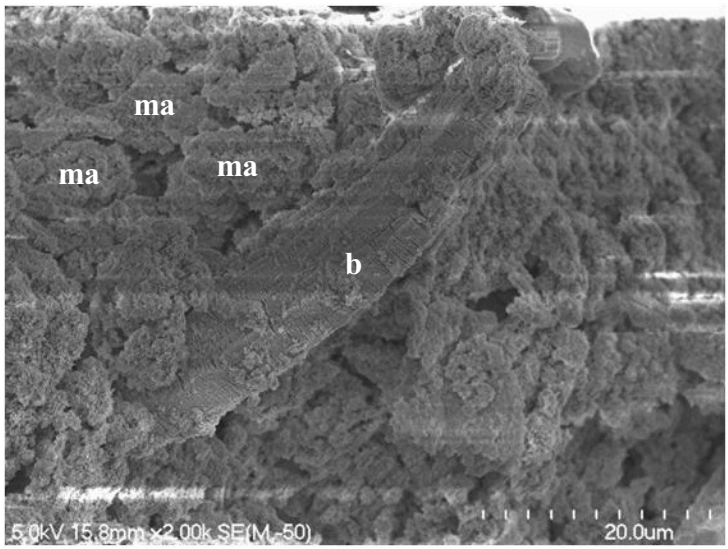

Figure 7.9: A large book **(b)** from TS1 with the lower section supported in, and the upper section radiating from, a background of clay minerals. To the left of the clay book appear a number of irregular and poorly defined microaggregates **(ma)**, which are linked by connectors of clay minerals. Porosity between the microaggregates is up to 5 µm.

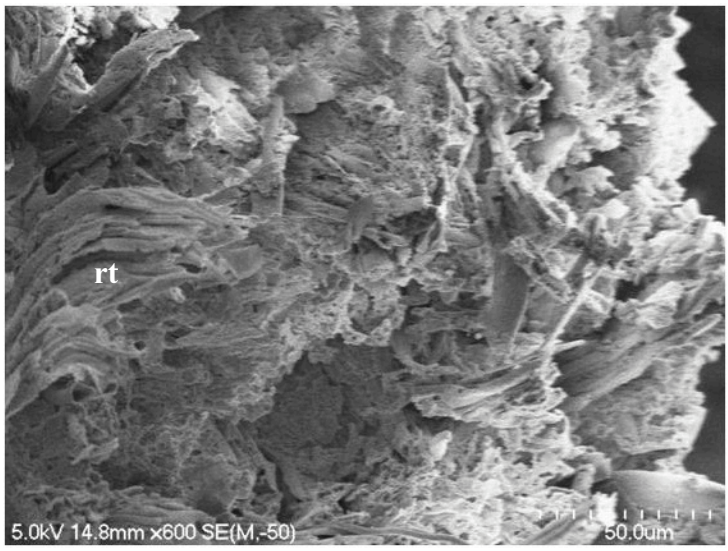

Figure 7.10: SEM image from TS1 displaying streaky and wavy material up to 70 µm long (**rt**). The streaky and wavy material comprises a number of tightly curved layers all orientated in the same direction overlying each other.

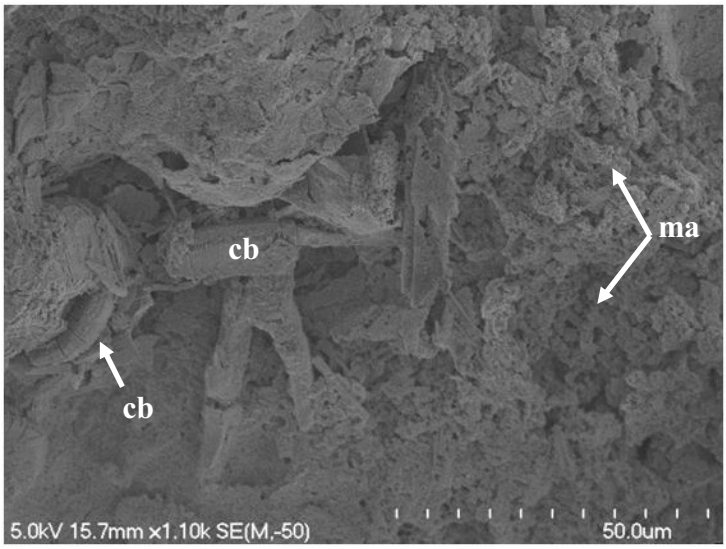

Figure 7.11: SEM image of irregularly shaped, poorly defined microaggregates (**ma**) from TS1 with porosities up to 5 µm occurring between them. A number of clay books (**cb**) are supported within and on the surface of the background material.

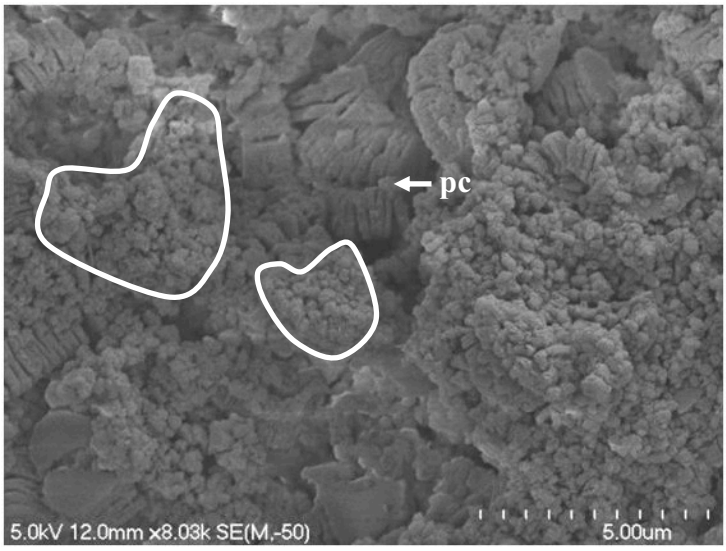

Figure 7.12: SEM image from TS3 showing clay books supported in small clay-sized material and also forming parallel contacts (**pc**) with each other. Aside from the books small microaggregates of clay material can be defined and these are circled. Porosity is dominated by interacting grains with sizes no more than 0.4 µm in diameter. Other larger pores occur but these are between clay books and aggregation of smaller clay-sized material.

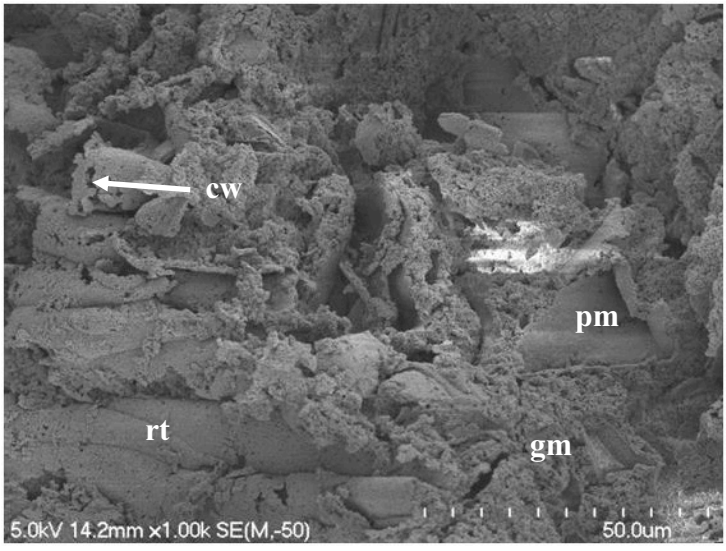

Figure 7.13: SEM image from TS1 of thin walled streaky and wavy material, with each broad roll aligned in the same direction (**rt**). The hollow nature and weakness of the streaky and wavy material is emphasised by the collapsed wall sections at **cw**. The streaky wavy material appears to grade into the groundmass material (**gm**) at the right of the image. A pluck mark appears in the groundmass which may indicate the location of a former mineral which was lost during sample preparation (**pm**).

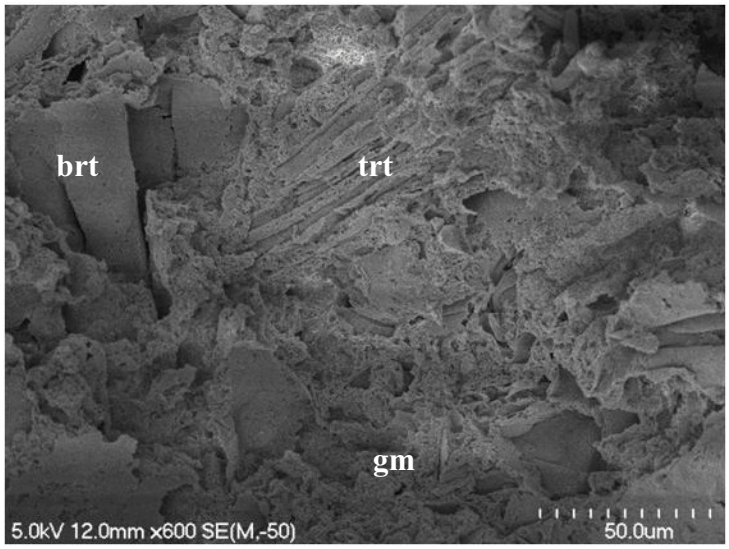

Figure 7.14: Streaky and wavy material from in TS2 with both broad (**brt**) and tight (**trt**) rolls orientated at almost right angles to each other. The streaky and wavy material appears to grade into the groundmass **(gm)** at the bottom of the image.

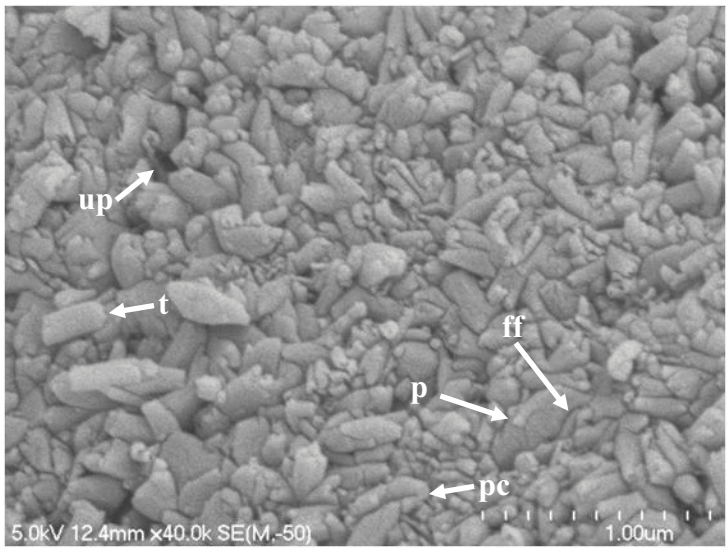

Figure 7.15: SEM image from TS1 showing the surface of streaky and wavy material, indicating it is comprised of predominantly of tubes **(t)** and to a lesser extent irregular plates **(p)**. Tubes are observed forming parallel face-to-face (**pc**) contacts and plates form a face-to-face (**ff**) contacts with other material. All material forms a flat surface; however, it is un-orientated across this surface. Very small (~ 0.1 μm) ultra-pores **(up)** occur between clay mineral particles.

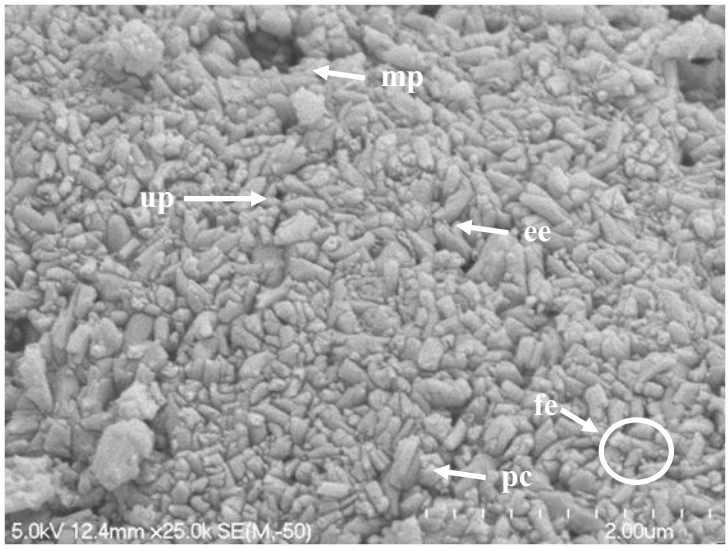

Figure 7.16: Surface of a relict texture from TS1, displaying parallel face-to-face (**pc**), edge-to-edge (**ee**) and face-to-edge (**fe**) contacts between tubes. Porosity is a result of the interaction between irregularly shaped clay minerals and forms inter granular ultra-pores (**up**). A larger micro-pore (**mp**) occurs at the top of the image; this is most likely a small collapsed wall section.

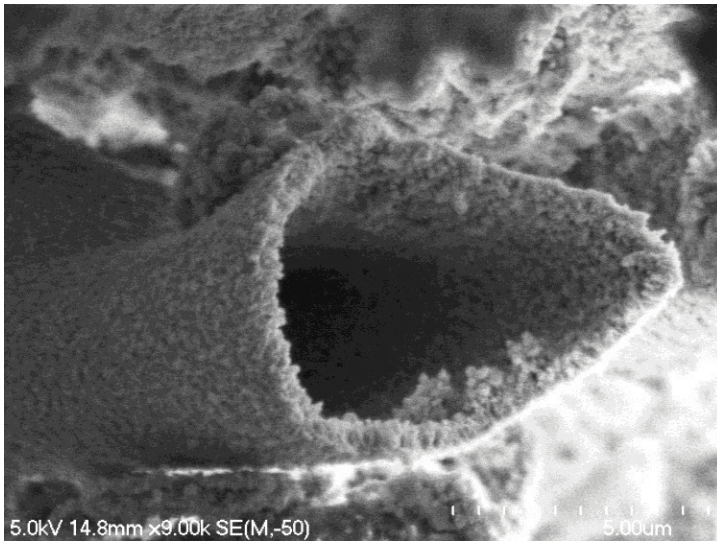

Figure 7.17: Long hollow tube from TS1 which is comprised of very small clay sized material. The tube has a diameter of ~ 7 µm and walls which are 0.5 µm thick.

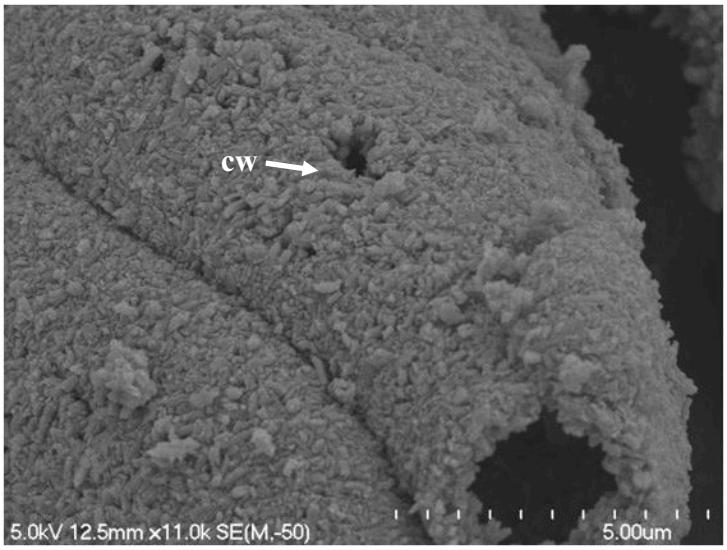

Figure 7.18: SEM image of a hollow tube from TS1. The opening of the tube is ~ 4 µm in diameter. The collapsed wall section at **cw** indicates the tubes delicacy.

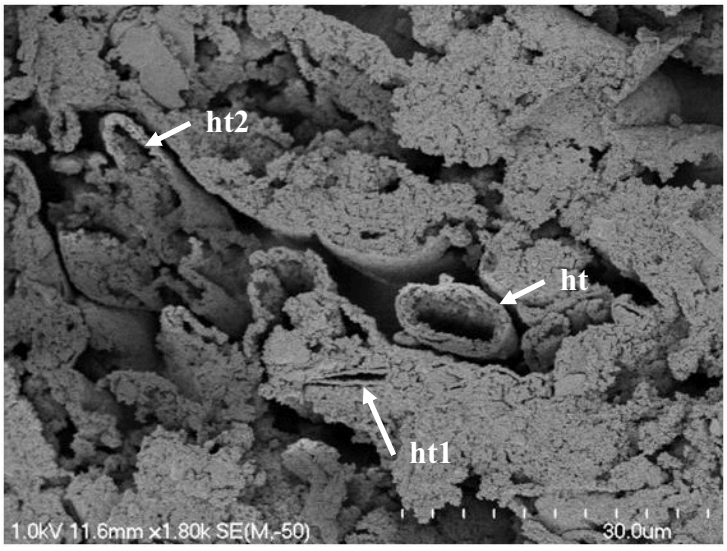

Figure 7.19: SEM image of at least one hollow tube from TS1, which is comprised of individual clay minerals (**ht**). The diameter of **ht** is 8 µm with walls 1 µm thick. The smeared faced of all other material is the result of sample preparation. The general structure appears very open with other tubes possibly present (**ht1 and ht2**).

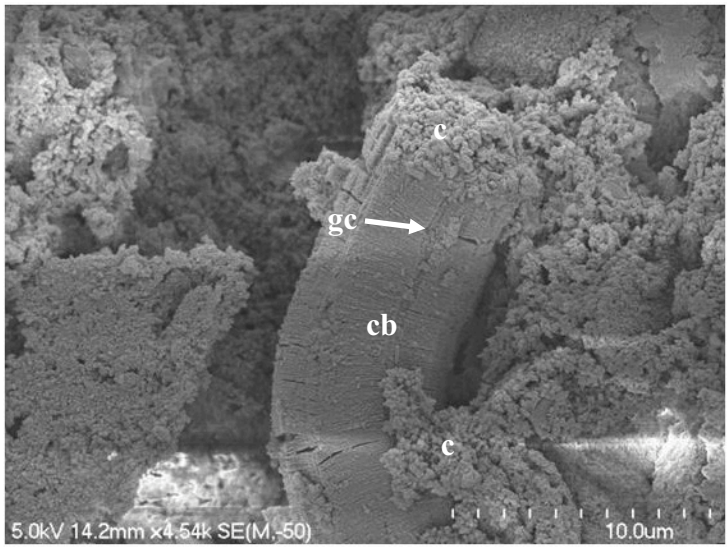

Figure 7.20: Single book **(cb)** from TS1, with very light grain coatings (**gc**), individually supported in a groundmass of plates, tubes and spheres. Connectors **(c)** are present between the groundmass material and the clay book.

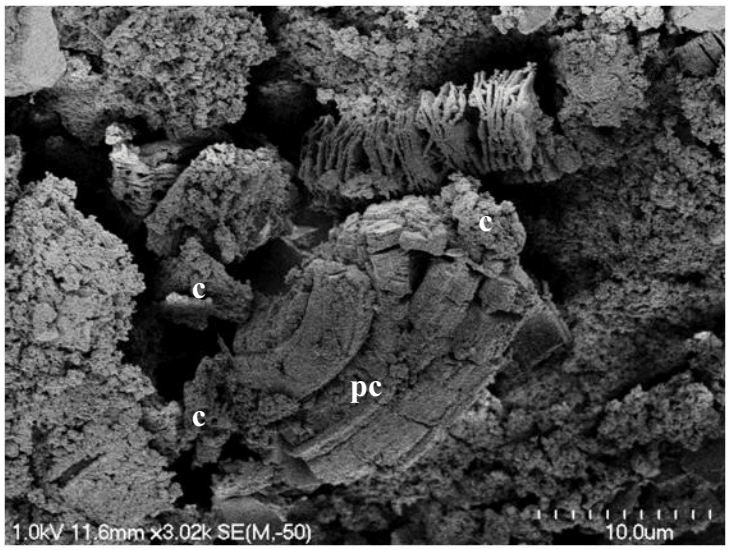

Figure 7.21: Books from TS1 in parallel contacts **(pc)** forming a much larger microaggregate. The microaggregate is supported within the microfabric by a series of connectors **(c)**.

Figure 7.22: SEM images from TS3 showing books forming edge-to-edge right angle contacts (**rc**).

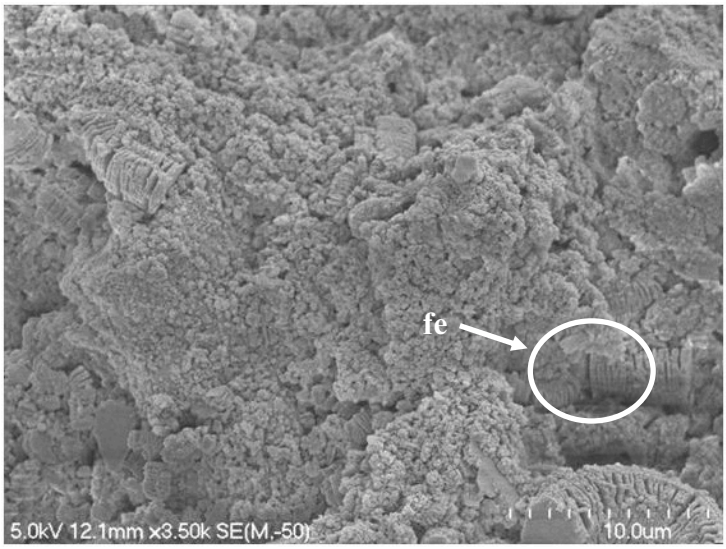

Figure 7.23: Books from TS3 fully immersed in groundmass material. The groundmass material laps against both the edges and faces of the books. Two books are observed meeting as face-to-edge contacts (**fe**).

7.3.3 Overall particle associations

Individual grains were typically embedded in the surrounding microstructure and clay sized material was observed lapping against the surface of the grain (Figures 7.6 and 7.7). Groundmass material was occasionally observed separating away from the face of the grain forming a loose contact (Figure 7.7). The separation may represent stress release upon overburden removal during sampling or the result of desiccation or fracture during sample preparation (Beattie 1990). However, the separation may also indicate weak contacts between the grain and background material. The contact between sand- and silt-sized grains and clay minerals were weak, indicated by the observation of pluck marks (Figure 7.13). Along the fracture surface, where the sample was split prior to investigation, mineral grains had moderate to minor coatings and volcanic glass was typically clean (Figures 7.7 and 7.24).

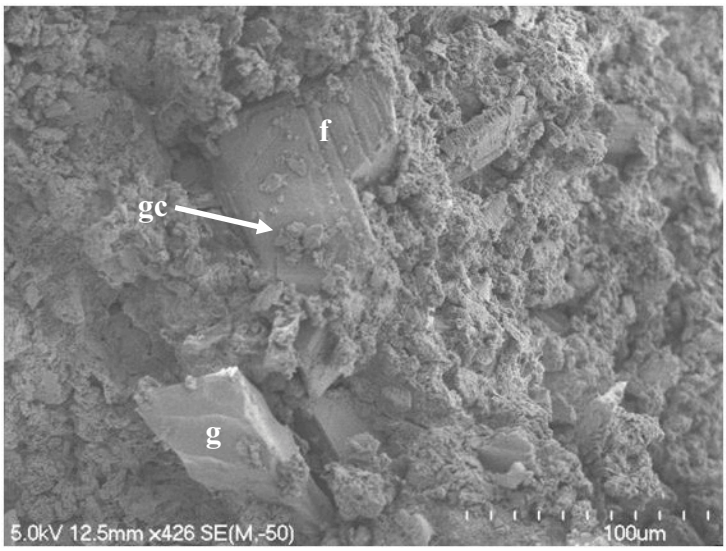

Figure 7.24: A feldspar grain **(f)** and a piece of volcanic glass **(g)** are in direct contact with the groundmass material of TS3. The feldspar grain appears to have a minor amount of grain coatings **(gc)** along the fracture surface.

Books were typically observed embedded in a background of smaller clay minerals (Figure 7.23). The smaller clay-sized material lapped both the face and edges of the book. However, books were also observed radiating from (Figure 7.9) and sitting on top of background material (Figure 7.11). Unlike grains, material was not typically observed separating away from the edge or face of individual books. Books typically had at least a small amount of grain coatings (Figures 7.9 and 7.20).

The paucity of large grains, poorly defined microaggregates, and the typical embedding of grains into a background of clay minerals meant connector assemblages were sparse and only observed in TS1 and TS2. Those present were comprised of clay sized tubular, spherical and platy material and formed structures up to 15 μm in length. Connectors were observed joining glass fragments (Figure 7.25), a book to groundmass material (Figure 7.20), and a microaggregate to a book and another microaggregate (Figure 7.21).

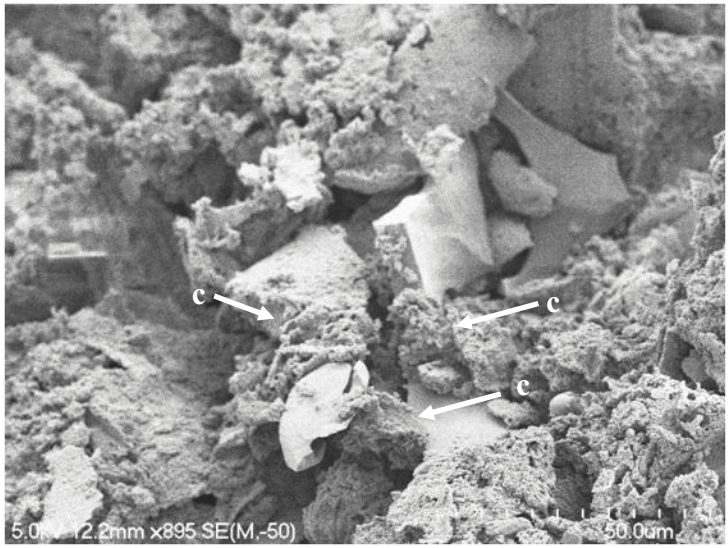

Figure 7.25: Connectors **(c)** comprised of small clay sized material from TS2 linking volcanic glass.

Poorly defined microaggregates, groundmass material and relict textures which were comprised of tubes, irregular polygonal spheres and small plates dominated the microstructure of TS1 and TS2 (Figures 7.7, 7.11 and 7.13). Whilst one could distinguish between the groundmass material and relict textures, a clear contact could not be defined. The relict textures appeared to simply grade into the groundmass material (Figures 7.13 and 7.14). Therefore particle arrangements of the observed clay minerals had no definable boundaries, formed a background and overall binder to the microstructure, and immersed larger grains and books. The

material from TS1 and TS2 fit with Beattie's (1990) description of a continuous groundmass. TS3 also had a continuous groundmass, with the smaller clay sized material acting as a binder. However, the predominance of relict textures observed in TS1 and TS2 was replaced by books in TS3 (Figures 7.12 and 7.23).

7.3.4 Pore sizes and shape

All samples from Tauriko were highly porous, with porosity values between ~ 62 and ~ 74% (Chapter 5). This was confirmed by SEM images, which showed an extremely open fabric.

In all samples the irregular shape of individual clay minerals, and their loose packing, resulted in a large amount of small pores between individual grains. These pores were typically ultra- and micro-pores up to 1 μm, with few larger than 0.7 μm (Figures 7.3, 7.4, 7.8 and 7.12). Pores between microaggregates are up to micro-pore size (5 μm in diameter) (Figures 7.9 and 7.11). Pores within the groundmass occurred up to macro-pore size (30 μm) (Figure 7.7), but were typically less than 15 μm (Figure 7.6).

Porosity associated with relict textures, which mostly affected TS1 and TS2, arose as a result of interaction between irregularly shaped clay minerals (Figures 7.15 and 7.16), collapsed wall sections (Figures 7.13 and 7.18), and within long hollow tubes (Figures 7.17, 7.18 and 7.19). Porosity between clay minerals was of similar size and shape to that described previously, but less frequent. Porosity in the collapsed wall sections was dominated by the size and shape of collapsed material and was observed up to meso-pore size, but pores were often only up to ~ 7 μm (Figure 7.13). Within the hollow tubes, meso-pores were typical but diameters never exceed 8 μm (Figures 7.17 and 7.19).

Porosity was observed between the individual plates of delaminating books (Figures 7.12 and 7.21) and also in the centre of small halloysite tubes.

The extent of connectivity between pores is largely unknown. However tubes in relict textures may extend to some depth into the sample, as do the void spaces around these tubes (Figure 7.19). Furthermore, the loose packing and

irregular shape of grains will increase the likelihood that the small pores between clay minerals are interconnected.

7.3.5 Remoulding

After remoulding, all Tauriko samples were completely altered from their undisturbed state. The structure was completely continuous and no micro-aggregates were observed. With the exception of a few remnants (Figure 7.26) relict textures were destroyed. Porosity was still abundant and dominated by that which occurred between irregular grains and within the groundmass. No macro-pores or fissure pores existed. The largest pore observed was a meso-pore (Figures 7.27 and 7.28).

Books typically remained intact following remoulding (Figure 7.29). Some delamination did occur (Figure 7.30) but this was only between two sheets and did not involve the whole book. Individual grains were observed individually and supported entirely by the groundmass (Figure 7.28). Individual books and grains remained embedded in the microstructure.

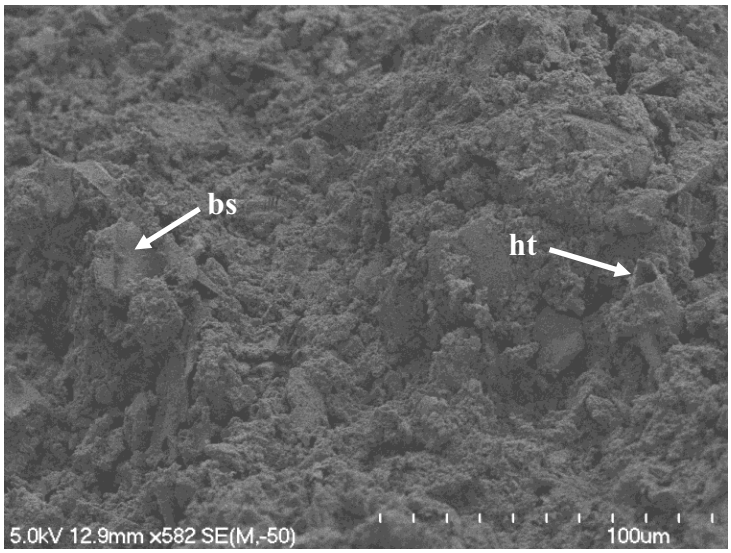

Figure 7.26: Remoulded sample from TS2 displaying a continuous structure with remnants of relict textures annotated as a broken sheets **(bs)** and hollow tubes **(ht)**.

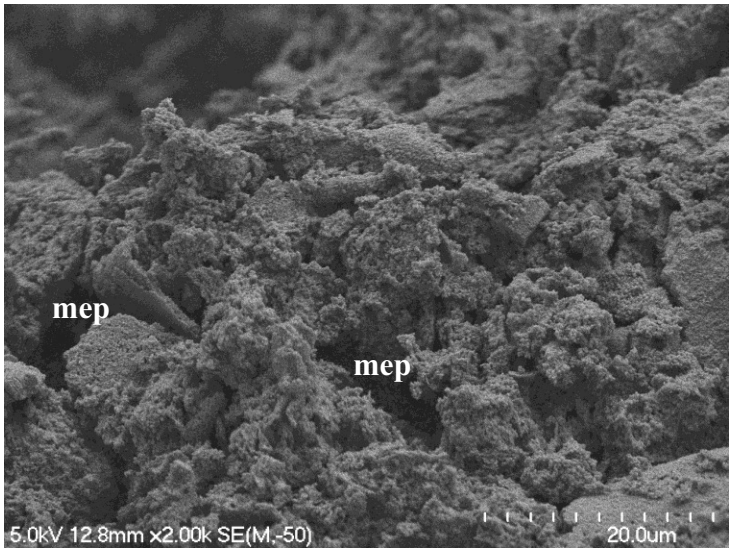

Figure 7.27: Remoulded material from TS2 displaying two meso-pores (**mep**) and the remainder of the groundmass dominated by micro-pores.

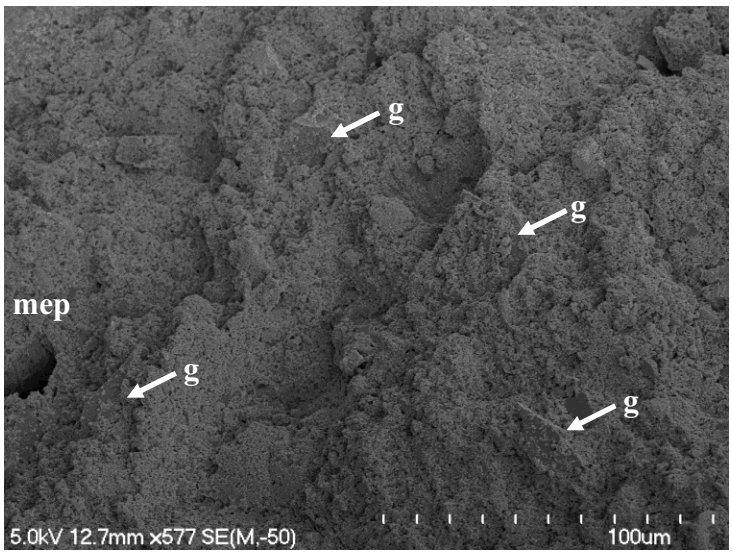

Figure 7.28: SEM image from TS3 showing grains (**g**) supported in a groundmass of clay minerals. A meso-pore is present at **mep**.

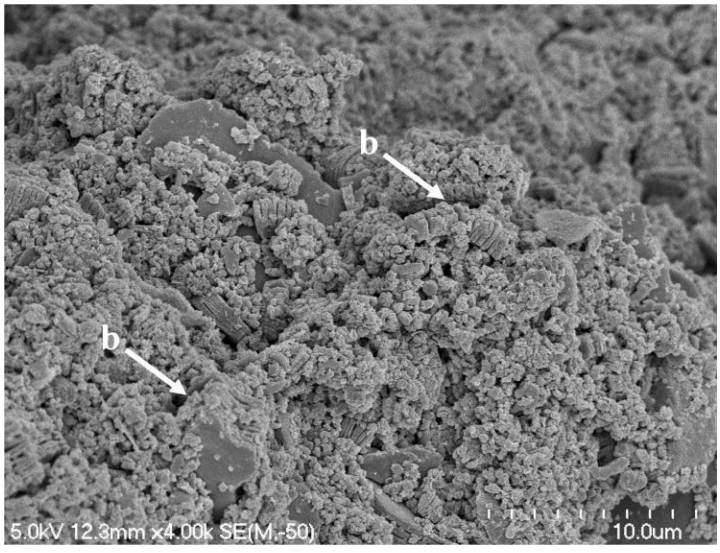

Figure 7.29: Halloysite books **(b)** from TS3 supported by a groundmass of clay minerals.

Figure 7.30: Remoulded material showing a halloysite book beginning to delaminate with sub-rounded spherical and ellipsoidal material between the platelets.

7.4 Otumoetai summary

The following describes microfabric components, particle arrangements, and pore size for samples from Otumoetai (OS1, OS2, OS3 and OS4).

7.4.1 Primary structural elements

7.4.1.1 Clay minerals

Halloysite was identified as the dominant clay mineral in samples from Otumoetai, although kaolinite was also present in OS3 (Chapter 6). The morphologies of individual clay minerals were comprehensively described in Chapter 6.

Halloysite tubes dominated all samples, long tubes were abundant in OS4 (up to 2μm) and shorter tubes in OS3 (mostly between 0.05 and 0.5 μm). OS1 and OS2 had a range of medium-sized tubes (few above 1 μm) (Figures 6.11, 6.12 and 6.13). Halloysite spheres occurred in all samples and OS2 had the highest abundance (Figure 6.20). Plates were observed in OS1, OS3 and OS4 (Figures 6.25, 6.26 and 6.27), but no books were observed.

7.4.1.2 Grains

Grains (non-clay material) were observed in both sand and silt size fractions for all samples, the abundance of which was least in OS3 and greatest in OS4. Plagioclase, quartz, and volcanic glass were observed, however their abundance was different to that recorded in Tauriko samples. Chapter 6 described the abundance, size and shape of all grains in detail. However, it should be noted

that both blocky and thin laminar type grains were observed in silt and sand size fractions. Furthermore, grains were least abundant in OS3.

Grains were typically observed individually and seldom came in contact with each other (Figure 7.31). When grains were close, they were separated by small clay-sized minerals (Figures 7.32 and 7.33). Grains typically did not display any dominant orientation (Figure 7.34). Small clay minerals were observed clothing larger sand- and silt-sized grains. For example, Figure 7.35 shows the outline of a biotite grain which is coated in clay.

Figure 7.31: SEM image from OS4 displaying sand grains (**sg**) supported individually in a groundmass of clay size material. The sand grains appear embedded in the surrounding material with the groundmass lapping against the edges of the grains.

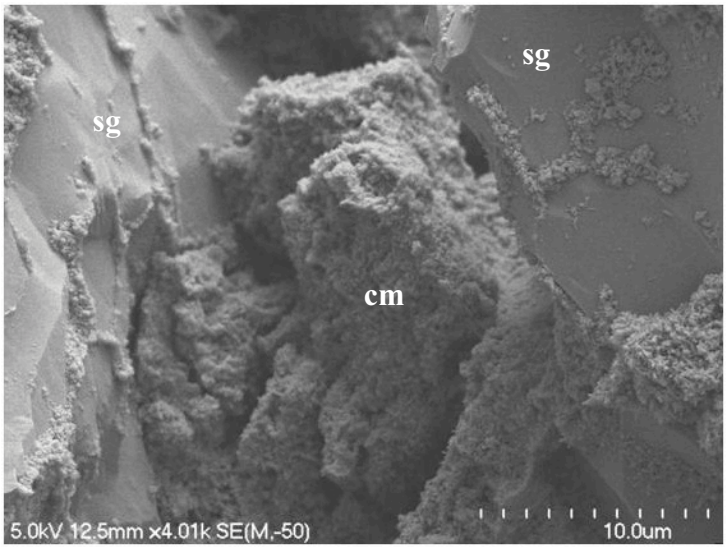

Figure 7.32: Clay minerals (**cm**), from OS2, forming a bridge between two large sand grains **(sg)**.

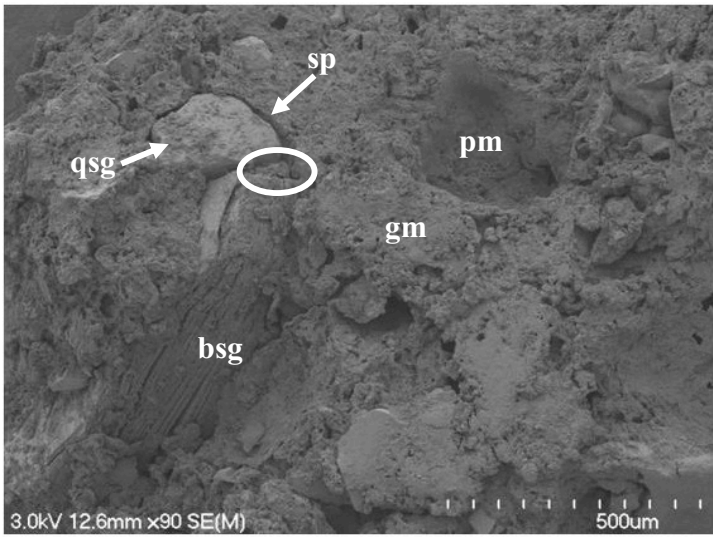

Figure 7.33: SEM image from OS4 showing clay sized material infilling the area between two sand grains (in oval), one is biotite (**bsg**) and the other is possibly quartz (**qsg**). The quartz grain has only minor grain coatings along the fracture surface. Groundmass (**gm**) material is observed separating (**sp**) away from the face of the sand grain forming a loose contact. A pluck mark (**pm**) is present in the top right hand corner of the image.

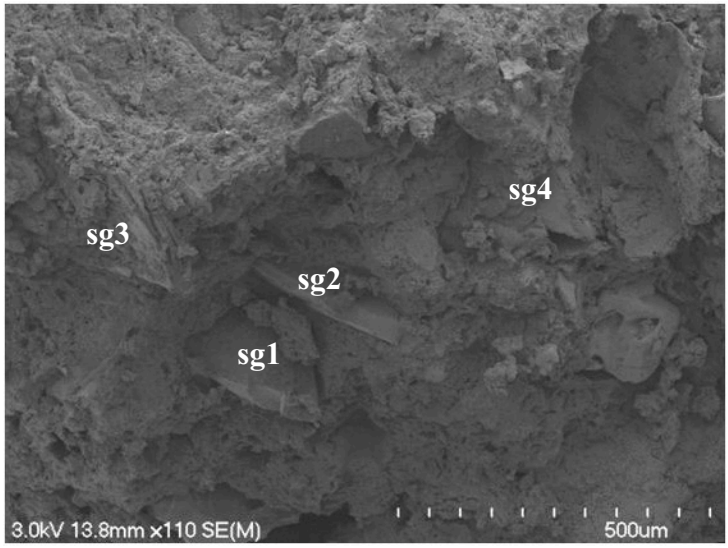

Figure 7.34: SEM image from OS4 showing large sand sized grains (**sg**) in a groundmass of smaller clay sized material. The grains are embedded in, and form a direct contact with, the groundmass material. The two sand grains (**sg1 & sg2**) in the centre of the image are orientated in the same direction; however those at **sg3** and **sg4** have faces which are at right angles to **sg1** and **sg2.**

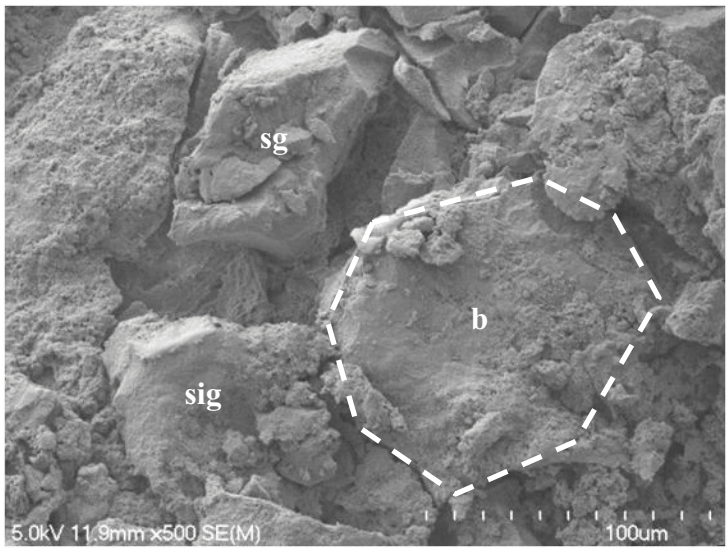

Figure 7.35: SEM image from OS1 showing sand **(sg)** and silt **(sig)** grains surrounding a biotite **(b)** grain clothed with clay sized material. The hexagonal edges of the biotite are indicated with a dashed line.

7.4.2 Elementary particle arrangements

7.4.2.1 Groundmass

In OS1, OS2, and OS4 halloysite tubes, which dominated the samples, were typically un-orientated over three dimensions forming a chaotic arrangement (Figure 7.36). The tubes were loosely packed and formed face-to-face (FF) contacts, which were either parallel or at right angles to each other (Figure 7.36). Face-to-edge (FE) contacts were also observed (Figures 7.36 and 7.37). FE or non-parallel FF contacts between tubes encouraged an open network type structure (Figures 7.36 and 7.37), which had a flocculated type appearance. The openness of this structure means there is a large proportion of void space surrounding the tubes.

In OS1, tubes were occasionally observed radiating from the fracture surface (Figure 7.38). It was unclear whether these tubes were radiating from aggregates or the surface of larger minerals.

In OS3, tubes were typically smaller and packed tighter than in OS1, OS2 and OS4 (Figures 7.39 and 7.40). The type of contacts between tubes described for OS1, OS2 and OS4 were present in OS3, but parallel FF contacts dominated (Figure 7.40). The orientation of tubes in OS3, whilst still random, was more subdued and had a flattened appearance when compared to other samples.

Small, irregular, polygonal shaped halloysite spheres were observed intermixed with tubes in OS1, OS2 and OS4 (Figure 7.41). Spheres were also observed individually in OS2 and OS4 (Figures 7.42 and 7.43). Because of their irregular and spherical shape, contacts were un-orientated.

In OS1, OS2 and OS4 observations indicated that tubes and spheres were typically observed together. This combination formed a very open delicate structure (Figures 7.44 and 7.45). In these samples, an increase in the abundance of irregular polygonal spheres relative to tubes caused a decrease in the openness of the structure (Figure 7.41), because the polygonal spheres were able to fill the gaps between tubes and pack more efficiently. The abundance of polygonal spheres was greatest in OS2, which resulted in large areas being devoid of tubes (Figure 7.43). Furthermore, structures formed by a combination of spheres and

tubes in OS2 (Figure 7.46) appeared less open than what was observed in OS1 and OS4. In OS1, a fine-grained gel-like material was infrequently observed coating arrangements of tubes and spheres (Figure 7.47). This coating will possibly act as a binding material.

In OS3, rather than and abundance of polygonal spheres intermixing with tubular material, plates were observed (Figure 7.40 and 7.48). However, the plates had little impact on the appearance of the structure because it was already tightly packed. Contacts between plates and tubes in OS3 were typically FF. Plates were also observed in FF contacts with each other (Figure 7.48). In OS3, large areas of sheet-like material were observed (Figure 7.48); whilst not well defined, contacts between plates within the sheets were EE.

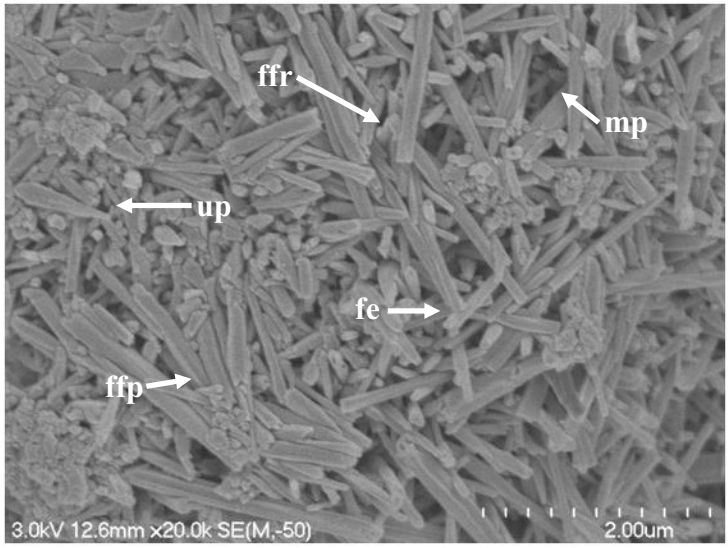

Figure 7.36: SEM image from OS4 showing un-orientated tubes with face-to-face contacts ranging between parallel (**ffp**) and right angles (**ffr**). Also observed are face-to-edge contacts (**fe**). Also present are abundant ultra **(up)** and micro **(mp)** pores. The largest pore is 0.5 μm in diameter.

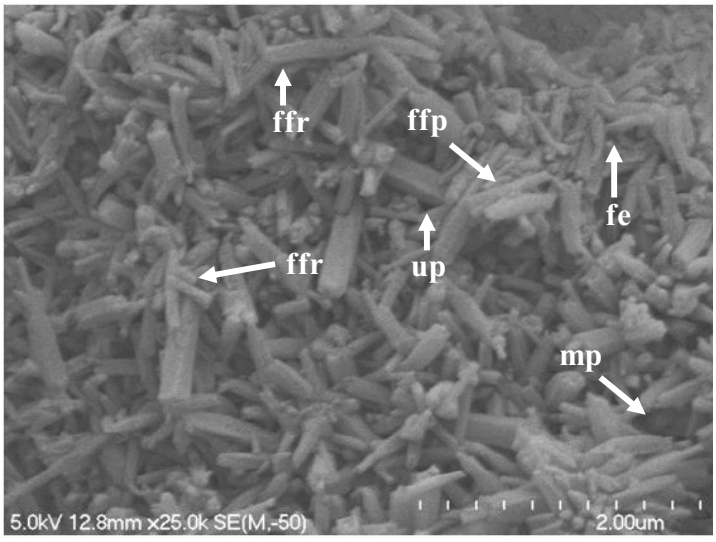

Figure 7.37: Tubes from OS2 arranged in an open structure. A range of tube contacts can be observed including; face-to-face contacts ranging between parallel (**ffp**) and right angles (**ffr**). Also observed are face-to-edge contacts (**fe**). Micro- **(mp)** and ultra-pores **(up)** are present.

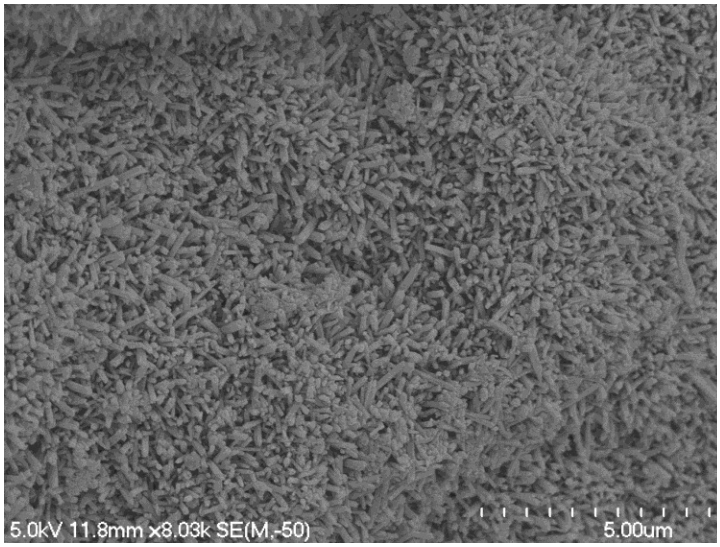

Figure 7.38: Halloysite tubes from OS1 radiating from the fracture surface created during sample preparation.

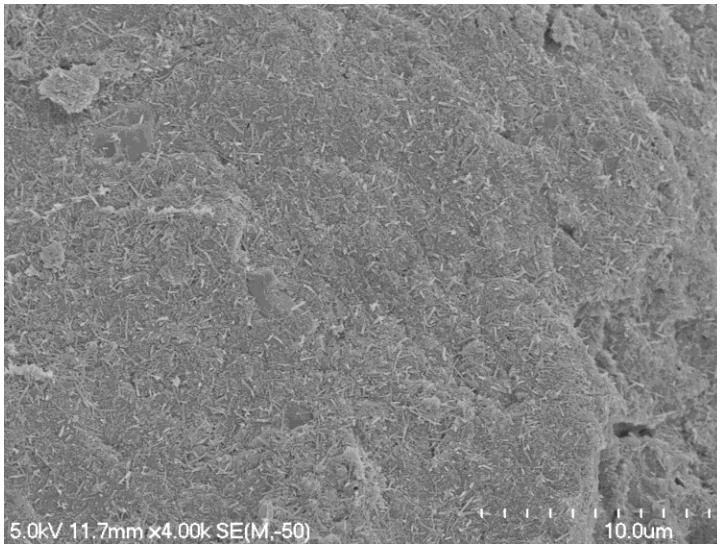

Figure 7.39: SEM image from OS3 showing tubes which are tightly packed.

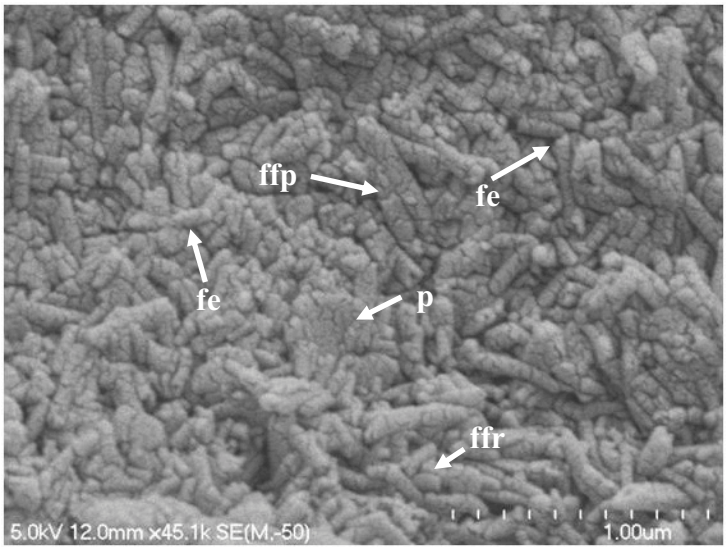

Figure 7.40: Tubes from OS3 tightly packed displaying face-to-face contacts ranging between parallel (**ffp**) and right angles (**ffr**). Also observed are face-to-edge contacts (**fe**). Included amongst the tubes are individual plates **(p)**. The mostly parallel contacts between tubes means only a small number of inter-particle ultra-pores are observed.

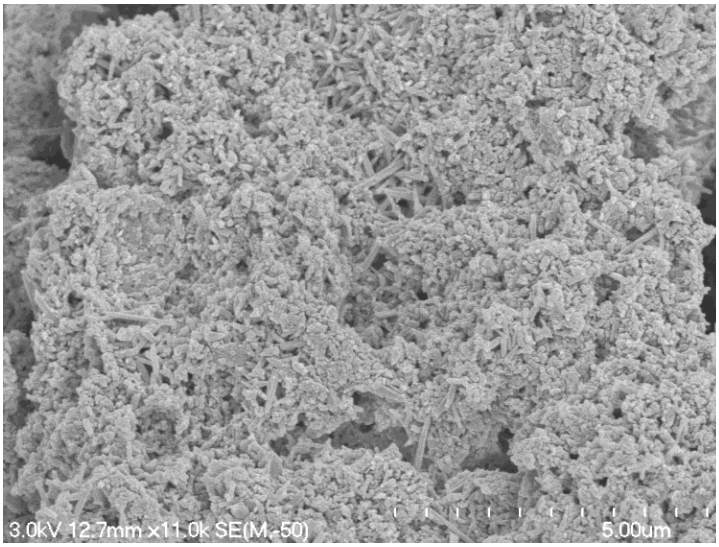

Figure 7.41: SEM image from OS4 displaying a large number of small polygonal spheres which appear to be overlying and interacting with tubes.

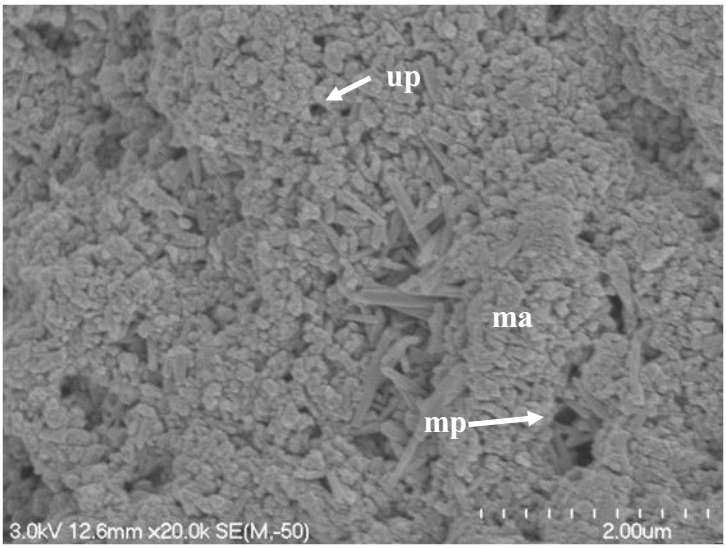

Figure 7.42: SEM image from OS4 displaying tubes and irregular spheres. The irregular spheres are observed clustering together to form small micro aggregates, ~ 2 μm in length **(ma)**. In this image inter particle ultra **(up)** and micro pores **(mp)** are observed between the small irregular polygonal spheres and around the tubes.

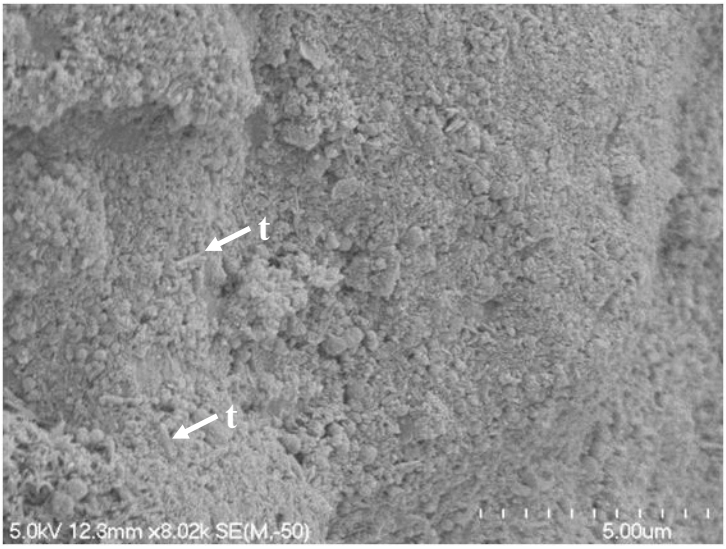

Figure 7.43: SEM from OS2 displaying a groundmass dominated by irregular polygonal spheres and a lesser amount of tubes **(t)**.

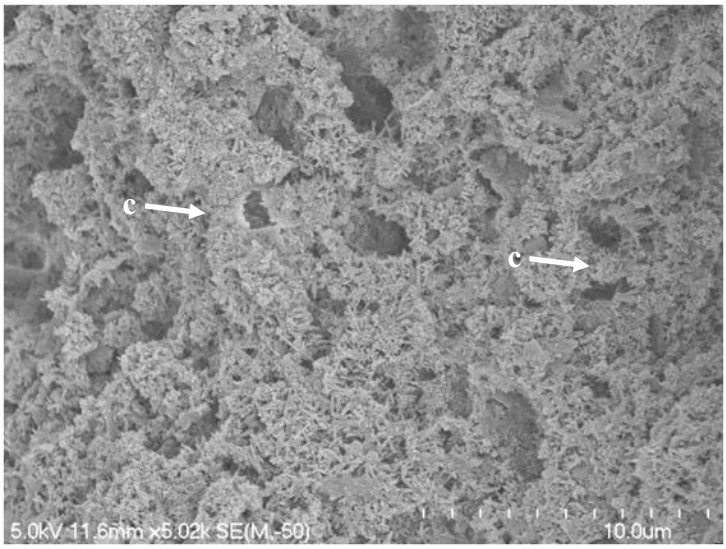

Figure 7.44: SEM image from OS1 displaying a combination of spheres and tubes forming a delicate open structure. Individual microaggregates are difficult to define, however, connectors **(c)** link clusters of tubes and spheres. Porosity is observed between individual clay minerals and within the groundmass, the maximum size is 2 µm.

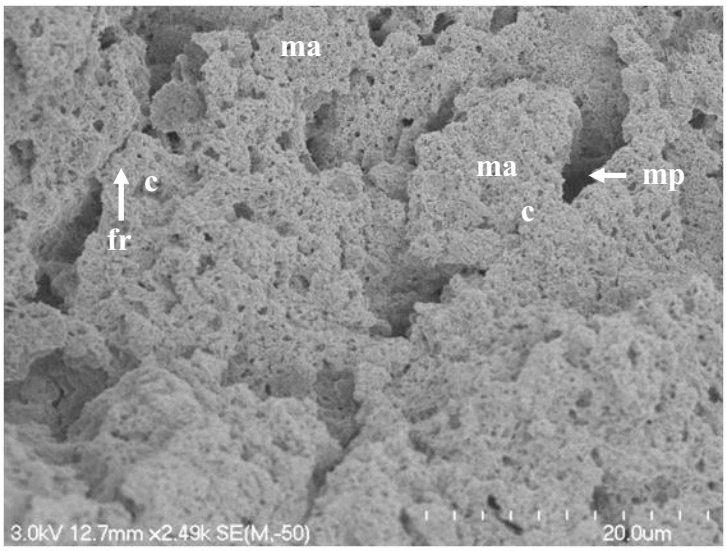

Figure 7.45: SEM image from OS4 displaying a combination of spheres and tubes which form a delicate, open structure. Poorly defined irregularly shaped micro aggregates (**ma**) up to 20 µm in length and associated connectors are present (**c**). Note the fracture (**fr**) in the top left hand corner. Pores between individual clay minerals and microaggregates are observed **(mp)**; the maximum size is ~ 4 µm.

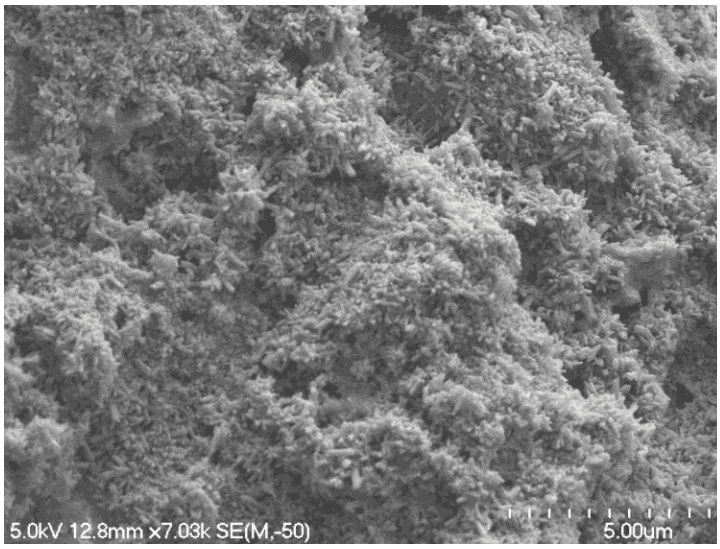

Figure 7.46: General structural image from OS2 displaying reduced porosity compared to OS1 and OS4.

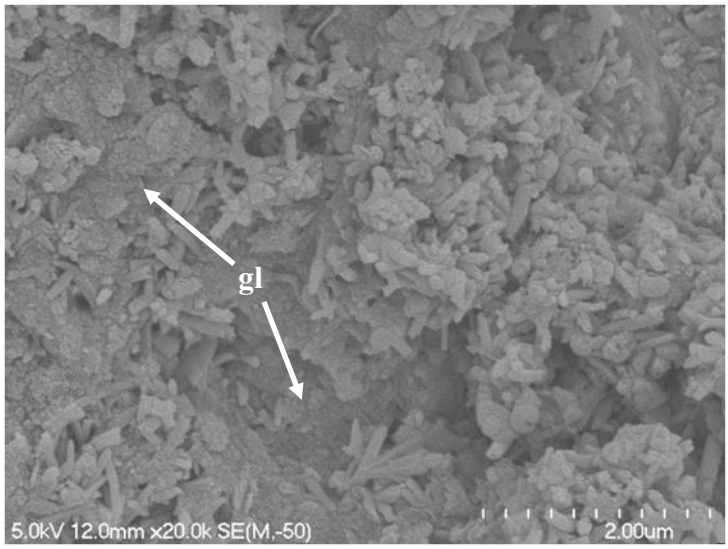

Figure 7.47: Tubes and spheres combining to form the typical structure observed in OS1. Covering this arrangement is a gel-like fine grained material which coats the tubes and spheres **(gl).**

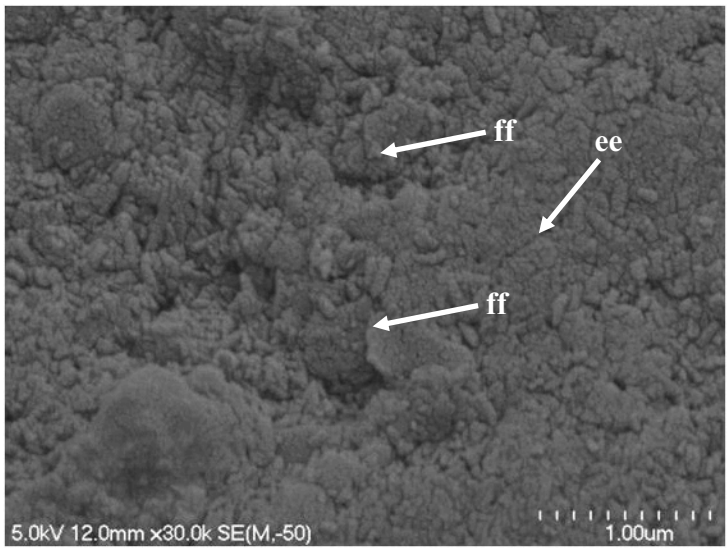

Figure 7.48: SEM image from OS3, showing plates in face-to-face contacts **(ff).** To the left of the image a large flat section is observed; whilst not well defined, individual plates which make up this section are in edge-to-edge **(ee)** contacts. Also observed in this image are ultra pores no larger than 0.1 µm.

7.4.2.2 Microaggregates

The clustering of spheres and tubes in differing amounts formed irregularly shaped microaggregates in OS1, OS2 and OS4 (Figures 7.45 and 7.49). However, similar to Tauriko samples, microaggregate boundaries were difficult to define and were possibly part of a much larger groundmass material. When definable, microaggregates were up to 20 µm in diameter (Figure 7.45). Larger, up to 80 µm, aggregates were sparsely observed, however, these may represent grains clothed in clay minerals.

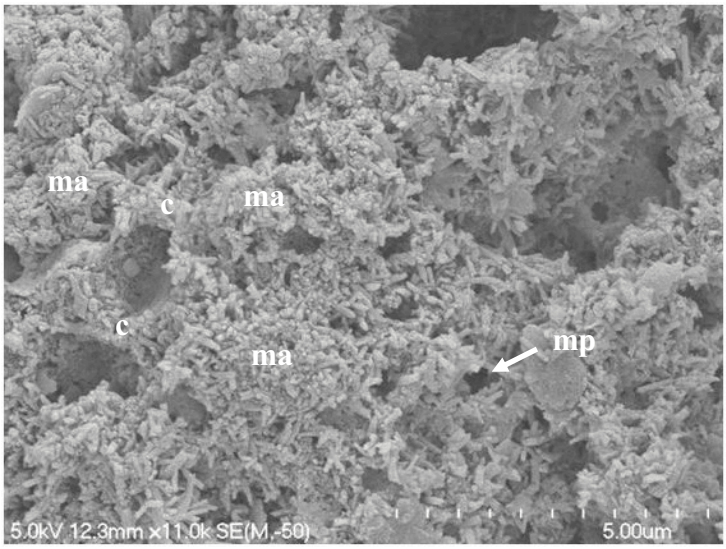

Figure 7.49: SEM image from OS1 showing poorly defined microaggregates **(ma)** up to 3.5 μm in diameter. Connectors (**c**) appear to link the poorly defined microaggregates. Porosity occurs between clay minerals and the microaggregates. Pores are typically micro-pores (**mp**) up to ~ 0.5 μm, the pore in the top right hand corner has a diameter of ~ 3 μm.

In OS4, dense microaggregates ~ 2 μm in diameter comprised of polygonal spheres (Figure 7.42) were observed. These were typically supported by tubular material. Whilst spheres appeared abundant in OS2, definable aggregate boundaries were not observed (Figure 7.43).

The tightly packed nature of OS3 meant that microaggregates were seldom observed.

7.4.3 Overall particle associations

The following describes the interaction between the general groundmass material, poorly defined aggregates and larger grains.

Grains were typically embedded in the surrounding groundmass (Figures 7.31 and 7.33) and groundmass material lapped against the surface of the grain (Figures 7.31 and 7.34). Along the fracture surface minor to abundant grain coatings (Figures 7.33 and 7.35) were observed, although some grains appeared clean (Figure 7.50). However, the linkage between groundmass and grains was weak because pluck marks were observed in OS2 and OS4 (Figure 7.33) and contacts were typically loose (Figures 7.33 and 7.51). OS3 was the only sample where grains were observed tightly bound into a background of clay minerals (Figure 6.49).

In OS1 and OS4 connectors were observed between microaggregates (Figures 7.44, 7.45) and joining large grains (Figure 7.32). All connectors were

comprised of the same clay minerals. However, the connectors were believed to be weak because fracturing was observed at contact points with microaggregates (Figure 7.45).

At Otumoetai, the groundmass and microaggregates were dominated by halloysite tubes, often with a lesser amount of spheres and plates. When combined, these particle arrangements appeared very similar and formed a background to the microstructure immersing large and often sparse grains. The overall structure in all samples had the appearance of a continuous groundmass; this was especially so in OS3.

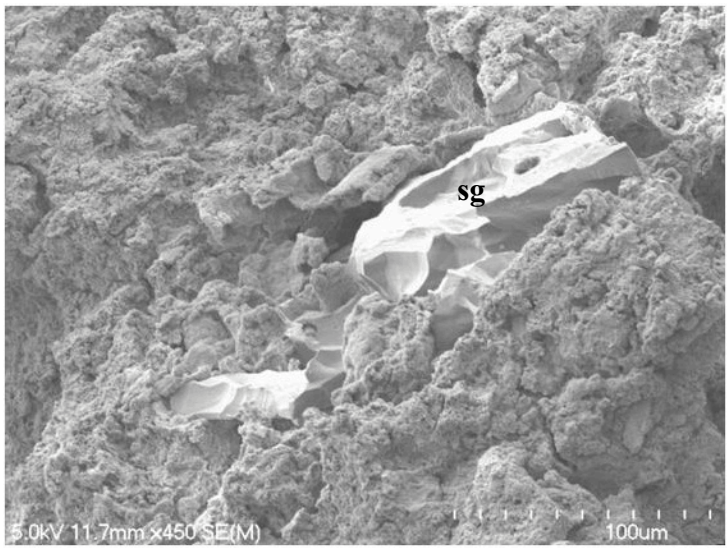

Figure 7.50: Sand-sized grain **(sg),** possibly quartz, from OS2 surrounded by a groundmass of clay-sized material. The sand grain is completely clean and does not have any grain coatings.

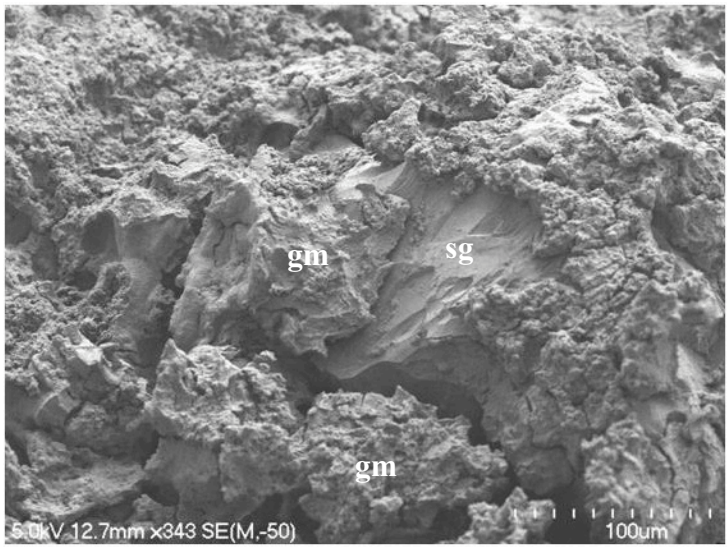

Figure 7.51: SEM image of groundmass material (**gm**) separating away from a sand grain (**sg**) forming a loose contact.

7.4.4 Porosity

Porosity in all samples was high, ranging between ~ 65 and ~ 75 %. As a result of the packing of particles, it was generally observed that OS3 was the least porous sample, OS1 and OS4 the most, and OS2 had intermediate porosity.

In all samples, pores (Figures 7.36, 7.37, 7.40 and 7.44) occurred as a result of the interaction between tubes, spheres and plates. These were observed within the poorly defined aggregates or groundmass material and were either ultra- or micro-pore size. In OS1, OS2 and OS4 these small pores were seldom larger than 0.5 μm (Figures 7.36 and 7.37) and in OS3, pore sizes were typically no larger than 0.1 μm, and were less abundant (Figures 7.40 and 7.48). Ultra-pores were dominant when irregular spheres interacted in OS1, OS2 and OS4 (Figure 7.42). This occurred most often in OS2 because spheres were frequently observed.

Pores which were not specifically a result of the interaction between clay minerals occurred in all samples. These pores occurred between microaggregates and within the groundmass, and were least abundant in OS3. Micro-pores were typical with a maximum size of ~ 4 μm (Figures 7.44 and 7.45). However, at low magnifications a number of meso-pores were observed (Figure 7.52), these were seldom larger than 20 μm. Macro-pores, whilst present, were rare in all samples, especially OS3.

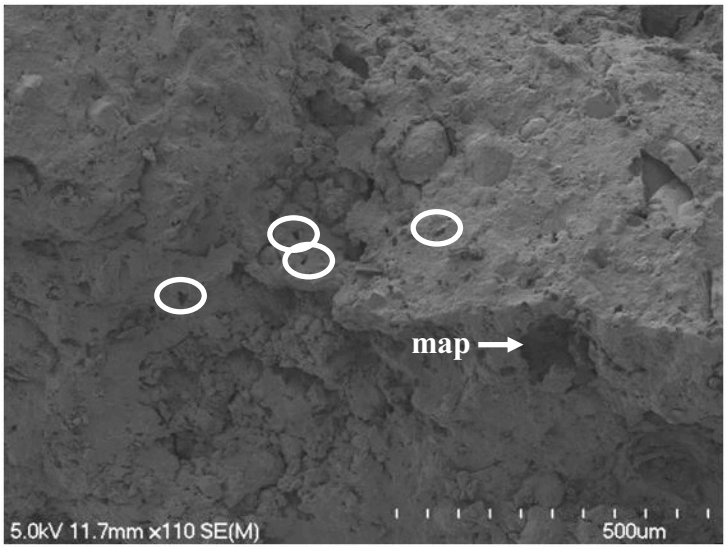

Figure 7.52: SEM image from OS3 showing a number of meso-pore (examples are circled) and a larger macro-pore (**map**).

Porosity within grains occurred within large sand and silt grains, for example Figure 7.33 gives an example of fissure like pores between delaminating sheets in a biotite mineral.

Like Tauriko the connectivity of pores in the Otumoetai samples was difficult to define, but the predominance of loosely packed tubes in OS1 and OS4 forming a network arrangement with a large amount of voids would promote interconnection of pores. However the large number of spheres in OS2 and the tight packing of tubes in OS3 not only reduced the openness of the structure but will also reduce the connectivity of pores.

7.4.5 Remoulded structure

Because of the practicalities of time, only remoulded material from OS3 and OS4 were viewed using the SEM.

No obvious change in microstructure was observed after remoulding of OS3. At high magnification the general microstructure was still observed as tightly packed and porosity was dominated by ultra-pores between individual clay particles (Figure 7.53). At low magnification there appeared to be a decrease in porosity (Figure 7.54), with most of the meso-pores observed in Figure 7.52 being completely destroyed.

OS4 retained a high proportion of inter-particle porosity after remoulding (Figures 7.55 and 7.56). Tubes were still observed intermixed with spheres (Figure 7.55). However, the delicate framework observed in undisturbed samples appeared less open (Figure 7.56) and the microaggregation of clay minerals had occurred (Figure 7.57). The microaggregates formed were at least 4 μm in diameter, represented a different structural arrangement and had reduced porosity compared to the undisturbed fabric of tubes and spheres.

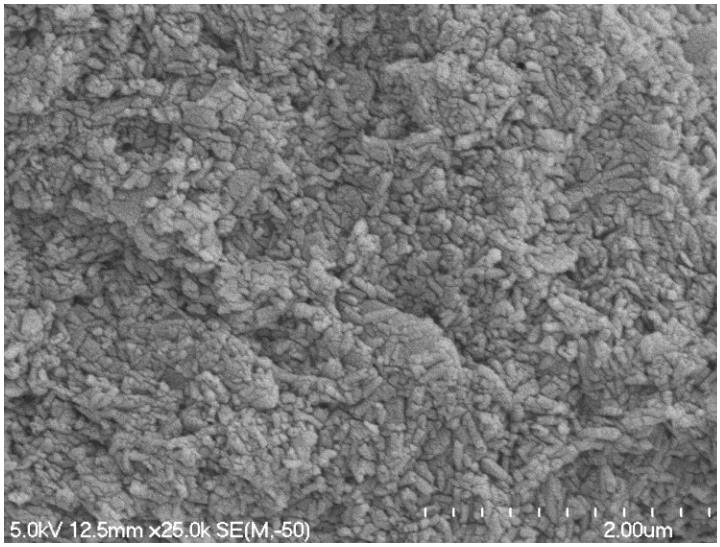

Figure 7.53: Remoulded material from OS3 tightly packed displaying porosity between clay minerals.

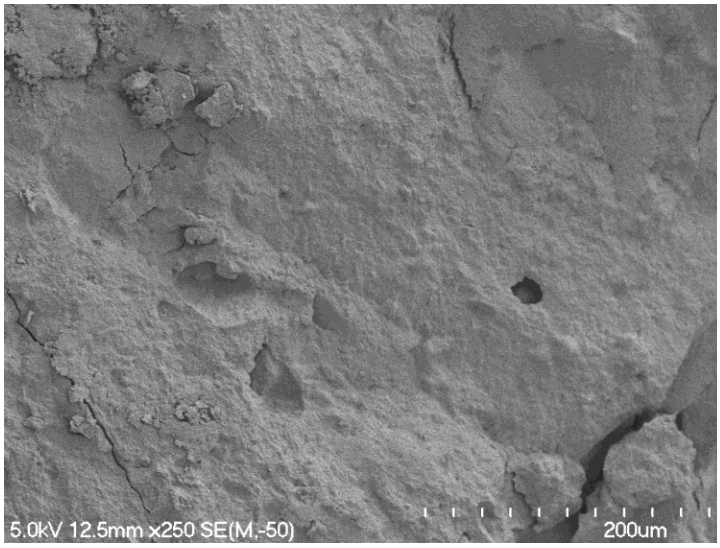

Figure 7.54: SEM image of remoulded material from OS3 displaying less porosity than what is observed in Figure 7.52. One pore is present with a diameter of ~ 22 µm.

Figure 7.55: SEM image of a remoulded sample from OS4 showing inter-particle porosity.

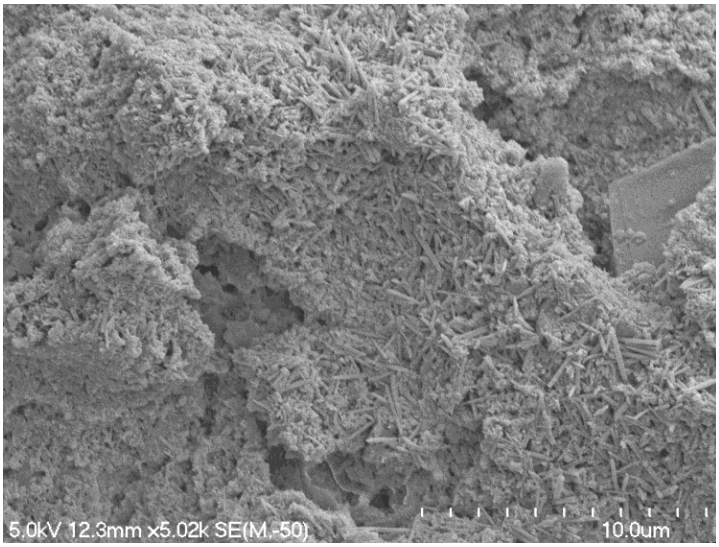

Figure 7.56: Remoulded SEM image from OS4 showing reduction of the previously observed open framework

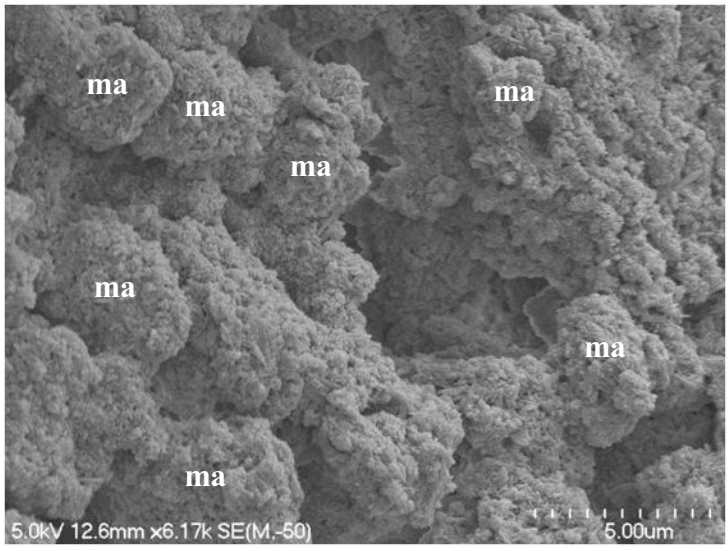

Figure 7.57: Remoulded SEM image from OS4 displaying microaggregates (**ma**) at least 4 µm in diameter

7.5 Overview of microfabric

Typically, sedimentary studies categorize observed microfabrics into geometric classifications often dictated by loading history and grain size distribution (Huppert 1986; 1988). Popular models to classify sedimentary deposits are that of Sergeyev (1980) and Grabowska-Olszewska *et al.* (1984). These classification systems divide microfabric into five groups, namely honeycomb, skeletal, matrix, turbulent and laminar microstructures.

Workers investigating volcanic soils have classified rhyolitc silts as honeycomb, mixed honeycomb skeletal, skeletal and mixed skeletal- matrix microstructures (Cong 1992; Keam 2008). Volcanic clay soils have been classified as matrix or mixed matrix – turbostratic (Keam 2008).

In this study, classification of microfabric type according to Sergeyev *et al.* (1980) and Grabowska-Olszewska *et al.* (1984) was difficult, if not impossible to apply. The classification systems of Sergeyev *et al.* (1980) and Grabowska-Olszewska *et al.* (1984) were based heavily on sedimentary deposits and included idealised microfabrics for deposits which may have experienced differing degrees of consolidation. The samples under examination in this study were normally consolidated pyroclastics, and the clays present occurred as a result of authigenic processes. The sedimentary classifications were also correlated with specific geomechanical data (see for example Sergeyev *et al.* 1980), which may not apply to volcanic deposits with similar microstructure. Attempting to force a sedimentary classification system, along with its associated properties, onto tephra derived deposits is unproductive and potentially misleading. The following will summarise the microstructural characteristics of samples observed in this study, and hence provide a summary to this chapter.

7.5.1 Tauriko

All Tauriko samples had a combination of polygonal spheres, tubes and individual plates which dominated the microfabric and formed irregular microaggregates, delicate relict textures and groundmass material. Halloysite books and larger grains were embedded within the background of clay minerals in all samples (Figure 7.58). Connector assemblages were few and the microfabric appeared continuous (Figure 7.58). As shown in Figure 7.58, the microfabric of TS1 and TS2 is slightly different to that of TS3. TS1 and TS2 were dominated by halloysite tubes; contrastingly, TS3 contained an abundance of irregular plates and polygonal spheres. Relict textures were most common in TS1 and TS2, yet books were more abundant in TS3. The abundant books were often observed forming parallel contacts and gave the microfabric in TS3 a less open appearance than in TS1 and TS2 (Figure 7.58).

In all samples, pores were dominantly ultra- and micro-pores, which occurred between clay minerals, microaggregates or within the groundmass. The hollow tubes of relict textures encouraged a large amount of porosity. Pores were typically meso-pores and only up 8 μm in diameter.

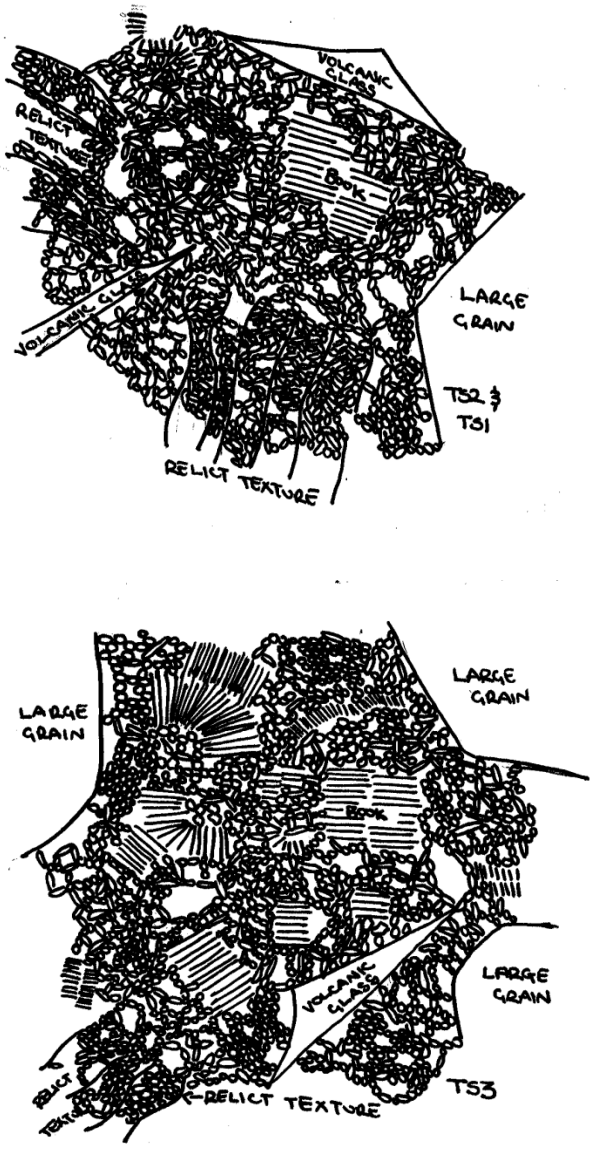

Figure 7.58: General microstructure for TS1 and TS2 (top) and TS3 (bottom) from Tauriko. Included in both images are small clay minerals which form the background to the microfabric, books, volcanic glass and larger grains.

The loose packing of tubes, spheres and individual plates in Tauriko samples resulted in an open microfabric where the clay minerals had few contacts compared to a more compact structure. Geometrically Figure 7.58 represents a 'skeletal' (Sergeyev *et al.* 1980) or 'honeycomb' type structure (Terzaghi 1925). Keam (2008) observed a similar structure in sensitive silts at Otumoetai however, he suggested the small irregular halloysite spheres and plates were crystalline quartz (Chapter 2).

7.5.2 Otumoetai

Most samples from Otumoetai were dominated by halloysite tubes, combined with a lesser amount of plates and spheres. OS2 being the exception with a large number of spheres. These minerals dominated the microfabric and combined to form groundmass material and microaggregates. The microfabric of all samples was continuous and grains were imbedded in background material (Figure 7.59).

Figure 7.59 indicates, whilst the components may be similar for all Otumoetai samples, their microfabric is different. OS1 and OS4 were similar, with a large amount of tubes in an open network appearance forming typically tangential contacts between each other. This openness was reduced with the inclusion of spheres. OS1 differed slightly from OS4 in the fact that tubes were typically slightly smaller and a fine grained coating was observed. While the fabric in OS2 included tubes and spheres in an open arrangement like that of OS1 and OS4, it had large areas of spheres in a dense arrangement giving it a slightly less open structure. OS3 contrasts with all other Otumoetai samples because small tubes were typically observed in tight parallel face-to-face contacts (Figure 7.59) and it contained the least amount of large grains.

Ultra or micro-pores dominated all samples, these occurred between clay minerals, microaggregates or within the groundmass. The tight packing of OS3 meant it had reduced porosity. Porosity in OS2 was reduced doe to its abundance of halloysite spheres. Larger pores were more common in OS1 and OS4, but least common in OS3. All samples had pores up to meso-pore size but macro-pores were seldom observed.

The open arrangement of tubes in OS1, OS2 and OS4 appeared much like the ‘flocculated’ structure presented by Lambe (1958). Tubes in a regular subdued fashion like that in OS3 were much like the “dispersed” arrangement of Lambe (1958) or the “matrix” structure presented by Sergeyev *et al.* 1980.

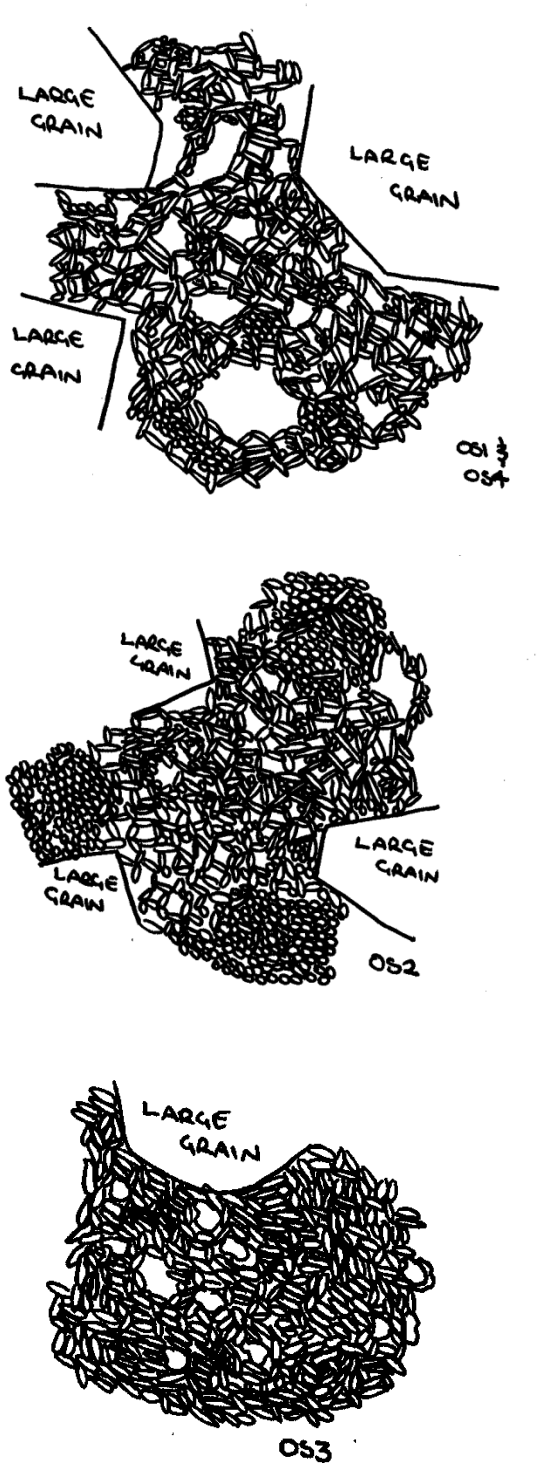

Figure 7.59: General microstructure for OS1 and OS4 (top), OS2 (middle) and OS3 (bottom) from Otumoetai. Included in both images are small clay minerals which form the background to the microfabric and larger grains.

Chapter 8
Discussion

8.1 Introduction

This chapter presents a discussion and synthesis of results from field, geomechanical, mineralogical, and microfabric investigations. It will discuss the origin of deposits sampled and their states of weathering and provide an explanation for halloysite formation and the unique morphology of halloysite books. The chapter will also make correlations between measured geomechanical properties and discuss interrelationships with microfabric. It will discuss the possible pathways which have contributed to the development of sensitivity.

8.2 Development of materials

8.2.1 History

All samples investigated in this study were ultimately volcanic (pyroclastic) in origin. Each sample contained volcanic glass, quartz and plagioclase, which are common in pyroclastic flow deposits, tephra deposits and in reworked ignimbrite material (Winter 2001; Roger Briggs *pers. comm.* 2008). Samples from both Tauriko and Otumoetai are likely to be rhyolitic in composition. Energy dispersive x-ray (EDX) analysis of material from Tauriko indicated that glass fragments had similar compositions to those of rhyolitic origin, and relict textures of pumice were also observed. At Otumoetai, the predominance of rhyolitic material in the Tauranga Basin (Chapter 2) would suggest that parent materials of this type are most likely. Furthermore, the dominance of hydrated halloysite in each sample may suggest a highly siliceous parent material, such as rhyolitic pyroclastic deposits. The following sections discuss the mode of deposition of the units at Tauriko and Otumoetai that were sampled.

8.2.1.1 Tauriko

Observations indicated that the mode of deposition for each site was different. All samples from Tauriko were primary tephra fall deposits. Glass shards observed during scanning electron microscopy were often thin, sharp and showed no obvious signs of abrasion or rounding (Chapter 6). Considering the delicacy of

the shards observed, one would expect them to be easily damaged if transported. These characteristics are indicative of primary deposition with limited or no reworking (Oborn 1988). Furthermore, during field investigation the clayey silt units from which TS1, TS2 and TS3 were sampled appeared massive and thick (0.5 – 1 m.), having no obvious fluvial bed forms (Chapter 4). An origin of primary tephra fallout was reflected in the void ratios of Tauriko samples, especially TS1 and TS2 and to a lesser extent TS3, with values of 2.86, 3.40 and 1.63, respectively. Light fallout deposition is enhanced by the irregular shape of pyroclastic material which would pack inefficiently and further support an open structure. This interpretation is supported by Rogers (1995), who stated that as the angularity of bladed loess increases so too will void ratio. By analogy sharp and irregularly shaped glass shards may have the same effect, an example being those presented in Figures 6.41 and 6.45. Pumice, a component typical of tephra or pyroclastic deposits, also adds to void ratio because of its vesicular nature. As the pumice weathers it may dissolve, becoming thin-walled and delicate and thus increasing void ratio. An example of this process is reflected by the relict textures observed in Figures 7.10, 7.13 and 7.14. The presence of relict textures lends support to Torrance`s (1992) hypothesis that void ratio may increase with diagenesis and weathering.

Given that the sensitive units from Tauriko were primary fall deposits, they could possibly represent pyroclastic units associated with the Te Ranga Ignimbrite (0.27 Ma; Briggs *et al.* 2005). The sensitive material may represent early fall deposits associated with the eruption of Te Ranga Ignimbrite because the minerals and textures observed were similar to those found in the Te Ranga Ignimbrite. Petrographical investigation indicated that glass textures in samples from Tauriko had curved and cuspate shapes exhibiting only moderate devitrification. Crystals (minerals) in the samples included plagioclase, hypersthenes, quartz and hornblende. All the above features have been previously described in the Te Ranga Ignimbrite (Briggs *et al.* 1996; 2005). However, the sensitive units may also represent material from an earlier eruptive event unrelated to the eruption of the Te Ranga Ignimbrite.

8.2.1.2 Otumoetai

Otumoetai samples did not have the same depositional history as material from Tauriko. Units at Tauriko were associated with the Te Ranga Ignimbrite (0.27 Ma) and therefore younger than those from Otumoetai, which lay below the Rangitawa tephra (0.34 Ma; Lowe *et al.* 2001). Furthermore, the paleosol (OS3) between OS2 and OS4 indicated that a long period of environmental stability, and hence time, occurred between depositional events at Otumoetai. The biotite observed in Otumoetai samples indicates an eruptive source which was rich in this mineral.

OS1 and OS4 were likely to be of fall origin, either as loess or tephra, because like Tauriko samples they have high void ratios of 3.02 and 2.62 respectively. The void ratio of OS3 may have been similar to ratios of OS1 and OS4. However, the void ratio has been overprinted in OS3 by pedogenic weathering whilst at the land surface. Considering that Rolo *et al.* (2004) reported void ratio values from Tierra Blanca pyroclastic deposits in El Salvador between 0.86 and 1.24. the lower void ratios values in TS3 (1.63) and OS3 (1.90) were still acceptable for materials of fall origin. If OS1, OS3 and OS4 are tephric then they represent members of the loosely defined Pahoia tuffs (0.35 – 2.18 Ma; Briggs *et al.* 1996), which in effect are part of the Matua subgroup (0.6 ka – 2.09 Ma; Briggs *et al.* 2006).

Petrological investigations suggested that the origin of OS2 was different from all other samples. Grain mount and x-ray diffraction (XRD) investigations (Chapter 6) indicated a concentration of heavy minerals in OS2, these being hornblende, titinomagnetite and pyroxene. Because of their high specific gravity (3.0 – 5.2) the relative abundance of these minerals indicated fluvial sorting. OS2 had a void ratio which was lower than those of TS1, TS2, OS1 and OS4. Such a low void ratio may indicate better sorting and packing in a wet fluvial environment as opposed to dry fallout deposition. In conclusion, OS2, was reworked and a member of the fluviatile Matua Subgroup (0.6 ka – 2.09 Ma).

Another major reason for the retention of high void ratios is that none of the samples had experienced extremely high rates of true geological consolidation. As a comparison, Beattie (1990) reported void ratios for fireclay in South Waikato

Tertiary coal measures between 0.29 and 0.65, and Chapman (1998) recorded void ratios between 0.1 and 0.56 in soil derived weathered from Tertiary Waitemata Group flysch deposits. Both of these materials have been consolidated.

8.2.2 Weathering environment

Samples from Otumoetai displayed evidence of greater weathering than those from Tauriko. Otumoetai samples were older than materials from Tauriko (section 8.2.1), potentially resulting in more time for weathering and argillisation processes to occur. Volcanic glass, which dissolves rapidly, and plagioclase were more abundant in samples from Tauriko. XRD analysis, through peak height (Table 6.7), indicated that highly resilient quartz was more abundant at Otumoetai than Tauriko. Furthermore, ferrihydrite and the broad Fe oxides, which are associated with weathering, had a greater presence at Otumoetai. These Fe minerals impart the light and dark brown colours observed in units from Otumoetai (McLaren & Cameron 1996), compared with the pale grey colour of material from Tauriko. If the samples from Tauriko were associated with the Te Ranga Ignimbrite then the sensitive units would have been rapidly covered by thick deposits of pyroclastic material, allowing little time for surface weathering.

At Otumoetai, OS3 showed evidence of a different and possibly stronger weathering environment. OS3 had high clay content (SEM observations), high liquidity and plasticity indexes, the largest XRD peak (bulk sample) for highly resilient quartz, and a high ratio of zircons, compared with other primary minerals. These features are typical of a highly weathered tephra deposit displaying strong soil formation (Shepherd 1984; Bakker *et al.* 1996). Being a paleosol, the advanced stages of weathering observed in OS3 were most likely a result of its past position at the land's surface. Therefore, biotic activity would have enhanced chemical weathering, an example being changes in pH which affects hydrolysis (McLaren & Cameron 1996). Biotic activity would have also encouraged soil mixing, creating a more developed soil structure than in other samples. Roots may have played an important role by compressing aggregates and causing differential dehydration (Hillel 2004). The darker colour of OS3 may indicate a slightly higher organic content than other units (Shepherd 1984). During particle size analysis, OS3 displayed the strongest reaction when H_2O_2 was added to remove organic matter.

High clay content in OS3 may have encouraged clay migration (illuviation) thus increasing the fine clay fraction in the lower portion of the unit (Bakker *et al.* 1996). Increasing the fine clay fraction would have impeded drainage, hence reducing the loss of Si in soil solution which encourages further halloysite formation, resulting in greater bulk densities (Parfitt *et al.* 1983; see also section 8.9). The dry bulk density in OS3 was high (920 kg m^{-3}) relative to all other samples (Table 5.2). Scanning electron microscope images of OS3 (Chapter 7) confirmed that the fabric in OS3 was different from that of all other samples, having short tightly packed halloysite tubes typically in a subdued parallel alignment.

8.2.3 Clay minerals

8.2.3.1 Formation

Clay mineral assemblages at both sampling sites were dominated by hydrated halloysite. Al-rich allophane was only a minor component in samples OS1, OS2 and OS3 (< 1.6 %) and was absent from OS4 and from Tauriko samples. The presence of both minerals was not unexpected considering the volcanogenic parent materials and likely drainage conditions (Chapter 2). As outlined in Chapter 2, it is likely that halloysite in this study has formed directly from primary minerals rather than neoformation from dissolved allophane.

The highly siliceous nature of the rhyolitic parent materials at both Tauriko and Otumoetai would have enhanced halloysite formation (Chapter 2). Further contributing to this are geological and climatic conditions. The vertical variability of geological units in the study area includes layers of low permeability, and OS3 may be one such example. These layers of low permeability create perched water tables and impede leaching conditions. Consequently, Si in soil solution remains high promoting halloysite formation (Chapter 2). These drainage conditions are supported by Bakker *et al.* (1996) who reported the formation of halloysite in soils with impeded drainage. Evidence of sustained saturation, either recently or in a past climate, is displayed by the presence of manganese concretions (pyrolusite) in all samples. Thus the soil has been saturated long enough for Mn reduction to

occur; subsequent drying, and hence oxidation, has resulted in the formation of MnO_2 (Vepraskas 1994).

Past climatic conditions may have also played a role in halloysite formation. For example, soils are sufficiently old (samples at Tauriko are > 0.27 Ma and those at Otumoetai are > 0.35 Ma) to have experienced cold and dry glacial climates (marine oxygen isotope stages 2, 6 and 8), which represent periods with reduced rainfall and likely reduced leaching (see references in Chapter 2).

Under current conditions, it is expected that halloysite formation is still occurring. Evidence of likely recent halloysite tube formation was observed during scanning electron microscopy in TS2 and OS3 (Figures 6.16 and 6.17). The thick overburden of material at each site, which is predominantly rhyolitic, will support a Si-rich environment, as silica in solution migrates down from upper horizons (Wada 1989; Lowe & Percival 1993). Combined with impeded drainage conditions, the fabric created by the formation of halloysite clays will encourage further halloysite formation by slowing the loss of silicon in solution. Scanning electron microscopy (Chapter 7) indicated that pore sizes were typically small (< 10 μm) in all samples, and few macro-pores (> 30 μm), which control water movement (McLaren & Cameron 1996), exist. This means that little water movement will occur, ensuring that Si in soil solution will remain high.

The small amounts (< 1.6 %) of Al-rich allophane in OS1, OS2 and OS3 mean that silica in solution has been high for prolonged periods to support the formation of halloysite (Chapter 2). However, for the small amount of allophane to form, the units which contain allophane would have had to experience periods with reduced Si concentration. This may have occurred during seasonal wetting, encouraging leaching which would lead to low Si concentrations in soil solution (Harsh *et al.* 2002). However, any influence of a wetting pattern is very weak because halloysite is by far the dominant clay mineral.

The small amount of kaolinite in OS3 may have derived by weathering (neoformation) from halloysite (McLaren & Cameron 1996). For example, Papoulis *et al.* (2004) suggested that as weathering advances, tubular halloysite converts to platy halloysite which then converts to kaolinite. Both tubes and plates were

observed in OS3. Churchman & Gilkes (1989) suggested that halloysite tubes could be altered to kaolinite as a result of prolonged desiccation. Prolonged desiccation may have occurred in a past drier climate or when OS3 was near the land surface. However, one would expect more of OS3 to have transformed to halloysite in this situation because the whole profile would have been affected. In contrast, Bailey (1990) stated that the structural difference between halloysite and kaolinite (i.e. tetrahedral rotations in kaolinite, Chapter 2) would require complete re-crystallisation for one to transform to the other. Churchman & Gilkes (1989) also indicated that halloysite tubes and kaolinite plates can form via separate pathways. For example, kaolinite can be formed from the intense weathering of biotite (Thompson & Ukrainczyk 2002). Biotite was observed in OS3. It was difficult to conclude which pathway was followed for kaolinite formation in OS3. However, the greater age and different weathering environments experienced by OS3 during glacial and interglacial conditions has resulted in a slightly more diverse range of clay minerals compared with those of other samples.

8.2.3.2 Halloysite

Within the samples examined, typical halloysite morphologies of tubes and spheres were observed, as was the lesser known plate-like morphology. All these morphologies had been previously observed in weathered volcanic material (Joussien *et al.* 2005). At Tauriko, especially TS3, halloysite in the form of books was observed (Figures 6.28 to 6.34). Book morphologies, which are traditionally associated with kaolinite (Dixon 1989; White & Dixon 2002), have never been previously reported for halloysite.

Energy dispersive x-ray analysis (EDX) suggested that the platy "sheet" or "leaf" morphologies, which make up each book, were influenced by high Fe content, because a high Fe content had prevented layer rolling from occurring within the plate of each book. Layer rolling takes place in hydrated halloysite in an attempt to correct the size misfit between the larger Si^{4+} tetrahedral sheet and the smaller Al^{3+} octahedral sheet (Chapter 2). Layer rolling has not occurred in the plate-like minerals because Fe^{3+} has isomorphically substituted Al^{3+} within the octahedral sheet, possibly during clay formation. Because the ionic radius of Fe^{3+} is larger than that of Al^{3+}, the length of the octahedral sheet will increase when substitution occurs. Therefore, the misfit in size between the tetrahedral and

octahedral sheets is corrected and flat plates occur within each book. Previous workers have suggested this phenomenon for individual plates (Churchman & Theng 1984; Noro 1986; Bailey 1990; Joussien *et al.* 2005). For example, Bailey (1990) stated that platy halloysite displays a negative relationship between layer curvature and Fe content. Thus platy halloysite has the most Fe content and less curvature than tubes. Furthermore, the Fe_2O_3 content of books (~ 5.2 %) measured here appeared to correlate well with that typically observed for plates (Figure 6.38).

EDX analysis indicated that tubes from Otumoetai had Fe contents (~ 3.2 %) at the high end of the typical values for large tubes and at the lower end of plates (Figure 6.38). On calculation of raw EDX values from Appendix 6.3, tubes had low *Al:Si* ratios with a value of 0.77. Soma *et al.* (1992) stated that a low *Al:Si* ratio indicates that the isomorphic substitution of Fe^{3+} for Al^{3+} in the octahedral sheet is non-stoichiometric, and that the loss of Al^{3+} is disproportionally higher than the gain in Fe^{3+}. This loss of Al^{3+} without replacement will promote layer curvature and thus tube formation. For example, Soma *et al.* (1992) indicated that a very low *Al:Si* ratio (0.67) explained layer curvature in halloysite spheres with high Fe content (4.59 %) in material from Opotiki (Bay of Plenty). Books also appear to be moderately depleted in Al with an *Al:Si* ratio of 0.81. However, this depletion is overcome by the large enrichment in Fe.

However, one must point out that samples in this study did not have iron impurities removed via deferration. Therefore it could be argued that Fe contents are slightly exaggerated. For example Soma *et al.* (1992) observed an ~ 80 % drop in Fe content, from 5.69 % to 1.22 %, following deferration of tubes. However, as stated in chapter 6, this has potentially been overcome by examining individual clay crystals rather than a bulk sample.

8.2.3.3 Genesis of books

The Fe content explains the plate-like morphology within individual books, but does not describe their genesis. Because the books are observed in a primary pyroclastic deposit, they have certainly been formed authigenically. A number of suggestions exist:

a) Individual plates may have electrostatically bonded together, thus forming the book-like features. Plates have been observed as an alteration product of pumice (Noro 1986) and pyroclastic material (Joussien *et al.* 2005);

b) Like kaolinite, the books may have formed from either a micaceous mineral or feldspar (Keller 1977; White & Dixon 2002). The micaceous mineral acts as template which subsequently results in the book-like structures (White & Dixon 2002). In the case of feldspar, the books are formed following destructive dissolution of the feldspar and then constructive crystallisation of the kaolinite (Keller 1977);

c) Individual halloysite tubes may have coalesced to form stacks which later became books. For example, Jeong (1998) described tubes coalescing to become plates and then later vermicular kaolinite. However, in this study such stacks must have remained as halloysite rather than becoming kaolinite.

It is unlikely that books were formed from the electrostatic attraction of plates, because the plates not included (i.e. those within the groundmass) were smaller than those in books. If the books represented individually stacked plates, one would expect their edges to be irregular, as the plates were generally of different geometries. Tubes coalescing to form plates and then books would invalidate the Fe content hypothesis, because Fe content would have been high during book formation resulting in plates rather than tubes. Transformation from a biotite mineral is possible because XRD analysis of the bulk soil sample indicated the possible presence of very thin flaked micaceous material (biotite) (Fanning *et al.* 1989) in TS1 and TS3 (Chapter 6, section 6.4.1.1). Whilst the typical micaceous lustre was not observed in hand specimens, it is possible most of the books represent halloysite, whilst some may represent mica intergrading into halloysite. Feldspar was recorded by XRD in Tauriko samples so transformation of this primary mineral into books is also possible. Why halloysite rather than kaolinite has formed may be linked to a poorly drained saturated environment.

8.3 Field variability

During field investigations at Otumoetai, large variability was observed both within and between stratigraphic units (Chapter 4). For example, peak vane strength in OS2 ranged from 78 to 172 kPa and remoulded strength was measured between 3 and 8 kPa using the adapted method, which in turn had an effect on sensitivity. Furthermore, sensitivities between units ranged from > 8 (OS3) to 52 (OS4) within a few metres, displaying very coherent (36 kPa) and almost liquid-like (2 kPa) remoulded strength, respectively. This was not unexpected, considering variability in engineering properties both between and within units has been reported on many occasions (see for example: Bird 1981; Briggs *et al.* 1996; Oliver 1997; Wesley 2007; Keam 2008). Variability arises because of the wide range of depositional environments (e.g. fallout pyroclastics, aeolian loess, fluvial reworking), weathering environments (e.g. climate, drainage) and a number of buried paleo-topographies. These features result in lateral changes in strength and abrupt vertical changes in grain size, soil type and a wide variety of water contents (Prebble 2001). For example, the high clay sample OS3 was less permeable than the overlying sample, OS2. In this instance, excess water will pond above OS3. This conclusion can be drawn because the thick layer of manganese oxide coatings (pyrolusite) between the two layers (Figure 4.11) indicated an extreme wetting and drying environment. This type of perched aquifer is not uncommon in the Tauranga region and may form basal slip planes (e.g. Gibb 1979; Bird 1981).

8.4 Geomechanical properties

The following section will discuss geomechanical properties for each sample, whilst taking into consideration observations during field testing, mineralogical investigations and scanning electron microscopy. Relationships between geomechanical properties will also be discussed.

8.4.1 Particle size

8.4.1.1 Measurement

Particle size analysis indicated that most samples had < 10 % clay content with the exception of OS3, which had ~ 35 %. Conversely, scanning electron microscopy (SEM) observations showed that the dominant microstructural material for all samples was clay. For example, OS3 was dominated by halloysite clay with very few primary grains observed. Therefore, based on SEM observations clay

content in OS3 could have possibly been more than 75 %, with all other samples having at least 20 % clay content. Thus, it was believed that the clay content in all samples has been underestimated by particle size analysis. Several other lines of evidence also suggest that clay content was underestimated as discussed below.

Halloysite tubes, spheres, plates and books were observed in great abundance during SEM observations, thus it was expected their activity would dominate samples. However, activity values for samples with low clay content were high, between 1.59 and 18.26, which suggests the presence of allophane (> 3) or montmorillonites (1.5 – 13), rather than halloysite (< 0.5) (Selby 1993). Montmorrillonites can be excluded because they were not observed during any analysis. Allophane was not generating the high activities because activities were still high in those soils with insignificant amounts of allophane (e.g. TS1, TS2, TS3 and OS4).

Grain mount investigation identified a high proportion of clay aggregates (~ 10 to ~ 25 %) in the fine sand fraction of all samples. This aggregation suggested that clays were not effectively dispersed during particle size investigations, because the dispersion methods for both analyses were similar (using H_2O_2, Calgon, and ultrasonication).

The relationship between liquid limit, plasticity index and clay content suggested that samples had not dispersed equally. Literature suggested that liquid limit and plasticity index are related to clay content (McLaren & Cameron 1996), as a result of increasing surface area. Therefore, a numerical relationship between clay content and these parameters was expected. However, this was not the case with correlation coefficients (r^2) of < 0.15. Poor correlations have been previously reported for soils which are dominated by allophane (Allbrook 1983) but not halloysite. One would still expect a relationship if the effect of non-dispersion was similar in each sample.

In volcanic-ash derived soils, problems with particle size results have been reported for allophanic soils following the preparation of samples by air drying (Wesley 1973; Allbrook 1983; Jacquet 1990). Quite the opposite affect has been recorded in soils with high halloysite content, where drying made aggregates less

stable (Churchman & Taite 1986). However, Shepherd (1984), who examined the Hamilton Ash formation, which are typically halloysite dominated, observed aggregated clay in the sand fraction during particle size analysis. He suggested that a number of processes, for example cementing and bonding of clay minerals with free sesquioxides, may cause aggregation.

The problems observed during particle size analysis arose because of inadequate dispersion (as seen by grain mount analysis observations). It was also possible that the calibration of the particle size analyser and the issues experienced concerning obscuration were also having an effect (Chapter 2). The calibration issues were a result of the wide range of materials, and hence differing optical properties, of each sample.

8.4.1.2 Strength and sensitivity

A weak positive relationship between silt content and adapted sensitivity is observed ($r^2 = 0.46$, Figure 8.1). However, no visual relationships existed for other sediment size classes, standard sensitivity, remoulded strength or peak strength. The correlation coefficient between particle size and the parameters mentioned above was typically low ($r^2 < 0.4$). Unfortunately, relationships may be over-shadowed by the problems with particle size measurements.

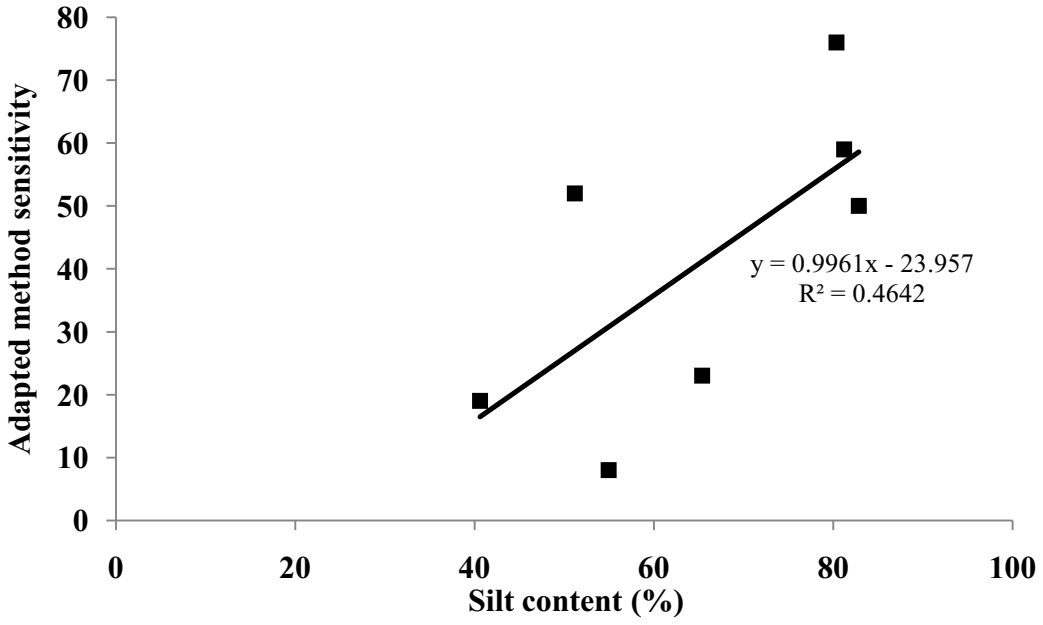

Figure 8.1: Relationship between silt content and sensitivity measured with the adapted method ($r^2 = 0.46$).

Further investigation indicated a weak relationship between adapted sensitivity and both liquid limit and plasticity index (Figure 8.2). The relationship suggests that as liquid limit and plastic index increase, sensitivity decreases. Considering liquid limit and plasticity index may represent clay content, then it could be suggested that as clay content increases, sensitivity decreases. This is logical considering the relationship with silt content.

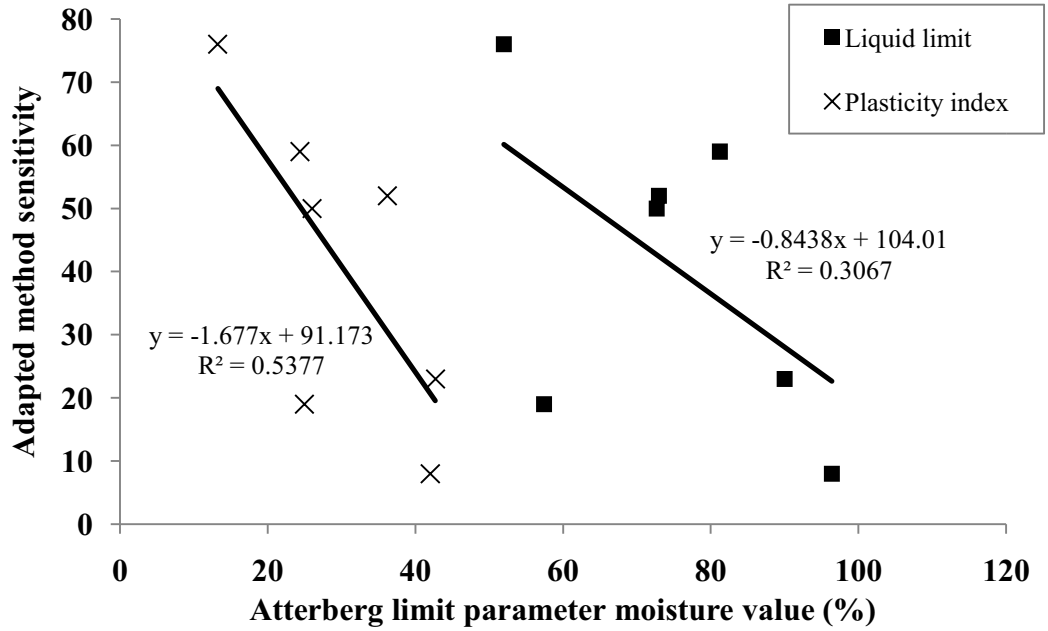

Figure 8.2: Relationship between liquid limit and sensitivity measured with the adapted method (r^2 = 0.31), and plasticity index and sensitivity measured with the adapted method (r^2 = 0.54).

8.4.2 Void ratio, porosity and bulk density

Void ratio, porosity and bulk density are related to a large number of parameters, including SEM observations, moisture content, peak vane strength and sensitivity. The following section will discuss these relationships. However, void ratio and porosity will be considered as one because both are interrelated (Chapter 3, equation 3.6). Furthermore, dry bulk density is inversely related to porosity (McLaren & Cameron 1996). In terms of making comparisons void ratio will be used because it is typically used in engineering studies. The void ratios discussed in this section are those obtained during initial investigations rather than those obtained from triaxial specimens.

8.4.2.1 Fabric

Section 8.2.1 made comment on the interrelationships between depositional method and void ratio. These events formed a base for void ratio, either high or

low, and are still represented in current values. However, what is observed now has been influenced by the way primary minerals have weathered to clay. Thus the following section will describe how current materials create the void ratios observed.

At Tauriko, void ratios follow the sequence TS2 (3.40) > TS1 (2.86) > TS3 (1.63). Scanning electron microscopy supported this observation. TS3 had the largest portion of dense books with plates in tight face-to-face contacts and TS1 had the least. Furthermore, TS1 and TS2 had a large proportion of hollow relict textures. TS3 had fewer relict textures and tubes, and instead had a larger amount of irregular spheres and few tubes. The irregular spheres are more likely to pack efficiently than relict textures. At Otumoetai, void ratio was highest in OS1 (3.02) and OS4 (2.62), yet lowest in OS2 (1.98) and OS3 (1.90). The higher void ratios in OS1 and OS4 were a result of halloysite tubes intermixed with small irregular spheres being arranged in an open network structure. The gaps between irregularly shaped aggregates of tubes and spheres also add to void ratio values. In OS2, a similar network of tubes and spheres occurred, but this was typically less open than in OS1 and OS4. Furthermore, sections of OS2 were dominated by regular spheres which, as in TS3, pack more efficiently than a combination of tubes and spheres. A low void ratio occurred in OS3 because the short halloysite tubes packed better those which were longer, as in OS1 and OS4. The tighter packing in OS3 has been explained by its prior position near the land surface (section 8.2.2).

In all samples, a large number of very small (< 1 μm) pores resulted from the interaction between irregularly shaped clay particles. In most samples, larger pores seldom had diameters > 20 μm. Considering that storage pores are less than 30 μm in diameter, and water is held more tightly as pore sizes decrease because of capillarity (McLaren & Cameron 1996), one can assume that water will be strongly held in all samples. Thus the high saturation states (83 to 102 %) observed in all samples, even at the end of summer, were a result of extremely small pore sizes. Because all soils are close to saturation an increase in void ratio results in an increase in moisture content ($r^2 = 0.87$) (Figure 8.3).

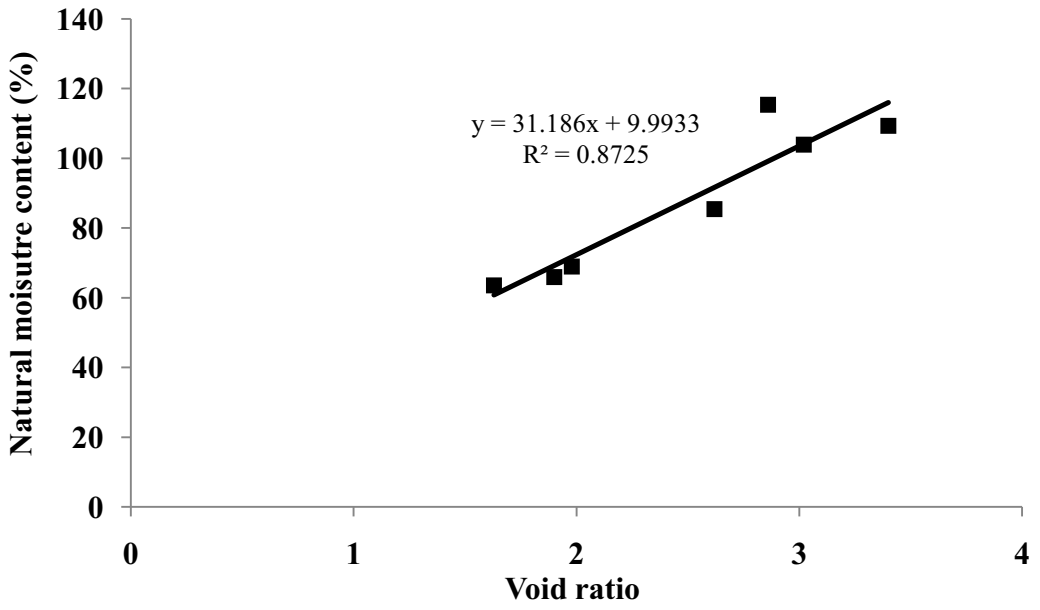

Figure 8.3: Relationship between void ratio and natural moisture content (%) ($r^2 = 0.87$).

The weathering from pyroclastic primary materials to clay has produced a clay groundmass in all samples. This alteration will have caused a change in the total porosity and its size distribution within each sample. For example, porosity is often higher in clay units than those dominated by larger grains (Selby 1993; McLaren & Cameron 1996). Small pores typically dominate clay, thus one typically observes a permeability decrease, from silts to clay (Selby 1993). This ability to store large amounts of tightly held water will certainly affect sensitivity. Clays also increase water retention through the process of adhesion, however much of this water would be tightly bound to the surface of the clay.

8.4.2.2 Peak vane strength and friction angle

Void ratio was negatively correlated with vane shear strength ($r^2 = 0.64$) (Figure 8.4). This relationship occurs because as the structure becomes more open or porous, the frictional contact between irregularily shaped clay minerals and large inert sand and silt grains decreases. Additionally, as clay minerals move further apart their electrostatic interaction becomes less.

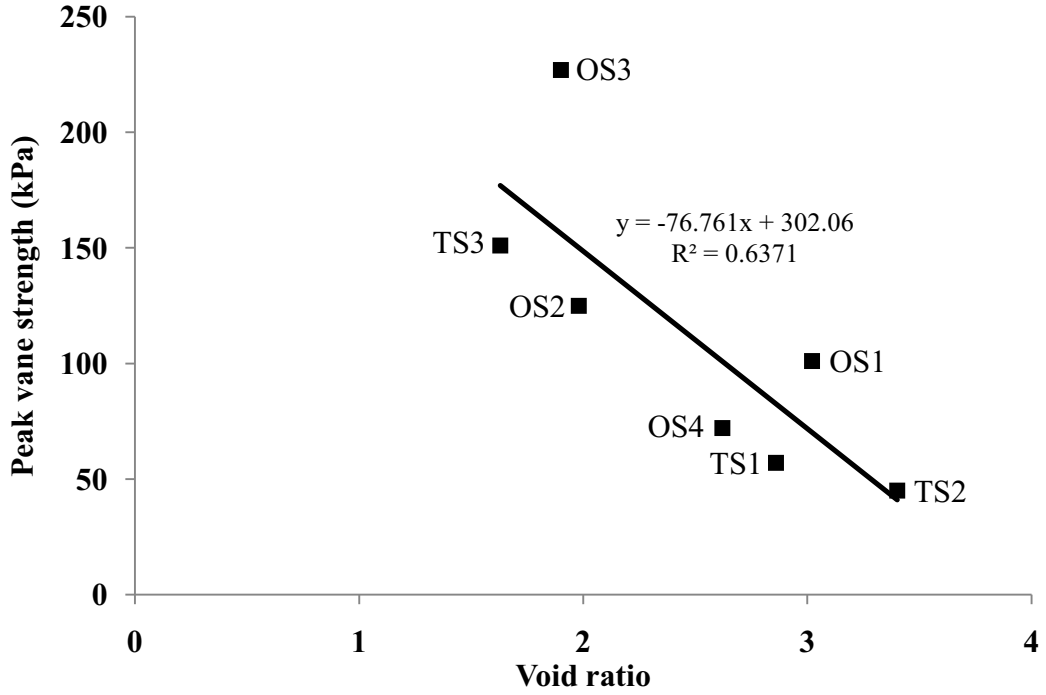

Figure 8.4: Relationship between void ratio and peak vane strength (kPa).

The high strength in OS3 (> 227 kPa) occured as a result of halloysite tubes being abundant in a subdued arrangement and typically in tight parrallel face-to-face contacts. These factors will increase the area available for electrostatic attraction between clay particles. The irregular shapes of clay particles mean they enhance frictional strength, so are more likely to interlock when sheared. Furthermore, larger non-clay minerals were strongly bound in the sorrounding groundmass of OS3. In contrast to OS3, the open chaotic framework of tubes in OS1 and OS4 typically meet tangentially as either face-to-edge or edge-to-edge contacts, which are weaker than those observed in OS3. The decrease in contact is not aided by the curved shape of halloysite tubes and spheres which share limited bonding surfaces. White & Dixon (2002) stated that this interlayer bond is weak and will promote slippage and failure under load. Secondly, the voids created by the irregular packing of tubes means less frictional resistance between materials. The strength in OS1 (101 kPa) was higher than in OS4 (72 kPa). This difference was a consequence of very fine material (Figure 7.47), either allophane, ferrihyrite or neo-formed halloysite, which acts as a cementing agent. Liquid limit was higher in OS1 (90.02 %) than in OS4 (76.96 %), which may indicate greater clay content, which promotes higher strength. The cementing material and higher clay contents may explain why OS1 had a high effective cohesion (34.5 kPa).

TS3 had the second highest strength (151 kPa), a result of the large number of books within the sample. The tight face-to-face contacts of plates within each book will form stronger bonds than other curved halloysite morphologies. However, one anticipates that this contact will be weaker than those in kaolinite books, because the interlayer water may lubricate each clay crystal, promoting slippage, as opposed to the tight hydrogen bonding within kaolinite. The tight face to face contacts between plates within books may account for the high effective cohesion of 24 kPa observed in TS3. TS3 had the least number of relict textures. The relict textures appeared hollow, delicate and weak; it is anticipated that they will easily crush when shearing forces are applied. Their delicacy was emphasised by the collapsed wall sections observed during SEM investigation and the lack of relict textures in remoulded specimens. This delicacy resulted in TS1 and TS2 having the lowest peak strengths at 57 and 45 kPa, respectively.

The small amount of ferrihydrite (< 0.5 %) in Otumoetai samples may explain why they have higher strength than TS1 and TS2; Jacquet (1990) stated that the presence of Fe oxides, especially ferrihydrite, will contribute to the strength properties of volcanic soils.

Even though the relationship between void ratio and friction angle was not particularly clear, samples OS3, OS2 and TS3 all had void ratios of < 2, and effective friction angles above 30º. In contrast, samples TS1, OS1 and OS4 had void ratios > 2.5 and friction angles of less than 30º. The relationship between void ratio and friction angle manifests through similar mechanisms as those presented for peak vane strength, especially grain interlocking as a consequence of tight packing causing high friction angle.

Because peak vane strength and moisture content are related to void ratio, it comes as no surprise that strength is correlated with moisture content ($r^2 = 0.65$) (Figure 8.5).

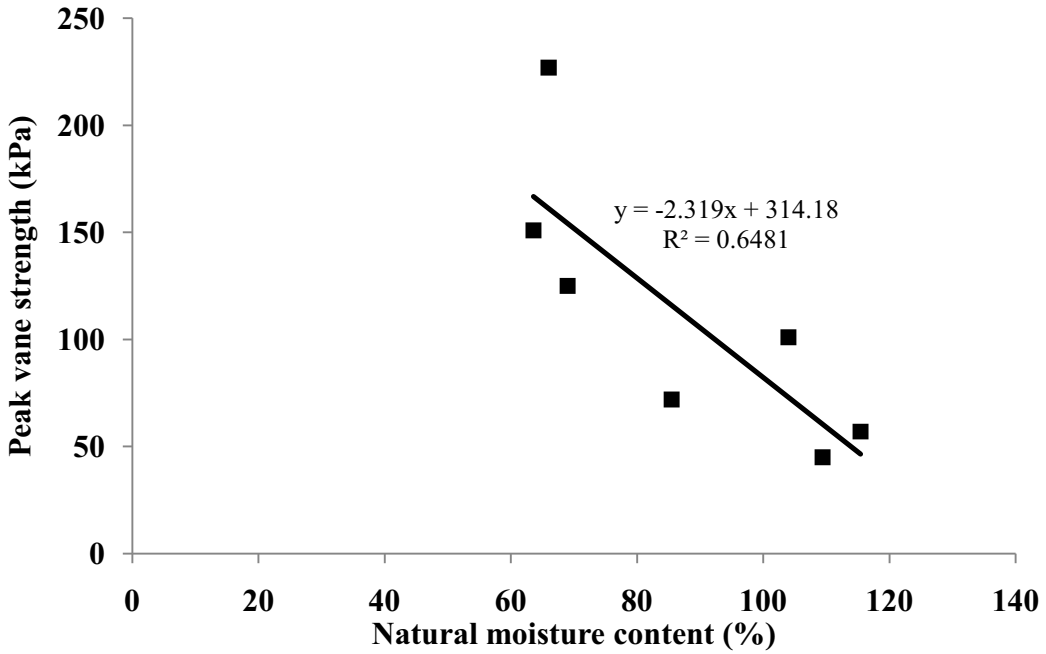

Figure 8.5: Relationship between natural moisture content (%) and peak vane strength (kPa) (r^2 = 0.65).

8.4.2.3 Liquid limit

Excluding OS3, a positive relationship exists between void ratio and liquid limit (r^2 = 0.67) (Figure 8.6).

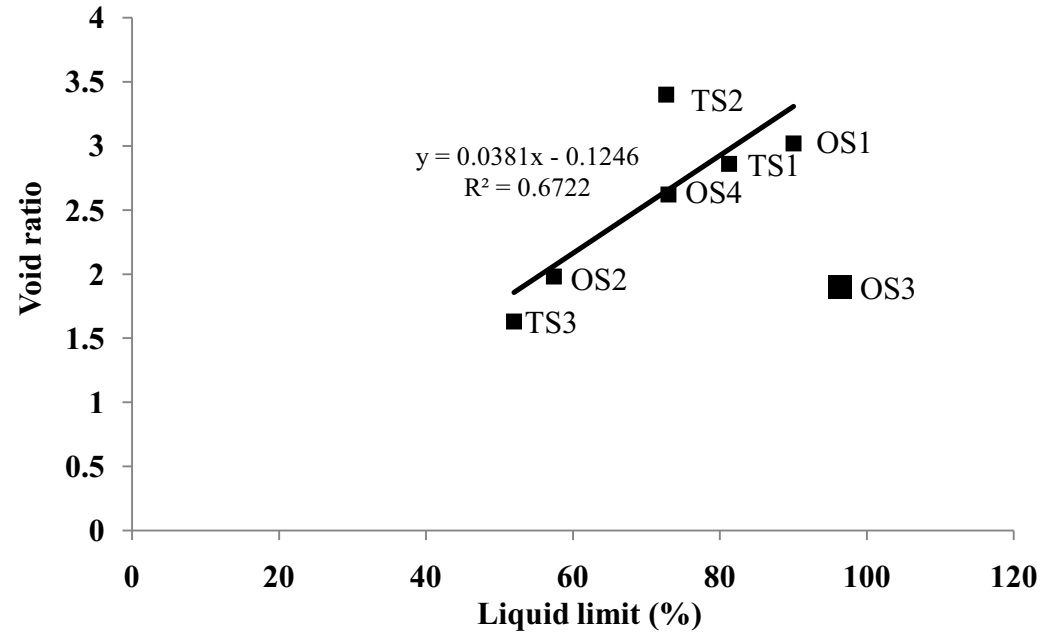

Figure 8.6: Relationship between liquid limit and void ratio (r^2 = 0.67). OS3 has been omitted from the correlation coefficient calculation (see text for explanation).

The typical relationship observed in Figure 8.6 was not reflected in OS3 because of its different weathering history compared with all other samples (section

8.2.2). This weathering history has promoted clay formation, increasing liquid limit, yet also resulted in a void ratio (1.90) at the lower end of the scale.

The relationship observed between other samples (excluding OS3) could indicate that as clay content increases so does void ratio. If this is the case it may indicate that an increase in void ratio is a result of diagenesis and weathering. This possibility was discussed by Torrance (1992) as a post-depositional factor which may affect sensitive volcanic soils. However, the correlation in Figure 8.6 may also be influenced by either clay type or morphology. For example, the surface area of kaolinite is typically less than that of halloysite, with values between 10 to 20 m^2 g and 35 to 70 m^2 g respectively (Selby 1993; Mitchell & Soga 2005). Because liquid limits are strongly correlated to surface area (Selby 1993) then a lesser liquid limit may be expected in kaolinite than halloysite. It is possible that because halloysite books represent one of the common kaolinite morphologies their surface properties may be similar. Thus, the high number of dense halloysite books in TS3 may result in low liquid limit and void ratio. At the other end of the scale, the small amount of allophane in OS1 (1.3 %) may foster a slightly higher liquid limit.

8.4.2.4 Sensitivity

A relationship exists between void ratio and standard remoulded strength ($r^2 = 0.71$) and senstivity ($r^2 = 0.52$). The relationships for remoulded strength and sensitivity are negative and positive, repsectively (Figure 8.7 A and B). This same correlation does not exist for adapted remoulded strength ($r^2 = 0.19$) nor adapted senstivity ($r^2 = 0.008$). However, a relationship exists between standard remoulded strength and peak strength ($r^2 = 0.88$) (Figure 8.8 A). A similar correlation is not observed for remoulded strength derived from the adapted method of sensitivity. The relationship observed in Figure 8.8 (A) possibly indicates that remoulding by rotating the vane 5 times does not completely destroy the structure of the specimen. Thus, the correlation between peak strength and void ratio (Figure 8.4) is overprinted onto remoulded strength, which has an affect on sensitivity. Because a relationship exists between void ratio and standard remoulded strength it comes as no surprise that a correlation is also observed between natural moisture content and standard remoulded strength ($r^2 = 0.63$) (Figure 8.8 B).

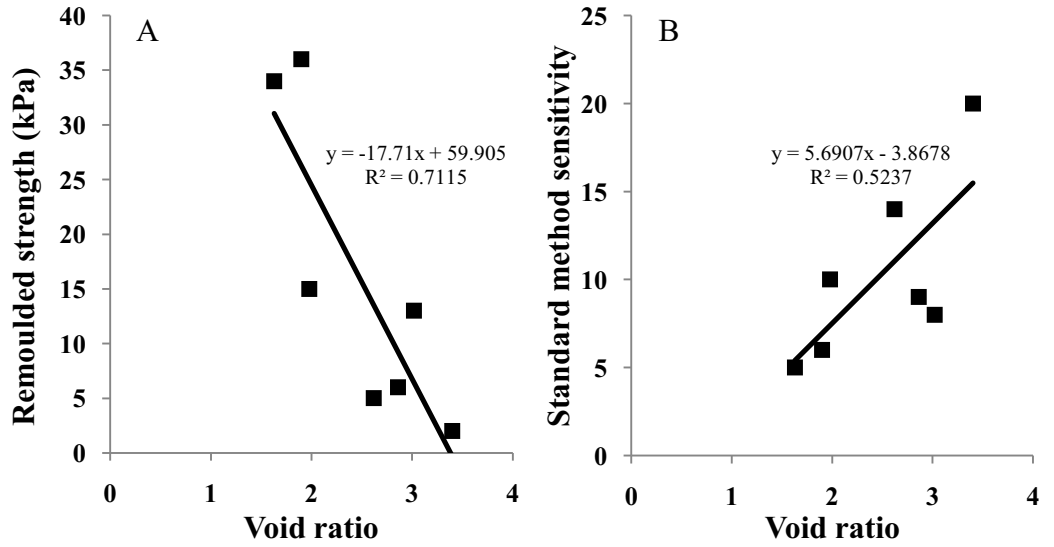

Figure 8.7: Relationships between: A) Void ratio and the standard method of sensitivity measurement remoulded strength (kPa) (r^2 = 0.71). B) Void ratio and the standard method of sensitivity measurement (r^2 = 0.52).

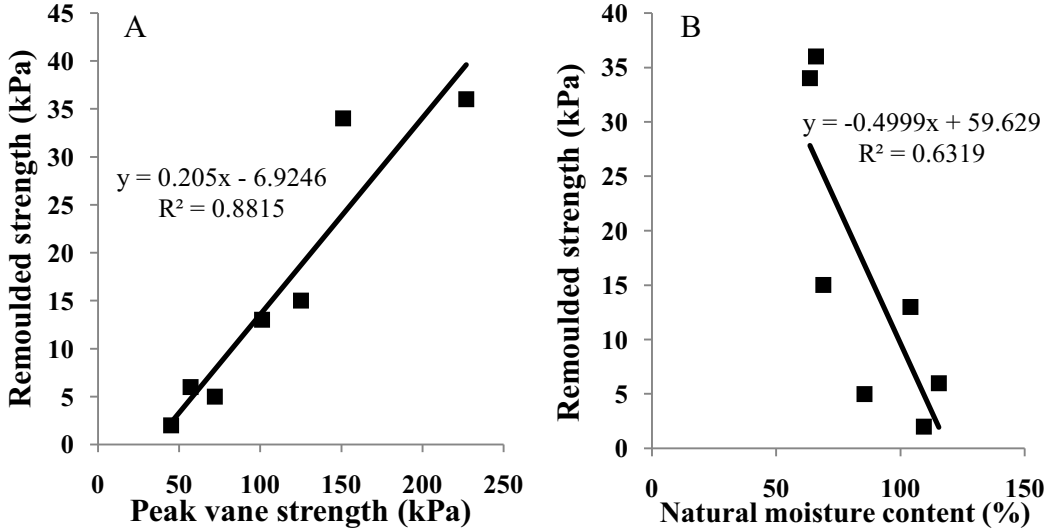

Figure 8.8: Relationship between: A) Peak vane shear strength (kPa) and the standard sensitivity method remoulded vane shear strength (kPa) (r^2 = 0.88). B) Natural moisture content (%) and the standard sensitivity method remoulded vane shear strength (kPa) (r^2 = 0.63).

8.4.3 Liquidity index

Most samples, except OS3, had natural moisture contents which exceeded their respective liquid limits, having liquidity index values between 1.33 and 2.39 (Table 8.1). High liquidity index values (> 1) have been previously reported in sensitive volcaniclastic deposits of the Tauranga region (Smalley *et al.* 1980; Hatrick 1982; Wesley 2007; Keam 2008). Soils which have moisture contents above the liquid limit are capable of liquefying when disturbed; these deposits may not only be highly sensitive but also extremely compressible (Hatrick 1982). Selby (1993) stated that soils with natural moisture contents at their liquid limit (liquidity

index = 1) will have remoulded shear strengths between 1 and 3 kPa. Therefore, soils with a liquidity index > 1 will potentially have even lower remoulded strengths than those suggested by Selby (1993).

Table 8.1: Liquidity index, void ratio, liquid limit, natural moisture content, and degree of saturation for all samples examined in this study.

Sample	Liquidity index	Void ratio	Liquid limit (%)	Natural moisture content (%)	Degree of saturation (%)
TS1	2.39	2.86	81.25	115	102.2
TS2	2.41	3.4	72.67	109	83.5
TS3	1.88	1.63	51.97	64	99.3
OS1	1.33	3.02	90.02	104	91.1
OS2	1.46	1.98	57.4	69	93.0
OS3	0.27	1.9	96.4	66	92.4
OS4	1.35	2.62	72.96	86	87.8

For liquidity index to be > 1, void ratio must be sufficiently high to allow natural moisture content to exceed liquid limit. For example TS1, TS2, OS1 and OS4 all had exceptionally high void ratios. Contrastingly, TS3 and OS2 had void ratios similar to OS3, yet they still have liquidity indexes which are > 1 (Table 8.1). The high liquidity indexes in TS3 and OS2 were a consequence of low liquid limits (Table 8.1). The low liquid limit in TS3 is possibly a result of halloysite books (Section 8.4.2.3) and in OS2 it may be a consequence of the abundance of heavy minerals (Table 6.7) and high sand content (Table 5.1). Other factors such as water availability and micro-structural characteristics (e.g. small pore sizes permitting strong water retention) are also important to ensure high liquidity indexes.

The liquidity index of OS3 contrasts to all other samples with a value of 0.27. This results from the combination of a high liquid limit and low void ratio (Table 8.1). Even if OS3 became fully saturated it would only be able to support a moisture content of ~ 71 %; this value is still below its liquid limit of 96.4 % (Table 8.1). The inability to exceed its liquid limit suggests that OS3 is unlikely to have extremely low remoulded strength on any occasion.

The benefit of liquidity index is that it normalises natural moisture content in regard to the liquid limit. This allows the comparison of natural moisture content of samples with other parameters, without the influence of clay content or type.

A positive relationship exists between adapted sensitivity and liquidity index for samples of this study (r^2 = 0.54). Furthermore, this correlation remains when other studies which report sensitivity in volcaniclastic materials are added (r^2 = 0.60). This relationship is presented in Figure 8.9 and the line-of-best-fit represents all points in the graph. Previous workers have reported this relationship for sensitive glaciomarine clays (Skempton & Northey 1952; Bjerrum 1954; Mitchell & Houston 1969, as cited in Lefebvre 1996). Mitchell and Houston (1969) suggested that retrogressive failure will develop in glaciomarine sediments when sensitivity is higher than 40 and liquidity index exceeds 1.5.

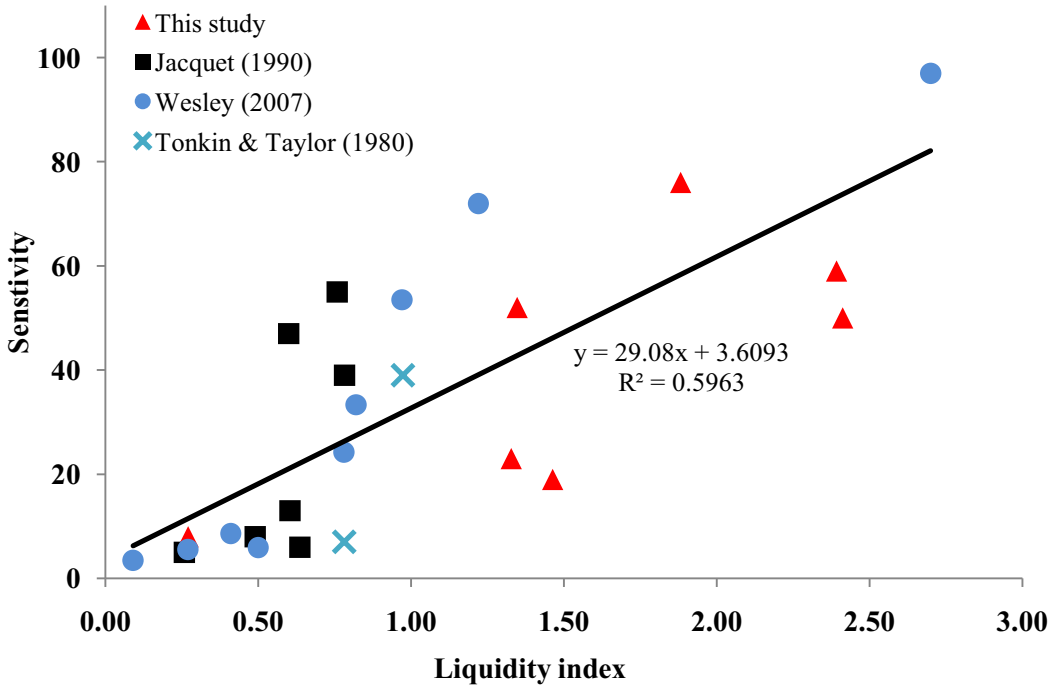

Figure 8.9: Relationship between liquidity index and sensitivity (r^2 = 0.60) for data from Tonkin & Taylor (1980), Jacquet (1990), Wesley (2007) and this study. The sensitivity values presented in the graph for this study are those derived from the adapted method.

When liquidity index and remoulded strength values from the same studies used to compile figure 8.9 are compared a power relationship exists (r^2 = 0.69) (Figure 8.10). This power relationship is presented as the solid line in Figure 8.10 and indicates an overall trend of decreasing remoulded strength as liquidity index increases (Figure 8.10). Furthermore, the largest change in remoulded strength occurs at liquidity indexes of < 0.5 (Figure 8.10).

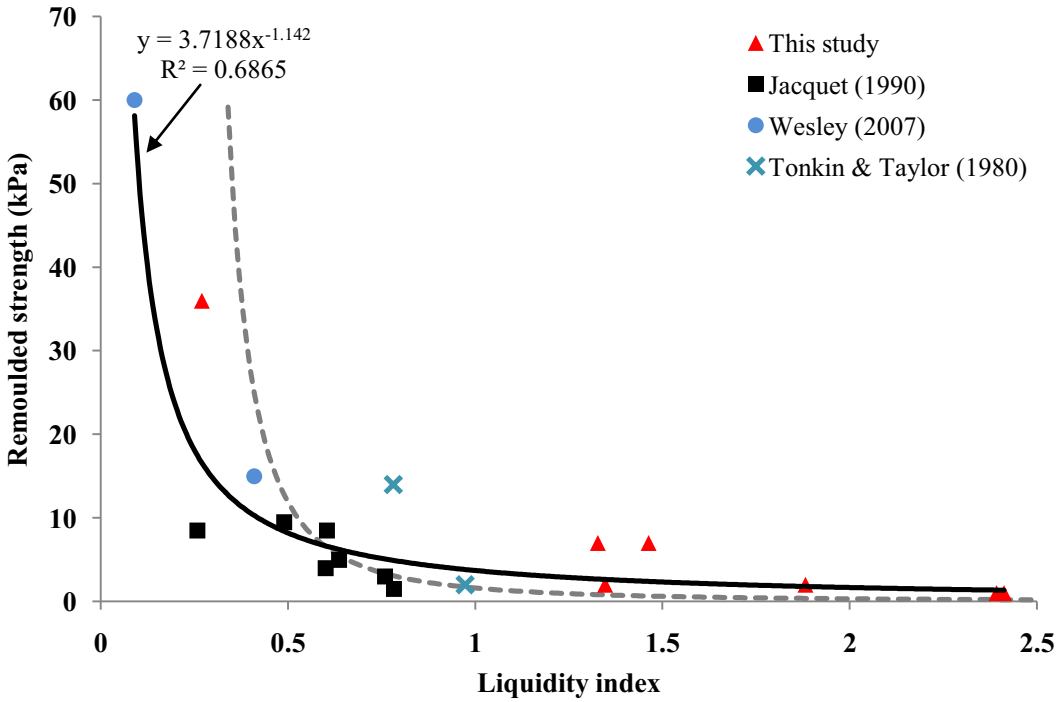

Figure 8.10: Relationship between liquidity index and remoulded shear strength (kPa) for data from Tonkin & Taylor (1980), Jacquet (1990), Wesley (2007) and this study (r^2 = 0.69). The solid line represents all data points presented on the graph and the dashed line represents the relationship of Mitchell & Soga (2005) which is presented in the text as equation 8.1. The remoulded shear strength values presented in the graph which represent this study are from the adapted method of sensitivity measurement. Most of the remoulded strength values from Wesley's (2007) study had to be omitted because they were derived from the equation of Sharma & Bora (2003; 2005) (Laurie Wesley *pers. comm.* 2008). Values from Jacquet (1990) were derived from analysis undertaken on a uniaxial compression apparatus so had to be converted to shear strength using equation 3.13 in chapter 3 before plotting on this graph.

The correlation presented in Figure 8.10 is not uncommon. For example, the remoulded strength calculation of Sharma & Bora (2003; 2005) is based on natural moisture content and its relationship between liquid and plastic limits (Chapter 3, equation 3.14). Furthermore, Mitchell & Soga (2005) presented an equation which links undrained shear strength of a remoulded clay and liquidity index. The relationship is derived from different clay types displaying a range of sensitivities and is presented as:

$$S_u = \frac{1}{(LI-0.21)^2} \qquad (8.1)$$

where:

S_u = undrained shear strength of remoulded clay;

LI = liquidity index.

Equation 8.1 is represented as a dashed line in Figure 8.10. The data from the relationship derived for volcanic deposits appears to track that of equation 8.1 reasonably well. However, the sharp increase in remoulded strength appears to occur at lower liquidity index values for soils of this study and those of other studies on volcanic soils (Tonkin & Taylor 1980; Jacquet 1990; Wesley 2007), than for the line from equation 8.1.

A relationship such as that presented in equation 8.1, and the power equation in Figure 8.10, may allow estimates of remoulded strength to be made when only Atterberg limit and natural moisture content data are available. Importantly, Figures 8.9 and 8.10 indicate that soils with high sensitivity and low remoulded strength are dictated by the extent to which natural moisture content exceeds liquid limit, which appears to be common in sensitive volcanic deposits of the Tauranga region (see chapter 2). The relationship between liquidity index and remoulded strength is a function of clay content, clay type, void ratio and saturation state.

Table 8.1 indicates that most soils with a liquidity index (< 1) were not quite saturated (< 100%). Therefore, during a precipitation event they are able to retain more water which would increase liquidity index causing a decrease in remoulded strength (Figure 8.10), enhancing sensitivity (Figure 8.9). However, it should be noted that samples in the field may never reach full saturation because pockets of air may remain in occluded pore spaces (Hillel 2004).

8.4.4 Peak, residual and remoulded strengths

8.4.4.1 Triaxial

Triaxial testing, especially pore water pressure (PWP) characteristics, indicated that OS3 was structurally different from all other samples. OS3 failed at very high strains and displayed dilation across all confining pressures. These characteristics arose from high clay content and dense packing of OS3 (section 8.4.2.1). The high strain at failure implies that OS3 was of a highly plastic nature where the halloysite tubes strongly interacted during shear. All other samples typically displayed characteristics of compaction rather than dilation during triaxial compression, which is a result of their open structure. Compaction during compression was observed as elevated values of the pore water pressure coefficient

A at failure (A_f), with values up to 1.09 reported in samples of this study. A_f values exceeding 0.75 can indicate high soil sensitivity (Head 1998). However, highly sensitive glaciomarine clays have been reported with A_f values of 2, indicating that PWP is twice the value of deviator stress (Mitchell & Soga 2005). All other samples typically failed at lower strains than OS3, which implies a more brittle failure. Brittle failure arises because the loose contacts between curved halloysite particles are minimal and large grains are only weakly bound into the groundmass. Therefore, this structural arrangement will have low ductility and hence contacts between grains will break suddenly and at lower strains (and potentially lower deviator stress) than those contacts observed in OS3. Failing at low strains in a brittle fashion is considered to be typical of highly sensitive clays (Mitchell & Soga 2005).

8.4.4.2 Ring Shear

Residual friction angle in most samples, except OS3, ranged between 26.56 and 33.13 °. These high friction angles are a result of irregularly shaped and bulky clay minerals (e.g. tubes and spheres) and large grains. Typically when platy particles dominate the sample (e.g. sedimentary deposits) they undergo reorientation during extended post-peak shearing forming, a smooth sliding plane which results in a large reduction in friction angle (Wesley 1992; Mitchell & Soga 2005). Because individual plates did not completely dominate any sample of this study, shear is more turbulent with particles preferring to roll. This rolling causes high residual friction angle (Mitchell & Soga 2005). Furthermore, remoulded material in OS4 formed rounded microaggregates, which may behave like large sand and silt grains during shear. In OS3 residual friction angle was the lowest at 19.34 °. The subdued arrangement and dominance of parallel face-to-face contacts between halloysite tubes following remoulding formed a flattened surface. This flattened surface, combined with the paucity of large grains observed in OS3, allows a closer representation of sliding shear, as previously described for plates.

Effective residual friction angles for samples TS1, TS3 and OS1 were higher than peak effective friction angles measured in the triaxial. This finding was thought to occur because, when remoulded, the open structure of most samples was destroyed and irregular clay minerals and grains were able to move closer together and hence interact more during ring shear testing than in triaxial testing.

8.4.4.3 Remoulded strength

An important feature of soils in this study is their remoulded strength because it determines whether material will flow on disturbance. Section 8.4.3 indicates a relationship between liquidity index and remoulded strength. However, the relationship does not explain structural changes during disturbance, which are considered to be important (Jacquet 1990). Table 8.2 presents each soil categorised on the basis of adapted remoulded strength. The following text then discusses possible relationships between these categories, other laboratory data and scanning electron microscopy observations.

Table 8.2: Remoulded strength (kPa) and sensitivity values for samples from Tauriko and Otumoetai. Samples are divided on the basis of remoulded strength. Both sensitivity and remoulded strength values are derived from the adapted method. Sensitivity values for each sample are presented in parenthesis.

Dilatent on remoulding		
Low remoulded strength	Moderate remoulded strength	High remoulded strength
TS1 - 1 kPa (59) TS2 - 1 kPa (50) TS3 - 2 kPa (76) OS4 - 2 kPa (52)	OS1 - 7 kPa (23) OS2 - 7 kPa (19)	OS3 - 36 kPa (8)

All samples from Tauriko and OS4 were very liquid-like following remoulding (Figure 8.11) thus displaying extreme dilatancy and very low remoulded strength (Table 8.2). Scanning electron microscopy (SEM) indicated that remoulding and hence destroying the typically open structure of material from Tauriko caused overall porosity to decrease. Remoulding also destroyed relict textures and microaggregates. Remoulding the open structured material from OS4 reduced porosity and caused small dense microaggregates to form. At both sites, weak contacts between grains and the background of clay minerals were also destroyed. Such changes in fabric can only occur through complete structural alteration and particle disassociation. The loose packing (encouraging an elevated void ratio) and typically curved shape of halloysite clay minerals encourages minimal contacts between grains making particle disassociation easier than if the material was tightly packed (see section 8.4.4.2). This conclusion can be drawn because peak strength was typically low in those samples with low remoulded strength. TS3 seems to be an exception, with comparatively high peak strength yet low remoulded strength. This may be explained by the abundance of books in TS3

both increasing peak strength and possibly reducing liquid limit. A reduced liquid limit makes it easier for liquidity index to be > 1.

Figure 8.11: Sample TS1 before remoulding (left) and after (right). Peak and remoulded strengths are 57 kPa and 1 kPa respectively.

The structural disturbance which occurred in these samples (TS1, TS2, TS3 and OS4) caused an abundant amount of tightly held water to be released (because liquidity index exceeds 1) from many small pores. The abundance of water suspends broken fragments of the destroyed microfabric (i.e. groundmass material and grains) and dilutes the plasticity of low activity binding clays (halloysite), causing a large reduction in strength and hence promoting high sensitivity (Table 8.2). Loss of plasticity was confirmed by the dilatent nature and minimal plasticity of samples during field investigations even though most samples have reasonably high liquid limits (typical value for hydrated halloysite is 50 – 70: Selby 1993; Mitchell & Soga 2005). These findings support those of Smalley *et al.* (1980) for soils at Omokoroa (Section 2.7.2).

OS1 and OS2 had slightly higher remoulded strength and hence lower sensitivity (Table 8.2) because of high liquid limit and low void ratio, respectively (Table 8.1). These factors resulted in a lower liquidity index than in TS1, TS2 and TS3 (Table 8.1). Thus, in OS1 and OS2, less water was available to support particles once fabric was destroyed, because the water was either tightly held to the surface of clays or simply not available.

OS3 contrasted with all other samples because it was plastic following remoulding (Figure 8.12) thus having high remoulded strength (Table 8.2). SEM

images indicated that the tightly packed structure of OS3 was little altered following disturbance. However, all the larger pores were destroyed so some structural alteration had occurred. Therefore, the strength reduction observed as a result of remoulding is a consequence of a minor loss of bonds and hence strength due to structural alteration (Jacquet 1990) and the release of a small amount of water from disturbed pores (Torrance 1992). However, the highly plastic nature following remoulding is a consequence of continued tight packing and hence electrostatic and physical interaction between clay minerals. Furthermore, the low liquidity index (< 1) means OS3 incapable of flowing on disturbance (Jacquet 1990) because water within the sample is either not present or bound to the surface of clay minerals.

Figure 8.12: OS3 following remoulding. Remoulded strength is 36 kPa.

8.5 Sensitivity classification

Chapter Two indicated that sensitivity in volcanic ash material was believed to manifest in high undisturbed strength (Jacquet 1990; Torrance 1992). In my study, this was certainly the case for OS3 (Table 8.2). However other samples especially TS1, TS2, TS3 and OS4 had sensitivity which manifested in low remoulded strength (Table 8.2). These samples were extremely dilatent and often liquid-like on remoulding (Figure 8.11). However, the highly dilatent samples could not confidently be called "quick clays" in an international sense because remoulded vane strength values did not fall below the upper limit of remoulded strength which is ~ 0.5 kPa (Chapter 2, section 2.2.2). The inability to record such low values may be a consequence of the shear vane used in this study being unable to measure strengths below 1 kPa. When remoulded strength was estimated using the equation of Sharma and Bora (2003; 2005) remoulded strength for most

samples except OS3 was between 0.6 kPa and < 0.3 kPa. Such values suggest that samples of this study may indeed have extremely low remoulded strength and be capable of flowing.

None of the soils of this study meet Soderblom's (1975) classification of "quick clays", which requires a rapidity number of 8 and sensitivity of ≥ 50. Most rapidity numbers were between 2 or 3, with TS2 recording a 4. Considering that a value of 10 indicates the soil has transformed into a liquid mass, it can be concluded that a lot of energy is required to transform samples into their dilatant remoulded state. This was confirmed by field observation, as it often took a lot of time and effort for a soil to become properly remoulded.

8.6 Geomorphology

In an undisturbed state even the most sensitive volcanic deposits were able to maintain coastal cliffs and cuttings some tens of metres high (Chapter 4). However, it is within these steep slopes where failures typically occur. For example, this study observed failures in steep hill slopes of ~ 30 º (Welcome Bay) and a relict coastal cliff section (Otumoetai). The ability to support such large cuttings is assisted by intervening high-strength layers, such as OS3. These intervening layers of high strength are one of the reasons why slips do not occur over the full height of slopes (Chapter 2). For example, OS2 was 100 kPa weaker than the underlying unit OS3.

Soils of this study were observed retaining a coherent structure *in situ* even when they were at or near full saturation and had a liquidity index > 1. Maintaining a coherent structure whilst saturated may indicate that these soils derive most of their strength from electrostatic attraction of halloysite clays rather than the forces of suction and capillarity. For example, Jacquet (1990) stated that capillarity has an effect on strength between saturation values of 73 and 87 % but not between values of 92 and 95 %. Only TS2 and OS4 were within the lower range of values (Table 8.1). Suction is an important control in soils which are moist but not saturated. In moist soils, an apparent cohesion is developed because PWPs are negative. However, when saturation occurs PWP becomes zero and suction or apparent cohesion is lost (Selby 1993). This would suggest that in the case of soils in this study, a significant triggering event (greater than simple soil saturation) would be

required to promote failure–for example, a large increase in PWP (causing it to become positive) due to heavy or prolonged rainfall.

High sensitivity and low remoulded strength becomes important once the landslide has been triggered. The energy created during the mass wasting event will cause the fabric of the normally coherent sensitive soils to be destroyed. In those soils with a high liquidity index (> 1), an abundance of water will be released from small pores and the flow-like nature of the mass wasting event will be promoted by those processes outlined in section 8.4.4.3. These processes include the dilution of plasticity and suspension of disturbed material. Furthermore, Keam (2008) added that both water held within pumice vesicules and halloysite tubes is released on disturbance. However, the water directly associated with halloysite, either within the tubes or on its surface will be tightly held and not easily released and therefore probably does not contribute to the flow like nature of mass wasting events.

This study indicates that the ability of deposits to flow on remoulding will be dictated by the volume of material which has a liquidity index that exceeds 1, and the degree to which this value is exceeded.

8.7 Comparison with classical "quick" clays

8.7.1 Geomorphology

Whilst failures in volcaniclastic deposits of the Tauranga region certainly flow following disturbance and show signs of retrogression (Chapter 2), geomorphic evidence suggests that they are different from the classical sensitive glaciomarine clays of Norway and Canada.

A classic example of failures in sensitive glaciomarine sediment was that at Rissa, Norway. The total slide, triggered by site loading, retrograded some 450 m inland from Lake Botnen and displaced 33 hectares of material from a slope of ~ 6 º (slope of 1:10) (Gregersen 1981). The failure did not occur as a single event but as a number of retrogressive and flake-type (large blocks raft out forming a new head scarp) episodes lasting less than an hour. Following the initial trigger, basal sediment collapsed and material flowed out into Lake Botnen under the weight of overlying sediment (Geertsema *et al.* 2006a). A more recent event is that at Mink

Creek, Canada, which was triggered by stream bank erosion. The Mink Creek event was also retrogressive and 23 hectares of material flowed from flat to rolling, gullied, terrain for a total distance of 1 km (Geertsema & Torrance 2005; Geertsema *et al.* 2006a; b).

The events of Rissa and Mink Creek indicate that the geomorphic appearance of mass wasting events in sensitive glaciomarine sediments clearly differs from those in sensitive volcaniclastic materials. For example, flow-like failures in sensitive volcaniclastic material typically occur as a single event in steep slopes and display minimal retrogression, and hence the size of the scarp is smaller and run-out distances are less than failures in sensitive glaciomarine sediments.

8.7.2 Geomechanics

The differences in geomorphic appearances between sensitive volcaniclastic and glaciomarine clays is a consequence of differences in geomechanical properties, most notably peak shear strength. Material at both Rissa and Mink Creek had low peak shear strength. Profiles from Rissa indicate that peak strength is typically less than 20 kPa down to a depth of 20 metres (Gregersen 1981). Mink Creek peak strength values ranged from 15 to 67 kPa over ~ 37 m with the majority of values less than 40 kPa. The main rupture surface at Mink Creek occurred in 4.5 m-thick sediment with peak strengths of 15 to 25 kPa and remoulded strength as little as 0.22 kPa (Geertsema & Torrance 2005; Geertsema et al. 2006b). Greertsema *et al.* (2006b) suggested that the material from Mink Creek could be of high rapidity. Data from my study indicates that highly sensitive volcanic deposits are typically stronger, are less rapid and have remoulded strength which may not be as low as sensitive glaciomarine sediments. The high peak strength means volcanic soil materials do not collapse under their own weight after support is removed during failure.

Adding to the differences in peak strength values between glacial marine clays and volcaniclastic deposits are other geomechanical properties. Table 8.3 indicates that volcaniclastic sediments of this study have higher moisture contents and higher liquid and plastic limits than those from glacial marine sensitive clay.

Table 8.3: Geomechanical properties for sensitive volcaniclastic materials of this study and those of sensitive glaciomarine sediments. Where *w* is natural moisture content, LL is liquid limit, PL is plasticity limit, PI is plasticity index, LI is liquidity index, Su is peak shear strength, Su_r is remoulded shear strength and St is sensitivity.

Location	*w* (%)	LL (%)	PL (%)	PI (%)	LI	Activity	Su (kPa)	Su_r (kPa)	St	Reference
Tauriko (project)	115 - 63	81 – 52	39 - 57	13 - 24	1.88 – 2.41	0.1 - 0.5[2]	45 – 151	< 2	50 - 76	This study
Otumoetai[1] (Landslide)	69 - 104	90 - 81	32 - 47	25 - 43	1.33 – 1.46	0.1 - 0.5[2]	72 -125	< 7	19 - 52	This study
Mink Creek British Columbia Canada (Landslide)	~ 32	30 - 35	17 - 22	10 - 18	-	0.26 -0.42	46 – 15[4]	0.65 – 0.22	118 - 20	Geertsema *et al.* (2006a;b); Geertsema & Torrance (2005)
Mangelerud Norway[3]	33.5	28	19	9	1.6	0.15	< 25	-	150	Mitchell & Soga (2005)
Outardes, Quebec, Canada (Project)	34- 50	32 - 45	17 - 20	12 - 29	0.88 – 1.97	-	57 -98[5]	1.6 – 6.6	13 - 33	Yong *et al.* (1979)
Vancover	38	28	22	6	2.7	0.22	~ 20		30	Gillot (1979)
Gloucester, Ontario (chaplain sea – Leda clay)	65	55	22	33	1.3	0.73	~ 20	-	100	Gillot (1979)
Rissa Valley (Landslide)	~ 20 - ~ 35	~ 22 - ~ 35	~ 18 - ~ 21	-	> 1	-	9 - > 30	-	100[6]	Gregersen (1981)

Note:

1) Does not include OS3.
2) Activity values are typical values for halloysite presented by Selby (1993)
3) Average values for profile from 11 m to 24 m. Note that above this depth the strength only was > 25 kPa in the top 5 m and even then the maximum strength was only ~ 60 kPa,
4) From examination of the profile data presented in Greertsema & Torrance (2005) down to 41 m depth, the peak strength typically ranges between ~ 15 and ~ 67 kPa however, one sample had a peak strength of ~ 95 kPa this sample was at a depth of 41m.
5) Taken from a depth between 2.4 – 3.3 m.
6) Sensitivities up to 100 were reported, but no remoulded strength value was given.

The lower moisture content of glacial clays is likely to arise from lower void ratios. For example, the material at Mink Creek was completely saturated, even at a moisture content of ~ 32 % (Marten Geertsema *pers. comm.* 2009), indicating a much lower void ratio (and hence possibly less open structure) than the volcaniclastic deposits of this study. Other differences result from clay mineral and grain size characteristics because these will affect Atterberg limits. For example, material at Mink Creek contains in order of abundance in the clay-size fraction (~ 43 %) chlorite > illite > kaolinite > feldspar > quartz; the silt (~ 57 %) fraction is dominated by quartz and feldspar (Geertsema & Torrance 2005). Similar material was observed in soils from Vancouver, Gloucestor Valley, and Outardes (Gillot 1979; Yong *et al.* 1979). Similarities do occur between sensitive volcaniclastic material and glaciomarine clay. These include high liquidity indexes, presence of low activity materials (halloysite in this study) (Table 8.3), characteristics of compaction during triaxial testing, and low strain at failure (section 8.4.4.1).

8.8 Are the soils in this study collapsible?

Collapsible soils are typically associated with loess deposits in arid environments (Selby 1993; Housten *et al.* 2002). However, the term "collapsible" has also been applied to volcaniclastic sediments (Clemence & Finbar 1981; Rogers 1995). More specifically, volcanic soils of the Tauranga region have been described as having collapsible characteristics (Prebble 1986; Keam 2008). Collapsible soils typically comprise silt and sand grains cemented together by either clay or chemical precipitates (Selby 1993; Housten *et al.* 2002). Thus, the fabric is highly porous (open) and consists of bulky irregular grains (Dudley 1970; Collins & McGown 1974). Wetting increases moisture content from a partially to a fully saturated state and collapse occurs as capillary strength is lost and cemented bonds soften (Housten *et al.* 2002). Furthermore, the collapsed soil will behave as a low strength suspension if void ratios are high enough to allow moisture content to exceed liquid limit (Selby 1993). Selby (1993) stated that collapsible soils typically have low clay content (2 to 20 %), low liquid limit (< 45 %), and low to high dry bulk densities (900 to 1500 kg m^{-3}).

The soils of this study certainly have an open structure, with the obvious exception of OS3. The open structure allows particles to lose volume and become

more closely packed on disturbance (Clemence & Finbar 1981; Rogers 1995). Scanning electron microscopy indicated that in samples from Tauriko and Otumoetai, large pores had been lost and material appeared more compact after remoulding. However, samples in this study did not collapse on wetting, as indicated by the capability to retain high amounts of water and have high saturation values (see section 8.6). Liquid limits in the soils of this study (Table 8.1) were much higher than those for typical collapsible soils. Some authors have argued for the inclusion of highly sensitive material under the umbrella of collapsible soils (e.g. Rogers 1995). However, such a term does not seem appropriate for the soils of my study. Whilst they may show characteristics of collapsible soils, the Tauranga soil materials certainly do not exhibit collapsible behaviour, in particular subsidence on wetting.

8.9 Development of sensitivity

Sensitivity in samples of this study was dominated by liquidity index, which is a function of void ratio, liquid limit and current moisture content. In this study, all the highly sensitive soils with low remoulded strength had liquidity indexes > 1. Typically as liquidity index increased so did sensitivity, and remoulded strength decreased.

Void ratio is important because a high value will allow a large amount of water to be retained, meaning low remoulded strength is more likely. Initial tephra fall deposition is a pathway for high void ratio and lack of geological consolidation ensures that this void ratio remains high with time. Weathering processes following fall deposition are also important. Material deposited during a period of rapid activity, either volcanic (tephra) or aeolian (tephric loess), will become buried within a short space of time. As activity continues the overburden becomes thicker and this subsequently leads to the land surface moving a greater distance above the deposited material. As this overburden increases pedogenesis will become increasingly weaker. Thus the deposits will become out of reach of biological cycles, experience reduced wetting and drying cycles, clay formation may be slowed and little illuviation will occur. The slowing of clay formation will also help keep liquid limit low. When burial occurs quickly enough, neoformation of clays may be dominated by a process of diagenesis rather than pedogenesis. The consequence is that material is able to maintain a high void ratio as it weathers to

clay. Hence the high void ratio increases the likelihood that liquid limit will be exceeded by natural moisture content.

Material which is deposited during a period of quiescence and remains at the surface for a long period of time will be subject to strong pedogenesis, involving high biological activity, desiccation, illuviation and advanced weathering. If these near-surface soil horizons are being formed during warm climates, then the higher temperatures will enhance biological and chemical activity (McLaren & Cameron 1996). The combination of these factors will result in a reduced void ratio, hence tighter packing. Furthermore, advanced weathering will promote clay formation and have a positive impact on both peak strength and liquid limit. An increase in liquid limit reduces the ability of the void ratio to maintain a liquidity index of > 1. Whilst the sample may be sensitive as a result of increased peak strength, it will have high remoulded strength and therefore will not flow on disturbance.

This same idea may also be true for a single thick deposit. Material deeper in the profile will experience less near-surface weathering than material near the land surface. This weathering gradient will result in material that is less sensitive or has higher remoulded strength near the top of the profile, yet more sensitive and dilatent material near the bottom. In this study, OS3 and OS4 may represent an example of the effects of this depth gradient.

The ideas presented above may explain why the Hamilton Ash beds in the Tauranga region are often associated with better engineering properties (e.g. elevated strength, higher dry bulk density and lower sensitivity) than the dilatent and highly sensitive material in this study (Hatrick 1982; Wesley 2007). One recent hypothesis for these better properties is that the Hamilton Ash beds were andesitic (e.g. NZ Soil Bureau 1968) whereas most of the other sub-surface material in the region was rhyolitic (Wesley 2007). However, Shepherd (1984; 1994) determined that the Hamilton Ash beds were largely rhyolitic in origin (Chapter 2). Therefore, the better engineering properties must be derived from other means. It is likely that the beds within the Hamilton Ash have experienced similar weathering patterns as explained for OS3 and have been subject to an extremely slow rate of up-building and hence strong (ongoing) pedogenesis. For example, the top member is a paleosol

(Chapter 4) and according to Briggs *et al.* (1996), the typical sequence in the Tauranga region is only ~ 1 m thick. Therefore the whole formation (apart from basal Rangitawa Tephra where present) effectively represents a deep soil with properties attained during upbuilding pedogenesis spanning up to ~ 300 ka and a number of glacial-interglacial cycles.

Based on micromorphological studies of the Naike and Patumahoe soils developed in Hamilton Ash beds, Bakker *et al.* (1996) showed that the soils, both dominated by halloysite, become more weathered with depth, quite likely a result of the accumulatory character of deposition of tephra materials combined with effectively continuous soil formation on them, i.e., upbuilding pedogenesis has dominated (Lowe 2000; 2008a). Large quantities of microlaminated, anisotropic clay coatings (probably halloysite) are present in Bt horizons of the Naike soil near Hamilton and are the result of clay illuviation, the migration of fine clay through the profile in suspension (fine clay: total clay ratios of 0.7 to 0.8 support this inference) (Bakker *et al.* 1996). The clay coatings have been responsible for impeding drainage and thus further reducing loss of Si and favouring more halloysite production, which thus imparts greater bulk densities (Parfitt *et al.* 1983) which exceed 1000 kg m^{-3} in Bt horizons (Lowe 2008a). Large amounts of Fe oxide coatings observed in both Patumahoe and Naike soils provide the reddish brown to strong brown colours in the Bt horizons of the Hamilton Ash-derived soils and are likely to be of similar levels in the Tauranga area.

The formation of halloysite is one feature common to materials of both high and low sensitivity. Otumoetai and Tauriko samples indicate that under the right weathering conditions, halloysite tubes, spheres and plates form an open microfabric with a large number of small pores. These arrangements have high sensitivity and typically low remoulded strength. However, under different weathering and clay neoformation conditions, these same materials become tightly packed with reduced porosity (OS3 is an example) and hence lower sensitivity and higher remoulded strength results. These findings indicate that the development of halloysite, in its own right, will not result in extremely high sensitivity which manifests as low remoulded strength. This conclusion is consistent with that of Jacquet (1990) who stated that the presence or abundance of either halloysite or allophane does not explain the level of sensitivity encountered.

The question remains that if another clay mineral, in this case allophane, were dominant would the sensitivity still be high, and in the case of TS1, TS2, TS3 and OS4, would remoulded strength be low (< 2 kPa)? Based on general statements, one could conclude that it is possible. For example, Prebble (1983; 1986) stated that soil fabrics dominated by halloysite **and allophane** clays are open, have few bonding points and contain much interstitial water. When disturbed, fabric is destroyed and a fluid material is produced. Furthermore, Frederickson (1988) concluded that if the soils in his study were saturated then their liquidity index would exceed 1, and sensitivity would be high. A more detailed study by Jacquet (1990) suggested that sensitivity in allophanic material can be up to 55 and remoulded shear strength can be as little as 3 to 4 kPa, but in his samples liquidity index was low at 0.6 to 0.76. The sample at 4 kPa was not fully saturated (85 %) and so remoulded strength could decrease on further wetting. However, Jacquet's (1990) samples only had between 14 and 28 % allophane and up to 7 % halloysite. In other samples with higher allophane contents (35 and 37 %), remoulded shear strength increased (8.5 and 9.5 kPa) and sensitivity decreased (8 and 13). The samples with higher allophane contents also had a higher liquid limit (127 to 133 %) than those samples with less allophane (63 to 86 %). The findings of Jacquet (1990) suggested that an increase in allophane may reduce sensitivity and increase remoulded strength.

Therefore, when allophane is the dominant clay mineral, sensitivity can be high but remoulded strength may not be extremely low, as observed in TS1, TS2, TS3 and OS4 (Figure 8.14). This is because the factors which control remoulded strength in halloysite (liquidity index, void ratio, saturation) are also important for allophane. However, the difference is that allophane can have extremely high liquid limits, compared to halloysite. For example, in allophanic soils liquid limits up to 250 % are possible and values > 100 % are not uncommon (Albrook 1983; Selby 1993; Mitchell & Soga 2005). Whilst allophane promotes an open structure, and often has high moisture contents, one expects that void ratio would have to be exceptionally high to allow natural moisture content to exceed liquid limit and hence cause remoulded strength to be low. This may be confirmed by Allbrook (1983) who examined the physical properties of 19 allophanic soils, of which none had liquidity indexes > 1. Consequently, soils dominated by allophane instead of halloysite may be sensitive but are unlikely to have extremely low liquid-like

remoulded strength because of the inability of moisture contents to easily exceed liquid limits.

In conclusion, the requirements for high sensitivity with low remoulded strength are:

- A void ratio which is sufficiently high to ensure liquid limit is capable of being exceeded by moisture content (liquidity index > 1). Tephra fall origin and deep weathering seem to ensure this occurs.

- The presence of halloysite, which will develop peak strength through electrostatic attraction and allow soils to remain in a coherent state even when saturated. Halloysite clays also mean that liquid limit can remain sufficiently low (unlike allophane) so it can be easily exceeded by natural moisture content. Deep burial may also sufficiently slow clay formation to help liquid limit remain low.

- An environment which encourages soils to be constantly saturated, ensuring high water contents. The typical stagnant or poorly drained conditions that promotes halloysite formation is conducive to this environment, as is the structure dominated by a large number of small pores following halloysite formation.

8.10 Summary

All soils in this study are ultimately volcanic in origin (pyroclastic) and have been deposited by either primary fall deposition or reworking. Samples at Otumoetai showed more advanced weathering than those at Tauriko. Compared to all samples collected, OS3 displays the greatest signs of weathering attributable to long periods of time spent near the land surface after deposition. This was reflected in it's tight packing, high undisturbed strength and dilatant characteristics during triaxial testing. Silica-rich rhyolitic parent material and impeded drainage conditions have meant halloysite was by far the dominant clay mineral in all samples. Consequently, a number of halloysite morphologies have been observed, including books. Such halloysite books have never been previously observed. Their structure may be a consequence of Fe substitution, allowing the normally curved halloysite morphologies (i.e. tubes) to lie flat.

All materials in this study were at least sensitive; field investigations indicated that this was a common property of soil material in the Tauranga region. However, sensitivity can be manifested as either low (< 2 kPa), moderate (7 kPa) or high remoulded strength (36 kPa). A common feature of those soils with low or moderate remoulded strength is that they have a liquidity index > 1. Those samples with low remoulded strength (TS1, TS2, TS3 and OS4) typically have an open structure, low peak strength and high void ratio. Samples with moderate remoulded strength (OS1, OS2) contained one factor (e.g high liquid limit or low void ratio) which negatively impacted on the rate which moisture content exceeds liquid limit. The only high remoulded strength sample, OS3, was tightly packed, had high clay content and moisture content which did not exceed liquid limit. Therefore, both peak and remoulded strength were high in the OS3 sample.

The consequence of those samples with high liquidity indexes (> 1) is that on disturbance in a mass wasting event, they will release excess water from small pores which was previously tightly held. This release of water dilutes the plasticity of low activity binding clays, supports grains and broken fragments of the clay materials, and allows material to flow.

Observations indicated that the depth of burial and time spent near the surface of a soil profile had an effect on the development of sensitivity, through different degrees of weathering. Those remaining near the land surface typically developed high peak strength and high remoulded strength (e.g OS3). Whilst the samples were still sensitive, they typically manifested sensitivity as high remoulded strength. Contrastingly material which was quickly buried were typically able to maintain higher void ratios hold greater amounts of water, thus increasing the likelihood of liquid limit being exceeded. If void ratio was low in these deeper samples, liquid limit was also low, this still allowed liquidity index to be > 1. If liquid limits are exceeded by natural moisture content, low remoulded strength and high sensitivity may result. Halloysite is an important contributor to sensitivity because it ensures that liquid limits remain low.

Chapter 9
Summary and conclusions

9.1 Summary of research findings

Field investigations indicated that sensitive soils are widespread through the Tauranga region. Sections at two sites with highly sensitive soils, Tauriko and Otumoetai, were investigated in detail using a combination of geomechanical, mineralogical and microstructural analysis. Using the information collected from investigations at the two sites, the following is a summary of research findings with special reference to the stated aim and objectives in Chapter 1.

9.1.1 Geomechanical properties of selected sensitive soils

Peak vane strength in samples from both sites ranged between 45 and 227 kPa. Using the adapted method of sensitivity, all samples were at least "sensitive" (> 8), with the highest value being 76. On extraction and remoulding, samples had either high (36 kPa), moderate (7 kPa), or low (≤ 2 kPa) remoulded strength. However, both peak and remoulded vane strengths were highly variable within samples, indicating heterogeneity not only between but also within geological units. Samples with moderate and low remoulded strength were dilatent when disturbed, with material becoming more liquid-like as remoulded strength decreased.

Low rapidity numbers (< 4), poor dispersion of clay during particle size analysis, and the considerable time and effort needed to liquefy samples whilst remoulding, indicated that a lot of energy is required to destroy the structure of each sample.

Moisture contents were typically high (> 60 %) with some samples having values exceeding 100 %. Because each sample was at or near full saturation *in situ* (saturation ratio ≈ 84 to 102 %), moisture content was positively correlated with void ratio ($r^2 = 0.87$).

The combination of low dry bulk density (656 kg m^{-3} to 966 kg m^{-3}) and relatively high particle densities (2532 kg m^3 to 2686 kg m^3) resulted in high values of porosity and void ratios compared with other weathered volcanic deposits. Porosity and void ratio values ranged between ~ 62 % and ~ 77 %, and 1.63 and 3.40, respectively. The observed void ratios and porosities can be explained by origin (pyroclastic fallout for most samples, or by fluvial reworking), morphology of clay minerals (spheres, tubes and books) and weathering histories (near surface or deep) of each unit sampled.

Peak vane strength was negatively correlated with void ratio (r^2 = 0.64). Microfabric observations suggested that the more porous structures were delicate and open resulting in reduced contacts between grains.

Liquid limits ranged between ~ 52 % and ~ 96 %, and plasticity indexes ranged from 13 % to 43 %. All samples plotted below the A line, in the typical range for halloysite clays. A positive correlation between liquidity index and sensitivity was observed (r^2 = 0.54). The relationship improved slightly when other studies on volcaniclastic deposits from New Zealand were included (r^2 = 0.60). A power relationship existed between remoulded strength and liquidity index (r^2 = 0.69). As liquidity index increased remoulded strength decreased. In those samples with low or moderate remoulded strength, natural moisture content exceeded the liquid limit, thus liquidity index was > 1.

Peak effective friction angles ranged between 25.7 º and 38.5 º. Friction angle was influenced by the irregular shape of particles (including clay, silt and sand) and void ratio. Low void ratios and hence tight packing relative to other samples resulted in greater grain interlocking, causing high friction angle, than in samples with high void ratio. Effective cohesion ranged between 4.7 kPa and 34.5 kPa. Halloysite books and cementing (observed as a coating of fine clay-like material) may have contributed to high the cohesion observed in some samples.

Pore water pressure conditions during triaxial testing indicated the structure of samples were different: two distinct groups could be defined. Samples with low to moderate remoulded strength failed at low strain (often < 5 %) and typically

displayed compaction during shear. Samples with high remoulded strength failed at high strains (> 13 %) and displayed dilation during shear.

Residual friction angles were between 19.34 º and 33.18 º. High residual friction angles were a result of irregular particle shapes and aggregates of clay particles rolling during shear. The lowest friction angle at 19.34 º was a consequence of halloysite tubes occurring in regular, parallel, face-to-face contacts with few large grains. This arrangement of particles formed a smooth sliding-type shear plane and hence lower residual friction angle.

Sensitive weathered volcanic deposits from the Tauranga region had peak strength, liquid limits, void ratios, and moisture contents which were higher than those of sensitive glacial marine clays in the Northern Hemisphere. Remoulded strength may also be higher in volcanic deposits. Higher peak strengths in weathered volcanic deposits mean that following initial failure, they do not collapse under their own weight, so large hectare-scale retrogressive mass wasting events like those observed in sensitive glacial marine clays, are not triggered in these materials.

9.1.2 Mineralogical properties of selected sensitive soils

All samples in this study were from weathered deposits of pyroclastic origin and rhyolitic composition. This origin was confirmed by the presence of glass, highly weathered pumice, plagioclase, and quartz. Other primary volcanogenic minerals in samples included hornblende, hypersthenes, and titanomagnetite. A dominance of rhyolitic materials in the Tauranga region had been demonstrated by previous stratigraphic work.

Delicate angular glass shards indicated that materials from Tauriko were primary fall deposits. One sample from Otumoetai had a concentration of heavy minerals (hornblende, titanomagnetite and pyroxene), which indicated fluvial reworking. This indicated that sensitivity can manifest in a range of depositional environments.

Clay contents in all samples exceeded 20 % with upper values of at least 75 % (based on SEM analyses). The clay mineralogy was completely dominated by hydrated halloysite and only a very small, insignificant amount of Al-rich allophane

was recorded. The dominance of halloysite was a consequence of the nature of the parent material (rhyolitic pyroclastics), slow to impeded drainage conditions (resulting in part from heterogeneity of underlying sediments), past climates that included prolonged periods of cold, dry glacial climates (and hence low rates of desilication), the microfabric formed by halloysite (i.e. many small pores), and a thick over-burden. The combination of these conditions ensured that silica in soil solution remained high, thereby encouraging the direct formation of halloysite rather than Al-rich allophane.

Halloysite morphologies were typically spheres, plates and tubes. However, a new and unique morphology of hydrated halloysite, in the form of clay books (vermiforms), was observed in samples from Tauriko. These books comprised individual "sheets" or "leaves". The books were unequivocally confirmed as halloysite with X-ray diffraction analyses of samples using various treatments. The morphology of the halloysite books was explained by high structural Fe content (~ 5 %) within "sheets" or "leaves", correcting the size misfit between the larger Si^{4+} tetrahedral sheet and the smaller Al^{3+} octahedral sheet.

Books contributed positively to peak vane strength and effective cohesion. The books may have assisted in low remoulded strength by suppressing the liquid limits of samples in which they were abundant.

9.1.3 Microfabric properties of selected sensitive soils

Hydrated halloysite in its various morphologies (e.g. tubes, spheres, books and plates) formed a background to the microfabric in all samples, acting as an overall binder. The microfabric of each sample was typically continuous, having poorly defined microaggregates and few connectors. Large grains of silt and sand sized material were supported within the background matrix of clay material.

Whilst individual components of the microfabric were similar in all samples, the overall structure of each sample was different. The microfabric of high remoulded strength samples was noticeably different to all other samples

Material which had high remoulded strength was dominated by short halloysite tubes which were closely packed, typically in parallel, face-to-face

contacts. The close packing meant porosity was low and dry density was high relative to other samples. The microfabric was dominated by ultra-pores, with a lesser number of micro- and meso-pores. Large grains were few and were tightly bound within the fabric. This structure changed little on remoulding, had high peak strength (> 227 kPa), liquidity limit (90.02 %) and clay content. High liquid limit and relatively low void ratio meant this structural type was unable to hold water above its liquid limit. The relatively dense microfabric resulted from an extended period of time at the land surface following deposition. Exposure to surface processes in the soil-forming environment has resulted in advanced pedogeneisis (e.g. high biological and chemical activity, and possibly clay illuviation). The good engineering properties (e.g. high bulk density) observed in the Hamilton Ash Formation in the Tauranga region seem to manifest from this structural type.

Typically the structures of low to moderate remoulded strength samples were more open than that of the high remoulded strength material. However this open structure was observed in different ways between sites. Material at Tauriko was dominated by loosely packed clay minerals (tubes spheres and plates) in a 'honeycomb' or 'skeletal'-type arrangement intermixed with delicate hollow textures (poossibly relict pumice). The delicate hollow textures added to structural openness. When the halloysite books increased in abundance at Tauriko, structural openness decreased. At Otumoetai structural openness was typically a consequence of halloysite tubes meeting at tangental contacts, having a 'flocculated'-type appearance. However, when the abundance of small irregular spheres increased at Otumoetai structural openness decreased. At both sites the loose packing meant a large number of ultra and micro-pores occurred between individual clay grains. Pores of all size classes were more abundant in these structural types than that with low remoulded strength. Grains were often only loosely bound into the microfabric.

These typically open structures which supported low to moderated remoulded strengths had a range of peak strengths (45 kPa to 151 kPa), liquid limits (51.97 % to 90.02 %) and void ratios (1.63 to 3.40). In all samples void ratio was sufficiently high to allow liquid limit to be exceeded by natural moisture content thus, liquidity index was > 1. Low to moderate remoulded strength samples with low void ratios had reduced liquid limits. The open structure was probably a result of quick burial of the deposits (by subsequent pyroclastic beds) and hence

weathering and synthesis of clays occurred as a result of subsurface diagenesis rather than via strong, near-surface pedogenic processes, as evident in the more compact, high remoulded strength structure.

The dominance of small pores in all samples was a consequence of clay formation. However, these small pores allowed the fabric to retain water tightly, near or at saturation, whilst maintaining a coherent structure. Water which was not bound to the surface of clay particles was available to be released on remoulding.

9.1.4 Key controls on sensitivity.

The dominant control on sensitivity was liquidity index, which is a function of void ratio, liquid limit and existing moisture content. All samples with high sensitivity and low remoulded strength had liquidity indexes > 1, yet material with higher remoulded strength and lower sensitivity had liquidity indexes < 1. The following section is an outline of the aspects of mineralogy, microstructure and geomechanics which cause this high sensitivity yet low remoulded strength to exist.

Void ratio must be high enough to ensure that liquid limit can be exceeded by natural moisture content. The fallout origin of material results in an initially open microfabric, and deep weathering (clay formation via mainly diagenesis rather than pedogenesis) without any geological consolidation preserves the open structure following deposition. This process ensures that void ratio typically remains high.

The formation of halloysite is important, because it promotes strength through electrostatic attraction enabling clays to remain coherent whilst saturated. Unlike allophane, halloysite clays typically have liquid limits which are able to be exceeded by natural moisture contents, without the sample requiring an excessively high void ratio.

Sensitive soils must remain in an environment where natural moisture contents are close to saturation. The typical ‘stagnant’ or slow to poorly drained conditions which promote halloysite formation, and the structure (dominated by small pores) which is subsequently formed, promotes a slow draining environment. This structure is able to tightly hold onto water which can be released on

remoulding. It will also reduce desilication encouraging further halloysite formation.

When these individual factors are combined, natural moisture content will exceed liquid limits. Therefore, within an energetic landslide, the microfabric of samples will be destroyed. The tightly held water within their small pores, which is not retained by the surface of clays or within their structure, will be released. This excess water will dilute the plasticity of inactive halloysite clays, and suspend aggregates of clay material and larger loosely held grains.

The combination of these factors (e.g. high void ratio, wet environment, presence of halloysite) will enable material to have dilatent properties and hence be more likely to flow on disturbance. The volume of material in which natural moisture content exceeds liquid limit, and the rate at which the liquid limit is exceeded, will determine the volume of material which is capable of flowing on failure.

9.2 Suggestions for future work

The following presents possible avenues of research into sensitive volcanic soils.

- Investigate the remoulded strength of samples which become liquid-like on disturbance with a Swedish drop cone or very sensitive shear vane, to get an accurate measure of strength.

- Examine the relationship between liquidity index of volcanic deposits and remoulded strength. Possibly by investigating a mathematical relationship between the two and possibly develop a predictor for remoulded strength from liquidity index. The relationship between sensitivity and liquidity index may also be investigated in a similar manner.

- Further investigate the origin and morphology of halloysite books, paying special attention to their Fe content.

- Investigate the contribution of sensitive soils to slope stability. One aspect may be to determine the possible contribution of increasing pore water to structural break down in sensitive soils.

- Further investigate the relationship between weathering processes and sensitivity. Such as, the nature of sensitivity in a chronosequence of volcanic soils.

References

Allbrook, R. F. 1983: Some physical properties of allophane soils from the North Island, New Zealand. *New Zealand Journal of Science 26:* 481 - 492.

Azizi, F. 2000, *Applied analysis in geotechnics*. E & F Spon, London.

Bailey, S. W. 1990: Halloysite - A critical assessment. *Sciences Geologiques 86:* 89 – 98.

Bakker, L.; Lowe, D. J.; Jongmans, A. G. 1996: A micromorphological study of pedogenic processes in an evolutionary soil sequence formed in late Quaternary rhyolitic tephra deposits, North Island, New Zealand. *Quaternary International 34 – 36:* 249 - 261.

Bareither, C. A.; Benson, C. H.; Edil, T. B. 2008: Reproducibility of direct shear tests conducted on granular backfill materials. *Geotechnical Testing Journal 31(1)*: 1 - 11.

Bates, T. F.; Hilderbrand, F. A.; Swineford, A. 1950: Morphology and structure of endellite and halloysite. *American Mineralogist 35:* 463 - 484.

Beattie, A. G. 1990: *Petrological controls on the geomechanical behaviour of coal measure soft rock, Waikato, New Zealand.* Unpublished MSc Thesis. University of Waikato, Hamilton, New Zealand.

Bell, D. H.; Pettinga, J. R. 1984: Presentation of geological data. *Proceedings of technical groups. The New Zealand Institute of Engineers 1984:* 4.1 - 4.36.

Bell, D. H.; Richards, L.; R. Thomson, R. 2003: Relict slip verification study – Tauranga District. *Geotechnics on the volcanic edge, Tauranga, March 2003, New Zealand Geotechnical Society Symposium. New Zealand geotechnical Society:* 281 – 289.

Bird, G. A. 1981: *The Nature and causes of coastal landsliding on the Maungatapu Peninsula.* Unpublished MSc Thesis. University of Waikato, Hamilton, New Zealand.

Berkman, D. A. 2001: *Field geologists manual*. The Australian Institute of Mining and Metallurgy Victoria, Australia.

Bishop, A. W.; Henkel, D. J. 1962: *The measurement of soil properties in the triaxial test.* Edward Arnold (Publishers) Ltd, London.

Bjerrum, L. 1954: Geotechnical properties of Norwegian marine clays. *Geotechnique 4:* 49 - 69.

Brand, E. W.; Brenner, R. P. 1981: *Soft Clay Engineering*. Elsevier, Amsterdam.

Briggs, R. M.; Hall., G. J.; Harmsworth., G. R.; Hollis., A. G.; Houghton., B. F.; Hughes., G. R.; Morgan. M. D.; Whitbread-Edwards., A. R. 1996: *Geology*

of the Tauranga Area – Sheet U14 1:50 000. Department of Earth Sciences, University of Waikato Occasional Report 22.

Briggs, R. M.; Houghton., B. F.; McWilliams, M.; Wilson, C. J. N. 2005: 40Ar/39Ar ages of silicic volcanic rocks in the Tauranga-Kaimai area, New Zealand: dating the transition between volcanism in the Coromandel Arc and the Taupo Volcanic Zone. *New Zealand Journal of Geology & Geophysics 48:* 459 - 469.

Briggs, R. M.; Lowe, D. J.; Esler, W. R.; Smith, R. T.; Henry, M. A. C.; Wehrmann, H.; Manning, D. A.; 2006: *Geology of the Maketu area, Bay of Plenty, North Island, New Zealand - Sheet V14 1:50 000.* Department of Earth Sciences, University of Waikato, Occassional Report 26.

Briggs, R. M.; Lowe, D. J.; Goles, G. G.; Shepherd, T. G. 1994: Intra-conference tour day 1: Hamilton - Raglan – Hamilton. In Lowe, D. J. (ed.): *Conference tour guides. International Inter-INQUA field conference and workshop on tephrochronology, leoss and paleopedology,* University of Waikato, Hamilton, New Zealand: 24 - 44.

Brindley, G. W.; Brown, G. 1980: *Crystal structure of clay minerals and their x-ray identification.* Mineralogical Society Monograph 5. Mineralogical Society, London.

Bromhead, E. N. 1986: *The stability of slopes* Surrey. University Press, Glasgow.

British Standard 1377 – 8 (BS1377), 1990: *Methods of test for soils for civil engineering purposes - part 8: shear strength tests (effective stress).* British Standards Authority, London.

Burn., D. A.; Cowburne., A. J. 2003: Engineering geological aspects of the Ruahihi Power scheme. *Geotechnics on the Volcanics Edge, Tauranga, March 2003, New Zealand Geotechnical Society Symposium*. New Zealand Geotechnical Society. 281 – 289.

Campbell, A. S.; Schwertmann, U. 1985: Evaluation of selective dissolution of extractants in soil chemistry and mineralogy by differential x-ray diffraction. *Clay Minerals 20:* 515 - 519.

Carr, R. G. 1981: A scanning electron microscope study of post-depositional changes in the Matahina Ignimbrite, North Island, New Zealand. *New Zealand Journal of Geology & Geophysics 24:* 429 - 434.

Chandler, M. P.; Rogers, N. W. 1980: *Triaxial and direct shear testing.* Department of Earth Sciences, University of Waikato internal report series in geomechanics no. 1. Unpublished Report University of Waikato. Hamilton.

Chapman, P. 1998: *The assessment of landslide mechanisms in the southern landslide zone, South Auckland, New Zealand.* Unpublished MSc Thesis. University of Waikato, Hamilton, New Zealand.

Churchman, G. J. 1990: Relevance of different intercalation tests for distinguishing halloysite from kaolinite in soils. *Clays and Clay Minerals 38 (6):* 591-599.

Churchman, G. J. 2000: The alteration and formation of soil minerals by weathering. In M. E. Summer (ed.), *Handbook of soil science*. CRC press, Boca Raton, Florida. F3 - F76.

Churchman, G. J.; Gilkes, R. J. 1989: Recognition of intermediataries in the possible transformation of halloysite to kaolinite. *Clay Minerals 24:* 579 - 590.

Churchman, G. J.; Taite, K. R.; 1986: Aggregation of clay in six New Zealand soil types as measured by disaggregation procedures. *Geoderma 37:* 207 - 220.

Churchman, G. J.; Theng, B. K. G. 1984: Interactions of halloysite with amides; minerological factors affecting complex formation. *Clay Minerals 19 (2):* 161 - 176.

Churchman, G. J.; Whitton, J. S.; Claridge, G. C.; Theng, B. K. 1984: Intercalation method using formamide for differentiating Halloysite from Kaolinite. *Clays and Clay minerals 32 (4)*: 241 - 248.

Clemence, S. P.; Finbarr, A. O. 1981: Design considerations for collapsible soils. *Journal of the geotechnical engineering division, Proceedings of the American Society of Civil Engineers 107 (GT3):* 305 - 317.

Collins, K. 1985: Towards characterisation of tropical soil microstructure. *First international conference on geomechanics in tropical lateric and saprolitic soils.* Brazilian Society for Soils Mechanics. 85 - 96

Collins, K.; McGown, A. 1974: The form and function of microfabric features in a variety of natural soils. *Geotechnique 24 (2):* 223 – 254.

Connell Wagner, 2000: *Geotechnical stability report for building 118 Ranganui Road Welcome Bay for WH & ZH White.* Unpublished report. Report number 7339-SH-01. Held on Tauranga City council files.

Connell Wagner, 2007: *Geotechnical completion report Rendale subdivision for Rendale estate limited.* Unpublished report. Report number T536-02-mo-03. Held on the Tauranga City council files.

Cong, S. 1992: *Engineering geology of rhyolitic silts in the upper Waitemata Harbour, Auckland, New Zealand.* Unpublished MSc Thesis. University of Auckland, Auckland, New Zealand.

Costanzo, P. M.; Guize, J. R. F. 1985: Dehydration of synthetic hydrated kaolonite: A model for dehydration of halloysite (10 Å). *Clays and Clay Minerals 33:* 415 - 423.

Craig, R. F. 1997, *Soil Mechanics*, E & FN Spon, London, United Kingdom.

Cruden, D., M.; Varnes, D. J. 1996: Landslide types and processes. In Turner A. K.; Schuster R. L. (eds.), *Landslides Investigations and Mitigation.* Special Report 247. Transportation Research Board, National Research Council. 36 – 71.

Dahlgren, R. A.; Shoji, S.; Nanyo, M. 1993: Mineralogical characteristics of volcanic ash soils. *Developments in Soil Science 21:* 101 - 143.

Dixon, J. B. 1989: Kaolin and serpentine minerals. In Dixon J. B.; Weed, S. B. (eds.), *Minerals in Soil Environments*, Soil Science Society of America Madison, Wisconsin. 467 – 519.

Dudley, J. H. 1970: Review of collapsible soils. *Journal the soil mechanics and foundations division proceedings of the American Society of Civil Engineers SM3 paper 7278:* 925 - 947.

Ece, O. I.; Schroeder, P. A. 2007: Clay mineralogy and chemistry of halloysite and alunite deposits in the Turplu area, Balikesir, Turkey. *Clays and Clay Minerals 55 (1): 18-35.*

Egashira, K.; Ohtsubo, M. 1982: Smectite in marine quick clays of Japan. *Clays and Clay Minerals 30:* 275 - 280.

Fanning, D. S.; Keramidas, V. Z.; El-Desoky, M. A. 1989: Micas. In Dixon J. B.; Weed, S. B. (eds.), *Minerals in soil environments*, Soil Science Society of America Madison, Wisconsin. 551 – 624.

Fields, M.; Perrot, K. W. 1966: The nature of allophane in soils - Part 3. *New Zealand Journal of Science 9:* 623 - 629.

Fredericksen, D. C. 1988: *A contribution to the geotechnical properties of allophanic soils from New Zealand.* Unpublished MSc Thesis. University of Waikato, Hamilton, New Zealand.

Froggatt., P. C.; Lowe., D. J. 1990: A review of late Quaternary silicic and some other tephra formations from New Zealand; their stratigraphy, nomenclature, distribution, volume and age. *New Zealand Journal of Geology and Geophysics 33:* 89 - 109.

Gardiner, V.; Dackombe, R. 1983: *Geomorphic Field Mapping.* George Allen & Unwin, London.

Geertsema, M.; Clague, J. J.; Schwab, J. W.; Evans, S. G. 2006a: An overview of recent large catastrophic landslides in northern British Columbia, Canada *Engineering Geology 83 (1-3):* 120-143.

Geertsema, M., Cruden, D. M. & Schwab, J. W. 2006b: A large rapid landslide in sensitive glaciomarine sediments at Mink Creek, northwestern British Columbia, Canada. *Engineering Geology 83 (1-3):* 36-63.

Geertsema, M.; Torrance, J. K. 2005: Quick clay from the Mink Creek landslide near Terrace, British Columbia: Geotechnical properties, mineralogy, and geochemistry. *Canadian Geotechnical Journal 42 (3):* 907-918.

Gibb, J. G. 1979: A coastal landslide. *Soil and Water, October:* 20 -21.

Gillot, J. E. 1979: Fabric, composition and properties of sensitive soils from Canada, Alaska and Norway. *Engineering Geology 14:* 149 -172.

Gonzalez, L. I.; Vallejo, J. A.; Jimenez, S.; Legeuy Jimenez, S.; 1981: Engineering geology of the tropical volcanic soils of La Guna, Tenerife. *Engineering Geology 17:* 1 - 17.

Grabowska-Olszewska, B.; Osipov, V.; Sokolov, V.; 1984: *Atlas of the microstructure of clay soils.* Panstwowe Wydamnictwo Naukowe, Warszawa.

Gregerson, O. 1981: The quick clay slide in Rissa, Norway. *Proceedings of the ICSMFE*, Stockholm. 421 - 426.

Harmsworth, G. R. 1983: *Quaternary stratigraphy of the Tauranga Basin. Unpublished MSc Thesis.* University of Waikato, Hamilton, New Zealand.

Harsh, J. B., Chorover, J.; Nizeyimana, E. 2002: Allophane and imogolite. In Dixon J. B.; Schulze D. G.; (eds.) *Soil mineralogy with environmental applications.* Soil Science Society of America, Madison, Wisconsin. 291 - 319.

Hatrick, A. V. 1982: *Report of committee to inquire into the failure of the Ruahihi Canal*. Unpublished Report. Ministry of Works and Development, New Zealand.

Head, K. H. 1992: *Manual of soil laboratory testing; volume 1: Soil classification and compaction tests.* Pentech Press, London.

Head, K. H. 1994: *Manual of soil laboratory testing; volume 2: Permeability, Shear strength and Compressibility tests.* John Wiley and Sons. West Sussex.

Head, K. H. 1998: *Manual of soil laboratory testing; volume 3: Effective stress tests.* John Wiley and Sons. West Sussex.

Hegan, B. D.; Wesley, L. R. 2005: *Tauranga storm event of 18 May, 2005: landslip issues.* Unpublished report for the Tauranga City Council. Held on Tauranga City Council files.

Heiken, G. 1972: Morphology and petrology of volcanic ashes. *Geological society of America Bulletin 83:* 1961 - 1988.

Heiken, G.; Wohletz, K. 1985: *Volcanic ash.* University of California Press, Los Angeles.

Hewitt, A. E. 1998: *New Zealand soil classification.* Landcare Research Science Series 1. Manaaki Whenua Press, Lincoln.

Hillel, D. 2004: *Introduction to environmental soil physics.* Elsevier, Burlington.

Houghton, B. F.; Hegan, B. D. 1980: *A preliminary assessment of geological factors influencing slope stability and landslipping in and around Tauranga City.* New Zealand Geological Survey, Lower Hutt.

Houston, S. L.; Houston, W. N.; Lawrence, C. A. 2002: Collapsible soil in hihgway infrastructure development. *Journal of Transportation Engineering (May – June):* 295 - 300.

Huppert, F. 1986: *Petrology of soft tertiary rocks and its relationship to geomechanical behaviour, Central North Island, New Zealand.* Unpublished PhD Thesis. University of Auckland, Auckland, New Zealand.

Huppert, F. 1988: Influence of microfabric on geomechanical behaviour of tertiary fine grained sedimentary rocks from central north Island, New Zealand. *Bulletin of the International Association of Engineering Geology 38:* 83 – 94.

Jacquet, D. 1987: *Bibliography on the physcal and engineering properties of volcanic soils in New Zealand*. New Zealand Soil Bureau bibliographic report, Lower Hutt.

Jacquet, D. 1990: Sensitivity to remoulding of some volcanic Ash Soils in New Zealand. *Engineering Geology 28:* 1 - 25.

Jeong, G. Y. 1998: Formation of vermicular kaolinite from halloysite aggregates in the weathering of plagioclase. *Clays and Clay Minerals 46 (3):* 270-279.

Johnson, S. L.; Guggenheim, S.; Koster van Groos, A. F.; 1990: Thermal stability of halloysite by high pressure differential thermal analysis. *Clays and Clay Minerals 38 (5)*: 477 - 484.

Joussein, E., Petit, S.; Churchman, J.; Theng, B.; Righi, D.; Delvaux, B. 2005: Halloysite clay minerals - A review. *Clay Minerals 40 (4):* 383 - 426.

Joussein, E.; Petit, S.; Fialips, C. I.; Vieillard, P.; Righi, D. 2006: Differences in the dehydration-rehydration behavior of halloysites: New evidence and interpretations. *Clays and Clay Minerals 54(4):* 473 - 484.

Karlsson, R.; Hansbo, S. 1989: Soil classification and identification *Byggforskningsradet Document D8*.

Keam, M. J. 2008: *Engineering geology and mass movement on the Omokoroa peninsula, Bay of Plenty, New Zealand.* Unpublished MSc Thesis, University of Auckland, Auckland, New Zealand.

Kear, D.; Schofield, J. C. 1978: *Geology of Ngauruwahia subdivision.* New Zealand Geological Survey Bulletin 88.

Keller, W. D. 1977: Scan electron micrographs of kaolins collected from diverse environments of origin - IV Georgia kaolin and kaolinizing source rocks. *Clays and Clay Minerals 25*: 311 - 345.

Kezdi, A. 1980, *Handbook of soil mechanics*. Elsevier, Amsterdam.

Kirkman, J. H. 1977: Possible structure of halloysite disks and cylinders observed in some New Zealand rhyolitic tephras. *Clay Minerals 12:* 199 - 215.

Kirkman, J. H. 1981: Morphology and structure of halloysite in New Zealand tephras. *Clays and Clay Minerals 29 (1):* 1 - 9

Kirkman, J. H.; Pullar, W. A. 1978: Halloysite in late Pleistocene rhyolitic tephra beds near Opotiki, coastal Bay of Plenty, North Island New Zealand. *Australian Journal of Soil Research 16:* 1 - 8.

Kohn, B. P.; Pillans, B.; McGlone, M. S. 1992: Zircon fission-track age for middle Pleistocene Rangitawa Tephra, New-Zealand - stratigraphic and paleoclimatic significance. *Palaeogeography Palaeoclimatology Palaeoecology 95 (1-2):* 73-94.

Lambe, T. W. 1958: The Structure of compacted clay. *Proceedings of the American Society of Civil Engineers 84 (SM2):* 1 - 34.

Lambe, T. W.; Whitman, R. V. 1979: *Soil Mechanics, SI Version*. John Wiley and sons New York.

Lancellotta, R. 1995: *Geotechnical engineering*. A.A. Balkema Publishers, Rotterdam, Netherlands.

Law, C. C. 1980, *Ring shear, vane shear, variable normal load direct shear and core samples for plain direct shear tests.* Department of Earth Sciences, University of Waikato internal report series in geomechanics no. 4. Unpublished Report University of Waikato. Hamilton.

Lee, I. K.; Ingles, O. G.; White, W. 1983, *Geotechnical Engineering.* Pitman, Boston.

Lefebvre, G. 1996, Soft Sensitive Clay. In Turner A. K.; Schuster R. L. (eds.), *Landlsides Investigations and Mitigation*. Special Report 247. Transportation Research Board. National Research Council. 607 – 617.

Lo, K. Y. 1962: Shear Strength of a sample of volcanic material. *Geotechnique 12:* 303 - 319.

Lowe, D. J. 1981: *Origin and composite nature of late Quaternary air fall deposits, Hamilton Basin, New Zealand.* Unpublished MSc Thesis, University of Waikato, Hamilton, New Zealand.

Lowe, D. J. 1986: Controls on the rates of weathering of clay mineral genesis in airfall tephra: A review and New Zealand case study. In. Colman, S. M.; Dethier, D. P. (eds.). *Rates of chemical weathering of rocks and minerals.* Academic Press. Orlando, Florida. 265 - 330.

Lowe, D. J. 1995: Teaching clays: from ashes to allophane. In Churchman, G.J.; Fitzpatrick, R.W.; Eggleton, R. A. (eds.). *Clays controlling the environment.* Proceedings of the 10th International clay conference 1996 vol 2 Oral papers. CSIRO Publishing Melbourne.

Lowe, D. J. 2000: Upbuilding pedogenisis in multisepaul tephra-derived soil in the Waikato region. In Adams, J. A.; Mehterell, A. K. (eds.). Soil 2000: *New horizons for a new century*. Proceedings, Australian and New Zealand 2nd

joint soils conference, Lincoln University. New Zealand Society of soil science. 183 - 184

Lowe, D. J. (ed.) 2008a: *Guidebook for pre-conference North Island field trip A1 Ashes and issues.* Australia and New Zealand 4th Joint Soils Conference, Massey University. New Zealand Society of Soil Science. 55 - 72.

Lowe, D. J.; Hogg, A. G. 1995: Letter to the editor - age of the Rotoehu ash. *New Zealand Journal of Geology and Geophysics 38:* 399 - 402.

Lowe, D. J.; Nelson, C. S. 1983: *Guide to the Nature and methods of analysis of tephras from the South Auckland Region, New Zealand*. Department of Earth Sciences, University of Waikato Occasional Report 11.

Lowe, D. J.; Percival, H. J. 1993: Clay mineralogy of the tephras and associated paleosols and soils, and hydrothermal deposits, North Island. *Guide book for the New Zealand Pre Conference field trip F.1.* 10th International Clay Conference. Adelaide, Australia.

Lowe, D. J.; Shane, P. A. R.; Alloway, B. V.; Newnham, R. M. 2008b: Fingerprints and age models for widespread New Zealand tephra marker beds erupted since 30,000 years ago: a framework for NZ-INTIMATE. *Quaternary Science Reviews 27 (1-2):* 95 - 126.

Lowe, D. J.; Tippett, M. J.; Kamp, P. J. J.; Liddell, I. J.; Briggs, R. M.; Horrocks, J. L. 2001: Ages on weathered plio pleistocene tephra sequences, Western North Island New Zealand. *Les Dossiers de l`Archeo-Logis 1:* 45 - 60.

Lowe, D. J.; Tonkin, P. J.; Palmer, A. S.; Palmer, J. (eds.) 2008c, *Dusty horizons (Loess).* Geological Society of New Zealand Miscellaneous Publication 124.

Malvern 1997, *Sample dispersion and refractive index guide.* Malvern Instruments Ltd, London.

Malvern 1999, *Operators guide* Malvern Instruments Ltd, London.

Manning, D. M. 1996: Middle Pleistocene tephrostratigraphy of the eastern Bay of Plenty, New Zealand. *Quaternary International 34 – 36:* 3 - 12.

McIntosh, P. D. 1979: Halloysite in a New Zealand tephra and paleosol less than 2500 years old. *New Zealand Journal of Science 22:* 49 - 54.

McLaren, R. G.; Cameron, K. C. 1996: *Soil science.* Oxford University Press, Auckland.

Meyer, V.; Larkin, T.; Pender, M. 2005: The shear strength and dynamic shear stiffness of some New Zealand volcanic ash soils. *Soils and foundations 45 (3):* 9 - 20.

Milne, J. D. G.; Clayden, B.; Singleton, P. L.; Wilson, A. D. 1995: *Soil description handbook.* Manaaki Whenua Press, Lincoln, Canterbury.

Mitchell, J. K.; Houston, W. N. 1969: The causes of clay sensitivity. *Journal of Soil Mechanics and Foundation Design, America Society of Civil Engineers 95 (SM3):* 845 - 871.

Mitchell, J. K.; Soga, K. 2005: *Fundamentals of soil behaviour*. John Wiley & Sons, Hoboken, New Jersey.

Molloy, L. 1998, *Soils in the New Zealand landscape: the living mantle.* New Zealand Society of Soil Science, Lincoln, Canterbury.

Moon, V. G. 1989: *Relationships between the geomechanics and petrography of ignimbrite.* Unpublished PhD Thesis, University of Waikato, Hamilton, New Zealand.

Moon, V. G. 1993: Microstructural controls on the geomechanical behaviour of ignimbrite. *Engineering Geology 35 (1-2):* 19-31.

Moore, D. M.; Reynolds, R. C. 1997: *X-ray diffraction and the identification and analysis of clay minerals*. Oxford University Press, New York.

Moore, P. J.; Styles, J. R. 1988: Some characteristics of a volcanic ash soil. *Proceedings of the second international conference on geomechanics in tropical soils Singapore.* A. A. Balkema, Singapore 161 - 165.

New Zealand Soil Bureau 1968: Soils of New Zealand Part 3. *New Zealand Soil Bureau Bulletin 26 (3):* 90 - 93.

Nicholson, C. M. 1986: *A Geomechanical Investigation of the Hamilton Ash formation using the Iowa borehole shear device and Selected laboratory tests.* Unpublished MSc Thesis, University of Waikato, Hamilton, New Zealand.

Noro, H. 1986: Hexagonal Platey Halloysite in an altered tuff bed, Komaki City, Aichi Prefecture, Central Japan. *Clay Minerals 21 (3):* 401 - 417.

Norsk Geoteknisk Forening 1974: *Retningslinjer for presntajon av geotekniske underskelser*. Oslo.

New Zealand Geotechnical Society (NZGS), 2001: *Guideline for hand held shear vane test*. New Zealand geotechnical Society.

New Zealand Geotechnical Society (NZGS), 2005: *Guidelines for the field classification and description of soil and rock for engineering purposes.* New Zealand Geotechnical Society.

New Zealand standard (NZS) 4402, 1986: *Methods of testing soil for civil engineering purposes.* The soil testing committee, (44/3), of the building and civil engineering division committee, (30/-) Standards Association of New Zealand. Wellington.

Oborn, L. E. 1988: Canal failure, Ruahihi hydro electric power scheme, Bay of Plenty, New Zealand. *Fifth Australia-New Zealand conference on geomechanics 1988 Barton, A.C.T.* Institute of Engineers, Australia. 574 - 584.

Oborn, L. E.; Northey, R. D.; Beetham, R. D.; Brown, I. R. 1982: *Engineering geological factors, related to collapse of Ruahihi canal*. Department of Scientific and Industrial Research, Wellington, New Zealand.

Ogura, Y.; Tanaka, R.; Takesako, H. 2008: Unique clay material formation in andisols derived from Holocene tephras of Mt Fuji. *Soil - the living skin of planet earth*. Australia and New Zealand 4th Joint Soils Conference, Massey University. New Zealand Society of Soil Science. 105.

Oliver, R. C. 1997: *A geotechnical characterisation of volcanic soils in relaton to coastal landslidng on the Maungatapu peninsula, Tauranga, New Zealand.* Unpublished MSc Thesis, University of Canterbury, Christchurch, New Zealand.

Olson, C. G.; Thompson, M. L.; Wilson, M. A. 2000: Phyllosilicates. In M. E. Summer (ed.). *Handbook of soil science.* CRC Press, Boca Raton, Florida. F125 - F180.

OPUS International consultants (OPUS) 1998: *Harini roundabout slip movement geotechnical assessment*. Unpublished report. Report number 9B03/E1. Held on the Tauranga City Council files.

OPUS International consultants (OPUS) 2006: *Pillans point storm water tunnel geotechnical factual report.* Unpublished report. Report number G2426. Held on Tauranga City Council files.

Papoulis, D.; Tsolis-Katagas, P.; Katagas, C. 2004: Progressive stages in the formation of kaolin minerals of different morphologies in the weathering of plagioclase. *Clays and Clay Minerals 52 (3):* 275 - 286.

Parfitt, R. L. 1990: Allophane in New-Zealand - a Review. *Australian Journal of Soil Research 28 (3):* 343 - 360.

Parfitt, R. L.; Childs, C. W. 1988: Estimation of forms of Fe and Al: A review, and analysis of contrasting soils by dissolution and mossbauer methods. *Australian Journal of Soil Research 26:* 121 - 144.

Parfitt, R. L.; Kimble, J. M. 1989: Conditions of formation of allophane in soils. *Soil Science Society of America 53:* 971 - 977.

Parfitt, R. L.; Furkert, R. J.; Henmi, T. 1980: Identification and structure of two types of allophane from volcanic ash soils and tephra. *Clays and Clay Minerals 28:* 328 – 334.

Parfitt, R.L.; Russell, M.; Orbell, G.E. 1983: Weathering sequence of soils from volcanic ash involving allophane and halloysite. *Geoderma 29:* 41-57.

Parfitt, R. L.; Saigusa, M.; Cowie, J. D. 1984: Allophane and halloysite formation in a volcanic ash bed under different moisture conditions. *Soil Science 138 (5):* 360 - 364.

Parton., I. M.; Olsen., A. J. 1980: Compaction properties of Bay of Plenty volcanic soils. *Proceedings of technical groups 6 (1G).* New Zealand Institute of engineers. 165 – 170.

Prebble, W. M. 1983: Investigations in an active volcanic terrain. *Proceedings of the symposium engineering for dams and Canals*. Institute of Professional Engineers New Zealand. 17.1-17.15.

Prebble, W. M. 1986: Geotechnical problems in the Taupo Volcanic Zone. *Volcanic hazard assesment in New Zealand.* New Zealand Geological Survey Record 10. 65 - 80.

Prebble, W. M. 2001: Geomechanics lecture 2001: Hazardous terrain - an engineering geological perspective. *New Zealand Geomechanics News 62:* 45 - 69.

Pullar, W. A.; Birrell, K. S. 1973: *Age and distribution of late quaternary pyroclastic and assoiated cover deposits of the Rotorua and Taupo area, North Island, New Zealand.* New Zealand soil Survey Report 1 & 2.

Pusch, R. 1962: Clay particles: their size shape and arrangement in relationship to some important physical properties of clay. *Statens rad for byggforskning 40.*

Rankka, K.; Andersson-Skold, Y.; Hulten, C.; Larsson, R.; Leroux. V.; Dahlin., T. 2004: *Quick clay in Sweden.* Swedish Geotechnical institute, Report 65.

Rao, S. M. 1995: Mechanistic approach to the shear strength behaviour of allophanic soils. *Engineering Geology 40 (3-4):* 215-221.

Robertson, I. D. M.; Eggleton, R. A. 1991: Weathering of granitic muscovite to kaolonite and halloysite and of plagioclase-derived kaolonite to halloysite. *Clays and Clay Minerals 39 (2):* 113 - 126.

Rogers, C. D. F. 1995: Types and distribution of collapsable soils. In Derbyshire, E.; Smalley I. J. (eds.), *Genesis and Properties of collapsable soils.* Kluwer Academic Publishers, Netherlands. 1 - 18.

Rolo, R.; Houghton, B. F.; Vallance, J. W.; Berdousis, P.; Mavrommati, C.; Murphy, W. 2004: Geological and engineering characterization of Tierra Blanca pyroclastic ash deposits. In Rose, W. I.; Bommer, J. J.; Lopez, D. L.; Carr M. J.; Major J. J. (eds.). *Natural Hazards in El Salvador: The Geological Society of America Special Paper 375.* The Geological Society of America Boulder, Colorado. 55 – 68.

Rosenqvist, I. T. 1953: Consideration on the sensitivity of Norwegian quick clays. *Geotechnique 3 (5):* 195 - 200.

Salter, R. T. 1979: *A Pedological Study of the Kauroa Ash formation at Woodstock.* Unpublished MSc Thesis, University of Waikato, Hamilton, New Zealand.

Selby, M. J. 1993: *Hillslope materials and processes.* Oxford University Press, Oxford.

Sergeyev, Y. M., Grabowska-Olszewska, B., Osipov, V., Sokolov, V. & Kolomenski, Y. N. 1980: The classification and microstructure of clay soils. *Journal of Microscopy 120 (3):* 237 - 260.

Sharma, B.; Bora, P. K. 2003: Plastic limit, liquid limit and undrained shear strength of soil - reappraisal. *Journal of Geotechnical and Geoenvironmental Engineering 129 (8):* 774 - 777.

Sharma, B.; Bora, P. K. 2005: Closure to "Plastic limit, liquid limit and undrained shear strength of soil - reappraisal" by Binu Sharma and Padma K. Bora. *Journal of Geotechnical and Geoenvironmental Engineering 131 (3):* 403 - 403.

Shepherd, T. G. 1984: *A pedological study of the Hamilton Ash group at Welches Road, Mangawara, North Hamilton.* Unpublished MSc Thesis, University of Waikato, Hamilton, New Zealand.

Shepherd, T. G. 1994: Paleoclimatic implications of clay minerals and paleosols within strongly weathered Plio-Pleistocene tephras of the Waikato region, central North Island, New Zealand. *Inter-INQUA Field Conference on Tephrochronolgy, Loess, and Paleopedology,* University of Waikato, Hamilton. 52 - 52.

Shepherd, T. G.; Gibbs, H. G. 1984: Mineralogical and chemical composition of the Hamilton Ash in the Waikato Basin. *New Zealand Soil News 32:* 183.

Shrimpton & Lipinski 1998: *Report on landslips Western Bay of Plenty July 1998.* Unpublished report. Held on Tauranga City Council files.

Schulze, D. G. 2002: An introduction to soil mineralogy. In Dixon J. B.; Schulze D. G.; (eds.) *Soil Mineralogy with environmental applications.* Soil Science Society of America, Madison, Wisconsin. 1 - 36.

Singh, B. 1996: Why does halloysite roll? - A new model. *Clays and Clay Minerals 44 (2):* 191 - 196.

Skempton, A. W. 1954: The pore pressure co-efficients A and B. *Geotechnique 4 (4):* 143 - 147.

Skempton, A. W. 1985: Residual strength of clays in landslides, folded strata and laboratory. *Geotechnique 35 (1):* 3 - 18

Skempton, A. W.; Northey., R. D. 1952: The sensitivity of clays. *Geotechnique 3 (1):* 30 - 53.

Smalley, I. J. 1971: Nature of quick clays. *Nature 231:* 310.

Smalley, I. J.; Fordham, C. J.; Callander, P. F. 1984: Discussion: Towards a general model of quick clay development. *Sedimentology 31 (4):* 595 - 598.

Smalley, I. J. R.; Ross. C. W.; Whitton, J. S. 1980: Clays from New Zealand support the inactive particle theory of soil sensitivity. *Nature 288*: 576 - 577.

Soderblom, R. 1966: Chemical aspects of quick-clay formation. *Engineering Geology 1 (6):* 415 - 431.

Soderblom, R. 1975: A new approach to the classification of quick clays. *Swedish Geotechnical Institute Preliminary Report 55:* 1 - 17.

Soma, M.; Churchman, G. J.; Theng, B. K. G. 1992: X-Ray photoelectron spectroscopic analysis of halloysites with different composition and particle morphology. *Clay Minerals 27 (4):* 413 - 421.

Sperazza, M.; Moore, J. N.; Hendrix, M. S. 2004: High-resolution particle size analysis of naturally occuring very fine grained sediment through laser diffractometry. *Journal of Sedimentary Research 74 (5):* 736 - 743.

Tauranga City Council (TCC). 2005: *Vale Street note remediation.* Unpublished report. Contract number 850843/1. Held on the Tauranga city council files.

Tergazhi, K. 1925: *Erdaumechanik auf Bodenphysikalischer Grundlage Deuticke*. Vienna.

Thompson, M. L.; Ukrainczyk, L. 2002: Micas. In Dixon J. B.; Schulze D. G.; (eds.) *Soil mineralogy with environmental applications.* Soil Science Society of America, Madison, Wisconsin. 431 - 467.

Tonkin & Taylor. 1980: *Omokoroa point land stability investigation.* Unpublished report. Report number 4487/2. Held on Tauranga City Council files.

Torrance, J. K. 1983: Towards a general model of quick clay development. *Sedimentology 30 (4):* 547 - 555.

Torrance, J. K. 1992: Discussion on sensitivity to remoulding of some volcanic ash soils in New Zealand, by D. Jacquet. *Engineering Geology 32 (1-2):* 101 - 105.

Torrance, J. K. 1996: On the development of high sensitivity: Minerological requirements and constraints. 7th *International Symposium on Landslides.* A. A. Balkema, Trondhiem. 491 - 496.

Torrance, J. K. 1987: Quick clays. In Anderson, M. G. Richards, K. S. (eds.) *Slope stability*. John Wiley & Sons. 447 - 473.

Torrance, J. K. 1995: Post-depositional processes in high-sensitivity, fine-grained, collapsible sediments. In Derbyshire, E.; Dijkstra, T.; Smalley. I. J. (eds.). *Genesis and properties of collapsible Soils.* Kluwer Academic Publishers 295 - 311.

Torrance, J. K.; Ohtsubo., M. 1995: Ariake Bay quick clays: a comparison with the general model. *Soils and Foundations 35 (1):* 11 - 19.

Vespraskas, M. J. 1994: *Redoximorphic features for identifying aquic conditions.* North Carolina Agricultural Research Service, North Carolina State University, Technical Bulletin 301.

Vickers, B. 1978: *Laboratory work in civil engineering, soil mechanics.* Granada Publishing, London, Great Britian

Wada, K. 1989: Allophane and imogolite. In Dixon J. B.; Weed, S. B. (eds.), *Minerals in soil environments*, Soil Science Society of America Madison, Wisconsin. 1051 – 1087.

Walker, G. P. L. 1979: A volcanic ash generated by explosions where ignimbrite entered the sea. *Nature 281:* 784 - 837.

Ward, T. W. 1967: Volcanic ash beds of the lower Waikato basin, North Island, New Zealand. *New Zealand Journal of Geology & Geophysics 10:* 1109 - 1135.

Wesley, L. 1973: Some basic engineering properties of halloysite and allophane clays in Java, Indonesia. *Geotechnique 23 (4):* 471 - 494

Wesley, L. 1977: Shear strength properties of halloysite and allophane clays in Java, Indonesia. *Geotechnique 27 (2):* 125 - 136.

Wesley, L. 1992: Some residual strength measurements on New Zealand soils. *Sixth Australia New Zealand conference on Geomechanics: geotechnical risk; identification, evaluation, and solutions*. New Zealand Geomechanics Society. 381 - 385.

Wesley, L. 2007: Slope behaviour in Otumoetai, Tauranga. *New Zealand Geomechanics News 74:* 63 - 75.

Wesley, L. D.; Matuschka, T. M. 1988: Geotechnical engineering in volcanic ash soils. *Proceedings of the second international conference on Geomechanic in tropical soils Singapore.* A. A. Balkema, Singapore 333 – 340.

White, N. G.; Dixon, J. B. 2002: Kaolin and serpentine minerals. In Dixon J. B.; Schulze D. G.; (eds.). *Soil mineralogy with environmental applications.* Soil Science Society of America, Madison, Wisconsin. 389 – 414.

Whitton, J. S.; Churchman, G. J. 1987: *Standard methods for mineral anaysis of soil survey samples for characterisation and classification.* New Zealand Soil Bureau Scientific Report 79.

Wilson, C. J. N.; Rhoades, D. A.; Lanphere, M. A.; Calvert, A. T.; Houghton, B. F.; Weaver, S. D.; Cole, J. W. 2007: A multiple-approach radiometric age estimate for the Rotoiti and Earthquake flat eruptions, New Zealand, with implications for the MIS 4/3 boundary. *Quaternary Science Reviews 26:* 1861 - 1870.

Winter, J. D. 2001: *An introduction to igneous and metamorphic petrology*. Prentice Hall, New Jersey.

Yong, R. N.; Sethi, A. J.; Booy, E.; Dascal, O. 1979: Basic characterization and effect of some chemicals on a clay from Outrades 2. *Engineering Geology 14:* 83 - 108.

Appendix 3.1

Soil description flow chart

1. Dominent Grain Size

Coarse Grained - fine, coarse, medium				Fine Grained		Organic Materials
Sand	Gravels	Cobbles	Boulders	Clay - plastic behaviour	Silt - quick dilatent behaviour	Organic Soils

Include subordinate and minor fractions, example; ***sandy fine to coarse GRAVEL with minor silt and clay*** **or** *clayey SILT with trace peat*

Coarse Grained Soils

2. Maximum Particle size - in (mm)

3. Grading - well graded **to** poorly graded, uniformly graded and gap graded.

4. Shape

Rounded	Subrounded	Subangular	Angular
			

5. Colour

1	2	3
light dark	pinkish reddish yellowish brownish greenish bluish greyish	pink red orange yellow brown green blue white grey black

6. Particle strength hardness, example; *easily broken by hand* **or** *can be broken by hammer*

7. Relative density ~ *loosley packed* ; can be removed by hand
~ *tightly packed* ; requires a pick for removal

8. Weathering

Completely weathered	Completely discoloured and altered no sign of original fabric
Highly weathered	Mostly altered and weakened, little traces of original fabric
Moderatly weathered	Large discoloured portions of original soil seperated by more altered material, significantly weakend
Slightly Weathered	Minor discolouration of some parts of the original soil, no loss of strength
Unweathered	Original soil with no discolouration, loss of strength or other affects due to weathering

9. Allophane content (see back)

10. Geological information, example *MT COOK GLACIAL OUTWASH*

Fine Grained Soils

2. Presence of course material - trace if less than 5%, subordinate if between 20 and 50%

3. Colour (see coarse grained soils)

4. Plasticity ~ *highly plastic* one that can be moulded and deformed over a range of moisture
~ *low plasticity* soils will show signs of dilatent or plastic behaviour.

5. Sensitivity (see back)

6. Strength

Descriptive Term	Undrained Shear Strength (kPa)	Diagnostic Features
Very soft	< 12	Easily exudes between fingers when squeezed
Soft	12 – 25	Easily indented by fingers
Firm	25 – 50	Indented by strong finger pressure and can be indented by thumb pressure
Stiff	50 – 100	Cannot be indented by thumb pressure
Very stiff	100 – 200	Can be indented by thumb nail
Hard	200 – 500	Difficult to indent by thumb nail

6. Structure, example; bedded, homogenous, fissured (see back)

7. If bedded, inclination and thickness (see back)

8. Moisture Content

Condition	Description	Granular Soils	Cohesive Soils
Dry	Looks and feels dry	Run freely through hands	Hard, powdery or friable
Moist	Feels cool, darkened in colour	Tend to cohere	Weakened by moisture, but no free water on hands when remoulding
Wet			Weakened by moisture, free water forms on hands when handling
Saturated	Feels cool, darkened in colour and free water is present on the sample		

10. Weathering (see coarse grained soils\)

11. Allophane content (see back)

12. Geological information, example *HAMILTON ASH*

Sensitivity

Descriptive Term	Shear Strength Ratio $\frac{\text{undisturbed}}{\text{remoulded}}$
Insensitive, normal	< 2
Moderately sensitive	2 – 4
Sensitive	4 – 8
Extra sensitive	8 – 16
Quick	> 16

Soil Structure

Term	Description
Homogeneous	The total lack of visible bedding and the same colour and appearance throughout
Bedding	The presence of layers
Fissured	Breaks along definite planes of fracture with little resistance to fracturing
Polished	Fracture planes are polished or glossy
Slickensided	Fracture planes are striated
Blocky	Cohesive soil that can be broken down into small angular lumps which resist further breakdown
Lensoidal	Discontinuous pockets of a soil within a different soil mass

Grain size

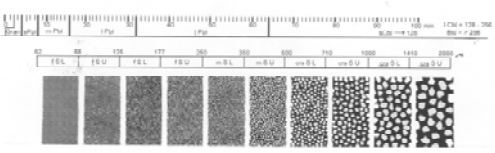

Sorting

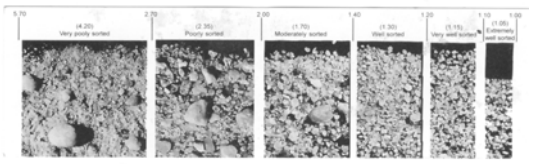

Bedding

Term	Inclination (degrees from
Sub - horizontal	0 - 5
Gently inclined	6 - 15
Moderatly inclined	16 - 30
Steeply inclined	31 - 60
Very steeply inclined	61 - 80
Sub - vertical	81 - 90

Term	Bed Thickness
Very thick	>2m
Thick	600mm - 2m
Moderatly thick	200mm - 600mm
Moderatly thin	60mm - 200mm
thin	20mm - 60mm
very thin	6mm - 20mm
Laminated	2mm - 6mm
thinly laminated	<2mm

Allophane

0	**Non reactive**	No colour change within 2 minutes
1	**Very weak**	Pale red or light red, just decernable within 2 mins
2	**Weak**	Pale red or light red within 1 minute
3	**Moderate**	Red or weak red within 1 minute
4	**Strong**	Dusky red or dark red after 10 seconds
5	**Very strong**	Dusky red or dark red within seconds

Organic soil discriptors

Term	Description
Topsoil	Surficial organic soil layer that may contain living matter. However top-soil may occur at greater depth, having been buried by geological proc-esses or man-made fill, and should then be termed a buried topsoil.
Organic clay, silt or sand	Contains finely divided organic matter; may have distinctive smell; may stain; may oxidise rapidly. Describe as for inorganic soils.
Peat	Consists predominantly of plant remains. Can be further described according to its degree of decomposition and strength. *Firm*: Fibres already compressed together *Spongy*: Very compressible and open structure *Plastic*: Can be moulded in hand and smears in fingers *Fibrous*: Plant remains recognisable and retain some strength *Amorphous*: No recognisable plant remains

Term	Description
Rootlets	Fine, partly decomposed roots, normally found in the upper part of a soil profile or in a redeposited soil (e.g. colluvium or fill).
Carbonaceous	Discrete particles of hardened (carbonised) plant material.

Appendix 3.2

The following presents information on material used for comparison testing. An image of the material sampled and the layout of the grid system used for comparison testing is presented in figure 1. Also presented are the raw undisturbed and remoulded strength values from comparison testing (table 1) and the sensitivity ratio derived from the data in table 1 (table 2).

Location: Tauriko (NZMS U14: 875 863)

Soil Description: Light whitish grey, silty CLAY, with black specs, no coarse material, moist, stiff, slightly plastic, homogenous.

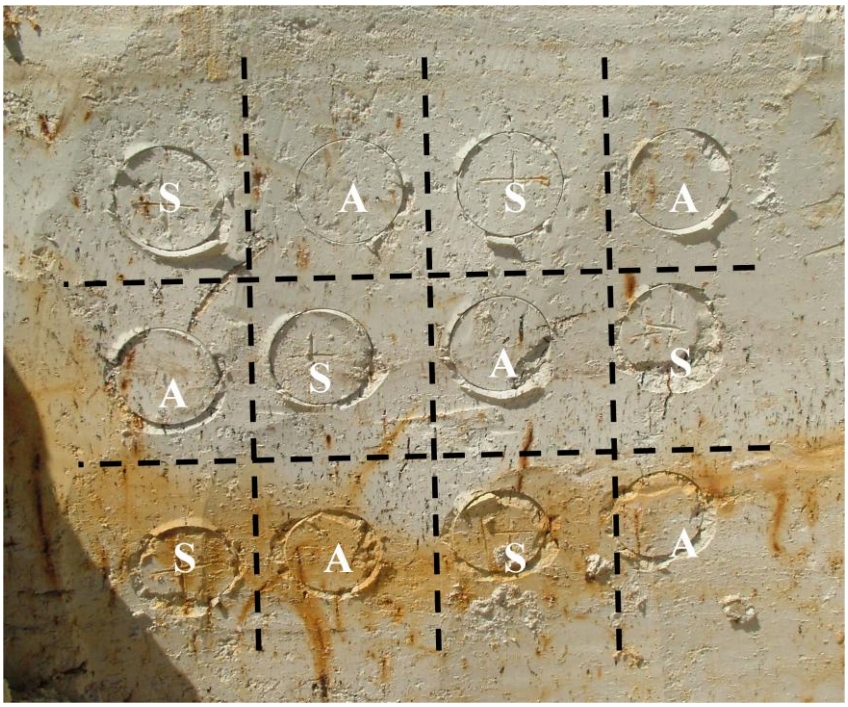

Figure 1: Grid overlaying area sampled for comparison testing using the standard (S) and adapted (A) methods of sensitivity testing.

Table 1: Undisturbed and remoulded shear data (kPa) from comparison testing using the standard (S) and adapted (A) methods of sensitivity testing.

Undisturbed / Remoulded strength (kPa)			
S	**A**	**S**	**A**
122/11	123/19	120/13	104/16
A	**S**	**A**	**S**
146/16	68/6	79/15	83/8
S	**A**	**S**	**A**
128/26	146/18	143/13	120/13

Table 2: Sensitivity values, derived from data in table 1, using the standard (S) and adapted (A) methods of sensitivity testing.

Sensitivity (ratio)			
S	**A**	**S**	**A**
11	7	9	7
A	**S**	**A**	**S**
9	11	5	10
S	**A**	**S**	**A**
5	8	11	9

T-test

The following presents t-test results for comparison peak strengths, remoulded strengths and sensitivity between the standard and adapted methods.

1. **Peak strength**

p = 0.58

Accept the null hypothesis; the two sets of data are from the same population and not significantly different

2. **Remoulded strength**

p = 0.29

Accept the null hypothesis; the two sets of data are from the same population and not significantly different

3. **Sensitivity**

p = 0.094

Accept the null hypothesis at 95 % confidence; the two sets of data are from the same population and not significantly different

T-test results indicate that from the data collected the standard and adapted methods give statistically the same results. Therefore, the adapted method is acceptable as an estimate of sensitivity.

Appendix 3.3

Geomorphic map symbol (from Gardiner & Dackombe 1983)

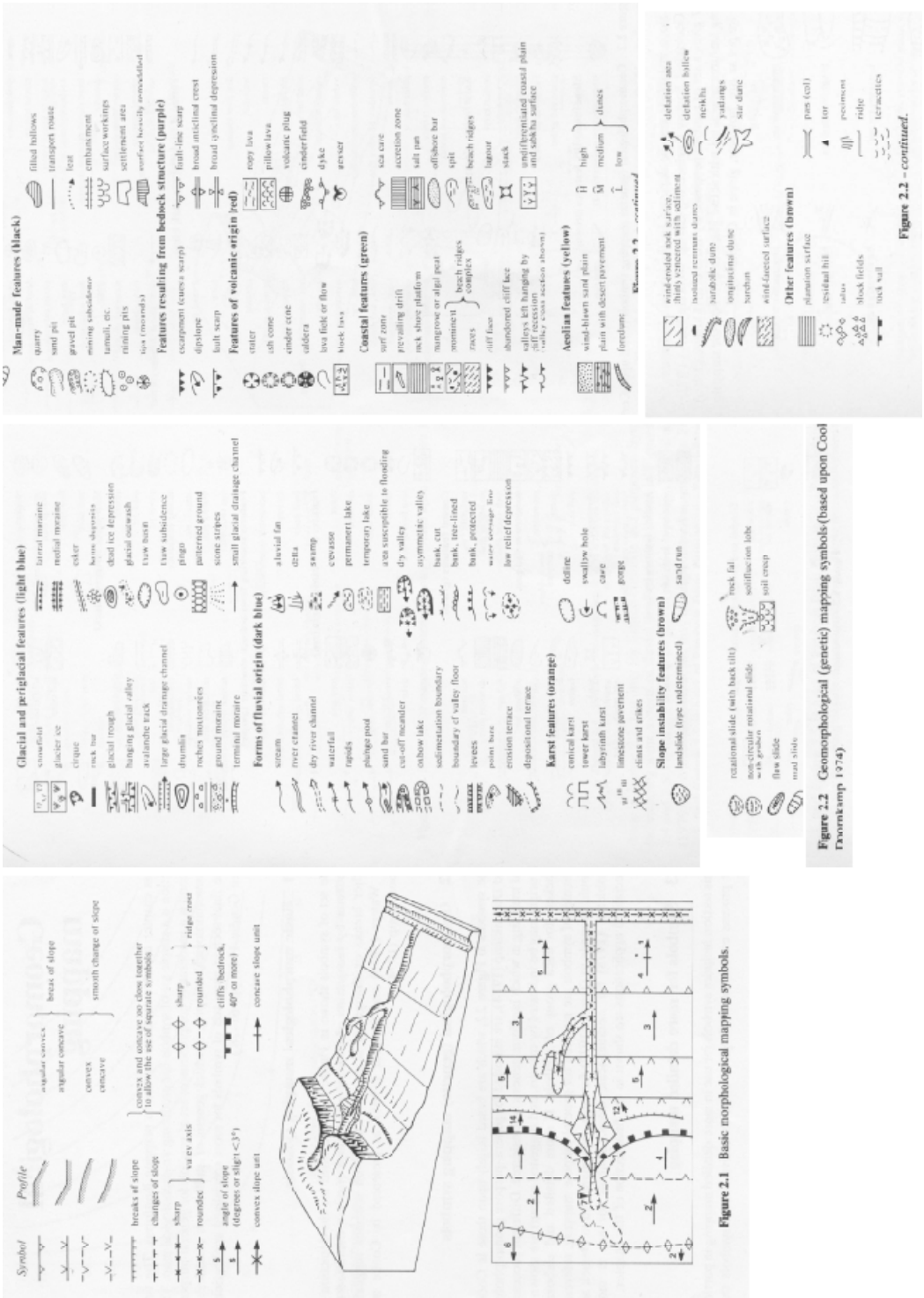

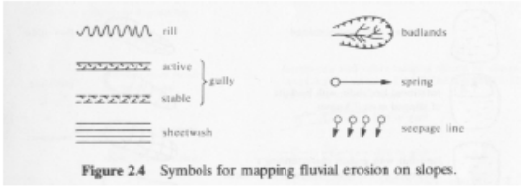

Figure 2.4 Symbols for mapping fluvial erosion on slopes.

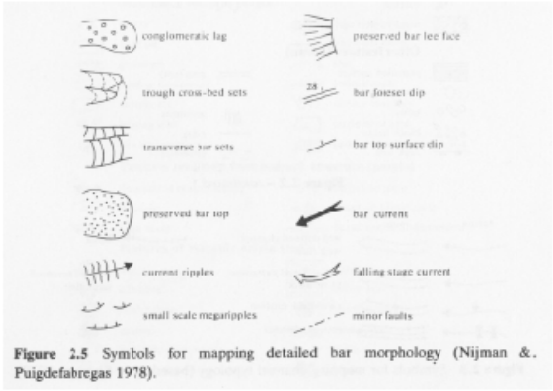

Figure 2.5 Symbols for mapping detailed bar morphology (Nijman &. Puigdefabregas 1978).

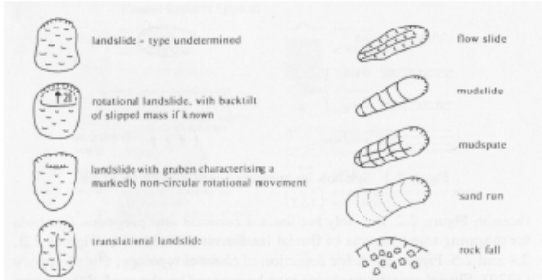

Figure 2.6 Symbols for detailed mapping of slope and mass-movement features and slope instability (Geological Society Engineering Group Working Party 1972).

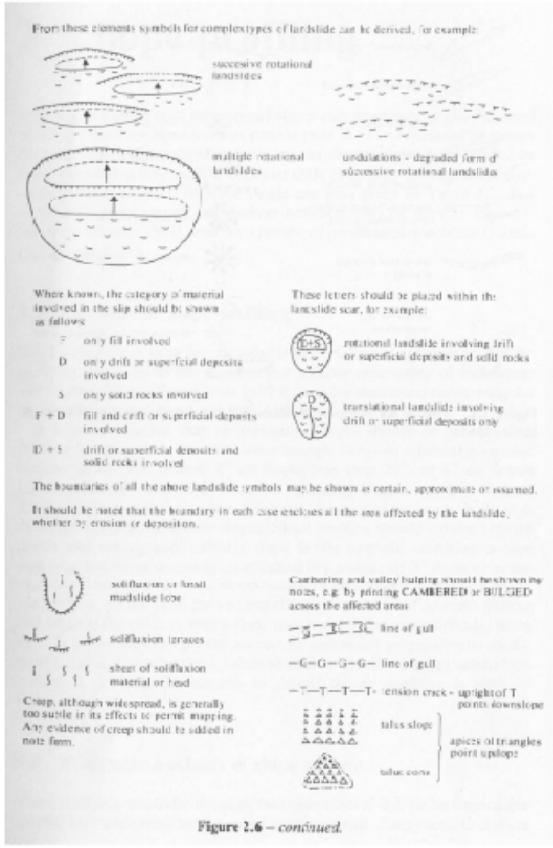

Figure 2.6 – *continued.*

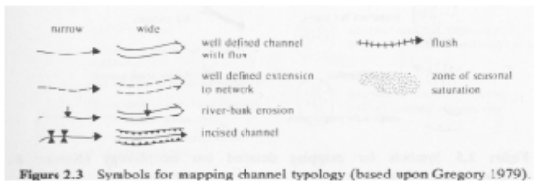

Figure 2.3 Symbols for mapping channel typology (based upon Gregory 1979).

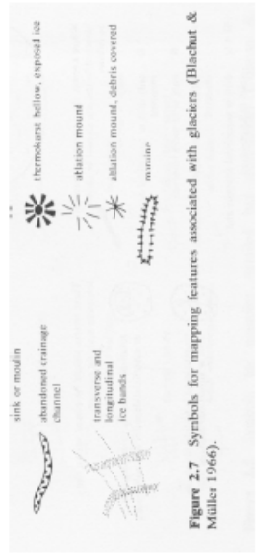

Figure 2.7 Symbols for mapping features associated with glaciers (Blachut & Müller 1966).

Appendix 3.4

The following presents a basic outline of the methods employed during sample collection. After retrieval all samples were stored in the laboratory in a large dark sealed drum until analysis.

Loose bulk sample – particle size, moisture, Atterburg limits, particle density, mineralogy and ring shear.

Material required for loose bulk samples was dug out from the unit under investigation, with either a spade or trowel, and placed in doubled plastic bags. In the laboratory these samples were stored in a large dark sealed drum until tested. Samples for moisture were tested as soon as possible.

Block bulk sample – scanning electron microscopy.

Scanning electron microscopy required intact samples to be collected. Typically a block of ~ 200 mm by ~ 200 mm was dug out ensure minimal disturbance and wrapped in doubled plastic bags.

Bulk density

Samples were typically collected in rings 70 mm high and 100 mm wide from the unit to be investigated. Unfortunately a hammer and dolly were not available for sample collection, as required by NZS4402 (1986). The bulk density rings were carefully inserted into the ground using a rubber mallet and wooden block. However care was taken to ensure that penetration was always perpendicular to the ground surface as the sampling ring was being inserted. Once all rings were inserted they were carefully dug out, and wrapped with plastic wrap. Typically 5 bulk density samples were taken from each unit and bulk density samples were tested as soon as possible on returning to the laboratory.

Shear box

Shear box samples were collected in steel rings 60 mm in diameter by 30 mm high. Samples were gently pushed into the unit under investigation and then dug out once all rings had been inserted into the ground. Samples were sealed in plastic film and then placed between two boards, wrapped with tap and then sealed in a plastic bag.

Triaxial samples

Samples were collected by slowly pushing 300 mm long by 50 mm wide lightly oiled sample tubes into the area to be investigated. Care was taken to ensure that the unit to be investigated was a least 300mm thick, to ensure that only the material in question was collected. The oiling of the tube was an attempt to reduce the resistance between the sampling tubes and the soil. Care was taken to ensure that the tubes were always perpendicular with the ground surface as they were being pushed in. If the surface of sample material within the tube was more than a few mm below the surrounding ground surface the sample was discarded and collected again. Once all tubes had been pushed into the unit under investigation they were carefully removed.

After digging out, samples were sealed in plastic film and placed in plastic bags to prevent moisture loss. Samples were wrapped in towels to provide protection during transportation. In the laboratory samples were stored in a large dark sealed drum until testing. Prior to testing samples were removed from the core using a hydraulic extruder. As the material was extruded it was collected in an appropriate sized split mould. Material located at either ends of the core was cut away and discarded, as it was thought this may have been compacted during sample collection and extraction. Thus samples were taken from a more central location in the core. Once extracted the sample was trimmed to 100 mm giving a height to diameter ratio of 2.

Appendix 3.5

The following appendix presents the preparation methods for particle size analysis which are based on an in house method at the University of Waikato.

1. A representative sub sample was air dried for at least overnight.

2. Once air dry the sample was passed through a 2mm sieve and a ≈ 5 gram sub sample was taken.

3. 10mls of hydrogen peroxide was added, to dissolve organic matter, and the sample was left overnight. The Grange Road samples were left longer and more hydrogen peroxide was added. More hydrogen peroxide was needed because not all organic matter was dissolved during the first treatment; this process was repeated for at least a week until the reaction subsided.

4. Over gentle heat a further 5mls of hydrogen peroxide was added, distilled water was used to wash any soil adhering to the sides of the beaker.

5. To **remove/dilute** the hydrogen peroxide the sample was reduced to a 5ml slurry and left to cool.

6. 10ml of Calgon was added to disperse clay particles; the sample was then left overnight.

7. Dispersion was assisted by placing the sample in an ultrasonic bath for 5 minutes prior to testing.

8. The samples were then tested in the Malvern lazer particle sizer.

Appendix 3.6

This appendix presents graphs of the median particle size of each sample across a range of obscuration values for each sample from Tauriko and Otumoetai.

These graphs helped determine the obscuration level to test each sample at during particle size analysis.

MASTERSIZER 2000

Trend Report

Sample Name:
OS1 - LORUN 1.52/0.01

Sample Source & type:

Sample bulk lot ref:

SOP Name:

Measured by:
jbw9

Result Source:
Edited

Measured:
Wednesday, 22 October 2008 12:26:18 p.m.

Analysed:
Sunday, 11 January 2009 12:48:51 p.m.

Particle Name:
soil 2

Particle RI:
1.520

Dispersant Name:
Water

Accessory Name:
None

Absorption:
0.01

Dispersant RI:
1.330

Analysis model:
General purpose

Size range:
0.020 to 2000.000 um

Sensitivity:
Normal

Result Emulation:
Off

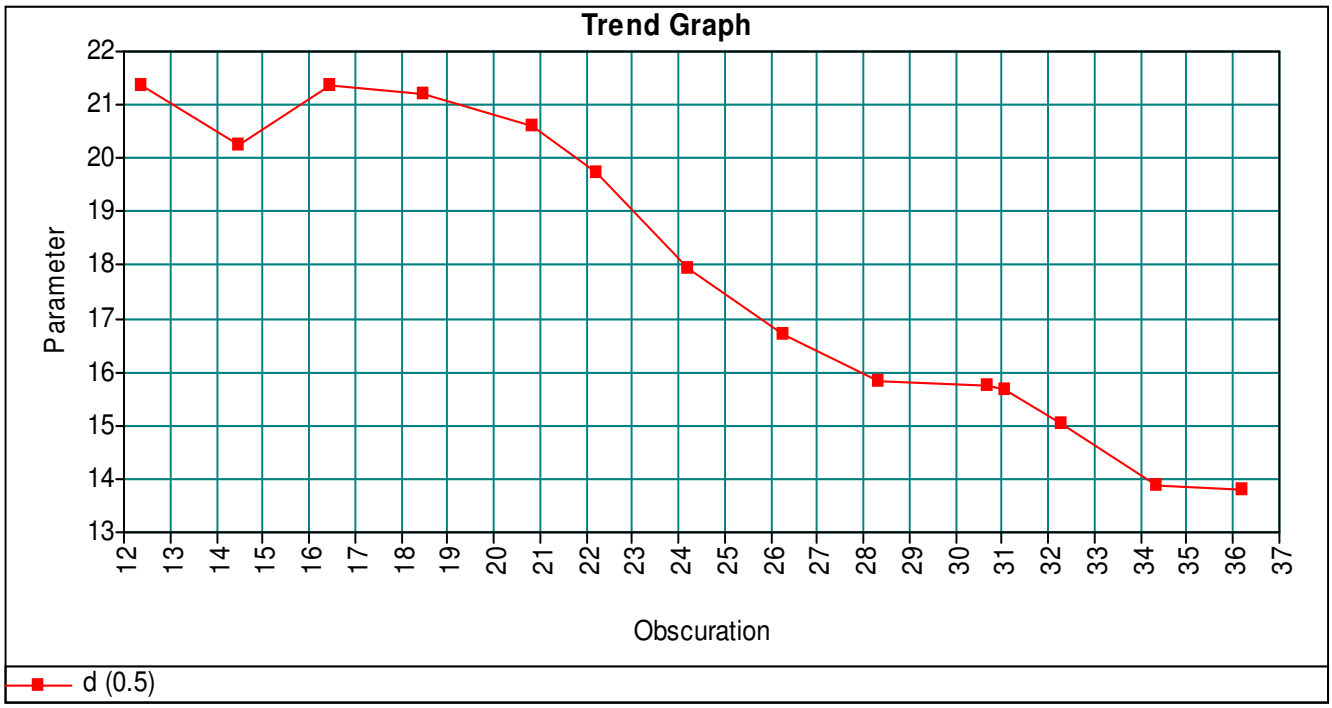

Operator notes:

MASTERSIZER 2000

Trend Report

Sample Name:
OS2 _ LO1.54/0.01

Sample Source & type:

Sample bulk lot ref:

SOP Name:

Measured by:
jbw9

Result Source:
Edited

Measured:
Sunday, 26 October 2008 12:42:23 p.m.

Analysed:
Sunday, 11 January 2009 12:50:25 p.m.

Particle Name:
Soil

Particle RI:
1.540

Dispersant Name:
Water

Accessory Name:
None

Absorption:
0.01

Dispersant RI:
1.330

Analysis model:
General purpose

Size range:
0.020 to 2000.000 um

Sensitivity:
Normal

Result Emulation:
Off

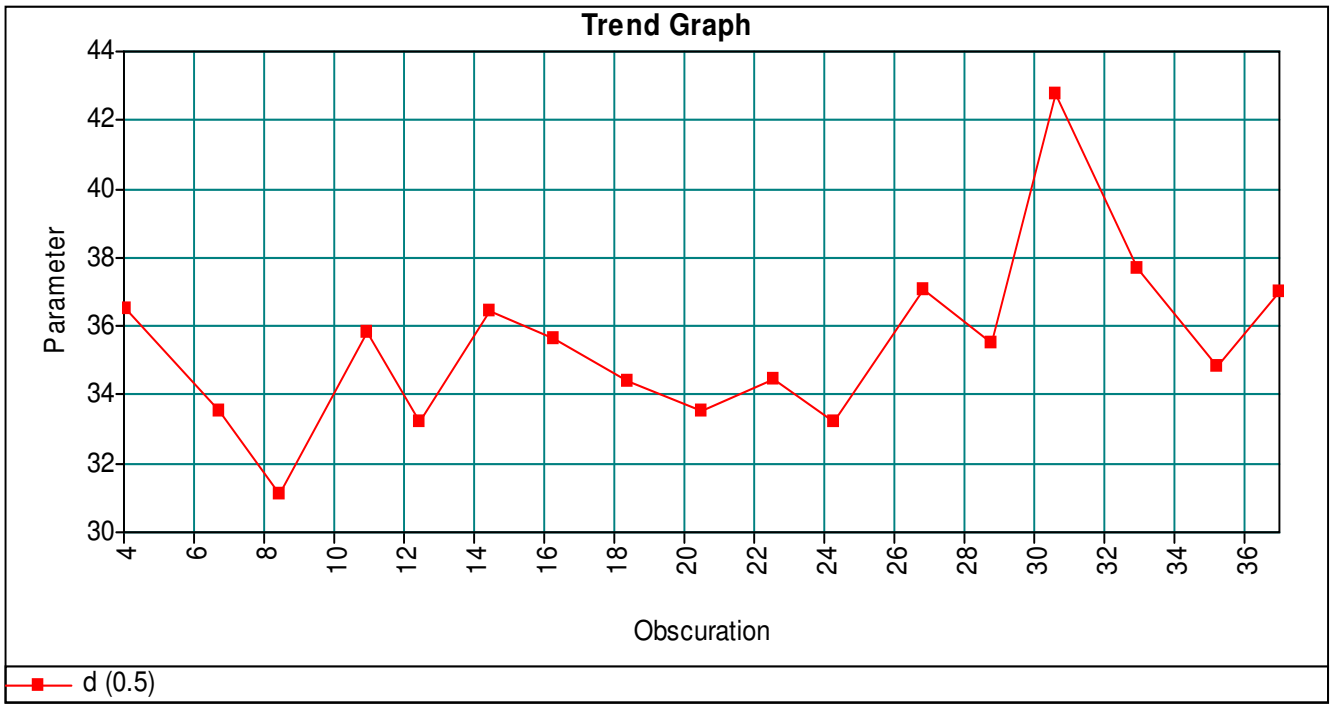

Operator notes:

MASTERSIZER 2000

Trend Report

Sample Name:
OS3 - 1.56/0.01

SOP Name:

Measured:
Sunday, 26 October 2008 2:46:29 p.m.

Sample Source & type:

Measured by:
jbw9

Analysed:
Sunday, 11 January 2009 12:52:34 p.m.

Sample bulk lot ref:

Result Source:
Edited

Particle Name:
soil 2

Accessory Name:
None

Analysis model:
General purpose

Sensitivity:
Normal

Particle RI:
1.560

Absorption:
0.01

Size range:
0.020 to 2000.000 um

Result Emulation:
Off

Dispersant Name:
Water

Dispersant RI:
1.330

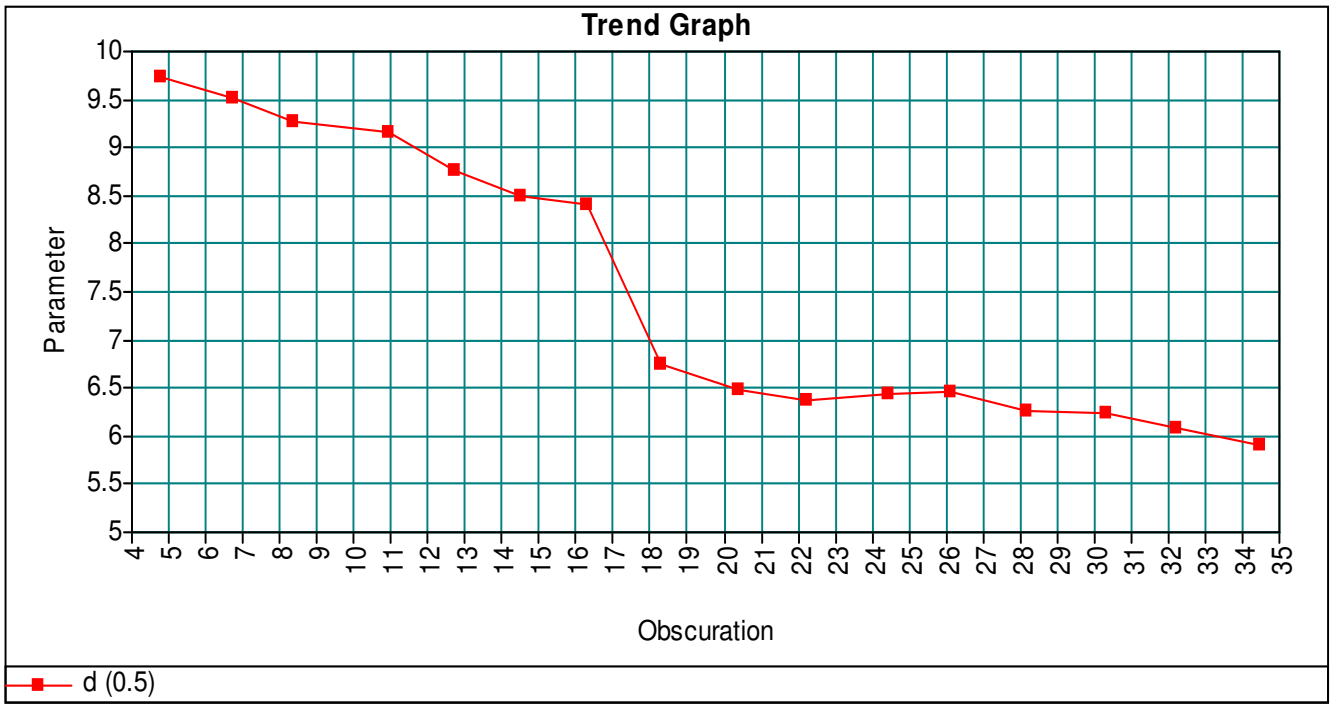

Operator notes:

Trend Report

Sample Name:
OS4-2B 1.55/0.01

Sample Source & type:

Sample bulk lot ref:

SOP Name:

Measured by:
jbw9

Result Source:
Edited

Measured:
Sunday, 26 October 2008 3:57:55 p.m.

Analysed:
Sunday, 11 January 2009 2:06:41 p.m.

Particle Name:
soil 2

Particle RI:
1.550

Dispersant Name:
Water

Accessory Name:
None

Absorption:
0.01

Dispersant RI:
1.330

Analysis model:
General purpose

Size range:
0.020 to 2000.000 um

Sensitivity:
Normal

Result Emulation:
Off

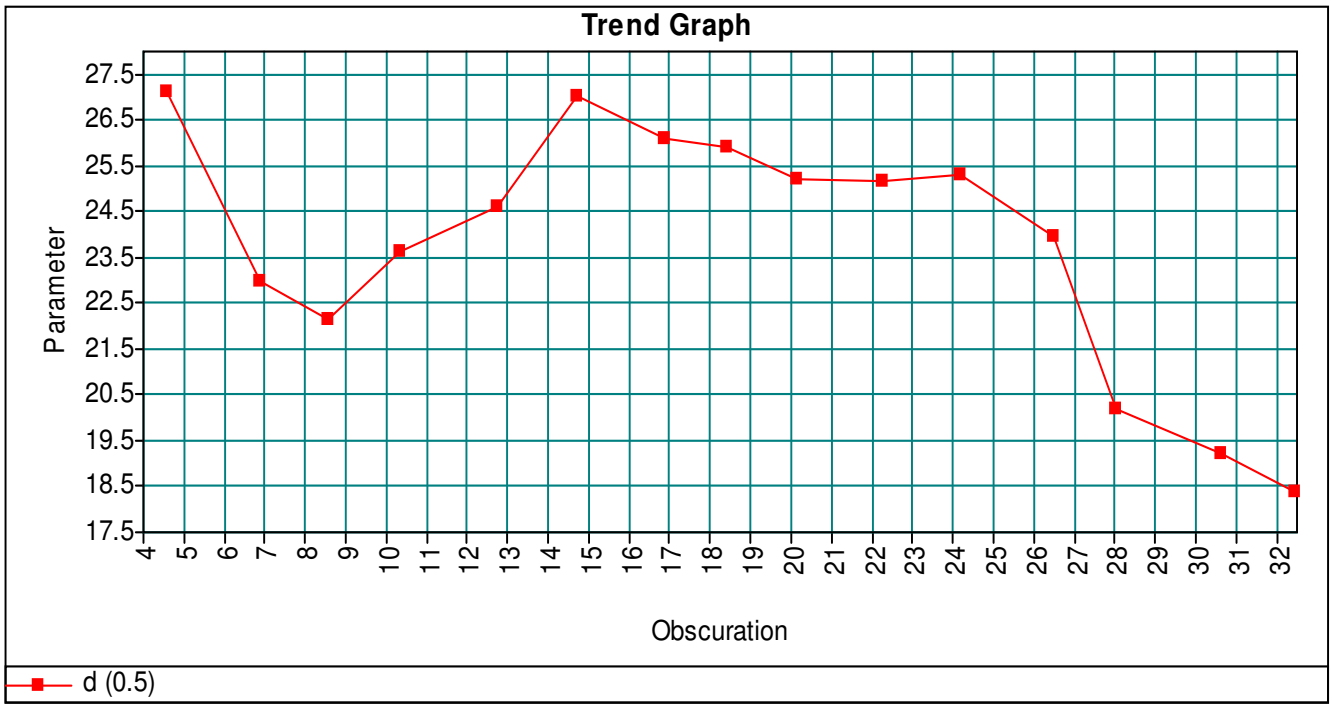

Operator notes:

MASTERSIZER 2000

Trend Report

Sample Name:
TS1 - manual measure 1.54/0.01

Sample Source & type:

Sample bulk lot ref:

SOP Name:

Measured by:
jbw9

Result Source:
Edited

Measured:
Friday, 17 October 2008 11:44:07 a.m.

Analysed:
Sunday, 11 January 2009 1:23:54 p.m.

Particle Name:
soil 2

Particle RI:
1.540

Dispersant Name:
Water

Accessory Name:
None

Absorption:
0.01

Dispersant RI:
1.330

Analysis model:
General purpose

Size range:
0.020 to 2000.000 um

Sensitivity:
Normal

Result Emulation:
Off

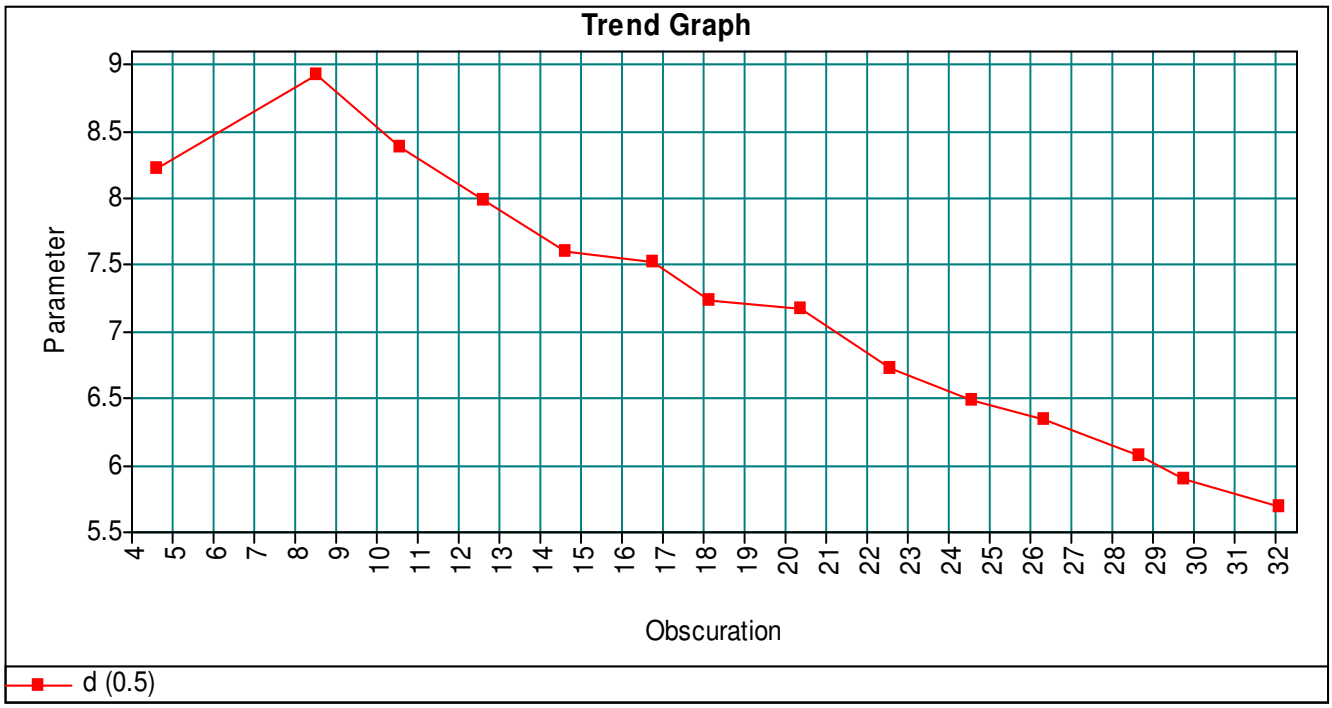

Operator notes:

MASTERSIZER 2000

Trend Report

Sample Name:
TS1 - 1.57/0.01

SOP Name:

Measured:
Friday, 17 October 2008 4:37:27 p.m.

Sample Source & type:

Measured by:
jbw9

Analysed:
Sunday, 11 January 2009 1:26:22 p.m.

Sample bulk lot ref:

Result Source:
Edited

Particle Name:
soil 2

Accessory Name:
None

Analysis model:
General purpose

Sensitivity:
Normal

Particle RI:
1.570

Absorption:
0.01

Size range:
0.020 to 2000.000 um

Result Emulation:
Off

Dispersant Name:
Water

Dispersant RI:
1.330

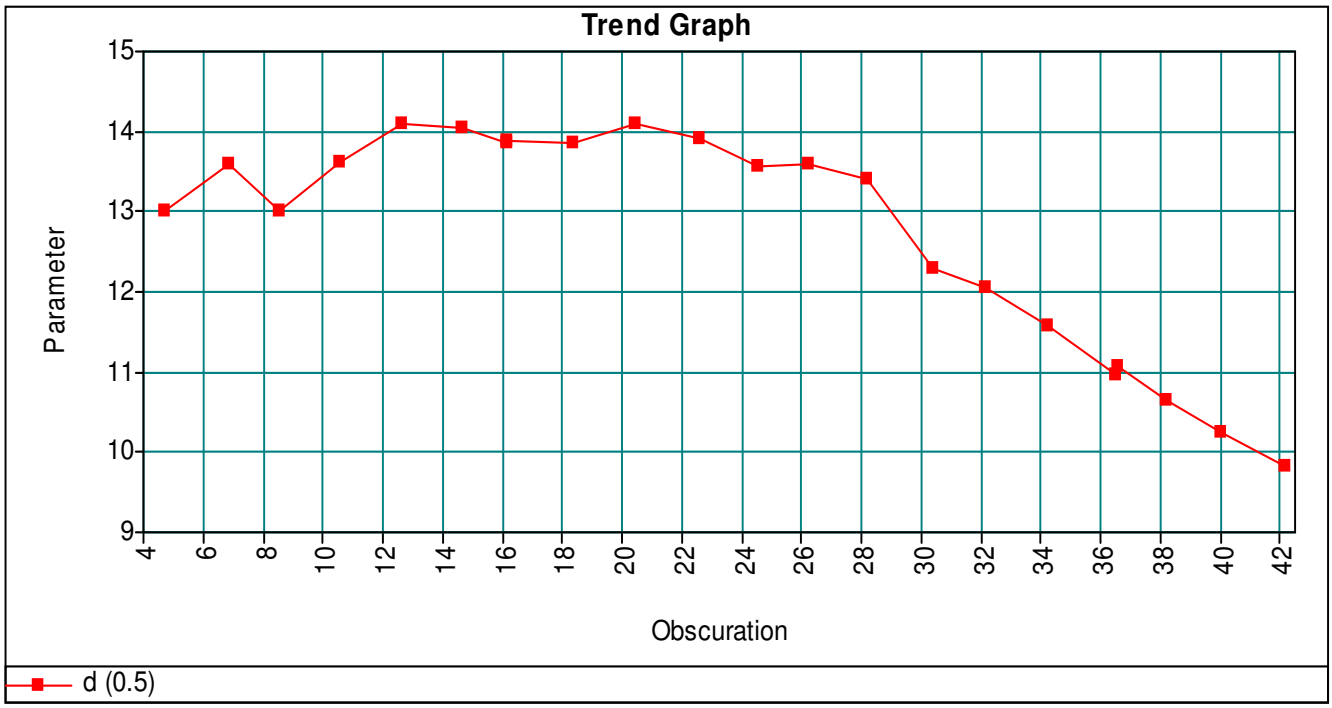

Operator notes:

MASTERSIZER 2000

Trend Report

Sample Name:
TS3 1.52/0.01

SOP Name:

Measured:
Friday, 17 October 2008 8:13:03 p.m.

Sample Source & type:

Measured by:
jbw9

Analysed:
Thursday, 11 December 2008 7:07:49 p.m.

Sample bulk lot ref:

Result Source:
Edited

Particle Name:
soil 2

Accessory Name:
None

Analysis model:
General purpose

Sensitivity:
Normal

Particle RI:
1.520

Absorption:
0.01

Size range:
0.020 to 2000.000 um

Result Emulation:
Off

Dispersant Name:
Water

Dispersant RI:
1.330

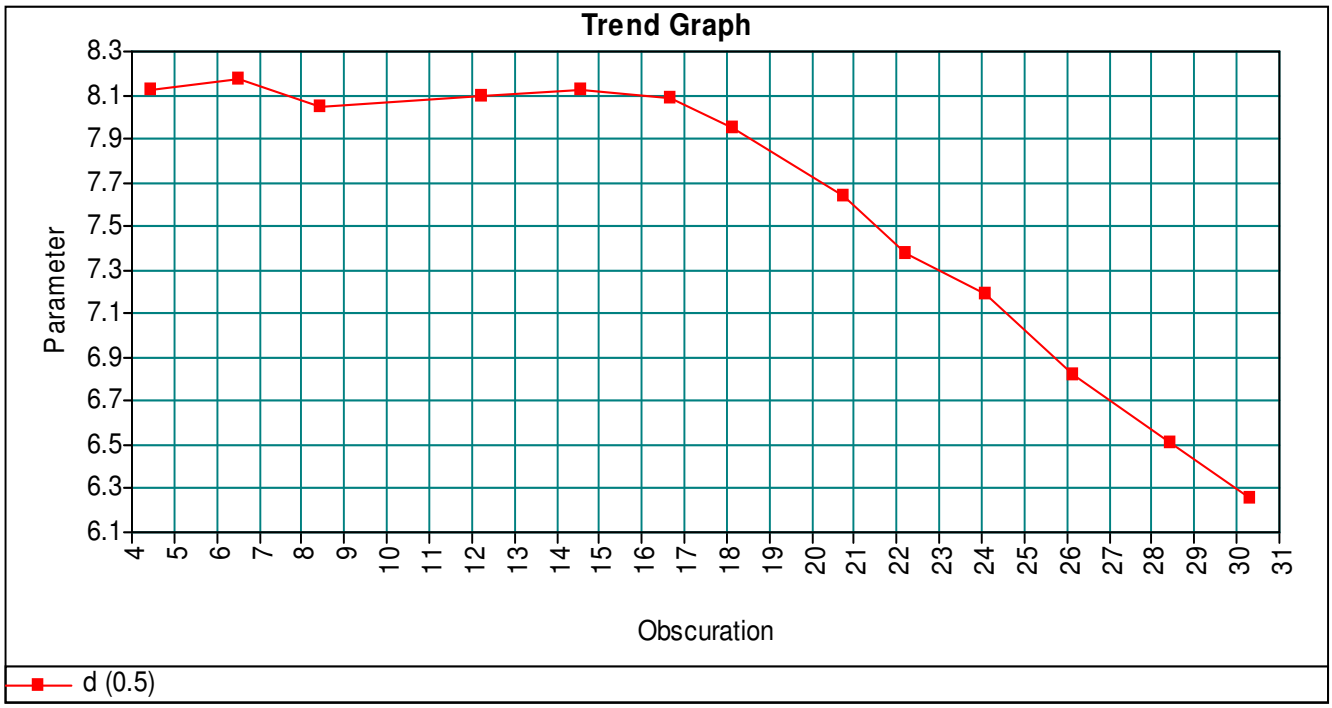

Operator notes:

Appendices 3.7

Normal force above each sample was calculated using the following equation:

$$\sigma_n = \gamma z \qquad (1)$$

Where:
σ_n = normal stress (kPa);
γ = unit weight of soil at field moisture (kPa);
z = depth to shear plane (m).

Because the triaxial is capable of applying pressure in terms of kPa the calculated value can be applied directly however for the shear box and ring shear these values need to be converted to a weight in terms of kg.

The shear box equation is as follows:

$$mass = \frac{\sigma_n A}{g}\ x\ 1000 \qquad (2)$$

Where:
Mass = weight which equals the calculated over burden (kg);
A = Area of the sample (m) in the case of the shear box it is 2.827 x 10^{-3} m^2;
g = gravity (m s^{-2}).

The equation used for the ring shear is similar to the shearbox. But because the ring shear has a 10:1 lever arm system the mass calculated in equation (2) should have the mass of the lever arm subtracted (1.143 kg) and then be divided by 10. Furthermore the area (A) of the ring shear sample is 40.07 x 10^{-4} m^2.

Appendix 4.1

The following appendix presents all soil logs compiled during the course of this study, these soil logs have been divided into three folders.

The folder labelled ‘Tauriko and Otumoetai logs’ contains the soil log sheets used to compile figures 4.4 and 4.5.

The folder titled ‘soil logs associated with geomorphic maps’ represents soil logs obtained from the slips presented as slip 1, slip 2 and main slip in appendices 4.2a and b.

The folder called ‘other general soil logs’ represents other soil logs compiled during the course of this study. One large log of note is called ‘Pyes Pa_log’.

Field Log Sheet

Location: Tauriko - Industrial area

Date 6 (day) 02 (month) 08 (year)

GPS: NZMS 260 U14 875 863

Notes: First page of Tauriko log.

Legend:
PR - Penetrometer (kg)
PVS - Peak vane shear strength (kPa)
P - Peak vane shear strength (kPa)
R - Remoulded vane shear strength (kPa)
S - Sensitivity (ratio = P/R)

Strat unit.	Depth (m)	Graphic Log	Description	PR	PVS	Sensitivity Standard P	Standard R	Standard S	Adapted P	Adapted R	Adapted S
Post Rotoehu Ash			Disturbed by earth works								
	1		Clayey SILT, trace fine sand, light brown with MnO flecks, firm, moist, moderately weathered.	6.5	91						
			Silty SAND, light brown coarse to fine pumecious sand, densely packed, moist, non bedded.	5.5	115						
Rotoehu Ash			SILT, light yellowish brown, very stiff, moist, non plastic, moderately weathered.	>10	>227						
	2		SAND, light yellow, densly packed, moist, well graded, pumecious	1	31						
Hamilton Ash formation			SILT, light pinkish brown, moist, moderately weathered.								
			CLAY, dark brown with MnO, firm, highly plastic, homogemous, highly weathered. - palesol	7	141						
			Silty CLAY, light orange brown with MnO flecks, very stiff, moist, highly plastic.	9	123						
	3		S andy SILT, trace clay, dark orange brown with MnO flecks, very stiff, moist, slighlty plastic, extra sensitive - quick, moderately weathered.	>10	>227						
				>10	UTP						
				>10	191	191	19	10	224	16	14
	4			>10	77	77	6	13			
				9.5	133	133	6	22	94	8	12
				7.5	87	87	8	11			
Undifferentiated material	5		Sandy SILT, dark brownish orange some MnO flecks, firm, dry, non plastic, extra senstive to - quick, moderately weathered.	6	65	65	5	13	65	6	11
				6	84	84	5	17			
				8	131	131	8	16	99	6	17
	6		Sandy SILT, trace clay, dark brownish orange with few MnO flecks, firm, dry - moist, extra sensitive - quick, moderately weathered.	8	76	76	8	9			
				8.5	81	81	5	16	76	6	13
				6	49	49	6	8			
	7		Clayey SILT, trace sand, dark brownish orange, firm, dry - moist, slightly plastic, extra sensitive - quick, moderately weathered.	7.5	71	71	6	12	71	6	12
				6.5	81	81	5	16			
			Clayey SILT, dark brownish orange with black MnO flecks, soft, moist, slightly plastic, extra sensitive, moderately weathered.	6	78	78	6	13	81	6	14
			Clayey SILT, with trace fine - medium sand, dark brown, few black MnO flecks, stiff, dry - moist, non plastic, sensitive - extra senstive.	>10	164	164	31	5			
	8			>10	160	160	11	15	128	13	10
				9	154	154	18	9			
				8	113	113	10	11	149	18	8
	9			8	147	147	15	10	151	16	9
				9.5	147	147	16	9			
				9.5	143	143	13	11			
				8	136	115	10	12	130	10	13
	10			7.5	115	115	10	12	130	10	13

Field Log Sheet

Location: Tauriko - Industrial area (2)

Date 6 (day) 02 (month) 08 (year)

GPS: NZMS 260 U14 875 863

Notes: Tauriko page 2 of log.

Legend:
PR - Penetrometer (kg)
PVS - Peak vane shear strength (kPa)
P - Peak vane shear strength (kPa)
R - Remoulded vane shear strength (kPa)
S - Sensitivity (ratio = P/R)

Strat unit.	Depth (m)	Graphic Log	Description	PR	PVS	Sensitivity Standard P	Standard R	Standard S	Adapted P	Adapted R	Adapted S
Undifferentiated material	11				117	117	8	15			
					97	97	13	7			
					115	115	6	19			
					128	128	10	13			
					117	117	8	15			
	12		Sandy SILT. dark brown with MnO flecks, stiff, moist, non plastic, extra sensitive, moderately weathered.		81	81	6	14	97	21	5
					94	94	10	9			
					125	125	10	13			
					99	99	11	9	110	28	4
	13				104	104	10	10			
					96	96	8	12			
					84	84	6	14			
	14				96	96	8	12			
			Clayey SILT, dark brown with MnO flecks, stiff, moist, slightly plastic, quick, slightly weathered.		86	86	3	29			
					86	86	6	14			
	15			>10	217	217	18	12			
				>10	191	191	15	13	191	18	11
				>10	>227				>227	32	>7
			Clayey SILT, trace sand, dark orange brown with MnO flecks, very stiff, dry, slightly plastic, sensitive, moderately weathered.	>10	>227						
	16			>10	>227						
				>10	>227	>227	42	<5			
				>10	>227	>227	47	<5			
	17		Silty CLAY, trace fine sand, dark brown orange with manganese flecks, stiff, moist, moderaetly plastic, sensitive - extra sensitive, moderately weathered.	>10	201	201	21	10	201	16-49 difficult to remould	4 - 13
				>10	194	194	29	7			
			Silty CLAY, dark orange brown, stiff, moist, moderatly plastic, sensitve - extra sensitive, moderately weathered.	>10	159	160	19	8	159	19	8
	18			10	165	165	15	11			
			Silty CLAY, light yellowish brown with MnO flecks, firm, moist, mod. plastic, sensitive, highly weathered.	10	100	100	15	7	87	8	11
			Silty CLAY, light brown, firm, moist, moderately plastic sensitive to extra sensitive.	>10	188	188	23	8			
				>10	177	177	15	12	186	39	5
	19		Silty CLAY, includes trace small to medium gravels (white grey and purple), light brown with MnO flecks, stiff, moist, moderately plastic, extra sensitive.	>10	160	160	16	10			
Te Ranga lg.			Silty SAND, subrodinate fine to medium gravel, fine to coarse grained sand, light yellowish brown, densly packed, moist, poorly sorted, sand so shear vane irrelevant, a number of thin black layers at base (manganese).	6.5	104	104	5	20			
				7.5	112	112	6	19			
	20		see over								

Field Log Sheet

Location: Tauriko - Industrial area (3)

Date 6 (day) 02 (month) 08 (year)

GPS: NZMS 260 U14 875 863

Notes: Tauriko page 3 of log.

Legend:
PR - Penetrometer (kg)
PVS - Peak vane shear strength (kPa)
P - Peak vane shear strength (kPa)
R - Remoulded vane shear strength (kPa)
S - Sensitivity (ratio = P/R)

Strat unit.	Depth (m)	Graphic Log	Description	PR	PVS	Sensitivity					
						Standard			Adapted		
						P	R	S	P	R	S
Te Ranga Ig.			Silty SAND,fine to coarse sand, light yellowish brown with MnO flecks, dense, moist to wet, non plastic, well sorted poorly graded, sand so shear vane irrelevant	8.5	115	115	6	19			
					100	100	8	13	100	3	33
	21		SAND, fine to coarse grained, trace small pumecious gravels, trace SILT, light pinkish grey, loosely packed, poorly graded, slightly weathered, large piece of charcol at base approxiamatly 0.3 m long sorrounded by a pink halo.	5							
Tephra fall deposits/ Matua subgroup			Clayey SILT, trace fine sand, light pink few MnO flecks, wet, soft, non plastic, quick, dilatent with out the addition of water, sticky.		34	34	2	17	34	1	34
	22		Clayey SILT, light brownish yellow overlain by orange band, firm, wet, non plastic								
			SILT, trace fine sand, light pinkish grey becoming yellow with depth with few MnO flecks, firm, wet, non plastic, moderately sensitive, dilatent without ad. water		98	98	26	4	98	2	49
					152	152	47	3	152	3	51
	23		SILT, light pink with few MnO flecks, stiff, wet, non plastic, sensitive, dilatent without the ad of water.		160	160	26	6	160	1	160
Matua subgroup			SAND, fine to coarse sub angular grains, light grey, dense, moist, moderaltly sorted, poorly graded.	8							
	24		SAND, light grey, loose, sub horizontal very thin bedding, corse and fine grained beds, coarse sand sub angular to sub rounded.								
			SAND, medium to corse grains, loose, massive, poorly sorted, coarse grains sub angular to sub rounded.								
			SAND, medium to coarse grain, trace fine gravels, light grey, massive, loosely packed.								
			SILT, light pink with few MnO flecks, non plastic, stiff.								
	25		SAND, fine to medium grained, light grey, dense, sub horizontal laminated bedding, moist, medium sands sub rounded and pumecious.								
			End of log at 24. 4 metres.								
	26										
	27										
	28										
	29										
	30										

Field Log Sheet

Location: Otumoetai - Grange Road (1)

Date 19 (day) 5 (month) 08 (year)

GPS: NZMS 260 U14 875 863

Notes: Page 1 of Otumoetai field log. Logging was undertaken in a slip on the lower section of a relict coastal cliff at 198 Grange Road.

Legend:
PR - Penetrometer (kg)
PVS - Peak vane shear strength (kPa)
P - Peak vane shear strength (kPa)
R - Remoulded vane shear strength (kPa)
S - Sensitivity (ratio = P/R)

Strat unit.	Depth (m)	Graphic Log	Description	PR	PVS	Sensitivity					
						Standard			Adapted		
						P	R	S	P	R	S
			Covered by grass and topsoil								
	8		S ilty CLAY, dark orangish brown with Mn flecks, no coarse material, soft - firm, moist, moderately plastic, sensitive, moderately weathered.		65	65	11	6	65	24	3
			CLAY, light greysih brown, homogoneous, stiff - very stiff, moist, highly plastic, sensitive, highly weathered.		110	110	18	6	110	47	2
Rangitawa teprha			Sandy SILT, light yellowish orange with many white and black flecks, also incl. golden coloured mica flakes, fine to coarse sand, stiff, moist, non plastic, extra sensitive, sand well to very well sorted, moderately weathered.		81	81	6	14			
	9				105	105	10	11	97	10	10
					149	149	10	15			
			CLAY, light brown with few Mn flecks, stiff, moist to wet, moderatly plastic, moderatly weathered, large gravel sized manganese.		109	109	11	10	109	18	6
	10		CLAY, dark brown, firm, moist, highly plastic, moderately weathered .		96	96	13	7	76	13	6
			CLAY, dark orange brown with Mn flecks, very stiff, moist, moderately plastic, sensitive, highly weathered. - paleosol	>10	164	164	29				
				>10	107	107	26	4	107	26	4
	11		Silty CLAY, dark greyish brown with manganese flecks, firm, moist, mod. plastic, sensitive, mod weathered.	>10	157	157	31	5	175	23	8
			Silty CLAY, light yellowish brown with Mn flecks, stiff, moist to wet, moderatly plastic, sensitive, highly weathered.	7.5	144	144	23	6	143	6	24
					105	105	10	11	96	5	19
	12		Silty CLAY, light yellowish brown with Mn flecks, some golden mica flakes, firm, moist to wet, slightly plastic, extra sensitive, moderately weathered, greasy, some roots.	5.5	112	112	11	10	120	13	9
				6.5	99	99	8	12	83	10	8
				7.5	97	97	15	6	130	18	7
			Clayey SILT, light yellowish orange, with Mn flecks, some golden mica flakes, firm, moist to wet, slightly plastic, extra sensitive, moderately weathered.	6.5	96	96	10	10	104	13	8
	13			8	123	123	16	8	117	19	6
			Clayey SILT, light orangish brown with Mn flecks, some golden mica flakes, firm - stiff, wet, slightly plastic, extra sensitive, looses volume on remoulding, moderately weathered.		144	144	13	11	117	10	12
					99	99	13	8	73	2	37
			CLAY, light pinkish brown, very stiff, highly plastic, includes large sheets of Mn.		144	144	19	8	146	13	11
	14		CLAY, dark brown, with Mn flecks, very stiff, moist, very plastic sensitive to extra senstive, homogenous, highly weathered - paelosol		214	214	32	8	110	23	5
				>10	UTP						
				>10	>227						
	15		as above but becomes light brown	>10	177	117	10	12	149	36	4
			CLAY, light yellowish brown with black Mn flecks, very stiff, moist, moderately plastic, highly weathered.	>10	>227						
	16		Clayey SILT, light yellowish brown with Mn flecks, some golden mica flakes, stiff, wet, slightly plastic, quick, dilatent without the addition of water,looses volume on remoulding.	9.5	107	107	5	21	87	3	29
				8.5	227	227	76	3	191	68	3
			CLAY, light orange brown with Mn flecks, stiff, moist, highly plastic, moderately sensitive. - paleosol?	6	84	84	16	5	65	16	4
	17		CLAY, light orange brown with Mn flecks, firm, wet, highly plastic, sensitivity, highly weathered.	5	75	75	13	6	71	16	4
			becomes most	5	126	126	29	4	118	28	4
					123	123	29	4	139	26	5

Field Log Sheet

Location: Otumoetai - Grange Road (2)

Date 19 (day) 5 (month) 08 (year)

GPS: NZMS 260 U14 875 863

Notes: Page 2 of Otumoetai field log.

Legend:
PR - Penetrometer (kg)
PVS - Peak vane shear strength (kPa)
P - Peak vane shear strength (kPa)
R - Remoulded vane shear strength (kPa)
S - Sensitivity (ratio = P/R)

Strat unit.	Depth (m)	Graphic Log	Description	PR	PVS	Sensitivity					
						Standard			Adapted		
						P	R	S	P	R	S
			CLAY, light orange brown with Mn flecks, firm, wet, highly plastic, sensitivity, highly weathered.	5	126	126	29	4	118	28	4
			becomes most		123	123	29	4	139	26	5
	18		becomes very wet		94	94	13	7	112	3	37
			End of log 18.5 m.								
	19										

Field Log Sheet

Location: Ranginui Road Slip

Date 21 (day) 01 (month) 08 (year)

GPS: NZMS 260: U14 927 817

Notes: This face log and augar log was underaken in the main slip as shaded in yellow in appendix 4.2a

Legend:
PR - Penetrometer (kg)
PVS - Peak vane shear strength (kPa)
P - Peak vane shear strength (kPa)
R - Remoulded vane shear strength (kPa)
S - Sensitivity (ratio = P/R)

Strat unit.	Depth (m)	Graphic Log	Description	PR	PVS	Sensitivity Standard P	Standard R	Standard S	Adapted P	Adapted R	Adapted S
			SILT, light orange brown, very stiff, dry, non-plastic, trace fine sand, slightly weathered.	9	UTP						
Post Rotoehu Ash			Sandy SILT, light brown, very stiff, dry, slightly weathered, few roots.	>10	UTP						
			SILT, light greyish-white, as above but coarse material increases with depth.	>10	UTP						
	1		SILT, light greyish-white with few black specs (MnO), stiff, extra sensitive non-plastic, slightly weathered.	>10	97	97	10	10			
			Silty SAND, light whitish-grey, very loosely packed, fine to coarse angular grains, well sorted, sensitive - extra sensitive unweathered.	2-3	49	49	6	8			
Rotoehu Ash			CLAY, dark brown with some orange flecks, very stiff, moist, highly plastic, moderately weathered.	>10	UTP						
Hamilton Ash paleosol			CLAY, light orange-brown, stiff, moist, highly plastic, sensitive, moderately weathered.	>10	UTP						
Hamilton Ash	2		CLAY, light orange-brown, moist to wet, subordinate subangular coarse sand and fine gravels of many colours - grey, red, apricot etc. moderately sensitive to sensitive.	>10	109	109	18	6			
				9.5	84	84	15	6			
			CLAY, light brown, stiff. moderatly sensitive to sensitive	8.5	87	87	16	5			
	3		CLAY, light yellowish brown, moderately plastic, moderatly sensitive black, white, grey and purple subordinate fine gravels.	9.5	100	100	23	4			
			CLAY, dark greyish-brown with black specs (MnO) and orangish brown streaks, sticky, very plastic, moderately sensitive to sensitive	7.5	133	133	34	4	143	29	5
			CLAY, light pinkish-orange with light orangish-brown streaks and black specs (MnO), sticky, wet, moderately sensitive, highly plastic, trace coarse sand, moderately weathered.	9.5	117	117	31	4	128	24	5
				8.5	104	104	31	3	117	23	5
	4		CLAY, light grey-brown, sticky, wet, very plastic, sensitive to moderatly sensitive.	5.5	50	50	6	8	55	2	28
				5	39	39	3	13	43	2	17
	5		CLAY, light yellowish-brown, stiff, very sticky, saturated, highly plastic, extra sensitive highly weathered. Water runs from cut face to fill 1mx1m hole to 30cm depth over few hours.		36	36	3	12	42	1	42
			Start of Auger log.								
			Sandy SILT, light orange-brown with some small black fragments, very loose, wet, with tracemedium sand,								
	6		Becomes saturated								
			CLAY, light grey intermixed with orange, stiff, hard orange grains, sticky, highly plastic, coarse sand, fine gravels.								
			Orange material decreased, some white to cream material appears white and fluffy, possibly pumiceous.								
			Clayey SILT material, loose								
	7		Firm base at 7.0 metres, UTP.								
			End of log.								
	8										
	9										
	10										

Field Log Sheet

Location: Welcome Bay Road- slip 1 (head of slip)

Date 30 (day) 11 (month) 07 (year)

GPS: Direct from GPS North: 638 1886 East: 279 3745

Notes: This log corresponds with slip 1 in appendix 4.2b, and represents a soil log undertaken at the head of the slip.

Legend:
PR - Penetrometer (kg)
PVS - Peak vane shear strength (kPa)
P - Peak vane shear strength (kPa)
R - Remoulded vane shear strength (kPa)
S - Sensitivity (ratio = P/R)

Strat unit.	Depth (m)	Graphic Log	Description	PR	PVS	Sensitivity					
						Standard			Adapted		
						P	R	S	P	R	S
			SILT with trace clay, dark brownish black, stiff to hard, dry, slightly plastic, sensitive, many roots (> 10 %), topsoil.	6.5	39	39	5	8			
			Silty CLAY, light yellowish orange, hard, dry, moderately plastic, vertical cracking, highly weathered.	> 10	NP						
				7	NP						
	1		Sandy SILT with trace fine sand light brown, stiff to hard, dry, non plastic, moderately weathered.	> 10	NP						
				> 10	NP						
	2		Slight break in slope								
			SILT with trace clay, light yellowish brown, firm - stiff, moist, slightly plastic, sensitive, moderately weathered.	8	110	110	15	7	110	16	7
				8	NP						
			SAND, light yellowish brown, fine to medium angular sand, loosely packed, dry, no obvious bedding. slightly weathered.	3	10						
	3			>10	NP						
			SILT with trace fine sand, light yellowish brown, stiff, moist, non plastic, moderately weathered.								
			End of log								
	4		Also undertook an auger log from break in slope (1.8m) sequence of units are presented below, and UTP occured at 4.4m								
			SILT with trace fine sand, dry to moist non plastic, light brown								
			Clayey SILT, light greyish brown, firm, moist, slightly plastic.								
			Silty CLAY, light yellowish brown, very firm, moderatly plastic, moist, moderately plastic.								
			SILT, light yellowish grey, dry to moist, non plastic.								
			UTP ~ 4.4 m								
	5										

Field Log Sheet

Location: Welcome Bay Road slip 1 _ log 2

Date 30 (day) 11 (month) 07 (year)

GPS: Direct from GPS North: 638 1886 East: 279 3745

Notes: This log was undertaken on the right hand side of the slip 1 (facing welcome bay road)

Legend:
PR - Penetrometer (kg)
PVS - Peak vane shear strength (kPa)
P - Peak vane shear strength (kPa)
R - Remoulded vane shear strength (kPa)
S - Sensitivity (ratio = P/R)

Strat unit.	Depth (m)	Graphic Log	Description	PR	PVS	Sensitivity Standard P	Standard R	Standard S	Adapted P	Adapted R	Adapted S
			Clayey SILT, dark brown, very stiff, dry, slightly plastic, horizontal and vertical cracks, highly weathered.								
	1		SILT with trace coarse sand and clay, light yellowish brown, firm, moist to dry, slightly plastic, moderately sensitive, moderately weathered.	6.5	29	29	16	2			
				6.5	47	47	16	3			
				5.5	34	34	10	3	34	6	6
			Silty CLAY with trace fine sand, dark brown, stiff, moist, moderately plastic, sensitive highly weathered.	9.5	175	175	34	5	131	21	6
	2			5.5	115	115	15	8			
			SAND, light yellowish brown, medium to fine coarse to sub angular sand, extra sensitive densly packed, well graded (coarse at top fine at bottom).	5.5	81	81	8	10			
				9.5	133	133	15	9			
			SILT, light yellowish brown, stiff, moist, non plastic, moderately weathered.	>10		Not able to get good penetration when undertaking shear vane readings.					
				10							
	3		SAND, yellowish grey, fine angular sand.								
			End of log 3.2 m.								
	4										

Field Log Sheet

Location: Welcome Bay Road drive way; slip 2

Date 11 (day) 12 (month) 07 (year)

GPS: From GPS: North: 638 1886 East: 279 3745

Notes: This Log is associated with slip 2 in appendix 4.2b

Legend:
PR - Penetrometer (kg)
PVS - Peak vane shear strength (kPa)
P - Peak vane shear strength (kPa)
R - Remoulded vane shear strength (kPa)
S - Sensitivity (ratio = P/R)

Strat unit.	Depth (m)	Graphic Log	Description	PR	PVS	Sensitivity Standard P	Standard R	Standard S	Adapted P	Adapted R	Adapted S
			SILT, dark brown, dry non plastic, topsoil.								
	1		Clayey SILT, dark brown, firm, moist, moderately plastic, moderately sensitive, moderately weathered.	9	194	194	62	3			
				8.5	81	81	19	4			
			SILT with trace medium to fine pumecious gravel, dark orange, firm, moist, non plastic, moderately sensitive to sensitive, well graded (fine material at top). slighly weathered.	5.5	65	65	16	4			
			SILT with trace fine to coarse sand, light orangish brown, firm, moist, non plastic, moderately sensitive to sensitive, moderately weathered.	7	55	55	13	4			
	2		SAND, dark orange, fine to coarse sub angular to angular sand, extra sensitive, loose, slighly weathered.	2	45	45	3	15			
				4	50	50	10	5			
			SILT, light yellow with black Mn flecks, soft to firm, moist, slightly plastic, sensitive.	4	62	62	10	6			
			Clayey SILT with trace fine sand, firm, light brown moist, slightly plastic, quick.	4.5	136	138	5	28	138	6	23
			Clayey SILT with trace fine to coarse sand, light grey, soft to firm, moist, slightly plastic, extra sensitive.		65	65	6	11			
			End of log 2.6m.								
	3										

Field Log Sheet

Location: Welcome Bay drive way; slip 2 - auger log

Date 11 (day) 12 (month) 07 (year)

GPS: From GPS: North: 638 1886 East: 279 3745

Notes: This Log is associated with slip 2 in appendix 4.2b, however this log is solely an auger log and was undertaken at the head of the slip in unfailed ground.

Legend:
PR - Penetrometer (kg)
PVS - Peak vane shear strength (kPa)
P - Peak vane shear strength (kPa)
R - Remoulded vane shear strength (kPa)
S - Sensitivity (ratio = P/R)

Strat unit.	Depth (m)	Graphic Log	Description	PR	PVS	Sensitivity					
						Standard			Adapted		
						P	R	S	P	R	S
			SILT, brownish black, slightly plastic, topsoil.								
			Clayey SILT, light orangish brown, soft, moist to dry, slightly plastic.								
	1		Silty CLAY, light orangish brown, moist, moderately plastic.								
			SILT with trace clay, dark brown, soft, wet, slightly plastic.								
			CLAY, light yellowish orange, stiff, moist, highly plastic.								
	2		CLAY, light grey, stiff, moist, moderatly plastic, includes trace subrounded small gravels which break up when pressure is applied.								
			SILT, yellowish brown, dry, non plastic, comes up as individual grains - augar unable to penetrate this material, it may represent the top of the ignimbrite located in a cutting near by.								
	3		UTP 2.6m.								

Field Log Sheet

Location: Behind shed log - top, bench 1 SH29 - Pyes Pa

Date 06/07 (day) 02 (month) 08 (year)

GPS: NZMS 260 U14: 846 807

Notes: This log was undertaken in the approximate area of Pyes Pa / Tauriko and was in a large cutting behind a shed which can be seen from state highway 29.

Legend:
PR - Penetrometer (kg)
PVS - Peak vane shear strength (kPa)
P - Peak vane shear strength (kPa)
R - Remoulded vane shear strength (kPa)
S - Sensitivity (ratio = P/R)

Strat unit.	Depth (m)	Graphic Log	Description	PR	PVS	Sensitivity: Standard P	Standard R	Standard S	Adapted P	Adapted R	Adapted S
Rotoehu and post-Rotoehu ash	1		Covered by vegetation, unable to be examined.								
			SILT, yellowish brown, trace sand, stif, dry, non-plastic, few roots, unweathered.		UTP		UTP				
	2		SILT, light yellowish brown, stiff, dry, non-plastic, some roots, unweathered, some orange staining.		113	113	10-16	11-7			
Rotoehu ash			SAND, lght yellowish brown, fine-medium grained, loosely packed, sensitive to extra sensitive, well sorted, pooly graded, unweathered.		39	39	6	7			
Hamilton ash paleosol			SILT, light yellowish brown, stiff, dry, non-plastic, unweathered, some orange staining.		104	104	16	7			
	3		SAND, light grey, fine to coarse grained,loosely packed, well sorted, poorly graded, coarse grains appear angular, sensitive, unweathered, many fine		>227						
			CLAY, dark brown, black flecks present (MnO), very stiff, dry, non-plastic, sensitive, homogeneous, highly weathered.		UTP						
			CLAY, dark brown, black flecks present (MnO), very stiff, dry, slightly plastic, homogeneous.		130	130	16	8			
	4		Clayey SILT, dark brown, very stiff, dry, non-plastic, homogeneous, no coarse material.		133	133	19	7			
			Sandy SILT, light yellowish brown, black flecks (MnO), very stiff, slightly plastic, sensitive medium to fine grained sand, trace clay.		143	143	16	9			
			Silty SAND, light yellow, densely packed, nonplastic, sensitive to extra sensitive, well sorted, poorly graded, black wavy lines in lower section.		130	130	19	7			
			Silty SAND, light yellow, loosely packed, dry-moist, non-plastic, extra sensitive poorly graded, coarse to fine grains.		143	143	16	9			
	5		Sandy SILT, light yellowish brown, sensitive to extra sensitive, fine to coarse grained sand, dry.		96	96	10	10			
			CLAY, light brown, black flecks (MnO), moist, moderately plastic, moderatly sensitive, fractured vertically and horizontlly, possible paleosol.		UTP						
			SAND, yellow, loosly packed, moderatly sensitive, well sorted, coarse to fine angular grains.		94	94	13	7			
	6		SAND, dark brown, loosely packed, moderately sorted fine to coarse grains, moderatly sensitive to sensitive, well graded coarsening up.		87	87	8	11			
			SAND, light yellow, densely packed, sensitive, coarse to fine grained, few subangular fine gravels, some grading.		104	104	31	3			
			SAND, light orange-brown, densely packed, fine to coarse grained, crumbles upon extraction.		47	47	13	4			
			SAND, dark brown, fine to coarse grained, tracefine angular gravels, poorly sorted, unweathered.		32	32	5	6			
	7		SAND, light orange-brown, densely packed, fine to coarse grained, crumbles upon extraction.		Very loose non-cohesive sediment						
			SAND, light yellowish-brown, moderately packed, coarse grained with trace angular gravel, grades to silty sand, sensitive to extra sensitive.		45	45	5	9			
			Silty SAND, dark brown-black, loosely packed.		62	62	10	6			
			Silty SAND, brown, densely packed, moist, trace fine pink-grey-white subangular pumecious gravels, poorly sorted, poorly graded, unweathered, crumbles upon extraction, sensitive to extra sensitive.		45	45	6	8			
	8		Silty SAND, light brown, coarse to fine grained, sensitive		87	87	10	9	83	19	4
			Silty CLAY, light whitish grey, firm, moist, moderately plastic, homogeneous.		73	73	11	7			
			Silty SAND, light orange, black flecks, moist to wet, gently inclined.		139	139	10	14			
	9		Silty SAND, light yellowish brown, firm, moist, non-plastic, sensitive, fine to coarse grained, trace clay with some dense clay lenses, orange staining, unweathered.		143	143	15	10	141	19	7
			Silty SAND, dark orange, firm, orange staining, underlain by a layer of whitish grey moist caly.		99	99	19	5	120	12	10
			Silty SAND, light grey, dense, moist, well sorted, large blob of greyish white clay, some black flecks (MnO), firm, moist, plastic, sensitive.		110	110	15	7			
	10				107	107	15	7			

Field Log Sheet

Location: Behind shed log - top, bench 1 SH29 - Pyes Pa

Date 06/07 02 08
day month year

GPS:

Notes: sheet 2 of log

Legend:
PR - Penetrometer (kg)
PVS - Peak vane shear strength (kPa)
P - Peak vane shear strength (kPa)
R - Remoulded vane shear strength (kPa)
S - Sensitivity (ratio = P/R)

Strat unit.	Depth (m)	Graphic Log	Description	PR	PVS	Sensitivity					
						Standard			Adapted		
						P	R	S	P	R	S
			CLAY, dark orange with black specs, firm, moist, moderately plastic, homogeneous.		123	123	10	12	113	19	6
			Silty CLAY, greyish white, few black specs (MnO), firm, moist, moderately plastic, homogeneous, extra sensitive		75	75	11	7	92	19	5
			SILT, light grey, very stiff, dry, non-plastic, trace fine to coarse sand, interbedded with fine sand with fine gravels, gravels pumecious, some orange staining, unweathered.		110	110	10	11	91	2	45
					UTP				81	3	27
	11				UTP						
			SAND, light orange, densely packed, poorly sorted, poorly graded, trace fine gravels, sub-horizontal laminated bedding.		UTP						
			Silty SAND, dark orange, gravel sized black flecks (MnO), dense, dry, fine to coarse grained, sub-horizontal laminated bedding, unweathered.								
					UTP						
	12		Clayey SILT, light grey, black flecks, very stiff, dry, slightly plastic, moderately weathered, intermixed with silty sand, densely packed, dry, fine to medium grained, sub-horizontal bedding, thinly laminated, extra sensitive		160	160	18	9			
			Silty SAND, light yellowish-brown, dense, dry, moderate sorting, trace fine gravels, slightly weathered.		UTP						
			SILT, light grey, stiff, dry, non plastic, layered with fine to coarse yellow brown sand.		UTP						
			SAND, orange, trace coarse gravels, intermixed with light grey clayey SILT, very stiff, slightly plastic, coarse material.		UTP						
	13		Sandy SILT, light yellowish brown, very stiff, moist, non-plastic, trace fine gravels, slightly weathered, trace fine gravels.		UTP						
			Silty SAND, light yellowish brown, some black flecks (MnO), dense, angular fine gravels (grey, red, purple), slightly weathered.	7	149	149	18	8			
			SAND, light grey with some orange staining, dense, poorly sorted, medium to fine grained, intermixed with a clayey SILT, light grey, firm, slightly plastic, very complex, sensitive to extra sensitive.	8.5	123	123	10	12			
	14		SILT, light greyish-white, few MnO flecks, stiff, dry, moderately plastic, trace clay, some orange staining, slightly weathered, sensitive to extra sensitive.	>10	86	86	6	14			
				8.5	225	225	28	8			
			SAND, dark orange, intermixed with silty CLAY at base, poorly sorted, trace angular to rounded fine gravels, subordinate black flecks. Very complex, extra sensitive.	8	112	112	15	7			
	15		SILT, light greyish-white with few black flecks (MnO), stiff, wet, non-plastic, intermixed with orange SAND	8	162	162	13	12			
			SILT, light greyish-white with few black flecks (MnO), soft, very wet, non-plastic, dilatent without water, feels sensitive, sensitive.	7	55	55	5	11			
			SILT, light greyish-white with few black flecks (MnO), soft, wet, sticky, slightly plastic, dilatent without water, trace clay, homogeneous, similar to above but not as wet, some orange staining, sensitive to extra sensitive	6	50	50	10	5	44	<1	>44
	16		SILT, light greyish-white with increasing black flecks (MnO), soft, moist, sticky, slightly plastic, dilatent without water, trace clay, extra sensitive, homogeneous, similar to above but not as wet, some orange staining tending to pink.	8.5	87	87	19	5			
				>10	157	157	16	10	156	3	52
			SILT, light grey, trace coarse sand in silt matrix, dense, heavily weathered pumecious material, poorly sorted, extra sensitive	>10	144	144	13	11	175	8	22
			SILT, light grey, moist, slightly plastic, trace coarse sand.	10	156	156	15	10			
	17		Sandy SILT, dark orange, firm, moist, non-plastic, trace coarse sand.								
			Clayey SILT, light grey grading to pink, stiff but soft on remoulding, wet, non-plastic,extra sensitive, dilatent without water, trace fine sand coarsening down, trace fine to coarse sub-angular gravel.	9.5	117	117	16	7	113	<1	>113
				9	190	190	32	6	128	2	64
			End of Log								
	18										
	19										
	20										

Field Log Sheet

Location: McLaren falls, base of cutting

Date 2 (day) 2 (month) 08 (year)

GPS: NZMS 260 U14: 782 724

Notes: This log represents a sensitive soil observed at the base of a small cutting. However, the majority of overlying material was covered in vegetation.

Legend:
PR - Penetrometer (kg)
PVS - Peak vane shear strength (kPa)
P - Peak vane shear strength (kPa)
R - Remoulded vane shear strength (kPa)
S - Sensitivity (ratio = P/R)

Strat unit.	thickness (m)	Graphic Log	Description	PR	PVS	Sensitivity					
						Standard			Adapted		
						P	R	S	P	R	S
			At base of cutting Clayey silt, light yellowish brown with black MnO flecks, soft, wet, slightly plastic, extra sensitive		62	62	5	12	63	2	32
			2m above the base of the cutting, similar material as above was observed, however this material was only moist.								
			An auger log was undertaken from the base of the cutting, the following presents the log from this.								
	0		Clayey SILT, light yellowish brown, soft, wet, slightly plastic, some orange staining.								
			Clayey SILT, greyish white with black MnO flecks, soft, wet, non plastic, dilatent without the addition of water.								
	1		Similar material to above but becomes very wet (saturated) and recovery in auger is only ~ 20 % of potential maximum.								
	2		Sandy SILT, ligth orange with black flecks, soft, wet, non plastic.								
			Auger UTP at ~ 2.3 m.								

Field Log Sheet

Location: Omanawa Road Slip

Date 22 (day) 11 (month) 07 (year)

GPS: N 6370193 E 2780979

Notes: Small slip on Omanawa Road 150m North of Peers Road intersection, easily rolling hill country.

Legend:
PR - Penetrometer (kg)
PVS - Peak vane shear strength (kPa)
P - Peak vane shear strength (kPa)
R - Remoulded vane shear strength (kPa)
S - Sensitivity (ratio = P/R)

Strat unit.	Depth (m)	Graphic Log	Description	PR	PVS	Sensitivity					
						Standard			Adapted		
						P	R	S	P	R	S
			SILT, brownish-black, siff, dry, non-plastic, homogeneous, strongly allophanic, smooth indistinct boundary.	8.5							
			SILT, reddish-brown, firm, dry to moist, non-plastic, some trace clay, strongly allophanic, diffuse boundary.	4	16	16	6	3			
	1		Clayey SILT, light yellow, very stiff, moist, moderately plastic, homogeneous, non-sticky, moderately sensitive, weakly allophanic.	9	121	121	34	4	121	35	4
	2		Clayey SILT, dull yellow-orange with few white pumice clasts increasing downward and black flecks with rust coloured smudge, firm, moderately plastic, moderately sensitive, moderately allophanic.	8	89	89	24	4			
	3		Clayey SILT, light yellow with black flecks (MnO), very stiff, moist, moderately plastic, moderately sensitive, grey 'clasts' increasing abundace downward.	7	62	62	16	4			
	4		Clayey SILT, light yellow, firm, moist, slightly plastic, non-sticky, sensitive homogeneous, very weakly allophanic.	8	93	93	16	6			
	5		SILT, bright yellowish brown with black flecks (MnO), very stiff, moist, non-plastic, sensitive, few light grey coarse material softer than matrix, homogeneous, very weakly allophanic.	>10	106	106	16	6	106	23	5
	6		End of Log 6.3m								
	7										
	8										
	9										
	10										

Field Log Sheet

Location: Omokoroa Coastal cliff single unit

Date 24 (day) 12 (month) 07 (year)

GPS: NZMS 260 U14: 794 927

Notes: A unit investigated early in the study to get an idea of how a typical sensitive soil in the Tauranga region my behave and what its appearance may be like.

Legend:
PR - Penetrometer (kg)
PVS - Peak vane shear strength (kPa)
P - Peak vane shear strength (kPa)
R - Remoulded vane shear strength (kPa)
S - Sensitivity (ratio = P/R)

Strat unit.	thickness (m)	Graphic Log	Description	PR	PVS	Sensitivity					
						Standard			Adapted		
						P	R	S	P	R	S
			SILT, light grey, soft, wet, slightly plastic, quick, dilatent without the addition of water, some weak orange staining.	3.5	28	47	3	16	49	< 1	49
	0.5		Silty CLAY, light yellowish brown, hard, moist, slightly plastic, sensitive to extra sensitive.	8.5	110	183	23	8	227	16	14
	1										
	3										

Field Log Sheet

Location: Oropi Road Roundabout

Date 16 (day) 11 (month) 07 (year)

GPS: N 6379948 E 2786928

Notes: This log was undertaken on the corner of Oropi Road and SH29, in a bowl shaped slip

Legend:
PR - Penetrometer (kg)
PVS - Peak vane shear strength (kPa)
P - Peak vane shear strength (kPa)
R - Remoulded vane shear strength (kPa)
S - Sensitivity (ratio = P/R)

Strat unit.	Depth (m)	Graphic Log	Description	PR	PVS	Sensitivity					
						Standard			Adapted		
						P	R	S	P	R	S
			SILT, black, very stiff, non-plastic, slightly allophanic.	8.5							
			Homogeneous reworked/disturbed material, very stiff, some vertical cracks.	>10							
			Thin, very stiff black layer.	>10							
			Yellowish brown, hard, dry, slightly plastic, homogenous.	>10							
	1		Light brown and black, hard, dry, plastic, small pumice clasts. Like a hardpan.	>10							
			Sandy SILT, greyish yellow, loosely packed, dry to moist, low plasticity, trace sand, lenses of clayey SILT.	>10							
				9							
	2			10							
				6	94	94	5	19	84	<1	>84
					55	55	5	11	84	3	28
			SILT, light grey, firm, wet, non-plastic, trace sand, remoulds to paste without addition of water, extra sensitive to quick.								
	3										
			SILT, light grey, stiff, wet, non-plastic, homogeneous, some fine roots, remoulds to a paste without the addition of water, extra sensitive to quick.	6	143	143	5	29	73	<1	>73
					71	71	5	14			
	4										
	5		SILT, light grey, stiff, wet, slightly plastic, slightly sticky, some roots, extra sensitive.	6	36	36	3	12	36	<1	>36
	6										
			Silty SAND, light grey, dry, sub-angular fine to medium and some coarse sand, possibly reworked material.	8							
			Sandy SILT, light grey, firm, non-plastic, some coarse material.	9							
			SILT, orange, moist, non-plastic.	>10							
	7		Unseen - covered with debris								
			SILT, grey, firm, moist, homogeneous, trace clay and fine sand, extra sensitive.	10	85	85	10	9			
			Sandy SILT, orange with grey material in lower 100mm, moist, non-plastic, extra sensitive, some coarse material.	10							
	8			8	164	164	13	12			
			Unseen - covered with debris								
	9										
			SILT, light yellow, very stiff, moist, moderately plastic, trace clay.	>10							
			Unseen covered with debris								
	10										

Field Log Sheet

Location: Oropi Road Roundabout

Date 16 (day) 11 (month) 07 (year)

GPS: N 6379948 E 2786928

Notes:

Legend:
PR - Penetrometer (kg)
PVS - Peak vane shear strength (kPa)
P - Peak vane shear strength (kPa)
R - Remoulded vane shear strength (kPa)
S - Sensitivity (ratio = P/R)

Strat unit.	Depth (m)	Graphic Log	Description	PR	PVS	Sensitivity					
						Standard			Adapted		
						P	R	S	P	R	S
			Unseen -covered with debris								
	11		SILT, light yellow, very stiff, moist, moderately plastic, trace clay, sensitive to extra sensitive.		169 156 78	169 156 78	29 23 8	6 7 10	169 120	29 8	6 15
			End of Log.								
	12										
	13										
	14										
	15										
	16										
	17										
	18										
	19										
	20										

Field Log Sheet

Location: Pyes Pa Road

Date 24 (day) 12 (month) 07 (year)

GPS: NZMS 260: U14: 846 774

Notes: This log is from an earth works site off Pyes Pa road, (approxiamatly 1 km south of Kennedy Road) where the new road linking state highway 29 and Pyes Pa Road was being constructed.

Legend:
PR - Penetrometer (kg)
PVS - Peak vane shear strength (kPa)
P - Peak vane shear strength (kPa)
R - Remoulded vane shear strength (kPa)
S - Sensitivity (ratio = P/R)

Strat unit.	Depth (m)	Graphic Log	Description	PR	PVS	Sensitivity					
						Standard			Adapted		
						P	R	S	P	R	S
			Silty Clay, light brown, stiff, moist, moderately plastic, sensitive.		126	126	23	5			
			Clayey SILT with trace fine sand, dark pin with MnO flecks, very stiff, moist to wet, slightly plastic, sensitive .		81	81	16	5			
					105	105	23	5	113	8	6
	1		Clayey SILT, brownish orange, few black MnO flecks firm, moist, slightly plastic, sensitive.		68	68	19	4	68	3	23
			Clayey SILT, yellowish brown some black MnO flecks, very stiff, moist, slightly plastic, sensitive.		110	110	15	7	84	3	28
			Clayey SILT with trace fine sand, light orangish yellow, very stiff, moist, slightly plastic, sensitive, subhorizontal bedding		66	66	10	7	63	2	32
			Clayey SILT wih trace fine sand, light orange with some black MnO flecks, stiff, moist, slightly plastic, sensitive.		81	81	10	8	81	3	27
			Silty CLAY with trace fine sand, dark orange with some black MnO flecks, stiff, moist to wet, moderately plastic, sensitive to extra sensitive, also included appears to be some large gravel charcoal pieces.		45	45	3	15	52	1	52
	2		Silty CLAY, firm, wet, moderately - highly plastic, extra sensitive, appears to be charcoal pieces as above.		28	28	3	9			
			End of log at 2.2m								
	3										

Field Log Sheet

Location: State highway 2, north of Pahoia and Omokoroa

Date 26 (day) 11 (month) 07 (year)

GPS: From GPS: North 639 0408 East 277 2200

Notes: This site is a cutting on SH2 approxiamatly 200 m north of the intersection with Turner Road. Note there is a section of ~ 3m above this log, however it was heavily vegetated, but appears to contain both the Hamilton and Rotoehu Ashes.

Legend:
PR - Penetrometer (kg)
PVS - Peak vane shear strength (kPa)
P - Peak vane shear strength (kPa)
R - Remoulded vane shear strength (kPa)
S - Sensitivity (ratio = P/R)

Strat unit.	Depth (m)	Graphic Log	Description	PR	PVS	Sensitivity					
						Standard			Adapted		
						P	R	S	P	R	S
			CLAY, light brownish orange, very stiff, dry, highly plastic, homogenous, highly weathered many, horizontal and vertical cracks.	>10	NP						
	1		CLAY, light grey with white and orange staining, very stiff, dry to moist, moderately plastic, moderately sensitive, highly weathered.	9	194	194	73	3	194	95	4
			CLAY with trace medium sand, light grey with orange flecks, very stiff, moist, highly plastic, sensitive, highly weathered.	>10	194	194	36	5			
				>10	178	178	42	4	178	36	5
				7	110	110	23	5	110	19	6
	2		Sandy SILT, light brownish yellow, very stiff, dry, non plastic, moderately weathered.	>10	NP						
			Sandy SILT with trace fine sand, dark orange, very stiff, dry, non plastic.	>10	NP						
			Sandy SILT, light yellowish orange, very stiff, moist, non plastic, extra sensitive, this unit includes coarse sand to small pebble size black flecks (possibly Mn).	>10	162	162	19	9	162	16	10
	3		Similar to above but lenses of softer material was observed.	7	136	136	19	7			
				9	162	162	16	10			
			End of log								

Appendix 4.2

This appendix presents the geomorphic maps which are found in the back pocket of this thesis and are labelled appendices 4.2a (Ranginui Road) and 4.2b (Welcome Bay Road). The soil logs for the slips presented in each of these maps can be found in appendix 4.1.

Appendix 4.3

The following appendix presents peak vane shear strength, remoulded strength, and sensitivity values derived using the standard and adapted methods of sensitivity measurement for all samples collected from Tauriko and Otumoetai.

Otumoetai

	Peak vane strength (kPa)	Standard method remoulded strength (kPa)	Standard method sensitivity	Adapted method remoulded strength (kPa)	Adapted method Sensitivity
OS1	110	10	11		
	123	23	5		
	94	10	9		
	73	10	7		
	115			11	10
	92			8	12
	99			5	20
	102			2	51
Mean	**101**	**13**	**8**	**7**	**23**
std dev	**15**	**7**	**2**	**4**	**19**
n	**8**	**4**	**4**	**4**	**4**
error	**6**	**4**	**1**	**2**	**11**
OS2	172	18	10		
	152	10	15		
	78	6	13		
	117	21	6		
	123	18	7		
	136	16	9		
	128			**6**	21
	134			8	17
	100			3	33
	104			8	13
	122			8	15
	136			8	17
Mean	**125**	**15**	**10**	**7**	**19**
std dev	**25**	**6**	**1**	**2**	**7**
n	**12**	**6**	**4**	**6**	**6**
error	**7**	**3**	**1**	**1**	**3**

OS3	> 227	36	6		
	> 227	37	6		
	> 227	34	7		
	> 227			49	5
	> 227			23	10
Mean	**227**	**36**	**> 6**	**36**	**> 7.5**
std dev	**0**	**2**	**1**	**18**	**4**
n	**5**	**3**	**3**	**2**	**2**
error	**0**	**1**	**0**	**18**	**4**

OS4	58	5	12		
	83	5	17		
	62			1	62
	84			2	42
Mean	**72**	**5**	**14**	**2**	**52**
std dev	**14**	**0**	**4**	**1**	**14**
n	**4**	**2**	**2**	**2**	**2**
error	**8**	**0**	**4**	**1**	**14**

Tauriko

	Peak vane strength (kPa)	**Standard method remoulded strength (kPa)**	**Standard method sensitivity**	**Adapted method remoulded Strength (kPa)**	**Adapted method Sensitivity**
TS1	49	5	10		
	60	6	10		
	62	8	8		
	52			1	58
	58			1	58
	60			1	60
Mean	**58**	**6**	**9**	**1**	**59**
std dev	**5**	**2**	**1**	**0**	**1**
n	**6**	**3**	**3**	**3**	**3**
error	**2**	**1**	**1**	**0**	**1**

TS2	39	2	20		
	50			1	50
Mean	**45**	**2**	**20**	**1**	**50**
std dev	**8**	**NA**	**NA**	**NA**	**NA**
n	**2**	**3**	**3**	**3**	**3**
error	**8**	**NA**	**NA**	**NA**	**NA**

TS3	149	34	5		
	152			2	76
Mean	**151**	**34**	**5**	**2**	**76**
std dev	**2**	**NA**	**NA**	**NA**	**NA**
n	**2**	**3**	**3**	**3**	**3**
error	**2**	**NA**	**NA**	**NA**	**NA**

Appendix 6.1

The following presents acid oxalate and pyrophosphate-extractable Fe, Al, and Si used for the determination of allophane and ferrihydrite.

Soil Analysis Results

Environmental Chemistry Laboratory

Client: Justin Wyatt, University of Waikat **Date In:** 6th October 08
Job No.: LJ08068 **Date Out:** 31st October 08

Client ID	Sample No.	Acid Oxalate-Extractable			rophosphate-Extracta	
		Fe	Al	Si	Fe	Al
		(method 164) (%)			(method 166) (%)	
OS1	M8/2295	0.29	0.48	0.19	0.05	0.08
OS2	M8/2296	0.25	0.43	0.16	0.04	0.07
OS3	M8/2297	0.28	0.19	0.08	<0.01	0.01
OS4	M8/2298	0.16	0.17	0.04	0.02	0.01
TS1 / 5	M8/2299	0.01	0.25	0.03	<0.01	0.02
TS2 / 6	M8/2300	< 0.01	0.27	0.04	0.01	0.03
TS3 / 7	M8/2301	< 0.01	0.22	0.04	0.01	0.02

Appendix 6.2

The following presents all the x-ray diffraction traces measured during the course of this study for samples from Tauriko and Otumoetai.

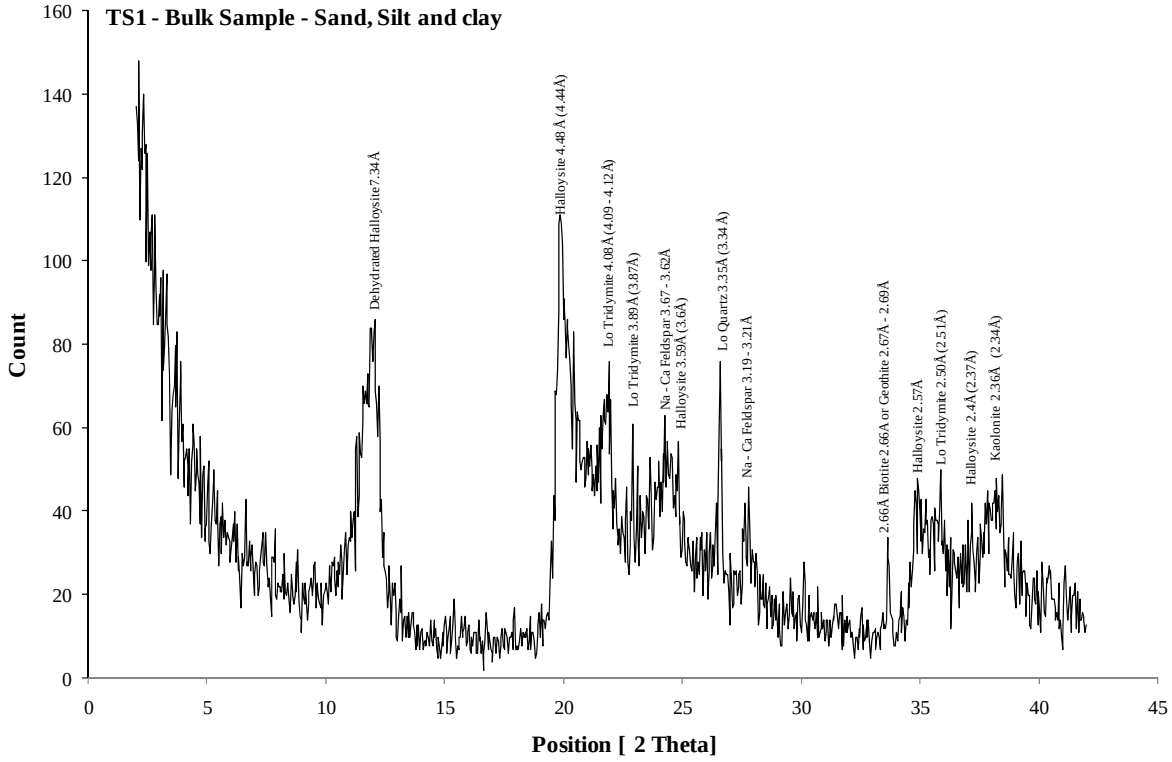

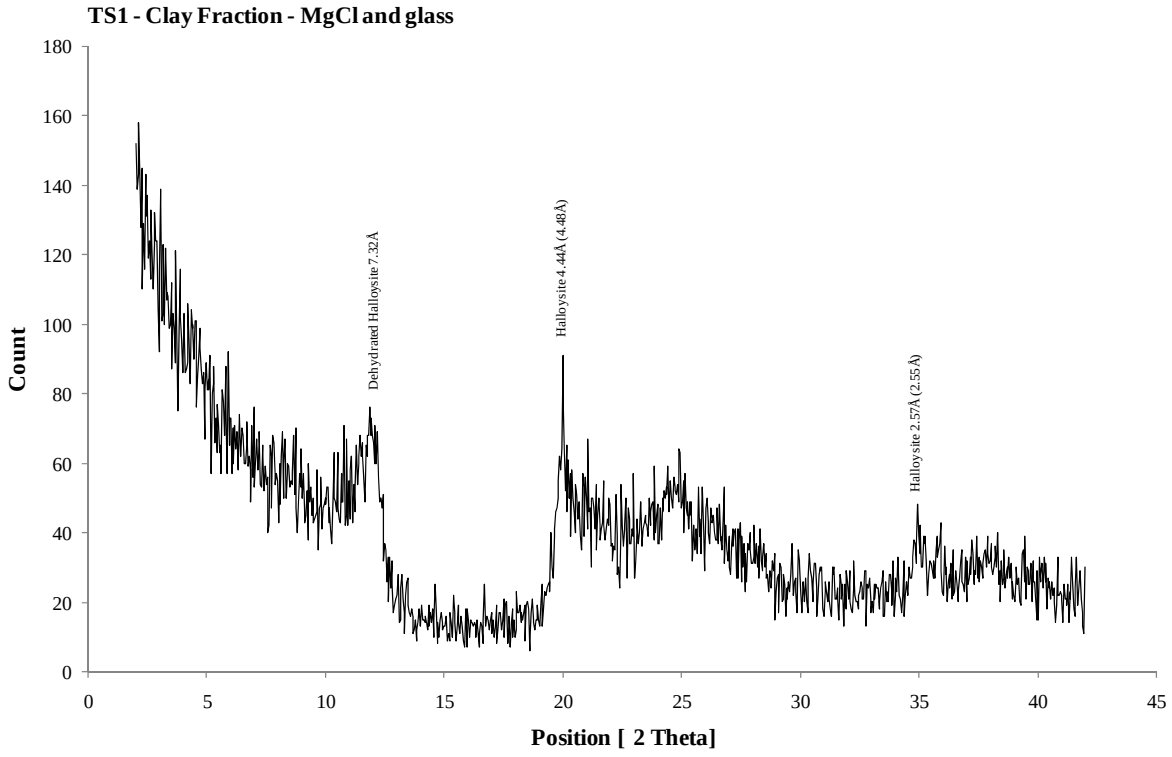

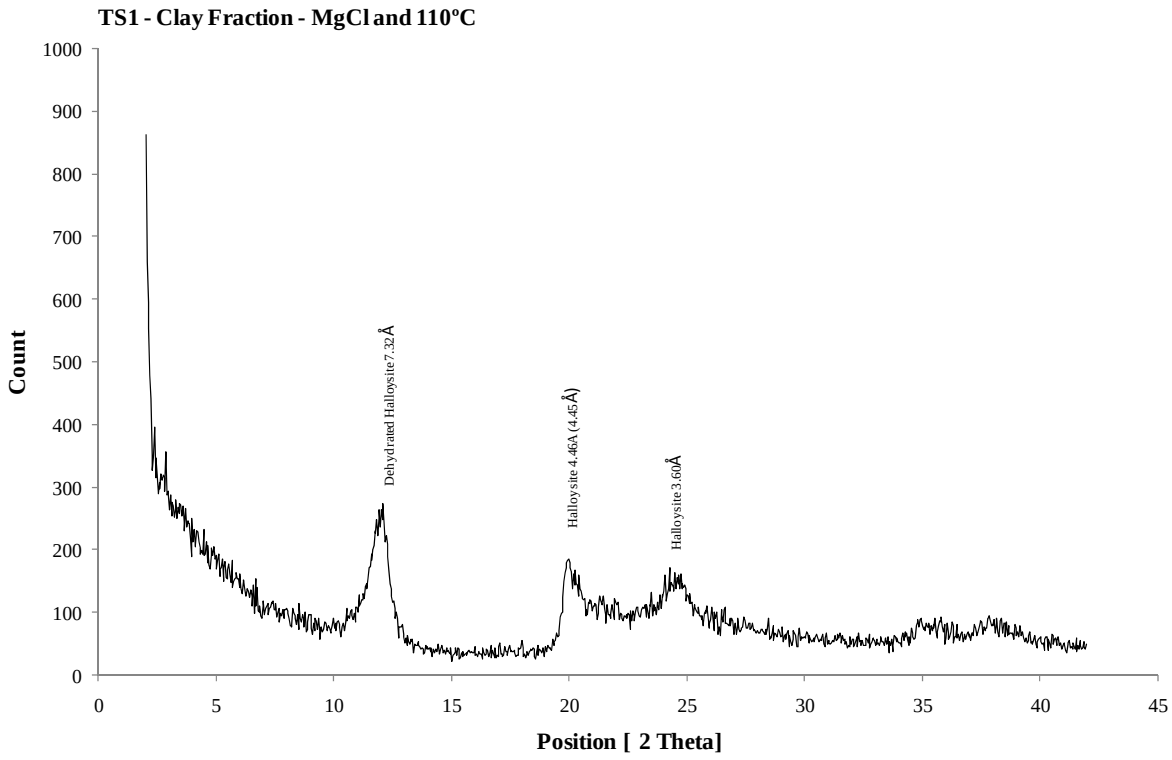
TS1 - Clay Fraction - MgCl and 110ºC
Count
Position [2 Theta]
Dehydrated Halloysite 7.32Å
Halloysite 4.46A (4.45Å)
Halloysite 3.60Å
0
100
200
300
400
500
600
700
800
900
1000
0
5
10
15
20
25
30
35
40
45

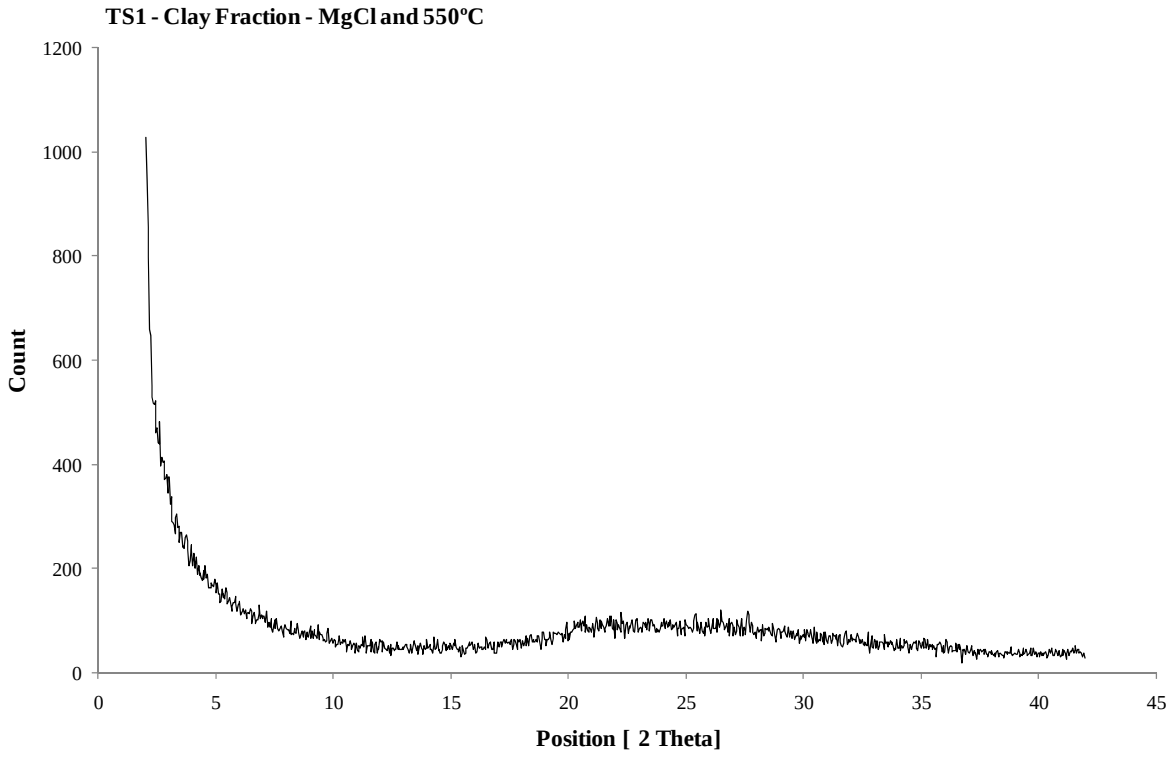
TS1 - Clay Fraction - MgCl and 550ºC
Count
Position [2 Theta]
0
200
400
600
800
1000
1200
0
5
10
15
20
25
30
35
40
45

TS1 - Clay Fraction - Ceramic tile and MgCl

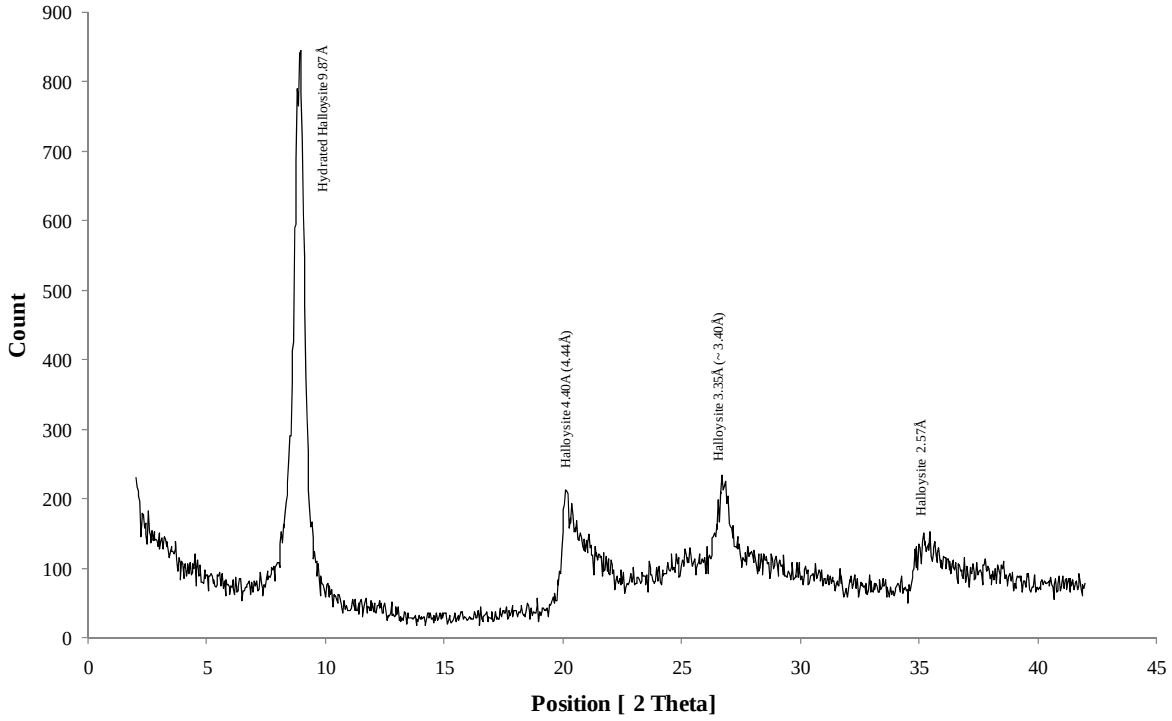

TS1 - Clay Fraction - ceramic tile, MgCl and formamide

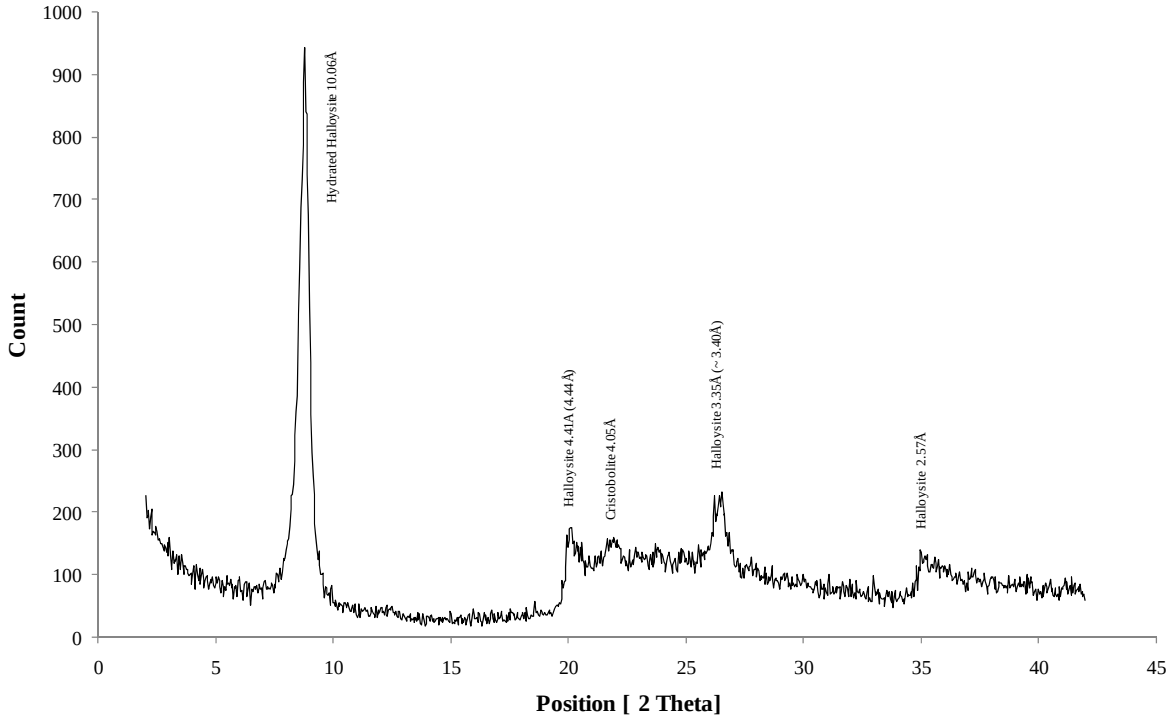

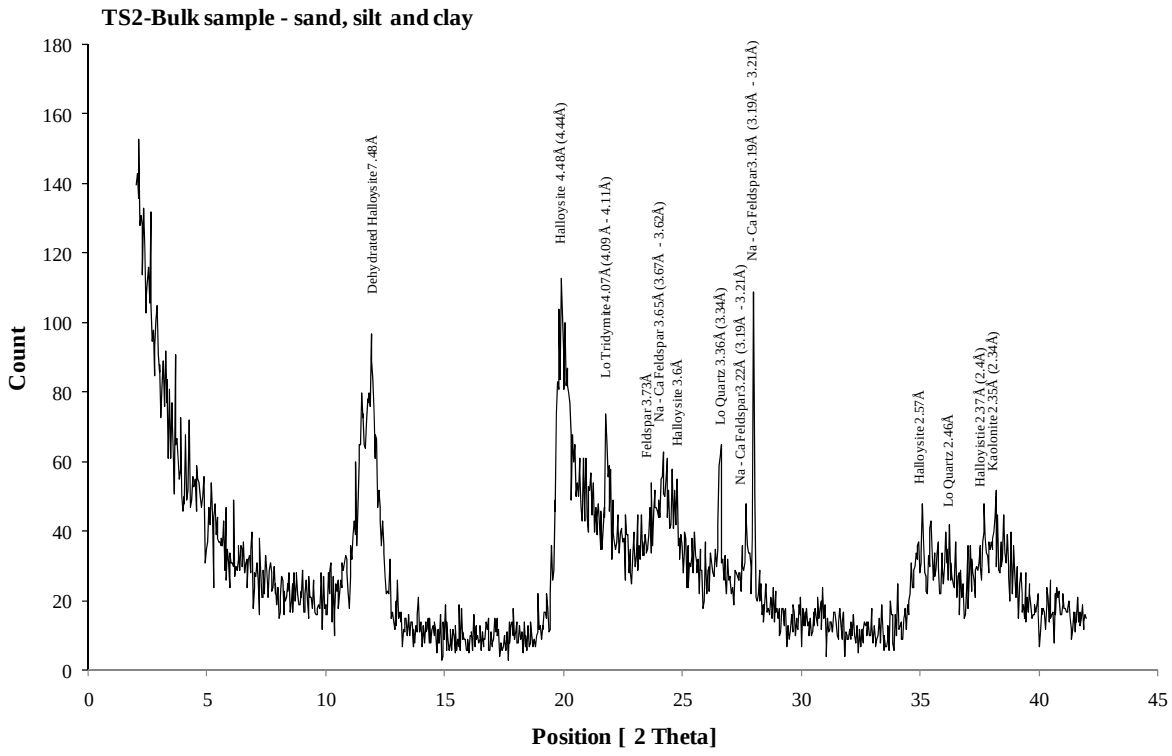
TS2-Bulk sample - sand, silt and clay
Count
Position [2 Theta]
Dehydrated Halloysite 7.48Å
Halloysite 4.48Å (4.44Å)
Lo Tridymite 4.07Å (4.09 A - 4.11Å)
Feldspar 3.73Å
Na - Ca Feldspar 3.65Å (3.67Å - 3.62Å)
Halloysite 3.6Å
Lo Quartz 3.36Å (3.34Å)
Na - Ca Feldspar3.22Å (3.19Å - 3.21Å)
Na - Ca Feldspar3.19Å (3.19Å - 3.21Å)
Halloysite 2.57Å
Lo Quartz 2.46Å
Halloysitie 2.37Å (2.4Å)
Kaolonite 2.35Å (2.34Å)

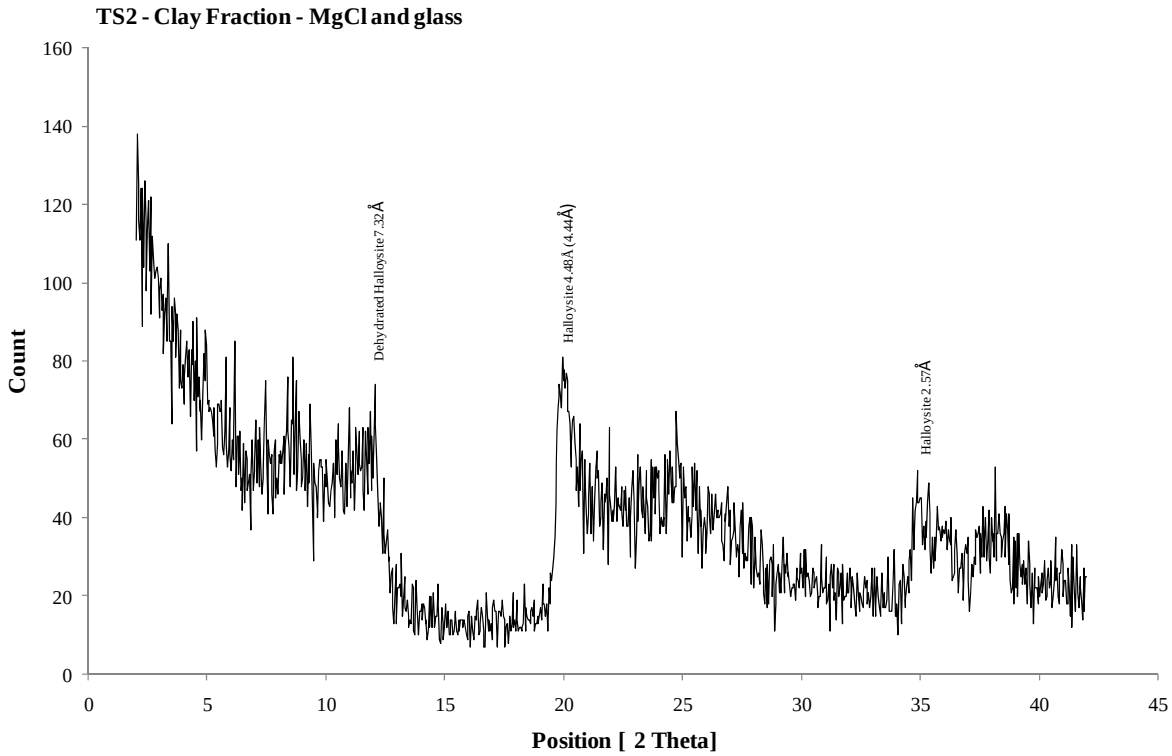
TS2 - Clay Fraction - MgCl and glass
Count
Position [2 Theta]
Dehydrated Halloysite 7.32Å
Halloysite 4.48Å (4.44Å)
Halloysite 2.57Å

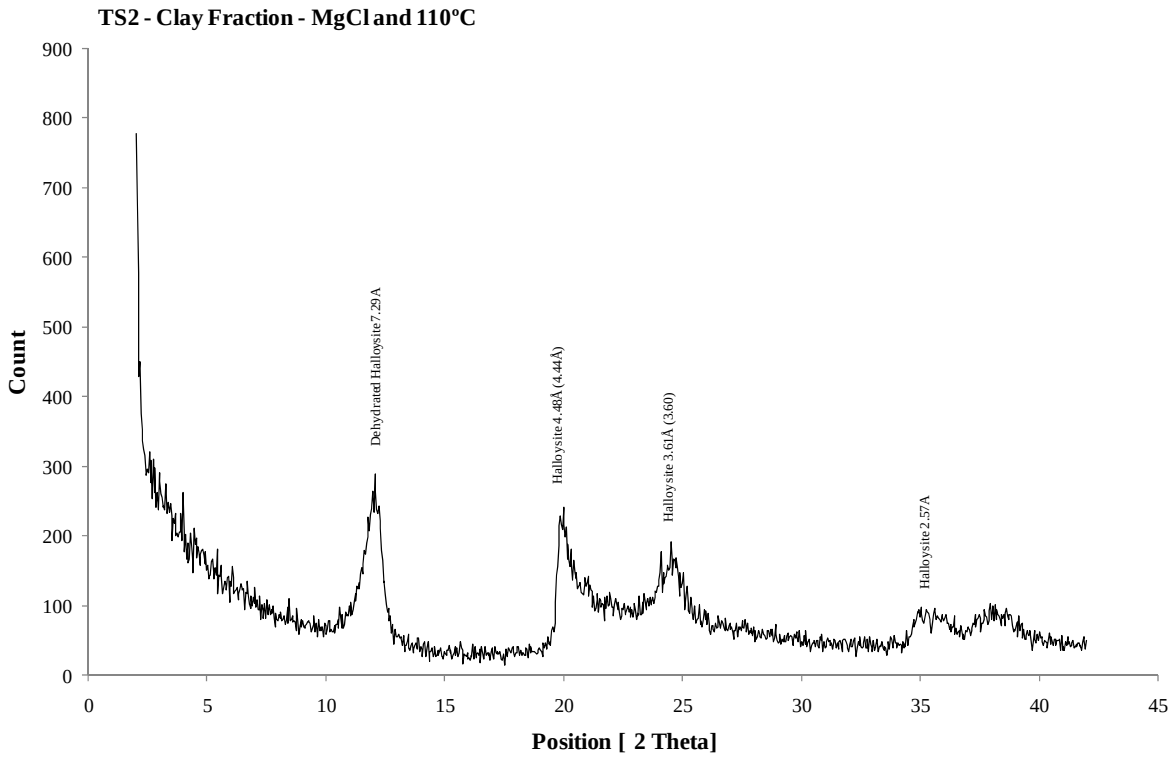
TS2 - Clay Fraction - MgCl and 110ºC
Count
Position [2 Theta]
Dehydrated Halloysite 7.29A
Halloysite 4.48Å (4.44Å)
Halloysite 3.61Å (3.60)
Halloysite 2.57A
0
100
200
300
400
500
600
700
800
900
0
5
10
15
20
25
30
35
40
45

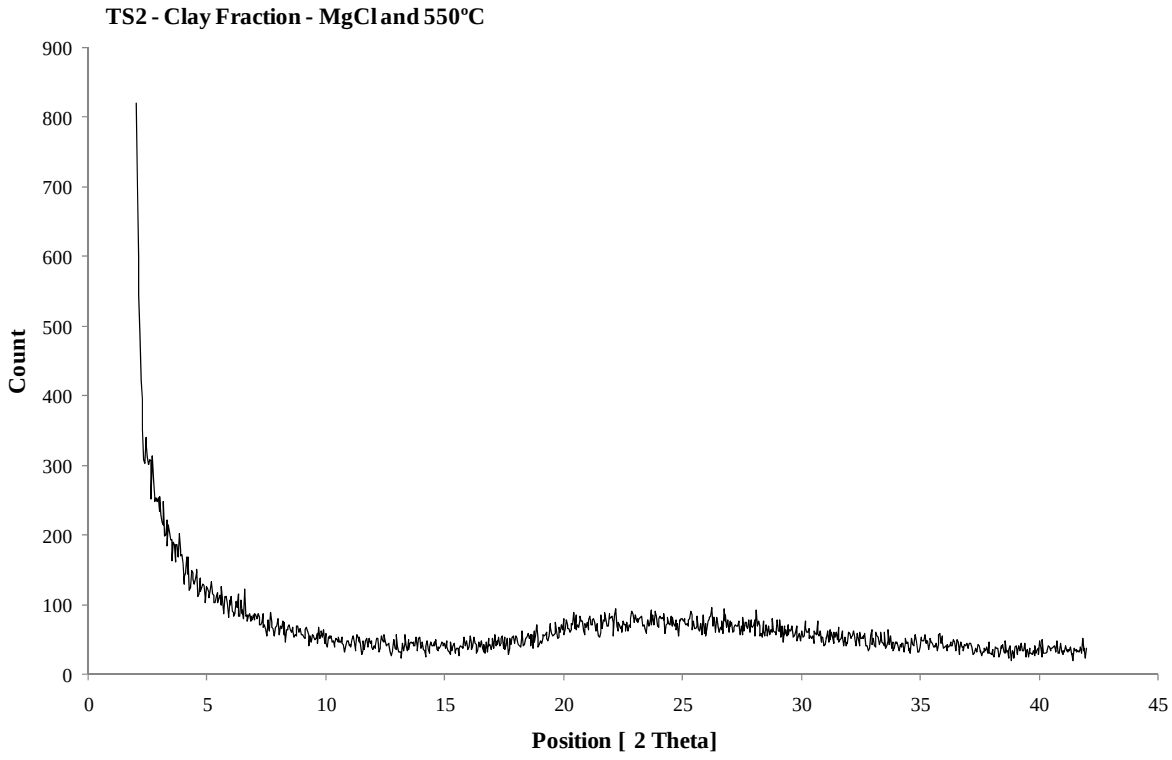
TS2 - Clay Fraction - MgCl and 550ºC
Count
Position [2 Theta]
0
100
200
300
400
500
600
700
800
900
0
5
10
15
20
25
30
35
40
45

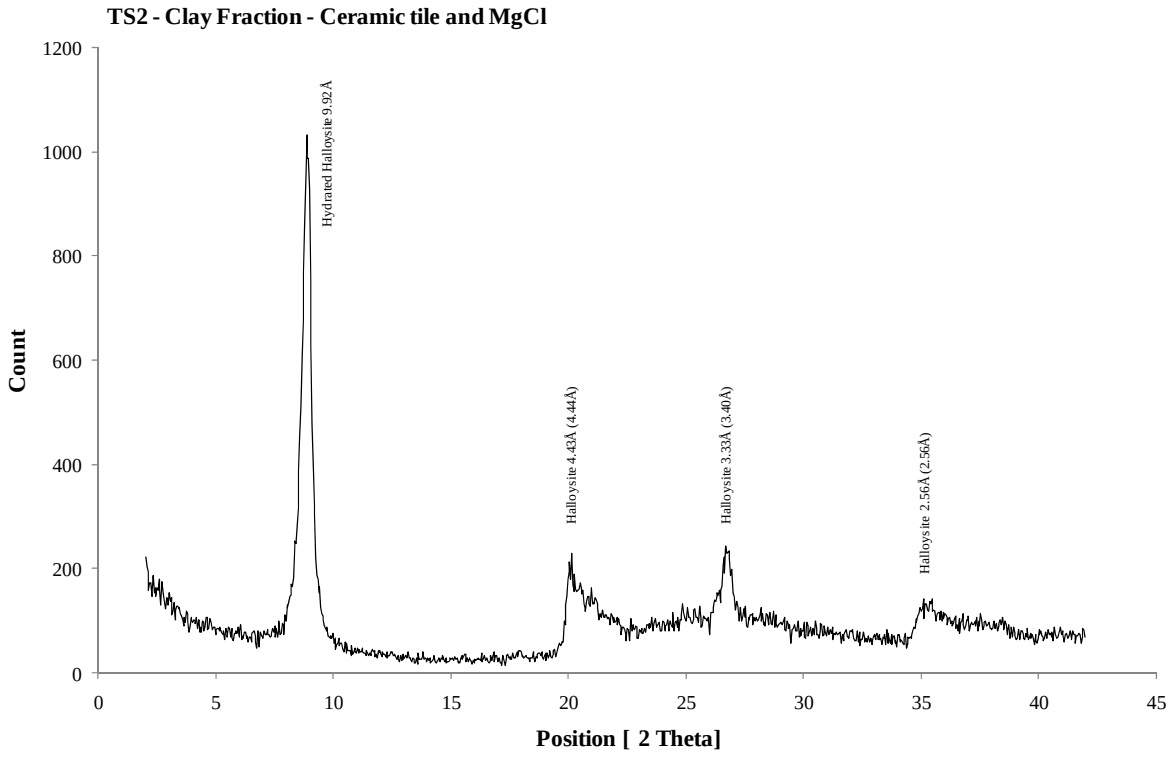
TS2 - Clay Fraction - Ceramic tile and MgCl
Count
Position [2 Theta]
Hydrated Halloysite 9.92Å
Halloysite 4.43Å (4.44Å)
Halloysite 3.33Å (3.40Å)
Halloysite 2.56Å (2.56Å)

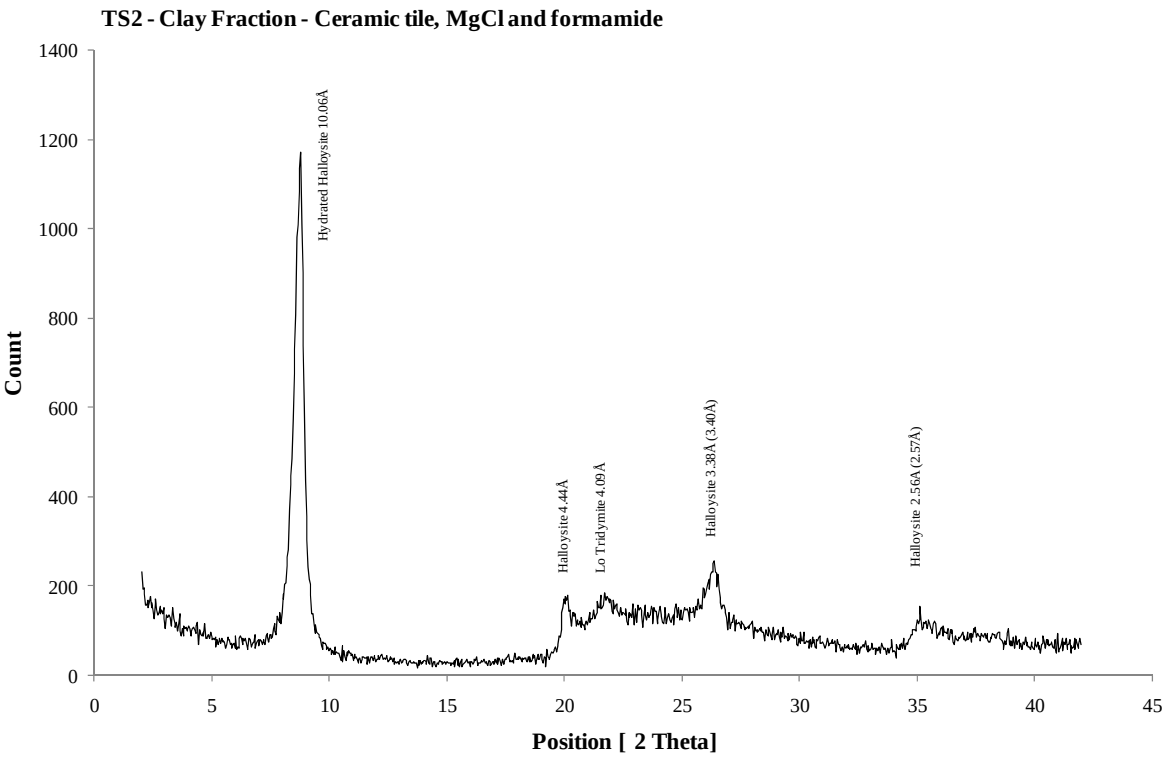
TS2 - Clay Fraction - Ceramic tile, MgCl and formamide
Count
Position [2 Theta]
Hydrated Halloysite 10.06Å
Halloysite 4.44Å
Lo Tridymite 4.09Å
Halloysite 3.38Å (3.40Å)
Halloysite 2.56Å (2.57Å)

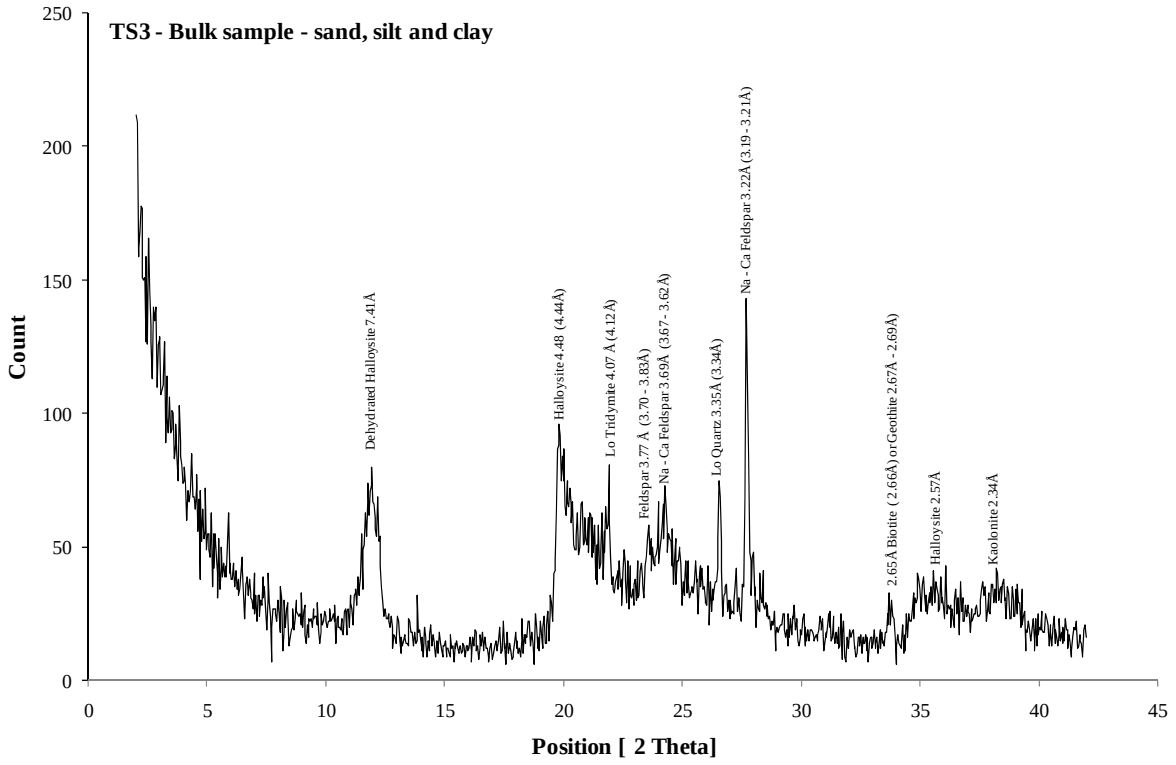
TS3 - Bulk sample - sand, silt and clay
Count
Position [2 Theta]
Dehydrated Halloysite 7.41Å
Halloysite 4.48 (4.44Å)
Lo Tridymite 4.07 Å (4.12Å)
Feldspar 3.77 Å (3.70 - 3.83Å)
Na - Ca Feldspar 3.69Å (3.67 - 3.62Å)
Lo Quartz 3.35Å (3.34Å)
Na - Ca Feldspar 3.22Å (3.19 - 3.21Å)
2.65Å Biotite (2.66Å) or Geothite 2.67Å - 2.69Å)
Halloysite 2.57Å
Kaolonite 2.34Å

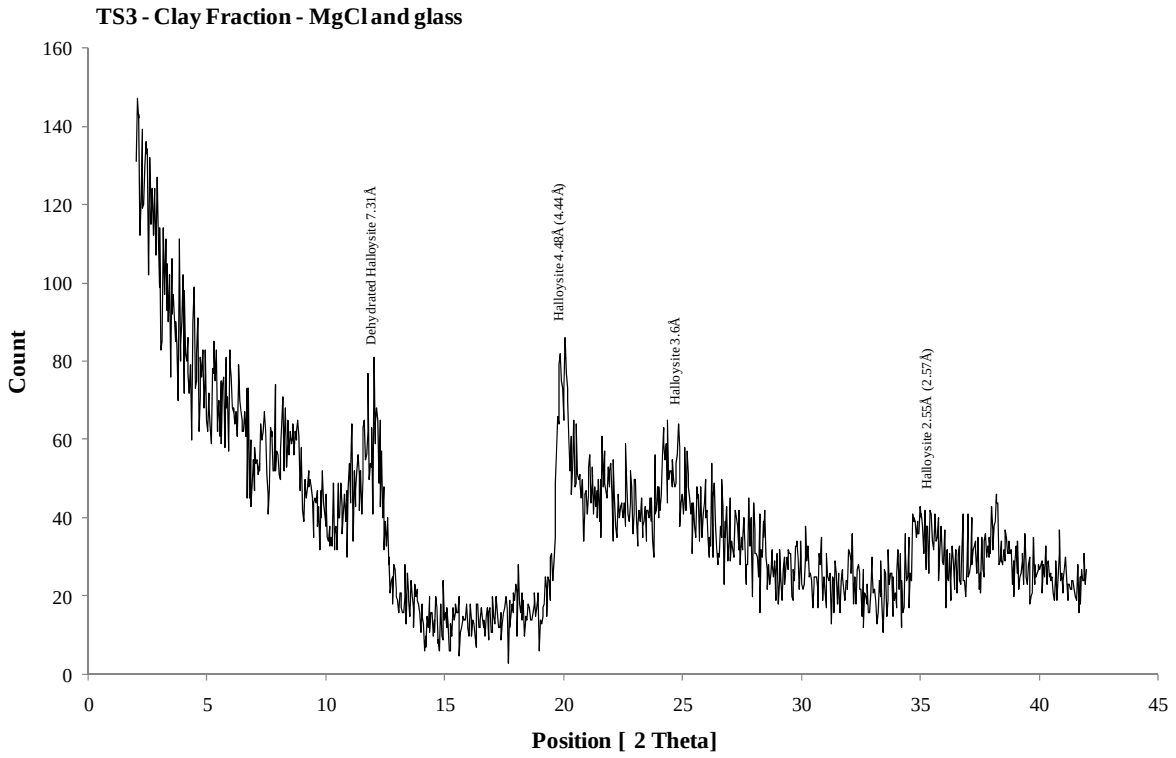
TS3 - Clay Fraction - MgCl and glass
Count
Position [2 Theta]
Dehydrated Halloysite 7.31Å
Halloysite 4.48Å (4.44Å)
Halloysite 3.6Å
Halloysite 2.55Å (2.57Å)

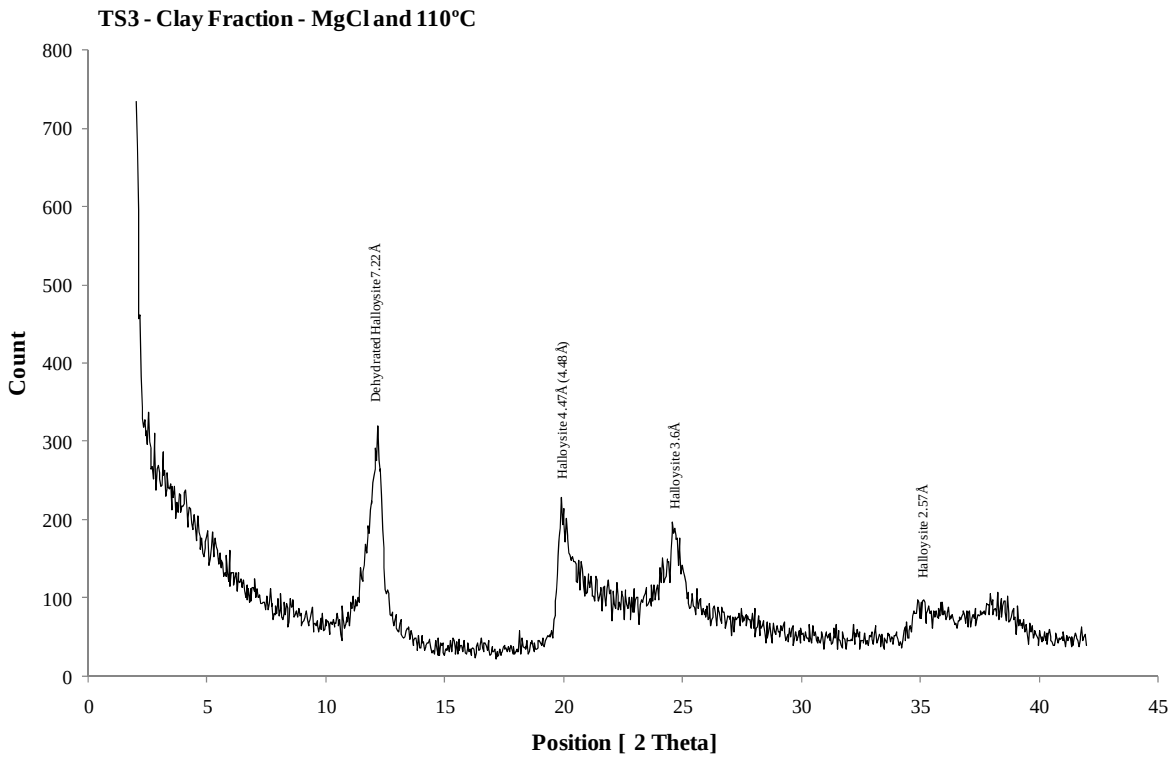
TS3 - Clay Fraction - MgCl and 110ºC
Count
Position [2 Theta]
Dehydrated Halloysite 7.22 Å
Halloysite 4.47Å (4.48 Å)
Halloysite 3.6Å
Halloysite 2.57Å
0
100
200
300
400
500
600
700
800
0
5
10
15
20
25
30
35
40
45

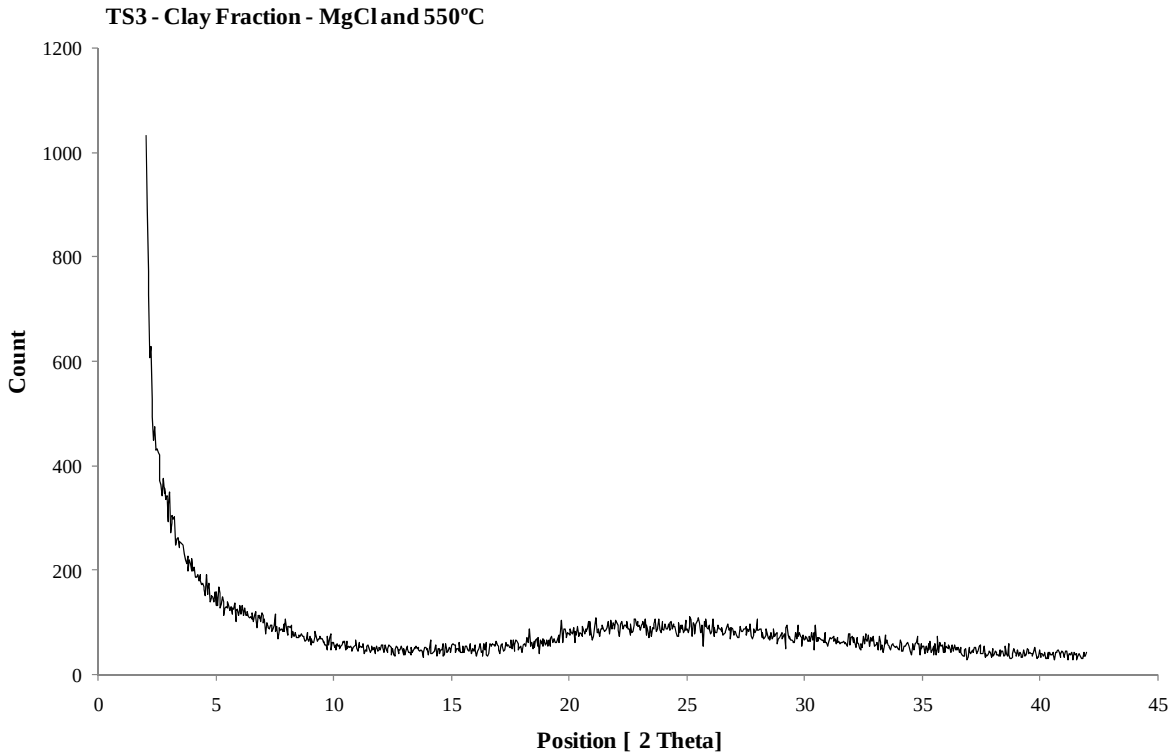
TS3 - Clay Fraction - MgCl and 550ºC
Count
Position [2 Theta]
0
200
400
600
800
1000
1200
0
5
10
15
20
25
30
35
40
45

TS3 - Clay Fraction - Porous ceramic tile and MgCl

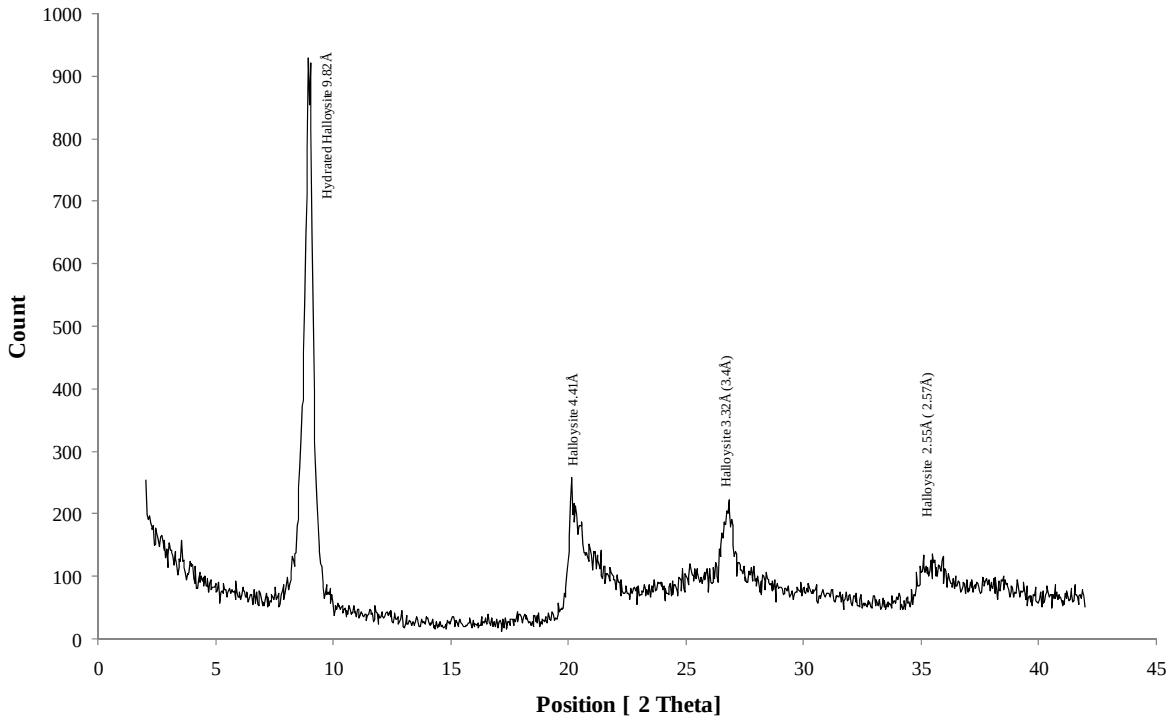

TS3 - Clay Fraction - Porous ceramic tile, MgCl and formamide

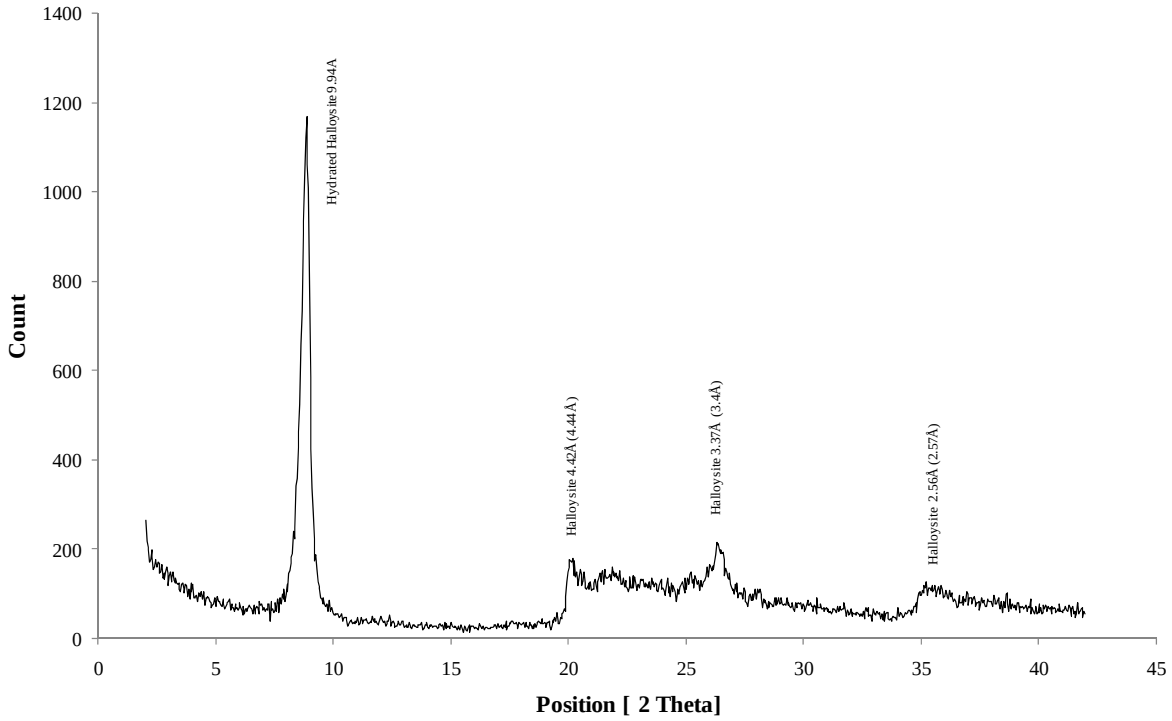

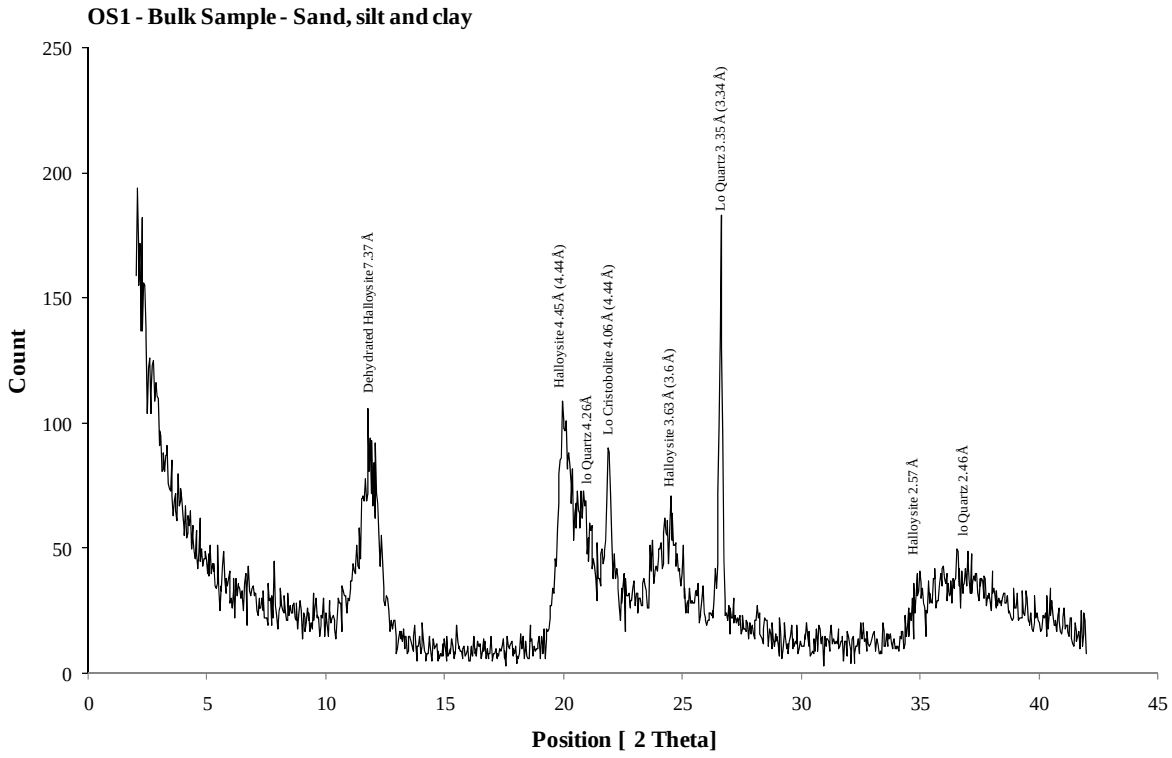
OS1 - Bulk Sample - Sand, silt and clay
Count
Position [2 Theta]
Dehydrated Halloysite 7.37 Å
Halloysite 4.45 Å (4.44 Å)
lo Quartz 4.26 Å
Lo Cristobolite 4.06 Å (4.44 Å)
Halloysite 3.63 Å (3.6 Å)
Lo Quartz 3.35 Å (3.34 Å)
Halloysite 2.57 Å
lo Quartz 2.46 Å

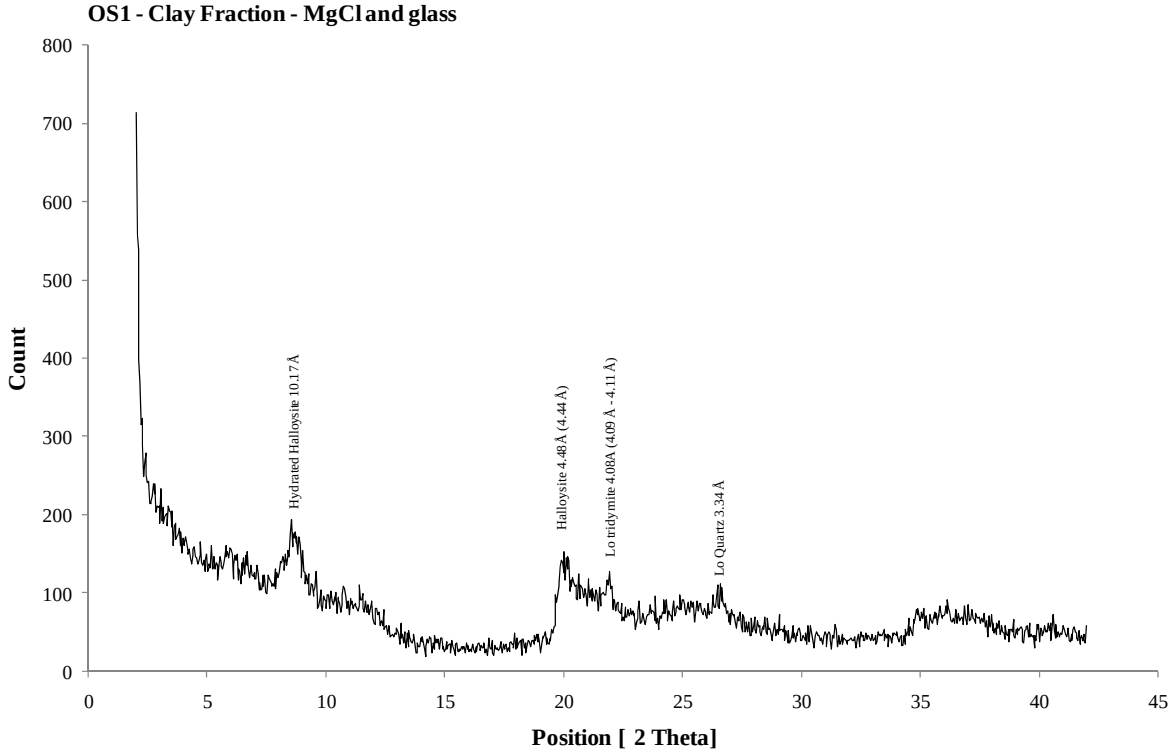
OS1 - Clay Fraction - MgCl and glass
Count
Position [2 Theta]
Hydrated Halloysite 10.17 Å
Halloysite 4.48 Å (4.44 Å)
Lo tridymite 4.08 Å (4.09 Å - 4.11 Å)
Lo Quartz 3.34 Å

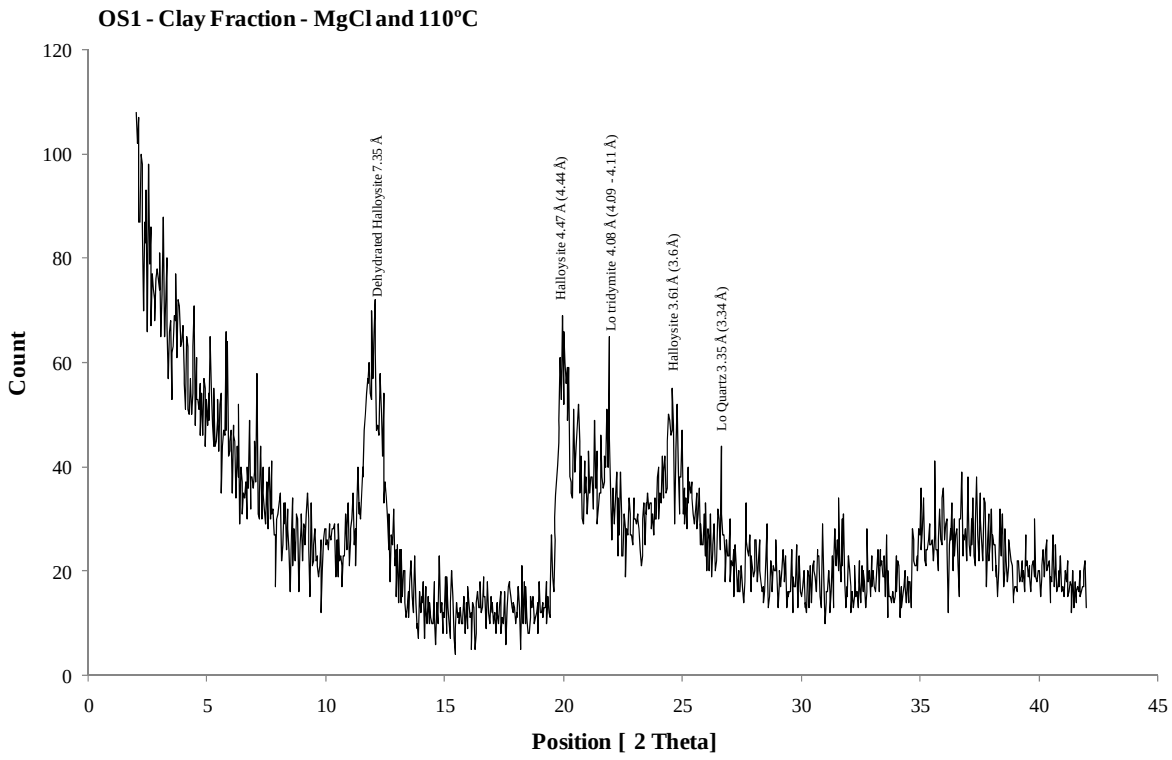
OS1 - Clay Fraction - MgCl and 110ºC
Count
Position [2 Theta]
Dehydrated Halloysite 7.35 Å
Halloysite 4.47 Å (4.44 Å)
Lo tridymite 4.08 Å (4.09 - 4.11 Å)
Halloysite 3.61 Å (3.6 Å)
Lo Quartz 3.35 Å (3.34 Å)

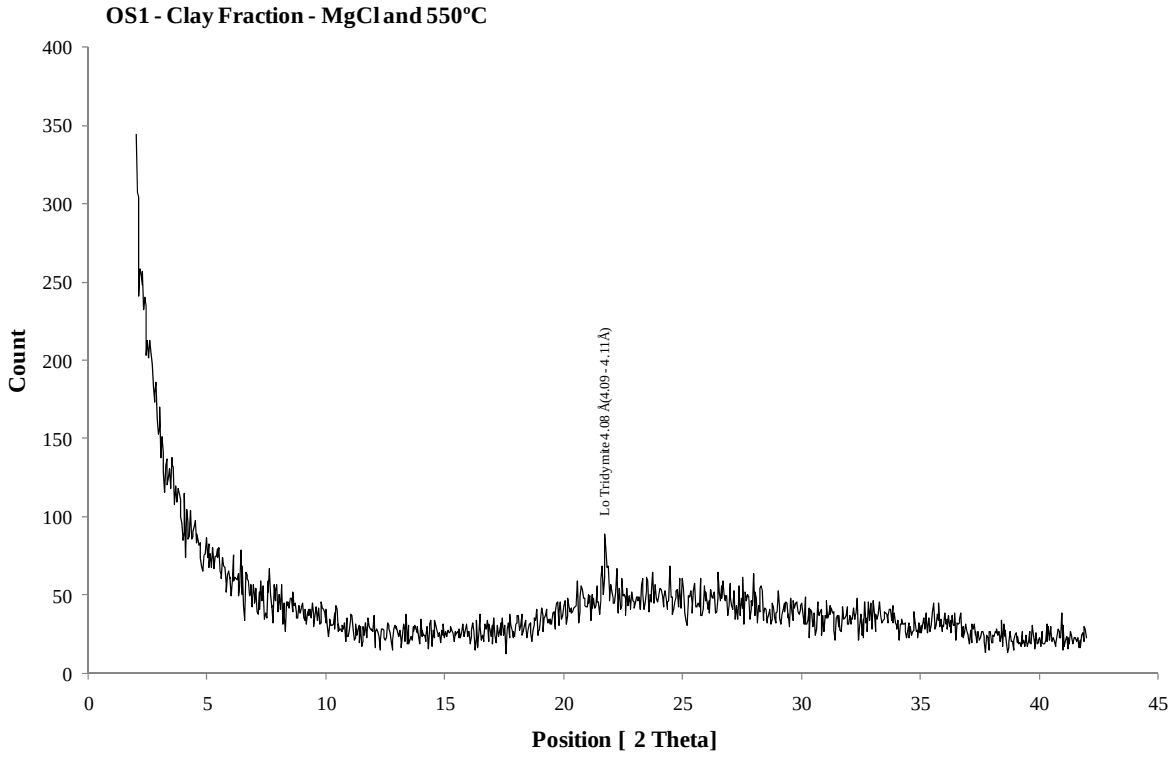
OS1 - Clay Fraction - MgCl and 550ºC
Count
Position [2 Theta]
Lo Tridymite 4.08 Å(4.09 - 4.11Å)

OS1 - Clay Fraction - Ceramic tile and MgCl

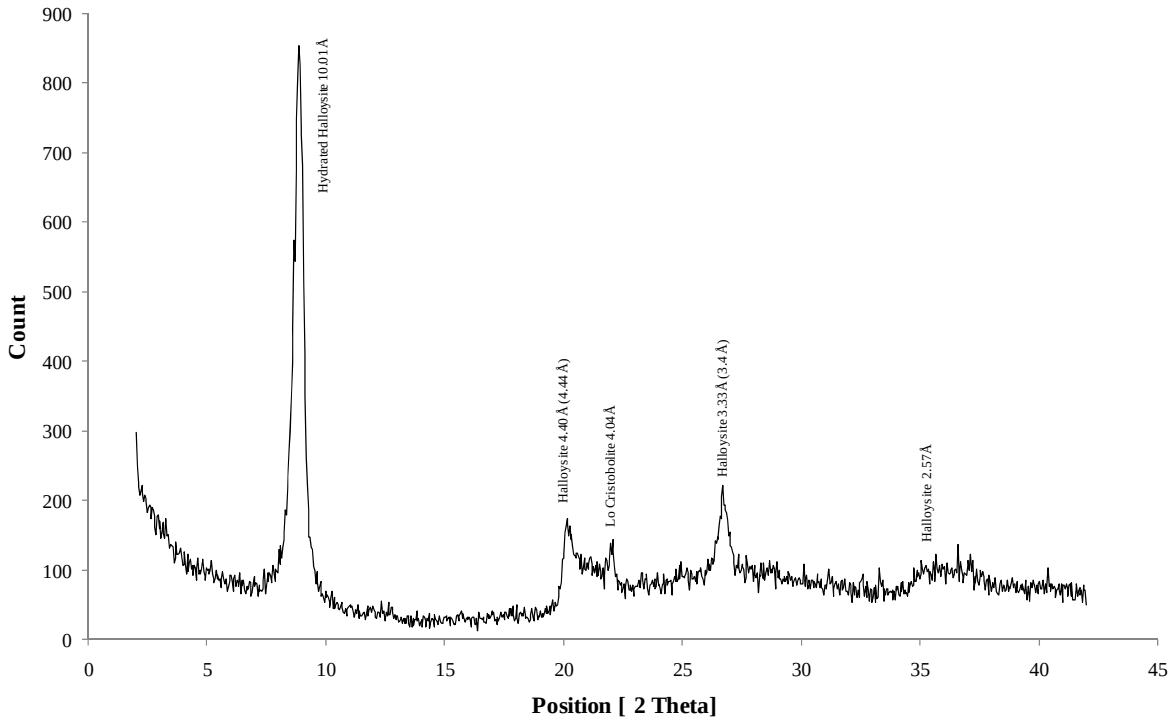

OS1 - Clay Fraction - Porous plate, MgCl and formamide

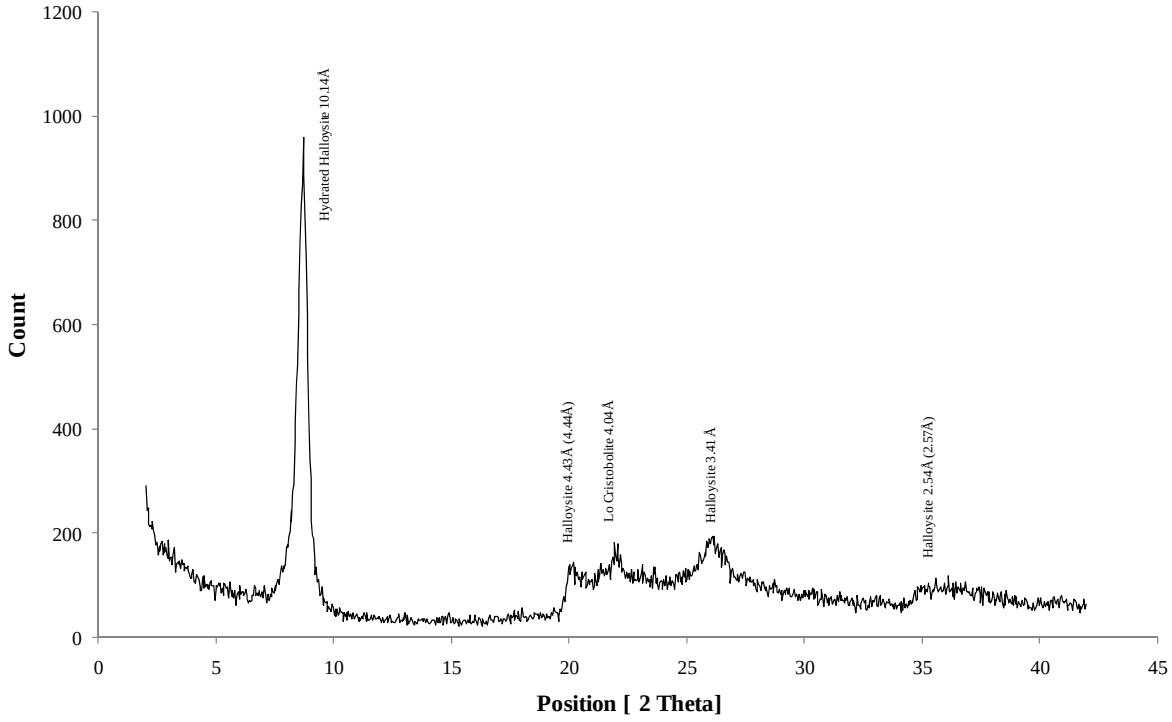

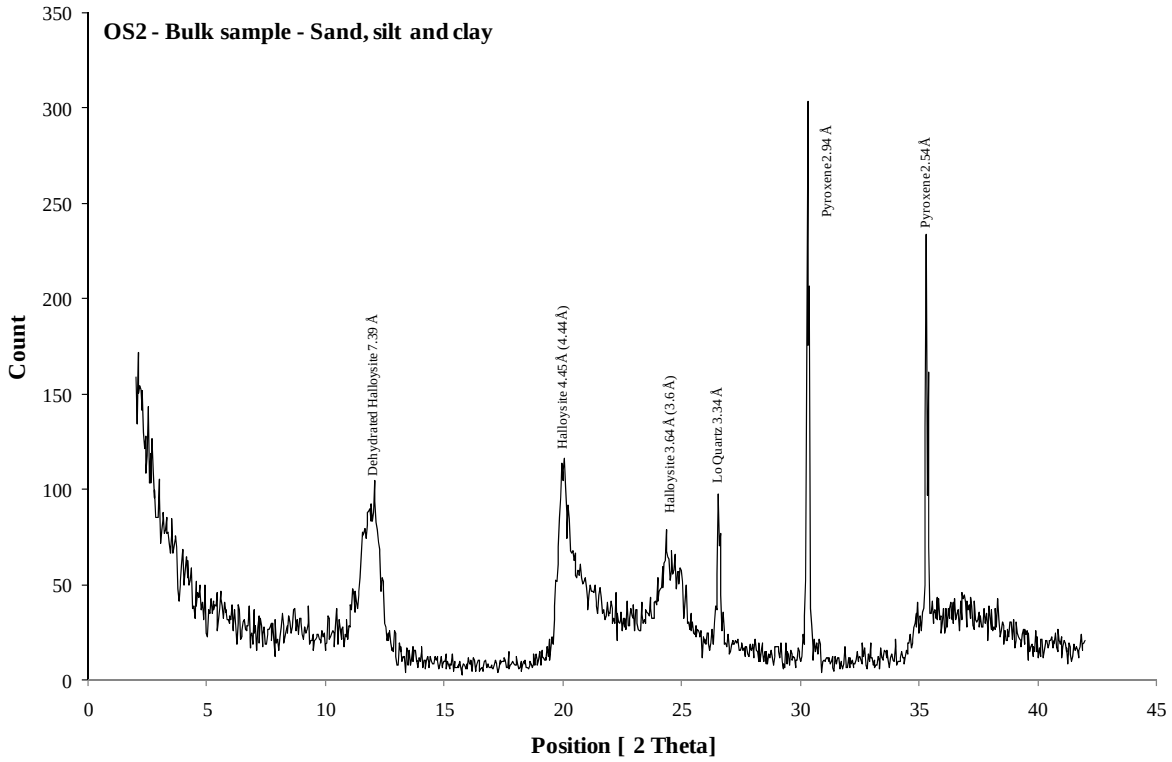
OS2 - Bulk sample - Sand, silt and clay
Count
Position [2 Theta]
Dehydrated Halloysite 7.39 Å
Halloysite 4.45Å (4.44Å)
Halloysite 3.64 Å (3.6 Å)
Lo Quartz 3.34 Å
Pyroxene2.94 Å
Pyroxene2.54Å

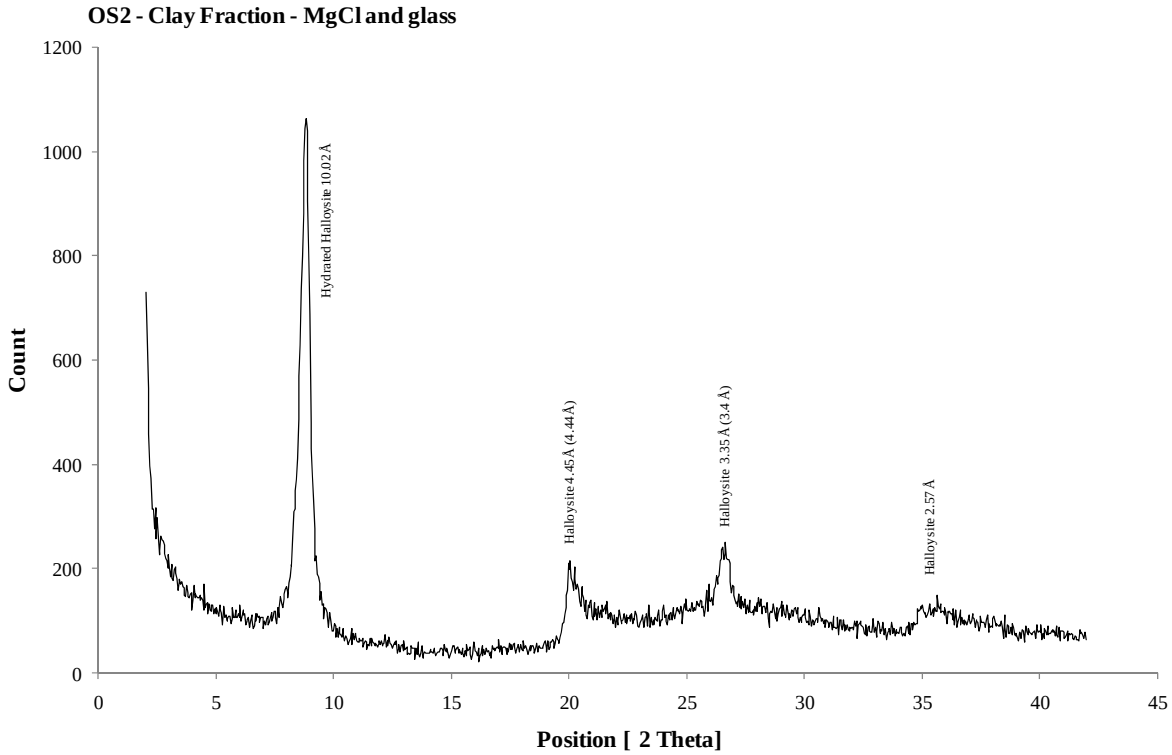
OS2 - Clay Fraction - MgCl and glass
Count
Position [2 Theta]
Hydrated Halloysite 10.02 Å
Halloysite 4.45Å (4.44Å)
Halloysite 3.35 Å (3.4 Å)
Halloysite 2.57 Å

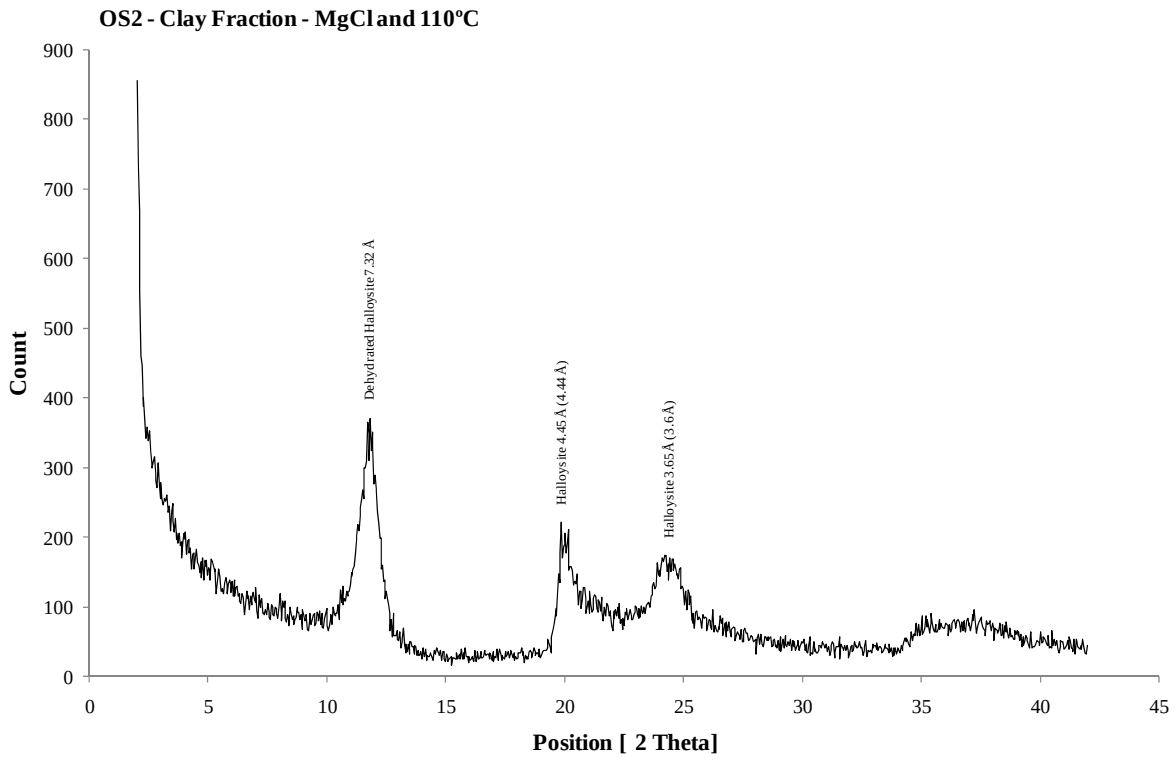
OS2 - Clay Fraction - MgCl and 110ºC
Count
Position [2 Theta]
Dehydrated Halloysite 7.32 Å
Halloysite 4.45 Å (4.44 Å)
Halloysite 3.65 Å (3.6 Å)

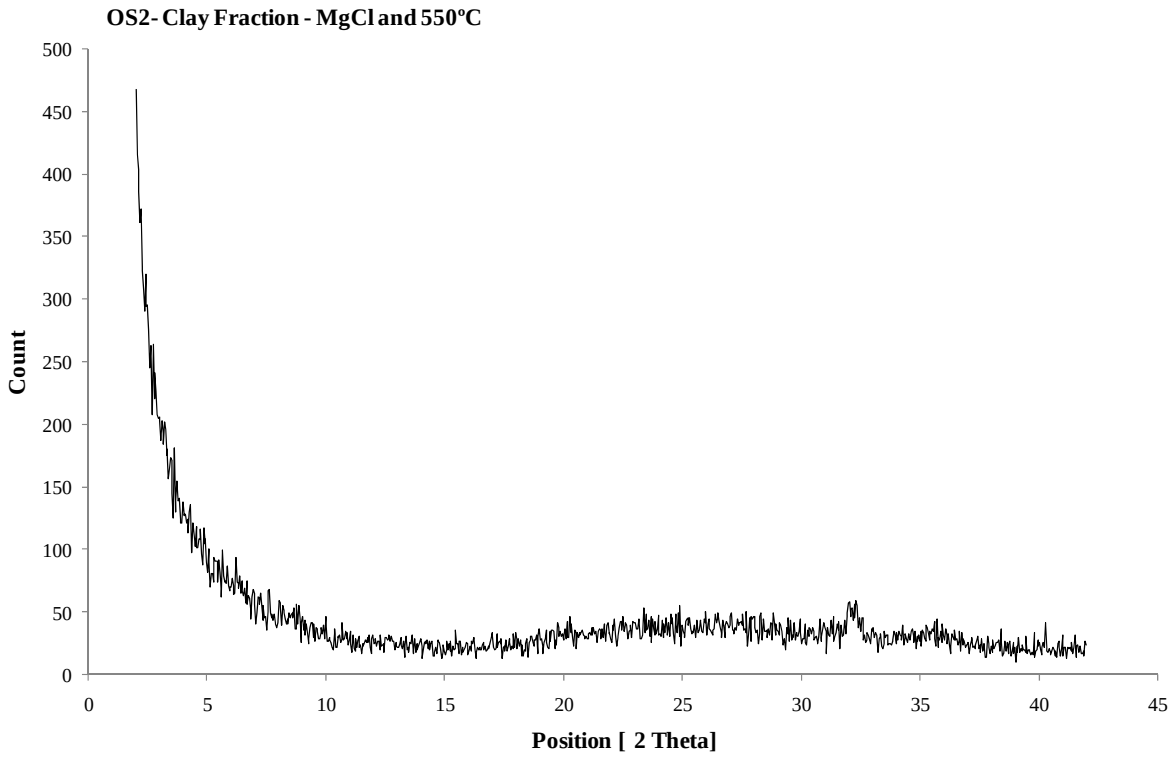
OS2- Clay Fraction - MgCl and 550ºC
Count
Position [2 Theta]

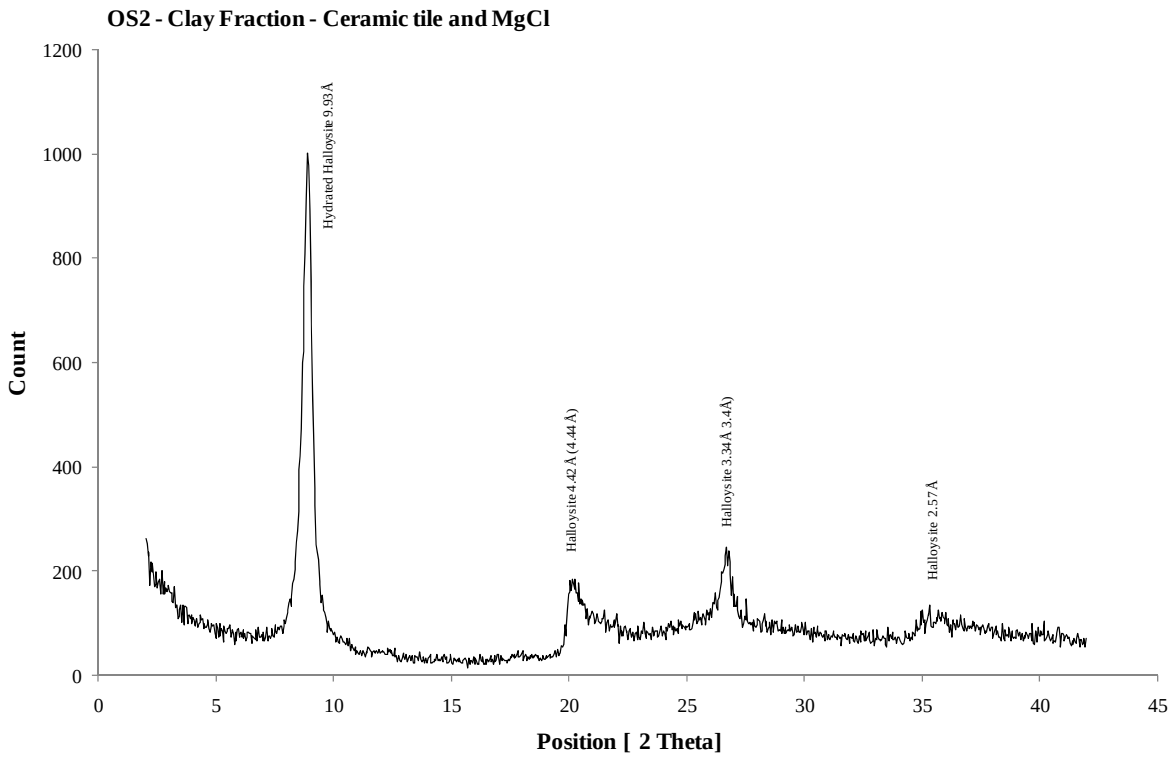
OS2 - Clay Fraction - Ceramic tile and MgCl
Count
Position [2 Theta]
Hydrated Halloysite 9.93Å
Halloysite 4.42 Å (4.44 Å)
Halloysite 3.34Å 3.4Å)
Halloysite 2.57Å

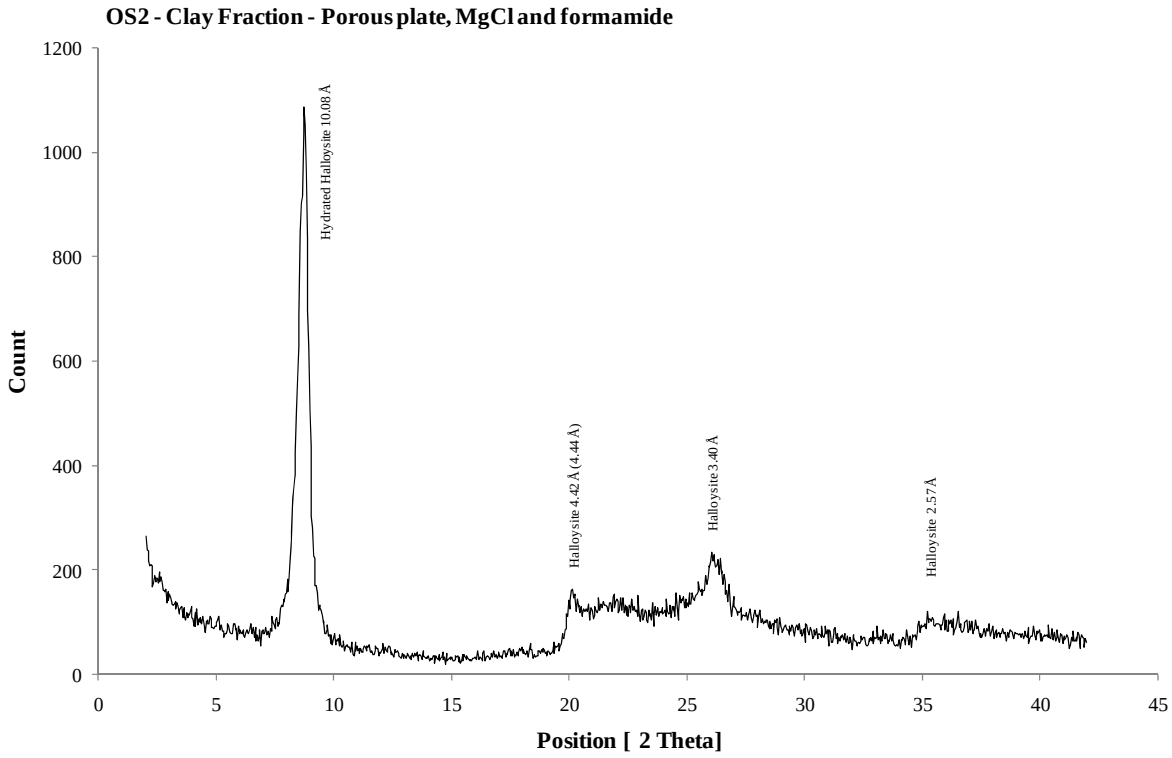
OS2 - Clay Fraction - Porous plate, MgCl and formamide
Count
Position [2 Theta]
Hydrated Halloysite 10.08 Å
Halloysite 4.42 Å (4.44 Å)
Halloysite 3.40 Å
Halloysite 2.57 Å

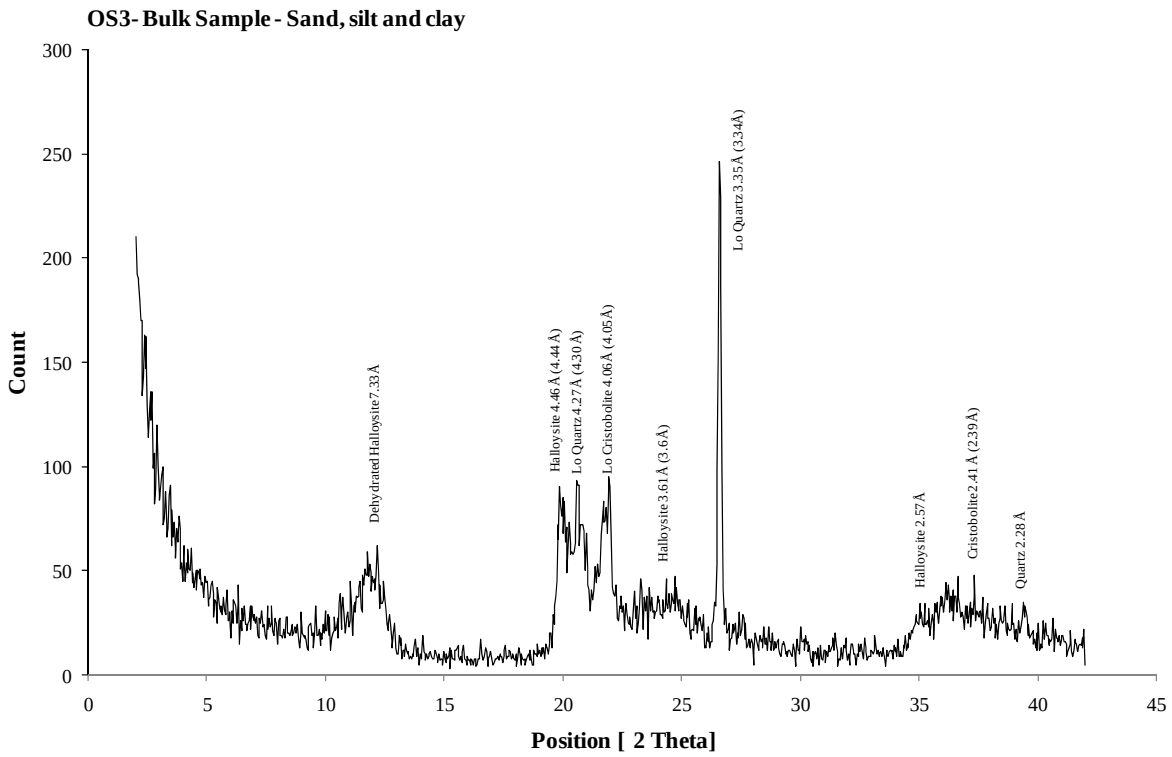
OS3- Bulk Sample - Sand, silt and clay
Count
Position [2 Theta]
Dehydrated Halloysite 7.33 Å
Halloysite 4.46 Å (4.44 Å)
Lo Quartz 4.27 Å (4.30 Å)
Lo Cristobolite 4.06 Å (4.05 Å)
Halloysite 3.61 Å (3.6 Å)
Lo Quartz 3.35 Å (3.34 Å)
Halloysite 2.57 Å
Cristobolite 2.41 Å (2.39 Å)
Quartz 2.28 Å

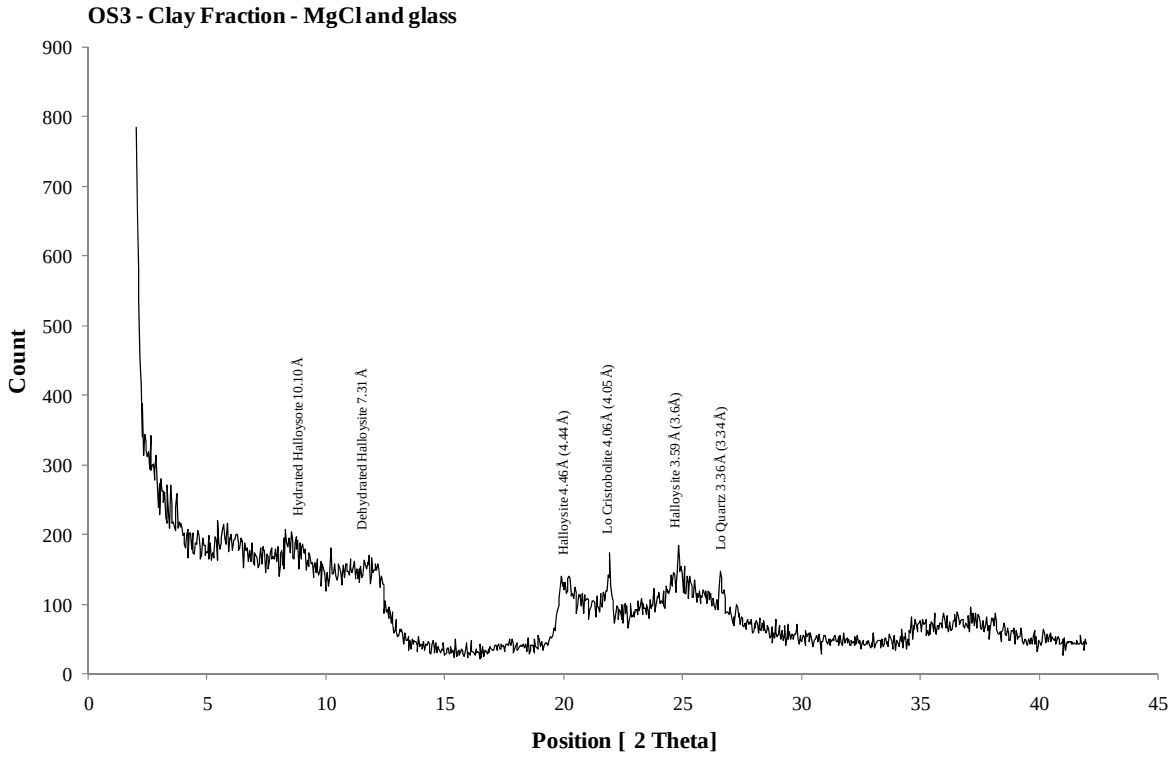
OS3 - Clay Fraction - MgCl and glass
Count
Position [2 Theta]
Hydrated Halloysite 10.10 Å
Dehydrated Halloysite 7.31 Å
Halloysite 4.46 Å (4.44 Å)
Lo Cristobolite 4.06 Å (4.05 Å)
Halloysite 3.59 Å (3.6 Å)
Lo Quartz 3.36 Å (3.34 Å)

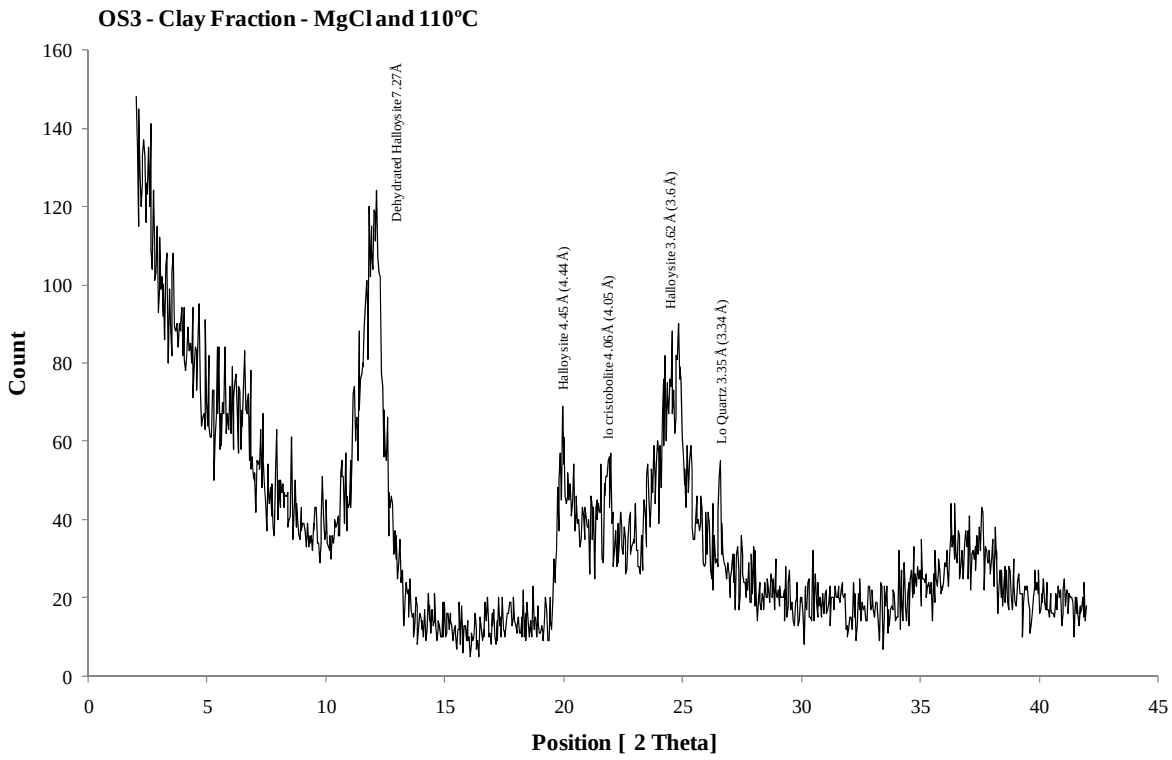
OS3 - Clay Fraction - MgCl and 110ºC
Count
Position [2 Theta]
Dehydrated Halloysite 7.27 Å
Halloysite 4.45 Å (4.44 Å)
Io cristobolite 4.06 Å (4.05 Å)
Halloysite 3.62 Å (3.6 Å)
Lo Quartz 3.35 Å (3.34 Å)

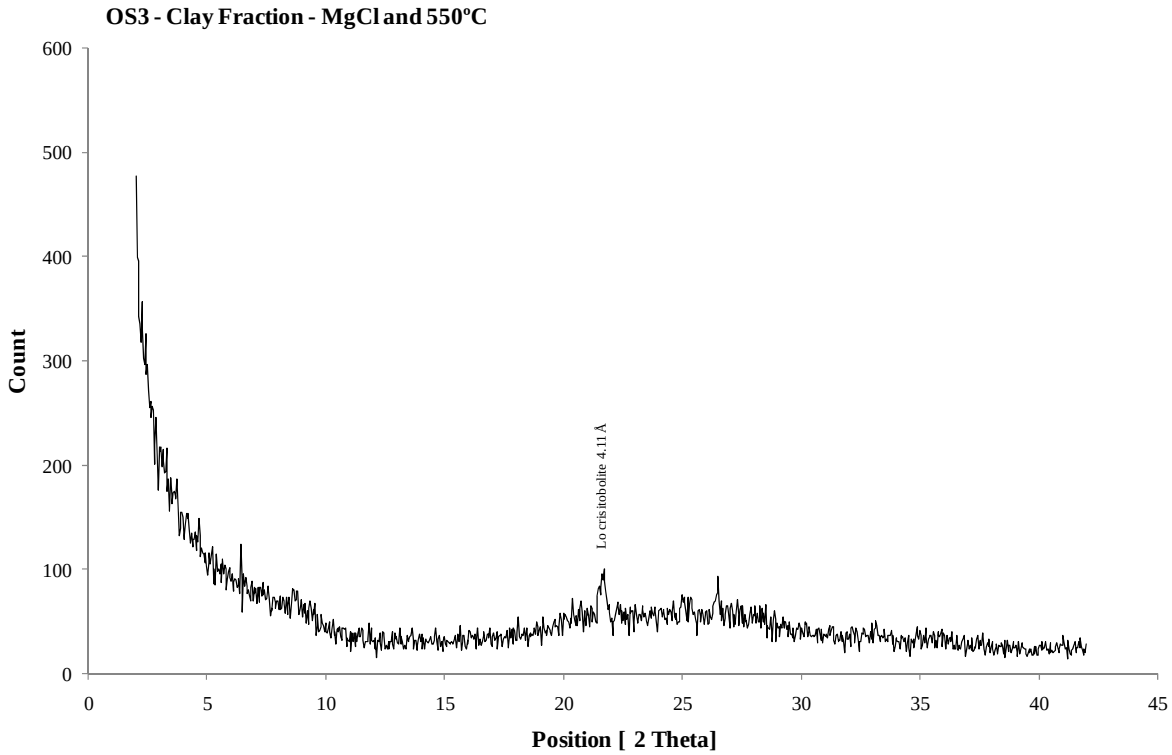
OS3 - Clay Fraction - MgCl and 550ºC
Count
Position [2 Theta]
Lo cristobolite 4.11 Å

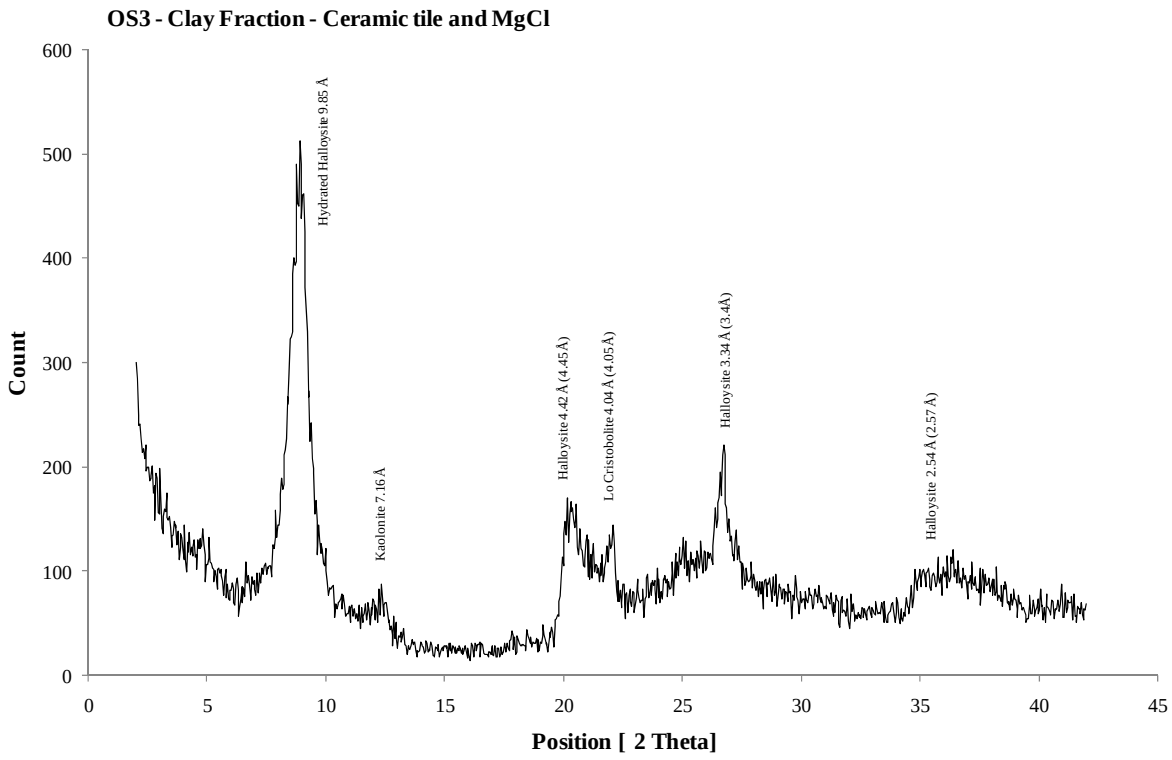
OS3 - Clay Fraction - Ceramic tile and MgCl
Count
Position [2 Theta]
Hydrated Halloysite 9.85 Å
Kaolonite 7.16 Å
Halloysite 4.42 Å (4.45Å)
Lo Cristobolite 4.04 Å (4.05Å)
Halloysite 3.34 Å (3.4Å)
Halloysite 2.54 Å (2.57 Å)

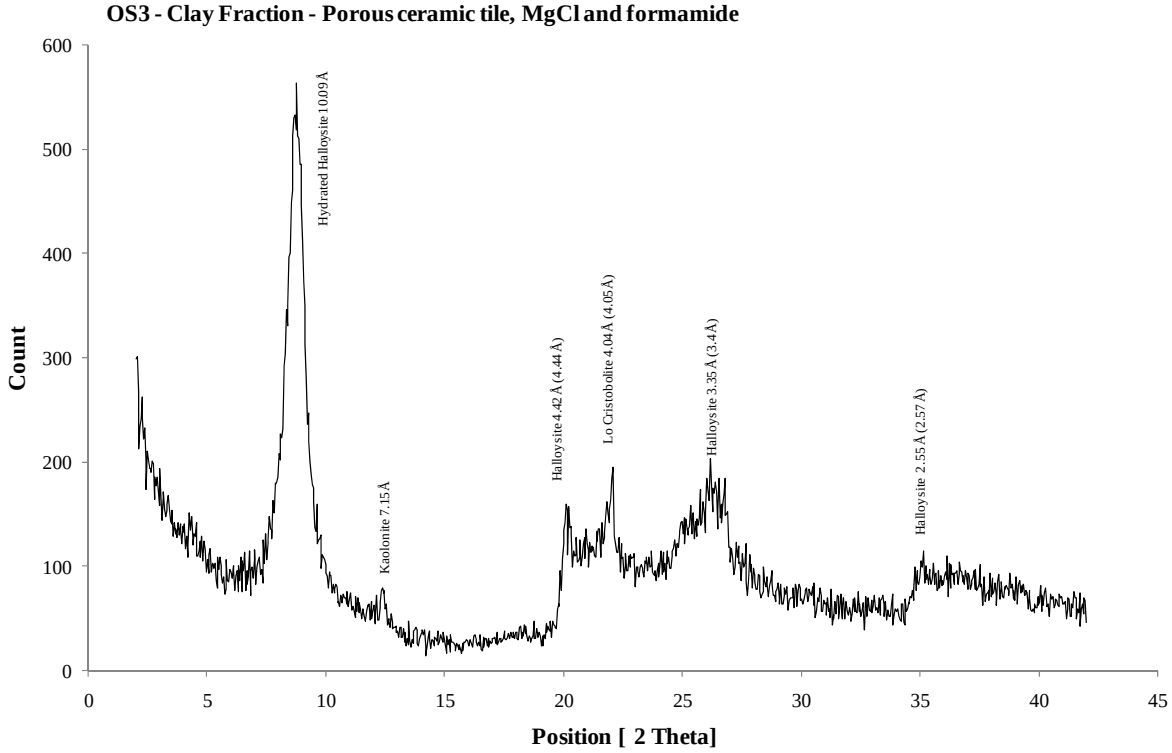
OS3 - Clay Fraction - Porous ceramic tile, MgCl and formamide
Count
Position [2 Theta]
Hydrated Halloysite 10.09 Å
Kaolonite 7.15 Å
Halloysite 4.42 Å (4.44 Å)
Lo Cristobolite 4.04 Å (4.05 Å)
Halloysite 3.35 Å (3.4 Å)
Halloysite 2.55 Å (2.57 Å)

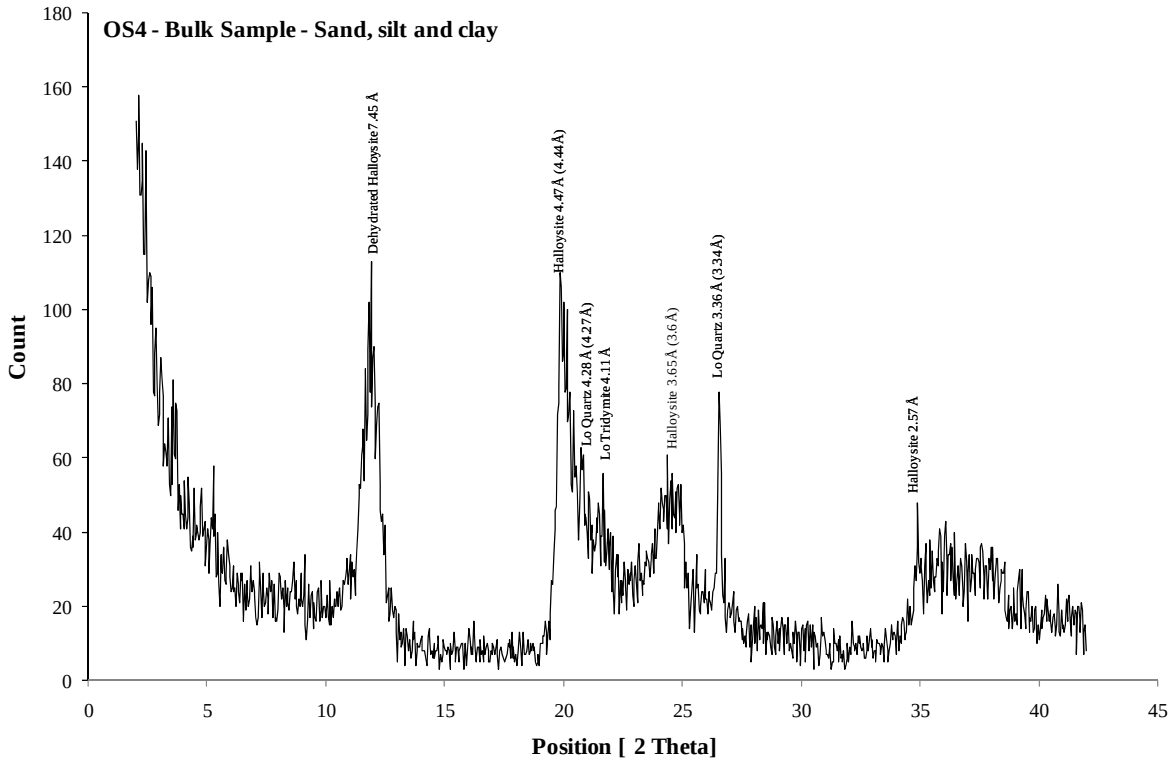
OS4 - Bulk Sample - Sand, silt and clay
Count
Position [2 Theta]
Dehydrated Halloysite 7.45 Å
Halloysite 4.47 Å (4.44Å)
Lo Quartz 4.28 Å (4.27 Å)
Lo Tridymite 4.11 Å
Halloysite 3.65 Å (3.6 Å)
Lo Quartz 3.36 Å (3.34 Å)
Halloysite 2.57 Å

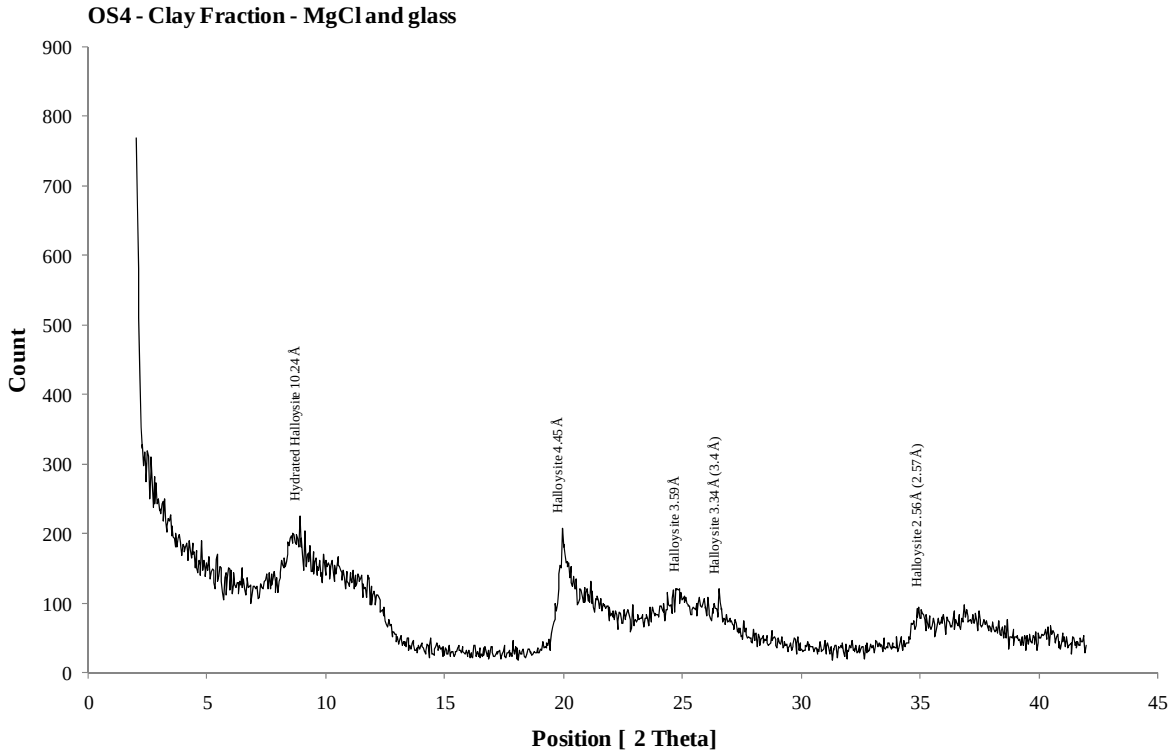
OS4 - Clay Fraction - MgCl and glass
Count
Position [2 Theta]
Hydrated Halloysite 10.24 Å
Halloysite 4.45 Å
Halloysite 3.59 Å
Halloysite 3.34 Å (3.4 Å)
Halloysite 2.56 Å (2.57 Å)

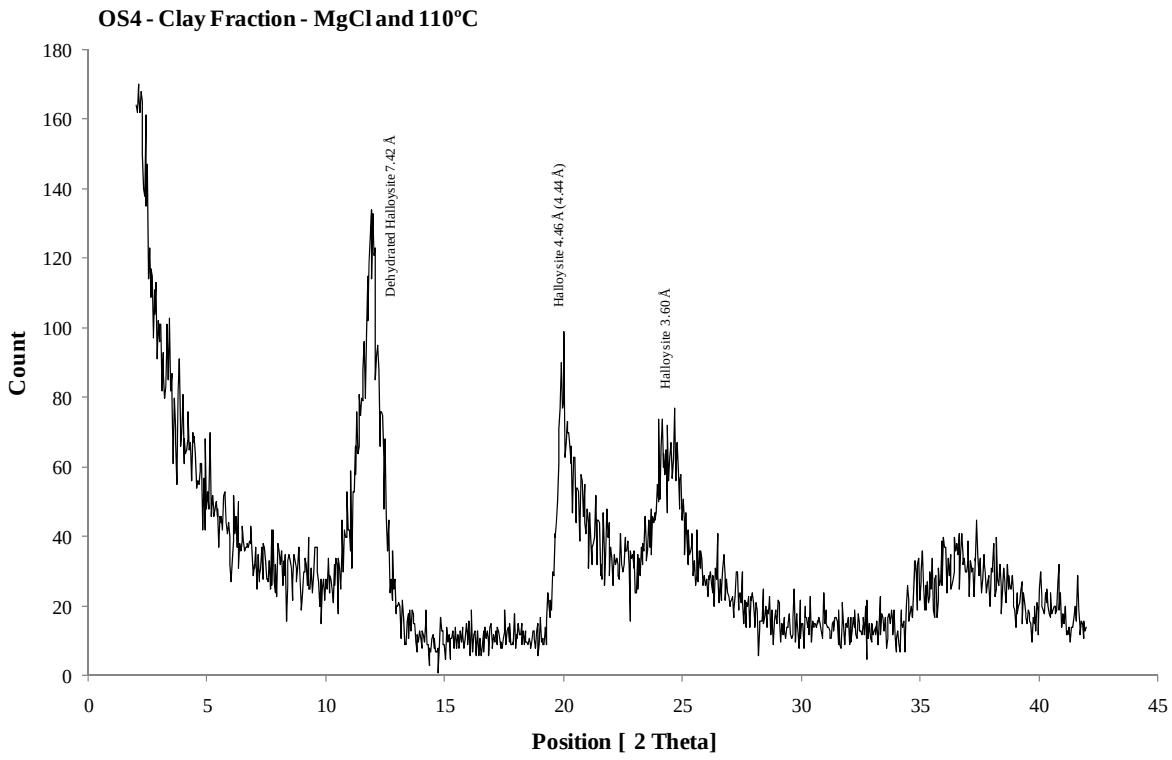
OS4 - Clay Fraction - MgCl and 110ºC
Count
Position [2 Theta]
Dehydrated Halloysite 7.42 Å
Halloysite 4.46 Å (4.44 Å)
Halloysite 3.60 Å
0
20
40
60
80
100
120
140
160
180
0
5
10
15
20
25
30
35
40
45

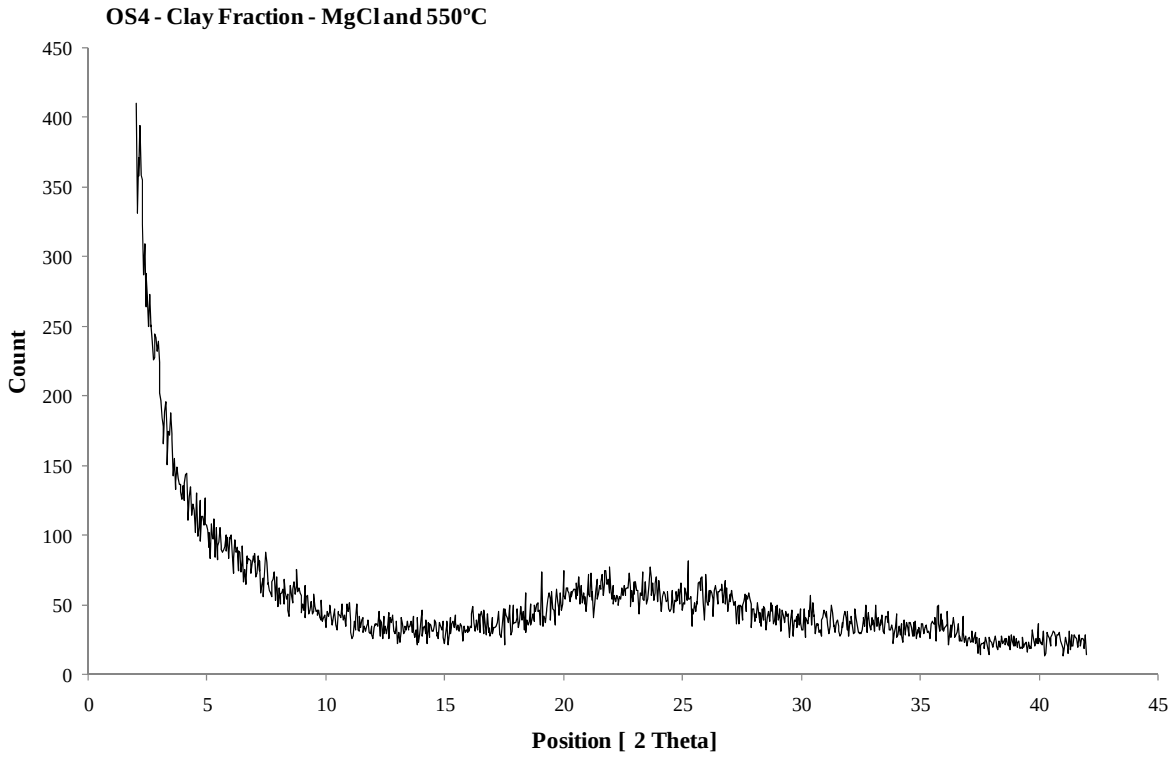
OS4 - Clay Fraction - MgCl and 550ºC
Count
Position [2 Theta]
0
50
100
150
200
250
300
350
400
450
0
5
10
15
20
25
30
35
40
45

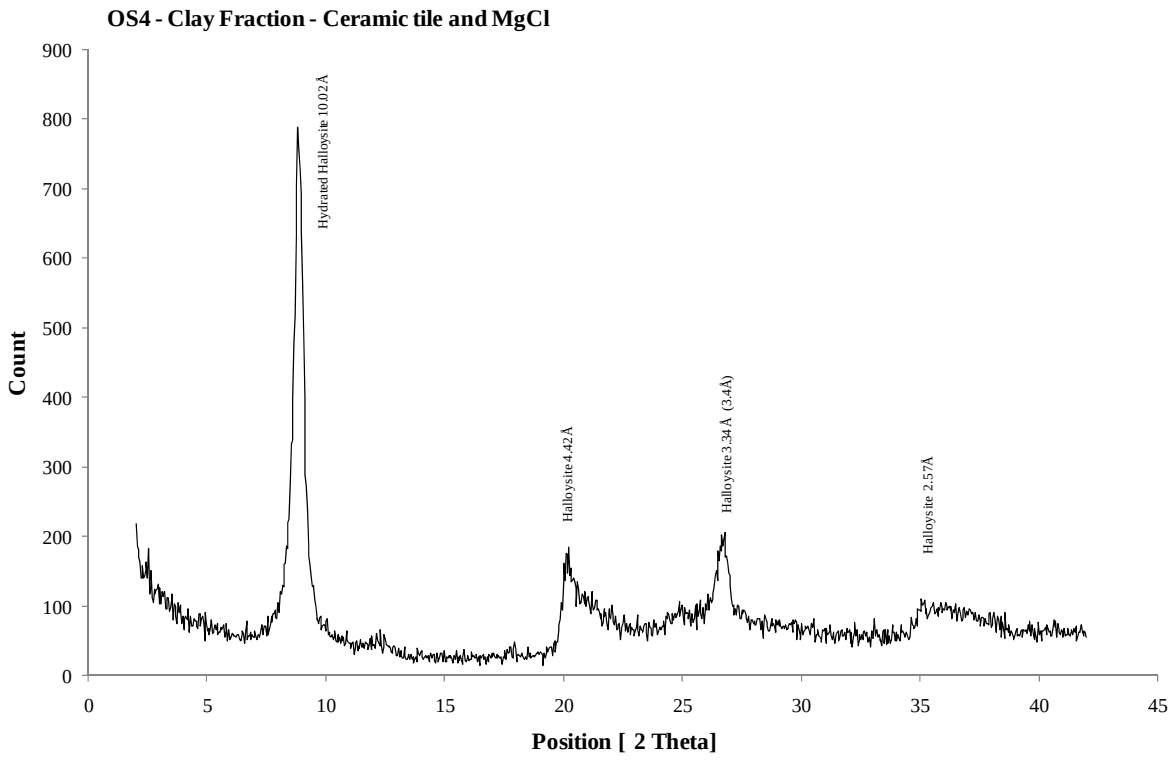
OS4 - Clay Fraction - Ceramic tile and MgCl
Count
Position [2 Theta]
Hydrated Halloysite 10.02Å
Halloysite 4.42Å
Halloysite 3.34Å (3.4Å)
Halloysite 2.57Å

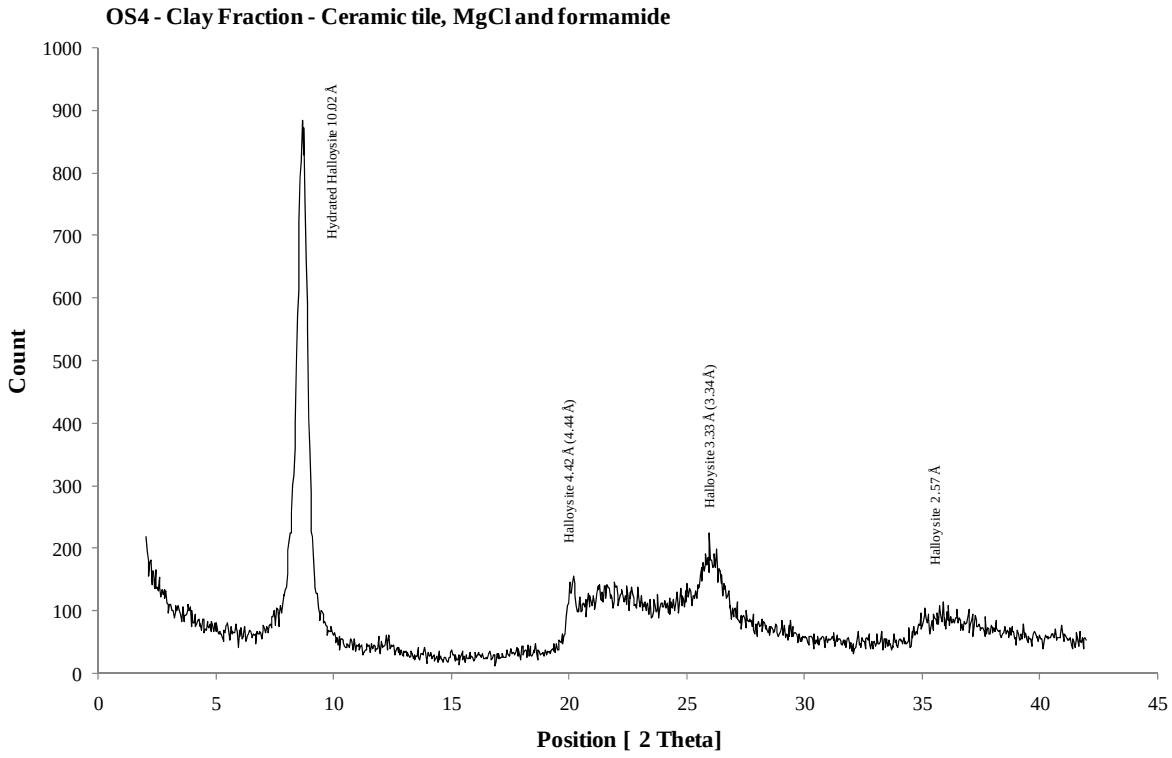
OS4 - Clay Fraction - Ceramic tile, MgCl and formamide
Count
Position [2 Theta]
Hydrated Halloysite 10.02 Å
Halloysite 4.42 Å (4.44 Å)
Halloysite 3.33 Å (3.34 Å)
Halloysite 2.57 Å

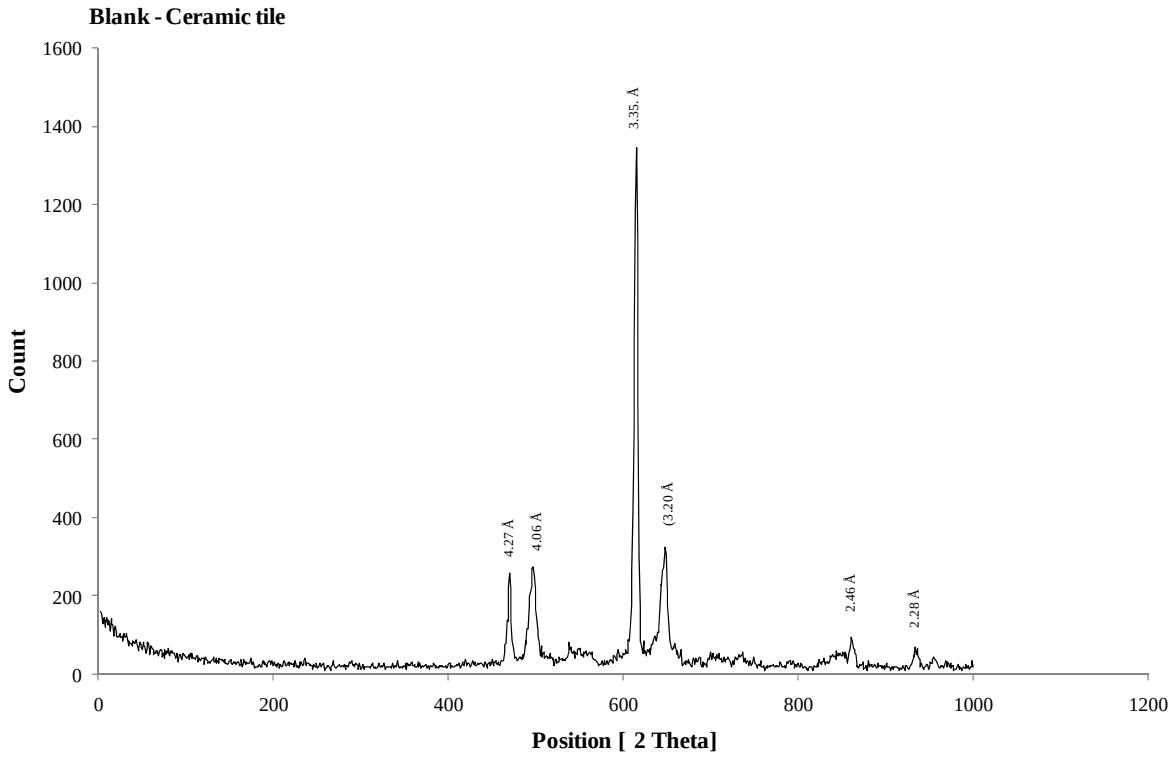
Blank - Ceramic tile
Count
Position [2 Theta]
1600
1400
1200
1000
800
600
400
200
0
0
200
400
600
800
1000
1200
4.27 Å
4.06 Å
3.35. Å
(3.20 Å
2.46 Å
2.28 Å

Appendix 6.3

The following presents raw and corrected EDX values from SEM analysis.

Raw tubes and books

Books

	Analy 19	analy 20	Analy 21	analy 22	analy 23	analy 28	analy 25	mean	error	std dev
O k	58.51	53.47	57.52	57.72	56.20	51.65	54.08	55.59	1.05	2.57
Al k	17.37	18.61	17.64	17.08	17.97	18.67	18.82	18.02	0.28	0.69
Si k	20.63	23.41	21.52	21.16	22.42	23.84	23.10	22.30	0.50	1.22
Ti l	0.00	0.00	0.00	0.00	0.00	0.00	0.00	0.00	0.00	0.00
Ti k	0.00	0.00	0.00	0.00	0.00	0.74	0.00	0.11	0.11	0.28
Fe k	3.49	4.19	3.32	3.18	3.41	4.34	3.47	3.63	0.18	0.45
Fe L	0.00	0.00	0.00	0.00	0.00	0.00	0.00	0.00	0.00	0.00
Ge K	0.00	0.00	0.00	0.00	0.00	0.00	0.00	0.00	0.00	0.00
Zn k	0.00	0.33	0.00	0.46	0.00	0.00	0.00	0.11	0.08	0.20
Mg k	0.00	0.00	0.00	0.00	0.00	0.76	0.53	0.18	0.13	0.32
Cl	0.00	0.00	0.00	0.40	0.00	0.00	0.00	0.06	0.06	0.15

tubes

	tube 1	tube 2	tube 3	tube 4	tube 7	tube 8	tube 9	tube 10	tube 11	tube 12	tube 7(2)	tube 9(3)	tube 9(2)	13	mean	error	std dev
O k	61.92	59.36	56.30	48.06	48.16	60.40	61.85235	57.31	46.43	63.01	49.31	60.26	57.00	58.98	56.31	1.68	5.81
Al k	14.62	17.95	18.61	21.14	21.06	16.55	15.87582	18.05	22.59	15.49	19.97	15.88	16.79	16.35	17.92	0.70	2.44
Si k	20.16	20.73	22.91	27.99	28.17	21.21	19.88371	23.05	29.63	19.95	26.90	21.61	23.93	21.63	23.41	0.98	3.38
Fe k	1.50	1.96	2.18	2.81	2.62	1.84	2.388122	1.60	1.35	1.55	3.82	2.25	2.27	3.05	2.23	0.20	0.69

Corrected tubes and books, and blank values

books

	Analy 19	analy 20	Analy 21	analy 22	analy 23	analy 28	analy 25	mean	Std dev	Error
Al203	32.81	35.16	33.33	32.26	33.95	35.26	35.56	34.05	1.31	0.53
SiO2	44.14	50.07	46.03	45.26	47.95	51.00	49.41	47.69	2.61	1.07
Fe2O3	4.99	5.98	4.75	4.55	4.88	6.21	4.96	5.19	0.64	0.26

tubes

	tube 1	tube 2	tube 3	tube 4	tube 7	tube 8	tube 10	tube 11	tube 12	tube 7(2)	tube 9(3)	tube 9(2)	13.00	mean	Std dev	Error
Al203	27.62	33.91	35.15	39.93	39.78	31.26	34.10	42.67	29.26	37.72	30.00	31.72	30.89	34.15	4.66	1.34
SiO2	43.12	44.34	49.00	59.87	60.26	45.37	49.30	63.38	42.67	57.54	46.22	51.19	46.27	50.66	7.18	2.07
Fe2O3	2.15	2.80	3.12	4.02	3.75	2.63	2.29	1.93	2.22	5.46	3.22	3.25	4.36	3.17	1.02	0.29

blank stub with carbon tape

C K	67.03
O k	21.08
Pt L	11.89

EDX values for volcanic glass found in Tauriko samples. Multipliers are from Berkman (2001).

		multiplier		
O	40.91			
Na	2.06	**x 1.348 =**	**Na_2O**	2.78
Al	7.24	**x 1.889 =**	**Al_2O_3**	13.67
Si	40.44	**x 2.139 =**	**SiO_2**	86.49
Cl	0.00			
K	5.02	**x 1.205 =**	**K_2O**	6.05
Ca	0.92	**x 1.399 =**	**CaO**	1.29
Fe	3.42	**x 1.286 =**	**FeO**	4.39